SCHOOL OF CHEMICAL ENGINEERING
UNIVERSITI SAINS MALAYSIA

2nd SChE POSTGRADUATE COLLOQUIUM 2020

UNIVERSITI SAINS MALAYSIA

APEX™

2nd SChE Postgraduate Colloquium 2020

School of Chemical Engineering

Universiti Sains Malaysia

23rd September 2020

Engineering Campus

Universiti Sains Malaysia

Published by,

School of Chemical Engineering
Engineering Campus
Universiti Sains Malaysia
14300, Nibong Tebal
Penang, Malaysia

ISBN xxxxxxxx

CONTENTS

FOREWORD FROM COLLOQUIUM ADVISOR

I would like to extend a warm welcome all participants of 2nd SChE Postgraduate Colloquium 2020 organized by the School of Chemical Engineering, Universiti Sains Malaysia. Let me take this opportunity to express my gratitude to the organizing committee in ensuring this colloquium a success. Congratulations!

Postgraduate students play the main backbone in the research area and are the important key to uphold the success and strive towards international ranking. This colloquium is designed to inculcate the research sharing among the postgraduate students by encouraging them to disseminate their research works through technical writings and presentations. Its main purpose is to showcase methodologies, applications and projects that bridge the gap between rudimentary research efforts and industrial applications, thus provoking advanced development in the research area. Participants from various disciplines in chemical engineering should use this opportunity to gain knowledge and be acquainted with other research areas from parallel sessions.

I am certain that this colloquium will see not only highly interesting presentations, but also venturing the new era of knowledge and research. In this spirit, I wish you all inspiring and fruitful colloquium.

Thank you.

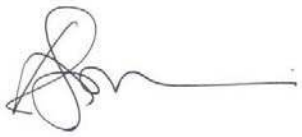

PROFESSOR IR. DR. ZAINAL BIN AHMAD
Dean, School of Chemical Engineering
Universiti Sains Malaysia

FOREWORD FROM COLLOQUIUM CHAIRMAN

It is a great pleasure for me to welcome all participants to the 2nd SChE Postgraduate Colloquium 2020. SChE 2020 is organized to bring together innovative postgraduate researchers in broad areas related to the Separation Process / Reaction Engineering, Biochemical/Environmental Engineering and Process Control / Modelling to a common forum. The primary goal of the colloquium is to promote R&D activities and exchange of scientific knowledge and research know-how among postgraduate researchers and academia. Postgraduate researchers are duly acknowledged and honoured in terms of their research efforts by presenting their work through this colloquium. About 45 participants participated in this event and 51 submitted the full paper.

On behalf of the organizing committee, I would like to express my thanks and appreciation to all those who are involved either directly as participants, speakers and committee members or indirectly for their effort in materializing the success of the SChEPC 2020.

Thank you.

PROFESSOR DR. MOHD AZMIER BIN AHMAD
Deputy Dean, School of Chemical Engineering
Universiti Sains Malaysia

ORGANIZING COMMITTEE

ADVISOR
Professor Ir. Dr. Zainal Ahmad
(Dean, School of Chemical Engineering, Universiti Sains Malaysia)

CHAIRMAN
Professor Dr. Mohd Azmier Ahmad
(Deputy Dean Research, Innovation & Industrial-Community Engagement,
School of Chemical Engineering, Universiti Sains Malaysia)

SECRETARY
Mira Edora Abdul Khani
Esah Abdul Manaf

TREASURER
Zuraida Mat Lazim

REVIEW COMMITTEE
Professor Dr. Mohd Azmier Ahmad (Head)
Dr. Lutfi Kurnianditia Putri
Dr. Nor Aini Ahmad
Dr. Nuur Fahanis Che Lah
Dr. Syahida Farhan Azha

PUBLICITY & PROMOTION COMMITTEE
Sofiah Mat Rasit

TECHNICAL & PHYSICAL COMMITTEE
Mohd Rasydan Omar
Mohammad Faizal Abu Bakar

DESIGNER
Dr. Nuur Fahanis Che Lah

FOOD & BEVERAGE COMMITTEE
Nur Aidila Mohd Lokman
Shaiful Musa

PUBLICATION COMMITTEE
Nur Husna Mansor

EVENT EMCEE
Danial Syakirin Zainal

JURY
Assoc. Prof. Dr. Suzylawati Ismail
Assoc. Prof. Dr. Vel Murugan Vadivelu
Assoc. Prof. Dr. Low Siew Chun

REGISTRATION COMMITTEE
Esah Abdul Manaf

SOUVINER COMMITTEE
Noor Hasliza Wan Chik
Norsiah Abd Rahman
Normie Hana A. Rahim

Dr. Azam Taufik Mohd Din
Dr. Irvan Dahlan
Dr. Masrina Mohd Nadzir
Dr. Norazwan Md Nor
Ir. Dr. Noorashrina A Hamid

SUBCOMMITTEE MEMBERS
Assoc. Prof. Dr. Syamsul Rizal Abd Shukor
Mohd Kamil Ashar

COLLOQUIUM PROGRAMME

<table>
<tr><th>Time</th><th colspan="4">WEDNESDAY
23rd SEPTEMBER 2020</th></tr>
<tr><td>0800 – 0815</td><td colspan="4" rowspan="3">Colloquium Registration</td></tr>
<tr><td>0815 – 0830</td></tr>
<tr><td>0830 – 0845</td></tr>
<tr><td>0845 – 0900</td><td colspan="4">Opening Ceremony
Professor Ir. Dr. Zainal Ahmad
(Seminar Room, SERC)</td></tr>
<tr><td>0900 – 0915</td><td rowspan="11">Group 1
Oral
Presentation
(Seminar Room, SERC)</td><td rowspan="11">Group 2
Oral
Presentation
(Training Room, SERC)</td><td rowspan="11">Group 3
Oral
Presentation
(Meeting Room 3, SERC)</td><td rowspan="11">Group 4
Oral
Presentation
(Meeting Room 4, SERC)</td></tr>
<tr><td>0915 – 0930</td></tr>
<tr><td>0930 – 0945</td></tr>
<tr><td>0945 – 1000</td></tr>
<tr><td>1000 – 1015</td></tr>
<tr><td>1015 – 1030</td></tr>
<tr><td>1030 – 1045</td></tr>
<tr><td>1045 – 1100</td></tr>
<tr><td>1100 – 1115</td></tr>
<tr><td>1115 – 1130</td></tr>
<tr><td>1130 – 1145</td><td colspan="4" rowspan="3">Sharing Session
Profesor Dr. Ahmad Zuhairi Abdullah
(Seminar Room, SERC)</td></tr>
<tr><td>1145 – 1200</td></tr>
<tr><td>1200 – 1215</td></tr>
<tr><td>1215 – 1230</td><td colspan="4" rowspan="3">Award Ceremony
“Best Presenter Award”
Professor Ir. Dr. Zainal Ahmad
(Seminar Room, SERC)</td></tr>
<tr><td>1230 – 1245</td></tr>
<tr><td>1245 – 1300</td></tr>
<tr><td>1300 – 1400</td><td colspan="4">LUNCH</td></tr>
</table>

Schedule of Parallel Oral

Presentation Sessions

ORAL PRESENTATION

VENUE: SEMINAR ROOM		
Time	**Paper ID**	**Title of Presentation**
0920 – 0930	PGC_SCHE USM_2020_01	**Physical Characterization of LSCF-NiO as Cathode Material for Intermediate Temperature Solid Oxide Fuel Cell (IT-SOFCs)** *A.Z. Rosli, M.R. Somalu, N. Osman, N.A. Hamid*
0930 – 0940	PGC_SCHE USM_2020_02	**Enhancement of Lanthanum, Strontium, Cobalt, Ferum perovskite with copper oxide (LSCF-CuO) infiltration as promising cathode for Intermediate Temperature Solid Oxide Fuel Cell (IT-SOFC)** *Ahmad Fuzamy Mohd Abd Fatah, Noorashrina A Hamid, Ahmad Azmin Mohamad, Andanastuti Muchtar*
0940 – 0950	PGC_SCHE USM_2020_03	**Polymer screening evaluation for nanofiber membrane** *A.I. Abdul Jalil, S. Ismail*
0950 – 1000	PGC_SCHE USM_2020_04	**The particle size of lignocellulosic biomass affects crystallinity: A review** *Abiodun Abdulhameed Amusa, Abdul Latif Ahmad*
1000 - 1010	PGC_SCHE USM_2020_05	**Hydraulic Fracturing Fluid Performance Using Encapsulated Borate-Crosslinked Fluid for Deepwater Application** *Nurul Syaza Mohamad, Suzylawati Ismail, Ling Kong Teng*
1010 – 1020	PGC_SCHE USM_2020_07	**Removal of Cu (II) from aqueous solution using composite adsorptive membrane** *Shazlina Abd Hamid, Suzylawati Ismail*
1020 – 1030	PGC_SCHE USM_2020_08	**Fabrication of Microcrystalline Cellulose (MCC) Incorporated Polyether Sulfone (PES) Membranes: Study of Different Concentration MCC on Hydrophilicity** *Amirul Islah Nazri, Abdul Latif Ahmad*
1030 – 1040	PGC_SCHE USM_2020_09	**New adsorbent development: Synthesis of cellulose-activated carbon hybrid fiber via Schweitzer's reaction** *Nur Azian Ahammad, Mohd Azmier Ahmad, Bassim H. Hameed, Azam Taufik Mohd Din*
1040 – 1050	PGC_SCHE USM_2020_10	**Fouling and performance study of marine fish farm water desalination using submerged vacuum membrane distillation** *Ying Shi Chang, Boon Seng Ooi*
1050 – 1100	PGC_SCHE USM_2020_11	**Concentrating Nutrients from Fish Farm Effluent via Forward Osmosis** *Aaron Koe Zhen Yao, Ooi Boon Seng*
1100 – 1110	PGC_SCHE USM_2020_12	**Hydrophobic PVDF membrane via dual soft non-solvent bath system for direct contact membrane distillation in desalination** *Lyly Leow, Ooi Boon Seng*
1110 – 1120	PGC_SCHE USM_2020_13	**Effect of reaction temperature on CO_2 hydrogenation to methanol using In_2O_3 catalyst** *Zaza Hazrina Hashim, Munirah Mohd Zain, Abdul Rahman Mohammad*

Schedule of Parallel Oral

Presentation Sessions

ORAL PRESENTATION

VENUE: TRAINING ROOM		
Time	**Paper ID**	**Title of Presentation**
0930 – 0940	PGC_SCHE USM_2020_14	**Preparation of ZnO for Photocatalytic Activity of Phenol That Exceed Acros ZnO** *B. M. Namoos, Abdul Rahman Mohamed*
0940 – 0950	PGC_SCHE USM_2020_15	**Membranes for Gadolinium Removal in Wastewater Treatment** *E. I. Oluwasola, A.L. Ahmad, A.A. Amusa, and M.K. Alsebaeai*
0950 – 1000	PGC_SCHE USM_2020_16	**Water Polishing Via Gravitational-Driven Ultrafiltration Membrane** *Nur Ir Imani Ishak, Ooi Boon Seng*
1000 - 1010	PGC_SCHE USM_2020_17	**Effect of process parameters on solid-liquid extraction of *Dillenia suffruticosa* leaves** *Nur Allia Asri, Khairiah Abd Karim*
1010 – 1020	PGC_SCHE USM_2020_18	**Preliminary Study on the Compatibility of P84 Polyimide (PI) Coated Polymethylpentene (PMP) Thin Composite Membrane** *Zulfida Mohamad Hafis Mohd Shafie, Abdul Latif Ahmad, Siew Chun Low, Sabine Rode, Bouchra Belaissaoui, Denis Roizard*
1020 – 1030	PGC_SCHE USM_2020_20	**PVDF blended PVDF-co-HFP enhanced Membrane Hydrophobicity for Desalination of Seawater via Direct Contact Membrane Distillation (DCMD)** *N. H. Mat Radzi, A. L. Ahmad*
1030 – 1040	PGC_SCHE USM_2020_21	**Single pot catalytic glycerol dehydration-oxidation: Sustainable production of acrylic acid** *Anas Abdullah, Ahmad Zuhairi Abdullah*
1040 – 1050	PGC_SCHE USM_2020_22	**Adhesion of Cylindrotheca *fusiformis* on Polyethersulfone Tubular Capillary Membrane in Suspended Culture System** *Siti Mariam Md Poad, Derek Chan Juinn Chieh*
1050 – 1100	PGC_SCHE USM_2020_23	**Anti-wetting properties of synthesis hydrophobic membrane by incorporation of clay particles for direct contact membrane distillation (DCMD)** *Wan Aisyah Fadilah Wae AbdulKadir, Abdul Latif Ahmad, Ooi Boon Seng*
1100 – 1110	PGC_SCHE USM_2020_24	**Thermal Effect on Algae, Biofilm and Their Composition towards Membrane Distillation Unit** *Yin Sim Ng, Derek Juinn Chieh Chan*

Schedule of Parallel Oral

Presentation Sessions

ORAL PRESENTATION

VENUE: MEETING ROOM 3		
Time	**Paper ID**	**Title of Presentation**
0920 – 0930	PGC_SCHE USM_2020_26	**Graphene Nanostructure Material for CO_2 Capture** *Rabita binti Mohd Firdaus Achutan, Abdul Rahman Mohamed*
0930 – 0940	PGC_SCHE USM_2020_27	**Plantwide Control of Biodiesel Production from Waste Cooking Oil** *Rasheed Olakunle Kelani, Zainal bin Ahmad, Dipesh Patle*
0940 – 0950	PGC_SCHE USM_2020_29	**Comparative study of carbon nanotube dispersion using binary mixed polymers** *J.G. Robinson, A.H. Kamaruddin, F.N. Gonawan*
0950 – 1000	PGC_SCHE USM_2020_30	**Surface modification of PTFE membrane for direct contact membrane distillation (DCMD) application.** *Mohamad Razif Mohd Ramli, Abdul Latif Ahmad*
1000 - 1010	PGC_SCHE USM_2020_31	**Development of Food Waste-Derived Biochar for CO_2 Capture at Ambient Condition** *Amirul Hazwan Nor Azazi, Abdul Rahman Mohamed*
1010 – 1020	PGC_SCHE USM_2020_37	**Screening of Natural Coagulant from Fruit Peels for Turbidity Removal** *Khadijah Md Noh, Suzylawati Ismail*
1020 – 1030	PGC_SCHE USM_2020_38	**Catalytic Co-pyrolysis of Plastic Waste and Biomass for the Production of Fuel Oil: Positive Synergistic Effect of Feedstock on Fuel Oil Yield and Quality –A Short Review** *A.W., Gin, M.A., Ahmad, A.T., Mohd Din*
1030 – 1040	PGC_SCHE USM_2020_40	**Quantifying Relationship between Chain Transfer Agent and Melt Flow Index for Low Density Polyethylene Tubular Reactor Production** *Dinie Muhammad, Zainal Ahmad, Norashid Aziz*
1040 – 1050	PGC_SCHE USM_2020_41	**Morphology Studies of Kaolin Hollow Fiber Membrane: Effect of Different Bore Fluid Rates** *M. I. M. Esham, A. L. Ahmad*
1050 – 1100	PGC_SCHE USM_2020_42	**Modelling Performance of *Spirodela polyrhiza*, *Salvinia molesta* and *Lemna minor* under Increasing Salinity** *Daniel Nesan, Derek Chan Juinn Chieh*
1100 – 1110	PGC_SCHE USM_2020_25	**Comparative study of the treatment of batik wastewater through electrocoagulation process using different types of metal waste-based electrodes** *Nurulhuda Amri, Ahmad Zuhairi Abdullah, Suzylawati Ismail*

Schedule of Parallel Oral

Presentation Sessions

ORAL PRESENTATION

VENUE: MEETING ROOM 4		
Time	**Paper ID**	**Title of Presentation**
0920 – 0930	PGC_SCHE USM_2020_44	**Biochar produce via liquid hot water (LHW) pretreatment and pyrolysis for CO_2 adsorption at low temperature** *Nurul Azrin Zubbri, Abdul Rahman Mohamed*
0930 – 0940	PGC_SCHE USM_2020_45	**Electrospun PET for Effective Air Filtration Media** *Wei Lin Ng, Soon Huat Tan*
0940 – 0950	PGC_SCHE USM_2020_46	**Elucidation of Kinetics and Mechanism of Uncatalyzed Esterification of Acetic Anhydride with Isoamyl Alcohol in a Microreactor System** *Cheong Sheng Lee, Syamsul Rizal Abd Shukor*
0950 – 1000	PGC_SCHE USM_2020_53	**Review of feedwater treatments for steam boilers at palm oil factory in Perak** *Muhammad Rufaizal Izham Rusdi, Zainal Ahmad*
1000 - 1010	PGC_SCHE USM_2020_56	**Preliminary studies on material selection for developing new polymeric water shut off agent emphasized on Malaysian average wellbore condition** *Siti Nuraffini Kamarulizam. Suzylawati Ismail*
1010 – 1020	PGC_SCHE USM_2020_57	**Co-Pyrolysis Process of Palm Kernel Shell and Polypropylene for Bio-Oil Production: Effect of Blending Ratio** *Aizatul Hikmah Zulkafli, Hamizura Hassan, Mohd Azmier Ahmad*
1020 – 1030	PGC_SCHE USM_2020_58	**Investigation on Activated Carbon Pre-treatment in Catalytic Cracking of Waste Cooking Oil** *Tavayogeshwary Thangadurai, Ching Thian Tye*
1030 – 1040	PGC_SCHE USM_2020_32	**Textured superhydrophobic membrane to treat high saline water via direct contact membrane distillation** *Teoh Guang Hui, Low Siew Chun*
1040 – 1050	PGC_SCHE USM_2020_33	**Surface coating rendered PP electrospun membrane superhydrophobic for desalination in membrane distillation** *Chin Jing Yi, Low Siew Chun*
1050 – 1100	PGC_SCHE USM_2020_43	**Effect of Particle Size on Bio-oil Production in Pyrolysis Process of Palm Wastes** *M.A. Al-Maari, M.A. Ahmad, A.M. Alsobaai, H. Hassan, A.T.M. Din*
1100 – 1110	PGC_SCHE USM_2020_06 (recording)	**Plant mediated synthesis of Titanium dioxide (TiO_2) nanoparticles: Mini review** *Mohammad Aslam, Ahmad Zuhairi Abdullah, Mohd Rafatullah*
1110 – 1120	PGC_SCHE USM_2020_48 (recording)	**Comparing Different Data Reduction Techniques in the Development of Water Quality Index (WQI) Prediction Model** *Danny Hartanto Djarum, Zainal Ahmad, Jie Zhang*

PGC_SCHE USM_2020_01

Physical Characterization of LSCF-NiO as Cathode Material for Intermediate Temperature Solid Oxide Fuel Cell (IT-SOFCs)

A.Z. Rosli[1], M.R. Somalu[2], N. Osman[3*], N.A. Hamid[1,*]
[1]School of Chemical Engineering, Engineering Campus, Universiti Sains Malaysia, 14300 Nibong Tebal Penang, Malaysia
[2]Fuel Cell Institute (Sel Fuel) Level 4, Research Complex, Universiti Kebangsaan Malaysia 43600 Bangi, Selangor, Malaysia
[3]Fakulti Sains Gunaan, Universiti Teknologi MARA Cawangan Perlis Kampus Arau, 02600 Arau, Perlis
E-mail: chrina@usm.my

Abstract. Fuel cell shows promising potential for energy production and solid oxide fuel cell (SOFC) is growing rapidly in the recent years. SOFC comprises of three parts; cathode, anode and electrolyte, and each of them have their own role. In intermediate temperature SOFC (IT-SOFC), cathode must provide triple phase boundary (TPB) for oxygen reduction reaction (ORR) to occur before the electron and ions can pass through. Therefore, $La_{0.6}Sr_{0.4}Co_{0.2}Fe_{0.8}$ (LSCF) composite with NiO was proposed as cathode material for IT-SOFC for its high electrical conductivity, high catalytic activity and high ORR. LSCF-NiO was synthesized through modified sol-gel method. A sample consisted of 1:1 ratio of LSCF and NiO was used for characterization with XRD and TGA/DTA. XRD result proved high purity and this finding affiliated that elevating calcining temperature eventually caused crystal size to be increased. TGA/DTA result showed that removal of organic compound occured at 200-400°C with peak at 250°C and the perovskite completely formed at 650ºC. As such, sample calcined at 700°C and above have good properties for IT-SOFC application. Characterization results of LSCF and NiO showed good compatibility. Therefore, LSCF-NiO is indeed have promising properties to be used as the cathode for intermediate temperature SOFC.
Keywords: *IT-SOFC; LSCF-NiO; physical characterization*

INTRODUCTION

Fuel cell is a contraption that converts chemical energy from fuels such as hydrogen and methane directly to electricity. Solid oxide fuel cell (SOFC) is one of the most common type of fuel cells being researched in the recent years since it possesses high conversion efficiency, low greenhouse gas emission and fuel flexibility [1]. However, it is desired to synthesize suitable material to allow SOFC to be operated at lower temperature [2], [3]. Recently, there are great attention on developing modified MIEC materials such as LSCF for SOFC because it is suitable for IT-SOFC cathode as it has enough required oxide ion and electron to operate efficiently at intermediate temperature [2]. Although, LSCF showed excellent performance but in exchange it has large thermal expansion coefficient compared to electrolyte and chemical instability when it is operated at high temperature. Volatility is also restricting the material from any practical application till now [4]. It is well known that LSCF possesses high ionic and electronic conductivity at intermediate temperature and shows impressive oxygen reduction reaction (ORR) catalytic activity [5].

However, its performance is bottle-necked by the transportation of oxygen ion. The development of LSCF is also being limited by the degradation of the material at its operating temperature [6]. Therefore, infiltration of noble metal was introduced into cathode surface layer to promote additional active sites at the B-site of the perovskite in order to improve its performable. The oxygen ion transportation also needs to be improved due to limiting factor of the LSCF performance. Fatah et al. [7] reported that the infiltration nobel metals such as CuO on the surface of the perovskite has improved the performance of the cathode. This proves that the infiltration of noble metal into the perovskite structure can improve its ORR activity at lower operating temperature. This is an interested topic to be focused on the development of improved version of LSCF cathode for IT-SOFC application. In this preliminary study, NiO would be infiltrated in the LSCF perovskite structure followed by characterization using TGA and XRD. Meanwhile, NiO was chosen due to cheaper material and good electric properties.

MATERIALS AND METHODS

La0.6Sr0.4Co0.2Fe0.8O3- (LSCF) sample was prepared by sol-gel method. The respective metal nitrates were dissolved with the ratio of 6:4:2:8 in the mixture of citric acid and ethylene glycol. The ratio of metals, citric

acid and ethylene glycol is 1:1:1. Citric acid acted as a chelating agent while ethylene glycol acted as a polymerizing agent. The mixture was stirred overnight, and then stirred at 100°C for 3 hours to form a gel. The gel was sintered at 600°C, 700°C, 800°C and 900°C for 6 hours, respectively. The char was crushed using agate pestle mortar and mixed with NiO at ratio of 1:1 and calcined again at their respective temperature for 6 hours. The sample was crushed again until a fine powder is formed.

X-ray diffraction (XRD) was used for phase composition characterization with Cu Kα from 10° to 70° for all samples using AXS Bruker GmbH. The raw data from XRD was taken and analyzed using Xpert-Highscore plus. The sample LSCF-NiO prepared at 800 °C was compared with the literature and synthesized LSCF and NiO at 800°C. Thermal decomposition behaviour was conducted using the Thermogravimetric analysis (TGA), Pelkin Elmer STA 600, starting from room temperature until 900°C with the air flowrate of 50cm^3/min and heating rate of 5°C/min in air.

RESULTS AND DISCUSSION

TGA was conducted to determine the optimum calcination temperature for LSCF-NiO powder synthesized. This analysis used to determine the temperature of the formation of lattice oxygen. Fig. 1 shows the TGA curve for the LSCF sample. The TGA result was divided into three sections, where the first section focuesed from room temperature to 150°C. Here, the removal of adsorbed water and nitrates from the metal nitrates occurred. This happened due to boiling point of water at 100°C and usually removal of nitrates happened at 70°C. As for second phase, range from 150°C to 500°C, a very steep TGA curve observed. Each organic compound makes two third of the total sample mass, so the steep curve was expected. Most of the weight reduced at 250°C where the removal of organic content took place. The steep curve started at around 200°C because the boiling point of polymerizing agent ethylene glycol at 197°C. As for the chelating agent citric acid, its boiling point at 320°C. However, it was expected to evaporate before it reaches the boiling point where it was removed along with the ethylene glycol as proven by the curve. Until the sample reached 450°C, the decomposition of combustion residue took place as its weight was constant. As for the third section from 500°C to 900°C, a sudden weight dropped as observed at 600°C. At this temperature formation of lattice took place. The similar pattern was achieved by several researchers on MIEC structure [8], [9]. From 650°C to 900°C, there no obvious slope observed indicating the complete formation of perovskite structure. The early conclusion that could be made where the LSCF perovskite structure could not completely form at 600°C.

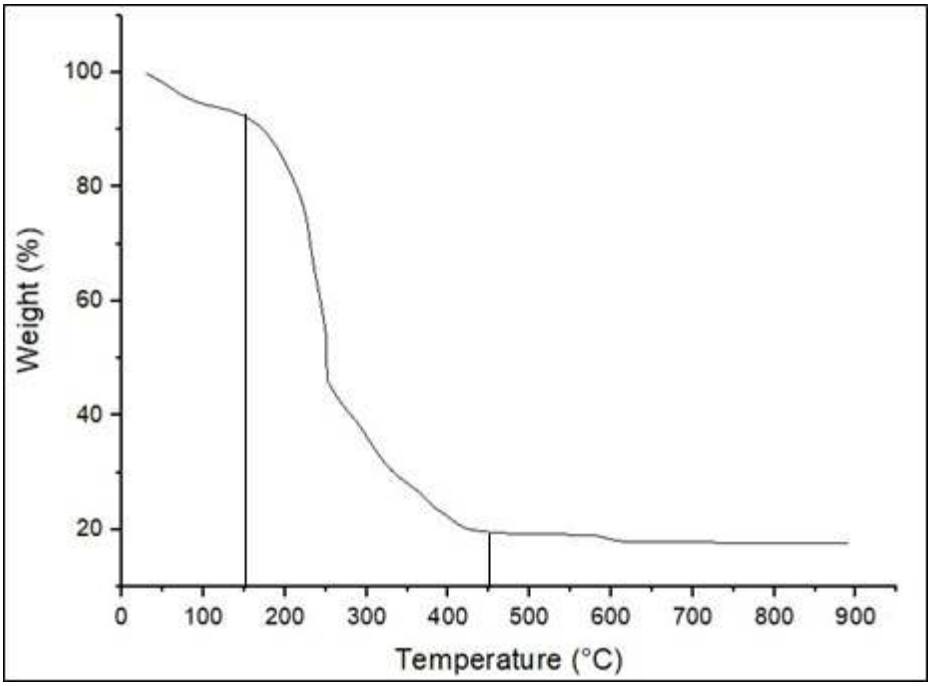

Figure 1. TGA curve of LSCF at precursor state

The XRD analysis was done to determine the phase composition with Cu K□ radiation from 10° to 70°. The data was analysed using Xpert-Highscore plus. The LSCF and NiO peak phases were also compared to the literatures. LSCF-NiO prepared at 800°C was chosen to compare with LSCF and NiO peaks. The comparison is shown in Fig. 2a. The entire peaks were identified as LSCF and NiO, and the peaks from both can be observed in

the LSCF-NiO 800 sample calcined at 800°C. When compared to peaks from other literature, it was found that the peaks of LSCF and NiO were identical. This also proved that the LSCF and NiO were indeed compatible with each other as it was able to form single phase perovskite structure at the synthesised temperature. Further study was done towards the XRD analysis regarding the comparison of LSCF-NiO peaks prepared at various calcination temperature. Based on Fig. 2b, the optimal calcination temperature of the LSCCF-NiO found at 700°C and due to the incomplete formation of LSCF perovskite structure as explained in TGA analysis in Fig. 1. From the TGA analysis, complete formation of perovskite and formation of lattice oxygen uncompleted at 600°C where the weight of the sample remained constant after 650°C indicates complete formation of perovskite.

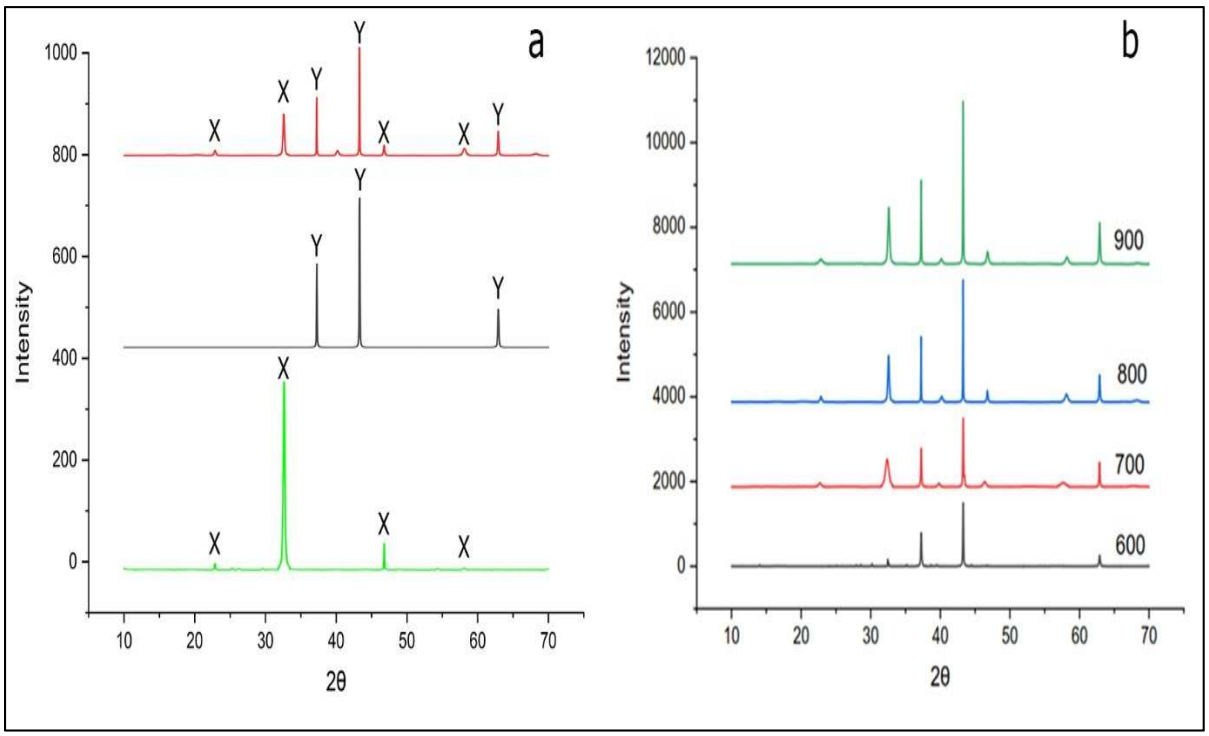

Figure 2. XRD analysis for LSCF, NiO and LSCF-NiO 800, 2b: LSCF-NiO prepared at 600, 700, 800, 900°C

CONCLUSION

Recent study was conducted to determine the compatibility of LSCF with NiO to be used as cathode in SOFC. Based on the results; LSCF and LSCF-NiO prepared using the modified sol-gel method shown positively outcome. The optimum calcination temperature found at 650°C for the complete perovskite structure to form via modified sol-gel method. The XRD result proved that the complete formation of LSCF structure when calcined at 700°C to 900°C due to no shifted peak was found from the analysis. The most obvious finding emerged from this study, sample calcined at 600°C did not have perovskite LSCF structure. The evidence from both analyses in this study suggested that NiO was indeed compatible with LSCF to be used as cathode for SOFC and the optimal calcining temperature was decided at 700°C.

ACKNOWLEDGEMENT

This research is fully funded under the Fundamental Research Grant Scheme (FRGS) sponsored by the Ministry of Higher Education of Malaysia (MOHE).

REFERENCES

[1] L. Lei, Z. Tao, T. Hong, X. Wang, and F. Chen, "A highly active hybrid catalyst modified (La0.60Sr0.40)0.95Co0.20Fe0.80O3-Δ cathode for proton conducting solid oxide fuel cells," *J. Power Sources*, vol. 389, no. March, pp. 1–7, doi: 10.1016/j.jpowsour.2018.03.058, 2018.

[2] S. A. Kumar, P. Kuppusami, and P. Vengatesh, "Auto-combustion synthesis and electrochemical studies of La0.6Sr0.4Co0.2Fe0.8O3-δ – Ce0.8Sm0.1Gd0.1O1.90 nanocomposite cathode for intermediate temperature solid oxide fuel cells," *Ceram. Int.*, vol. 44, no. 17, pp. 21188–21196, doi:

10.1016/j.ceramint.2018.08.164, 2018.

[3] M. Letilly, O. Joubert, and A. Le Gal La Salle, "Characteristics and performance improvement of anode supported solid oxide fuel cells based on BaIn 0.3Ti 0.7O 2.85 (BIT07) as electrolyte, BIT07-Ni as anode and La 0.58Sr 0.4Co 0.2Fe 0.8O 3-δ (LSCF) as cathode," *J. Power Sources*, vol. 206, pp. 210–214, doi: 10.1016/j.jpowsour.2012.01.138, 2012.

[4] H. Xu, H. Zhang, and A. Chu, "An investigation of oxygen reduction mechanism in nano-sized LSCF-SDC composite cathodes," *Int. J. Hydrogen Energy*, vol. 41, no. 47, pp. 22415–22421, doi: 10.1016/j.ijhydene.2016.09.153, 2016.

[5] L. Wang *et al.*, "A novel core-shell LSCF perovskite structured electrocatalyst with local hetero-interface for solid oxide fuel cells," *Int. J. Hydrogen Energy*, vol. 45, no. 20, pp. 11824–11833, doi: 10.1016/j.ijhydene.2020.02.130, 2020.

[6] M. Letilly, O. Joubert, and A. L. G. La Salle, "Characterisation and optimisation of the cathode/electrolyte couple for SOFC LSCF/BIT07," *J. Power Sources*, vol. 212, pp. 161–168, doi: 10.1016/j.jpowsour.2012.03.042, 2012.

[7] A. F. Mohd Abd Fatah and N. A. Hamid, "Physical and chemical properties of LSCF-CuO as potential cathode for intermediate temperature solid oxide fuel cell (IT-SOFC)," *Malaysian J. Fundam. Appl. Sci.*, vol. 14, no. 3, pp. 391–396, doi: 10.11113/mjfas.v14n3.1220, 2018.

[8] Z. Shao, G. Xiong, J. Tong, H. Dong, and W. Yang, "SeparationPurificationTech25_2001_419," vol. 25. pp. 419–429, 2001.

[9] D. Li, W. Liu, H. Zhang, G. Jiang, and C. Chen, "Fabrication , microstructure , mechanical strength and oxygen permeation mixed-conducting composites," *Materials Letters*, vol. 58. pp. 1561–1564, doi: 10.1016/j.matlet.2003.10.026, 2004.

PGC_SCHE USM_2020_02

Enhancement of Lanthanum, Strontium, Cobalt, Ferum perovskite with copper oxide (LSCF-CuO) infiltration as promising cathode for Intermediate Temperature Solid Oxide Fuel Cell (IT-SOFC)

Ahmad Fuzamy Mohd Abd Fatah[1], Noorashrina A Hamid[1,*], Ahmad Azmin Mohamad[2], Andanastuti Muchtar[3]

[1]School of Chemical Engineering, Engineering Campus, Universiti Sains Malaysia, 14300 Nibong Tebal, Pulau Pinang, Malaysia

[2]School of Material and Mineral Source, Engineering Campus, Universiti Sains Malaysia, 14300 Nibong Tebal, Pulau Pinang, Malaysia.

[3]Department of Mechanical & Manufacturing Engineering Faculty of Engineering & Built Environment, Universiti Kebangsaan Malaysia, 43600 UKM Bangi Selangor, Malaysia.

Email: chrina@usm.my

Abstract. $La_{0.6}Sr_{0.4}Co_{0.2}Fe_{0.8}O_3$ (LSCF) doped with copper oxide (CuO) is an attractive yet promising cathode material for IT-SOFC owing to its distinguished properties including high electrical conductivity and high catalytic activity for the oxygen reduction reaction. The study was conducted to investigate the potential of composite LSCF-CuO as cathode material for IT-SOFC using enhanced modified citrate method under controlled condition. Results from XRD showed high purity of as-synthesized samples since no shifted peak detected after being calcined at 800°C. XRD analysis also showed enhanced modified citrate method able to reduce the crystalline size as showed from Scherrer equation calculation compared to conventional method. Moreover, it found that the addition of copper oxide on the cathode layer greatly influenced the electrochemical performance, which was in line with physical characterization results. EIS analysis further verified the polarization resistance of sample calcined at 800°C was as small as 0.299 Ω as compared to conventional LSCF which is 0.418Ω.
Keywords: *LSCF-CuO cathode, Intermediate Temperature Solid Oxide Fuel Cell*

INTRODUCTION

Solid Oxide Fuel Cell is an electrochemical device that convert chemical energy into electrical energy. SOFCs consist of three main components which are cathode, anode and electrolyte and required oxygen to act as a fuel for oxygen reduction reaction process. Mixed ionic electronic conducting (MIEC) type material is one of the cathode compositions that usually being relate with SOFCs that operate at intermediate temperature. It is noteworthy that mixed ionic-electronic conducting (MIEC) oxides, especially perovskite and Ruddlesden-Popper oxides with both high electronic and ionic conductivities, have been recognized as the potential material to prepare oxygen separation membranes due to their high permeability and phase.

Previous study has revealed that MIEC type material suitable to be applied in IT-SOFCs due to their excellent metal traits and have a great chemical composition among themselves. However, as the temperature increase, the grain sizes also increase and the electro-catalytic activity to be decrease[1]. Therefore, addition of another element into the cathode matrix is highly advantages in order to improve the electrocatalytic activity. Copper oxide is one of the good elements that can be composited with the LSCF due to its unique chemical composition which has a good chemical compatibility with most element in transition metal[2]–[4]. Application of CuO composite toward various types of cathode were proved as it has a capability as good catalyst for chemical reaction and effective sintering aid of ceramics as reported previously[1]. It is due to the catalytic property of cathode affected by two possible processes which are oxygen reduction reaction (ORR) and the diffusion of copper oxide into the LSCF lattice.

MATERIALS AND METHODS

The starting materials for sol-gel route were lanthanum nitrate hexahydrate ($La(NO_3)_3 \cdot 6H_2O$, CAS, 10277-43-7 MERCK®, 99%), strontium nitrate ($Sr(NO_3)_2$, Grade AR, Friendemann Schimdt Chemical, 99%), cobalt nitrate-hexahydrate ($Co(NO_3)_2.6H_2O$, ChemAR®, 99%), ferum nitrate-nonahydrate ($Fe(NO_3)_3.9H_2O$, ChemPur®, 99%), citric acid monohydrate ($C_6H_8O_7.H_2O$, R&M Chemicals, 99%) and ethylene glycol ($C_2H_6O_2$, Grade A.R, R&M Chemicals, 99%). The chemical involved in symmetric cell processing were ethylenediaminetetraacetic acid ($C_3H_3N_2O$, CAS, 60-00-4 Sigma Aldrich®, 99%), terpienol ($C_{10}H_{18}O$, CAS, 8000-41-7 Sigma Aldrich®, 99%), ethyl cellulose ($C_{23}H_{24}N_6O_4$, CAS, 9004-57-3 Sigma Aldrich®, 99%), copper

nitrate ($Cu(NO_3)_2 \cdot 3H_2O$ CAS, 10031-43-3 Sigma Aldrich®, 99%) and cerium (CeO_2/Sm, CAS, 734624 Sigma Aldrich®, 80% Cerium, 20% samarium).

The $La_{0.6}Sr_{0.4}Co_{0.2}Fe_{0.8}O_3$- (LSCF) and CuO powder was synthesized by sol-gel method. The sol-gel method followed the enhanced modified polymerized complex method and conventional Pechini method which has been discussed elsewhere [1]. Enhanced modified polymerized complex method was done by introducing EDTA as new chelating agent in sol-gel processing. Metal nitrate, citric acid and EDTA were mixed with ratio 1:1:1 with addition of reasonable ratio of ethylene glycol as solvent. The pH solution was controlled at pH 7 using ammonium solution and was stirred for 3 hours until homogeneous mixture formed. The resulted solution was heated at 100ºC until gel formation occurred. Gel contained LSCF was calcined at 800ºC for 6 hours and the resulted sample was mixed with copper oxide at weight ratio of 95:5. The mixture powder was calcined at 800ºC. Slurry cathode was formed by ratio of 30:19:1 of LSCF-CuO, terpineol and ethyl cellulose. Symmetric cell was formed by applying the slurry cathode at both side of SDC pellet and platinum paste was coated at cathode side to act as a current collector layer.

The phase composition was characterized by using X-ray diffraction (XRD) with Cu Kα radiation from 10 θ to 90 θ for the entire sample by using an AXS Bruker GmbH. The raw data from the XRD analysis was analyzed using Xpert-Highscore Plus. The main sample of LSCF- CuO at 800ºC was compared with literature and from synthesized LSCF and CuO sample with same temperature. The electrochemical impedance spectra analysis was conducted on EIS with furnace system (model ZIVE SP2). Silver wires were attached to the electrodes surface which had been coated with platinum paste. The temperature for EIS measurement was varied between 800ºC to 600ºC with same frequency range from 0.1Hz to 1MHz with signal amplitude of 10 mv and 5 mv for each sample. The polarization cell was measured using type-K thermocouple and recorded on Digi-Sense digital thermocouple meter (Eutech Instrument). ZMAN 2.4 (ZIVE LAB) software was used to fit the experimental data to the equivalent circuit and each of them was plotted in Sigma Plot software version 11. The analysis was conducted in open air.

RESULTS AND DISCUSSION

XRD analysis of LSCF-CuO synthesized using modified as well as Pechini sol-gel is shown in Fig. 1. The LSCF structure was defined using comparison and analysis method which has been discussed elsewhere [1]. Based on Fig. 1, the LSCF-CuO able to achieve a single-phase perovskite since there was no major shifted peak detected. The optimal calcination temperature for LSCF-CuO usually achieve at 800ºC based on the TGA analysis beforehand so comparison was made between samples and literature produced a precise data for phase comparison [1]. Based on the XRD analysis, all peaks were defined as single phase perovskite. The peak of LSCF showed that it was shifted toward the high-angle indicating that the inter-diffusion of La^+ ions in LSCF. The entire peaks have been identified as LSCF and CuO and similar finding was presented in several articles those analyzed the XRD results towards LSCF which described the highest intensity achieved at 2θ in between 30º to 40º [5]–[8]. It also being described from previous study that addition of CuO able to reduce the required calcination temperature from 800ºC to 700ºC due to the infiltration on the B-site of the perovskite [1].

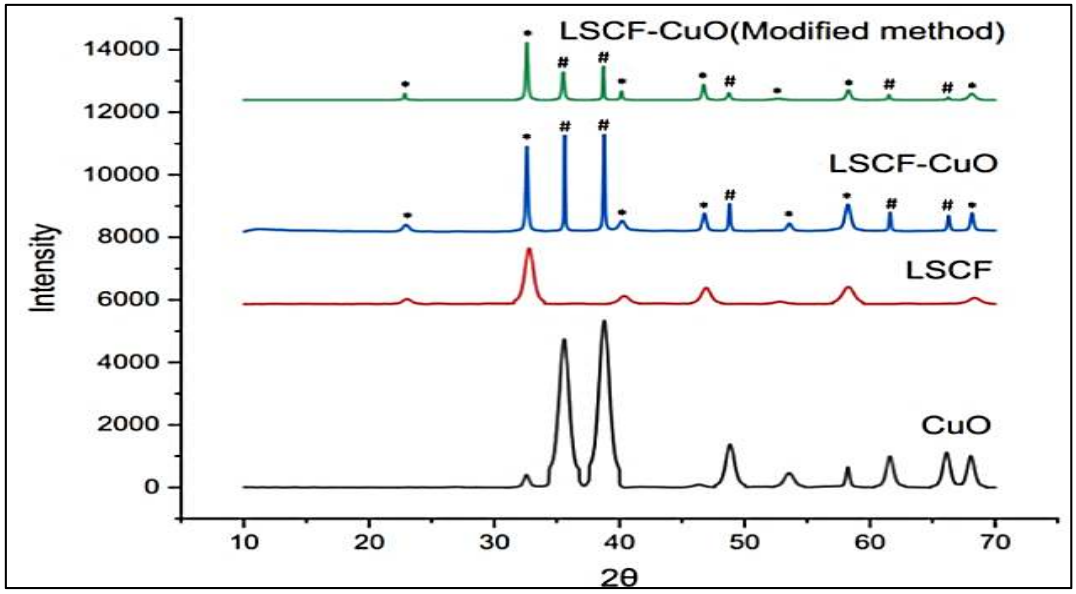

Figure 1. XRD analysis of LSCF-CuO by enhanced modified method vs conventional method

The XRD analysis continued by comparison of crystallites size calculated via Scherrer equation for both synthesizing routes. From data in Table 1, it is apparent that enhanced modified method able to reduce the crystallites size of LSCF-CuO from 90.49nm to 40.67nm. It could be explained further that the addition of EDTA further improved the formation of perovskite as EDTA considered as better chelating agent in wastewater treatment. High acidity solution in sol-gel processing was desirable in order to ensure all metal clusters together to form a perovskite formation. However, highly acidity solution was undesirable due to metal degradation in SOFCs perspective. Therefore, addition of ammonium solution was needed to control the pH value of the solution in the formation of LSCF.

Table 1. Crystallites sized of LSCF-CuO by respective method.
(Calcination temperature = 800 ºC, LSCF:CuO ratio = 95:5)

Sample	Crystal Size (nm)
Pechini Method	90.49
Enhanced modified method	40.67

Further experiment was conducted to measure the polarization resistance of LSCF-CuO as shown in Fig. 2. The equivalent circuit and fitting parameters generated by the ZMAN software, the parameters were determined as L_s, R_s, R_1, Q_1 indicating the inductance attributed to the silver current-voltage probes or high frequency phase shift of the EIS equipment. R_s was categorised as the R_Ω where it represented the electrolyte resistance and the connection silver wire resistance. Meanwhile, R_1, and Q_1 represented low frequency arc where R represented the resistance at the frequency region while Q represented the arc resistance constant phase element (CPE) of the respective frequency region[9]. This equivalent circuit was chosen due to the application of symmetrical cells which contributed to the measurement of polarization resistance in cathode side only.

Further investigation on the addition of copper oxide towards the cathode surface found that the polarisation resistance for LSCF-CuO was smaller than that of the LSCF which is 0.299Ω and 0.418Ω. The value of activation energy proved that the addition of CuO indeed acted as a synergistic catalyst since the activation from pure LSCF was reduced based on Arrhenius equation where LSCF-CuO activation energy at 122.20 kJ/mol while conventional LSCF activation energy at 144.25 kJ/mol. This could be explained as the addition of CuO towards MIEC type cathode improved the electrochemical performance by increasing the electro-catalytic activity of the cathode. It showed that the connections among grains were better in LSCF-CuO composite cathode, thus improving the charge transfer. However, it has been stated that increasing of high calcining temperature affected the grain boundary, thus reducing the ORR kinetic of the sample. Moreover, it has been reported that optimal calcining temperature for LSCF was at 800ºC for conventional method. However, comparison needed to be made for LSCF-CuO and LSCF. Therefore, the calcination and sintering were decided to be done at 800ºC. In further review, the addition of CuO was able to help in increasing the surface energy of the cathode and the grain boundary speed movement, which would result in the reduction in optimal calcining temperature. It has been that the addition of CuO in SOFCs perspective was able to perform a stable operation for long time [10].

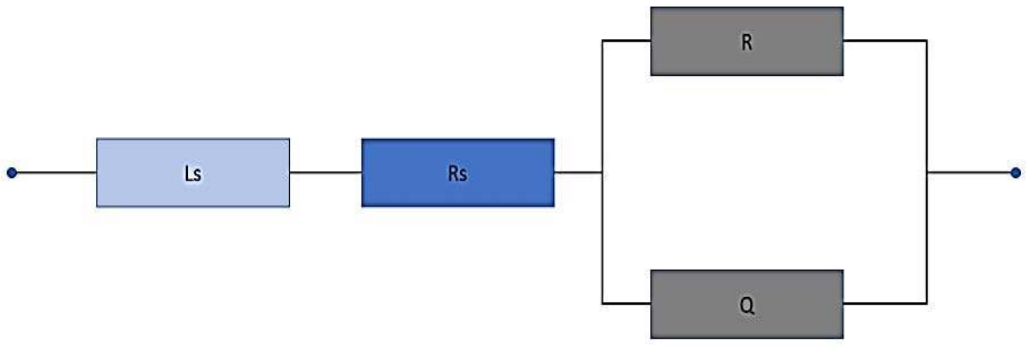

Figure 2. Equivalent circuit in Z-man Software

CONCLUSION

Infiltration of copper oxide towards LSCF found capable to improve the electrocatalytic activity of the cathode. On tio of that, copper oxide also proved to have a good chemical compatibility with LSCF by the XRD analysis. Effect of calcining temperature toward the electrochemical performance was conducted beforehand and it was found that reducing calcining temperature improved the EIS result. It could be explained that the reduction

of the temperature causes the particle size of the cathode decreased due to the properties of the metal. In order to improve the cathode, CuO infiltration was implemented and resulted improving the electro catalytic activity. Hence, activation energy and the grain boundary which subsequently improve the electron transfer inside the electrode.

ACKNOWLEDGEMENT

This work was financially supported by the Ministry of Science, Technology & Innovation (MOSTI) Malaysia under Fundamental Research Grant Scheme Malaysia and all the research works conducted in Universiti Sains Malaysia (USM).

REFERENCES

[1] A. F. Mohd Abd Fatah and N. A. Hamid, "Physical and chemical properties of LSCF-CuO as potential cathode for intermediate temperature solid oxide fuel cell (IT-SOFC)," *Malaysian J. Fundam. Appl. Sci.*, vol. 14, no. 3, pp. 391–396, doi: 10.11113/mjfas.v14n3.1220, 2018.

[2] A. A. Baqer *et al.*, "Synthesis and characterization of binary (CuO)0.6(CeO2)0.4 nanoparticles via a simple heat treatment method," *Results Phys.*, vol. 9, pp. 471–478, doi: 10.1016/j.rinp.2018.02.079, 2018.

[3] C. Xu, X. Hao, M. Gao, H. Su, and S. Zeng, "Important properties associated with catalytic performance over three-dimensionally ordered macroporous CeO2-CuO catalysts," *Catal. Commun.*, vol. 73, pp. 113–117, doi: 10.1016/j.catcom.2015.10.025, 2016.

[4] C. Nicollet *et al.*, "Gadolinium doped ceria interlayers for Solid Oxide Fuel Cells cathodes : Enhanced reactivity with sintering aids (Li , Cu , Zn), and improved densi fi cation by in fi ltration," *J. Power Sources*, vol. 372, no. November, pp. 157–165, doi: 10.1016/j.jpowsour.2017.10.064, 2017.

[5] A. P. Jamale, C. H. Bhosale, and L. D. Jadhav, "Electrochemical behavior of LSCF/GDC interface in symmetric cell: An application in solid oxide fuel cells," *J. Alloys Compd.*, vol. 623, pp. 136–139, doi: 10.1016/j.jallcom.2014.10.122, 2015.

[6] M. Nadeem, B. Hu, and C. Xia, "Effect of NiO addition on oxygen reduction reaction at lanthanum strontium cobalt ferrite cathode for solid oxide fuel cell," *Int. J. Hydrogen Energy*, vol. 43, no. 16, pp. 8079–8087, doi: 10.1016/j.ijhydene.2018.03.053, 2018.

[7] S. A. Muhammed Ali, M. Anwar, N. Ashikin, A. Muchtar, and M. R. Somalu, "Influence of oxygen ion enrichment on optical, mechanical, and electrical properties of LSCF perovskite nanocomposite," *Ceram. Int.*, vol. 44, no. 9, pp. 10433–10442, doi: 10.1016/j.ceramint.2018.03.060, 2018.

[8] L. Zhang, T. Hong, Y. Li, and C. Xia, "CaO effect on the electrochemical performance of lanthanum strontium cobalt ferrite cathode for intermediate-temperature solid oxide fuel cell," *Int. J. Hydrogen Energy*, vol. 42, no. 27, pp. 17242–17250, doi: 10.1016/j.ijhydene.2017.05.207, 2017.

[9] Özden Çelikbilek, E. Siebert, D. Jauffrès, C. L. Martin, and E. Djurado, "Influence of sintering temperature on morphology and electrochemical performance of LSCF/GDC composite films as efficient cathode for SOFC," *Electrochim. Acta*, vol. 246, pp. 1248–1258, doi: 10.1016/j.electacta.2017.06.070, 2017.

[10] K. Raju and D. Yoon, "Reactive air brazing of GDC – LSCF ceramics using Ag – 10 wt % CuO paste for oxygen transport membrane applications GDC-LSCF GDC-LSCF Filler," *Ceram. Int.*, vol. 42, no. 14, pp. 16392–16395, doi: 10.1016/j.ceramint.2016.07.042, 2016.

PGC_SCHE USM_2020_03

Polymer Screening Evaluation for Nanofiber Membrane

A.I. Abdul Jalil, S. Ismail*
School of Chemical Engineering, Engineering Campus, Universiti Sains Malaysia,
14300 Nibong Tebal, Pulau Pinang, Malaysia.
Email: *chsuzy@usm.my

Abstract. Screening of different types of polymers; polyacrylonitrile (PAN), polyvinylidene fluoride (PVDF), chitosan (CS) and polyvinyl alcohol (PVA)) as the backbones of nanofibrous membranes were investigated. The nanofibrous membrane was fabricated using electrospinning process. The applied voltage, polymer flow rate, tip-to-collector distance and the drum collector rotation speed were the process conditions tested in this current work. A crosslinking process was further performed via heat treatment for PAN and PVDF polymers, while glutaraldehyde for CS and PVA, to improve the nanofiber stability. The morphology of nanofiber structures was analysed using SEM to identify the nanofiber distribution, structure and bead formation. The best nanofiber membrane showed the shortest spinning time, centred nanofiber dispersion position, nano-sized fiber and did not disintegrate when in contact with water.
Keywords: *Electrospinning, nanofiber, PAN, PVDF, CS, PVA*

INTRODUCTION

Electrospinning is recognised as a suitable technique for the fabrication of polymer nanofibers [1]. Many researchers exploited electrospinning in order to produce micro- to nano-sized fibers. These micro- and nano-sized fibers exhibit sizeable specific surface areas, porous structure and modifiable surface physical and chemical properties [2]. The use of these nanofibers is extensively used in textile, filtration, electrical, wastewater, medical, tissue engineering and membrane industries [3]. In electrospinning process, the knowledge of the polymer solution and the electrospinning conditions are crucial as they affect the fiber diameter and morphology [4].

Several types of polymers had been studied to produce these nanofibers such as PAN, PVDF, CS and PVA. PAN is a polymer composed of acrylonitrile monomers. It has excellent physicochemical properties such as high mechanical strength, good chemical resistance, thermally stable and easy to be electrospun. The nitrile group presents in PAN can be hydrolysed and involved in chemical reactions with metal ions complexing agents [5]. Meanwhile, PVDF is a polymer that contains -CH_2-CF_2- groups which provide high mechanical strength, high chemical resistance, antioxidative abilities and high thermal and hydrolytic stabilities [6]. CS is a natural copolymer that is soluble in acidic condition solvents due to -NH_2 protonation. The functional groups of -NH_2 and -OH in CS provide adsorption capability to the polymer. CS has a unique nature of being polyelectrolyte where it is challenging to be electrospun without the help of another polymer such as PVA to stabilise it. PVA is a non-ionic polymer that has excellent spinnability [7]. The PVA molecular chain has large numbers of hydroxyl groups, which is vital in adsorption of ions in wastewater via hydrogen bonding and crosslinking.

In this study PAN, PVDF, CS and PVA were electrospun. The nanofiber is crosslinked via thermal treatment crosslinking or crosslinking via glutaraldehyde. The desired nanofiber characteristic is abundant, shortest time to produce, smallest in diameter, and water-resistant.

MATERIALS AND METHODS

PAN with MW of 150 000 g/mol, PVDF with MW of 534 000 g/mol, CS with MW of 310 000 g/mol – 375 000 g/mol and PVA with MW of 85 000 – 124 000 g/mol and glutaraldehyde were purchased from Biotek Abadi Sdn. Bhd. Acetone and dimethyl sulfoxide (DMSO) were acquired from BT Science Sdn. Bhd. The solvent used in this work was distilled water.

The concentration and solvent for each polymer are shown in Table 1. PAN was dissolved in DMSO under room temperature until a homogenous solution was formed. The solvent for PDVF was a mixture of acetone and DMSO with the ratio 40/60. PVDF powder was added and stirred at room temperature until homogenous. CS was prepared as a mixture of CS and PVA. CS was prepared by dissolving CS powder in distilled water under 90°C heat until homogeneity. Meanwhile, PVA was prepared by dissolving PVA powder in distilled water under 110°C heat. The CS/PVA polymer was mixed with a 20/80 ratio and stirred overnight. Pure PVA was prepared similarly as the previous CS/PVA but only with PVA polymer and at a higher concentration. 4 mL was set as the volume for each polymer. The electrospinning process was run with the electrospinning parameters as shown in Table 1. The produced nanofiber undergoes crosslinking after the electrospinning process. PAN and PVDF were crosslinked via thermal treatment and CS and PVA were crosslinked using glutaraldehyde vapour.

Table 2. Polymer preparation and electrospinning parameters

Polymer	Concentration (%)	Solvent	Electrospinning parameters		
			Voltage (kV)	Flow rate (mL/hr)	Tip-to-collector (cm)
PAN	10	DMSO	16	0.8	15
PVDF	15	Acetone/DMSO	15	1	10
CS	3% CS/8% PVA	Distilled water	23	0.7	10
PVA	10	Distilled water	15	1	15

The electrospinning process relied on the polymer concentration, voltage supplied, polymer flow rate, and tip-to-collector distance. Figure 1 shows the graphical image of an electrospinning equipment set-up in the Chemical Engineering Integrated Research Space, School of Chemical Engineering, USM.

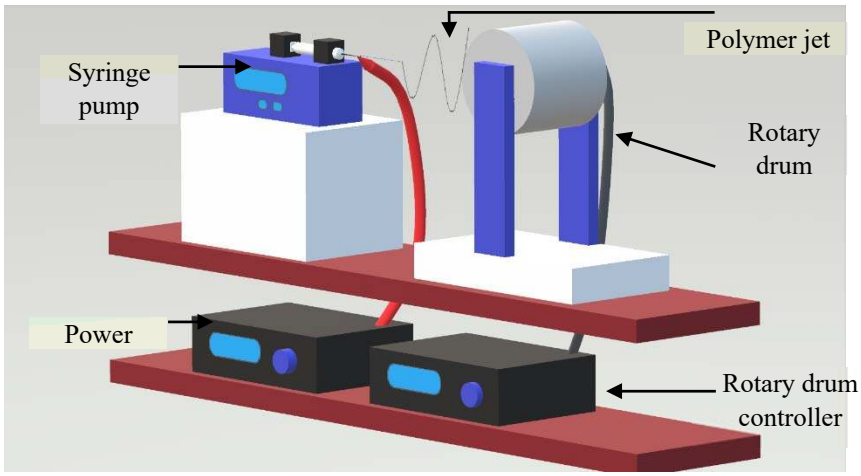

Figure 1: Electrospinning equipment set-up

The surface morphologies of the polymers were characterised by Scanning Electron Microscope, SEM (Hitachi TEM3000) with 3000x magnification. The contact angle was determined using LAUDA Surface Analyzer (LSA100).

RESULTS AND DISCUSSION

In this study, four types of polymer were electrospun and crosslinked. Table 2 shows the results of electrospun nanofibers for their mass, area, time taken for nanofiber completion, nanofiber size and the contact angle. Meanwhile, the morphology of each polymer was observed by SEM and illustrated in Figure 2. PAN produced neat fibers with linear, round and smooth surfaces, with no bead formations. The diameter of PAN nanofiber was 689.33 nm as comparable to [8]. The contact angle of PAN was 119.2° which shows hydrophobicity. The next polymer which produced the heaviest and biggest nanofiber mat had nanofiber diameters of 1370 nm. The closest nanofiber with 16% concentration formed by [9] with 1291 nm diameter. The contact angle by PVDF nanofiber was 124.5° , which showed ultra-hydrophobicity [10]. The PVDF nanofiber produced linear, thick and smooth fibers with no bead formations.

CS prepared with PVA acted as copolymer to induce the electrospinning process. The nanofibers formed with CS/PVA produced non-linear, fibrous, and with some bead formation. Polymer smears appeared in some parts of the nanofiber mat. This might be caused by solvents that did not fully evaporate during the nanofiber formation in electrospinning. CS/PVA produced a slightly hydrophobic polymer; however, it quickly loses its hydrophobicity as time pass, dropped to 55° after 1 minute. Lastly, PVA formed similarly to CS/PVA, but with more bead formation. Polymer smears were also seen in the PVA nanofibers. PVA also produced the smallest mat of the nanofiber. PVA initially showed hydrophobic nature but the contact angle also dropped to 80° after 1 minute. From here it could be inferred that PAN produced the best nanofiber mat, with its small, uniform nanofiber, smooth and non-beaded surface, and relatively short electrospinning process. In addition, PAN nanofiber was water resistant.

Table 3. Electrospun nanofiber results

Polymer	Concentration (%)	Electrospun nanofiber				
		Mass (g)	Area (cm^2)	Time for nanofiber completion (hrs)	Nanofiber diameter (nm)	Contact angle (°)
PAN	10	0.289	245.9	5	689.33	119.2
PVDF	15	0.715	357.95	4	1370.00	124.5
CS	3% CS/8% PVA	0.296	76.4	5.7	1432.67	91.7
PVA	10	0.324	30.133	4	1156.00	90.6

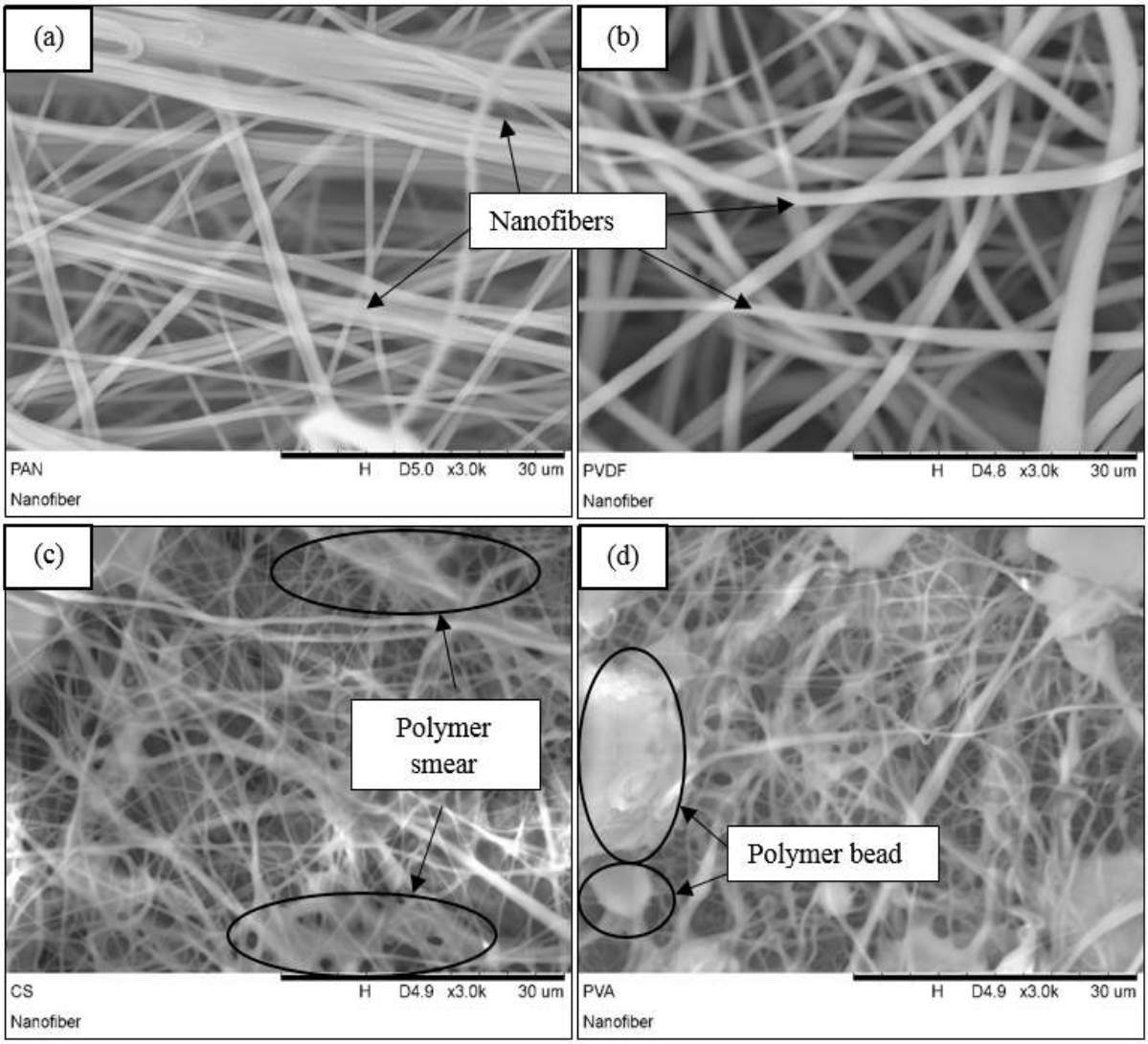

Figure 2. SEM images: (a) PAN nanofiber, (b) PVDF nanofiber, (c) CS nanofiber and (d) PVA nanofiber

CONCLUSION

In this work, PAN, PVDF, CS and PVA nanofibers were successfully electrospun with nanofiber diameter size ranging from 689.33 nm to 1432.67 nm. PAN and PVDF produced smooth and linear nanofibers while CS and PVA produced beaded and has polymer smears. All electrospun polymers showed the ability to resist water. Lastly, the best polymer in this screening was PAN with the smallest nanofiber diameter, uniformed, non-beaded nanofiber and its high-water resistance.

ACKNOWLEDGEMENT

The authors would like to acknowledge the Ministry of Higher Education of Malaysia (MOHE) for funding this research project under the Fundamental Research Grant Scheme (203/PJKIMIA/6071413).

REFERENCES

[1] Z. M. Huang, Y. Z. Zhang, M. Kotaki, and S. Ramakrishna, "A review on polymer nanofibers by electrospinning and their applications in nanocomposites," *Compos. Sci. Technol.*, vol. 63, no. 15, pp. 2223–2253, 2003.

[2] S. Zhang, Q. Shi, G. Kor, C. Christodoulatos, and H. Wang, "Chromate removal by electrospun PVA / PEI nano fi bers : Adsorption , reduction , and e ff ects of co-existing ions," vol. 387, no. November 2019, 2020.

[3] A. Alliyehyousefi, Z. Hamid, and K. Saied Nouri, "Characterization of Electrospinning Parameters of Chitosan/Poly(vinyl alcohol) Nanofibers to Remove Phenol via Response Surface Methodology," *Polym. Sci.*, vol. 04, no. 01, pp. 1–9, 2018.

[4] D. A. Gopakumar, V. Arumukhan, R.V. Gelamo, D. Pasquini, L.C. de Morais, S. Rizal, D. Hermawan, A. Nzihou, P.S.A. Khalil, "Carbon dioxide plasma treated PVDF electrospun membrane for the removal of crystal violet dyes and iron oxide nanoparticles from water," *Nano-Structures and Nano-Objects*, vol. 18, p. 100268, 2019.

[5] P. R. Sruthi and S. Anas, "An overview of synthetic modification of nitrile group in polymers and applications," *J. Polym. Sci.*, vol. 58, no. 8, pp. 1039–1061, 2020.

[6] S. A. Haddadi, S. Ghaderi, M. Amini, and A. R. S. A, "ScienceDirect Mechanical and piezoelectric characterizations of electrospun PVDF-nanosilica fibrous scaffolds for biomedical applications," *Mater. Today Proc.*, vol. 5, no. 7, pp. 15710–15716, 2018.

[7] H. Tian, L. Yuan, J. Wang, H. Wu, H. Wang, A. Xiang, B. Ashok, A. V. Rajulu ., "Electrospinning of polyvinyl alcohol into crosslinked nanofibers: An approach to fabricate functional adsorbent for heavy metals," *J. Hazard. Mater.*, vol. 378, no. February, p. 120751, 2019.

[8] L. Hao, W. Gao, S. Yan, M. Niu, G. Liu, and H. Hao, "Functionalized diatomite / oyster shell powder doped electrospun polyacrylonitrile submicron fi ber as a high-ef fi ciency adsorbent for removing methylene blue from aqueous solution : Thermodynamics , kinetics and isotherms," *J. Mol. Liq.*, vol. 298, p. 112022, 2020.

[9] Ç. Akduman, "PVDF nanofiber membranes produced by electrofiltration method for microfiltration: The effect of pore size and thickness on membrane performance," *Eur. J. Sci. Technol.*, no. 16, pp. 247–255, 2019.

[10] N. Nuraje, W. S. Khan, Y. Lei, M. Ceylan, and R. Asmatulu, "Superhydrophobic electrospun nanofibers," *J. Mater. Chem. A*, vol. 1, no. 6, pp. 1929–1946, 2013.

PGC_SCHE USM_2020_04

The particle size of lignocellulosic biomass affects crystallinity: A review

Abiodun Abdulhameed Amusa, Abdul Latif Ahmad, Adewole K. Jimoh
School of Chemical Engineering, Engineering Campus, Universiti Sains Malaysia,
14300 Nibong Tebal, Pulau Pinang, Malaysia
E-mail: chlatif@usm.my

Abstract: Lignocellulosic biomass (LCB) is readily available in areas with constant rainfall like Malaysia. Agro-based wastes are discarded as instead of being used as resources for other high-value materials/chemicals. Gas separation, water purifications, and others require that fillers should be less crystalline for effective incorporation into polymers matrix. Therefore, in this review, sieves with different mesh sizes between 710 and 30 microns were used after the biomass was air-dried and ground using a ball mill. The results show justifications for researchers changing to nano-sized materials with reduced crystallinity for various applications.
Keywords: *Lignocellulosic biomass, crystallinity, pretreatment, particle size, ball milling.*

INTRODUCTION

LCB signifies the surplus renewable resources from agricultural wastes which can be used to sustain human beings when converted to other products. Cellulose, hemicellulose, and lignin are the major constituents of LCB. The proportions of these components vary based on factors like the type of biomass (hard or soft), the part (seed, leave, stem, bark), etc. The main factor limiting LCBs valorization is the complexity of its structure associated with plant cell wall recalcitrance. Therefore, size reduction is the first pretreatment technique to enhance accessibility to embedded functional groups and further processing such as enzyme hydrolysis as shown in Figure 1.

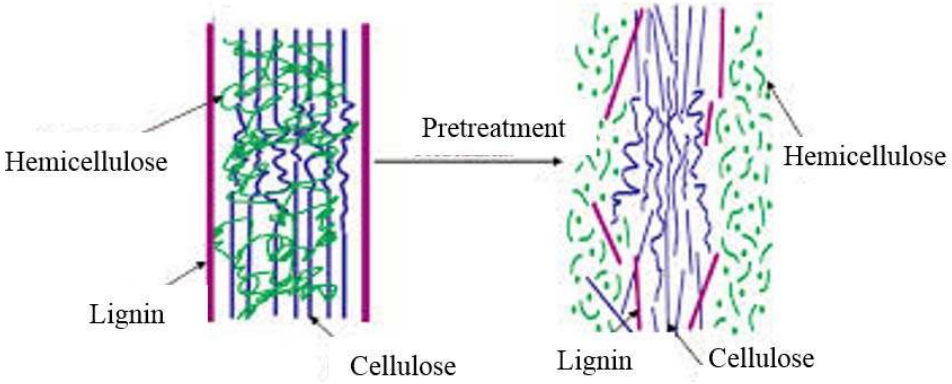

Figure 1. The pretreatment role on LCB [1]

Grinding (mechanically) of biomass materials via some methods such as shipping and milling to size range of 10-30 mm and up to 0.22 mm, respectively. Limitations on the biomass from mass and heat transfer can be reduced by shipping while effective particle size reduction is easily using grinding and milling. The milling type and duration will affect the overall specific surface area of the biomass. Taherzadeh and Karimi [2] reported that varying methods of milling such as the hammer, vibratory, two-roll, and colloid, yield different results. Although, most efficient and effective are via vibratory ball milling compared to other ordinary millings. Milling of LCB to fine powders is environmental-friendly free from usage of hydroxymethyl furfuraldehyde or levulinic acid toxic that are toxic substances. It shows that the milling as the first preliminary pretreatment method among researchers and the excellent performance from milling is attributed to generate shear forces. A combination of alkaline pretreatment with milling will produce better results (Figure 2) as reported by Zakaria et al. [3] which improved the enzymatic hydrolysis of biomass with the aid of these combination.

RESULTS

The efficiency of enzymes saccharification and other applications such as biofuel production are dependent on LCB feedstock crystallization [5]. Dougherty et al. [6] reported the increasing in yield of sugar due to the varied particle sizes which resulted in a reduction in crystallinity (Table 1).

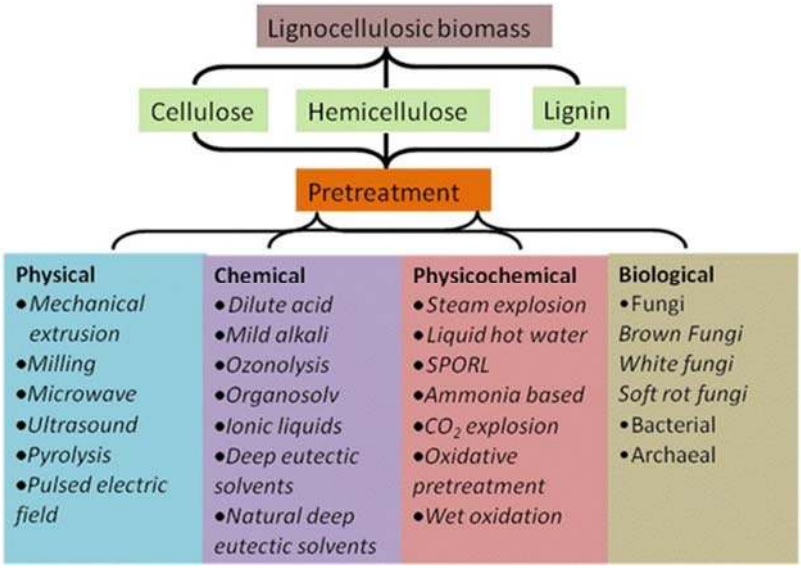

Figure 2. Lignocellulosic biomass pretreatment techniques [4]

Table 1. LCB particle size, BET surface area, and crystallinity index

Particle size (Mesh)	BET Surface area (m^2/g)				Crystallinity Index			
	Untreated	Pretreated			Untreated	Pretreated		
		Dilute Acid	Ammonia fiber expansion (AFEX)	Ionic Liquid		Dilute Acid	Ammonia fiber expansion (AFEX)	Ionic Liquid
>200	0.29	0.65	0.99	2.56	0.51	0.48	0.36	0.20
75-100	0.56	0.76	0.96	2.82	0.41	0.44	0.30	0.18
32-50	0.52	0.84	1.03	3.19	0.34	0.41	0.30	0.15

The values are taken from [6]

CONCLUSION

Cellulose and hemicellulose usages are hindered with lignin presence. This implies that delignification is highly paramount. However, crystallinity inhibits this process due to the influence of strong covalent/hydrogen bonding. The physical pretreatment of lignocellulosic biomass to fine particles would reduce its crystallinity which enhanced other processes and applications such as hemicellulose/cellulose extractions and hydrolysis, biofuel production.

REFERENCE

[1] Otieno, Z. Pretreatments to Enhance the Digestibility of Wheat Straw. *Int. J. Renew. Sustain. Energy* **3** 26,2014

[2] Taherzadeh, M. J. and Karimi, K. Pretreatment of lignocellulosic wastes to improve ethanol and biogas production: A review. *Int. J. Mol. Sci.* **9** 1621–51, 2008

[3] Zakaria, M. R., Fujimoto, S., Hirata, S. and Hassan, M. A. Ball milling pretreatment of oil palm biomass for enhancing enzymatic hydrolysis. *Appl. Biochem. Biotechnol.* **173** 1778–89, 2014.

[4] Kumar, A. K. and Sharma, S. Recent updates on different methods of pretreatment of lignocellulosic feedstocks: a review *Bioresour. Bioprocess.* **4,** 7, 2017.

[5] Kumar, R., Mago, G., Balan, V. and Wyman, C. E. Physical and chemical characterizations of corn stover and poplar solids resulting from leading pretreatment technologies *Bioresour. Technol.* **100** 3948–62, 2009.

[6] Dougherty, M. J., Tran, H. M., Stavila, V., Knierim, B., George, A., Auer, M., Adams, P, D. and Hadi, M. Z. Cellulosic Biomass Pretreatment and Sugar Yields as a Function of Biomass Particle Size. Ed A C Marr *PLoS One* **9** e100836, 2014.

PGC_SCHE USM_2020_05

Hydraulic Fracturing Fluid Performance Using Encapsulated Borate-Crosslinked Fluid for Deepwater Application

Nurul Syaza Mohamad[1], Suzylawati Ismail[1,*], Ling Kong Teng[2]
[1]School of Chemical Engineering, Engineering Campus, Universiti Sains Malaysia, 14300 Nibong Tebal, Pulau Pinang, Malaysia
[2]Client Support Laboratory (CSL), Schlumberger, Jalan P. Ramlee, 50250 Kuala Lumpur, Malaysia
E-mail: [,]chsuzy@usm.my*

Abstract. The application of borate-crosslinked fluids has increased in usage for fracturing treatments in this past few decades because of its low potential to formation damage and economically viable. Recent advances in borate fluid chemistry have resulted in new techniques to minimize friction and treating pressure using chemically delayed borate crosslinker. The introduction of encapsulation method provides a comprehensive solution to cater the common challenges faced in deepwater completion by delaying the viscosity enhancement in controllable manner, usually until it reaches 2/3 of the tubing. Substantially, this facilitates in reducing the treatment cost and extended the application of borate-crosslinked fluids in deeper wells with higher bottom hole temperature. While emphasizing on the effectiveness of this method, this research aims to thoroughly evaluate the advancement application of crosslinked fluid with delayed mechanism and investigate the parameters controlling its behaviour. This paper also presents the research progresses in the area of development of hydraulic fracturing treatment fluid, as well as the context of challenges and breakthrough that are presently serving as bottlenecks in deepwater fracturing. In this review, we focused on borate-guar crosslinked fluid to keep the subject under discussion.
Keywords: *crosslink; deepwater; encapsulation; hydraulic fracturing*

INTRODUCTION

The needs to exploit inaccessible fossil fuel reserves has made hydraulic fracturing to be used by the oil and gas industry as an approach to boost up hydrocarbon production since 1947 [1]. Along with the hydraulic fracturing widespread, this well stimulation technique has led to massive research efforts in optimizing fracturing fluid formulation. Overall, fracturing fluid design should have the ability to transport proppant effectively and break efficiently to encourage flowback of the fluid to the surface, and ultimately the effectiveness of the formulated fluid when applying to the targeted well with specific temperature and pressure setting. Researches predicted the ultimate hydrocarbon production through well stimulation could increase by more than 30% driven by crosslinked fracturing fluid with the aid of advanced gel breaker technology. However, the complexity of the fracturing fluid design associated with its rheological properties, fluid stability, crosslinking behaviour, breaker performance, shear insensitivity and compatibility of the fluid with formation fluid is very challenging. If the breaker reduces the viscosity of the fracturing fluid prematurely, fracture formation, proppant transport capability as well as fluid leakage control into the formation can all be impaired. Meanwhile, the crosslinking process needs to take place at a designated time to ensure proppant is delivered effectively. Clearly, striking a balance between effectiveness and timeliness on the action of breaker and crosslink are crucial and difficult. These concerns prompted the industry to improvise the existing fluid system, hence delayed crosslinked fluid system through the encapsulation method was introduced.

Deepwater fracturing requires higher pump rate to generate enough bottom hole treating pressure (BHTP) to create a hydraulic fracture without exceeding the limits of the hydraulic equipment at the surface while effectively create a fracture height that covers all multiple pay zones. However, pumping a viscous fluid at high rate inevitably lead to an increase in friction and treating pressure. Crosslinking agent such as borate is added to permit the fracturing fluid to be pumped at a lower initial viscosity, thus reducing the friction pressure in the tubing, while the fluid viscosity subsequently increases to the desired level after crosslinking begins. However, in fracturing operations the crosslinking often occurs at an undesirable time. If the process happens too early, the pressure builds up will cause completion issues however if it occurs too late, proppant placement will be an issue. For years, these limitations had served as barriers in designing an optimum fluid profile that satisfies the well configuration. Later, encapsulation method was brought forward as the solution to extend delayed mechanism in crosslinking time to address the challenges faced in deepwater completions. However, the extent of delay time has raised questions on the parameters that trigger the release of borate. Most importantly, the expected delayed action takes place in time by controlling these parameters. Thus, the focus of this research is to formulate a hydraulic fracturing treatment fluid for high temperature reservoir using the application of encapsulated borate-crosslinked gel system and examine its behaviour under simulated deepwater setting (40-350 °F).

In deep water, travel distance to the mudline is longer and fluids are exposed with extreme tubular friction pressure if crosslinking process is done at the pumping stage. Other than extreme temperature exposure that could compromise the crosslink performance, another reason to delay the crosslinking of these fluids is because of the high shearing rates while transiting the well tubulars and passing through the perforations [2]. Recent advances of delayed crosslinked gel system are introduced in approach to retard the reaction rates of the crosslink sites on the polymer backbone. Delaying the crosslink provides the means to maintain the friction pressure at acceptable levels by minimizing the time the fluid spends in the tubing at high viscosities [3]. From a practical standpoint, this holds very important implications for deep wells with high temperature setting. After substantial progress in this area, benefits of a slowed crosslinked reaction became apparent [4].

To address the concerns governing deepwater fracturing in high temperature field with absolute shear stress, encapsulation method is proposed to provide a mechanism to delay crosslinking or gel-breaking process in a controllable fashion. In the encapsulation process, the crosslinker or breaker is coated with a film of inert coating that acts as a barrier between the active content and the fracturing fluid [1] and later degrades or is slowly permeated by the carrier fluid in order to release the breaker or crosslinker into the fracturing fluid to deliver their purpose respectively. Typically, this delay time can be adjusted so that crosslinking occurs at a desirable time (about 2/3 of the pipe time). Multiple tests were conducted to ascertain the release profile of the breaker and crosslinker to understand the release mechanism. Still *et al*. [5] claimed that one way to minimize hydrostatic release is to increase the encapsulation coating thickness, in which by thickening the coating improves fluid stability during pumping as well as providing some protection from thermal breakdown of the oxidizer. They found that the hydrostatic release profiles as a function of encapsulation thicknesses are shown in Fig. 1.

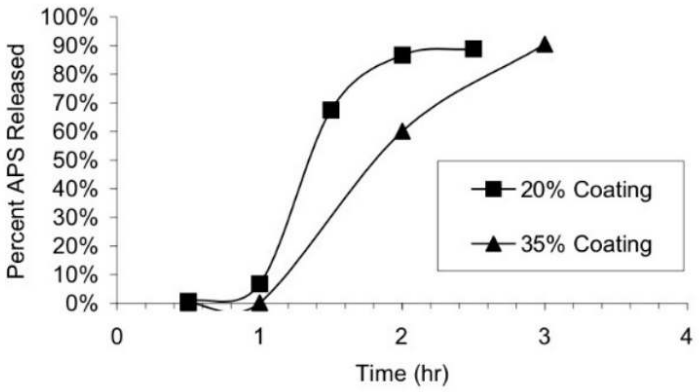

Figure 3. Hydrostatic release of ammonium persulfate (APS) breaker as a function of coating thickness at 225°F under atmospheric conditions [6]

MATERIALS AND METHODS

Encapsulated Crosslinked fluid delay time

The crosslink delay time of the frac fluid was quantitatively measured by recording the time for the crosslinking process started to take place at deepwater temperature range (40-350 °F). Using the cup-to-cup method, crosslink delay time was defined as the time required for the fluid to form a strong lip. A control fluid without encapsulant was run at first as a baseline, and the test was next run using different range of temperature, pH, brine density, coating thickness and friction pressure. Three forms of encapsulated borate-crosslinked fluid; 10%, 20% and 30% coated were used for this study. The results of using uncoated crosslinked fluid and the delay time for each concentration used were observed and recorded to evaluate the range of delay time when using different coating thickness.

Shear sensitivity test

During the travel to perforations, fracturing fluids were subjected to high shearing in the wellbore. The shear sensitivity of the designed fluid was tested in a shear history simulator at ambient temperature, at 40 °F to represent mudline conditions and at 300 °F to simulate bottomhole static condition. The fluid was dynamically injected into a rheometer at a controlled shear rate to simulate travel time. The procedures included the continuous shearing of the fluid at 100 s^{-1} with periodic shear ramps every 30 minutes by changing the shear rate through 100-, 75-, 50-, 25-, 50-, 75-, and 100 s^{-1} shear stages to obtain the rheological properties. To qualify as shear tolerant, the designed fluid was expected to fulfil these criteria when cooled down to a simulated mudline temperature of 40 °F; (1) After 5 minutes, the fluid had at least 100 cP at 100 s^{-1} (2) At 10 minutes, the fluid

viscosity was greater than 160 cP at 100 s^{-1}. (3) At 15 minutes, the fluid viscosity was greater than 70% of the static test at 100 s^{-1}. (4) At 30 minutes, the fluid viscosity was greater than 80% of the static test at 100 s^{-1} [3].

Coreflow

Coreflow test was performed to evaluate fluid leakoff and clean-up in the fracturing fluid. Test was performed using a core sample from representative well of deepwater setting. Leakoff test was simulated by injecting the fracturing fluid at a constant differential pressure. The leakoff rate was measured as a function of the square root of time to calculate the spurt loss and leakoff coefficient. The core was then shut in at 300 °F and a confining pressure of 2,500 psi was applied for 24 hours to simulate the after-fracturing completion work. After shutting in, brine solution was injected in the production direction to simulate the flowback and the retained permeability was measured.

RSM Modelling

Response surface methodology (RSM) was used for optimization of fracturing fluid performance across a targeted range of parameters. A 3D model was generated to demonstrate the interactive effects between individual parameters. The effects of temperature, pH, brine density, coating thickness and friction pressure on the release rate of boric acid was investigated. In the preliminary work, the effect of the independent parameters on response was investigated by varying one factor at a time while keeping the others constant. With the visualization of predicted model to observe the overview of the relationship among the independent parameters on the response to simulate real data of deep well profile and identify the optimal operating conditions for productivity forecast. The model clarified the effects for binary combination of the independent parameters.

CONCLUSION

The fracturing fluid system used in this project was encapsulated borate-crosslinked fluid with different coating thickness, which kept the fluid stable at very high temperatures (up to 350 °F). With wells being drilled deeper with extreme temperatures exposure, it was concluded that a high-temperature encapsulated crosslinked fluid was important for optimum fracturing fluid performance in a way that the encapsulant 1) provided a shield to retard the crosslink reaction to take place, which helped to control crosslinking and gel breaking time 2) limiting the tubing friction and treating pressure by delaying the viscosity enhancement 3) enables crosslinked fracturing fluid stability for a longer time than designed 4) minimizes residual mass and 5) prevent shear degradation.

The fluid was expected to demonstrate compatibility with all selected additives and brine solution, and to remain stable at mudline temperatures as low as 40 °F, and effective at bottom-hole temperatures of at least 250 °F. The encapsulated crosslinker was expected to provide extended crosslink delay times in the range of 2 to 20 minutes depending on the encapsulant thickness, by slow dissolution of the coating without affecting fluid stability. The extended delay time allow in limiting the tubing friction and treating pressure. The formulation designed was anticipated to reduce the treating pressure by at least 20% depending on the wellbore configuration. Based on the past researches conducted, that the rate of boric acid releases is a function of coating thickness, temperature, pH, brine density and friction pressure. In this context, the rate of dissolution of the encapsulation was controlled by manipulating the encapsulant thickness to adjust the range of delay times.

ACKNOWLEDGEMENT

The authors would like to thank USM and Mr. Ling Kong Teng from Schlumberger for his assistance in guiding the research workflow of this project

REFERENCES

[1] R. Barati and J. T. Liang, “A review of fracturing fluid systems used for hydraulic fracturing of oil and gas wells,” *J. Appl. Polym. Sci.*, vol. 131, no. 16, pp. 1–11, doi: 10.1002/app.40735, 2014.

[2] C. L. J., “A New Method for Determining the Rheology of Crosslinked Fracturing Fluids,” 1983.

[3] J. Bagal, N. M. Gurmen, R. A. Holicek, B. R. Gadiyar, and C. N. Fredd, “Engineered application of a weighted fracturing fluid in deep water,” *Proc. - SPE Int. Symp. Form. Damage Control*, vol. 2006, pp. 791–806, 2006, doi: 10.2523/98348-ms, 2006.

[4] D. C. Gardner and J. V. Eikerts, “Rheological characterization of crosslinked and delayed crosslinked fracturing fluids using a closed-loop pipe viscometer,” *Proc. - SPE Annu. Tech. Conf. Exhib.*, vol. 1983-October, doi: 10.2523/12028-ms, 1998.

[5] J. W. Still, S. B. McConnell, and M. J. Miller, “An Improved Encapsulated Breaker to Decrease Hydrostatic Release and Increase Thermal Stability,” *SPE Int. Symp. Oilf. Chem.*, pp. 173–181, doi: 10.2523/80220-ms, 2003.

PGC_SCHE USM_2020_06

Plant mediated synthesis of Titanium dioxide (TiO_2) nanoparticles: Mini review

Mohammad Aslam[1], Ahmad Zuhairi Abdullah[1,*], Mohd. Rafatullah[2]
[1] School of Chemical Engineering, Universiti Sains Malaysia,14300 Nibong Tebal, Penang, Malaysia
[2] School of Industrial Technology, Universiti Sains Malaysia,11800 Penang, Malaysia
Email: [*]chzuhairi@usm.my

Abstract: Nanotechnology is a rising star with many prospective applications in the research horizon and promises to deliver. This involves in the design, synthesis, characterization, and application of materials and devices whose smallest functional organization, in at least one dimension, is in the nanometer scale or billionth of a meter. Most of these materials are usually generated by physical and chemical processes which are hazardous and toxic, but recent advances on plant mediated synthesis are simpler, safer and scalable. Plant mediated synthesis of nanoparticles is shown to be beneficial compared to microbes, because the existence of large variety of biomolecules in plants can serve as a capping and reducing agents and therefore increases the rate of nanoparticles reduction and stabilization. Among all the nanoparticles, titanium dioxide (TiO_2) nanoparticles have been mostly exploited in various applications. This review is dedicated to phyto-based biosynthesis of TiO_2 nanoparticles along with the focus on bioreduction ability of different plant extracts against TiO_2 under various experimental conditions.
***Keywords**: Nanotechnology; nanostructures; titanium dioxide; biomolecules*

INTRODUCTION

Nanotechnology is primarily concerned with the synthesis and potential use of nanoparticles (NPs) of varying dimensions, structures, chemical compositions and controlled dispersion. NPs are usually defined as particles with sizes in the range of 1 to 100 nm. These particles are remarkable, because they exhibit unique physical and chemical properties that are substantially different compared to their macro components [1]. Among all metal oxides, TiO_2 NPs are the important scientific concern with a photo catalytic, antimicrobial and antibacterial successful applications based on their activities [2, 3]. Though pure and well-defined nanoparticles may successfully produce by chemical and physical methods, but they are very expensive and potentially harmful to the environment. An alternative to chemical and physical methods for producing nanoparticles in an environmentally friendly way could be through the usage of biological organisms such as microorganisms, plant extracts or plant biomasses [4, 5].

The green synthesis of metal / metal-oxide nanoparticles (NPs) has attracted considerable attention to explore the potential application of bio-based nanotechnology. A quick, environmentally friendly and less toxic way to synthesize NPs from plant extracts are such a motivation to many material scientists [6]. It has been reviewed that green sources always act as both stabilizing and reducing agent for the synthesis of shape and size-controlled nanoparticles. In comparison to conventional industrial manufacturing process, synthesis methods using plant extracts seem to have advantages in terms of reagents handling and process safety [7]. The fact that many of the recent works concerning the NPs ' synthesis have described plant extracts as the key reagents to be in time with this future prospect. Moreover, phytochemicals are generally thought to effectively produce NPs, although the precise mechanism is yet to be satisfactionally explained.

GREEN SYNTHESIS OF TIO_2 NPS USING PLANT EXTRACTS

Preparation of plant extract

A common way for the plant extract is prepared from the desired plant part via washing and mixing with the distilled water followed by boiling for a few minutes, filtered and finally the filtrate can be quickly used or stored for further use at a low temperature. The complete process of extract preparation is shown in Figure 1. For increasing, the efficiency of phytochemicals, proficient extraction of plants should be carried out by potential methods. Longer solvent exposure to plants can lead to chemical content in the extract [8]. The selection of the appropriate solvent also affects the rate of extraction. Generally, the enhanced phytochemical content presents in alcoholic and phenolic extracts.

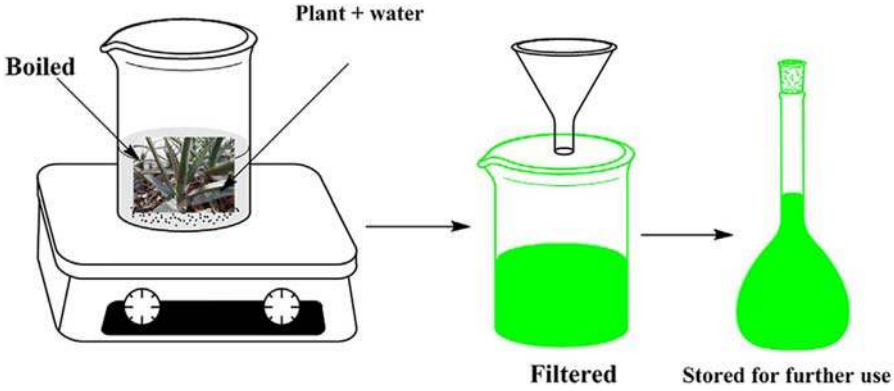

Figure 1. Method for preparation of plant extract

Preparation of TiO_2 nanoparticles

The process to synthesize TiO_2 NPs starts with forming a solution of titanium precursor such as TTIP, $TiCl_4$, $TiO(OH)_2$, $TiO(SO)_4$ and TiO_2 bulk particles in the desired solvent (ethanol or distilled water). The prepared extract is added drop wise to this solution and the mixture is stirred at constant room temperature. The synthesized nanoparticles are then filtered, washed, dried and then calcined with distilled water. The change in the color of the solution indicates the synthesis of TiO_2 NPs. The general mechanism of green synthesis of TiO_2 NPs is shown in Fig.2. Calcination is generally carried out from 400 to 800 °C for the removal of organic groups. Phytochemicals present in plant are supposed to perform either of roles; reduction of metal salts, hydrolysis of the Ti(IV) antecedent, solubilizing, and polymerization of the different intermediates [9]. The obtained NPs were then characterized by various instrumental techniques such as XRD, TEM, FESEM, Light Scattering (LS) and FTIR.

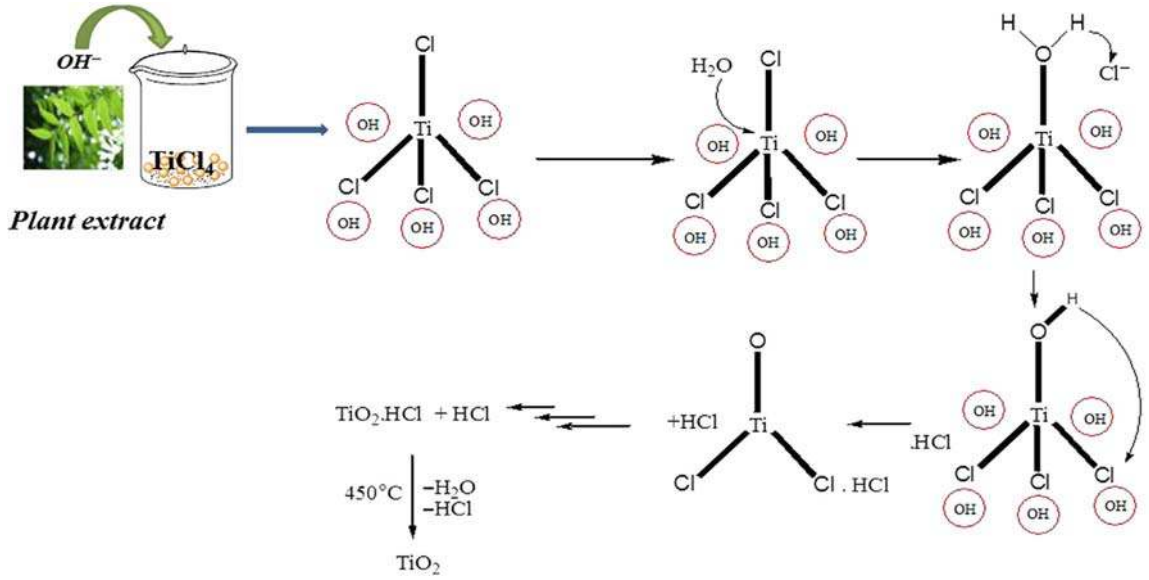

Figure 2. General mechanism of TiO_2 NPs synthesis

Synthesis techniques

Table 1 highlights the current NP synthesis findings using various plant extracts. The composition of biomolecules in plant extracts gives rise to the bio reduction of NPs. However, the reduction phenomenon is still not fully addressed fundamentally. A leaf extract (prepared from finest powder) of Nyctanthes Arbor-tristis (night flowering jasmine) was reported as the first attempt for green and rapid synthesis of titania nanoparticles (TiO_2) using titanium tetraisopropoxide (TTIP) as a precursor. They stated that this route is suitable for quick NPs synthesis. The finest Nyctanthes leaves powder was used to prepare the extract. It has been observed from the SEM images that the NPs obtained were pure and crystalline with uniform shapes. The resulting nanoparticles were between 100-150 nm in size [10]. Another group of authors reported TiO_2 NPs synthesized using an extract from Hibiscus rosa-sinensis flowers and 500 mM titanium oxysulfate as titanium precursor at pH 7. Their XRD data suggested an average particle size for 7 nm of their NP's. Morphologically, their spherical NPs were monodispersed without an aggregation under SEM. The FTIR data suggested that the capping agents were the phytochemicals mainly containing phenolic and amines groups [11].

Table 1. Various plant extract used to synthesize TiO_2 NPs

No.	Plant	Capping agent	Titanium precursor	Morphology	Characterization	Ref.
1.	*Acanthophyllum laxiusculum*	Roots extract	TTIP	20-25nm; Spherical	XRD, FTIR and TEM	[16]
2.	*Ageratina altissima (L.)(White snakeroot)*	Leaves extract	$TiO(OH)_2$	60-100nm; spherical	XRD, FTIR and FESEM	[17]
3.	*Annona squamosal (Sugar apple)*	Peel extract	$TiO(OH)_2$	23-25nm; Spherical & rutile	EDS, UV-Vis, TEM, SEM and XRD	[18]
4.	*Aloe Vera*	Leaves extract	$TiCl_4$	32nm; Irregular structure	TEM, XRD and TG/DTA	[19]
5.	*Azadirachta Indica (Neem)*	Leaves extract	TTIP	124nm; Spherical & interconnected	FESEM, EDAX, XRD, UV–Vis and FTIR	[20]
6.	*Bauhinia variegate*	Leaves extract	$TiCl_4$	6-20nm; Irregular shape	XRD and UV-Vis	[21]
7.	*Calotropis gigantean (Crown flower)*	Flower extract	$TiO(OH)_2$	160-220nm; Spherical oval	FTIR, EDS, XRD and SEM	[22]
8.	*Cinnamomum tamala*	Leaves extract	TiO_2	8-20nm	FESEM,TEM and FTIR	[23]
9.	*Dandelion*	Pollen extract	$TiCl_3$	Rod shaped	XRD, FSEM and TEM	[24]
10.	*Echinacea purpurea (L.)*	Whole plant	TiO_2	120nm; Polydisperse	TXRF, SEM and XRD	[25]
11.	*Hibiscus rosa-sinensis*	Flower extract	Titanium oxysulphate	7nm; Spherical	SEM, XRD and FTIR	[11]
12.	*Jatropha curcas*	Latex extract	$TiO(OH)_2$	25-50nm; Spherical	TEM, SAED, XRD FTIR and EDAX	[26]
13.	*Nyctanthes (Night-flowering Jasmine)*	Leaves extract	Titanium tetraisopropoxide	100-150; Spherical	XRD, SEM and PSA	[10]
14.	*Psidium guajava (Guava)*	Leaves extract	$TiO(OH)_2$	32.58nm; Spherical	XRD, FTIR, FESEM and EDX	[12]
15.	*Vigna radiate (L.)*	Legume extract	TiO_2	Oval	SEM and FTIR	[27]

The leaf extract of guava (Psidium Guajava) produced TiO_2 NPs' the exhibited antioxidant and antimicrobial properties. Aqueous P. Guajava leaf extract was prepared from freshly collected leaves (20 g). They were initially washed with tap water and immersed in 250 mL of double-distilled water at 60 °C for 15 minutes. Then, the filtered extract was mixed with 80 mL of $TiO(OH)_2$ at 25 °C for 24 hours until green coloured of TiO_2 NP's were obtained. The leaf extract was found to contain alcohol as well as primary and aromatic amines that contributed to the TiO_2 NPs synthesis. The synthesized TiO_2 NPs' XRD result indicated the presence of both anatase and rutile forms. Moreover, the EDX studies showed that the synthesized TiO_2 NP's were crystalline in nature [12]. Meanwhile, the other author used leaf extract of Catharanthus roseus to synthesize TiO_2 NPs with the size range of 25 to 110 nm and of irregular shapes. The average size of the NPs' was measured and found to be 65 nm. The extract of C.roseus leaves was then utilized for the preparation of a broth solution and after extraction of the phytochemicals from the leaf, filtration was carried out and the extract was allowed to mix with the precursor TiO_2 followed by stirring in order to get the TiO_2 nanoparticles. The XRD, FTIR, SEM, AFM analyses were then performed to reveal the exact characteristics and morphology of the synthesized TiO_2 NPs [13].

Plant extracts are widely considered as good sources of both capping and reducing agents in the biological synthesis of nanoparticles. Another leaf extracts i.e. Eclipta prostrata L. which is also known as false daisy was used to prepare TiO_2 NPs' using aqueous reduction method. An aqueous containing the leaves of Eclipta prostrata L. was first boiled, filtered and mixed with $TiO(OH)_2$ and then stirred to produce the nanoparticles that were verified by color change at room temperature to indicate the successful synthesis of TiO_2 NPs. The synthesized TiO_2 NPs were then subjected to different analyses like FTIR, XRD, AFM, and FESEM. Spherically shaped NPs' were obtained with a size range of 36 to 68nm and an average particle size of 49.5nm [14]. It has been observed that the leaf extract of Syzygium cumini also used as reducing and stabilizing agent for the synthesis of TiO_2 NPs. Syzygium cumini leaves were thoroughly washed with double distilled water to remove any dirt adhered to the surface. Leaf extract was prepared by mixing 20 g of powder with 100 mL of distilled water and heating the mixture at 80 °C for 60 minutes. The aqueous extract was then reacted with 80 mL of 5 mM TTIP solution to 80 mL of Syzygium cumini extract at the ratio of 1:1 (volume/volume) followed by continuous stirring at room temperature for 8 hours. After stirring, the mixture was centrifuged at 9000 rpm for 10 min to separate the nanoparticles. The TiO_2 NPs obtained were dried for one night at 100 °C followed by calcination in a muffle oven for 3 hours at 570 °C. The average crystalline size, surface area, pore size diameter and total pore volume of TiO_2 NPs are 10 nm, 105 m^2/g, 10.50 nm, and 0.278 cm^3/g, respectively [15].

CONCLUSION

During the last decade, green synthesis using an environmentally friendly approach has been the matter of great interest in research field. There will be numerous active biomolecules present in a plant extract. The desired active agents can be isolated from the mixture using the suitable solvents. Hydroxyl and carbonyl groups are the major components of plant extract and help in the reducing and capping of the NPs. This technique can help the researchers to achieve the controlled characteristics such as size, morphology, desired crystalline structure of the TiO_2 NPs. However, few plants are used so far for the phytosynthesis of TiO_2 NPs and a plenty of works are still waiting in this area.

ACKNOWLEDGEMENT

The authors are thankful to the financial support provided by Long Term Research Grant Scheme (LRGS) (67215001) sponsored by the Ministry of Higher Education of Malaysia.

REFERENCES

[1] L-S. Li, J. Hu, W. Yang, A.P. Alivisatos. Band gap variation of size- and shape-controlled colloidal cdse quantum rods. Nano Lett, 1:349–51, (2001).

[2] R.N. Bharagava, G. Saxena, A.K. Yadav, V. Singh, K.B. Thapa, S.P. Goutam. Green synthesis of TiO_2 nanoparticles using leaf extract of Jatropha curcas L for photocatalytic degradation of tannery wastewater Chem. Eng. J., 336, 386–9, (2017).

[3] V. Patidar, J. Preeti. Green Synthesis of TiO_2 nanoparticle using Moringa oleifera leaf extract Int. Res. J. Eng. Technol., 4, 470–3, (2017).

[4] D. Bhattacharya and G. Rajinder, Nanotechnology and potential of microorganisms. *Crit Rev Biotechnol* 25:199–204, (2005).

[5] P. Mohanpuria , N.K. Rana and S.K. Yadav, Biosynthesis of nanoparticles: technological concepts and future applications. *J Nanopart Res,* 10:507–517, (2008).

[6] C.P. Devatha, A.K. Thalla, S.Y. Katte. Green synthesis of iron nanoparticles using different leaf extracts for treatment of domestic wastewater, J. Clean. Prod., 139 1425–1435, (2016).

[7] S. Iravani. Green synthesis of metal nanoparticles using plants. Green Chem., 13:2638–50, (2011).
[8] A. Amid, R.J.M. Salim, M.I. Adenan, The factors affecting the extraction condition for neuroprotective activity of Centella asiatica evaluated by metal chelating activity assay. J. Appl. Sci., 10(10), 837–842, (2010).
[9] O.V. Kharissova, H.V.R. Dias, B.I. Kharisov, B.O. Pérez, V.M.J. Pérez, The greener synthesis of nanoparticles. Trends Biotechnol., 31(4), 240–248, (2013).
[10] M. Sundrarajan, S. Gowri, Green synthesis of titanium dioxide nanoparticles by Nyctanthes arbor-tristis leaves extract. Chalcogenide Lett., 8(8), 447–451, (2011).
[11] N. Azwanida. A review on the extraction methods use in medicinal plants, principle, strength and limitation. Med. Aromat. Plants, 4(196), 2167-0412, (2015).
[12] T. Santhoshkumar, A.A. Rahuman, C. Jayaseelan, G. Rajakumar, S. Marimuthu, A.V. Kirthi, K. Velayutham, J. Thomas, J. Venkatesan, Se-K Kim. Green synthesis of titanium dioxide nanoparticles using Psidium guajava extract and its antibacterial and antioxidant properties. Asian Pac J Trop Med, 968-976, (2014).
[13] K. Velayutham, A.A. Rahuman, G. Rajakumar, T. Santhoshkumar, S. Marimuthu, C. Jayaseelan, A. Bagavan, A.V. Kirthi, C. Kamaraj, A.A. Zahir, G. Elango. Evaluation of Catharanthus roseus leaf extract-mediated biosynthesis of titanium dioxide nanoparticles against Hippobosca maculata and Bovicola ovis. Parasitol Res, 111:2329–2337, (2012).
[14] G. Rajakumar, A.A. Rahuman, B. Priyamvada, V.G. Khanna, D.K. Kumar, P.J. Sujine. Eclipta prostrata leaf aqueous extract mediated synthesis of titanium dioxide nanoparticles. Mater. Letters 115–117, (2012).
[15] N. K. Sethy, Z. Arif, P.K. Mishra, P. Kumar. Green synthesis of TiO_2 nanoparticles from Syzygium cumini extract for photo-catalytic removal of lead (Pb) in explosive industrial wastewater. Green Process Synth, 9: 171–181, (2020).
[16] Z. Madadi, T.B. Lotfabad. Aqueous extract of Acanthophyllum laxiusculum roots as a renewable resource for green synthesis of nano-sized titanium dioxide using sol-gel method. Adv. Ceram. Prog., 2 (1), 26, (2016).
[17] S. Ganesan, I.G. Babu, D. Mahendran, P.I. Arulselvi, N. Elangovan, N. Geetha, P. Venkatachalam. Green engineering of titanium dioxide nanoparticles using Ageratina altissima (L.) King & HE Robines. Medicinal plant aqueous leaf extracts for enhanced photocatalytic activity. Ann. Phytomedicine – Int. J., 5, 69–75, (2016).
[18] S.M. Roopan, A. Bharathia, A. Prabhakarn, A.A. Rahuman, K. Velayutham, G. Rajakumar, R.D. Padmaja, M. Lekshmi, G. Madhumitha. Efficient phyto-synthesis and structural characterization of rutile TiO2 nanoparticles using Annona squamosa peel extract. Spectrochim Acta A Mol Biomol Spectrosc, 98:86–90, (2012).
[19] K.G. Rao, C. Ashok, K.V. Rao, C.H.S. Chakra, P. Tambur. Green synthesis of TiO_2 nanoparticles using Aloe vera extract. Int. J. Adv. Res. Phys. Sci., 2(1A), 28–34, (2015).
[20] R. Sankar, K. Rizwana, K.S. Shivashangari, V. Ravikumar. Ultra-rapid photocatalytic activity of Azadirachta indica engineered colloidal titanium dioxide nanoparticles. Appl Nanosci, 5, 731–736, (2015).
[21] V. Galstyan, E. Comini, C. Baratto, G. Faglia, G. Sberveglieri. Nanostructured ZnO chemical gas sensors. Ceram Int., 41:14239–44, (2015).
[22] S. Marimuthu, A.A. Rahuman, C. Jayaseelan, A.V. Kirthi, T. Santhoshkumar, K. Velayutham, A. Bagavan, C. Kamaraj, G. Elango, M. Iyappan, C. Siva, L. Karthik, K.V. Rao. Acaricidal activity of synthesized titanium dioxide nanoparticles using Calotropis gigantea against rhipicephalus microplus and haemaphysalis bispinosa. Asian Pac J Trop Med, 6:682–8, (2013).
[23] G.K. Naik, P.M. Mishra, K. Parida. Green Synthesis of Au/ TiO2 for effective dye degradation in aqueous system. Chem. Eng. J., 229, 492–497, (2013).
[24] S.-J. Bao, C. Lei, M.-W. Xu, C.-J. Cai, D.-Z. Jia. Environment friendly biomimetic synthesis of TiO2 nanomaterials for photocatalytic application. Nanotechnology, 23 (20), 205601, (2012).
[25] R. Dobrucka. Synthesis of titanium dioxide nanoparticles using Echinacea purpurea herba. Iran. J. Pharm. Res., 16, 756–762, (2017).
[26] M. Hudlikar, S. Joglekar, M. Dhaygude, k. Kodam. Green synthesis of TiO2 nanoparticles by using aqueous extract of Jatropha curcas L. latex. Mater Lett, 75, 196–9, (2012).
[27] A. Chatterjee, D. Nishanthini, N. Sandhiya, J. Abraham. Biosynthesis of titanium dioxide nanoparticles using Vigna radiata. Asian J Pharm Clin Res., 9 (4), 1–4, (2016).

PGC_SCHE USM_2020_07

Removal of Cu (II) from aqueous solution using composite adsorptive membrane

Shazlina Abd Hamid, Suzylawati Ismail*
School of Chemical Engineering, Engineering Campus, Universiti Sains Malaysia,
14300 Nibong Tebal, Pulau Pinang, Malaysia.
*E-mail: *chsuzy@usm.my*

Abstract. A flat sheet of composite adsorptive membrane was fabricated via simple blending process and phase inversion method for the removal of Cu (II) from aqueous solution. The characterization techniques such as Scanning Electron Microscopy (SEM), Energy Dispersive X-ray Spectroscopy (EDX) and Fourier-Transform Infrared Spectroscopy (FTIR) were performed to determine the changes in morphology, elements and functional groups of the composite adsorptive membrane after adsorption. Results obtained from SEM, EDX and FTIR showed that Cu (II) was successfully adsorbed on the membrane after undergoing the adsorption process.
Keywords: *Composite adsorptive membrane; Adsorption; Cu (II) removal*

INTRODUCTION

Over the past few years, researchers have shown their great interest in adsorptive membrane technology, especially in water and wastewater treatment area. It provides many benefits such as high removal capacity, reusability, stability, faster kinetics, lower pressure drop, higher flow rate and ease of scale-up [1]. The adsorptive membrane utilizes a combination of adsorption and filtration processes in a one-unit operation. In most studies, the adsorbent was embedded into the polymer matrices to adsorb the valuable target compounds. In this study, a composite adsorptive membrane was prepared by impregnating zeolite into the PSf polymer matrix specifically to remove Cu (II). This paper aims to characterize the membrane sample before and after adsorption using important characterization methods (SEM, EDX and FTIR) in order to investigate the capability of the membrane to remove Cu (II) ions by adsorption process.

MATERIALS AND METHODS

A dope solution was prepared by dissolving 2 wt% SDS in 65 wt% NMP solvent for 1 h under agitation (Wisestir) at 300 rpm and 3 wt% PVP was added into the mixture. Then, 15 wt% zeolite was added into the mixture and it was further sonicated (Ultrasonic, Elma S80H) for 1 h. Afterwards, 15 wt% PSf polymer was gently mixed into the solution and stirred at 500 rpm using a temperature of 60°C, overnight. Then, the mixture was sonicated and degassed for 1 h to remove the air bubbles from the dope solution. The polymer solution was casted on a glass plate (250 µm film thickness) using an automatic film applicator at room temperature. Next, the casted membrane was immediately immersed into a water coagulation bath in order to allow the phase inversion to occur. The membrane was finally dried at room temperature and stored in a closed container until it was ready to be used.

For batch adsorption studies, the membrane was cut into a rectangular size (0.17 m x 0.04 m) and immersed in a beaker containing 10 mg/L of Cu (II) ion solution (200 mL) at pH 5. Adsorption experiments were carried out for 24 h at room temperature. The surface and cross-sectional morphology and elements present in composite adsorptive membrane before and after adsorption were analysed using a Scanning Electron Microscope (SEM) and Energy Dispersive X-Ray Spectroscopy (EDX) (Quanta Feg 450, FEI). The changes on the surface chemistry of adsorptive membranes before and after adsorption were measured using Fourier-transform infrared spectroscopy (FTIR) (FTIR-NICOLET iS10).

RESULTS AND DISCUSSION

Figure 1 shows the SEM morphology of the top surface and cross-section of the composite adsorptive membrane before and after Cu (II) ion adsorption. Before the metal adsorption, a smooth membrane surface with the presence of some pores was obtained (Figure 1-a1). However, the surface texture of the membrane changed drastically after adsorption. It was clearly seen that the membrane surface was loaded with Cu (II) ions, as shown in Figure 1-b1. It seems that the membrane surfaces and pores were covered by metal ions. The asymmetric membrane contained porous skin layer with a finger-like structure that was observed in the cross-section of the membrane (Figure 1-a2). It resulted of the phase inversion technique applied in this study for membrane fabrication. The finger like pores promoted to increase its water permeability. Moreover, it was identified that the zeolite particles were distributed inside the membrane's pore because of blending mixtures. After adsorption, the pores were filled with Cu (II) ions,

which proved that the adsorption not only took place on the surface of the membrane but got into the membrane's pore as well.

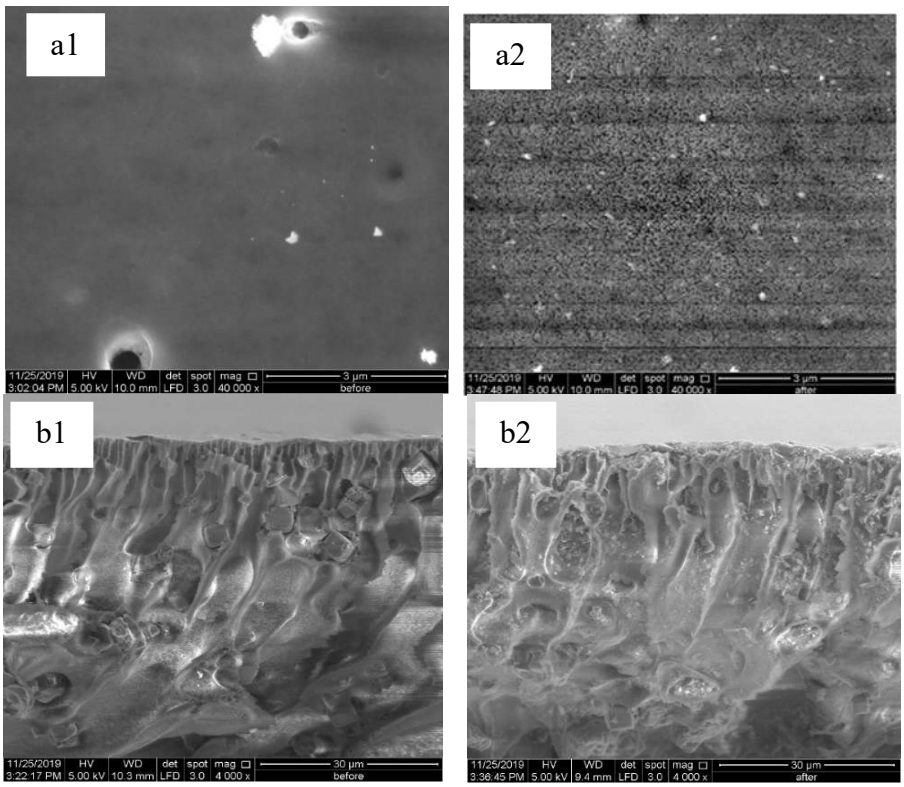

Figure 1. SEM images of surface and cross-section of the composite adsorptive membrane (a1, a2) before and (b1, b2) after adsorption of Cu (II) ions. Magnification: 40,000x.

Results of EDX spectra are presented in Figure 2 where each element contained in the samples, before and after adsorption, are observed. It was identified that Al, Si, C, O and Na were present in composite adsorptive membrane before adsorption. Zeolite is a porous aluminosilicate material that is composed of SiO_4 and AlO_4 tetrahedral structures of a three-dimensional network. The existence of trivalent Al atoms in the structure provided an anionic character that was neutralised by additional cations such as magnesium (Mg^{2+}), calcium (Ca^{2+}) and sodium (Na^{+}). The element sodium (Na^{+}) shown in the graph came from zeolite and SDS surfactant. Initially, the element Na^{+} was present in raw membrane. However, it was absent after adsorption. Note that an ion exchange mechanism could be the cause as to why the metal cations might be exchanged with the additional framework cations, which has been considered as the primary mechanism of metal adsorption with zeolites [2]. Besides that, the sulphur element was identified in the membrane sample originating from PSf and SDS, which was introduced into membrane formulations. As expected, the copper element appeared in the spectra after adsorption. The presence of this metallic element on the surface of membrane indicated that Cu (II) ion was successfully adsorbed onto the membrane.

The surface functional groups of composite adsorptive membrane before and after the Cu (II) ion adsorption were identified by FTIR spectroscopy and are illustrated in Figure 3. FTIR spectra of membrane samples before and after adsorption of Cu (II) ion were similar. However, after the loading of this metal on the membrane surface, some vibration bands shifted to a slightly lower frequency. The changes of magnitude and shifts identified for some absorption bands were attributed to the interaction of Cu (II) ions with adsorbent functional groups. The broad band at 3100 - 3500 cm^{-1} of FTIR spectra was assigned to –OH stretching [3]. This could be cause of the characteristic of zeolite, which has a hydrophilic nature and is able to adsorb water molecules via hydrogen bonding. The identification of O-H band on FTIR spectra indicated that O-H functionalities of the membranes played an important role in the adsorption process [4]. After metal adsorption, the band shifted towards a slightly lower frequency from 3402 to 3395 cm^{-1}. This result suggested the involvement of hydroxyl groups in the binding of Cu (II) ions and it could be a reason for the decreasing in O-H bond strength. Besides that, the presence of zeolite particles on the membrane surface was associated with the bands at 970 – 1000 cm^{-1}, which was referred to the Si-O-Al species. It was observed that there was a slight shift in vibrations from 965 cm^{-1} to a lower frequency that is 932 cm^{-1} after adsorption thus demonstrating the successful loading of Cu (II) ions into the zeolite structure [5]. These changes occurred due to the binding of Cu (II) ions with silica and alumina functional groups of zeolite. Thus, the band shifting confirmed that the adsorption of metal ions on the surface of the membrane. The band at 1660 cm^{-1} corresponded to vinyl group of PVP additive. The

bands reflected in the spectrum at 1322 cm^{-1} were associated with C-N and carbonyl groups, C=O stretching from mixing of PSf and PVP [6]. At 1487 cm^{-1}, the band of aromatic benzene ring was also detected. The bands at 1500 cm^{-1} and 1504 cm^{-1} corresponded to asymmetric and symmetric stretching vibrations of ether-O and aromatic C=C groups, which were derived from the PSf membrane [7]. The signal of S=O stretching from the vibration of sulfone groups SO_2 was displayed at 1150 cm^{-1} due to the presence of SDS surfactant and PSf in the membrane structure.

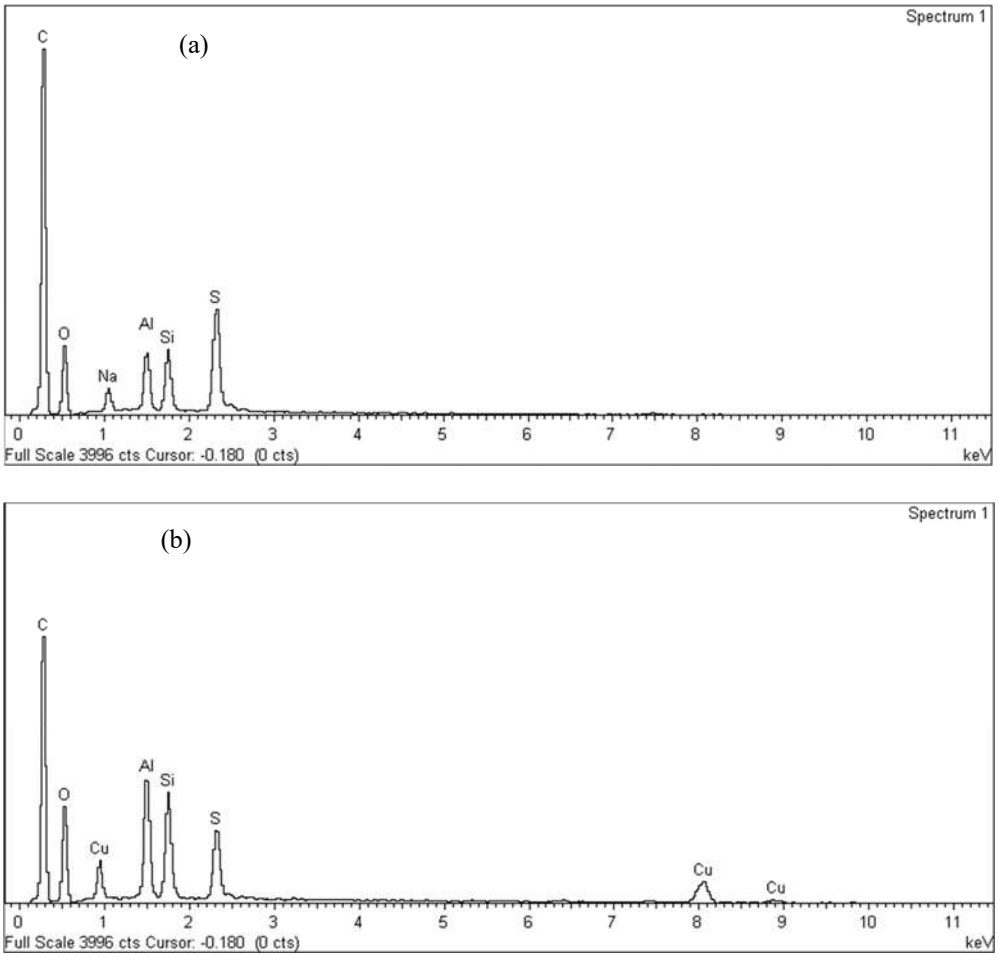

Figure 2. EDX analysis spectra of composite adsorptive membrane (a) before and (b) after adsorption of Cu (II) ions.

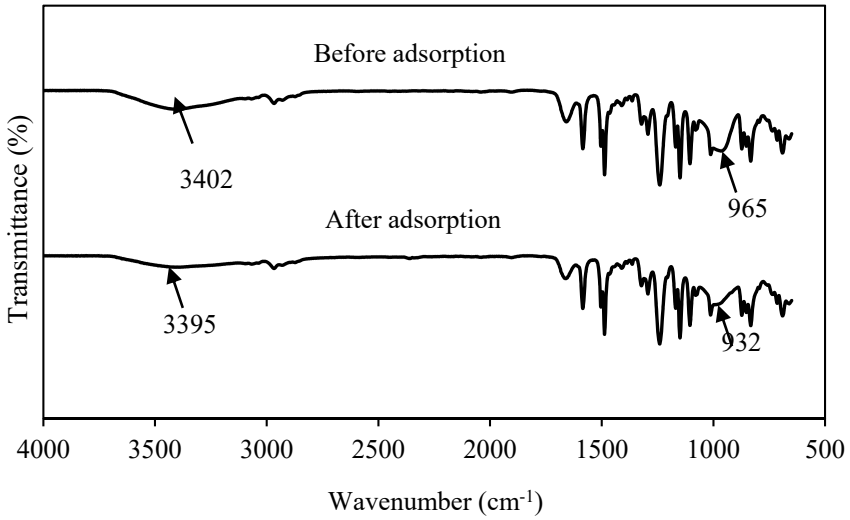

Figure 3. FTIR spectra of composite adsorptive membrane used for the adsorption of Cu (II) ions from aqueous solution.

CONCLUSION

A composite adsorptive membrane was successfully prepared by a simple synthesis method, which involved blending and phase inversion process to remove Cu (II) ions from aqueous solution. Characterization results of SEM showed that Cu (II) ions were successfully adsorbed on the membrane surface and pore. Results from FTIR and EDX studies confirmed that the composite adsorptive membrane containing the main functional groups $Si\text{-}O^-$ and $Al\text{-}O^-$ which were relevant for the Cu (II) ion adsorption. In conclusion, the composite adsorptive membrane can be utilized for the removal of cationic metal species or for future industrial applications.

ACKNOWLEDGEMENT

The authors would like to acknowledge the Ministry of Energy, Science, Technology, Environment and Climate Change, Malaysia (MESTECC) in providing the financial support through R & D Fund (305/PJKIMIA/6013394) for this research project.

REFERENCES

[1] Y. G. A. El-reash, A. M. Abdelghany, and A. A. Elrazak, "Removal and separation of Cu (II) from aqueous solutions using nano-silver chitosan/ Polyacrylamide membranes," *Int. J. Biol. Macromol.*, vol. 86, pp. 789–798, 2016.

[2] B. Biškup and B. Suboti, "Kinetic analysis of the exchange processes between sodium ions from zeolite A and cadmium, copper and nickel ions from solutions," *Sep. Purif. Technol.*, vol. 37, pp. 17–31, 2004.

[3] J. He, Y. Song, and J. P. Chen, "Development of a novel biochar/PSF mixed matrix membrane and study of key parameters in treatment of copper and lead contaminated water," *Chemosphere*, vol. 186, pp. 1033–1045, 2017.

[4] N. Abdullah *et al.*, "Polysulfone/hydrous ferric oxide ultrafiltration mixed matrix membrane: Preparation, characterization and its adsorptive removal of lead (II) from aqueous solution," *Chem. Eng. J.*, vol. 289, pp. 28–37, 2016.

[5] F. T. Fanta, A. A. Dubale, and D. F. Bebizuh, "Copper doped zeolite composite for antimicrobial activity and heavy metal removal from waste water," *BMC Chem.*, vol. 13, pp. 1–12, 2019.

[6] A. Pagidi, R. Saranya, G. Arthanareeswaran, A. F. Ismail, and T. Matsuura, "Enhanced oil – water separation using polysulfone membranes modified with polymeric additives," *Desalination*, vol. 344, pp. 280–288, 2014.

[7] S. S. Kumar and H. Vurimindi, "Synthesis of polysulfone and zirconium oxide coated asbestos composite separators for alkaline water electrolysis," *Chem. Eng. Process Tech.*, vol. 3, p. 1035, 2017.

PGC_SCHE USM_2020_08

Fabrication of Microcrystalline Cellulose (MCC) Incorporated Polyether Sulfone (PES) Membranes: Study of Different Concentration MCC on Hydrophilicity

Amirul Islah Nazri, Abdul Latif Ahmad*
School of Chemical Engineering, Engineering Campus, Universiti Sains Malaysia,
14300 Nibong Tebal, Pulau Pinang, Malaysia.
*E-mail: *chlatif@usm.my*

Abstract. Hydrophilic polyether sulfone (PES) membranes were prepared via dry-wet phase inversion technique using different concentration of microcrystalline cellulose (MCC) as additive. In this study, dimethylacetamide/lithium chloride (DMAc/LiCl) co-solvent was used to assist MCC dissolution into the dope solution. The prepared membranes were characterized for the chemical and hydrophilicity properties using Attenuated Total Reflectance Fourier Transform Infrared Spectroscopy (ATR-FTIR) and water contact angle techniques. The ATR-FTIR and water contact angle measurements indicated that the membranes exhibited improvement in hydrophilicity when incorporated with MCC due to presence of hydroxyl functional groups towards the surface.
Keywords: *Polyether sulfone; Microcrystalline Cellulose; DMAc/LiCl co-solvent; membrane morphology; hydrophilicity.*

INTRODUCTION

Polyethersulfone (PES) is one of many polymeric materials being used for the preparation of microfiltration (MF) and ultrafiltration (UF) membranes. PES possesses remarkable properties including toughness, resistance to mineral acids and high thermal stability. However, the hydrophobicity of PES limits its application especially for the water treatment process. Membranes with hydrophobic properties promote non-specific solutes adhesion on their surface, leading to fouling. Membrane fouling causes decline in flux due to generation of extra resistance against transport of water through the membrane. As the result, higher applied pressure is needed to compensate this flux reduction and membrane cleaning becomes necessary, leading to higher operating cost. In addition, fouling phenomena also leads to membrane degradation cause to reduction of membrane's selectivity and shorter membrane's lifetime [1]. Microcrystalline cellulose (MCC) is a derivation of cellulose obtained from purified and partially depolymerized cellulose. It possesses the advantages of the most abundant organic raw material in the world. Cellulose is renewable, good thermal stability, low price, specific strength and stiffness and biodegradable [2, 3]. MCC consists of (i) crystalline phase, which comprises of tight bundles of microcrystal in a rigid linear arrangement, and (ii) paracrystalline area composes of amorphous cellulose chains. The amorphous phase is readily hydrolyzed when subjected to acid hydrolysis and resulted in shorter and more crystalline fragment. The diameters of these crystallites are the same order as the diameter of the cellulose nanofibrils and it formed by cellulose chains due to van Waals and hydrogen bonding interactions [4]. By chemical structure, each monomeric unit of MCC consists of three hydroxyl groups which make it hydrophilic and easily to be functionalized [3, 5]. The good hydrophilicity of MCC can make up for the hydrophobicity of PES membranes and reduce the fouling effects [2]. However, due to abundance amount of hydroxyl groups, MCC tends to form inter- and intra- hydrogen bonding between themselves thus making them agglomerated and hard to dissolve in common solvents [5, 6].

Many works have been done to tackle the cellulose insolubility issues. Some researchers had modified the cellulose properties by grafting/crosslinking different functional groups onto cellulose surface via surface modification techniques [3, 6]. By doing so, cellulose and its derivatives dispersed well in the common solvents. However, it leads to reduction in amount of hydroxyl group thus reducing the hydrophilicity of the resulting membrane. Recently, some researchers studied the dissolution of cellulose using co-solvent system such as dimethyl acetamide/lithium chloride (DMAc/LiCl), sodium hydroxide (NaOH)/urea, DMSO/tetrabutylammonium fluoride, N-methyl morpholine oxide (NMMO) and ionic liquid [5]. Among of all co-solvents listed, DMAc/LiCl is favourable as both DMAc and LiCl are commonly used as solvent and pore former in membrane fabrication processes. To date, only few studies have implemented the co-solvent system in the fabrication of PES/MCC mixed matrix membranes. In this study, DMAc/LiCl co-solvent was used to fabricate PES/MCC mixed matrix membrane using different concentration of MCC as fillers.

MATERIALS AND METHODS

Commercialize microcrystalline cellulose (MCC) was purchased from Sigma Aldrich, USA and directly be used without further treatment. The dope solutions were prepared via blending process using DMAc/LiCl co-solvent based on the composition shown in Table 1. MCC was properly dissolved into the mixture of LiCl and DMAc at 110

°C for 50 mins, prior to blending with PES at 60 °C for 24 hours. The dope solutions were continuously stirred at 500 rpm throughout the whole blending processes. To remove air bubbles, the dope solutions were degassed in an ultrasonic bath for 1 hour. The dope solutions were then casted on a glass plate by using a film applicator with ~250 µm thickness. Subsequently, the casted membranes were left open air for 45 seconds and then immersed into a water coagulation bath for 24 hours for the phase inversion process to occur. After 24 hours, the membranes were washed with running water and remained dipped in the water bath until further use. The fabricated membranes were characterized for surface chemistry and hydrophilicity by using Fourier Transform Infrared Spectroscopy (FT-IR) and contact angle analysis, respectively.

Table 1. Composition of prepared dope solutions (Total mass of dope = 30g)

Sample	PES[a] [g]	MCC[b] [g]	Co-Solvent	
			LiCl[c] [g]	DMAc[d] [g]
S0	5.175	0	0	24.825
S1	5.175	0.3	1.962	22.563
S3	5.175	0.9	1.914	22.011
S5	5.175	1.5	1.866	21.459

[a] PES maintained at 17.25 wt.%.
[b] MCC varied for 0, 1, 3, 5 wt. %.
[c] LiCl calculated from 8 wt.% of total amount of co-solvent used.
[d] DMAc calculated from 92 wt.% of total amount of co-solvent used.

RESULTS AND DISCUSSION

FT-IR analysis of commercial MCC (Sigma Aldrich), pristine PES membrane (S0) and MCC-incorporated membranes (S1, S3, S5) were carried out and the spectra are shown in Figure 1. The spectra were recorded in transmittance mode in the range of 4000-400 cm $^{-1}$. The spectra of MCC is comparable to pure cellulose and cellulose nanocrystals (CNC) as reported previously in literatures [7]. The wide peak at ~ 3300 cm^{-1}, ~ 2900 cm^{-1} and ~1600 cm^{-1}, later will be mentioned as regions of (i), (ii) and (iii), are corresponding to -OH stretching vibration, C-H stretching vibration, and absorption of water molecules due to strong interaction between cellulose and water, respectively. In addition, the peak at ~ 1426 cm^{-1} assigned to a symmetric -CH_2 bending vibration and this band is known as the crystallinity band. The peaks at approximately 892 cm^{-1} and 1063 cm^{-1} are associated with cellulosic β-glycosidic linkages and the pyranose ring ether band of cellulose, respectively.

For the fabricated membranes, all the MCC-incorporated PES membranes (S1. S3, S5) showed similar spectra as the pristine PES membrane (S0) especially at the wavenumber between ~1500 cm^{-1} down to 500 cm^{-1}. This indicated that the MCC-incorporated membranes were sustaining the PES characteristic even after being incorporated with MCC. In addition, the presence of additional peaks in regions of (i), (ii) and (iii) in Figure 2 indicated that MCC was successfully being incorporated onto the PES matrix, thus forming a new mixed matrix PES/MCC membrane. This is possible since MCC able to dissolute in the dope solutions in the presence of co-solvent DMAc/LiCl. During the dissolution process, the breaking of the intra and inter hydrogen bonds between hydroxyl groups of MCC by the co-solvent happened [8] and those hydroxyl groups were then able to make new hydrogen bonds with the PES. Besides that, the effect of increasing the MCC loading into the dope solutions could directly be interpreted in Figure 1 by the increasing of peak intensity at wavenumber ~3300 cm^{-1} in region (i), wavenumber ~2900 cm^{-1} in region (ii) and wavenumber ~1600 cm^{-1} in region (iii). As more loading of MCC added, the peaks intensity in those three regions was also increased and membrane S5 showed the highest increment amongst the others. This is due to the increasing amount of hydroxyl groups being deposited on the PES as the result from increasing the MCC loadings. This can be further proved by the water contact angle analysis.

Contact angle was used to determine the effect of different loading of MCC on the surface hydrophilicity of the fabricated PES membranes. The analysis was carried out using water as the wetting agent. The results are shown in Figure 3. It can clearly be seen in Figure 2 that the membranes S1, S3 and S5 show lower water contact angle than the pristine PES membrane (S0). This indicated that the hydrophilicity of the fabricated membranes increased and MCC was successfully incorporated into the PES membrane with the presence of co-solvent. The increment in hydrophilicity is due to the presence of hydrophilic hydroxyl groups from MCC on the PES membrane, that attract water towards the surface of the membrane. Water then tends to spread on the membrane surface thus resulting in lower contact angle. Aside from that, the result showed the increment in hydrophilicity due to increment of MCC loadings. It proved that the more MCC being used, more hydroxyl groups were available on the membrane surface, thus the higher hydrophilicity. Membrane S5 showed the lowest contact angle reading up to 34.6° compared to the other membranes.

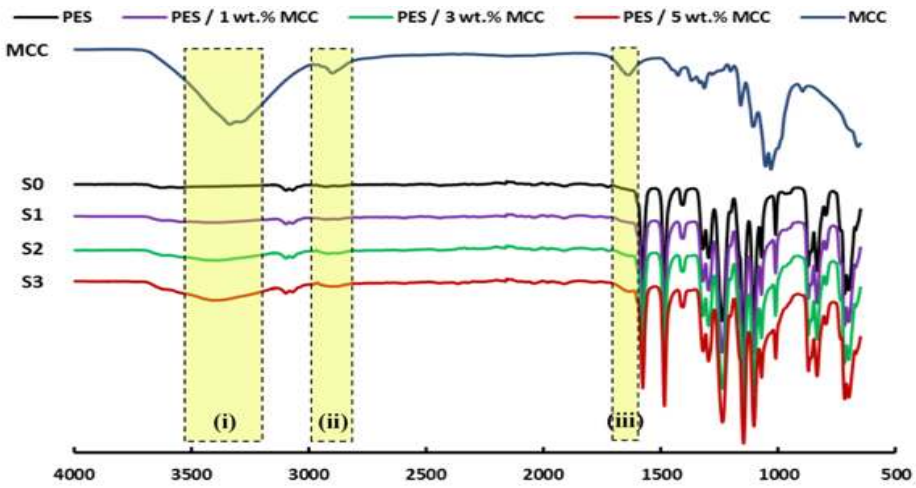

Figure 1. FT-IR spectrum of MCC, pristine PES (S0) and MCC-incorporated PES membrane (S1, S3, S5)

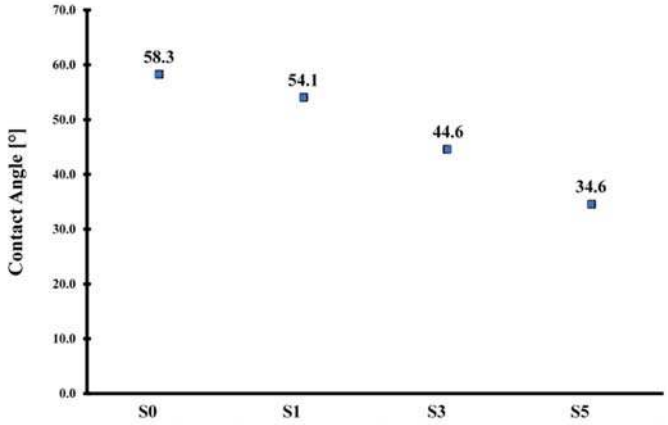

Figure 2. Contact angle for pristine PES (S0) and MCC-incorporated PES (S1, S3, S5) membranes

CONCLUSION

The study concluded that the hydrophilicity of PES membrane increased by incorporating MCC into PES matrix. The presence of hydroxyl peak at wavenumber ~3300 cm^{-1} in FT-IR spectra indicated the presence of co-solvent DMAc/LiCl, thus MCC were successfully be incorporated onto the PES membrane. Aside from that, contact angle analysis indicated that PES membrane incorporated with MCC showed higher hydrophilicity than the pristine PES membrane. In addition, more hydrophilic membrane with the lowest contact angle of 34.6° was successfully fabricated with the increasing MCC loading up to 5 wt.%.

REFERENCES

[1] D. Zhang, A. Karkooti, L. Liu, M. Sadrzadeh, T. Thundat, Y. Liu and R. Narain, J. Membr. Sci. **549** 350-356 (2018).
[2] S. Wang, S. Xiaoming and C. Fushan, Cell. Chem. Technol. **52(3-4)** 265-270 (2018).
[3] M. Jonoobi, A. Ashori and V. Siracusa, Polym. Test. **76** 333-339 (2019).
[4] D. Trache, M. H. Hussin, C. T. Hui Chuin, S. Sabar, M. R. Fazita, O. F. Taiwo, T. M. Hassan and M. K. Haafiz, Int J Biol Macromol. **93** 789-804 (2016).
[5] L. El Hamdaoui, M. El Bouchti and M. El Moussaouiti, Polym. Bull. **75(2)** 769-779 (2017).
[6] H. Khanjanzadeh, R. Behrooz, N. Bahramifar, W. Gindl-Altmutter, M. Bacher, M. Edler and T. Griesser, Int J Biol Macromol. **106** 1288-1296 (2018).
[7] M. H. Hussin, N. A. Pohan, Z. N. Garba, M. J. Kassim, A. A. Rahim, N. Brosse, M. Yemloul, M. R. Fazita and M. K. Haafiz, Int J Biol Macromol. **92** 11-19 (2016).
[8] C. Zhang, R. Liu, J. Xiang, H. Kang, Z. Liu and Y. Huang, J. Phys. Chem. B. **118(31)** 9507-14 (2014).

PGC_SCHE USM_2020_09

New adsorbent development: Synthesis of cellulose-activated carbon hybrid fiber via Schweitzer's reaction

Nur Azian Ahammad[1], Mohd Azmier Ahmad[1], Bassim H. Hameed[2], Azam Taufik Mohd Din[1,*]
[1]School of Chemical Engineering, Engineering Campus, Universiti Sains Malaysia, 14300 Nibong Tebal, Pulau Pinang, Malaysia
[2]Department of Chemical Engineering, Engineering College, Qatar University, Doha, Qatar.
Email: [*]chazam@usm.my

Abstract. In 1859, the Swiss chemist Matthias Eduard Schweizer invented Schweitzer's reagent or schweizer's reagent. Schweitzer's reagent is the traditional chemical for the direct dissolution of cellulose in a copper (II) hydroxide ammonial solution that developed the chemical complex tetraamminediaquacopper dihydroxide, $[Cu(NH_3)_4(H_2O)_2](OH)_2$. The aim of this research was to develop a new hybrid adsorbent made up of cellulose/carbon fiber using direct dissolution of the cellulose and powdered activated carbon (PAC) in the Schweitzer's reagent. Effect of powdered activated carbon (PAC) loading (0.5g, 1.5g and 2.5g) onto Schweitzer 's reagent was studied. It was observed that the cellulose and PAC adsorbent shrinking after 24 hours of drying under room temperature. The synthesised of cellulose-powdered activated carbon hybrid fiber were characterised using a scanning electron microscope (SEM) and an energy dispersive x-ray spectroscope (EDX). SEM proved that increasing the carbon load could provide and enhanced more specific surface areas and active sites for adsorption process. The EDX image presented the existence of carbon (C), oxygen (O), copper (Cu) and silicon (Si) on the surface of CPAC fiber.
Keywords: *Schweitzer's reagent; cellulose/carbon fiber; adsorbent.*

INTRODUCTION

Environmental pollution induced by manufacturing and agriculture is growing as a consequence of its rapid expansion, including emerging contaminants, dyes compounds, toxic heavy metals [1]. In the past few decades, few techniques have been introduced to overcome this pollution, which adsorption, chemical precipitation, redox, membrane system, and electrolysis [2], [3]. Adsorption is a viable technique compared to others. In industry, the adsorption process usually used activated carbon as an adsorbent because of its capacity to adsorb a number of organic and inorganic contaminants, polar and non-polar compounds in aqueous or gaseous environments [4]. Activated carbon can come in many different forms, i.e., powdered, granular, coating and clothe [5]. However, activated carbon powder type has few drawbacks, such as hard to recover after the adsorption process and may float in the solution during the adsorption process. At the same time, granular activated carbon may cause adsorbent performance changes as it may cause pressure drop in dynamic column adsorption. Coating and clothe type of activated carbon has a high possibility of leaching. Thus, in this study, the integration of carbon into fiber carbon will ensure carbon is held firmly to stand high flow resistance and high pressure of operation. Therefore, the production of carbon fiber adsorbent can be easily customized to the required specification. The main objective of this research was to develop cellulose/carbon fiber using direct dissolving of the cellulose and powdered activated carbon (PAC) in the Schweitzer's reagent. The adsorbent was forms by simultaneous forming of the cellulose and powdered activated carbon fiber in the sulphuric acid solution [6].

MATERIALS AND METHODS

Commercial powdered activated carbon (PAC) was purchased from Century Chemicals Sdn.Bhd while copper(II) hydroxycarbonate ($CH_2Cu_2O_5$) and sulphuric acid (H_2SO_4) were purchased from Sigma and ammonium solution (NH_4OH) were purchased from Merck. Firstly, a volume of aqueous ammonia solution was added to an amount of $Cu(OH)_2$ solid powder. The solution was mixed for 30 min (until fully dissolved) and an amount of cellulose was added to Schweizer's reagent and mixed for 30 min again. Next, after the cellulose was dissolved, powdered activated carbon with different carbon loading (0.5, 1.5 and 2.5 g) was added into the mixture. Then, mixed solutions of cellulose/PAC blended were injected slowly using syringe to a solution of sulphuric acid. The fiber were rinsed using distilled water and dried for 48 h at 30 °C. Next, the adsorbent was characterized using Scanning Electron Microscope (SEM Quanta FEG450, USA) and Energy Dispersive X-Ray analysis (EDX).

RESULTS AND DISCUSSION

It was observed that the cellulose and PAC adsorbent shrinking after 24 hours of drying under room temperature as in Figure 1. Scanning electron microscopy (SEM) analysis was carried out to observe the morphology of (CPAC) fiber synthesized adsorbent and their surface structures for different carbon loading. The analysis provided illustrations of the pore structure, surface structure and arrangement of the pores. Figure 2 shows structural morphologies of CPAC fiber for (a) 0.5g, (b) 1.5g and (c) 2.0g of powdered activated carbon at 1000x magnification. It is noticed that the structural morphologies of Figure 2(a) were smooth for 0.5 g of carbon loading and had some cracks on the surface of the sample which exhibit low porosity. While, for 1.5 g and 2.5g of carbon loading as in Figure 2(b) and Figure 2(c) has changed the morphology of the sample with huge alteration formation of the pores, rough surface and emerged more porous cavities. However, 2.5g of carbon loading showed clearly the morphology of the adsorbent by increasing the number and volume of active sites compared to 1.5g carbon loading. Therefore, increasing the carbon load could provide more specific surface areas and active sites that are advantageous for adsorption process [3].

Figure 1. Inverted images of cellulose and PAC (a) after immersion in distilled water once the cellulose and PAC formed, (b) after dried for 24 hours.

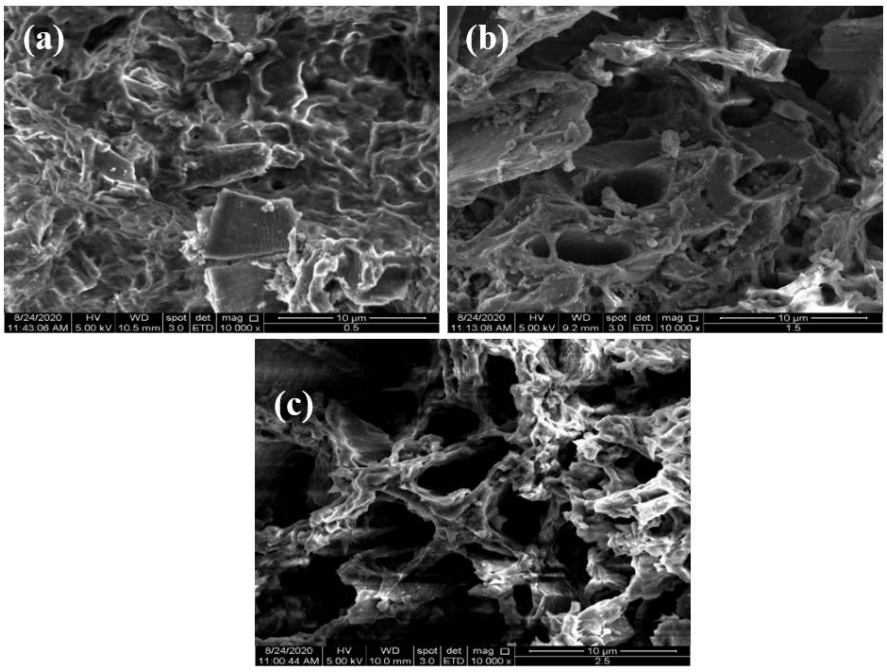

Figure 2. Structural morphologies of CPAC fibers for (a) 0.5g, (b) 1.5g and (c) 2.0g of powdered activated carbon at 1000x magnification**.**

On site, EDX as an auxiliary analysis provided by SEM was used to estimate the presence of element in the materials. Figure 3 displays EDX spectra analysis for (a) 0.5g, (b) 1.5g and (c) 2.0g of powdered activated carbon, where each element in the samples present. The EDX image presents the existence of carbon (C), oxygen (O), copper (Cu) and silicon (Si) on the surface of CPAC fiber. The percentage of carbon inside CPAC fiber increased with increasing in carbon loading. Moreover, the percentage of copper and oxygen inside CPAC fiber decreased with

increasing in carbon loading. Figure 3(a) showed that at 0.5g carbon loading the percentage of oxygen (37.34%) and copper (39.66%) were higher compared to percentage of carbon (22.76%). Whereas, Figure 3(c) showed that at 2.5g carbon loading the percentage of carbon (60.05%) were higher compared to percentage of oxygen (31.32%) and copper (8.37%). Thus, increased in carbon loading due to an efficient adsorption process.

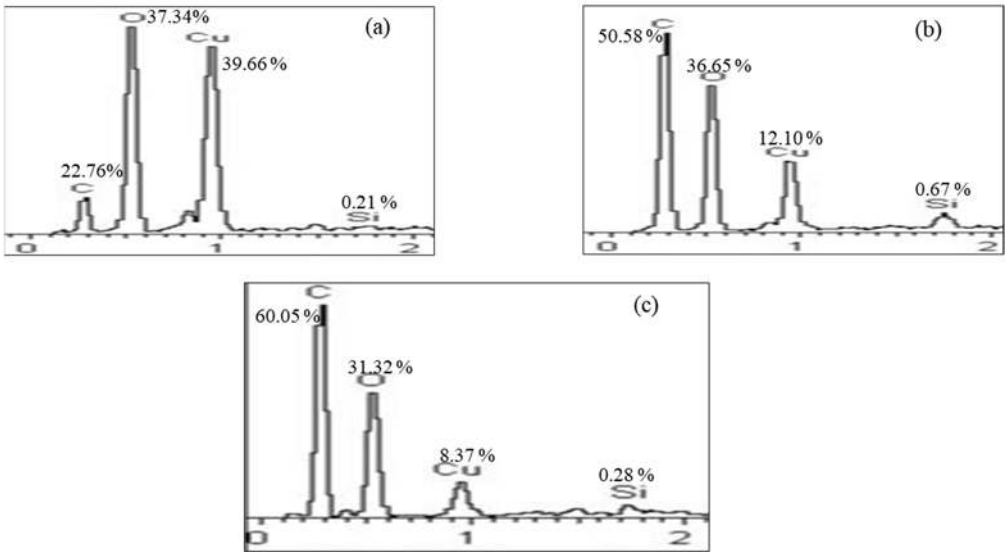

Figure 3. EDX spectra analysis for (a) 0.5g, (b) 1.5g and (c) 2.0g of powdered activated carbon

CONCLUSION

In conclusion, a new hybrid adsorbent made up of cellulose/carbon fibers using direct dissolution of the cellulose and powdered activated carbon (PAC) in the Schweitzer's reagent was successfully developed. Study of the process parameter on the effect of carbon loading in the aqueous solution of the Schweitzer reagent concluded that 2.5 g of carbon loading enhanced the formation of the pores and could provide more specific surface areas and active sites that are beneficial for the adsorption process.

ACKNOWLEDGEMENT

Authors would like to acknowledge Universiti Sains Malaysia for providing scholarship through USM Fellowship Program to Master of Science candidate, Nur Azian Ahammad. This work was also supported by the Research University Incentive Grant (1001/PJKIMIA/8061604).

REFERENCES

[1] H. Jiang *et al.*, "Preparation of a novel bio-adsorbent of sodium alginate grafted polyacrylamide/graphene oxide hydrogel for the adsorption of heavy metal ion," *Sci. Total Environ.*, vol. 744, p. 140653, Nov. 2020.

[2] R. Mu, B. Liu, X. Chen, N. Wang, and J. Yang, "Adsorption of Cu (II)and Co (II) from aqueous solution using lignosulfonate/chitosan adsorbent," *Int. J. Biol. Macromol.*, vol. 163, pp. 120–127, Nov. 2020.

[3] J. Feng, J. Zhang, W. Song, J. Liu, Z. Hu, and B. Bao, "An environmental-friendly magnetic bio-adsorbent for high-efficiency Pb(II) removal: Preparation, characterization and its adsorption performance," *Ecotoxicol. Environ. Saf.*, vol. 203, p. 111002, Oct. 2020.

[4] M. Kwiatkowski and E. Broniek, "An analysis of the porous structure of activated carbons obtained from hazelnut shells by various physical and chemical methods of activation," *Colloids Surfaces A Physicochem. Eng. Asp.*, vol. 529, pp. 443–453, Sep. 2017.

[5] M. Jekel *et al.*, "Anthropogenic organic micro-pollutants and pathogens in the urban water cycle: Assessment, barriers and risk communication (ASKURIS)," *Environmental Sciences Europe*, vol. 25, no. 1. Springer Verlag, p. 20, 08-Aug-2013.

[6] "Adsorptive removal of chloramphenicol from wastewater by NaOH modified bamboo charcoal | Elsevier Enhanced Reader." [Online]. Available: https://reader.elsevier.com/reader/sd/pii/S096085241000731 5?token=12D712C91C5A732567CC0C9295EF1707ADC19FF80CEF0F05A0F3552000519F4D2770B752A64D5467CC3C6A9154389816.

PGC_SCHE USM_2020_10

Fouling and performance study of marine fish farm water desalination using submerged vacuum membrane distillation

Ying Shi Chang, Ooi Boon Seng*
School of Chemical Engineering, Engineering Campus, Universiti Sains Malaysia,
14300 Nibong Tebal, Pulau Pinang, Malaysia.
*E-mail: *chobs@usm.my*

Abstract. This study investigates the fouling behaviour and performance of a hydrophobic commercial polypropylene (PP) hollow fibre membrane for desalination from a local marine fish farm. Permeation and jar test studies were employed to investigate the effect of feed temperature on the permeate flux and salt rejection of the membrane and its fouling propensity. The fouled membrane was subjected to SEM-EDS analysis. Results obtained showed that the permeate flux of marine fish farm water was reduced after 6th hour operation with significant fouling by magnesium-based deposits observed at feed temperatures above 60℃.
Keywords: *Membrane distillation; Hydrophobic; Fouling; Salt rejection.*

INTRODUCTION

One of the main problems that restricts the application of membrane distillation in desalination is membrane fouling or scaling [1-3]. Scaling happens when the accumulation of salt precipitates and crystals on the surface of membrane. These precipitates could reduce the flux and the hydrophobicity degree of membranes. The internal scaling where the crystals accumulated in the large pores will induce membrane wetting and consequently contaminate permeate quality [3]. The marine fish farm water which contains large amount of sparingly soluble mixed salts has high potential to cause membrane scaling due to their solubilities decrease with the elevated feed temperature.

In the current work, marine fish farm effluent was treated in a submerged vacuum membrane distillation system by using a hydrophobic commercial polypropylene (PP) hollow fibre membrane. To identify the major foulants on membrane and the threshold temperature that caused fouling, the effluent was stirred at 100 rpm in jar testing under elevated temperature range from 25 to 70 ℃. The effluent was then used as feed in a submerged vacuum membrane distillation (VMD) system to study the temperature effect on the membrane flux performance and salt rejection.

MATERIALS AND METHODS

Jar test study

The purpose of carrying out the jar test study is to investigate the physicochemical interaction between the inorganic salts with the membrane at the elevated temperature. The hydrophobic commercial PP hollow fibres (ACCUREL PP S6/2 from Membrana, GmbH, Germany) with area of 0.000531 m^2 were soaked in a beaker containing 100 ml marine fish farm water which is heated by a hot plate stirrer at 100 rpm. The testing was studied with the feed temperature range from 25 to 70 ℃ for duration of 72 hours. The fouled hollow fibres were taken out from the beaker and then rinsed three times with deionized water and dried under ambient condition. All the beakers were sealed with parafilm and aluminium foils to prevent evaporation to surrounding.

Experimental set-up of submerged vacuum membrane distillation

A commercial PP membrane bundle contains 4 fibres with the length of 25 cm (effective area of 0.0085 m2). The hydrophobic membrane bundle was dead-end sealed and potted to the cover of a stainless-steel feed tank. The membrane bundle with the tank cover was placed vertically and closed tightly in the tank to allow full immersion of membrane in the feed solution. The feed tank was pumped in 6.8 L of marine fish farm water using a peristaltic pump (Cole-Parmer Masterflex L/S). The solution was heated by the internal coil where hot water circulation inside by means of a hot water bath (Protech Model HC20). The inlet and outlet temperatures of water circulating in the coil were measured by two temperature indicators. The feed temperature inside the tank was monitored by a thermocouple thermometer (UNI-T UT320D). Then, the water vapour that generated from the hollow fibre lumen was sucked by vacuum pump at 3 kPa absolute (Edwards Model XDS5). It was then condensed in a vacuum glass trap which is immersed in a chilled water bath (Protech Model 653DX) at 6 ℃. The experiments were conducted at the feed temperature of 55, 60 and 65 ℃. The mass and conductivity of the permeate were measured for every 15 minutes interval. The permeate flux was calculated based on the permeate mass, active membrane area, and the time used to produce permeate in the submerged VMD process.

Marine fish farm water analysis

The marine fish farm water was collected from surface water of Straits of Malacca, which is 6 km away from the coastal Sungai Udang Port area. The conductivity of the marine fish farm water and permeate was measured by a

conductivity meter (Ohaus Starter 300C). A pocket salt meter (Atago PAL-ES3) was used to measure the salinity of marine fish farm water while its pH was measured by a pH meter (Extech Instruments ExStik II). Sodium (Na), magnesium (Mg), and calcium (Ca) that present in the water were measured by atomic absorption spectroscopy (AAS) (Shimadzu AA-6650) using air-acetylene flame. Chloride (Cl), sulphate (SO_4), total Ca hardness, phosphate (PO_4), silica (SiO_2), ammonia (NH_3), nitrite (NO_2), and nitrate (NO_3) of the water were measured by a digital photometer (Lovibond Maxi Direct).

Table 1. The quality parameters of the marine fish farm water

Characteristics	Value
Total dissolved solid, TDS of brackish water (mg/L)	17530.00±63.77
Conductivity of brackish water (mS/cm)	35.10 ±0.09
pH	8.09±0.02
Salt content %	2.68±0.04
Sodium, Na (mg/L)	11884.80±367.93
Magnesium, Mg (mg/L)	2328.30±290.89
Calcium, Ca (mg/L)	578.40±9.99
Chloride, Cl (mg/L)	19733.30±984.32
Sulphate, SO_4 (mg/L)	2946.70±221.56
Total calcium hardness (mg/L)	207.70±3.09
Phosphate, PO_4 (mg/L)	3.70±0.47
Silica, SiO_2 (mg/L)	below 1.0
Ammonia, NH_3 (mg/L)	below 1.2
Nitrite, NO_2 (mg/L)	below 0.03
Nitrate, NO_3 (mg/L)	below 4.0

Membrane characterization

Scanning Electron Microscopy (SEM) and energy dispersive spectroscopy (EDS). The fouled membrane samples were analyzed by a FEI Quanta 450 SEM analyzer to study its surface morphology and fouling condition.

RESULTS AND DISCUSSION

In this work, the purpose of carrying out jar test study is to determine the major foulants formed on the membrane and investigate the temperature threshold limit that caused onset fouling occurred. The effluent was then employed as the feed in the submerged vacuum membrane distillation (VMD) system to study the effect of temperature on the membrane flux performance and fouling propensity.

Jar test findings

The extent of elevated temperature on the crystal formation on the membrane surface was investigated via jar test. Figure 1 shows that the surface pores of the membranes using marine fish farm water as feed solution at 25, 40, and 50℃ were clean while the membrane surface was deposited by salt crystals at 60 and 70 ℃. The quantity and size of the Mg, S and Si microcrystalline scales increased with increased in temperature (Table 2). The onset of scaling occurred at 60 ℃. The sparingly soluble mixed salts that present in the fish farm water are insoluble at higher temperature. Magnesium silicate and magnesium sulphate could be the major precipitates formed on the membrane.

Submerged VMD experiments

In a continuous 12 hours submerged VMD operation, the fish farm water was used as a feed solution and the transmembrane permeate flux was observed for the commercial hydrophobic PP hollow fibre membranes at different feed temperatures of 55, 60 and 65 ℃. As shown in Figure 2. At 55℃, the permeate flux was almost stable over 12 hours operation, whereby no fouling observed under SEM image in Figure 3(a). It can be also observed that the flux at 60 and 65 ℃ started to reduce after 6th hour, due to the severe fouling on the membrane surface. Based on the SEM observation in Figure 3 (b) and (c), the magnesium based scalants at feed temperature of 65 ℃ was found to be more

serious with obvious pores blocking compared to that of 60℃. However, pore wetting did not occur as no contamination in permeate with the evidence of above 99.9% salt rejection.

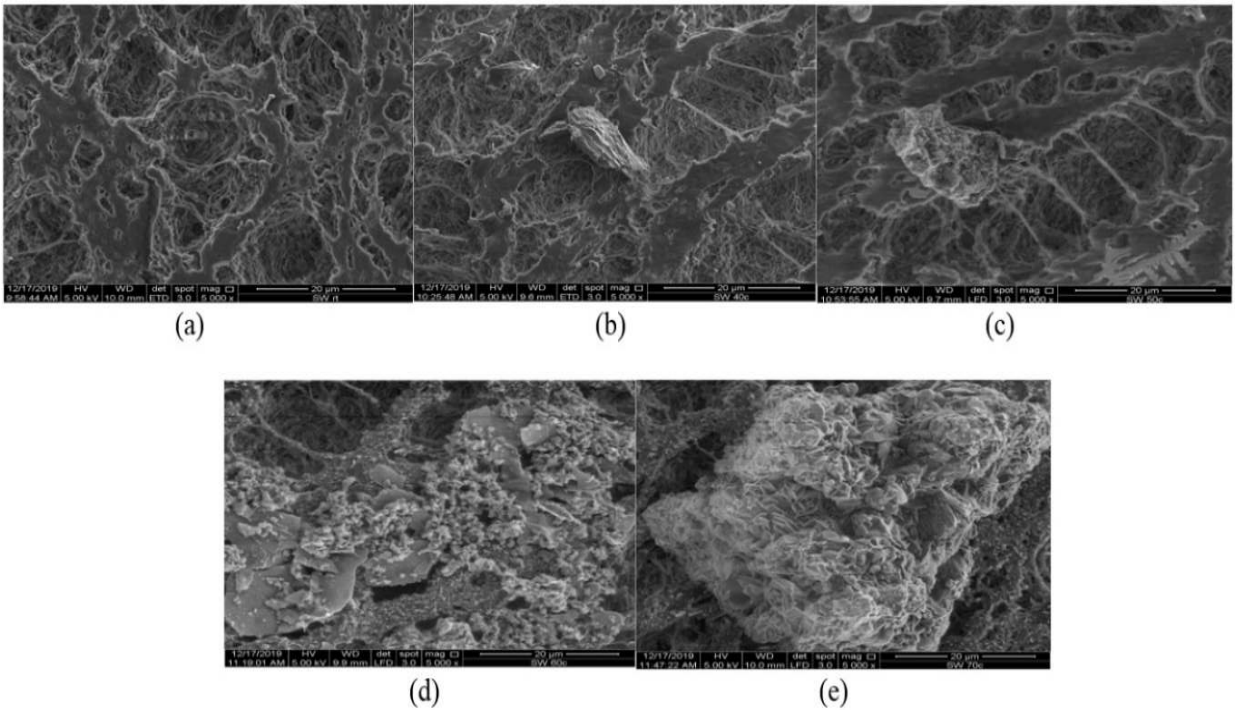

Figure 1. SEM images of magnesium-based deposits on membrane surface using marine fish farm water as feed solution at (a) 25, (b) 40, (c) 50, (d) 60, and (e) 70 ℃.

Table 2. EDS elemental analysis results of the scales formation on membrane surface using marine fish farm water as feed solution with temperature range of 25-70 ℃.

Weight of elements (%)	C	O	Na	Mg	Al	Si	S	Cl	Ca
Feed at 25℃	97.32	2.43	0.05	0.05	0.05	0.06	-	0.04	0.01
Feed at 40℃	95.39	4.17	0.02	0.07	0.25	0.05	-	0.07	0.02
Feed at 50℃	86.54	12.84	0.19	0.07	0.02	0.08	0.06	0.18	0.01
Feed at 60℃	83.07	14.56	0.41	0.81	0.03	0.54	0.15	0.41	0.04
Feed at 70℃	77.76	19.62	0.21	1.07	0.07	0.75	0.20	0.28	0.03

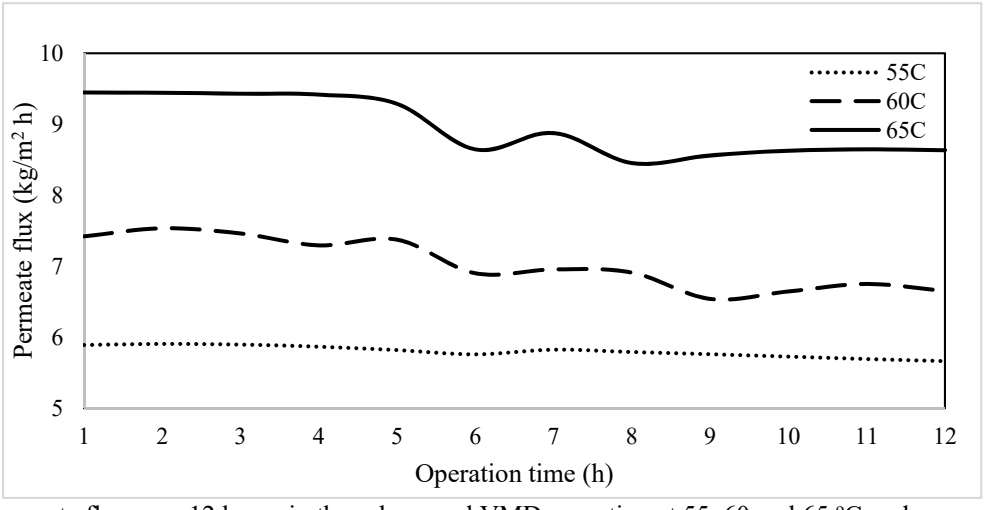

Figure 2. Permeate flux over 12 hours in the submerged VMD operation at 55, 60 and 65 ºC under constant vacuum of 3 kPa absolute.

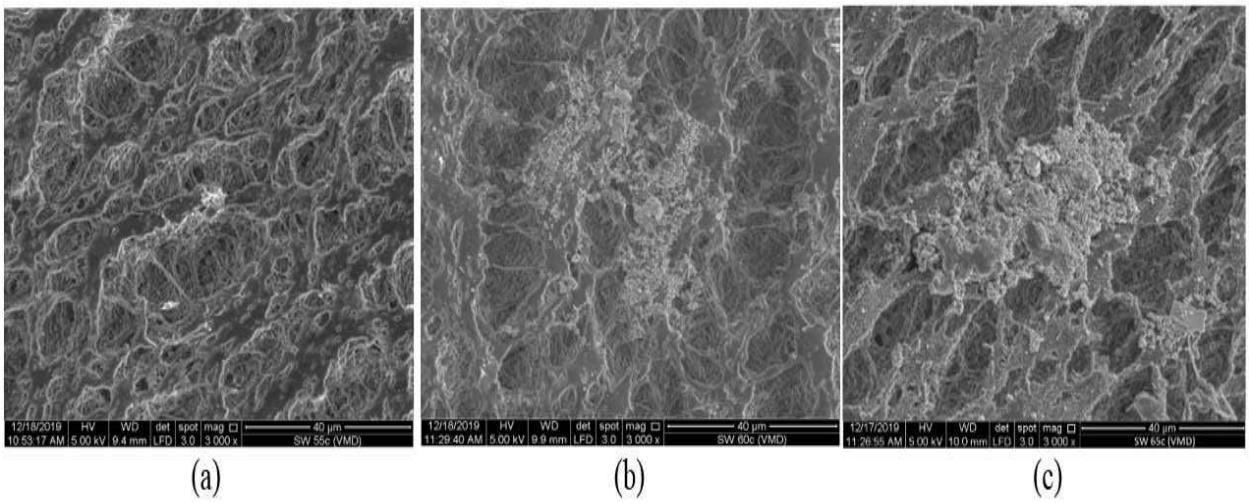

Figure 3. SEM images of magnesium-based deposits formed on membrane surface after 12 hours submerged VMD process at constant 3 kPa vacuum using marine fish farm water at (a) 55, (b) 60, and (c) 65 °C.

CONCLUSION

In this work, the extent of fouling by the inorganic salts in the fish farm water on the surface of membrane was investigated. The main deposited found on the membrane was magnesium foulants. The operating temperature of the submerged VMD should be operated below 60 °C to reduce the fouling intensity.

ACKNOWLEDGEMENT

This work was supported by the Transdisciplinary Research Grant Scheme (TRGS) (67612002), Ministry of Higher Education of Malaysia.

REFERENCES

[1] Y.S. Chang, H.T. Lyly Leow, B.S. Ooi, Membrane Distillation for Water Recovery and Its Fouling Phenomena,
J. Membr. Sci. Res. **6,** 107-124 (2020).
[2] D. Warsinger, J. Swaminathan, E. Guillén-Burrieza, H. Arafat, J. H. Lienhard, Scaling and Fouling In Membrane Distillation for Desalination Applications: A Review, Desalination. **356,** 294-313 (2015).
[3] G. Naidu, S. Jeong, S. Vigneswaran, T.M. Hwang, Y.J. Choi, S.H. Kim, A review on fouling of membrane distillation, Desalination and Water Treat. **57,** 10052-10076 (2016).

PGC_SCHE USM_2020_11

Concentrating Nutrients from Fish Farm Effluent via Forward Osmosis

Aaron Koe Zhen Yao, Ooi Boon Seng*
School of Chemical Engineering, Engineering Campus, Universiti Sains Malaysia,
14300 Nibong Tebal, Pulau Pinang, Malaysia.
*E-mail: *chobs@usm.my*

Abstract. The potential of incorporating Forward Osmosis (FO) to treat fish farm effluents was tested with a lab-scale setup using an asymmetric cellulose triacetate (CTA) FO membrane. FO technology can provide a sustainable wastewater treatment method due to the low energy requirement and less fouling tendency. The treatment performed was focused on recovering nutrient loads, namely ammonium and phosphate, present in the wastewater. FO can recover resources by solely depending on the osmotic pressure difference between the draw solution and feed solution. Different concentrations (0.5 to 2.0 mg/L) of magnesium chloride, $MgCl_2$, solution was used to test the water flux and concentrating efficiency of ammonium and phosphate. Synthetic wastewater containing 10 mg/L of ammonium was tested with $MgCl_2$ followed by synthetic wastewater with 20 mg/L of phosphate. The average water flux for both cases showed similar results with highest flux (13.95 and 15.00 L/ (m^2 h) for ammonium and phosphate respectively) when 2.0 M $MgCl_2$ was used as draw solution. The concentrating factor for ammonium peaked at 1.41 (2.0 M $MgCl_2$) and showed only 1.03 when 0.5 M of $MgCl_2$ was used. The concentrating factor for phosphate showed lower result with 1.31 for 2.0 M $MgCl_2$. The highest reverse salt flux (Mg^{2+} ions on feed side) when ammonium was used as feed was when 1.0 M of $MgCl_2$ was used. The concentration of Mg^{2+} was 158.86 mg/L. When phosphate feed was used, the reverse salt flux decreased at high concentration of $MgCl_2$ draw solution (19.08 mg/L of Mg^{2+} ions). The reverse salt flux also peaked at 101.58 mg/L with 1.0 M $MgCl_2$. The presence of Mg^{2+} ions was needed at the feed side for the formation of struvite ($NH_4MgPO_4 \cdot H_2O$). Real wastewater from fish farm (initial concentration of 11.0 and 35.7 mg/L for phosphate and ammonium) was treated for 6 hours with 1.0 M $MgCl_2$ as draw solution. The concentrating factor achieved was 1.72 and 1.24 for phosphate and ammonium respectively. Fouling in CTA FO membrane was evaluated by a 6-hours operation with concentration of draw solution remaining constant at 1.0 M $MgCl_2$ throughout the experiment. Two different wastewaters were tested, namely mixed (ammonium and phosphate) synthetic solution, and real fish farm effluent. For mixed synthetic solution, the water flux experienced a steady decline over time (from 10.95 to 10.17 L/ (m^2 h)). The decrease in water flux was expected to be caused by the bidirectional cation diffusion across the membrane that gradually lowered the osmotic pressure difference. Real fish farm effluent showed a decrease (from 8.68 to 8.34 L/ (m^2 h)) in water flux over time. It was deduced that bidirectional cation diffusion and presence of suspended solid in feed solution caused the drop in water flux. CTA FO membrane proved to be capable of recovering ammonium and phosphate from fish farm effluents with minimal fouling occurrence.
Keywords: *Aquaculture Effluent, Forward Osmosis, Ammonia Recovery, Phosphate Recovery*

INTRODUCTION

Aquaculture has seen great growth throughout the years due to an increase in demand for fisheries. The increased reliance on aquaculture implies that there would be an increase in amount if aquaculture effluent generated annually. Aquaculture effluent is a nutrient-rich effluent that consists of dissolved components, mainly nitrogen, phosphorus and suspended solids [1]. The direct discharge of these effluents is detrimental to the environment as it decreases water quality and causes eutrophication. With main focus shifting from removal to recovery of wastes, forward osmosis (FO) systems have gained much interest in the application of wastewater treatment. FO operates by having a semi-permeable membrane in between two liquid mediums with different osmotic pressures. Water diffuses through the membrane toward the side with higher osmotic pressure by osmosis. The solution with higher osmotic pressure is known as the draw solution while the other is the feed solution. FO has the ability to reject and concentrate many contaminants, such as solutes and suspended solids, in the absence of hydraulic pressure [2]. By operating in the absence of hydraulic pressure, the system will have low energy requirement and low fouling propensity. The low concentration of nutrient wastes in aquaculture effluent makes it difficult to concentrate and recover them with conventional methods [3]. Therefore, the incorporation of FO in treatment of aquaculture effluent has potential to provide good water and resource recovery. The study aimed to evaluate the performance of FO system in treating aquaculture wastewater. The performance was evaluated by average water flux, concentration factor of ammonium and phosphate, and reverse salt concentration. The fouling study was also conducted with different feed solutions.

MATERIALS AND METHODS

FO Membrane and Setup

The FO membrane used was an asymmetric cellulose triacetate (CTA) FO membrane supplied by Sterlitech and manufactured by FTS H2O. The lab-scale FO system was operated in a counter current crossflow filtration with active layer facing the feed side (AL-FS) orientation. The feed solution was placed on a magnetic stirrer and was pumped with a peristaltic pump while the draw solution was placed on a measuring balance and pumped by a gear pump. Both these solutions were circulated to the FO membrane cell with a constant flow rate of 8 GPH. The feed and draw solutions were separated by the thin CTA FO membrane in a unit cell. The unit cell from Sterlitech, has outer dimensions of 12.7 x 10 x 8.3 cm and provided an active membrane area of 42 cm^2. All inlets and outlets of the FO membrane cell has a diameter of ¼ inch. For the start-up of the experiment, 300 mL of the feed and draw solution of desired concentration was pre-circulated for 30 minutes before proceeding with the real operation. At the end of each testing, the feed and draw solution were drained from the FO membrane cell. Distilled water was circulated in the system for cleaning to prevent any residual draw solution from corroding the FO set up.

Feed and Draw Solution

The draw solution used for this research was magnesium chloride, $MgCl_2$ solution. The draw solution was prepared by dissolving $MgCl_2$ powder (98%) from Sigma-Aldrich in distilled water. 400 mL of draw solution was used at the start of each experiment. For feed solutions, synthetic ammonia and phosphate solutions were prepared by ammonium chloride, NH_4Cl powder (99.5%) and potassium dihydrogen phosphate, KH_2PO_4 powder (99.5%), respectively. For synthetic ammonia solution, the initial concentration of ammonia used was 10 mg/L while initial concentration of phosphate was 20 mg/L. An initial volume of 500 mL was used for the feed solution.

Forward Osmosis Performance and Fouling Study

The performance of CTA FO membrane was evaluated using two different feed solutions, namely synthetic ammonia solution and synthetic phosphate solution. Each feed solution was tested with different concentrations of $MgCl_2$ (0.5 M, 1.0 M, 1.5 M, and 2.0 M) as draw solutions. The average water flux and concentrating factor of ammonia and phosphate were calculated to evaluate the FO performance under various draw solution concentration and feed solution. The FO performance study was conducted for a two-hour period. For FO fouling study, the system was operated for six hours long. For the 6-hours long operations, the concentration of draw solution was maintained at 1.0 M. The dilution effect was nullified by manually adding 10 mL of 2.0 M $MgCl_2$ solution for every 10 g increase in the weight of the draw solution. 10 mL of feed solution was also added every 10 g of water loss to prevent drainage on the feed side. Various feed solutions were examined for the FO fouling study, namely synthetic ammonia solution, synthetic phosphate solution, mixed synthetic solution and real fish farm effluent. The average water flux was calculated by using Equation 1.

$$Water\ flux, Jw\ \left(\frac{L}{m^2.h}\right) = \frac{m_{DS}}{\rho_{FS} A_m t} \quad (1)$$

Where m_{DS} is the change in mass of draw solution (g), ρ_{FS} is the density of feed solution (g/L), A_m is the area of membrane (m^2) and t is the duration of operation (hr). The rejection of ammonia and phosphate on feed side were expressed as concentration factor which is calculated with Equation 2.

$$Concentrating\ Factor = \frac{Concentration\ at\ time\ t}{initial\ concentration} \quad (2)$$

RESULTS AND DISCUSSION

Forward Osmosis (FO) Performance Study

The effect of different draw solution (DS) concentration on pure ammonium and pure phosphate solution were first tested out to evaluate the performance on different feed solutions. The evaluation of FO performance was focused on three main parameters namely, average water flux across the FO membrane, concentrating factor for either ammonium of phosphate on the feed side and reverse salt concentration (Mg^{2+}) at the end of operation. The comparison of average water flux for ammonium and phosphate solutions at different DS concentration are displayed in Figure 1. When 0.5 M magnesium chloride, $MgCl_2$ solution was used, ammonium solution showed higher water flux compared to phosphate solution with values of 7.22 L/(m^2•hr) and 6.07 L/(m^2•hr), respectively. The difference in average water flux between the two feed solutions can be explained by the difference in molar concentration [4]. Phosphate feed solution has higher molar concentration which caused the increase in osmotic pressure on the feed side. This causes the difference in osmotic pressure across the FO membrane to be lower and hence lowering the average water flux. As the concentration of DS increases, the average water flux between the two feed solutions became comparable. When the DS concentration went up to 2.0 M, the average water flux for phosphate feed solution peaked at 15.00 L/(m^2•hr) while ammonium feed solution peaked at 13.95 L/(m^2•hr). The higher average water flux for phosphate feed solution justified by comparing the reverse salt concentration for each case. The Mg^{2+} concentration on feed side is

displayed in Figure 2. The difference in reverse salt concentration between the two feeds is related to their water flux performance. At 0.5 M DS concentration, there was only a slight difference in reverse salt concentration. Therefore, ammonium feed solution resulted in greater average water flux compared to phosphate feed solution. The difference in Mg^{2+} concentration in feed side increased greatly as DS concentration increases. The difference in reverse salt concentration for 1.0 M, 1.5 M and 2.0 M were 57.28 ppm, 54.17 ppm and 78.87 ppm, respectively. With higher Mg^{2+} concentration on feed side, the water flux decreased due to the drop in osmotic pressure difference.

For all DS concentrations, ammonium feed solution showed greater value in Mg^{2+} concentration compared to phosphate feed solution. The higher reverse salt concentration for ammonium feed solution explained by the occurrence of bidirectional cation diffusion between ammonium ions and Mg^{2+} ions across the FO membrane [5]. As DS concentration increases from 0.5 M to 1.0 M, the reverse salt concentration increased from 98.51 ppm to 158.86 ppm when ammonium solution was used as feed. The reverse salt concentration when phosphate solution was at feed side increased only slightly from 96.54 ppm to 101.58 ppm. For these cases, the reverse salt concentration obeys Fick's Law which states that reverse salt flux increases as concentration difference across membrane increases [4]. When DS concentration goes up to 1.5 M and 2.0 M, Mg^{2+} concentration on feed side decreased for both ammonium and phosphate feed solutions which did not obey Fick's Law.

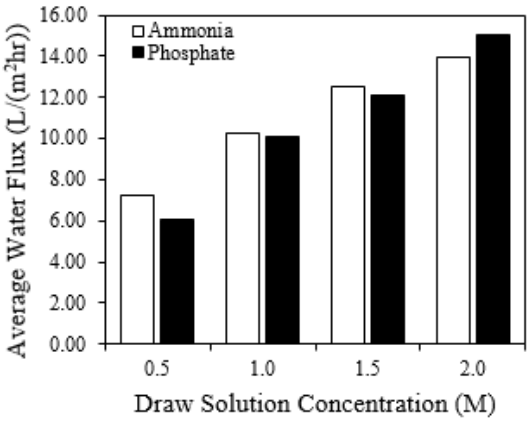

Figure 1. Average water flux of ammonium and phosphate solutions at different DS concentrations (0.5 M, 1.0 M, 1.5 M and 2.0 M)

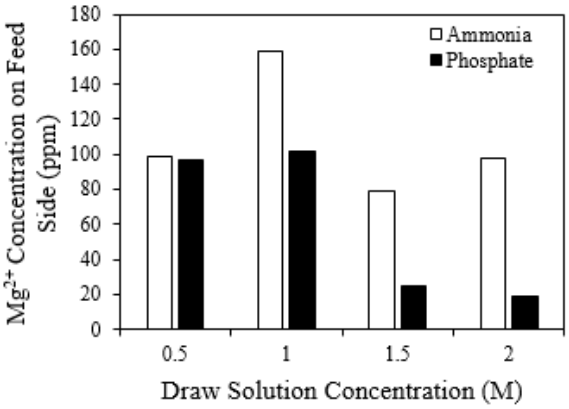

Figure 2. Magnesium ion, Mg^{2+} concentration on feed side for ammonium and phosphate solutions at different DS concentrations (0.5 M, 1.0 M, 1.5 M and 2.0 M)

The concentration of ammonium and phosphate on feed side is expressed as concentration factor as illustrated in Figure 3. Both ammonium and phosphate synthetic solutions showed an increase in concentration factor as the DS concentration increases. This is mainly attributed to the increased water flux across the membrane. The concentration factor for ammonium is higher than phosphate at all different DS concentrations except for 0.5 M DS concentration. The lower concentration factor value for phosphate is due to the higher initial concentration for synthetic phosphate solution. With this, CTA FO membrane has the potential to concentrate ammonium and phosphate on the feed side which implies that resource recovery from FO systems is possible.

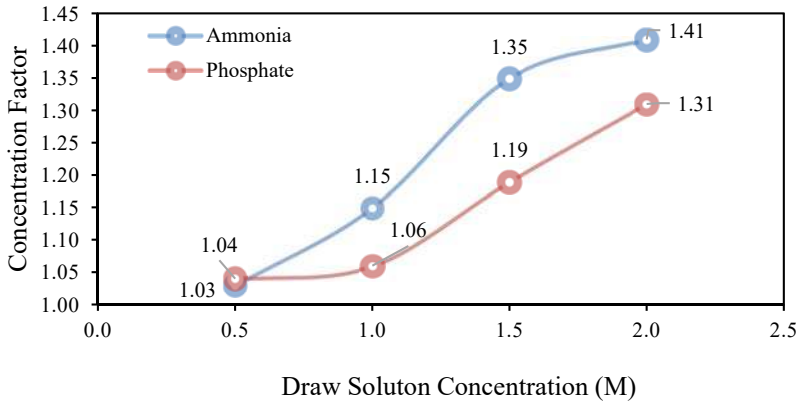

Figure 3. Concentration factor for ammonium and phosphate solutions at different DS concentrations (0.5 M, 1.0 M, 1.5 M and 2.0 M)

Forward Osmosis (FO) Fouling Study

The FO fouling study was evaluated by conducting a 6-hours long operation for a mixed synthetic solution and real fish farm effluent. The average water flux for both these solutions are displayed in Figure 4. Both solutions showed a slight decrease in average water flux during the FO operation. The gradual decreased was caused by the dilutive internal concentration polarization on the draw side of the FO membrane. As water permeates through the FO membrane, the concentration of DS was diluted which lowers the osmotic pressure difference across the membrane. Real fish farm effluent exhibited lower average water flux from the start. This phenomenon is explained by the higher initial concentration of ammonium with value of 35.7 mg/L compared to 10 mg/L for the synthetic solution. The presence of other solutes in real fish farm effluent also plays a part in lowering the osmotic pressure difference. Hence, real fish farm effluent has lower initial average water flux compared to the mixed synthetic solution. From the 6-hour long operation, no fouling was observed based on the average water flux performance. The ammonium and phosphate in real fish farm effluent was concentrated from 35.7 mg/L to 44.6 mg/L and 11.0 mg/L and 19.0 mg/L, respectively.

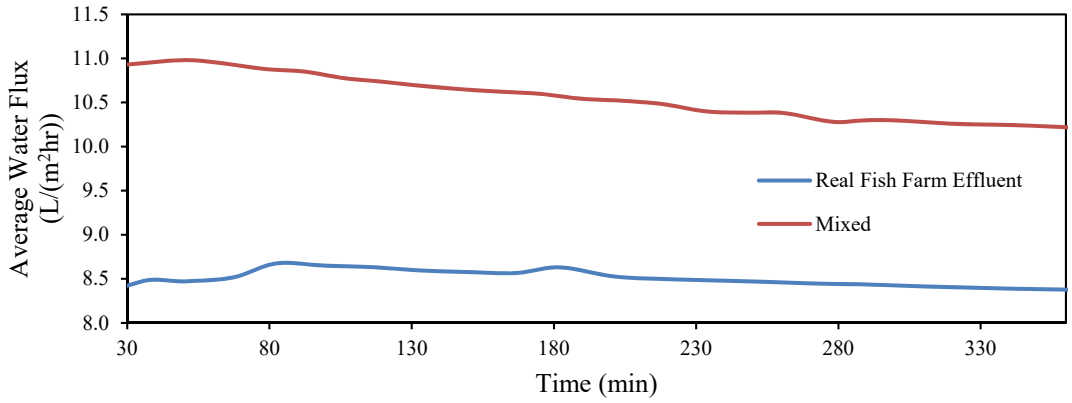

Figure 4. Average water flux for real fish farm effluent and mixed synthetic solution for 6-hours long operation

CONCLUSION

CTA FO membrane has shown potential for the treatment of aquaculture effluent. The FO system managed to concentrate main nutrient wastes, which are ammonium and phosphate, on the feed side. This indicated that FO systems can recover resources from low concentration feed, such as aquaculture effluent. Although the average water flux obtained when treating real fish farm effluent was not impressive, the low fouling tendency of the FO membrane provides sufficient reason to further study on the capabilities of FO systems in aquaculture effluent treatment.

REFERENCES

[1] M. Nurul, A. Sikder, W. W. Min, A. O. Ziyad, P. Prem, and R. D. Kumar, "Sustainable Treatment of Aquaculture Effluents in Future-A Review," *International Research Journal of Advanced Engineering and Science,* vol. 1, pp. 190-193, 2016.

[2] W. Suwaileh, N. Pathak, H. Shon, and N. Hilal, "Forward osmosis membranes and processes: A comprehensive review ofresearch trends and future outlook," *Desalination,* vol. 485, p. 21, 2020.

[3] A. E. Turcios and J. Papenbrock, "Sustainable treatment of aquaculture effluents-What can we learn from the past for the future?," *Sustainability* vol. 6, pp. 836-856, 2014.

[4] M. Qasim, N. A. Darwish, S. Sarp, and N. Hilal, "Water desalination by forward (direct) osmosis phenomenon: A comprehensive review," *Desalination,* vol. 374, pp. 47-69, 2015.

[5] X. Lu, C. Boo, and M. Elimelech, "Bidirectional Diffusion of Ammonium and Sodium Cations in Forward Osmosis: Role of Membrane Active Layer Surface Chemistry and Charge," *Environmental Science & Technology,* vol. 48, pp. 14369-14376, 2014.

PGC_SCHE USM_2020_12

Hydrophobic PVDF membrane via dual soft non-solvent bath system for direct contact membrane distillation in desalination

Lyly Leow, Ooi Boon Seng*
School of Chemical Engineering, Engineering Campus, Universiti Sains Malaysia,
14300 Nibong Tebal, Pulau Pinang, Malaysia
*E-mail: *chobs@usm.my*

Abstract. In this study, hydrophobic PVDF membranes were fabricate using dual non-solvent bath system via phase inversion technique. The durations of first soft non-solvent bath were varied before immersed in the second hard non-solvent bath for further phase inversion process. Membrane analysis tests such as Scanning Electron Microscope (SEM) and Water Contact Angle (WCA) were performed. It was observed that the duration of the first soft non-solvent bath had significant effects on the surface morphology and surface WCA of the membrane. Membrane that immersed in the first soft non-solvent bath for 2 seconds followed by second hard non-solvent bath for 1 day exhibits the highest WCA of 141.62.28±5.46° with nodular structure on the membrane surface.
Keywords: *Polyvinyldene fluoride, dual non-solvent bath system, membrane distillation*

INTRODUCTION

Polymers with hydrophobic property were very crucial in Membrane Distillation (MD) process because during MD process, aqueous solutions need to be prevented to pass through the membrane pores [1]. PVDF polymer has been chosen in most of the MD study as the hydrophobic polymer base in fabrication of membrane due to its lower surface energy (25mN/m) and good chemical, physical and mechanical properties [2]. Besides, compare with other polymers, PVDF is soluble in numerous organic solvents such as Dimethyl Acetamide (DMAc), Dimethyl Formamide (DMF), Dimethyl sulfoxide (DMSO), N-methylpyrrolidone (NMP) and Triethylphosphate (TEP) and it can be prepared by using phase separation methods. During membrane fabrication via phase inversion process, dual non-solvent bath system was performed to create rougher membrane surface which lead to higher WCA [3].

MATERIAL AND METHODS

PVDF (Mw = 250,000 – 450,000, Alfa Aesar), was used as polymer base. NMP (anhydrous, 99.5%, Merck) was used as solvent for polymer solution preparation. Methanol (industrial grade, Revlogi Materials) was used as the first soft non-solvent bath while deionized water was used as the second hard non-solvent bath in phase inversion process. All solvent and chemicals were used as received.

16% of PVDF polymer was dissolved in 84% of NMP organic solvent by heating and stirring on the hot plate in a sealed beaker. The stirring speed and temperature were controlled at 250rpm and 60℃ respectively. After PVDF fully dissolved in NMP solvent, the polymer solution was cooled down to room temperature prior to casting.

The prepared PVDF solution was manually cast on top of fabric with a thickness of 400μm which supported by glass plate. The membrane immediately immersed into the first soft non-solvent bath that consists of methanol for a predetermined time followed by immersion in the second hard non-solvent bath that consists of deionized water for 1 day. After 1 day, the formed membrane was rinsed with DI water and dried in air. The synthesized membrane was kept in zipper bag prior for testing and use in DCMD.

RESULTS AND DISCUSSION

Figure 1 shows the surface morphology of 16% PVDF hydrophobic membrane that prepared via dual non-solvent bath system by immersing the nascent cast film into the first non-solvent that consists of fully methanol bath for (a) 2 seconds, (b) 5 minutes, (c) 1 hour, (d) 24 hours and (e) 36 hours and followed by second non-solvent water bath for 1 day. It was observed that as the immersion time in the first non-solvent methanol bath became longer, the nodular structure of the membrane became bigger which promote bigger pore size on the membrane surface. Polymer underwent instantaneous crystallization process during 2 seconds of immersion in the methanol bath and underwent precipitation process in the second non-solvent bath which then results in smallest nodular structure as shown in Figure 1(a). Nevertheless, prolonged period of immersion in the methanol bath has allowed the solidification of crystallite structure which result in bigger nodular structure formed on the membrane surface [4] as shown in Figure 1(b) and (c) where Figure 1(c) that has immersed for 1 hour in methanol bath has bigger nodule structure compared to Figure 1 (b) that has immersed for 5 minutes in methanol bath. On the other hand, as the membrane immersed for 1 day in the first

methanol bath followed by the second water bath for another 1day, solidification of the polymer was dominant and result in the biggest nodule structure as shown in Figure 1(d). Precipitation in the second non-solvent water bath did not contribute significant changes in the surface morphology of the membrane in Figure 1(d) because phase inversion process has completed in the first non-solvent methanol bath. This can be further proven in Figure 1(e), where same surface morphology was obtained as Figure 1(d) after immersed for 36 hours in the first non-solvent methanol bath followed as compared to 1 day in second non-solvent water bath.

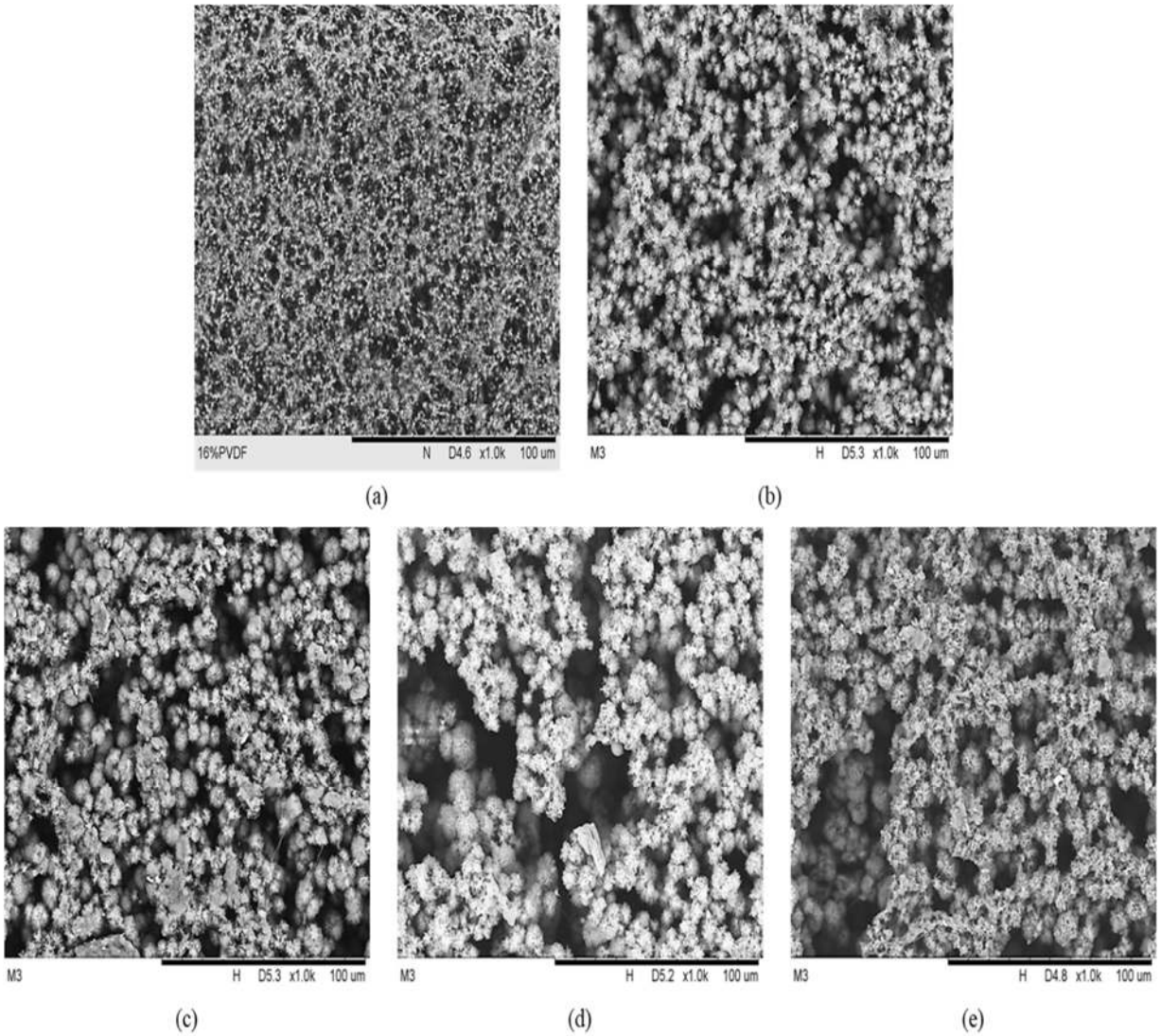

Figure 1. Surface morphology of fabricated 16%PVDF hydrophobic membrane that immersed (a) 2 seconds, (b)5 minutes, (c) 1 hour, (d) 24 hours and (e) 36 hours in first non-solvent bath under 1,000 magnifications.

Surface water contact angle (WCA) of each fabricated membrane was tested and the result was presented in Figure 2. It was observed that the WCA decreased from 141.62.28±5.46° to 112.18±4.89° when the immersion time in the first non-solvent methanol bath increased form 2 seconds to 36 hours. However, when the immersion time for the first methanol bath was more than 1 day, the WCA were almost similar to each other. The WCA result was agreed with the surface morphology obtained in Figure 1, whereby Figure 1(d) and Figure 1(e) that has the same crystallite structure have almost same WCA value. The size of the nodular formed on the membrane surface affect the measured WCA. Smaller nodular structure promotes rougher surface as shown in Figure 1(a), hence, the membrane has higher WCA. Membrane with the highest WCA was tested in DCMD. However, membrane wetting occurs after operating for 1 hour which suggest that nodular structure membrane surface was not suitable in DCMD although it has the highest WCA (141.62.28±5.46°).

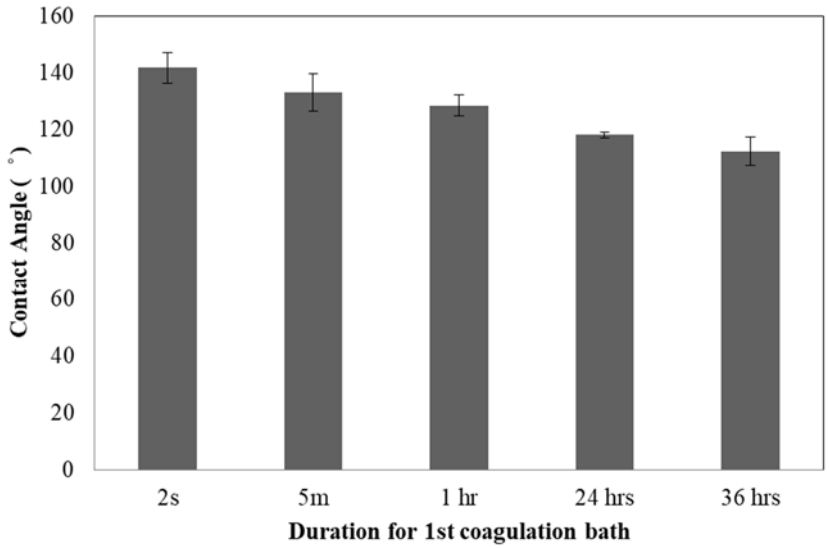

Figure 2. Hydrophobicity of membrane at various duration of first non-solvent methanol bath in a dual bath system

CONCLUSION

In conclusion, hydrophobic membrane can be produced via dual non-solvent bath system via phase inversion process without any additives or chemical modification. The immersion time in the first non-solvent bath is the key to produce hydrophobic surface on the membrane while the second non-solvent bath will promote porous structure by allowing precipitation to occur. The shorter the immersion time in the first soft non-solvent bath, the produced membrane was more hydrophobic. However, the phase inversion process completed after 1 day, hence, the second non-solvent bath does not have any significant change if the membrane was immersed in the non-solvent bath for more than 1 day. The fabricated membranes have nodular structure whereby it might not suitable for DCMD process because wetting of the membrane started to occur after 1 hour although the membrane was hydrophobic in nature.

ACKNOWLEDGMENT

The authors are thankful to the financial support provided by Fundamental Research Grant Scheme (FRGS) (203/PJKIMIA/6071395), Ministry of Education Malaysia.

REFERENCES

[1] A.L. Ahmad, W.K.W. Ramli, Hydrophobic PVDF membrane via two-stage soft coagulation bath system for Membrane Gas Absorption of CO2, Sep. and Purif. Technol., 103, 230-240, (2013).
[2] J.A. Kharraz, A.K. An, Patterned superhydrophobic polyvinylidene fluoride (PVDF) membranes for membrane distillation: Enhanced flux with improved fouling and wetting resistance, J. of Membr. Sci., 595, 117596, (2020).
[3] M. Tian, S. Yuan, F. Decaesstecker, J. Zhu, A. Volodine, B. Van der Bruggen, One-step fabrication of isotropic poly(vinylidene fluoride) membranes for direct contact membrane distillation (DCMD), Desalination, 477, 114265, (2020).
[4] B.S. Ooi, N.S.M. Yatim, A.L. Ahmad, S.O. Lai, Preparation of polyvinylidene fluoride membrane via dual coagulation bath system and its wettability study, J. of Appl. Polym. Sci., 124, E225-E232, (2012).

PGC_SCHE USM_2020_13

Effect of reaction temperature on CO_2 hydrogenation to methanol using In_2O_3 catalyst

Zaza Hazrina Hashim, Munirah Mohd Zain, Abdul Rahman Mohammad*
School of Chemical Engineering, Engineering Campus, Universiti Sains Malaysia,
14300 Nibong Tebal, Pulau Pinang, Malaysia
*Email:*chrahman@usm.my*

Abstract. Indium oxide has come to light as a surprisingly effective methanol synthesis catalyst through CO_2 hydrogenation reaction. In this study, we investigated the effect of temperature ranges from 180°C-300°C to synthesis methanol by CO_2 hydrogenation. These results established an assuring basis for the development of catalyst for methanol synthesis.
Keywords: *Carbon dioxide, Hydrogenation, Methanol, Indium oxide*

INTRODUCTION

The increase of carbon dioxide concentration as one of the main Green House Gases (GHGs) in the atmosphere is relentless. Various strategies are currently studied to alleviate the emission of CO_2 into the atmosphere or to convert it into valuable chemical products. The uses of CO_2 as a feedstock for the synthesis of value-added chemicals is a promising alternative for CO_2 abatement [1]. Industrial methanol synthesis is performed by catalytic hydrogenation of syngas (H_2/CO/CO_2) over Cu-ZnO/Al_2O_3-type catalyst. Unfortunately, the industrial Cu-ZnO/Al_2O_3 catalyst is neither active nor selective in CO_2 hydrogenation. Previous published research studies demonstrated that the use of industrial catalysts brings to very low hydrogenation conversions of CO_2 to methanol. When CO_2 replaces CO, this experience serious short comings because CO_2 is more inert than CO, leading to lower CO_2 conversion [2]. Recently, indium oxide (In_2O_3) has been studied as a catalyst in CO_2 hydrogenation to methanol due to its simpler system. As studied by Martin et al. [3], In_2O_3 has showed high activity and selectivity in multiple catalytic transformations involving CO_2.

MATERIAL AND METHODS

Indium (III) nitrate hydrate ($In(NO_3)_3 \cdot xH_2O$) purity of 99.99% and zirconium (IV) oxide(ZrO_2) purity of 99% were used as a metal precursor and support, respectively, were obtained from Sigma Aldrich, USA. Citric acid for sol gel synthesis method was obtained from Merck, Germany.

Catalyst preparation

The catalysts were prepared using citric acid-base sol gel method. The mol ratio of citric acid to the metal precursor was 3:1. It was stirred continuously at 250 rpm until the suspension become gel-like. The gel like product was dried in an oven at 105°C for 24 hours. It was grounded and calcined at 500°C for 5 hours.

Catalytic activity testing

The CO_2 hydrogenation was carried out in a fixed-bad micro reactor. 160 mg of the catalyst was loaded into the reactor and the reactant gases, H_2 and CO_2, were fed into the reactor with flow rate ratio of 3:1. All experiments were conducted at 280°C, 4 MPa and weight hourly space velocity (WHSV) of 15000 mL/g_{cat}.h.

RESULT AND DISCUSSION

The effect of reaction temperature on the performance of catalyst was investigated in the range of 180°C-300°C while WHSV and pressure were held constant at 15 L/min.g_{cat} and 4 Mpa, respectively. The CO_2 conversion, methanol selectivity and methanol yield are shown in Figure 1. The CO_2 conversion improved as expected with the increasing of reaction temperature. When the temperature of the reaction increased, more external energy was generated for CO_2 activation. The CO_2 conversion rate expanded quickly at temperature of 180°C-260°C. The reduction of the CO_2 conversion leads to the probability that the catalyst may incur from deactivation due to the loss of indium surface area when the reaction temperature raised above 260°C.

The temperature ranges studied had a significant impact on product selectivity. The selectivity of methanol grown massively from 92% to 96% with the increased temperature of reaction from 180°C-260°C. This is due to the activation of CO_2 by higher temperature reaction. The heat supplied enable the breaking of the C-O bond and forming C-H bond. Methanol selectivity decreased above optimum temperature (>260°C-280°C) as estimated by theoretical

equilibrium trend. The CO_2 hydrogenation reaction to methanol is exothermic, therefore the low temperature was favored. The methanol yield was increased correspond with temperature due to the rapid increased of CO_2 conversion and methanol selectivity. Nevertheless, the methanol yield was decreased with further rise of temperature (>260°C-300°C) due to the lower selectivity of methanol and CO_2 conversion. The highest methanol yield (14.94) was achieved at 260°C, whereby a balance between CO_2 and methanol selectivity was attained.

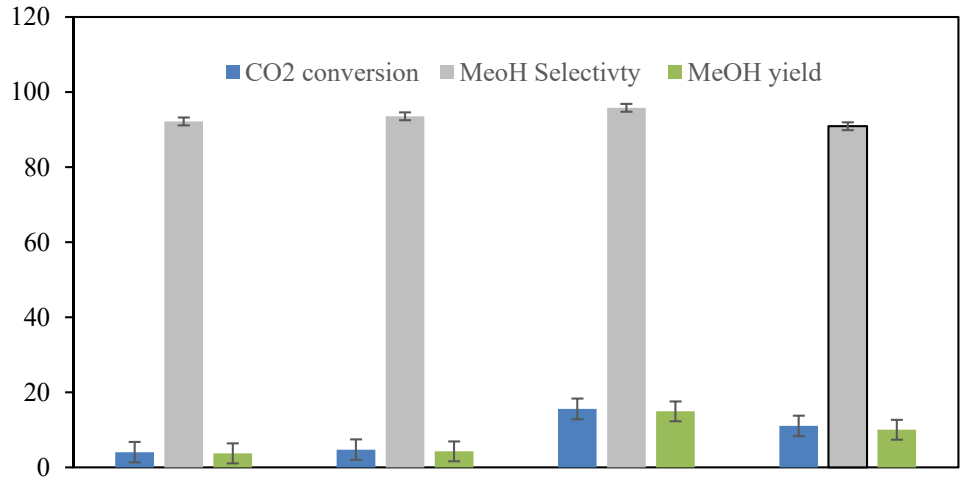

Figure 1. Effect of reaction temperature on CO_2 hydrogenation to MeOH using In_2O_3 catalyst

CONCLUSION

From the study, the optimum temperature reaction was 260°C for the methanol synthesis. Above the optimum temperature, the methanol selectivity decreased as the CO selectivity increased by RWGS reaction. Direct CO_2 hydrogenation to methanol has been the subject of many CO_2 utilization studies over the past few decades, continuous research is still required for decentralization of the technology and developing new and efficient catalysts is as a useful approach in resolving the present limitation.

ACKNOWLEDGMENT

This work was supported by USM-NanoMITE under Long-Term Research.Grant Scheme (LRGS, 203/PJKIMIA/6720009).

REFERENCES

[1]. Allam, D., et al., *Improved Cu- and Zn-based catalysts for CO_2 hydrogenation to methanol.* Comptes Rendus Chimie. **22**(2): p. 227-237, 2019.
[2]. Fang, X., et al., *Improved methanol yield and selectivity from CO_2 hydrogenation using a novel Cu-ZnO-ZrO_2 catalyst supported on Mg-Al layered double hydroxide (LDH).* Journal of CO_2 Utilization. **29**: p. 57-64, 2019.
[3]. Martin, O., et al., *Indium Oxide as a Superior Catalyst for Methanol Synthesis by CO_2 Hydrogenation.* Angewandte Chemie International Edition. **55**(21): p. 6261-6265, 2016.

PGC_SCHE USM_2020_14

Preparation of ZnO for Photocatalytic Activity of Phenol That Exceed Acros ZnO

B.M. Namoos, Abdul Rahman Mohamed*
School of Chemical Engineering, Engineering Campus, Universiti Sains Malaysia,
14300 Nibong Tebal Penang, Malaysia
Email: chrahman@usm.my

Abstract. This work aimed to synthesize zinc oxide (ZnO) with high activity to degraded phenol in wastewater, purchased ZnO from Acros photocatalytic activity were tested offering 90.4% degradation of 10 ppm phenol, it used as a benchmark for this study. The zinc oxide (ZnO) powders were prepared by three different methods, different pH values and calcination temperature were tested and studied, the effect of zinc salt on the quality of Zinc oxide been also studied in this work. The photocatalytic activity of the synthesized optimum ZnO powder was tested under UV-light. After one hour, the degradation efficiency for 10 ppm phenol were tested for the synthesized ZnO by methods 1, 2, and 3 showing 33.5%,45%, 93.8% respectively.
Keywords: *Zinc oxide; phenol; photocatalytic, wastewater*

INTRODUCTION

During 1972, Honda and Fujishima find out that TiO_2 had the faculty on water splitting. Since then it consider the beginning of a new age in Photocatalyst field[1]. Photocatalyst processes produced the benefit of fast reaction velocity, moderate reaction conditions, and high selectivity, adding to all of these a non-hazardous nature. In semiconductors like ZnO, the performance of the photocatalyst depends on the production of hydroxide radicals which is the strongest oxidant in nature[2]. energy electron-hole e-/h+ pairs can generates when the photons energy exceeds the bandgaps value, the electron (e-) will settle in the conduction band (CB) after leaving its place in valance band (VB) producing a hole (h^+) in the VB[3]. When the e^-/h^+ pairs go to the surface, the whole h^+ in VB will lead to oxidation reaction for water to produce hydroxide radicals while electron in CB will lead to reduction reaction to produce superoxide[4].

$$\text{Photocatalyst} + hv \longrightarrow (e^-/h^+) \text{ producing}$$
$$h^+ + H_2O \longrightarrow OH^- + H^+$$
$$e^- + O_2 \longrightarrow O^{-2}$$
$$O^{-2} + H_2O \longrightarrow H_2O_2 \longrightarrow 2\ .OH$$
$$\text{Dye pollutant} + OH^- \longrightarrow CO_2 + H_2O$$
$$\text{Dye pollutant} + h^+ \longrightarrow \text{products of oxidation}$$
$$\text{Dye pollutant} + e^- \longrightarrow \text{products of reduction}$$

MATERIALS AND METHODS

The chemicals used were zinc oxide (Acros Organics), zinic chloride ($Zn(Cl)_2$,Merck Chemicals), sodium hydroxide (NaOH, Across Organics) and zinc acetate dehydrate ($(CH_3COO)_2Zn*2H_2O$, Merck Chemical). Three different methods were used to synthesis ZnO. For the first method, synthesis of ZnO was conducted using simple precipitation method. Zinc chloride and zinc acetate were used as zinc salts. Then, 0.2 M of sodium hydroxide solution was added drop wise to 0.1 M of zinc salt solution under constant stirring till the pH value reached 8, 10, and 11. EUTECH (model: pH700) pH meter was used for the measuring of pH value. The first pH value for zinc chloride solution was 5.65 while for Zinc acetate was 6.64. The pH for both zinc solutions started to increase gradually with the addition of NaOH. Combination of both zinc solutions required the formation of the precipitation. White precipitations were obtained under continuous mixing by MTOPS (model: MS300) Magnetic stirrer plate. The white precipitate had been centrifuged at 650 rpm for 12 minutes and dried under 100°C for overnight. The samples were calcined at 400, 450, and 500°C for 2 hrs.

For the second method, thermal precipitation method was used to synthesis ZnO. 4.9996 gm of NaOH was dissolved in 50 mL deionized water (DI) and heated at 70°C under stirring condition. Then, 6.5375 gm of $Zn(NO_3)_2{\cdot}6H_2O$ was added dropwise into the NaOH solution and stirred for 7 hrs. The resultant mixture was cooled, filtered, washed with deionized water. It was dried at 60 °C in air for 15 hrs before calcined at 400°C for 2 hrs.

For the third method, ZnO was synthesized using the modified thermal precipitation method. NaOH was dissolved in 50 ml of DI until reached pH≈11.5. Then, the aqueous NaOH solution was heated at 70 °C under stirring condition. 3.4072 gm of $Zn(Cl)_2$ was added dropwise into the NaOH solution and stirred for another 5 hrs. The

resultant mixture was cooled, filtered, washed with deionized water. It was dried at 60 °C in air for 24 hrs and finally calcined at 400 °C in air for 2 hrs.

Every photocatalyst experiment was performed in a 250 ml circular beaker. A 120 Watt of PAR 38 incandescent lamp which supplied by Firefly was used. The lamp was placed 10 cm above the reaction solution surface with 30° of light flood. The reaction was held inside an acrylic black box to prevent any stray light from interacting with the Philips lamp during reaction. Flow meter was used to control the amount of air that entered to the reaction system. Cooling fan was used to reduce the temperature inside the reactor. The solution was stirred with a hot plate stirrer to form homogeneous mixture with the Photocatalyst.

RESULTS AND DISCUSSION

ZnO produced by using Method 1 had been synthesized from different Zinc salts ($(CH_3COO)_2Zn*2H_2O$ and $Zn(Cl)_2$) and various pH values and calcination temperature had been tested. The results (Fig. 1 (a), (b), and (c)) showed that increasing of pH synthesizing value led to increment of the photocatalytic activity of the produced ZnO. It was attributed to the surface morphology, in which pH value during synthesizing affected severely on the face morphology of the generated ZnO. Besides that, it affected on the range of e^-/h^+ recombination and the ZnO activity[5]. Increasing degree of alkaline medium during the synthesizing of ZnO promoted the formation of the wurtzit crystal structure which known as the most stable kind of ZnO crystalline in nature[6]. While, increasing the calcination temperature reduced the photocatalytic activity due to the agglomeration problem. Agglomeration particles reduced the effective surface area and reduced ZnO performance. The optimum condition to produce ZnO was at pH 11 and and calcined in 400°C.

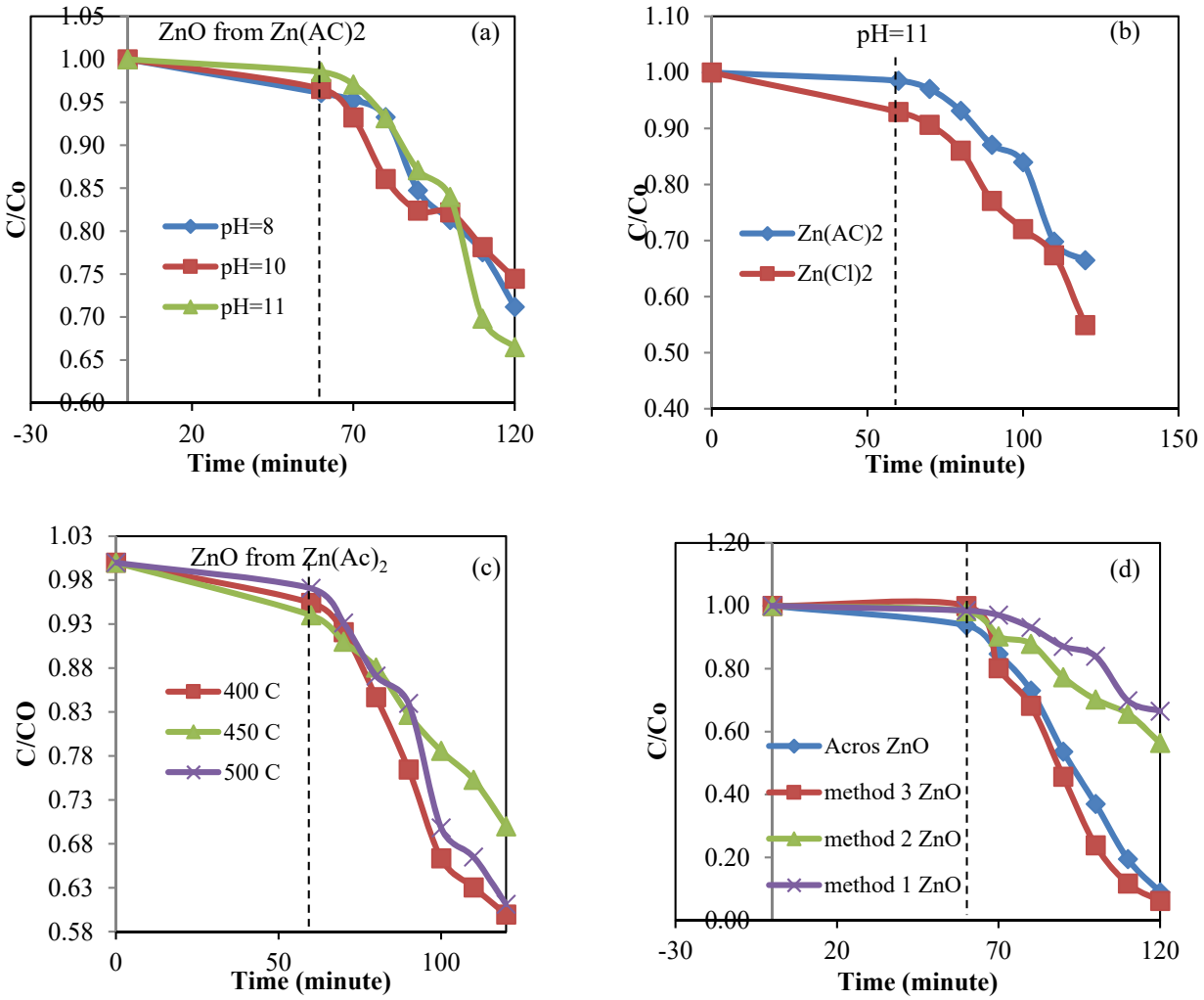

Figure 1. ZnO synthesis and calcined at different conditions; (a) ZnO synthesized at different pH values by method 1, (b) ZnO synthesized from different precursors by method 1, (c) ZnO calcined at different temperatures by method 1 and (d) phenol degradation in wastewater for synthesized and Acros ZnO

The ZnO that synthesized by method 2 didn't show a good result as shown in Fig. 1 (d). The synthesized ZnO by method 3 showed the higher activity compared to Acros one (Figure 1 (4)). After an hour under PAR 38 incandescent lamp, the synthesized ZnO caused 15% of phenol degradation. Meanwhile, the Acros ZnO estimated only 13% left. The increment of ZnO activity was expected due to the lager surface area when the particle size decreased. Thus, reduction of activation energy (E_{bg}) which made the electrons transfered towards the CB much easier and faster hence increased the number of e^-/h^+ and ZnO activity.

CONCLUSION

This study showed that, the ZnO activity affected by synthesis conditions. Increasing of pH value caused the ZnO synthesis in more alkaline and increased the ZnO photocatalytic activity. It also was proved that 400°C was the best calcination temperature for ZnO. This study also showed that precursors affected on the quality of the photocatalyst produced even by using the same synthesizing method. This study showed that, the synthesized ZnO is more efficiency than Zn Acros.

REFERENCES

[1] Linsebigler, A. L., Lu, G. & Yates, J. T. Photocatalysis on TiO_2 Surfaces: Principles, Mechanisms, and Selected Results. *Chem. Rev.* **95**, 735–758 (1995).

[2] Castellote, M. & Bengtsson, N. Applications of Titanium Dioxide Photocatalysis to Construction Materials. *Appl. Titan. Dioxide Photocatal. to Constr. Mater.* (2011). doi:10.1007/978-94-007-1297-3

[3] Submitted, T. Synthesis of Sol-gel Based Titanium dioxide Photocatalyst : Investigations on their Modification , Interaction with Metal ions , and Antimicrobial Activity DESAI VILAS SHIVAJI Under the Supervision of. (2013).

[4] Linden, K. G. & Mohseni, M. *2 . 8 Advanced Oxidation Processes : Applications in Drinking Water Treatment*. *Comprehensive Water Quality and Purification* **2**, (Elsevier Ltd., 2014).

[5] Paper, R. *et al.* Effect of the pH Value of Synthesis Conditions on the Phase Structure and Photocatalytic Properties of Bismuth Molybdates Synthesized Using a Hydrothermal Method Regular Paper. 4–9 (2015). doi:10.5772/61294

[6] Cao, D., Gong, S., Shu, X., Zhu, D. & Liang, S. Preparation of ZnO Nanoparticles with High Dispersibility Based on Oriented Attachment (OA) Process. (2019).

PGC_SCHE USM_2020_15

Membranes for Gadolinium Removal in Wastewater Treatment

E. I. Oluwasola[1,2], A.L. Ahmad[1,*], A.A. Amusa[1], M.K. Alsebaeai[1,3]
[1]School of Chemical Engineering, Engineering Campus, Universiti Sains Malaysia, 14300 Nibong Tebal, Pulau Pinang, Malaysia.
[2]Food Technology Department, The Federal Polytechnic Ado Ekiti, Ekiti state 360231, Nigeria
[3]Department of Chemical Engineering, Faculty of Engineering and Petroleum, Hadhramout University, Hadhramout, Yemen
E-mail: [*]chlatif.usm.my

Abstract. Membrane for wastewater treatment plays a very crucial role in minimizing the levels of harmful metallic contaminants in reclaimed water. It is superior to conventional water treatment systems, especially for the removal of polar organic pollutants because of their relatively high aqueous solubility. Gadolinium (a rare earth element) is a Contaminant of Emerging Concern (CEC) that has attracted research interest in the last two decades. It was first introduced as Gd-based contrast agents for use in magnetic resonance imaging (MRI) in 1988 and has since been employed in the diagnosing of vascular myocardial, orthopedic, oncologic, inflammatory, and neurological diseases, among others. Anthropogenic Gd is traceable to the increasing use of gadolinium-based contrast agents (GBCA) in magnetic resonance imaging (MRI). The chelated metal was initially regarded as safe until Paramagnetic Gd chelates were detected as a microcontaminant in water resources in the mid-1990s in Germany (Berlin river). Anomalous Gd-concentration in surface waters has been reported worldwide from the river and estuarine waters, coastal seawater, groundwater, tap water, and soft drink. The anthropogenic Gd chelates are also being considered as a potential tracer for emerging microcontaminants such as steroids, pharmaceuticals, and personal care products. Contrary to earlier reports restricting Gd contamination to megacities with highly evolved health care systems, recent research had shown that Gd contamination can also be found in wastewater drained from rural communities without MRI equipment or with less developed health facilities. To date, there are insufficient bioaccumulation data to enable concerned regulatory authorities to set a permissible limit for Gd in water and food. Everyone is likely exposed to a minute quantity of Gd daily through the in-advert consumption of contaminated drinking water, soft drink, and ingredients (meat, seafood, and vegetables). The quantity ingested in this way may be considerably higher for safety. Unfortunately, conventional waste-water treatment does not reduce anthropogenic Gd-concentration significantly. It is therefore crucial to regularly monitor Gd species in the environment and seek efficient methods for its removal in wastewater treatment. Removal of Anthropogenic Gd is essential to prevent potential accumulated ingestion of gadolinium metal, prevent exposure to its ecotoxicity and adverse human health effects. Therefore, this paper focus on a review of the advances in the technologies for Gds removal in different aqueous media and the prospect for efficient membrane for gadolinium removal in wastewater treatment.
Keywords: *membranes; anthropogenic; gadolinium; wastewater; treatment*

INTRODUCTION

The rare-earth elements (REEs) plays a very significant role in our industrial world due to the growing increase in their demand and for their critical and indispensable use in many high-tech industries. The use of rare earth elements (REE) in new technologies has strongly increased over the last three decades [1]. This growing demand for REEs has led to increased environmental exposure and water pollution from numerous REEs commercial products and as a result, the recovery of REEs is a significant issue that requires appropriate consideration [2]. Gadolinium is a naturally occurring element usually referred to as Rare earth elements (REEs). It is a silver-white, malleable, and ductile heavy metal with an atomic number of 64 [3]. Stable gadolinium (Gd) complexes have been used as paramagnetic contrast agents for magnetic resonance imaging (MRI) for over 20 years, but have recently been identified as environmental contaminants [4]. Gd (III) is regarded as a fission product; that may trickle to the surrounding environment and cause many risks, therefore, it is regarded as a hazardous material. To avoid the toxicity of the Gd ion, it is used under a chelated form called Gd-based contrast agents (Gd-CA) [6]. However, contrary to the previous assumptions that GBCAs are stable throughout the water cycle, it is degradable. Degradation products in drinking water supplies can increase the risk of adverse health effects. GBCAs concentrations in aquatic systems are often referred to as anthropogenic gadolinium [7]. The long-term effects of the anthropogenic Gd anomaly, especially on aqueous ecosystems, are still largely unknown [8] and [9] therefore its remained unregulated either in its ionic or in its chelated form by any environmental or waste- / drinking water standard, however, the lack of regulation does not rule out the need for concern about its safety even at its lowest level concentrations [10]. Many forms of organocomplexed gadolinium (Gd) contrast agents have recently been linked to a debilitating and potentially fatal skin disease called nephrogenic systemic fibrosis (NSF) in patients with renal failure. Free Gd released from these

complexes via transmetallation is believed to be the most important trigger for NS [11]. Similarly, Gadolinium based contrast agents (GBCAs) has been linked to toxicity in patients, regardless of having impaired or normal renal function and Presently, no therapy is considered effective enough for the removal of gadolinium (Gd) from the body [12]. From the foregoing, it is imperative to search for an enhanced wastewater treatment processes that are capable of removing the stable contrast agents [13]. Many Several methods for the recovery of REEs has been researched and these include precipitation, filtration, solvent extraction etc. [14]. The present paper attempt to review some of the technologies that have already been used to remove gadolinium in different aqueous media and the prospect for efficient Membrane for gadolinium remediation.

GADOLINIUM REMOVAL IN DIFFERENT AQUEOUS MEDIA

Some of the techniques used for Gd (III) removal from different aqueous solutions include chemical precipitation, filtration, coagulation, ion exchange, evaporation, adsorption, liquid-liquid extraction, solid-phase extraction, electrochemical processes, and membrane technology [15], [16], [17], [18] and [19] as reported by [20].

Chemical precipitation technique

[21] developed a simple and inexpensive injection of sodium hydroxide, NaOH, into $GdCl_3$ solution to effectively precipitate $GdCl_3$ which resulted in a near-instantaneous dropout of >99% of the gadolinium. At the pH of 11 and above the dissolved gadolinium forms insoluble Gd $(OH)_3$ which can then be removed from the water by the use of simple settling tanks, continuous-process cyclonic separation, filter presses, vacuum filtration, and even magnetic filtering. Similarly, chemical precipitation to remove gadolinium from heavy water containing large concentrations of gadolinium was demonstrated by [22]. The removal of the gadolinium by precipitation before nitrate removal was carried out by precipitation with sodium phosphate and potassium dihydrogenphosphate. Dry or wet sodium phosphate worked equally well for the precipitation of Gadolinium as $GdPO_4$. The yield was close to 100% in both cases.

The chemical reactions in precipitation as follows:

$$Gd(NO_3)_3 + Na_3PO_4 \rightarrow GdPO_4 + 3NaNO_3$$ molar ratio of 1:1

$$Gd(NO_3)_3 + 3KH_2PO_4 \rightarrow Gd(H_2PO_4)_3 + 3KNO_3$$

The experiment was tested several times at room temperature with different quantities of Gd $(NO_3)_3$ ranging from 100 mg to 2.0 g. It was reported that virtually all dissolved gadolinium can be precipitated in a single precipitation step (100% yield) within minutes using either a solid or liquid solution form of the precipitating agents [22].

Ion exchange technique

The removal of Uranium and Gadolinium from aqueous solution using sonicated emulsion polymer (synthetic zeolite A) synthesized by ultrasonic irradiation technique has been reported by [23]. The synthetic sonicated emulsion polymer was employed as an organic ion exchange material for the removal of the lanthanides. [20] also showed that Dowex HCR S/S a commercial cation exchange resin can be used as an effective and low-cost sorbent for the removal of Gd(III) from aqueous solution. A series of cesium molybdo vanado phosphate (CsMVP) supported on platelet SBA-15 (SBA-15–% x CsMVP, x = 20, 30, 40 and 50 wt.%) was synthesized as an efficient inorganic composite ion-exchanger for gadolinium ion removal from aqueous solution. The SBA-15–30 % CsMVP weight fraction was reported to have the maximum adsorption capacity toward gadolinium removal while the adsorption capacity of metal ions onto the adsorbent varies directly with the system temperature. [24]

Sorption technique

[25], synthesized a nanocomposite pellet obtained from banana peels (BPNC) and used it for the removal of REEs and radioactive minerals from wastewater. It was reported that BPNC exhibited a high affinity for U, Th, Gd, and La in the real mine water sample. Similarly, Nanostructured banana peel was employed as an adsorbent for REEs removal from mine water. The results obtained revealed that banana peels have a high affinity for Sm, Eu, Nd, Pr, Gd, Tb, and Lu compared to other lanthanides present in the mine water samples [26]. The adsorptive removal feasibility of trace Gd(III) from aqueous solutions using colloidal aqueous suspensions of GO loaded in dialysis bag was evaluated by Chen, Wanga, Zhuoa, Liua, Yiping, and Li. The maximum adsorption capacity of Gd(III) on GO was found to be 286.86 mg g−1 at the pH of 5.9 and at 303 K which was higher than any other previously reported values for GO adsorbent before their work [27]. However, in more recent work using Hydrosols of facilely prepared carbon nanotubes/graphene oxide (CNTs/GO) sealed in dialysis bags adsorption capacity of 534.76 mg·g−1 at the pH of 5.9 and 303 K has been reported for the highly efficient and re- pollution-free removal of trace Gd(III) from water by [28]. A novel hydrophilic, three-dimensionally cross-linked, aliphatic backbones with pendant hydroxamic acid (HA)

group as functional moiety was synthesized for the removal of gadolinium [Gd(III)] from laboratory waste aqueous effluent. The sorption study showed that PHA is an effective matrix for Gadolinium Gd(III), Elution study indicated that gadolinium can be recovered and with almost 98 % elution factor the sorbent matrix can be regenerated and reused [29]. [30] used three carbon samples, including commercial (1690 m^2 g^{-1}), activated carbon prepared from guava seeds (637 m^2 g^{-1}), and activated carbon prepared from avocado kernel (1068 m^2 g^{-1}), to study the adsorption of gadolinium-based contrast agents (GBCAs): gadoterate meglumine Dotarem®, gadopentetate dimeglumine Magnevist®, and gadoxetate disodium Primovist®. The carbon materials activation was optimized with H_3PO_4 using a Taguchi methodology to obtain mesoporous materials. The tested carbon samples were able to adsorb 70– 90% of GBCA in aqueous solution but less in model urine due to some competitive adsorptive urine components that inhibit the adsorption. The highest removal was achieved by the commercial carbon sample followed closely by the Avocado carbon, with average removals of 80%, in which mesoporosity prevails over microporosity was reported to have the best removal efficiency by a square meter in a batch system in aqueous solution and model urine. An unsuccessful attempt was made by [31] to use four different aquatic plant species (Lemna gibba, Ceratophyllum demersum, Elodea nuttallii, E. canadensis) as biological filters for the removal of commonly used but structurally different GBCA- s (Omniscan, Dotarem) from water. The result strangely showed that none of the four investigated macrophytes had any significant impact on the Gd-concentration despite having high bioaccumulation removal activity for other heavy metals (e.g. Mn, Cr, Pb, Ni, Cd).

Membranes for Gadolinium Removal In Wastewater

The membrane as a water treatment technology gained recognition in the late 1950s. It is a process that removes unwanted constituents from water through a barrier that allows certain substances to pass through while blocking others. The goal is to produce potable water for industry and for drinking which is now a global burden. Membrane either as a solid or in liquid form can be described as a thin layer of material that is capable of separating materials as a function of their physical and chemical properties when a driving force is applied across the membranes [32]. Most research on Gadolinium removal are based on non-aquatic media samples and in metallurgical extractive applications. To date, only a few research efforts have addressed its removal in wastewater. Recently Asadollahzadeh et al., (2020) reported the separation of gadolinium by a supported liquid membrane. The Adsorption process is generally regarded as a promising method for the recovery of rare earth metals because of its simplicity, high efficiency, and low cost [14]. Removal of gadolinium chelates through adsorption on activated carbon in wastewater, as well as in drinking water is ineffective because of the poor absorbability of gadolinium chelates on activated carbon [10]. [21] suggested using a suitable sequence of filters, and introducing nanofiltration (NF), a new membrane intermediate in pore size between reverse osmosis (which rejects all $GdCl_3$ and everything larger) and ultrafiltration (which passes all GdCl3 and everything smaller) to selectively extracts GdCl3 from a water stream. Reserve osmosis membranes have been suggested as an effective technique to remove Gd-based contrast agents from wastewater [9]. Similarly, [34] suggested reverse osmosis purification as an effective mechanism to remove stable anthropogenic (micro) contaminants from tap water. Reverse osmosis membrane has been reported to remove 99.85% anthropogenic Gd in an advanced water treatment plant [4]. Therefore, Research effort is required to develop appropriate, effective, and economical nanofiltration, ultrafiltration or reverse osmosis membranes to remove the controversial anthropogenic metal which also have the potential of being used as a tracer for the presence of pharmaceuticals microcontaminants in waste water because of its persistence , reliability and, ability to be measured cheaply and accurately at very low concentrations [4]

REFERENCES

[1] Thomas G. Goonan, «Rare Earth Elements—End Use and Recyclability», in *Scientific Investigations Report 2011–5094*, 2011.

[2] O. Pereao, C. Bode-Aluko, O. Fatoba, K. Laatikainen, eta L. Petrik, «Rare earth elements removal techniques from water/wastewater: A review», *Desalin. Water Treat.*, 71–86, 2018.

[3] Greenwood N.N.; eta A. Earnshaw, *Chemistry Elements*. 1997.

[4] M. G. Lawrence, J. Keller, eta Y. Poussade, «Removal of magnetic resonance imaging contrast agents through advanced water treatment plants», *Water Sci. Technol.*, libk. 61, zenb. 3, or. 685–692, ots. 2010,

[5] E. A. El-Sofany, «Removal of lanthanum and gadolinium from nitrate medium using Aliquat-336 impregnated onto Amberlite XAD-4», *J. Hazard. Mater.*, libk. 153, zenb. 3, or. 948–954, 2008.

[6] M. F. Bellin eta A. J. Van Der Molen, «Extracellular gadolinium-based contrast media: An overview», *Eur. J. Radiol.*, libk. 66, zenb. 2, or. 160–167, 2008, doi: 10.1016/j.ejrad.2008.01.023.

[7] R. Brünjes eta T. Hofmann, «Anthropogenic gadolinium in freshwater and drinking water systems», *Water Res.*, libk. 182, ira. 2020, doi: 10.1016/j.watres.2020.115966.

[8] M. Birka, C. A. Wehe, O. Hachmöller, M. Sperling, eta U. Karst, «Tracing gadolinium-based contrast agents from surface water to drinking water by means of speciation analysis», *J. Chromatogr. A* libk. 1440, or. 105–111, Apr. 2016, doi: 10.1016/j.chroma.2016.02.050.

[9] H. S. Thomsen, «Are the increasing amounts of gadolinium in surface and tap water dangerous?», *Acta radiol.*, libk. 58, zenb. 3, or. 259–263, 2017, doi: 10.1177/0284185116666419.
[10] M. Cyris, «Behavior of Gadolinium-based Diagnostics in Water Treatment», 2013.
[11] W. Yantasee *et al.*, «Novel sorbents for removal of gadolinium-based contrast agents in sorbent dialysis and hemoperfusion: preventive approaches to nephrogenic systemic fibrosis», *Nanomedicine Nanotechnology, Biol. Med.*, libk. 6, zenb. 1, or. 1–8, 2010, doi: 10.1016/j.nano.2009.05.002.
[12] W. Ngamcherdtrakul *et al.*, «Removal of a gadolinium-based contrast agent by a novel sorbent hemoperfusion in chronic kidney disease (CKD) rodent model», *Sci. Rep.*, 1–9, abe. 2019.
[13] P. Ebrahimi eta M. Barbieri, «Gadolinium as an emerging microcontaminant in water resources: Threats and opportunities», *Geosci.*, libk. 9, zenb. 2, or. 93, ots. 2019, doi: 10.3390/geosciences9020093.
[14] I. Anastopoulos, A. Bhatnagar, eta E. C. Lima, «Adsorption of rare earth metals: A review of recent literature», *J. Mol. Liq.*, libk. 221, or. 954–962, ira. 2016, doi: 10.1016/j.molliq.2016.06.076.
[15] A. D. Ebner, J. A. Ritter, eta J. D. Navratil, «Adsorption of cesium, strontium, and cobalt ions on magnetite and magnetite - Silica composite», *Ind. Eng. Chem. Res.*, libk. 40, zenb. 7, or. 1615–1623, martx. 2001.
[16] B. Alyüz eta S. Veli, «Kinetics and equilibrium studies for the removal of nickel and zinc from aqueous solutions by ion exchange resins», *J. Hazard. Mater.*, libk. 167, zenb. 1–3, or. 482–488, 2009.
[17] B. A. Fil, A. E. Yilmaz, R. Boncukcuoğlu, eta S. Bayar, «Removal of divalent heavy metal ions from aqueous solutions by Dowex HCR-S synthetic resin», *Bulg. Chem. Commun.*, 201–207, 2012.
[18] C. Xiong, J. Zhu, C. Shen, eta Q. Chen, «Adsorption and desorption of praseodymium (III) from aqueous solution using D72 resin», *Chinese J. Chem. Eng.*, libk. 20, zenb. 5, or. 823–830, 2012.
[19] M. A. Khan *et al.*, «Adsorption of Cobalt Onto Graphite Nanocarbon-Impregnated Alginate Beads: Equilibrium, Kinetics, and Thermodynamics Studies», *Chem. Eng. Commun.*, l 403–418, 2014.,
[20] M. M. Hamed, S. E. Rizk, eta A. A. Nayl, «Adsorption kinetics and modeling of gadolinium and cobalt ions sorption by an ion-exchange resin», *Part. Sci. Technol.*, libk. 34, zenb. 6, or. 716–724, aza. 2016.
[21] M. R. Vagins, «A Scientific/Technical Report for the Advanced Detector Research Program Selective Filtration of Gadolinium Trichloride for Use in Neutron Detection in Large Water Cherenkov Detectors», 2007.
[22] E. W. Wilde, C. J. Berry & Mudlagiri, eta B. B. Goli, «Method for Removing Gadolinium from Used Heavy Water Reactor Moderator», *Nucl. Technol.*, libk. 144, zenb. 1, or. 141–143, 2003.
[23] A. M. El-kamash, E. H. Borai, M. G. Hamed, eta M. M. Abo-Aly, «Fixed Bed Sorption Studies On The Removal Of Uranium And Gadolinium Ions From Aqueous Solution Using Sonicated Emulsion Polymer», *Int. J. Innov. Res. Growth*, libk. 8, zenb. 4, 2019, doi: 10.26671/ijirg.2019.4.8.101.
[24] H. Aghayan, A. R. Khanchi, eta A. R. Mahjoub, «Synthesis and characterization of cesium molybdo vanado phosphate immobilized on platelet SBA-15: An efficient inorganic composite ion-exchanger for gadolinium ion sorption», *Appl. Surf. Sci.*, libk. 274, or. 7–14, 2013, doi: 10.1016/j.apsusc.2013.02.005.
[25] O. Atiba-Oyewo, M. S. Onyango, eta C. Wolkersdorfer, «Synthesis and application of alginate immobilized banana peels nanocomposite in rare earth and radioactive minerals removal from mine water», 2019.
[26] O. A. Oyewo, M. S. Onyango, eta C. Wolkersdorfer, «Lanthanides removal from mine water using banana peels nano sorbent», *Int. J. Environ. Sci. Technol.*, libk. 15, zenb. 6, or. 1265–1274, 2017.
[27] W. Chen, L. Wang, M. Zhuo, Y. Liu, Y. Wang, eta Y. Li, «Facile and highly efficient removal of trace Gd(III) by adsorption of colloidal graphene oxide suspensions sealed in dialysis bag», *J. Hazard. Mater.*, libk. 279, or. 546–553, 2014, doi: 10.1016/j.jhazmat.2014.06.075.
[28] L. Guo *et al.*, «Highly efficient removal of Gd(III) using hybrid hydrosols of carbon nanotubes/graphene oxide in dialysis bags and synergistic enhancement effect», *Chem. Eng. J.*, 535–545, 2018.
[29] M. Singha, S. Pal, K. N. Hareendran, eta S. B. Roy, «Poly-hydroxamic acid (PHA) matrix for gadolinium pre-concentration and removal», *J. Radioanal. Nucl. Chem.*, libk. 302, zenb. 2, or. 961–966, urr. 2014.
[30] M. P. Elizalde-González, E. García-Díaz, M. González-Perea, eta J. Mattusch, «Removal of gadolinium-based contrast agents: adsorption on activated carbon», *Environ. Sci. Pollut. Res.*, libk. 24, zenb. 9, or. 8164–8175, 2017, doi: 10.1007/s11356-017-8491-x.
[31] M. Braun, G. Zavanyi, A. Laczovics, E. Berényi, eta S. Szabó, «Can aquatic macrophytes be biofilters for gadolinium-based contrasting agents?», *Water Res.*, libk. 135, or. 104–111, mai. 2018.
[32] I. G. Wenten, Membrane in Water and Wastewater Treatment, 2015, zenb. November.
[33] M. Asadollahzadeh, R. Torkaman, eta M. Torab-Mostaedi, «Recovery of gadolinium ions based on the supported ionic liquid membrane: parametric optimization via central composite design approach», *Int. J. Environ. Sci. Technol.*, libk. 17, zenb. 9, or. 3983–3996, 2020, doi: 10.1007/s13762-020-02743-8.
[34] K. Schmidt, M. Bau, G. Merschel, eta N. Tepe, «Anthropogenic gadolinium in tap water and tap water-based beverages from fast-food franchises in six major cities in Germany», *Sci. Total Environ.*, libk. 687, or. 1401–1408, urr. 2019, doi: 10.1016/j.scitotenv.2019.07.075.

PGC_SCHE USM_2020_16

Water Polishing Via Gravitational-Driven Ultrafiltration Membrane

Nur Ir Imani Ishak, Ooi Boon Seng*
[1]*School of Chemical Engineering, Engineering Campus, Universiti Sains Malaysia,*
14300 Nibong Tebal Penang, Malaysia
*E-mail: *chobs@usm.my*

Abstract. The demand of clean water for daily activities is crucial for remote area whereby the water treatment and transportation facilities are limited. Water polishing using membrane technology is an energy saving and efficient method under such condition. In this work, water filtration via gravity-driven ultrafiltration membrane (GDU) was tested using hollow fibre PVDF membrane. Its removal efficiency towards three common contaminants in surface water namely humic acid, calcium carbonate and yeast solution has been investigated. It was found that the highest removal efficiency of the GDU system towards humic acid, calcium carbonate and yeast solution were 95.56 %, 99.22 % and 99.85 %, respectively. Different feed solutions exhibited different fluxes declination profiles due to their fouling characteristic. The obtained results showed that GDU is an effective method for polishing the water by removing the microbes, colour and turbidity. The reclaimed water could be used as non-potable water for daily activities during flood or for the remote area whereby accessibility to the electric power is limited.
Keywords: Water reclamation, gravity-driven membranes, ultrafiltration, hollow fibre PVDF membrane, non-potable water.

INTRODUCTION

Reclaiming potable and non-potable water during flood or for the remote area are essential to maintain the basic operation of life. Such process demands for constraint space as well as electricity supply limitations. To date, various methods had been introduced to polish the water such as filtration, membrane separation, adsorption, coagulation and even ozonation [1]. Membrane separation processes have been cited as a suitable process for water treatment, since it can provide an absolute barrier for bacteria and viruses, besides removing turbidity and colour. However, most membrane pressure process requires electricity power to provide the driving force or the trans-membrane pressure which might be unavailable for the remote area. Alternatively, gravity-driven membrane system can be designed to operate based on the hydrostatic pressure. Gravity-driven ultrafiltration membrane (DGU) play an utmost important role in both advanced wastewater and household tap water treatment. As energy-saving approach, studies about fouling mechanism in GDU system will provide the fundamental information for optimizing and achieving its practical application [2]. In this work, a bench top gravitational driven ultrafiltration membrane was tested on its separation efficiency on removing three major contaminants in the surface water namely humic substance, calcium carbonate and yeast that represent hardness and microbes, respectively.

MATERIALS AND METHODS

Experimental setup

The bench top gravitational driven membrane ultrafiltration system was set up as shown in Figure 1. The membrane column consists of 30 pieces of hollow fibre membranes with a length 60 cm packed in the tubular column of 30 cm height in two-pass to give total filtration area of 0.078585 m^2. The hollow membrane had an internal diameter of 0.6 mm and external diameter of 1.2 mm and placed vertically. The filtration was carried out in the batch mode with the solution level was maintained at 40 cm from the electronic balance to ensure the same hydrostatic pressure. The permeate was collected at the bottom of the column by measuring using an electronic balance connected to data-acquisition software called Rs Weight.

Separation Efficiency Study

Three different type of feeds namely humic acid, calcium carbonate and yeast solution were fed to the top of the membrane module periodically. The feed level in the membrane module was kept constant at 80 mL of each feeds which being poured at one time into the filtration module. The membrane flux was calculated by dividing the collected weight over the predetermined time and the filtration area. The rejection of the membrane was calculated by the following equation:

$$\mathrm{R} = 1 - \frac{C_p}{C_f}$$

Whereby R is rejection, C_p and C_f are the concentration of contaminants in the permeate and feed, respectively. The turbidity of the calcium carbonate solution (before and after) the filtration was monitored using a

Turbidimeter (Hach, US). The absorbance reading of humic acid and yeast solution was obtained using UV-Vis Spectrophotometer model (Shimadzu, Japan). Both the humic acid and yeast were measured at the wavelength of 540 nm and 290 nm, respectively.

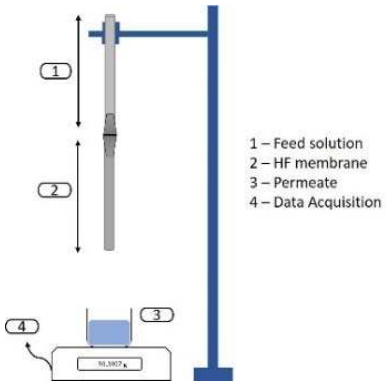

Figure 1. The bench top gravitational driven membrane ultrafiltration system

Membrane Characterization

The images of the layered membrane surface before and after undergoing the ultrafiltration process were obtained using scanning electron microscopy (SEM, S-3000N, Hitachi company) coupled with energy dispersion spectrometry (EDS, EDAX company, USA). All the samples were coated with gold under low vacuum. The images also studied at varies magnification in range of 1000 x – 10 000 x magnification.

RESULT AND DISCUSSION

Membrane Characterization

Figure 2 shows the SEM images of the pristine hollow fibre PVDF membrane surface before and after undergoing the ultrafiltration. SEM micrograph for the membrane surface (a) shows the clean and fresh hollow fibre membrane. Meanwhile (b) shows the structure of humic substances deposited on the outer layer of membrane surface.

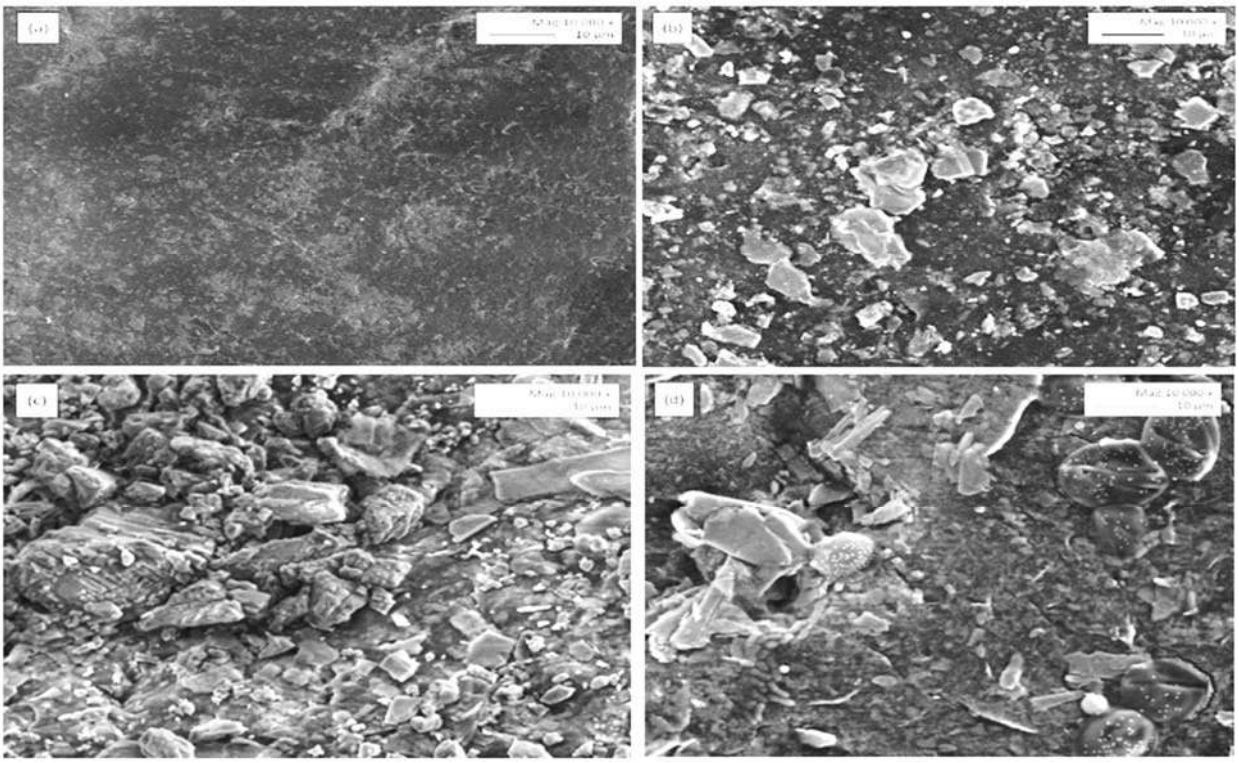

Figure 2. SEM images of Morphology of hollow fibre PVDF membrane (a) before filtration (b) after filtration of humic acid (c) after filtration of calcium carbonate (d) after filtration of yeast solution.

It was loosely packed and dispersive compared to figure (c) which represented the precipitation of $CaCO_3$ on the membrane surface. The precipitation of $CaCO_3$ salts take place due to the decomposition of bicarbonate ions. In figure (d), there was yeast molecules found on membrane surface which exist in round shape with spots structure. This is because of the immediate contact between the yeast molecule in the aqueous solution and coagulant as it exits from the membrane filtration. Apart from that, there was also precipitation of other soluble salts ions caused by the rapid coagulation process of the isotonic medium for the yeast solution.

Removal efficiency of Humic Acid

The membrane performance for humic acid (HA) removal was investigated under different feed concentrations. Membrane fouling was aggravated with increase in humic acid concentration and resulting in lower flux and poorer rejection. Results showed that membrane fouling caused considerable humic acid permeation that indicated the reduction in terms of rejection capability due to the cake formation. Based on Figure 3, the corresponding highest removal efficiency of HA was 95.56 % when 10 mg/L of initial HA concentration was filtered. Figure 4 shows that the highest initial flux was 2.066 kg/m^{2}s with feed concentration of 10 mg/L humic acid. In the real surface water, humic acid concentration is ranging from 0.01 to 1.2 kDa. Most of the organic substances in humic substances occurred in dissolved form, whose fraction in TOC was in the range of 5.51-21.23 gC/m^3 [3].

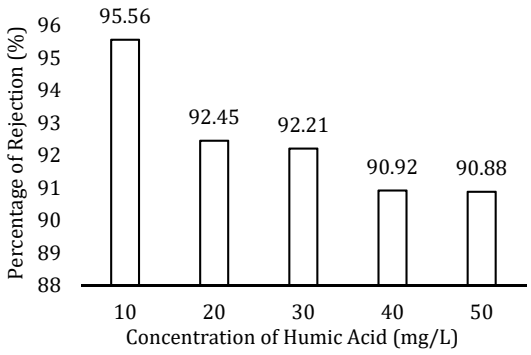

Figure 3. Percentage of Rejection (%) at different concentration of humic acid

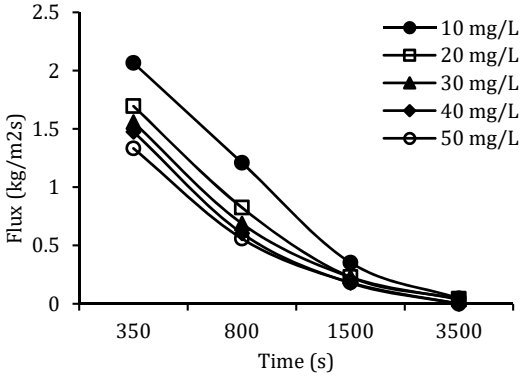

Figure 4. Flux profiles at different humic acid concentration (mg/L)

Removal efficiency of Calcium Carbonate

The membrane has better removal of the hardness compared to the humic acid. However, Figure 5 shows the rejection percentage significantly decreased from 99.22 % to 97.45% when the concentration of $CaCO_3$ was increased from 0.1 to 0.5 wt %. This can be understood as the higher the calcium carbonate, the tendency for it to scale the membrane become higher. As for the permeate fluxes (Figure 6), the highest flux obtained was 3.7106 kg/m$_2$s when 0.1 wt % $CaCO_3$ solution was filtered. Meanwhile, the flux for the other four different $CaCO_3$ solution concentration were almost the same in the ranged of 3.1151 – 2.7944 kg/m$_2$s. Once the concentration of calcium carbonate content exceeds this limit, the surface scaling will be immediately taken place and the flux will be reduced drastically. The initial flux of the $CaCO_3$ is higher compared humic acid. However, the scaling rate of the $CaCO_3$ is also higher than the humic acid filtration.

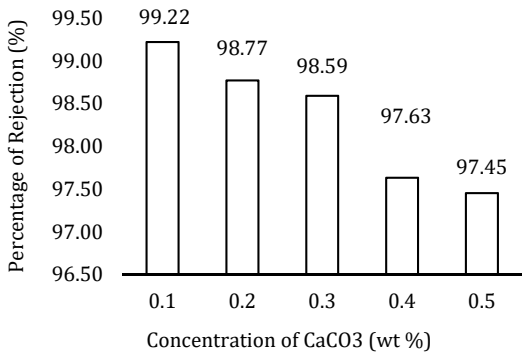

Figure 5: Percentage of Rejection (%) at Calcium Carbonate concentrations

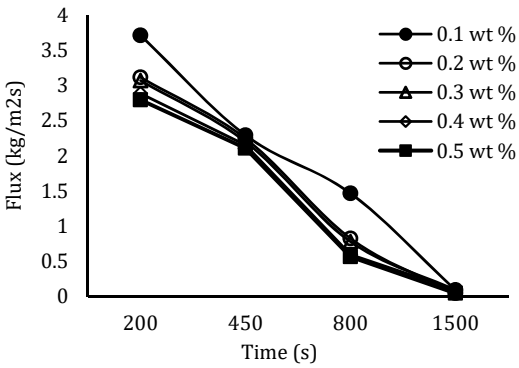

Figure 6: Flux profiles at different calcium different carbonate concentrations (wt %)

Removal efficiency of Yeast Solution

From the observation, it was found that the separation efficiency of the membrane towards yeast is good as compared to humic substance and hardness. As the yeast solution concentration increases, the percentage of rejection was slightly decreased but maintaining the overall performance of more than 99%. Overall yeast solution recovery efficiencies ranged from 99.63 % to 99.85 %. These results demonstrate that the ultrafiltration was effective for microbial removal using the isothermal process. The obtained results show that the filtration of yeast solution using commercial hollow fibre PVDF membrane with gravity driven pressure can produce stable removal efficiency. Figure 8 shows that there are insignificant changes in term of their flux profile for yeast at different concentrations. For example, for 0.2 g/L and 0.4 g/L yeast solution concentration, there had only slightly difference in filtration flux which was 1.8003 kg/m^{2}s and 1.7866 kg/m^{2}s respectively. Meanwhile, the filtration flux of 0.6 g/L, 0.8 g/L and 1.0 g/L yeast solution concentration produced almost the same filtration flux.

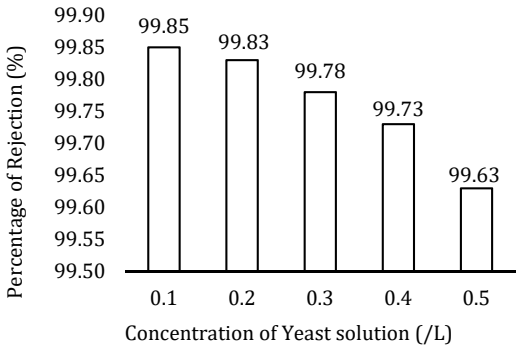

Figure 7. Percentage of Rejection (%) towards different concentration of Yeast solution (g/L)

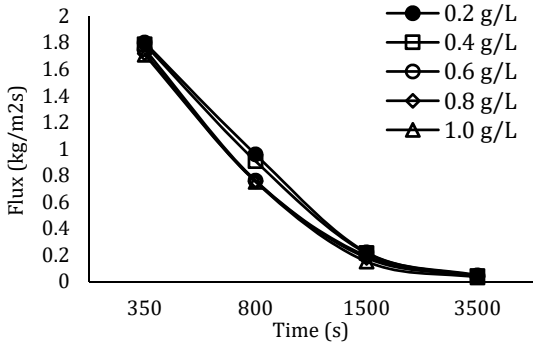

Figure 8. Flux profile at different concentration of Yeast solution (g/L)

CONCLUSION

In this study, a gravitational driven ultrafiltration system was used to polish the water contaminated with humic substance, hardness and microbes. It was observed that the PVDF ultrafiltration membrane could highly reject the yeast solution, followed by calcium carbonate then humic acid. The feed solution that produced the highest flux was the feed solutions with the lowest concentration. The initial flux of the membrane was within 3.7106 kg/m^{2}s, 2.066 kg/m^{2}s and 1.8003 kg/m^{2}s for humic acid, calcium carbonate and yeast solution respectively. Membrane fouling is inevitable especially with higher feed solution concentrations. By polishing the contaminated water with the UF membrane, the reclaimed water is suitable for daily non-potable usage.

ACKNOWLEDGEMENT

This work was supported by the Malaysia Research University Network (MRUN) Collaborative Research Program (203/PJKIMIA/67216003), Ministry of Education Malaysia.

REFERENCES

[1] Matilainen, A., Gjssing, E. T., Lahtinen, T., Hed, L., Bhatnagar, A., and Sillanpaa, M., 2011. An overview of the methods used in the characterization of natural organic matter (NOM) in relation to drinking water treatment. Chemosphere, 83, 1431-1442.

[2] Wang, Y., Fortunato, L., Jeong, S., and Leiknes, T., 2017. Gravity-driven membrane system for secondary wastewater effluent treatment: Filtration performance and fouling characterization. Separation and Purification Teachnology 184: 26-33.

[3] Rucka, K., Solipiwko-Piescik, A., and Wolska, M., 2019. Effectiveness of humic substance removal during the coagulation process. Sringer Nature Journal 1:535.

PGC_SCHE USM_2020_17

Effect of Process Parameters on Solid-Liquid Extraction of *Dillenia Suffruticosa* Leaves

Nur Allia Asri, Khairiah Abd Karim*
School of Chemical Engineering, Engineering Campus, Universiti Sains Malaysia
14300 Nibong Tebal Penang Malaysia
E-mail: **chkhairiah@usm.my*

Abstract. *Dillenia suffruticosa* or known as *simpoh air* is a plant species of Dilleniaceae that has been studied to be a popular medicinal plant in Malaysia especially in treating cancerous diseases. It is believed that the presence of phenolic compounds in this plant have a protective mechanism. Limited research has been carried out on this plant species hence this study aims to investigate the ability of *D. suffruticosa* leaves extract in preventing corrosion of metals. In this preliminary study, various Soxhlet extraction apparatus was used to investigate various extraction related parameters such as extraction temperature (65 – 85˚C) ethanol concentration (50 – 95% (v/v)) and extraction time (1 – 5 hours) on the yield of extract. The results showed that the maximum of *D. suffruticosa* extract yield of 16.57 ± 2.49% was achieved at 80˚C, ethanol concentration of 70% (v/v) and extraction time of 3 hours.
Keywords: *Dillenia suffruticosa, phenolic compound, soxhlet extraction*

INTRODUCTION

In recent years, green corrosion inhibitors extracted from plants have been receiving researchers' attention due to their bioactive compounds that satisfies the criteria as corrosion inhibitor. Bioactive compounds commonly found in plants includes phenolic compounds, carotenoid, anthocyanins and tocopherol [1]. Phenolic compounds are secondary metabolites produced by plants generally play a role in plant adaptations to environmental stress conditions [2]. *Dillenia suffruticosa* or locally known as "simpoh air" is a medicinal plant species of Dilleniaceae found abundantly on alluvial places such as swamps, mangroves, riversides or eroded soil, wasteland, forest edges, and native to Malaysia, Singapore, Brunei, Indonesia, and Sri Lanka [3], [4]. *D. suffruticosa* is one of the plants reported to have high values of phenolic and flavonoids [3]. Studies proved that *Dillenia* sp. have been used for various medical purposes as *Dillenia* sp. leaves extract has also been studied for its antioxidants and cytotoxic properties against cancer [3] [4]. However, there is yet any studies on the ability of *Dillenia* sp. plant extracts as corrosion inhibitor in aggressive environment. Thus, the ultimate aim of this study is to investigate the ability of *Dillenia* sp. leaves extract in hindering corrosion of metals in aggressive media.

In order to yield the phenolic compound in *Dillenia* sp. leaves responsible for inhibiting properties, extraction method is used as first imperative step. There are several factors to be considered that can affect the extraction efficiency before commencing the extraction process such as method of extraction, selection of type and concentration of extracting solvent, particle size of plant materials, solid to liquid ratio, extraction time and temperature and extraction pH [5]. Conventional method of extraction such as soxhlet extraction method have been used for several years and yet, it is the most regularly used extraction technique due to its simplicity and easy to run [6], [7]. This preliminary study aims to maximize the extract yield of *Dillenia* sp. leaves by varying the extraction parameters such as solvent concentration, extraction temperature and extraction time.

MATERIALS AND METHODS

D. suffruticosa leaves were collected from a property located in Kamunting, Perak (4.91˚N 100.72 ˚E. The leaves were cleaned under running tap water to remove dirts and were dried in an oven at temperature of 50˚C for 24 hours to remove moisture content. The dried leaves were then ground into powder using a commercial blender and sifted into uniform size of 350-500 µm. The dried sample (5 g) was weighed and loaded into Soxhlet extractor thimble and placed in the extraction apparatus. Ethanol (300 mL) at various concentration of 50, 60, 70, 80 to 95% (v/v) was used in the study and was added into 500 mL round bottom flask. The sample was extracted at varied temperature of 65, 70, 75, 80, 85˚C. On the effect of extraction time, extraction process was conducted at different extraction time of 1, 2, 3, 4 and 5 hours. After the extraction process, ethanol was removed from the extract using rotary evaporator under reduced pressure at 30˚C and the dried sample was scrapped off from the flask and then stored in an airtight container at 4˚C until further use. The extract obtained after evaporation was weighed and the percentage yield of the extract was calculated as follows:

$$\text{Yield (\% w/w)} = \frac{W_e}{W_l} \times 100\ \% \qquad \text{--- (1)}$$

where:
W_e is the mass of dried extract (g)
W_l is the mass of dried leaves sample (g)

RESULTS AND DISCUSSION

Effect of extraction temperature

In Soxhlet extraction process, temperature is one of the key factors that is affecting the yield of phenolic compound from *D. suffruticosa* leaves. According to Krishna et al. [8], improved extraction is achieved at higher extracting temperature due to faster diffusion and improved solubility of compound from plant material in the solvent, hence increasing the percentage yield of extracts. Figure 1 shows that the highest percentage yield of *D. suffruticosa* leaves of 11.93 ± 1.24% was obtained at 80˚C and the yield was reduced afterward. Despite the positive effect of increasing temperature on extraction yield, the stability of phenolic compound might also be affected by high temperature [8], [9]. Temperature of 80˚C was chosen for extraction of *D.suffruticosa* leaves as the stability of extracted compound was affected at high temperature beyond 80˚C.

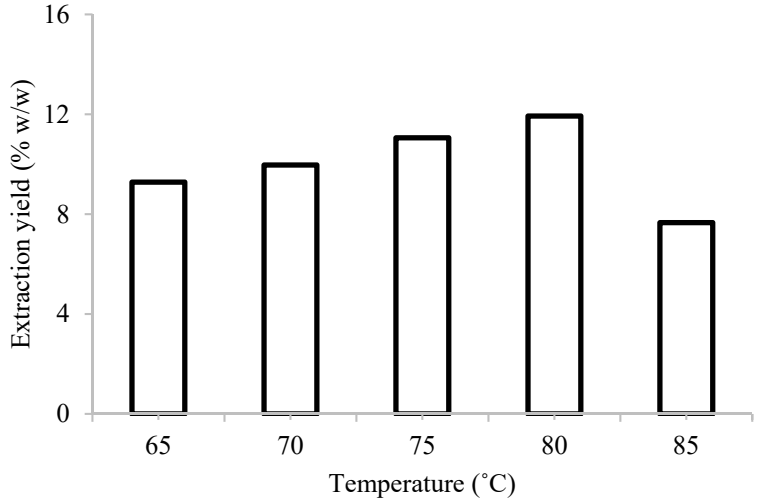

Figure 1. Effect of extraction temperature on percentage yield of *D. suffruticosa* leaves extract (Conditions of extraction: ethanol concentration: 95%, extraction time: 3 hours)

Effect of ethanol concentration

The selection of extracting solvent is dependent on the polar properties of the extracted phytochemicals [10]. Water-ethanol is selected as extraction solvent in this study because of the possibility of mixing them in any proportion, both solvents are less toxic and safer for human consumption compared to other organic solvent [11]. From Figure 2, it depicts that the percentage yield of *D. suffruticosa* leaves extract increased with increasing ethanol concentration and reached the maximum at 70% (v/v) with the yield of 15.72 ± 1.70%. Different polarities in extracting solvent may have facilitated the extraction process due to the presence of water as swelling agent in *D. suffruticosa* leaves, hence promotes the surface contact area between the extracting solvent with plant matrix [12], [13]. This explains why the extraction yield beyond 70% (v/v) of ethanol concentration has declined as very little water present for swelling of cell [14]. Ethanol concentration of 70% (v/v) is chosen as for extraction of *D. suffruticosa* leaves.

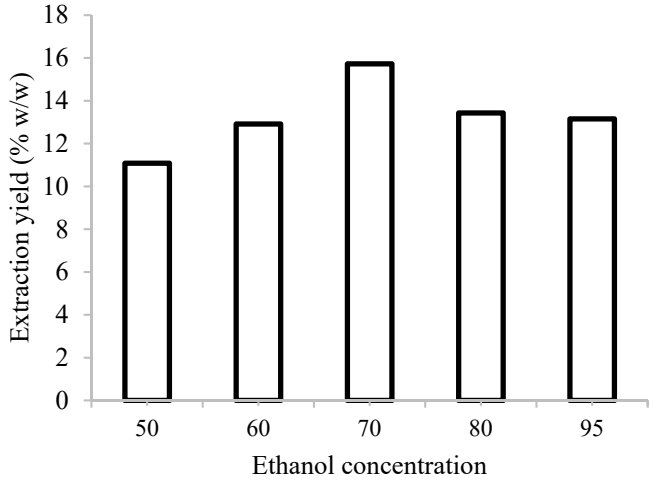

Figure 2. Effect of ethanol concentration on percentage yield of *D. suffruticosa leaves* extract (Conditions of extraction: extraction temperature: 80˚C, extraction time: 3 hours)

Effect of extraction time

Extraction time is important in solvent extraction as appropriate extraction time can reduce the cost and energy of the extraction process. Extraction time also plays an imperative role in percentage yield obtained throughout the process. Bunansari et al., stated that longer extraction time will surge the amount of extracted compound [15]. The influence of extraction time can be observed from Figure 3 where the percentage yield has gradually increased as the extraction time was prolonged. The highest yield obtained after 3 hours of extraction with 16.57 ± 2.49% yield. Significant reduction in percentage yield is observed with prolonged extraction time. This phenomenon can be explained by Fick's second law of diffusion where equilibrium of solution concentration in solvent and *D. suffruticosa* leaves matrix was attained after a period of time [11]. Therefore, extraction time of 3 hours was selected as the optimum temperature to extract compounds from *D. suffruticosa* leaves.

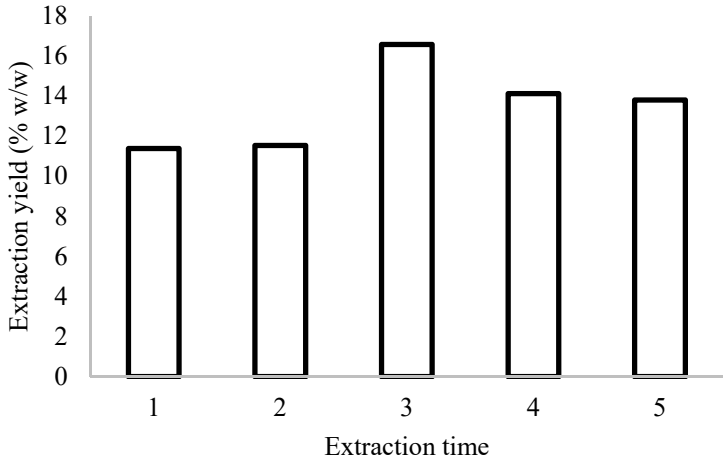

Figure 3. Effect of extraction time on percentage yield of *D. suffruticosa leaves* extract (Conditions of extraction: ethanol concentration: 70% (v/v), extraction temperature: 80˚C)

CONCLUSION

This study investigated the process parameters affecting solid-liquid extraction using Soxhlet apparatus factors, namely: extraction temperature, ethanol concentration and extraction time on the yield percentage of the extract of *Dillenia* leaves. The highest extraction yield of 16.57 ± 2.49% was obtained using extraction temperature of 80 ˚C, ethanol concentration of 70% and extraction time of 3 hours. Thus, *Dillenia* leaves extract can be further studied on its ability inhibiting corrosion of metal in destructive environment.

ACKNOWLEDGEMENT

This research is funded under financial support provided by USM Bridging Grant (304/PJKIMIA/6316535).

REFERENCES

[1] A. Altemimi, N. Lakhssassi, A. Baharlouei, D. G. Watson, and D. A. Lightfoot, "Phytochemicals: Extraction, isolation, and identification of bioactive compounds from plant extracts,"Plants, **6(4)** 56–78 (2017).

[2] H. Zhao, "Effects of processing stages on the profile of phenolic compounds in beer," in Processing and Impact on Active Components in Food, V. Preedy, Ed. Elsevier Inc., 533–539 (2015).

[3] M. Dawood Shah, J. Seelan Sathiya Seelan, and M. Iqbal, "Phytochemical investigation and antioxidant activities of methanol extract, methanol fractions and essential oil of *Dillenia suffruticosa* leaves," Arabian Journal Chemistry, (2020).

[4] N. Armania, L.S. Yazan, S.N. Musa, I.S. Ismail, J.B. Foo, K.W. Chan, H. Noreen, A.H. Hisyam, S. Zulfahmi, and M. Ismail, "*Dillenia suffruticosa* exhibited antioxidant and cytotoxic activity through induction of apoptosis and G2/M cell cycle arrest,"Journal of Ethnopharmacology, **146(2)** 525–535 (2013).

[5] W. Aida, "Effect of ethanol concentration, extraction time and extraction temperature on the recovery of phenolic compounds and antioxidant capacity of *Orthosiphon stamineus* extracts phenolic content (TPC), total flavonoid content (TFC), condensed tannin content," International Food Research Journal,**18(4)** 1427–1435 (2011).

[6] O. R. Alara, N. H. Abdurahman, and C. I. Ukaegbu, "Soxhlet extraction of phenolic compounds from *Vernonia cinerea* leaves and its antioxidant activity," Journal of Applied Research on Medicinal and Aromatic Plants, **11** 12-17 (2018)

[7] G. B. Yenge, V. L. Kanawade, C. A. Nimbalkar, R. N. Kenghe, and A. P. Patil, "Optimization of soxhlet extraction of garden cress oil by response surface methodology," **5(2)** 526-530 (2017).

[8] M. L, A. Krishna, J. Reddy, and G. S. Nirmala, "Optimization studies on extraction of phytocomponents from betel leaves," Resource-Efficient Technologies, **3(4)**, 385–393 (2017).

[9] S. R. Shirsath, S. S. Sable, S. G. Gaikwad, S. H. Sonawane, D. R. Saini, and P. R. Gogate, "Intensification of extraction of curcumin from *Curcuma amada* using ultrasound assisted approach: Effect of different operating parameters," Ultrasonics Sonochemistry, **38** 437–445 (2017).

[10] C. W. I. Haminiuk, M. S. V. Plata-Oviedo, G. de Mattos, S. T. Carpes, and I. G. Branco, "Extraction and quantification of phenolic acids and flavonols from *Eugenia pyriformis* using different solvents," Journal of Food Science and Technology, **51(10)** 2862–2866 (2014).

[11] K. K. Chew, S. Y. Ng, Y. Y. Thoo, M. Z. Khoo, W. M. Wan Aida, and C. W. Ho, "Effect of ethanol concentration, extraction time and extraction temperature on the recovery of phenolic compounds and antioxidant capacity of *Centella asiatica* extracts," International Food Research Journal **18(2)** 571–578 (2011).

[12] S. Hemwimon, P. Pavasant, and A. Shotipruk, "Microwave-assisted extraction of antioxidative anthraquinones from roots of *Morinda citrifolia*," Separation and Purification Technology **54(1)** 44–50 (2007).

[13] W. Xiao, L. Han, and B. Shi, "Microwave-assisted extraction of flavonoids from *Radix Astragali*," Separation and Purification Technology **62(3)** 614–618 (2008).

[14] T. W. Charpe and V. K. Rathod, "Effect of ethanol concentration in ultrasound assisted extraction of glycyrrhizic acid from Licorice root," Iranian Journal of Chemical Engineering **11(4)** 21–30 (2014).

[15] B. Buanasari, W. T. Eden, and A. I. Sholichah, "Extraction of phenolic compounds from petai leaves (*Parkia speciosa* Hassk.) using microwave and ultrasound assisted methods," Jurnal Bahan Alam Terbarukan, **6(1)** 25-31 (2017)

PGC_SCHE USM_2020_18

Preliminary Study on the Compatibility of P84 Polyimide (PI) Coated Polymethylpentene (PMP) Thin Composite Membrane

Zulfida Mohamad Hafis Mohd Shafie[1,2], Abdul Latif Ahmad[1,*], Siew Chun Low[1], Sabine Rode[2], Bouchra Belaissaoui[2], Denis Roizard[2]

[1] School of Chemical Engineering, Engineering Campus, Universiti Sains Malaysia, 14300, Nibong Tebal, Penang, Malaysia

[2] Laboratoire Réactions et Génie des Procédés (LRGP) (UMR 7274), Université de Lorraine / CNRS, ENSIC, 1, rue Grandville – BP 20451, 54001 Nancy Cedex, France

*E-mail: *chlatif@usm.my*

Abstract. In this study, the polymer compatibility of polymethylpentene (PMP) membrane as the base substrate with P84 PI coating was elucidated. P84/PMP composite was fabricated in dense flat sheet configuration. SEM and FTIR were utilised to characterize the composite layers, while peeling test was conducted to verify the peelability of the P84 on PMP. Results suggested a good adhesion of P84 on PMP layer, but the adhesion is irreversible when the composite was peeled off. The wettability of P84 PI solution on low surface energy PMP layer may also become a considerable limitation for a defect-free thin coating in gas separation membrane fabrication.

Keywords: *P84 polyimide coating; polymethylpentene substrate; thin composite membrane*

INTRODUCTION

Fabrication of membranes with thin selective layer can be traced back to the year 1963 with the success of Sidney Loeb & Srinivasa Sourirajan from UCLA in fabricating asymmetric polymeric membranes [1]. The membrane, which consist of a thin surface layer and a thick-porous sublayer made up of the same polymer were made through phase inversion; a common methodology in membrane research nowadays but was a breakthrough during that period. Nevertheless, the use of this methodology is with one significant limitation; inability to separate the materials between the supporting layer and its selective layer. While not being a significant problem in lab scale, commercial potential of the membranes would highly depend on the material cost and its mechanical viability, particularly when utilizing the expensive high-performance membrane. Using the same concept, approach to separate the layers were made to better control the properties of the membrane by laminating together separate specialized layers to create what is called as composite membrane. Eventually, thin film composite (TFC); first developed by Peter S. Francis from North Star Research and Development Institute for reverse osmosis membranes were born and became the new contender to the original Loeb – Sourirajan's anisotropic polymeric membranes [2, 3]. The idea was then adapted for gas separation membrane, with Jay M.S. Henis and Mary K. Tripodi from Monsanto Company (now part of Air Products and Chemicals Inc.) to first made asymmetric and TFC membrane economically feasible for industrial application [4, 5].

The discrete fabrication methodology of the selective layer and the support layer is beneficial in optimizing the layers to its full potential, based on its intended application [6]. It is also beneficial as an engineering solution for some of the high potential polymers to be used as selective layer, since it may not be suited to be fabricated in asymmetric membrane morphology due to its intrinsic weak mechanical properties [7], on top of substantially reducing the cost of the expensive specialized polymers [8]. Composite membranes generally aim to improve gas transport properties with negligible resistance on the porous support layer [9, 10]. Hence, three parameters would need to be optimized in order to theoretically maximize the separation performance: (i) selectivity & (ii) permeance for the surface selective layer, and (iii) gas transport resistivity for the support layer. Membrane should exhibit high selectivity to have the required product purity, while having high permeance to reduce the capital cost by increased membrane area [11]. The thin selective film is thus the heart of the composite membrane; being the site for molecular separation to take place.

Increasing the membrane's flux can be achieved through three methods; (i) increase in the driving force (partial pressure) or surface area, (ii) improvement of the selective layer's gas permeability, and (iii) lowering the selective layer's thickness. Option (i) however is limited to real world practicality especially by the increase in capital cost with larger membrane area, making option (ii) and (iii) as the methodology of choice for membrane research. The permeance of the selective layer is hence can be increased with thinner selective layer, or with better selective layer's permeability [8].

Polyimide (PI), being one of the materials of choice for CO_2 separation processes at the industrial level is a good candidate as the base matrix of a mixed matrix membrane (MMM). Nevertheless, PI such as P84 is highly selective yet low in permeability to be used as a thick dense membrane layer with acceptable level of mechanical integrity especially in hollow fiber configuration. While commercial P84 based hollow fiber membranes such as

Sepuran by Evonik Industries AG has been available and performing well since 2012, this membrane is asymmetric in nature. High cost of the fillers of mixed matrix membranes such as functionalized graphene oxides and metal organic frameworks means that its usage needs to be minimize only at the surface selective dense layer of the membrane where the benefit is maximum and the material cost is minimum. This is further complicated by the limited solvation of P84, which are known to be best dissolved in N-methyl-2-pyrrolidone (NMP), a common polar aprotic solvent for other base polymer used in membrane fabrication. Hence, in this study, the polymer compatibility of polymethylpentene (PMP) membrane as the base substrate with P84 PI coating is elucidated. Results from this preliminary study would verify the feasibility for composite membrane fabrication and gives an insight for fabrication methodology of a working PMP/P84 composite membrane in future works.

MATERIALS AND METHODS

PMP – P84 PI composite dense flat sheet membranes were synthesized through thermal induced phase inversion process. Approximately 3g of 2wt. % PMP solution in CCl_4 and 10 wt.% P84 PI solution in NMP was poured onto a clean petri dish 8.7 cm in diameter. It is then placed in a pre-heated oven at 60 °C and left overnight to dry to form a thin dense layer. The PMP & P84 PI solution was poured stepwise (PMP first or P84 PI first) with drying in between, or both together back-to-back, depending on the samples. The prepared samples were then left to cool slowly and then immersed in water for a while to remove solvent residues. The layers were then peeled from the petri dish and dried under room temperature for several days.

RESULTS AND DISCUSSION

Figure 1 represents the resulting PMP/P84 PI composite made under different fabrication sequences. Good composite layers were formed when PMP solution was poured on the dried P84 layer [image (a)], but not the other way around [image (b)]. Low surface tension CCl_4 was able to wet well the dried P84 layers, forming a good composite layer. On the other hand, P84 PI solution did not wet well the dried PMP layer in (b) due to the low surface energy of PMP (21.0 mJ/m^2) below the surface tension of NMP solvent (40.8 mN/m). This could be a major problem in fabricating PMP/P84 composite membrane as the high permeability PMP would become the substrate, which may complicate the fabrication process. While surface modification of PMP such as through plasma/heat treatment [12] has been reported to increase its surface energy, these methods are destructive and may not bode well for scale up. Nevertheless, fabrication through dip coating of PMP fibers can be a simple solution. On the other hand, back-to-back P84 and PMP fabrication caused premature phase inversion due to the miscibility of the solvent used in the study (CCl_4 & NMP).

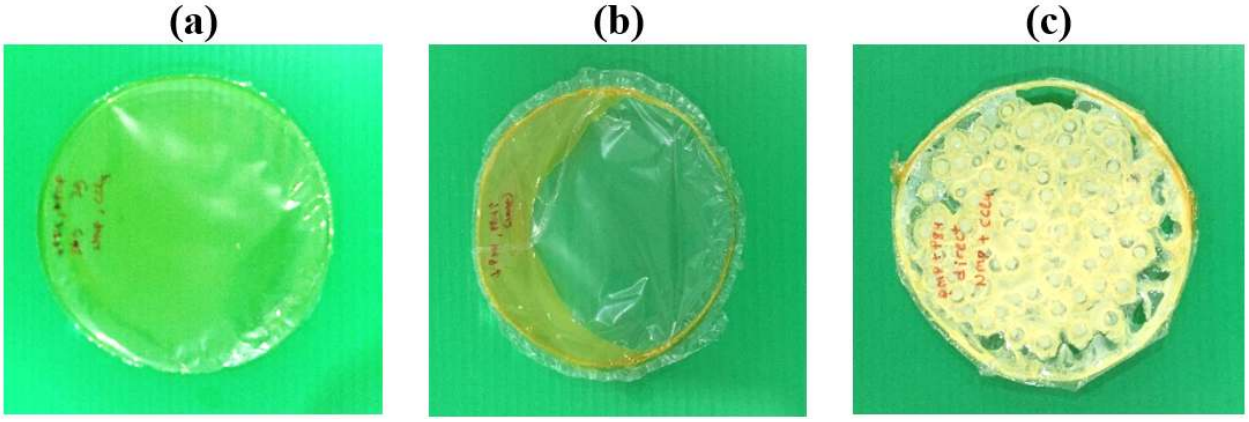

Figure 1. PMP/P84 PI composite made under different fabrication sequences. (a) P84 solution, dried, then PMP solution [P84 – PMP], (b) PMP solution, dried, then P84 solution [PMP – P84], (c) P84 and PMP solution back-to-back [P84 + PMP]

FTIR was utilized to validate the composite layer formed in image (a). Figure 2 represents the FTIR spectrum of the composite layer from both sides, as compared to the FTIR spectrum of the unprocessed PMP & P84 PI polymers. Signature peaks of PMP at 2800 - 3000 cm^{-1} for C-H stretching and 1383 & 1465 cm^{-1} for C-H bending [13] were visible for composite (top) layer, while signature peaks of P84 PI at 1780 cm^{-1} for C=O asymmetric stretching, 1715 cm^{-1} for C=O symmetric stretching and 1356 cm^{-1} for C-N stretching [14] were visible for composite (bottom) layer, suggesting the composite has been fabricated successfully. As the composite spectrum were not or minimally superimposed, this suggested that the layers did not blends nor chemically changed during fabrication.

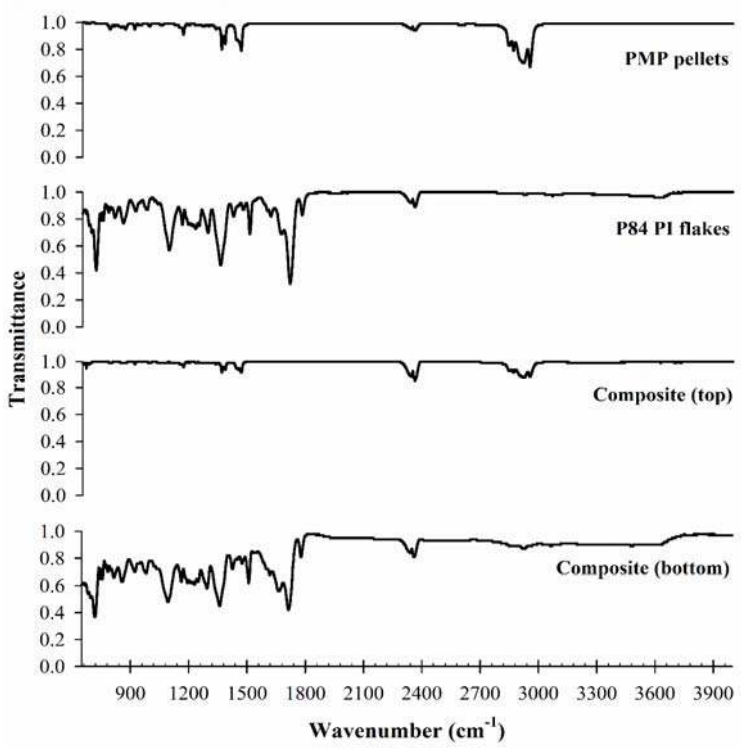

Figure 2. FTIR spectrum of PMP pellets, P84 PI flakes, PMP/P84 PI composite (top), and PMP/P84 PI composite (bottom) for P84 – PMP composite sample

SEM and EDX were also utilised to visualize the cross section of the composite, as illustrated in Figure 3. Two distinctive layers could be seen while the elemental mapping of O atom (in green) which is concentrated on the bottom layer is in line with the P84 PI's chemical structure [15]. Nevertheless, it is worth to note that the layers separated when cracked in liquid nitrogen and hence could only be cut using a sharp knife. The separated layers could not be fused afterwards. While this is merely a methodological difference, this suggested that the coating is physically adhered, not through chemical means.

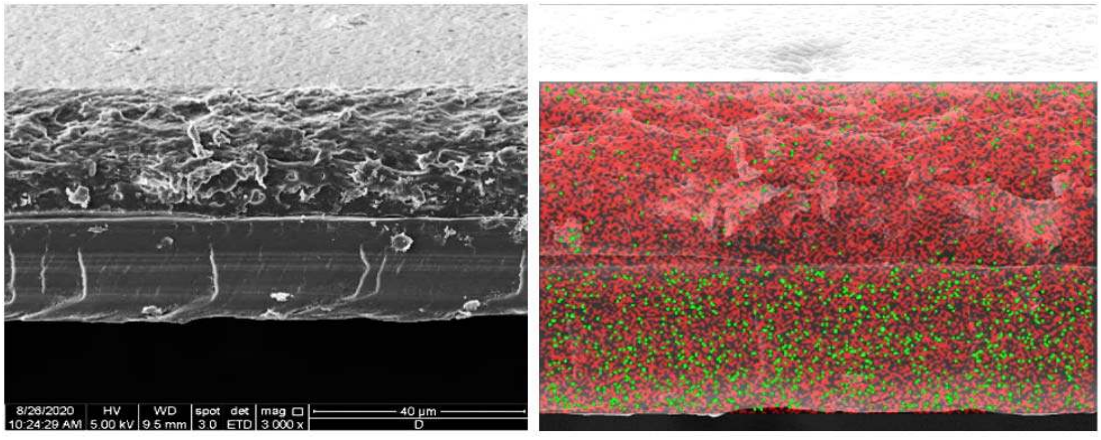

Figure 3. Cross section of the PMP/P84 PI composite for P84 – PMP composite sample. (Left) Micrograph at x3k magnification. (Right) Superimposed EDX mapping at x4k magnification, where red = carbon atom & green = oxygen atom

Peeling test conducted by modified X-cut method confirmed the peeling of the layer even when subjected to the shearing of knife. Figure 4 represents the SEM micrograph and light microscope image near the cutting line, confirming the peeling of the layers. Nevertheless, no air bubbles could be seen on the layers other than near the cutting line, suggesting that the coating was firmly held together unless being stressed in a specific condition. It is unclear what will contribute to the separation of the layers and how the layers adhere in the first place, but the coating did not peel easily even when pulled by force, which suggesting that the composite membrane is weak to shear. To

verify this claim, pull off tensile test was conducted by sandwiching the membrane between two stubs of 1.9 cm in diameter using epoxy and let hanged with certain weight to induce tensile force between the layers. Interestingly, the layers did not separate even under a maximum of 40N of force for more than 1 h. A more proper testing is to be conducted in the future.

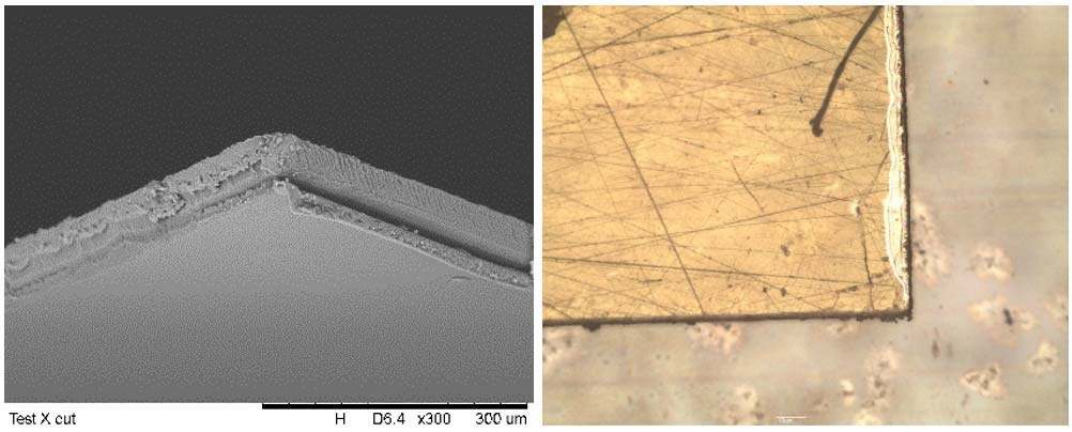

Figure 4. Adhesibility and peeling test observation. (Left) SEM micrograph cross section of X-cut at x300 magnification. (Right) Light microscope image near the cut border. Separated layer can be clearly seen on the cutting line and absent everywhere else

CONCLUSION

PMP/P84 PI composite was fabricated using thermal induced phase inversion process. The membranes did not undergo chemical changes and suggested good compatibility. Good adhesion was noted between the layers, although the layers did not adhere back once peeled. The wettability of P84 PI solution on low surface energy PMP layer may become the main concern for a defect free thin coating in gas separation membrane fabrication.

ACKNOWLEDGEMENT

This research is supported by Universiti Sains Malaysia USM-RUI grant (Grant no: 1001/PJKIMIA/8014063). Zulfida Mohamad Hafis Mohd Shafie would like to express his thanks to USM Fellowship and the Government of France through the French Embassy in Malaysia/Campus France for financing his study & research mobility.

REFERENCES

[1] Loeb, S. and S. Sourirajan, Advances in Chemistry. **38** 117-132 (1963).
[2] Cadotte, J.E. and R.J. Petersen, ACS Symposium Series. **153** 305-326 (1981).
[3] Francis, P.S., F.C.D. Luzio, W.S. Gilla, and A. Kotch, Office of Saline Water United States Department of the Interior **177** 1-60 (1966).
[4] Henis, J.M.S. and M.K. Tripodi, Journal of Membrane Science. **8(3)** 233-246 (1981).
[5] C&EN, Chemical & Engineering News Archive. **58(20)** 57-60 (1980).
[6] Wong, K.C., P.S. Goh, and A.F. Ismail, International Biodeterioration & Biodegradation. **102** 339-345 (2015).
[7] Salih, A.A.M., C. Yi, H. Peng, B. Yang, L. Yin, and W. Wang, Journal of Membrane Science. **472** 110-118 (2014).
[8] Tsai, F.J., D. Kang, and M. Anand, Separation Science and Technology. **30(7-9)** 1639-1652 (1995).
[9] Pinnau, I. and W.J. Koros, Industrial & Engineering Chemistry Research. **30(8)** 1837-1840 (1991).
[10] Wijmans, J.G. and P. Hao, Journal of Membrane Science. **494** 78-85 (2015).
[11] Kattula, M., K. Ponnuru, L. Zhu, W. Jia, H. Lin, and E.P. Furlani, Scientific Reports. **5** 15016 (2015).
[12] Slepička, P., S. Trostová, N. Slepičková Kasálková, Z. Kolská, P. Malinský, A. Macková, L. Bačáková, and V. Švorčík, Polymer Degradation and Stability. **97(7)** 1075-1082 (2012).
[13] Michaljaničová, I., P. Slepička, J. Hadravová, S. Rimpelová, T. Ruml, P. Malinský, M. Veselý, and V. Švorčík, RSC Advances. **6(79)** 76000-76010 (2016).
[14] Omidvar, M., C.M. Stafford, and H. Lin, J Memb Sci. **575** (2019).
[15] Soroko, I., Y. Bhole, and A.G. Livingston, Green Chem. **13(1)** 162-168 (2011).

PGC_SCHE USM_2020_19

Synthesis and characterization of hydrophobic PVDF-SiO_2 mixed matrix hollow fiber membrane for desalination through direct contact membrane distillation

Mohammed Karama Alsebaeai, Abdul Latif Ahmad*
School of Chemical Engineering, Engineering Campus, Universiti Sains Malaysia,
14300 Nibong Tebal, Pulau Pinang, Malaysia.
*E-mails: *chlatif@usm.my*

Abstract. Polyvinylidene fluoride (PVDF)/SiO_2 hollow fiber (HF) composite membranes were prepared for direct contact membrane distillation (DCMD) by the dry-wet phase inversion immersion precipitation process. The effect of blending hydrophobic nano fumed silica (SiO_2) particles into the PVDF dope solution was investigated. The loading of the nanoparticles in the dope solution was varied at different wt.% (1.5, 3, 4.5 and 6 wt.%). The prepared HF membranes were characterized by water contact angle, porosity, liquid entry pressure (LEP_W,). In addition, membrane distillation experiments of 3.5 wt.% NaCl solutions were carried out in pristine and modified Polyvinylidene fluoride (PVDF)/SiO_2 hollow fiber membrane. The results indicated that the fabricated HF mixed matrix membrane could be of great potential in the desalination through DCMD.
Keywords: *Hydrophobic silica; membrane distillation; desalination.*

INTRODUCTION

As water scarcity is the major concern nowadays all over the world. The increase in freshwater demand is driving the interest in using desalination applications [1]. However, the conventional and membrane-based desalination technologies such as electrodialysis and reverse osmosis (RO) are considered impractical to supply the fresh water requirements efficiently [2–4]. MD is a temperature–driven separation technology which relies on the vapor pressure difference between the feed side and the permeate side across the micro-porous hydrophobic membrane which provides the driving force in MD. This technique results in a highly pure permeate solution and a highly concentrated feed solution where the non-volatile substances are retained [5].

MD performance depends on the characteristics of the developed membrane and the structure of the membrane module [6]. Nevertheless, developing an ideal MD membrane for desalination and high permeation performance is still being investigated[7]. Therefore, in order to obtain an ideal membrane for better MD performance, an effective and improved approach should be developed to gain the optimum characteristics for the targeted membrane. The key factors that membrane should have for an effective MD process are higher hydrophobicity , high porosity, optimal thickness, good chemical resistance strength, acceptable mechanical strength, anti-fouling characteristic, high liquid entry pressure (LEP_w) , narrow pore size distribution, low vapor transport resistance and reduced thermal conductivity[8,9]. Hollow fiber membranes are the preferable choice by researchers in compared to the flat sheet membranes in MD applications due to their less sensitivity to temperature polarization, flexibility, self -supporting property, and large surface area per unit volume [10,11].

Currently, poly(vinylidene fluoride) (PVDF) is the commonly used hydrophobic polymer to fabricate flat sheet and hollow fiber membranes. In order to improve the anti-wetting property of the PVDF membranes, a lot of investigations have been done by researchers to modify the surface of PVDF with low surface energy material and /or prepare micro/nano -scale surface structure [12]. Among the polymers that have been used in this particular purpose are FEP [13,14], Hyflon AD60 [15], ECTFE [16], PTFE [17], PDMS [18]. Therefore, the objective of this research is to study the effect and performance of blending various amount of silica nano particles with PVDF using dry- wet phase inversion method to fabricate PVDF/SiO_2 HF membrane and test it using direct contact membrane distillation (DCMD)

MATERIALS AND METHODS

PVDF hollow fiber membranes (HF) were synthesized using dry-wet spinning technique. PVDF powder was dried in oven for 24 h at 100 °C to remove the moisture content. The spinning dope solution was prepared by mixing the dried PVDF powder with solvent (DMAc) and non-solvent additives mixture (PEG1500 and LiCl. The predetermined amount of hydrophobic nano- fumed silica was then added into the solution. The mixture was subjected to continuous mechanical stirring for 24 h at 60°C. Afterwards, the stirring was stopped, and the homogenous solution was degassed for 1 h to release the gas bubbles prior to spinning process. The PVDF/SiO_2 mixed matrix hollow fiber membranes were fabricated via dry-jet wet phase inversion process. The homogenous dope solution was transferred into the reservoir tank and was extruded out through a spinneret under nitrogen pressure of 0.15 MPa. The dope flowrate was adjusted by the speed of the gear pump. Distilled water was used as bore fluid and simultaneously fed to

the spinneret under the same pressure condition to make a lumen of the hollow fiber. After squeezing out from the spinneret, the hollow fiber falls along the air gap before immersed into the external coagulation bath (tap water). The produced fibers were rolled up by take up drum to be collected and immersed in changeable water for 3 days at time interval 1 day to remove the residual solvent before air drying for 2 days at room temperature

RESULTS AND DISCUSSION

Anti-pore wetting is one of the main parameters that needed to be achieved by increasing the hydrophobicity of the HF membranes. As a result, high permeate flux, and desalination performance could be enhanced in DCMD [19]. Table 1 shows the results of the water contact angle measurements of the hollow fiber membranes. It is anticipated that the hydrophobicity of the HF membranes will be increased due to the hydrophobic nature of the mixed SiO_2 nanoparticles in compared with the pristine PVDF membrane [20]. As the loading of nano fumed silica particles increased from (M-1 to M-4), the hydrophobicity of the SiO_2 mixed composite HF membrane has been enhanced from 85° to 96°. Basically, surface energy and the engineering structure of the material embedded (nano fumed silica) plays a crucial role in promoting the surface hydrophobicity of the membrane [20,21].

However, the effect of increasing the concentration of SiO_2 on the membrane porosity has been also investigated. The pristine membrane presented the highest porosity value of 85% while a clear decreasing trend in membrane porosity is observed by increasing the mass ratio of SiO_2 nanoparticles as shown in Table 1. The reason behind that is increasing the viscosity of the dope which caused the formation of denser sponge like pores instead of the finger like pores [22]. Apparently, dropping the membrane porosity is caused by the formation of dense membrane which led to reducing the micro-voids. The measured LEP of the hollow fiber membranes were above 3.0 bar as presented in Figure 1 which gives indication of anti-wetting property of the pores [23]. The variation of the pore size distribution of the nanocomposite membrane effectively lead to a change in water resistance in penetrating the membrane pores.

Table 1. Effects of different silica loadings on Porosity, contact angle, LEP

Membrane	Contact angle (°C)	Porosity (%)	LEP (bar)
M-0	82	85	3.9
M-1.5	85	80	3.5
M-3	87	74	4.2
M-4.5	91	68	4.3
M-6	96	62	4.5

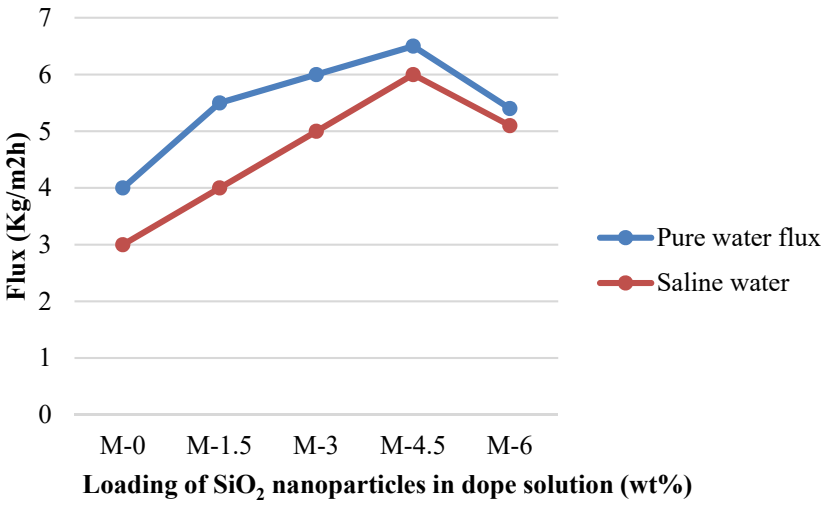

Figure 1. Permeation flux of DCMD as a function of nanoparticles concentration in dope solution

The performance of the fabricated hollow fiber membranes was tested for DCMD for distilled water and 3.5 wt.% NaCl solution. Salt rejections were above 99.9% for all HF membranes in our experiments. It can be observed that the membrane permeate flux enhances over the pristine membrane (M-0). The observation showed that membranes permeate flux exhibited higher flux with increasing the dosage of nano-fumed silica (SiO_2) with a peak value at 4.5 wt.% (M-4.5) with maximum permeate flux about 6.5 and 6 kg/m^2 h for saline and pure water respectively.

This may attribute to the increased hydrophobicity which could also reduce temperature polarization effect and higher pore size [15,20] in addition to the liquid entry pressure (LEP) enhancement that improves the anti-wetting property of the membrane [25].

CONCLUSION

(PVDF)/SiO_2 hollow fiber (HF) composite membranes were synthesized successfully. The study concluded that PVDF blended with SiO_2 nanoparticles is suitable for DCMD processes for desalination application.

ACKNOWLEDGEMENT

The authors would like to acknowledge the support by the Ministry of Education Malaysia for the Trans-disciplinary Research Grant Scheme (TRGS), TRGS/1/2018/USM/01/5/1.

REFERENCES

[1] G. Amy,, N. Ghaffour,, Z. Li,, L. Francis,, R.V. Linares,, T. Missimer,, S. Lattemann, Desalination 401 (2017) 16–21.
[2] A. Deshmukh,, C. Boo,, V. Karanikola,, S. Lin,, A.P. Straub,, T. Tong,, D.M. Warsinger,, M. Elimelech, Energy Environ. Sci. 11(5) (2018) 1177–96.
[3] A.L. McGaughey,, R.D. Gustafson,, A.E. Childress, J. Memb. Sci. (2017). 10.1016/j.memsci.2017.08.040.
[4] A. Criscuoli,, M.C. Carnevale, Desalination (2015). 10.1016/j.desal.2015.03.003.
[5] S. Meng,, J. Mansouri,, Y. Ye,, V. Chen, J. Memb. Sci. 450 (2014) 48–59. 10.1016/j.memsci.2013.08.036.
[6] J.A. Prince,, V. Anbharasi,, T.S. Shanmugasundaram,, G. Singh, Sep. Purif. Technol. 118 (2013) 598–603. https://doi.org/10.1016/j.seppur.2013.08.006.
[7] M. Yao,, J. Ren,, N. Akther,, Y.C. Woo,, L.D. Tijing,, S.-H. Kim,, H.K. Shon, Chemosphere 230 (2019) 117–26. 10.1016/j.chemosphere.2019.05.049.
[8] K.J. Lu,, J. Zuo,, T.S. Chung, J. Memb. Sci. (2016). 10.1016/j.memsci.2016.04.058.
[9] H. Qiu,, Y. Peng,, L. Ge,, B. Villacorta Hernandez,, Z. Zhu, Appl. Surf. Sci. (2018). 10.1016/j.apsusc.2018.03.004.
[10] Y. Huang,, C. Xiao,, Q. Huang,, H. Liu,, J. Zhao, Chem. Eng. J. 403 (2021). 10.1016/j.cej.2020.126295.
[11] T. Turken,, R. Sengur-Tasdemir,, E. Ates-Genceli,, V.V. Tarabara,, I. Koyuncu, J. Water Process Eng. 32 (2019). 10.1016/j.jwpe.2019.100938.
[12] C.R. Szczepanski,, F. Guittard,, T. Darmanin, Adv. Colloid Interface Sci. (2017). 10.1016/j.cis.2017.01.002.
[13] K. Chen,, C. Xiao,, Q. Huang,, H. Liu,, H. Liu,, Y. Wu,, Z. Liu, Desalination 375 (2015) 24–32. https://doi.org/10.1016/j.desal.2015.07.021.
[14] Y. jie Wu,, Q. lin Huang,, C. fa Xiao,, K. kai Chen,, X. feng Li,, N. na Li, Desalination 353 (2014) 118–24. 10.1016/j.desal.2014.09.010.
[15] D. Tong,, X. Wang,, M. Ali,, C.Q. Lan,, Y. Wang,, E. Drioli,, Z. Wang,, Z. Cui, Sep. Purif. Technol. 157 (2016) 1–8. https://doi.org/10.1016/j.seppur.2015.11.026.
[16] J. Pan,, C.F. Xiao,, Q.L. Huang,, H.L. Liu,, J. Hu, J. Mater. Chem. A 3 (2015) 23549.
[17] Li,, D. Rana,, T. Matsuura,, C.Q. Lan, Sep. Purif. Technol. 226 (2019) 192–208. https://doi.org/10.1016/j.seppur.2019.05.102.
[18] D. Sun,, M.Q. Liu,, J.H. Guo,, J.Y. Zhang,, B.B. Li,, D.Y. Li, Desalination (2015). 10.1016/j.desal.2015.05.017.
[19] M.K. Alsebaeai,, A.L. Ahmad, J. Ind. Eng. Chem. 86 (2020) 13–34. 10.1016/j.jiec.2020.03.006.
[20] J.E. Efome,, M. Baghbanzadeh,, D. Rana,, T. Matsuura,, C.Q. Lan, Desalination (2015). 10.1016/j.desal.2015.07.002.
[21] Z.Q. Dong,, X.H. Ma,, Z.L. Xu,, Z.Y. Gu, RSC Adv. 5(83) (2015) 67962–70. 10.1039/c5ra10575g.
[22] H. Fan,, Y. Peng, Chem. Eng. Sci. (2012). 10.1016/j.ces.2012.05.052.
[23] D. Winter,, J. Koschikowski,, M. Wieghaus, J. Memb. Sci. 375(1–2) (2011) 104–12. 10.1016/j.memsci.2011.03.030.
[24] A. Razmjou,, E. Arifin,, G. Dong,, J. Mansouri,, V. Chen, J. Memb. Sci. 415–416 (2012) 850–63. 10.1016/j.memsci.2012.06.004.
[25] J.A. Kharraz,, A.K. An, J. Memb. Sci. 595 (2020). 10.1016/j.memsci.2019.117596.

PGC_SCHE USM_2020_20

PVDF blended PVDF-co-HFP enhanced Membrane Hydrophobicity for Desalination of Seawater via Direct Contact Membrane Distillation (DCMD)

N.H. Mat Radzi, A.L. Ahmad*
School of Chemical Engineering, Engineering Campus, Universiti Sains Malaysia,
14300 Nibong Tebal, Pulau Pinang, Malaysia.
*E-mail: *chlatif@usm.my*

Abstract. Polyvinylidene fluoride (PVDF) blended polyvinyledene fluoride-co-hexafluoropropylene (PVDF-co-HFP) membranes were fabricated via the Double Casting Phase Inversion (DCPI) method, which consisted of a nanocomposite layer on the top while pristine membrane layer at the bottom. 0.5% ZnO nanoparticles (NPs) were loaded into the casting solution together with the PVDF and PVDF-co-HFP. The morphology of the top layer was changed when ZnO NPs and PVDF-co-HFP were loaded, which was more rigid, porous, and sponge-like. The blending of the PVDF-co-HFP in the nanocomposite layer increased the water contact angle, which was from 135° to 146°. Moreover, the liquid entry pressure of water (LEPw) for the DL membrane with top layer consist of PVDF-co-HFP blended PVDF/ZnO membrane was 1 bar. Furthermore, the presence of PVDF-co-HFP also improve membrane porosity and reduced the pore size. The efficiency of the fabricated double-layer membranes for the membrane distillation (MD) was evaluated by using the Direct Contact Membrane Distillation (DCMD) unit. The desalination of saltwater was undergone for 6 hours of operation. The optimal membrane maintained a stable flux of 9.41 L/m^{2}h and 99% salt rejection and has anti-fouling properties.
Keywords: *Double-layer membrane, hydrophobic, desalination*

INTRODUCTION

Clean and high quality of water is very essential to all living things. Seawater is one of the vast water resources that can be treated to produce a high quality of water and can be used in daily life. One of the methods for seawater treatment that arises nowadays is the membrane distillation (MD) process. MD is a thermally-driven process, where a hydrophobic microporous membrane is used as the barrier to separate the volatile compound of the hot feed and then condensed in the cold permeate [1], [2]. Direct Contact Membrane Distillation (DCMD) is one of the configurations in MD, whereby hot liquid stream on the feed side, while cold liquid stream on the permeate side. The temperature difference in the feed and permeate stream creates a vapour pressure gradient which contributed to the water vapour passes through the membrane pores [3]. The membrane for DCMD does not only require a hydrophobic surface, but also require good properties of the inner membrane's layers, including morphology, pore size, and pore size distribution [3]. Instead of using a conventional single-layer (SL) membrane, fabricating a double-layer (DL) membrane is getting the attention of the researchers. The intention of fabricating DL membrane is to locate the nanoparticles (NPs) on the top layer only, thus it can enhance the performance and rejection of the desalination process. Double casting phase inversion (DCPI) is one of the unique methods to fabricate the DL membrane [4]. The top layer of the DL membrane must be a superhydrophobic layer, whereas less hydrophobic or hydrophilic layer for the bottom layer [3], [5]. It is to accelerate the water vapour movement and indirectly enhance the flux performance of the DCMD process [5]. However, the incorporation of the NPs on the top layer may weaken the mechanical properties of the membrane [6]. Therefore, in this study, the PVDF-co-HFP was blended with PVDF to improve the membrane's strength as the PVDF-co-HFP has good tensile strength and higher hydrophobicity than the PVDF. It is due to the presence of fluoropropylene (HFP) into the vinylidene fluoride (VDF) blocks [7]. The blended PVDF and PVDF-co-HFP were implemented on the top later of the DL membrane. Thus, the study on surface hydrophobicity and flux performance enhancement were evaluated.

MATERIALS AND METHODS

Two casting solutions were prepared, Solution A (without nanoparticles) and Solution B (with ZnO nanoparticles and blended with PVDF: PVDF-co-HFP (7:3)). The composition of each solution was presented in Table 1. The solutions were cast twice, begin with solution A with thickness 350 µm and then Solution B was cast in duration 30s with gap clearance 50 µm [3], [4]. Then, the cast membrane was immersed in non-solvent ethanol for 20 minutes before immersing in distilled water for 24 hours. After that, the membrane was dried at room temperature before further analysis. The hydrophobicity of the membranes was measured by water contact angle measurement through a sessile drop method by a goniometer (Rame-Hart 250-FI, USA) instrument. A syringe pump was used to drop 6µL of deionised (DI) water on different points of the membrane and the water contact angle was recorded. Moreover, further analysis of membrane hydrophobicity was analysed based on the liquid entry pressure of water (LEPw) and pore size

distribution using a porometer (Porolux 1000, Benelux Scientific, Belgium). DI water was filled up on the membrane surface and the pressure needed for DI water to penetrate the biggest pore size was recorded, while the membrane pore size distribution was analysed by immersing the membrane in porefil (pore wetting agent) and then results were recorded. Furthermore, the efficiency of the membranes in membrane distillation (MD) was analysed by using the Direct Contact Membrane Distillation (DCMD) lab-scale unit. The MD process for desalination of seawater was undergone for 6 hours of operation and the flux performance was recorded every hour as well as seawater conductivity.

Table 1. Dope solutions composition

Dope solution	Membranes	PVDF (wt%)	PVDF-HFP (wt%)	ZnO (wt%)	NMP (wt%)
(Solution A) as bottom layer	-	17	-	-	83
(Solution B) as top layer	D	17	-	0.5	82.5
	DB	11.9	5.1	0.5	82.5
*Solution B for single layer	S	17	-	0.5	82.5

RESULTS AND DISCUSSION

Effects of fabricating double-layer membrane on the water contact angle, liquid entry pressure of water (LEPw), porosity, and pore size were shown in Table 2. The hydrophobicity of the fabricated membranes was improved slightly when the DCPI method was implemented, which is from 135° to 139° for membrane S and D, respectively. This was due to the increasing of the surface roughness of the membrane, where the NPs loading on the D membrane only located on the top layer, while for the S membrane majority of the NPs were like to locate in the middle of the membrane [6]. Furthermore, when the PVDF-co-HFP was blended in the top layer membrane, the water contact angle increases to 146° (membrane DB). This indicated that the presence of HFP at VDF bond thus helped in improving the hydrophobicity of the membrane's surface [7]. Further analysis of the membrane wettability was evaluated based on the LEPw. The LEPw result on the DB membrane was the highest, which was 1.0 bar compared to the membrane without blended with PVDF-co-HFP. However, the LEPw for membrane D was lower than the membrane DB. This is because when the DCPI method was applied, the pore size of the bottom layer was large compared to the single-layer membrane [3][8]. In addition, the pore size of the DL membrane was reduced, especially when PVDF-co-HFP was blended in the top layer, which was 0.54 μm (membrane DB). Moreover, the porosity of the membranes increased significantly as the NPs was loaded at the top layer only, which was from 70% to 86%. The porosity of the membrane D and DB did not have significant changes although PVDF-co-HFP was loaded in the top layer. The high porosity of membrane tends to achieve high flux performance.

Table 2. Water contact angle, LEPw, porosity and pore size.

Membranes	Contact angle ($\theta, °$)	LEPw (bar)	Pore size (μm)	Porosity (%)
S	135	0.69	0.95	70
D	139	0.6	0.87	87
DB	146	1.0	0.54	86

The morphology of the fabricated membrane was presented in Figure 1. It shows that the NPs located at the top layer when the DCPI method was implemented as shown in figure 1(b) (c) compared to figure 1(a). Besides that, the effect of DL membrane changed the morphology of the top and bottom layer, which can be seen in figure 1(b). The top layer was more rigid than the bottom layer, thus it can accelerate the water vapour during the DCMD process. However, when PVDF-co-HFP was blended in the top layer solution, the morphology was uniform. This could be due to the increment of the molecular weight of the polymer content on the top layer, thus affected the membrane morphology [9]. Therefore, the movement of the water vapour to pass through the membrane layer might be slow.

The desalination of the seawater via DCMD was analysed based on the fabricated membranes. The permeation flux performance for each membrane was presented in Figure 2. It was found that the flux for membrane S was the lowest compared to the other DL membrane, which was only 4.14 L/m^{2}h. This can be related to the lower porosity of the membrane. Furthermore, the permeation flux for DL membrane was high, especially for membrane D, which was 9.41 L/m^{2}h. However, when PVDF-co-HFP was blended with PVDF (membrane DB), the permeation flux was only 6.14 L/m^{2}h. This agrees with Wu et. al (2018), where the PVDF-co-HFP have lower tendency to get high flux for DCMD [7]. Although the PVDF-co-HFP was blended with PVDF, the performance flux was not higher than the membrane D. In addition, the conductivity of the permeate solution was reduced after 6 hours DCMD operation as well as the removal of salt, whereby almost 99% of salt has been removed.

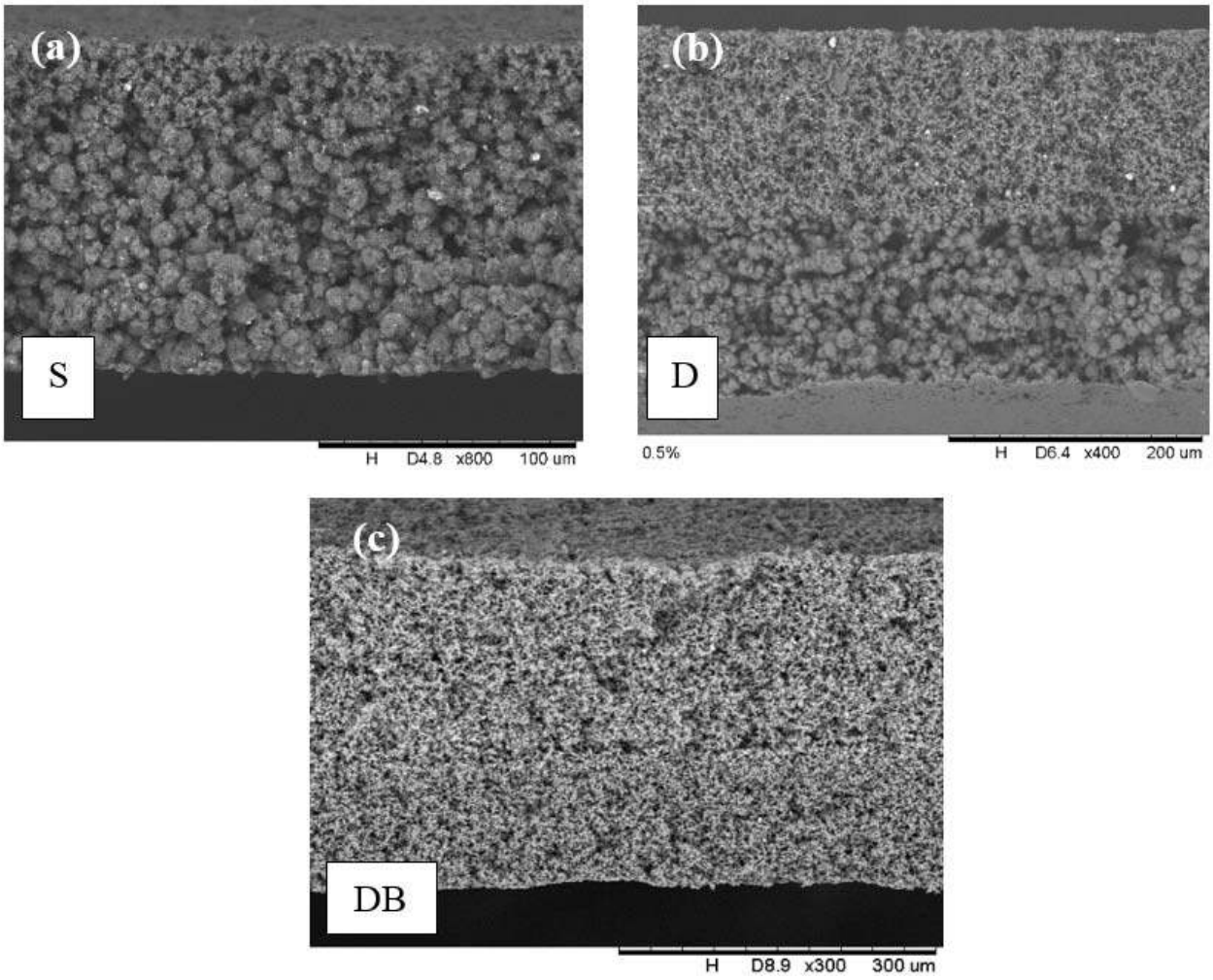

Figure 1. The SEM image of the cross-section view for the SL membrane (a) S, DL membrane (b) D, and DL membrane blended PVDF-co-HFP in the top layer (c) DB.

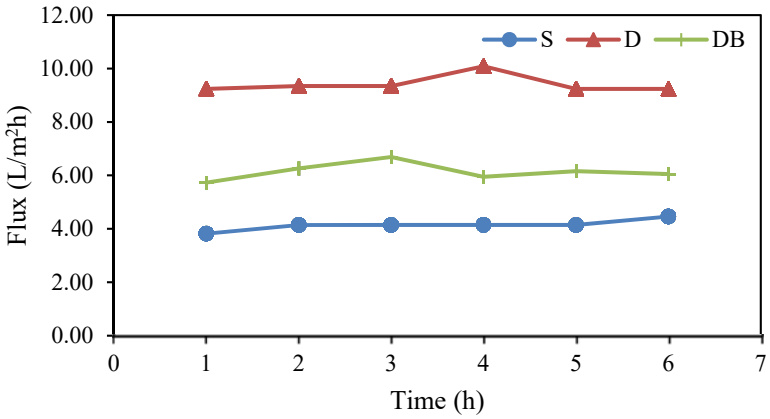

Figure 2. Permeation flux for desalination of the fabricated membrane.

CONCLUSION

In conclusion, the effect of fabricated DL membrane via DCPI method improved the membrane hydrophobicity, porosity and the flux performance in DCMD operation. The presence of PVDF-co-HFP blended with PVDF improved

the membrane hydrophobicity to 146°. However, it contributed to the reducing of the flux performance as explained by the morphology of the membrane shown in SEM images.

.

ACKNOWLEDGEMENT

The authors would like to acknowledge the Ministry of Higher Education Malaysia for providing the Trans-disciplinary Research Grant Scheme (TRGS) grant TRGS/1/2018/USM/01/5/1 and Long Term Research Grant Scheme 1/2018, LRGS (203/PJKIMIA/67215002). The authors also appreciate the financial support by Universiti Sains Malaysia under the Graduate Assistant (GA) Scheme.

REFERENCES

[1] A. Bamasag, T. Alqahtani, S. Sinha, N. Ghaffour, and P. Phelan, "Experimental investigation of a solar-heated direct contact membrane distillation system using evacuated tube collectors," *Desalination*, vol. 487, no. March, p. 114497, 2020.

[2] Q. Zhao, H. Zhang, Z. Hu, and S. Hou, "A solar driven hybrid photovoltaic module/direct contact membrane distillation system for electricity generation and water desalination," *Energy Conversion and Management*, vol. 221, no. March, pp. 113146–113161, 2020.

[3] N. H. Mat Radzi and A. L. Ahmad, "Effect of ZnO nanoparticles loading in double-layer polyvinylidene fluoride membrane for desalination via direct contact membrane distillation," *Asia-Pacific Journal of Chemical Engineering*, no. July, pp. 1–12, 2020.

[4] O. T. Mahlangu, R. Nackaerts, J. M. Thwala, B. B. Mamba, and A. R. D. Verliefde, "Hydrophilic fouling-resistant GO-ZnO/PES membranes for wastewater reclamation," *Journal of Membrane Science*, vol. 524, no. August 2016, pp. 43–55, 2017.

[5] H. Attia, D. J. Johnson, C. J. Wright, and N. Hilal, "Comparison between dual-layer (superhydrophobic – hydrophobic) and single superhydrophobic layer electrospun membranes for heavy metal recovery by air-gap membrane distillation," *Desalination*, vol. 439, no. August, pp. 31–45, 2018.

[6] Q. Xia, M. Liu, Y. Wang, and W. Xing, "Structure design and applications of dual-layer polymeric membranes," *Journal of Membrane Science*, vol. 562, no. April, pp. 85–111, 2018.

[7] P. Wu, L. Y. Jiang, and B. Hu, "Fabrication of novel PVDF/P(VDF-co-HFP) blend hollow fiber membranes for DCMD," *Journal of Membrane Science*, vol. 566, no. May, pp. 442–454, 2018.

[8] R. Roshani, F. Ardeshiri, and M. Peyravi, "Highly permeable PVDF membrane with PS/ZnO nanocomposite incorporated for distillation," *RSC Advances*, vol. 8, no. June, pp. 23499–23515, 2018.

[9] I. Ali *et al.*, "Assessment of Blend PVDF Membranes, and the Effect of Polymer Concentration and Blend Composition," *Membranes*, vol. 8, no. 1, pp. 13–31, 2018.

PGC_SCHE USM_2020_21

Single pot catalytic glycerol dehydration-oxidation: Sustainable production of acrylic acid

Anas Abdullah, Ahmad Zuhairi Abdullah*
School of Chemical Engineering, Engineering Campus, Universiti Sains Malaysia,
14300 Nibong Tebal, Pulau Pinang, Malaysia.
*E-mail: *chzuhairi@usm.my*

Abstract: The use of biomass resources in the present decade has garnered much attention. The biomass route provides an ideal alternative to eliminate the dependence on the polluting and now-renewable fossil fuel routes. Glycerol is produced as a by-product during biodiesel production. Acrylic Acid is an important chemical obtained from propylene. Acrylic acid can also be produced from glycerol. Various catalysts have been developed to study the glycerol oxydehydration process. In this review different catalysts used for the glycerol oxydehydration process are summarized. The advantages as well as the challenges associated with different catalyst types are briefly discussed.
Keywords: *Glycerol, Acrylic acid, Oxydehydration, Catalyst.*

INTRODUCTION

The dwindling availability of fossil fuels and climate change policies have led to the development and implementation of renewable energy sources. Biofuels have emerged in this scenario and have been extensively studied and developed in recent decades. Biodiesel is a replacement for fossil-derived diesel with comparable characteristics. Its production is based on transesterification of vegetable oils from various sources and generates large amounts of glycerol as a by-product [1]. Surplus supplies and the subsequent decline in prices have centred on glycerol studies to produce additives, polymers and fuels. Upgrading glycerol is a favourable way to compare biodiesel and conventional diesel gains, increase competition and the present scenario may be the perfect point for a full transition from refinery to biorefinery. The production of acrylic acid from glycerol involves the development and synthesis of suitable catalyst design. The work involves elements that bring Bronsted acid and oxidising properties to the material to directly convert glycerol into acrylic acid through oxidative dehydration in a single bed reactor. MoVWO mixed oxides, VO/zeolites, and MoVO/heteropolyacids are usually studied as catalysts, combining acidity and the oxidant property of vanadium. Recent research has identified Bronsted acidity over niobium and vanadium active sites caused by dissociative water adsorption. The need for water in the process may be helpful to add functionalities in vanadium catalytic sites for acrolein dehydration. The new method of processing glycerol-acrylic acid under development can further be divided into two kinds: a catalytic two-bed system and a catalytic one-bed system. Glycerol undergoes dehydration to acrolein in a two-bed catalytic system, accompanied by acrolein oxidation to acrylic acid or deoxy-dehydration to allyl alcohol first and subsequent acrylic acid oxidation. The catalytic two-bed system normally requires two reactors. On the other hand, one reactor is very economical. The development of the catalytic one-bed system, particularly catalysts, is difficult. The glycerol oxidation catalysts for a one-step acrylic acid must be multifunctional. In general, catalysts should have synergistic acid and redox catalytic sites. In addition, it is important to tailor the particle size, morphology, and porosity of the catalysts. Moreover, the mechanical characteristics and the lifetime of the catalysts from an engineering perspective should satisfy the need for service and profitability.

ONE BED CATALYTIC SYSTEM

The catalytic one-bed method for direct oxidation of glycerol and acrylic acid in a single reactor has been responsible for controlling the research and the reaction over the last two decades. Particular attention has been paid to it, as it is much more economical than a 2-phase reactor or 2-bed reactor operation. A single reactor is clearly advantageous for simplifying the reactor design and operation, increasing efficiency and reducing investment [2]. If only one catalyst is used, all acid sites for glycerol dehydration to acrolein and redox sites for in situ acrolein to acrylic acid oxidation should be included. Glycerol dehydration is an endothermic (Eq. 1) reaction, and acrylic oxidation is an exothermic reaction (Eq. 2). Therefore, the reactor design and configuration should use its endothermic dehydration and exothermic oxidation characteristics, to achieve a thermal equilibrium and increase energy efficiency. Various catalysts were investigated for glycerol oxydehydration to acrylic acid. Studies have indicated that V, W, Mo are typically active species for the glycerol oxydehydration. [3] The catalysts may typically be categorised as single oxide, binary oxide, ternary oxide and heteropoly acids.

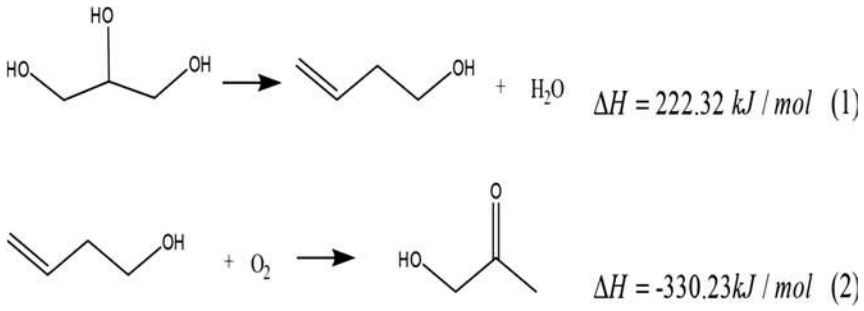

HETEROPOLYACID CATALYSTS

Heteropoly acids, which include heteropoly anions and counter cations (H+, H3O+, H5O2), are well known catalysts with very powerful Bronsted sites. Keggin unit consists of a central atom (usually P, Si, or Ge) in a tetrahedral arrangement to oxygen atoms, that is then surrounded by 12 oxygen octahedra which mainly contain tungsten or molybdenum. The unique structure shows an extremely high mobility of protons and a "pseudo-liquid step." Vanadium has been used earlier to replace Mo or W in keggin-type heteropoly acid cesium salts as catalysts for glycerol acrylic acid oxidation. The acid base and redox properties can be varied across a wide range by adjusting the composition of chemicals such as $Cs_{2.5}H_{0.5}PW_{12}O_{40}$. Li et al. [3] doped V into $H_3PMo_{12}O_{40}$ cesium salts to a achieve 60% acrylic acid yield with a complete conversion over the $H_{0.1}Cs_{2.5}(VO)_{0.2}(PMo_{12}O_{40})_{0.25}(PW_{12}O_{40})_{0.75}$ catalyst. The combined solid solutions resulted in variations in catalytic oxidation potential and surface acidity, and consequently substantial improvement in acrylic acid selectivity. The substitution of vanadium in the secondary structure of Keggintype HPCs such as CsPMo or CsPW increased the catalyst 's oxidation power and facilitate the formation of acrylic acid in the oxidation process. Suganuma et al. [4] used heteropoly acid, together with ZSM-5, for direct oxydehydration of glycerol as a bifunctional catalyst. Scattered on ZSM-5 zeolite $H_5PV_2Mo_{10}O_{40}$ and $H_6PV_3Mo_9O_{40}$ are stable. Hence, Bi-functional catalyst is the synthesis of an oxidation catalyst (heteropoly acid) and an acid catalyst (zeolite). Acrylic acid was observed at 30 selectivity % after 6 h at 350 °C. Glycerol oxidation required the weak acid catalyst and high oxidative capacity. Catalysts supported by alumina-polyoxometalates (POM support Al_2O_3) are utilised in a one-pot process for the fluid-phase conversion of glycerol to low-temperature acrylic acid (90 ° C). At 90 ° C, the maximum acrylic acid yield of 36.2% is achieved over 6% V-$H_3SiW_{12}O_{40}$ / HZSM-5 at 6 h. The kinetic studies of the one pot glycerol oxidation of this catalyst showed that the rate of glycerol conversion was based on the pseudo-first - order concentration of glycerol, just slightly on the concentration of H_2O_2 [4].

Table 1: Different catalysts studied for the glycerol oxydehydration process

Catalyst	Glycerol conversion	Acrylic acid yield (%)	Ref
Cu/ SiO_2–MnO_2	77.1	57.6	[5]
W–V–Nb–O	100	59.2	[6]
$H_{0.1}Cs_{2.5}(VO)_{0.2}(PMo_{12}O_{40})_{0.25}(PW_{12}O_{40})_{0.75}$	100	60%	[4]

COKING OF CATALYST

Although important progress has been made on the conversion of glycerol and the yield of acrylic acid in the catalytic oxydehydration of acrylic acid in a single bed method, a major challenge remains to solve catalyst disabilities. There are: (i) coking, (ii) burning, (iii) thermal degradation, and (iv) attrition / crushing the causes for catalyst deactivation. Coking is the main factor leading to deactivation of the catalyst for oxidation of glycerol. Moreover, coking is normally thought to occur primarily during the dehydration process of glycerol. According to the studies reported in the literature, coking of the abovementioned catalysts cannot be completely avoided. In the aspects of catalysts, some methods, including doping catalysts with many more metallic elements or adjusting the surface acidity and pore structure of the solid catalysts, have been proposed for coking inhibition. In addition, in view of the reaction conditions, increasing water concentration, feeding oxygen, and adjusting reaction temperature has proven to mitigate coking. Fig. 1 shows the mechanism of coking and regeneration of the catalyst.

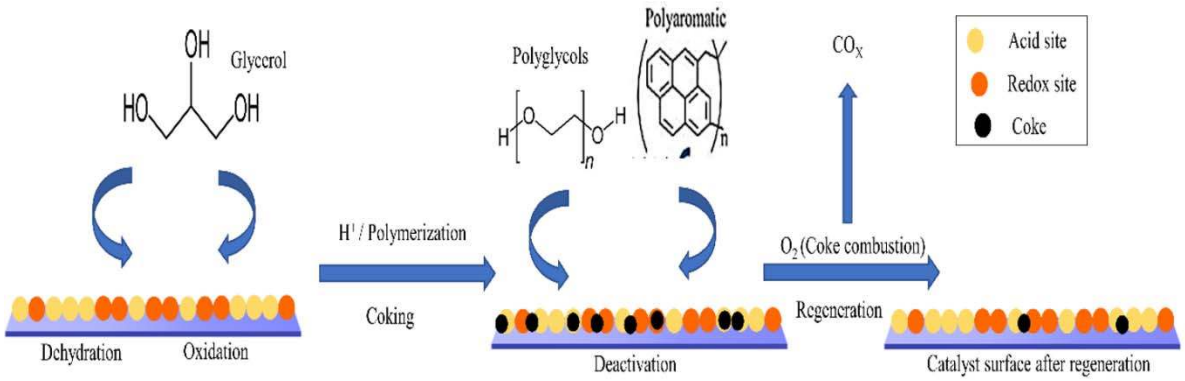

Figure 1. Mechanism of coke formation and regeneration of the catalyst

CONCLUSION

In summary, while the conversion of glycerol into acrylic acid is attractive and progress has been made in a single reactor, there are still various difficulties and challenges in further investigations. In most papers, studies are focused on continuous steaming processes, with many advantages in industrial applications. Unlike the vapor-phase process the fluid-phase process can be carried out at lower temperatures, whereas acrylic acid is subject to low selectivity or organic limitations. In vapor-phase reactions, since the feed of O_2 is successful to inhibit the catalytic deactivity of glycerol dehydration in an acrolein, hence, the one-stage oxidative dehydration of glycerol to acrylic acid in an O_2-containing flow in order to inhibit the catalytic deactivation is advantageous. It is also conceivable that the intermediate acrolein can be converted to acrylic acid immediately in one-step before it participates in coke formation, but there is not enough proof of this hypothesis. The idea to dehydrate glycerol in a single bed vapor phase to acrylic acid centres on the preparation of catalysts capable of both glycerol dehydration and acrolein oxidation through acrylic acid. Vanadium and molybdenum are generally used as an effective component for different oxidation reactions in most efficient catalysts. MoVO and MoVWO catalysts for acrolein oxidation to acrylic acid have shown good results. Catalysts for the oxidative dehydration of one-bed glycerol are therefore usually a mixture of vanadium and / or molybdenum with acid catalysts like WOx, zeolites and heteropolyacids. So far, Heteropolyacids have shown the highest yield among all the reported catalysts. The problem is however that the two sorts of components with separate roles usually engage not only in the continuous dehydration of glycerol and acrolein oxidation, but also in unpredictable reactions like glycerol condensation. As a result, acrylic acid selectivities in most studies were poor. The stacked catalyst method, on the other hand, is beneficial for the continuing oxidative dehydration of glycerol into acrylic acid. However, since there are two forms of reactions under uniform conditions of reaction, both the top and bottom layer catalysts should be active. Hence, if problems like catalyst deactivation, low acrylic acid yield and reusability of the catalyst can be addressed, the dehydration-oxidation of glycerol to acrylic acid will be the renewable, green industrial process.

ACKNOWLEDGEMENT

The authors greatly acknowledge USM for the financial support (RUI grant 8014059) to this work.

REFERENCES

[1] R. Sindhu, P. Binod, A. Pandey, S. Ankaram, Y. Duan, and M. K. Awasthi, *Biofuel Production From Biomass*. Elsevier B.V., 2019.

[2] M. B. dos Santos, H. M. C. Andrade, and A. J. S. Mascarenhas, "Oxidative dehydration of glycerol over alternative H,Fe-MCM-22 catalysts: Sustainable production of acrylic acid," *Microporous Mesoporous Mater.*, vol. 278, no. January, pp. 366–377, 2019.

[3] A. Chieregato *et al.*, "Structure–Reactivity Correlations in Vanadium-Containing Catalysts for One-Pot Glycerol Oxidehydration to Acrylic Acid," *ChemSusChem*, vol. 10, no. 1, pp. 234–244, 2017.

[4] X. Li and Y. Zhang, "Oxidative Dehydration of Glycerol to Acrylic Acid over Vanadium-Substituted Cesium Salts of Keggin-Type Heteropolyacids," *ACS Catal.*, vol. 6, no. 5, pp. 2785–2791, 2016.

[5] B. Sarkar, C. Pendem, L. N. Sivakumar Konathala, R. Tiwari, T. Sasaki, and R. Bal, "Cu nanoclusters supported on nanocrystalline SiO2-MnO 2: A bifunctional catalyst for the one-step conversion of glycerol to acrylic acid," *Chem. Commun.*, vol. 50, no. 68, pp. 9707–9710, 2014.

[6] K. Omata, K. Matsumoto, T. Murayama, and W. Ueda, "Direct oxidative transformation of glycerol to acrylic acid over Nb-based complex metal oxide catalysts," *Catal. Today*, vol. 259, pp. 205–212, 2016.

PGC_SCHE USM_2020_22

Adhesion of Cylindrotheca *fusiformis* on Polyethersulfone Tubular Capillary Membrane in Suspended Culture System

Siti Mariam Md Poad, Derek Chan Juinn Chieh*
School of Chemical Engineering, Engineering Campus, Universiti Sains Malaysia,
14300 Nibong Tebal, Pulau Pinang, Malaysia.
*E-mail: *chderekchan@usm.my*

Abstract. Microalgae has received increasing interest as valuable feedstock for biofuels and biobased product. As the conventional microalgae cultivation system can be very costly, alternative methods which use solid or semi-solid materials has gained focus as it offers more benefits over the current conventional system. Thus, this study was intended to study the adhesion of microalgae cells onto the surface of solid material. Cylindrotheca *fusiformis* was used to study the capability of polyethersulfone (PES) capillary membrane as materials for microalgae cultivation system. The adhesion of microalgae onto the membrane surface was identified using dry weight determination and microscopic imaging. The result obtained showed positive result and may help in future microalgae cultivation system.
Keywords: Microalgae, tubular capillary membrane

INTRODUCTION

Microalgae are currently considered as a promising feedstock for biofuels and other biobased products. Apart from the low competition with food industry as microalgae is not a common source of food, it can also be cultivated and harvested irrespectively of the season and microalgae can grow without using wide fertile land [1], [2]. To date, the microalgae are cultivated and maintained in liquid suspensions are commonly operated in open ponds and in various design of closed photobioreactors [2].

Natural waters and artificial pond are categorized as open ponds are easier and less expensive to build and operate, and more durable than closed system [3], [4]. Closed photobioreactors refers to a closed system which having no direct gas exchange and contaminants with the environments [4]. However, these two system have drawbacks such as risk of contamination, lower biomass productivity caused by inefficient stirring as well as the increase of operational cost and operational cost by the needs of mixing and aerating [5][6]. To cater the problem from suspension cultivation methods, the usage of solid or semi-solid materials as an alternative has received increasing interest [7]. This type of cultivation methods offer benefits such as less water and space required and the contamination can be controlled [2], [8]. In this study, a tubular capillary membrane was used to study the adhesion of microalgae cells onto its surface.

MATERIALS AND METHODS

The benthic species, Cylindrotheca *fusiformis* (UTEX 2085) purchased from UTEX culture collection of algae, University of Texas at Austin was sub-cultured in artificial sea water enriched with f/2 Medium. The medium was sterilized by autoclaving at 121 °C for 15 min prior to use. The microalgae strains were maintained under photoautotrophic system, kept at 25°C ± 2°C and placed under cool-white fluorescent lamp with a 12 h:12 h light/dark cycle with an average light intensity of 1500 lux. The polyethersulfone (PES) capillary membrane was purchased from 3M Company to study its ability in microalgae cultivation. The membrane is hydrophilic with the wall thickness of 100 ± 25 µm and a maximum pore size of 0.5 ± 0.1 µm.

Figure 1 showed the setup of the experiment which consist of 250 ml flask filled with 200 ml of f/2 medium and 3 strings of capillary membrane each having approximately 27 cm of length. Then 10 ml of cell culture with an initial dry weight of 0.03 ± 0.01 g was poured inside the flask. One end of each membrane was kept outside the flask to provide aeration before the flask was covered with cotton and aluminium foil. The experimental temperature was kept at 25°C ± 2°C and maintained under cool-white fluorescent lamp with a 12 h:12 h light/dark cycle with an average light intensity of 1500 lux. The experiment was done in triplicate. After 7 days, the capillary membranes were removed from the flask and washed with distilled water to remove all soluble nutrients from the microalgae culture. The capillary membranes were then dried at 60°C overnight. The attachment of Cylindrotheca *fusiformis* on the surface of the membrane was evaluated by determining the dry weight using an analytical scale after it was cooled in a desiccator. The image of the capillary membrane was microscopically observed at 4.5x to observe the attachment of the cells on the surface of the membrane.

Figure 1: Setup of the experiment

RESULTS AND DISCUSSION

Table 1 display the result on the dry weight obtained after 7 days of cultivation. The dry weight obtained is 0.0026 ± 0001 g, which indicates that without initial inoculation directly on the surface of the membrane, a part of the microalgae cells was able to adhere on the surface of the membrane. The initial adhesion of the cells to the surface of the membrane may occur at the beginning of the experiment when the suspension culture was poured inside the flask by gravitational forces or hydrodynamic forces [9]. Figure 2 display the images of the pristine capillary membrane and the capillary membrane after the experiment with cell on its surface under microscopic view at 4.5x magnification. The image b) c) d) was taken from different section of a membrane and it showed that there is the presence of cells on the surface of the membrane. However, the microalgae cells attachment and the thickness are not uniform along with the membrane.

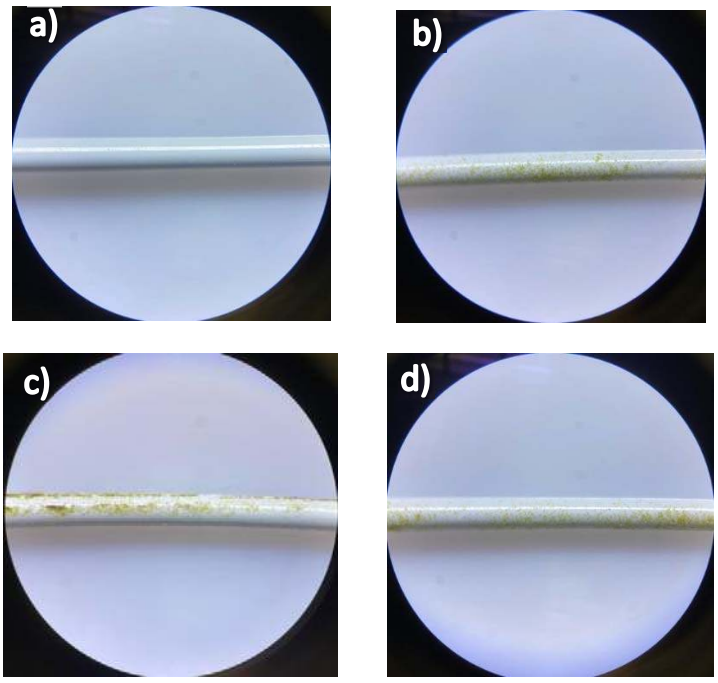

Figure 2. The image of the capillary membrane under microscope at 4.5x magnification. a) The image of a pristine capillary membrane before the experiment. b), c), d) The image of the capillary membrane with cells after the experiment at different section.

Table 1. Final dry weight result obtained on the adhesion of Cylindrotheca fusiformis on the surface of PES capillary membrane.

Flask	Dried Cell (g)	Average weight of dried cells (g)
1	0.0036	
2	0.0024	0.0026
3	0.0019	

CONCLUSION

A simple setup was done to study the adhesion of Cylindrotheca *fusiformis* onto the surface of PES capillary membrane. Both dry weight result and microscopic view showed positive result which indicated that the microalgae cells were adhered onto the surface of the membrane with a different degree of attachment.

ACKNOWLEDGEMENT

This research is funded under the Research University grant no. 1001/PJKIMIA/8014065.

REFERENCES

[1] Y. Sano and A. Horibe, "Microalgal Culture for Chlorella sp. using a Hollow Fiber Membrane Module," *J. Membr. Sci. Technol.*, vol. 06, no. 01, pp. 1–6, 2016.

[2] T. Liu, J. Wang, Q. Hu, P. Cheng, B. Ji, J, Liu, Y. Chen, W. Zhang, X. Chen, L. Chen, L. Gao C Ji. and H. Wang, "Attached cultivation technology of microalgae for efficient biomass feedstock production," *Bioresour. Technol.*, vol. 127, no. April, pp. 216–222, 2013.

[3] G. C. Zittelli, N. Biondi, L. Rodolfi, and M. R. Tredici, "Photobioreactors for Mass Production of Microalgae," in *Handbook of Microalgal Culture*, Wiley-Blackwell, 2013, pp. 225–266.

[4] R. N. Singh and S. Sharma, "Development of suitable photobioreactor for algae production - A review," *Renew. Sustain. Energy Rev.*, vol. 16, no. 4, pp. 2347–2353, 2012.

[5] H. Hamano, S. Nakamura, J. Hayakawa, H. Miyashita, and S. Harayama, "Biofilm-based photobioreactor absorbing water and nutrients by capillary action," *Bioresour. Technol.*, vol. 223, pp. 307–311, 2017.

[6] P. L. Gupta, S. M. Lee, and H. J. Choi, "A mini review: photobioreactors for large scale algal cultivation," *World J. Microbiol. Biotechnol.*, vol. 31, no. 9, pp. 1409–1417, 2015.

[7] J. Wang, W. Liu, and T. Liu, "Biofilm based attached cultivation technology for microalgal biorefineries—A review," *Bioresour. Technol.*, vol. 244, pp. 1245–1253, 2017.

[8] L. Zhuang, D. Yu, J. Zhang, F. Liu, Y. Wu, and T. Zhang, "The characteristics and in fl uencing factors of the attached microalgae cultivation : A review," vol. 94, no. May, pp. 1110–1119, 2018.

[9] J. H. Wang, L. L. Zhuang, X. Q. Xu, V. M. Deantes-Espinosa, X. X. Wang, and H. Y. Hu, "Microalgal attachment and attached systems for biomass production and wastewater treatment," *Renew. Sustain. Energy Rev.*, vol. 92, no. May, pp. 331–342, 2018.

PGC_SCHE USM_2020_23

Anti-wetting properties of synthesis hydrophobic membrane by incorporation of clay particles for direct contact membrane distillation (DCMD)

Wan Aisyah Fadilah Wae AbdulKadir, Abdul Latif Ahmad*, Ooi Boon Seng
School of Chemical Engineering, Engineering Campus, Universiti Sains Malaysia,
14300 Nibong Tebal Penang, Malaysia
E-mail: *chlatif@usm.my*

Abstract. Wetting resistance of membrane surface has been broadly investigated for hydrophobic membrane. Recently, it is widely studied to meet the requirement of membrane distillation (MD). In this study, two different clay particles – montmorillonite (MMT) and halloysite nanotube (HNT) were used after wax functionalization – in fabrication of polyvinylidene fluoride (PVDF) MD membrane. Membrane with HNT obtained higher contact angle of 137º compared to membrane with MMT (122º). In direct contact membrane distillation (DCMD) process, the addition of HNT particles in the PVDF membrane not only improved the contact angle but also achieved the highest water flux and seawater permeate flux of 11.63 L/m^{2}h and 7.30 L/m^{2}h, respectively. This membrane showed a respectable reusability of water vapor flux after 16 h usage (8 h water and 8 h real seawater) with 99.9% salt rejection. The incorporation of HNT decreased its liquid entry pressure (LEP) from 3.10 bar to 2.69 bar while adding MMT improved up to 4.04 bar. This study suggests that the applicable anti-wetting properties for long-term MD operation should consider higher LEP (>1 bar) for DCMD.
Keywords: *Anti-wetting, hydrophobic membrane, clay, DCMD*

INTRODUCTION

Anti-wetting properties is a crucial factor for the development of hydrophobic membrane, particularly in membrane distillation (MD). In this process, hydrophobicity of the membrane plays an important role to ensure only water vapor molecules penetrate the pores [1]. The MD membranes have to meet several requirements including hydrophobic, thin, small pore size (0.1 to 0.5 µm), highly porous, low surface energy of membrane surface (high contact angle), high liquid entry pressure (LEP), high permeability and applicable for long term performance, respectively [2]. Among these requirement, LEP is a critical property to determine the ability of continuous long permeation in MD process. Therefore, two types of clay particles, montmorillonite (MMT) and halloysite nanotube (HNT) were utilized in this work to be improved into an effective hydrophobic membrane for desalination by the most simplest process of direct contact membrane distillation (DCMD). This effort not only provide an alternative pathway to produce reusable water sources but also help in developing cost-effective membranes. Since addition of nanoparticles into the membrane matrix offered an efficient way to achieve more effective antifouling membrane, clays particles, specifically with silicates layer have ability of being dispersed into polymeric matrices at nanoscale [3]. Thus, this present work was aimed to study the effect of functionalized MMT and HNT on the anti-wetting properties of the developed hydrophobic polyvinylidene fluoride (PVDF) membrane. The selected anti-wetting properties measurements (e.g. contact angle, LEP, porosity,morphology) of the membranes were investigated to establish the correlation with the membrane performance efficiency.

MATERIAL AND METHODS

Functionalization of MMT and HNT particles

MMT and HNT powders were functionalized with carnauba wax. The carnauba wax was added in N-hexane and heated at 85 ºC until well-dissolved. A specific amount of MMT was added in 5 wt.% wax solution and continuously stirred for 24 h at ambient temperature. Then, the functionalized MMT was filtered and annealed in a vacuum oven at 100 ºC for 1 h. The similar process was carried out for HNT powder.

Membrane preparation

Fabrication of hydrophobic membranes was carried out using triethyl phosphate (TEP) as solvent, polyvinylidene fluoride (PVDF) polymer and functionalized clays, f-MMT and f-HNT, respectively. PVDF polymer was added in TEP at 70 ºC under constant stirring until obtained homogeneous solution. Meanwhile, the f-MMT particles was sonicated at 40 ºC for 2 h. After PVDF solution was well-dissolved, the sonicated f-MMT was put in the homogenous PVDF solution and kept stirring for 24 h. The PVDF/f-MMT dope solution was degassed for 1 h and left at ambient temperature for another 30 min to avoid the presence of air bubbles within the solution. Then, the dope solution was casted with 500 µm of thin film applicator onto a glass plate. The immersion precipitation process was carried out in pure methanol for 15 min after 30 s of air exposure and continued in water bath of 20 – 25 ºC for 24 h.

The fabricated membrane was dried via dual-drying method to reduce shrinkage of PVDF/f-MMT membrane. Similar fabrication process was carried out for PVDF/f-HNT membrane.

Membrane characterization

Pore size and water liquid entry pressure (LEP_w) were measured by Porolux 1000 porometer (Benelux Scientific, Belgium). To measure pore size, membrane was fully wetted by porefil solution and placed in the 20 cm sample holder. Then, nitrogen gas was flowed in the chamber until it recorded the reading. For LEP_w measurement, non-wetted membrane was placed in the same holder filled with deionized water and flowed the nitrogen gas in the chamber. The first flow of the water penetrated the pore was obtained as the LEPw reading.

The porosity of membranes (ε_m) was carried out using porefil. The membrane was immersed in porefil for 1 h and dried in the oven for 24 h. The porefil density is 1.87 g/cm^3 and D_p is the PVDF polymer density of 1.78 g/cm^3. Contact angle was measured by sessile drop method using goniometer (Rame-Hart 250 F-1, USA). A 6 µL of water droplet was dropped with micro-syringe on different area of the membrane surface and the readings were recorded. A hydrophobic surface should obtain a contact angle more than 90º. Membrane morphology was characterized using scanning electron microscope (SEM, HITACHI S-3000N, Hitachi Ltd. Japan). The membranes were first fractured in liquid nitrogen and coated by gold. Both surface and cross section of each membranes were analyzed.

DCMD performance test

Performance test for each membrane was studied using DCMD process. The water flow rates were adjusted to 4 GPH using peristaltic pump on the hot side (feed) and centrifugal pump on the cold side (permeate). Distilled water was heated at 70 ºC and circulated to crossflow membrane module with effective area of 47.5 cm^2. After penetration of water vapor at the cold side of 20 ºC, the condensation of water vapor caused the formation of water droplet and flowed to the cold tank as a clean permeate. The continuous DCMD process was run for 8 h. The same piece of membrane was used for real aquaculture seawater sample for another 8 h after drying in several days. The permeate weight was recorded in the computer and measured the conductivity of permeate after 8 h. The flux permeation and salt rejection were calculated by Eq. 1.

$$J = \frac{\Delta W}{A.\Delta t} \quad (1)$$

where J is the flux in L/m^{2}h, ΔW is the weight of permeate (L), A is the effective area of membrane (m^2) and Δt is the time (h).

RESULTS AND DISCUSSION

Effect of functionalized MMT and HNT on anti-wetting properties

The effect of different types of clay particles on the anti-wetting properties for the fabricated PVDF membranes were characterized using several types of analyzer to identify the possible wetting resistance of each membranes as shown in Table 1. From the contact angle measurement, the incorporation of f-HNT in PVDF membrane showed a significant improvement on the membrane surface. It achieved the highest contact angle of 137˚.

Table 1. Anti-wetting properties of the fabricated PVDF membranes

Membrane	Contact angle (˚)	LEP_w (bar)	Mean pore size (µm)	Porosity (%)	Thickness (µm)
PVDF	112	3.10	0.21	87	217
PVDF/f-MMT	122	4.04	0.16	82	215
PVDF/f-HNT	137	2.69	0.14	85	245

The presence of f-HNT in the polymer matrices encouraged the formation of lower surface energy of membrane surface compared to f-MMT. It might be due to the well-dispersion of nanomaterial (HNT) in the polymer matrix, which lead to the change of membrane pores size. The introduction of f-HNT in the polymer matrix proved an ability to form a smaller inner pore size with LEP of 2.69 bar compared to f-MMT. Even though, the pore size between both fillers shows insignificant difference, PVDF/f-HNT membrane still able to obtain higher surface porosity than PVDF/f-MMT membrane. This was suggested due to the unstacked nanotubes structure that caused a well-dispersion of HNT to single particles compared to the platy montmorillonite particles [4]. The structure of clay particles induced different behavior of prepared membranes, which affected their structure and morphology. The unstacked nanotubes particles might facilitate the acceleration of solvent and non-solvent exchange during phase inversion process even it has thicker membrane layer compared to platy montmorillonite membrane. Moreover, the addition of f-MMT experienced a slight decrease in surface porosity which might be due to the agglomeration and the

small size of pore, which clarified in previous study of 5 wt% MMT in hollow fiber PVDF membrane [5]. Among the anti-wetting properties of prepared membranes, PVDF/f-HNT membrane shows applicable properties to meet the requirement of MD membrane. The performance test was proved to achieve a good performance compared to other prepared membranes.

Flux permeation and salt rejection of the fabricated PVDF membranes

The performance of pristine PVDF, PVDF/f-MMT and PVDF/f-HNT membranes were carried out for water and real aquaculture seawater. Although the incorporation of f-HNT increased the membrane thickness, both water and seawater permeate flux of PVDF/f-HNT membrane were 11.63 L/m^{2}h and 7.30 L/m^{2}h, which is the highest and most consistence fluxes within 16 h runs. The remarkable result of f-HNT in polymer matrix might be due to the different surface chemistry at the inner and outer sides of the nanotubes particles. The dielectric characteristic of carnauba wax, which carries permanently both positive and negative charges [6] surrounded on incorporated HNT might facilitate the water vapor permeation of PVDF/f-HNT membrane during DCMD process. Additionally, this PVDF/f-HNT membrane might form a complex electrostatic surface due to the implication of unique HNT structure and dielectric characteristic of carnauba wax and caused high water vapor permeation. However, the permeate flux shows a slight reduction compared to water flux as real seawater contains numerous types of molecules, which could block the surface pores of PVDF/f-HNT membrane. Hence, reduced the permeation rate of water vapor. A different flux behaviour was shown for pristine PVDF membrane after running with real seawater. The permeate flux was not consistence compared to other prepared membranes with clays. This phenomenon could be suggested due to unstable structure of pristine PVDF membrane, which required more time to achieve consistency in flux permeation. Therefore, the introduction of clays as filler in PVDF membrane matrix has proved to enhance their ant-wetting resistance with applicable flux permeation.

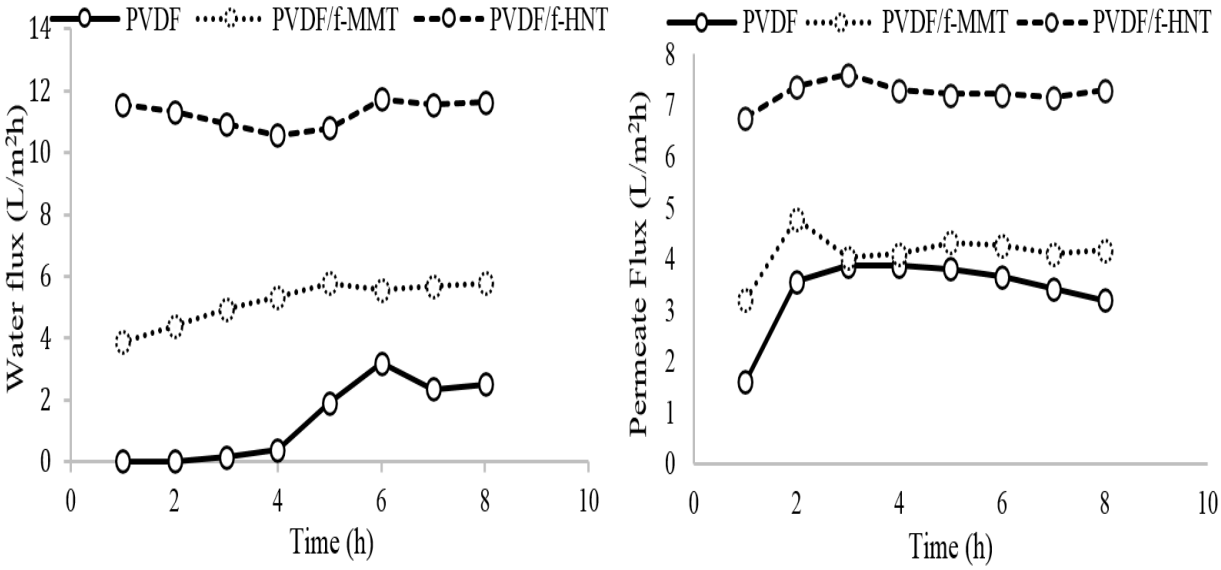

Figure 1. Flux permeation of fabricated PVDF membranes for water and real aquaculture seawater sample

CONCLUSION

In the present study, the effect of the different clay particles on the prepared membranes of both f-MMT and f-HNT were examined. The incorporation of f-HNT was found to be the potential filler for hydrophobic membrane, particularly in MD due to the hydrophobicity, small pores, high porosity and gave a positive effect on both water and permeate fluxes. Besides, it obtained a good consistency of flux permeation throughout 16 h. In contrast, contact angle of f-MMT is less twice the contact angle of pristine PVDF membrane compared to f-HNT. The contact angle contributed to a better water vapor permeation while withstanding longer DCMD operation as LEP of this membrane met the MD requirement. On top of that, this PVDF/f-HNT membrane also presents a slightly higher removal efficiency as compared to the PVDF/f-MMT membrane. In summary, the introduction of fillers is necessary to improve anti-wetting properties as both fillers could transform the PVDF membrane into an efficient MD membrane for desalination of real aquaculture seawater. Each of the fillers offered different impacts on the anti-wetting properties depending on the interaction between PVDF matrix and functionalized fillers, which significantly contributed to the removal efficiency of salt in the DCMD process.

ACKNOWLEDGMENT

The authors gratefully acknowledge the financial support received from the Ministry of Education (MOE) of Malaysia, TRGS (203.PJKIMIA.67612001) as well as LRGS (203/PJKIMIA/67215002) throughout this study.

REFERENCES

[1] J. A. Prince, D. Rana, G. Singh, T. Matsuura, T. J. Kai, and T. S. Shanmugasundaram, "Effect of hydrophobic surface modifying macromolecules on differently produced PVDF membranes for direct contact membrane distillation," *Chem. Eng. J.*, vol. 242, pp. 387–396, 2014, doi: 10.1016/j.cej.2013.11.039.

[2] M. M. A. Shirazi and A. Kargari, "A review on applications of membrane distillation (MD) process for wastewater treatment," *J. Membr. Sci. Res.*, vol. 1, pp. 101–112, 2015.

[3] H. Rajabi, N. Ghaemi, S. S. Madaeni, P. Daraei, M. Ali, and M. Falsafi, "Nanoclay embedded mixed matrix PVDF nanocomposite membrane: Preparation, characterization and biofouling resistance," *Appl. Surf. Sci.*, vol. 313, pp. 207–214, 2014, doi: 10.1016/j.apsusc.2014.05.185.

[4] Y. Lvov and E. Abdullayev, "Functional polymer-clay nanotube composites with sustained release of chemical agents," *Progress in Polymer Science*, vol. 38, no. 10–11. pp. 1690–1719, 2013, doi: 10.1016/j.progpolymsci.2013.05.009.

[5] M. Rezaei, A. F. Ismail, S. A. Hashemifard, and T. Matsuura, "Preparation and characterization of PVDF-montmorillonite mixed matrix hollow fiber membrane for gas-liquid contacting process," *Chem. Eng. Res. Des.*, vol. 92, no. 11, pp. 2449–2460, 2014, doi: 10.1016/j.cherd.2014.02.019.

[6] E. R. Muniz *et al.*, "Carnauba wax enhances the insecticidal activity of entomopathogenic fungi against the blowfly Lucilia sericata (Diptera: Calliphoridae)," *Journal of Invertebrate Pathology*, vol. 174. 2020, doi: 10.1016/j.jip.2020.107391.

PGC_SCHE USM_2020_24

Thermal Effect on Algae, Biofilm and Their Composition towards Membrane Distillation Unit

Yin Sim Ng, Derek Juinn Chieh Chan*
School of Chemical Engineering, Engineering Campus, Universiti Sains Malaysia,
14300 Nibong Tebal, Pulau Pinang, Malaysia.
*E-mail: *chderekchan@usm.my*

Abstract. Membrane distillation has lower operating temperature and potential to recycle waste heat for desalination, catching much attention of the researchers in the recent years. However, the biofouling is still a challenging hurdle to be overcome for the applications. Membrane distillation is a thermally driven separation, so the increase of temperature in the seawater feed could influence the extent of biofouling on the unit parts. In this review, we present the effect of temperature on algal growth, the range of temperature the microbes, marine algae and planktons are able to survive, and the changes to those planktons once it has exceeded the critical temperature. Thermal effect on the biofilm, its composition and properties are discussed as well, with association of the biofilm secreting microbes, but the study related to membrane distillation unit seems to be lacking. Characterizations of the algae, biofilm and EPS that govern biofouling are summarized. This information not only will help in designing future studies to fill up the knowledge gaps in biofouling of membrane distillation, but also to some extent, assist in pointing out possible fouling factors and predicting the degree of biofouling in the membrane distillation unit.
Keywords: *Heat; Algae; Membrane distillation.*

INTRODUCTION

Membrane distillation is an attractive technology for desalination since it offers lower operating pressure than the pressure driven membranes and lower operating temperature compared to conventional distillation. It can also couple with solar energy for treating saline water and further lowers the energy requirement. However, biofouling could happen in the membrane distillation unit since their parts are contacted with the seawater. It has been causing significant problems to various sectors. It is the accumulation of a colony of microorganisms and other living things with the biofilms on the surface that can reduce the functionality and impede normal operation of the system. Biofilms are microbial secretion when microbes encounter environmental stress, in which they have evolved and cooperate to improve their chances of survival. It allows them to grow and thrive under challenging conditions as in marine environment. By adhering their cells to the developing biofilm or specifically extracellular polymeric substances (EPS) forming communities, the microbes are protected against temperature and pH fluctuations, UV exposure, changes in salinity, depletion of nutrients, antimicrobial compounds, and predation. Some symbiosis is also shown between the autotropic cells and heterotrophic cells in the biofilms. The strategy of survival has led to their success in the marine habitat and colonization on nearly all man-made surfaces in contact with seawater [1]. However, humans treat the biofilm and the nuisance it caused as biofouling. Biofouling has been causing problems to mariculture, desalination, medical, shipping and power sectors which incurs significant economic impact and loss, and in some other case, leading to possible health risks.

TYPICAL TEMPERATURE FOR MEMBRANE DISTILLATION

Typical temperature for membrane distillation is 30-60^{o}C [2], 60-85 ^{o}C in Gryta [3] study, 60-80 ^{o}C for a desalination solar-driven membrane distillation plant [4]. Alkhudhiri, Darwish [5] summarized the temperature studied in the available researches are from 5 to 80 ^{o}C. So, typical working temperature should fall between the range of 30 - 85 ^{o}C. This temperature range would have significant effect on the algal and microbial growth and composition, biofilm secretion and biofouling formation in the membrane distillation unit.

CATEGORY OF MICROBES

Microbes can be roughly categorized into psychrophile, mesophile, thermophile and hyperthermophile, according to their temperature requirement for growth. Psychrophiles are microorganisms that can grow at 0 °C and below, have an optimum growth temperature close to 15 °C, and usually do not survive at temperatures above 20 °C. Mesophiles (“middle loving”) are adapted to moderate temperatures, with optimal growth temperatures ranging from temperature about 20 - 45 °C.

Organisms that grow optimally from temperatures of 50 °C to 80 °C, are called thermophiles ("heat loving"). They do not multiply at room temperature. Thermophiles are widely distributed in hot springs, geothermal soils, and garden compost piles. (eg. *Thermus aquaticus* and *Geobacillus* sp.). Beyond 80 °C to a maximum of 110 °C, the organisms are considered as hyperthermophiles, with some extreme examples that survive temperatures above 121 °C (autoclave temperature). Microbes isolated from extreme environment surrounding the hydrothermal vents at the bottom of the ocean, with temperature up to 340 °C, could achieve optimal growth at temperatures higher than 100 °C. The examples are *Pyrobolus* and *Pyrodictium*, archaea that grow at 105 °C and survive autoclaving.

Thermophilic algae and fungi can tolerate about 60 °C, and eubacteria about 70 °C. But by far the most extreme thermophiles are among the archaea; the current record is held by a species known as 'strain 121', also a hydrothermal vent species, which grows at 121 °C and survives 131 °C [6].

The growth rates of the organisms are the highest at optimum growth temperature, while the rates decrease as they approach minimum and maximum growth temperature (or the lowest and highest temperature the organism can survive and replicate).

BIOFILM SECRETING MICROBES

In the study of Pavlovsky, Sturtevant [7], after 1 hour heat treatment at 45ºC, cell reproduction of *Staphylococcus epidermidis* ceased, and its cell viability was significantly reduced at 60ºC. The relative concentrations of the polysaccharide, protein, and DNA components of the EPS were unchanged by the heat treatment at 45 and 60 °C, which suggest that EPS molecular constituents are not significantly degraded by the temperature treatment. Some aggregation on the scale of 100 nm was found by dynamic light scattering at 60 °C. Relative to control biofilms maintained at 37 °C, an order of magnitude reduction in the biofilm yield stress was observed after 60 °C temperature treatment, whereas at 45ºC, no such difference was found. It means that temperature increment can weaken mechanical integrity of *S. epidermidis* biofilms. Another similar study from Pijls, Sanders [8] on *S. epidermidis* showed that total eradication was observed at 65°C or higher for 3.5 minutes followed by 24 hours of vancomycin 10 mg/l and rifampicin 1 mg/l. Heat treatment at 60°C for 3.5 minutes followed by 24 hours of vancomycin 1 mg/l and rifampicin 1 mg/l followed by another thermal shock of 60°C for 3.5 minutes (two thermal shocks) can achieve total eradication as well. *Staphylococcus aureus* formed porous biofilm at higher temperature (45°C), where porosity allows *S. epidermidis* to colonize more of the surface, resulting in detectable *S. epidermidis* biomass. In the study of thermal deactivation of *Pseudomonas aeruginosa* biofilm [9], it observed that the viability decreased with temperature of thermal shock and time of heating, but complete deactivation was never achieved at 80°C for 30 minutes.

CHARACTERIZATION OF THE ALGAE AND BIOFILM

The information regarding characterization of the algae and biofilm that govern biofouling in membrane distillation are limited compared to the one in conventional pressure driven membrane and shows some similarity. The techniques for characterization of algae and biofilm in conventional pressure driven membrane are more matured and thus presented. Nguyen, Roddick [10] had summarized and made comprehensive review on the characterization techniques as follows

Microbial analysis such as heterotrophic plate counts, total direct cell counts and physical and (bio)chemical analysis such as total wet weight deposits, adenosine triphosphate, EPS and proteins have been used to determine the active biomass on spiral wound membranes. Common microscopy methods for morphological observation of biofilms include epifluorescence microscopy (EFM), confocal laser scanning microscopy (CLSM) and electron microscopy. EFM coupled with staining methods can provide information on microbial activity, total cell counts and the 2-dimensional distribution of bacteria in the biofilm. CLSM provides information about the 3-dimensional structure of biofilms and has the ability to identify different components of the biofilms either by autofluorescence (for algae) or by using specific fluorescent dyes (for bacterial DNA or EPS glycoconjugates). Electron microscopy methods such as scanning electron microscopy (SEM) and transmission electron microscopy (TEM) have been employed for elucidating biofilm structure. SEM is capable of imaging complex structures of the biofilm while TEM can visualise the cross-sectional detail of individual microorganisms and their relationship to each other. Due to the high vacuum conditions required for SEM, sample preparation such as drying and coating of the samples with a conductive material is necessary. Environmental scanning electron microscopy (ESEM) can be used for the observation of hydrated samples (i.e., in their natural state) and it does not require such sample preparation. ESEM has been used to observe polysaccharide (alginate) fouling on a microporous membrane.

Scanning transmission X-ray microscopy (STXM) can be used for examining hydrated biofilms due to the ability of soft X-rays to penetrate water. STXM, CLSM and TEM were employed to map the distribution of macromolecular subcomponents (e.g., polysaccharides, proteins, lipids, and nucleic acids) in a biofilm and demonstrated that this combination of multi-microscopy analysis can be used to create a detailed correlative map of biofilm structure and composition.

Other microscopy methods such as atomic force microscopy can be used for eliciting biofilm surface topography or analyzing the EPS on the surfaces of bacterial biofilms. Soft X-ray microscopy can be used for elucidating the initial steps of bacterial colonization. Digital time-lapse microscopy can be used for in-situ study of growth and detachment of biofilms in flow cells, and near-field scanning optical microscopy can be used for examining the bacterial community composition and structures of biofilms.

Fourier transform infrared (FTIR) spectroscopy has been employed for analyzing microbial aggregates on membrane surfaces and can provide information about the chemical nature of the fouling layer. It allows one to distinguish the different kinds of fouling on the same membrane but cannot provide information about biofilm thickness. Nuclear magnetic resonance (NMR) microscopy has been utilized to study biofouling of industrial spiral wound RO modules. NMR microscopy can provide a non-invasive quantitative measurement of RO membrane biofouling and its impact on hydrodynamics and mass transport in RO systems.

Surface-enhanced Raman spectroscopy (SERS) could be used as a new and versatile tool for examining the fouling of protein on polyvinylidene fluoride (PDVF) membranes. The fouled area can be visualized by a combination of Raman mapping and silver staining. The fouling potential of different proteins could be identified by comparing their relative SERS intensities on a glass slide before and after the mixture was filtered through the PVDF membrane. A combination of molecular (such as fluorescence in situ hybridization, denaturing gradient gel electrophoresis) and microscopy techniques can be employed to study the biofilm formation by *Sphingomonas* spp. on RO membranes. However, these techniques can only be used when doing a destructive membrane autopsy.

Characterization of EPS usually involves its extraction from the biofilm and quantification of the components. EPS extraction is important for studying the physicochemical properties and their impact on contaminants in the aquatic environment. A good EPS extraction method should not alter its characteristics or cause cell lysis and should collect all of the EPS components. Techniques for EPS extraction can be divided into three categories: physical and chemical methods, and a combination of the two. Common physical methods include centrifugation, dialysis, filtration and sonication, ion exchange and heating. Chemical methods utilize chemical agents such as ethylenediamine tetraacetic acid (EDTA), formaldehyde, sodium hydroxide and ethanol for the extraction of EPS from the microorganisms. Physical methods usually yield less than chemical methods although they have the advantage of minimal contamination from reagents and minimal cell lysis. The combination of chemical and physical methods is more effective as a high yield can be obtained without excessive contamination and cell lysis due to the reagents. There are numerous techniques available for analyzing and quantifying EPS components such as colorimetry, FTIR spectroscopy, X-ray photoelectron spectroscopy, high performance size exclusion chromatography, high performance liquid chromatography, gas chromatography-mass spectrometry, deoxyribonucleic acid (DNA) assays and proton nuclear magnetic resonance.

AVAILABLE RELATED BIOFOULING STUDIES

To date, only few membrane distillation studies were focused on biofouling in the seawater and brackish water feed. Krivorot, Kushmaro [11] were using direct contact membrane distillation (DCMD) at 40 °C for 14-19 days under intermittent analysis and indicated that slightly higher temperature would make the membrane less fouled, and temperature cycling to 70 °C or using top brine with 70 °C or higher temperature would reduce biofilm formation on membrane running at 40 °C. Another study using similar membrane at 50 °C [12] pointed that flux decline mainly caused by scaling and biofouling, and biofouling exist after long term operation although high temperature and salinity can inhibit bacteria, and biofouling might accelerate inorganic scaling formation. Therefore, elevated temperature and salinity would have limitation in role of anti-biofouling. *Proteobacteria, Bacteroidetes, Firmicutes and Planctomycetes* were found to be the most abundant phyla. Some thermophilic and halotolerant bacteria, eg. *Bacillus*, can be positively selected by the hot and hypertonic environment, and these bacteria would cause significant flux drop. *Proteobacteria* (eg. *Rhodobacteraceae* and *Hyphomonadaceae*), *Planctomycetes* and *Bacteroidetes* played important roles in microbial community succession in biofilm formation. Firmicutes was found abundantly in concentrating mode. Naidu, Jeong [13] examined the interaction of humic substances on organic and biofouling during the treatment of seawater using DCMD at 70 °C. it showed that the organics penetrated through the membrane pores and seawater organic fouling was irreversible. Humic substances and low molecular weight (LMW) organics are dominant organic contents in seawater. Humic substances were thermally converted to LMW–humic organics and it is more prominent in the presence of salt (NaCl), while inorganic scalant (CaSO4) reduced the conversion due to the binding effect. The assimilable organic carbon (AOC) concentration is closely associated with biofilm growth (biofouling). The AOC concentration increased as the concentration of LMW–humic organics increased and would possibly leading to increased biofouling in the feed and on the membrane. Zodrow, Bar-Zeev [14] observed a steady decline in bacteria concentration (nearly 2 orders) in the membrane distillation feed reservoir, over the course of 4 days. Despite the drop in planktonic bacteria, significant biofilm formation was observed. The biofilms formed were heterogeneous and contained several colonies. Phylogenetic analysis using next-generation sequencing of 16S rDNA showed significant shifts in the microbial communities. Bacteria representing the orders *Burkholderiales*, *Rhodobacterales*, and *Flavobacteriales* were most abundant in the biofilms. Nthunya, Gutierrez [15] found that higher organic content of

the low salinity feed worsened the fouling and wetting in both pristine and modified membranes (i.e., flux decays of up to 73.6% in uncoated membrane samples). They also pointed out that adsorption of hydrophobic contaminants (e.g., colloidal silica and organic compounds in the feed) on membrane distillation surface induces fouling and thus severe decrease in water flux. Although many membrane biofouling bacteria do not thrive under high temperatures and salinity, it is otherwise for thermophilic bacteria.

The study of the thermal effect on the biofilm, its composition and properties in the membrane distillation are limited in the current literature.

CONCLUSION

The membrane distillation studies which focused on biofouling in the seawater and brackish water feed are lacking. Their thermal effect on the biofilm, its composition and properties are limited too. From the information obtained, biofouling is unavoidable and can be severe in the membrane distillation unit even under elevated temperature. The microbial diversity and population in the ocean from different marine geographical origins can vary greatly. The microbial population, strains and abundance, concentration of assimilable organic carbon, presence of inorganic, nutrient level in the feed, membrane surface and abiotic factors in the configured membrane unit could affect severity of the biofouling and organic fouling in the unit itself.

REFERENCES

[1] de Carvalho, C.C.C.R., *Marine Biofilms: A Successful Microbial Strategy With Economic Implications.* Frontiers in Marine Science, 2018. **5**(126).
[2] Curcio, E. and E. Drioli, *Membrane Distillation and Related Operations—A Review.* Separation & Purification Reviews, 2005. **34**(1): p. 35-86.
[3] Gryta, M., *Effectiveness of water desalination by membrane distillation process.* Membranes, 2012. **2**(3): p. 415-429.
[4] Banat, F., et al., *Performance evaluation of the "large SMADES" autonomous desalination solar-driven membrane distillation plant in Aqaba, Jordan.* Desalination, 2007. **217**(1): p. 17-28.
[5] Alkhudhiri, A., N. Darwish, and N. Hilal, *Membrane distillation: A comprehensive review.* Desalination, 2012. **287**: p. 2-18.
[6] Fath, B.D., *Encyclopedia of ecology*. 2018: Elsevier.
[7] Pavlovsky, L., et al., *Effects of temperature on the morphological, polymeric, and mechanical properties of Staphylococcus epidermidis bacterial biofilms.* Langmuir : the ACS journal of surfaces and colloids, 2015. **31**(6): p. 2036-2042.
[8] Pijls, B.G., et al., *Induction heating for eradicating Staphylococcus epidermidis from biofilm.* Bone & joint research, 2020. **9**(4): p. 192-199.
[9] O'Toole, A., E.B. Ricker, and E. Nuxoll, *Thermal mitigation of Pseudomonas aeruginosa biofilms.* Biofouling, 2015. **31**(8): p. 665-675.
[10] Nguyen, T., F.A. Roddick, and L. Fan, *Biofouling of water treatment membranes: a review of the underlying causes, monitoring techniques and control measures.* Membranes, 2012. **2**(4): p. 804-840.
[11] Krivorot, M., et al., *Factors affecting biofilm formation and biofouling in membrane distillation of seawater.* Journal of Membrane Science, 2011. **376**(1): p. 15-24.
[12] Jiang, L., L. Chen, and L. Zhu, *Fouling process of membrane distillation for seawater desalination: An especial focus on the thermal-effect and concentrating-effect during biofouling.* Desalination, 2020. **485**: p. 114457.
[13] Naidu, G., S. Jeong, and S. Vigneswaran, *Interaction of humic substances on fouling in membrane distillation for seawater desalination.* Chemical Engineering Journal, 2015. **262**: p. 946-957.
[14] Zodrow, K.R., et al., *Biofouling and Microbial Communities in Membrane Distillation and Reverse Osmosis.* Environmental Science & Technology, 2014. **48**(22): p. 13155-13164.
[15] Nthunya, L.N., et al., *Fouling-resistant PVDF nanofibre membranes for the desalination of brackish water in membrane distillation.* Separation and Purification Technology, 2019. **228**: p. 115793.

PGC_SCHE USM_2020_25

Comparative study of the treatment of batik wastewater through electrocoagulation process using different types of metal waste-based electrodes

Nurulhuda Amri[1,2], Ahmad Zuhairi Abdullah[1,*], Suzylawati Ismail[1]
[1]School of Chemical Engineering, Engineering Campus, Universiti Sains Malaysia, 14300 Nibong Tebal, Penang, Malaysia
[2]Faculty of Chemical Engineering, Universiti Teknologi MARA (UiTM), Cawangan Pulau Pinang, 13500 Permatang Pauh, Penang, Malaysia
*E-mail: *chzuhairi@usm.my*

Abstract. Batik industries generate large quantities of effluent with high concentrations of contaminants such as organic dyes, waxes and sodium silicate that require a proper treatment prior to discharge into the environment. To address this issue, a batch monopolar electrocoagulation (EC) process was conducted for the treatment of colour, COD and silica from a batik effluent using two different types of waste-derived metal electrodes i.e waste aluminium can (WAC) and waste steel container (WSC). The suitability of the WAC and WSC electrodes for the treatment of batik wastewater was investigated. Findings revealed that WAC electrode was more effective than WSC as it resulted in higher removals of pollutants. The removal efficiencies for WAC and WSC electrodes on the colour, COD and silica were 81.6 % and 40.0 %, 56.0 % and 34.0 %, and 100.0 % and 98.9 %, respectively. The superior performance of WAC in colour and COD removals was attributed to the generation of aluminium hydroxide ($Al(OH)_3$), which was responsible for the adsorption of dyes to produce virtually colourless treated wastewater. Meanwhile, slight lower colour and COD removals as shown by the yellowish treated wastewater by the WSC electrode was due to the formation of iron particles in the solution. The low settleability of iron hydroxide ($Fe(OH)_3$) particles in the solution also complicated the separation of the sludge. As for silica, both electrodes demonstrated high removal efficiencies due to an active reaction between the respective metal oxides and/or metal hydroxides with silica at neutral pH condition to form precipitates. In short, for the treatment of batik wastewater via the EC process, WAC electrode was an efficient electrode which produced a better-quality treated wastewater and allowed easier sludge separation.
Keywords: *Batik wastewater, waste aluminium cans, waste steel container, colour, COD, silica.*

INTRODUCTION

Batik industry is one of the growing textile-based industries in Malaysia that contributes positively to Malaysia's economic development. The main problem related to the batik industry is the discharge of the effluent from the soaking, boiling and rinsing processes without a proper treatment system. Among all the processes, the largest volume of wastewater is produced from the rinsing step. This type of wastewater usually contains high amounts of organic dyes, waxes and sodium silicate that contribute to the high colour intensity, COD, silica and pH of the effluent. Organic dyes released into the nearby water stream may contain chemicals that are toxic, carcinogenic or mutagenic to aquatic life [1]. Meanwhile, long-term exposure to silica has been reported to increase the risk of lung diseases such as tuberculosis, silicosis, chronic bronchitis and lung cancer in humans [2]. Therefore, there is a critical need to explore the effective treatment for batik wastewater before been discharged into the water bodies to reduce its adverse effects on human and aquatic life. In recent years, electrocoagulation (EC) appears to be a promising technology due to its simple, inexpensive and effective method in treating various pollutants simultaneously. Thus, this study aimed to demonstrate the suitability of waste aluminium cans (WAC) and waste steel container (WSC) electrodes for the treatment of batik wastewater using an EC process. The efficiency of the electrodes in removing colour, COD and silica was compared and discussed. SEM-EDX analysis was also carried out on both generated flocs to elucidate the removal mechanism of the pollutants.

MATERIALS AND METHODS

Sample Collection

The batik wastewater was collected from a batik factory located in Batu Ferringhi, Penang. The sample was manually collected in a 10 L of polytetrafluoroethylene (PTFE) container from the rinsing tank and preserved in a cold room at 4 ºC in accordance with the Standard Methods for the Examination of Water and Wastewater [3]. The characterization analysis was carried out within 24 hours of the collection period to identify the main characteristics

of the batik wastewater. The sample was then filtered before being used in the EC process to remove solid wax. Meanwhile, the initial pH of the sample was adjusted to pH of 7 using 0.1 M of HCl.

Batch EC system

Batch monopolar EC experiments were carried out in a 1.1 L rectangular reactor with two pieces of WAC and WSC plain electrodes. The electrodes were placed at the centre of the cell with the inter-electrode distance (IED) of 0.5 cm. The area of each electrode dipped into the solution was 6 cm x 7 cm. The electrodes were connected to a DC power supply (Dazheng PS - 305D, 0 - 5 A, 0 - 30 V) in order to supply and control the required current during the experiment. 800 mL of the batik wastewater was initially fed into the EC cell and the current density was set at 25 mA/cm^2 for 30 minutes. The wastewater was continuously stirred during the experiment to get a homogeneous solution. Samples of the treated wastewater were taken after the EC process and filtered through a 0.45 µm Whatman filter paper prior to its colour, COD and silica measurements. Meanwhile, the WAC and WSC flocs with batik pollutants were collected by vacuum filtration pump, dried at 105 ^{O}C and subjected to SEM-EDX analysis. Each EC run was conducted in duplicate and the average removal efficiency was calculated to ensure the reproducibility of the experimental data.

The colour of the batik wastewater (in ADMI unit) was analysed using the Standard Method 2120 F [4]. Meanwhile, COD concentration (mg/L) was analysed using the Standard Method 5220 D [5], a closed reflux method. Silica concentration was analysed using the Method 8185 (Silicomolybdate method) [6] using a high-range silica reagent set (1 – 100 mg/L SiO_2). All the analyses were conducted using a Hach™ DR6000 UV VIS spectrophotometer (USA). The colour, COD and silica removal efficiencies are calculated using Eq. (1):

$$\text{Removal Efficiency, \%} = \frac{C_0 - C_f}{C_0} \times 100\% \quad (1)$$

Where, C_0 is the initial value (ADMI)/concentration (mg/L) and C_f is the value (ADMI)/concentration (mg/L).

The surface morphology and elemental composition of the produced WAC and WSC flocs were examined by means of a scanning electron microscope (SEM) equipped with an energy dispersive X-ray spectroscopy (EDX) facility (Quanta 450 FEG, FEI, Netherlands) operated at an accelerating voltage of 5 kV.

RESULTS AND DISCUSSION

Characteristic of the batik wastewater

The characteristics of the batik wastewater from the rinsing process are shown in Table 1. Results demonstrated that the batik wastewater was high in colour, COD, silica and pH which did not comply with the discharge standard for the industrial effluent as stated in the Malaysian's Fifth Schedule of Environmental Quality (Industrial Effluent) Regulation 2009 [7]. The COD values were in the range of 300 to 350 mg/L which were much higher than those of Standard A (80 mg/L) and B (250 mg/L). Meanwhile, colour was found to be in the range of 270 – 296 (in ADMI unit) which was almost triple that of standard A. Furthermore, a high silica concentration of more than 600 mg/L was detected in the batik wastewater and it originated from sodium silicate used as a colour stabilizer. This sodium silicate also contributed to the high pH of the batik wastewater (pH ~10.75), far above the current regulatory limits.

Table 1. Characteristics of batik wastewater from the rinsing process.

Parameters	Value	Discharge standard	
		Standard A	Standard B
COD (mg/L)	300-350	80	250
Colour (ADMI)	270-296	100	200
Silica (mg/L)	610-680	-	-
Temperature (^{O}C)	25.4	40	40
pH	10.75	6.0-9.0	5.5-9.0
Conductivity	940.7µS/cm	-	-

*Standard A: used for effluents discharged into inland waters within catchment areas as specified in the Sixth Schedule of the Environmental Quality Act., *Standard B: used for effluents discharged into any other inland waters or Malaysian waters.

Performance of WAC and WSC electrodes for the treatment of batik wastewater

Proper selection of the electrode material is crucial as it could significantly affect the efficiency of the EC process. Thus, the effect of different types of metal waste-based electrodes (WAC and WSC) for the treatment of batik wastewater was investigated in this study. The batch EC study was conducted at optimum process conditions obtained from previous study using Acid Red 18 (AR18) dye at a current density of 25 mA/cm^2, a pH of 7, an NaCl dosage of 0.2 g/L, an IED of 0.5 cm and a reaction time of 30 min. The colour, COD and silica removal efficiencies of WAC and WSC electrodes are shown in Table 2.

Table 2. Removal efficiencies and characteristics of batik wastewater after the EC process using WAC and WSC electrodes.

Parameters	WAC	WSC
Colour removal, % (ADMI)	81.6	40.0
COD removal, %	56.0	34.0
Silica removal, %	100.0	98.9
Final pH	8.2	5.4
Apparent colour	Colourless	Light yellow

It was revealed that the WAC electrodes performed better than those made of WSC with higher colour, COD and silica removal efficiency of 81.6 %, 56.0 % and 100.0 %, respectively. The superior performance of WAC was attributed to the formation of larger amount of aluminium hydroxide ($Al(OH)_3$) and aluminium oxide (Al_2O_3) at neutral pH condition. At a pH of 7, most of the $Al(OH)_3$ precipitated as aluminium coagulants that actively adsorbed the dye molecules [8]. Thus, a colourless treated wastewater could be obtained after the EC process as shown in Figure 1 (a). Furthermore, the formation of silicon dioxide ($SiO_{2(am)}$) as the dominant silicon-containing component of the sodium silicate aqueous solution under pH neutral conditions [9] also contributed to a complete silica removal. At this condition, the aluminium species ($Al(OH)_3$) and/or Al_2O_3) could effectively combine with $SiO_{2(am)}$ to form aluminium silicate ($Al_2O_3.SiO_2$). The formation of large amount of $Al_2O_3.SiO_2$ flocs could be visibly observed floating at the top of the EC cell (Figure 1 (a)).

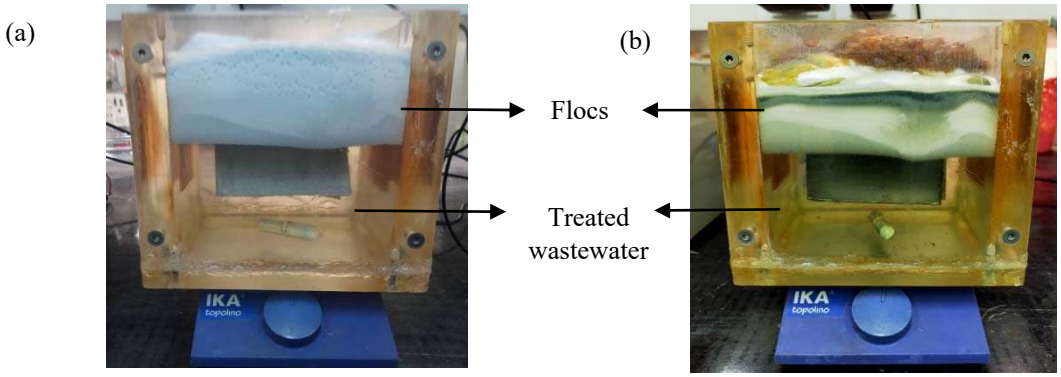

Figure 1. The treated batik wastewater after the EC process for (a) WAC electrodes and (b) WSC electrodes. **(**Current density=25 mA/cm^2, pH=7, NaCl dosage= 0.2 g/L, IED=0.5 cm and reaction time=30 min)

Meanwhile, the WSC electrodes demonstrated slightly lower colour and COD removal efficiencies of 40.0 % and 34.0 %, respectively. The lower colour and COD removal efficiencies were consistent with the yellowish treated wastewater due to the presence of Fe^{3+} ions in the solution [10]. The fine Fe^{3+} ions would then eventually form $Fe(OH)_3$ particles (brownish in colour) in the solution with low sedimentability. Due to this reason, it was noticed that the filtration of treated wastewater from the sludge was more difficult than WAC electrodes. In contrast, silica was found to be effectively removed by the WSC electrode with 98.9 % removal resulting in a large flocs formation (Figure 1(b)). Nevertheless, the silica removal was still higher with WAC as it could eliminate this pollutant under the same operation conditions. The similar finding was reported by Zhang et al. [11] as they revealed that Al^{3+} was more effective than Fe^{3+} in removing the dissolved silica from the water.

Flocs Characteristics

The surface morphology and elemental composition of the generated WAC and WSC flocs from the EC were analysed using SEM-EDX. Figure 2 (a) and (b) exhibit the surface morphology of WAC and WSC flocs at magnifications of 500x, respectively. Meanwhile, the EDX results of the produced flocs are shown in Table 3. The SEM images reveal that the both generated flocs were composed of irregular particles sizes indicating their amorphous nature [12]. However, it was clearly observed that the surface of WAC floc was more porous than the WSC floc which significantly enhanced the colour removal via adsorption mechanism. Furthermore, based on the EDX analysis, Al, Fe and O were identified as the predominant elements to suggest a large formation of $Al(OH)_3$ and $Fe(OH)_3$ as coagulants in both WAC and WSC flocs, respectively. These coagulants were primarily responsible for the adsorption and/or entrapment of batik dyes by the generated flocs. Higher composition of Si in WAC floc than WSC by 4.6 % also confirmed that WAC electrodes could remove silica better due to the effective reaction between Al and silica to form $Al_2O_3.SiO_2$ precipitate. Meanwhile, the existence of Na and Cl was attributed to the addition of NaCl as a supporting electrolyte in the process.

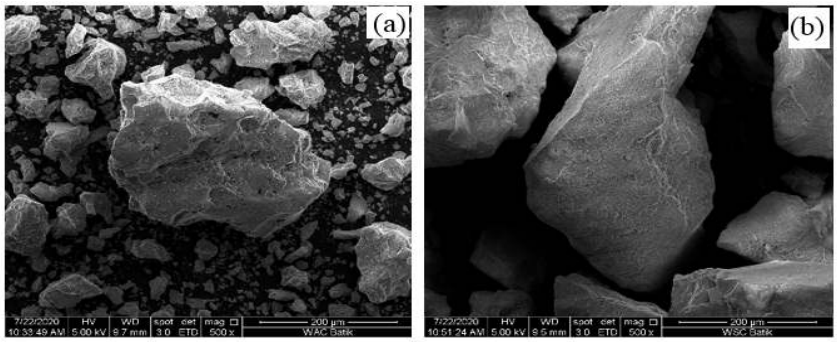

Figure 2. SEM-EDX images of flocs produced after the EC process at a magnification of 500 x using (a) WAC electrodes and (b) WSC electrodes.

Table 2. Elemental compositions of the generated flocs by the WAC and WSC electrodes.

Elements	WAC floc Weight %	WSC floc Weight %
C	9.2	11.2
O	56.6	55.6
Na	3.4	0.3
Al	15.8	-
Fe	-	24.0
Si	13.2	8.6
Cl	1.8	0.3

CONCLUSION

This study demonstrated a comparison study between WAC and WSC electrodes for the treatment of batik wastewater through EC process. Findings revealed that the WAC electrode was more suitable for the treatment of batik wastewater due to its higher colour, COD and silica removal efficiencies to produce a better quality treated wastewater (in terms of apparent colour and final pH) with an additional advantage of easier sludge separation than WSC. Further investigation on the optimization conditions of EC process for the treatment of batik wastewater using WAC electrodes need to be done to maximize the removal efficiency of pollutants as well as to minimize the energy consumption of the EC process.

ACKNOWLEDGEMENT

The authors gratefully acknowledge the financial support received from the Ministry of Higher Education (MOHE) of Malaysia (LRGS Grant Project number 67215001) as well as Universiti Teknologi MARA (UiTM) for the study leave of the first author.

REFERENCES

[1] V. Khandegar and A. K. Saroha, J. Environ. Manage., **128**, 949–963 (2013).
[2] L. F. Castañeda, O. Coreño, and J. L. Nava, J. Environ. Chem. Eng., **7(5)**, 1–7 (2019).
[3] Standard Methods for the Examination of Water and Wastewater, 23rd ed. Washington D.C: American Public Health Association, (2017).
[4] Hach, "Color, ADMI Weighted Ordinate Method," **7**, 1–6 (2019).
[5] Hach, "Chemical Oxygen Demand, USEPA and Reactor Digestion Method," **10**, 1–10 (2014).
[6] Hach, "Method 8185 Powder Pillows - Silicomolybdate Method," **1**, 1–6 (2014).
[7] Ministry of Natural Resources and Environment Malaysia, (2010). [Online]. Available: http://www.doe.gov.my/eia/wp-content/uploads/2012/03/A-Guide-For-Investors1.pdf.
[8] A. G. Khorram and N. Fallah, J. Environ. Chem. Eng., **6**, 635–642 (2018).
[9] J. Kang, R. Fan, Y. Hu, W. Sun, R. Liu, Q. Zhang, H. Liu and X. Meng, J. Clean. Prod., **195**, 280–288 (2018).
[10] F. Hussin, F. Abnisa, G. Issabayeva, and M. K. Aroua, J. Clean. Prod., **147**, 206–216 (2017).
[11] X. Zhang, M. Lu, M. A. M. Idrus, C. Crombie, and V. Jegatheesan, Process Saf. Environ. Prot., **126**, 18–24 (2019).
[12] S. U. Khan, D. T. Islam, I. H. Farooqi, S. Ayub, and F. Basheer, Process Saf. Environ. Prot., **122**, 118–130 (2019).

PGC_SCHE USM_2020_26

Graphene Nanostructure Material for CO_2 Capture

Rabita Mohd Firdaus Achutan, Abdul Rahman Mohamed*
School of Chemical Engineering, Engineering Campus, Universiti Sains Malaysia,
14300 Nibong Tebal, Pulau Pinang, Malaysia.
*E-mail : *chrahman@usm.my*

Abstract. Modification of the graphene based macroscopic materials (GBMs) adsorbent by selecting the right functional groups through impregnation or grafting method has been recommended to enhance the ability of CO_2 adsorption and to facilitate the mass transfer of CO_2 to adsorbents. Two common functional groups, which are alkaline carbonate and amine, are normally used to modify the adsorbent surface. Influenced by the most relevant amine-based chemical absorption technologies for CO_2 capture, the production of potential amine-functionalized adsorbents is an alternative approach to resolve problems due to this conventional technique, such as low gas-liquid contact area, low CO2 loading and serious absorbent corrosion. It is believed that the addition of amine to the adsorbent surface will enhance the basic active sites that help facilitate interaction with acidic CO_2 adsorbents.
Keywords: *Graphene; functionalization; adsorption,* CO_2 *capture*

INTRODUCTION

The steady increase in atmospheric greenhouse gases (GHG) concentration is the biggest environmental concerns leading to global warming [1]. Global warming is also referred to as climate change because it leads to alter the geology of the Earth and other environmental changes. Global warming occurs when carbon dioxide (CO_2) or other air pollutants and GHG collect in the atmosphere and absorb sunlight and solar radiation that have bounced off the earth's surface. Normally, this radiation would escape into space - but these pollutants, which can last for years to centuries in the atmosphere, trap the heat and cause the planet to get hotter [2]. Further increases are expected as the annual burning of fossil fuels is likely to continue to rise steadily to meet the spiralling energy demand of an increasing human population. Thus, significant attempts must be taken to reduce the volume of CO_2 entering the atmosphere. As a potential technology to mitigate CO_2 emissions, carbon capture and storage (CCS) is gaining considerable attention from scientists and researchers [3]. CCS is conceptually a simple approach where it involves capturing, transporting, and storing CO_2. However, much effort is needed to study, develop, and implement this technology in industrial settings to cut the operating cost and energy penalty of this technology [4]. From the various strategies (e.g. pre-combustion, post-combustion and oxy-fuel combustion) and multiple techniques (e.g. absorption, adsorption, membrane separation, and cryogenic distillation) actively being explored to adsorb CO_2 from fossil-fueled power plants and other large industrial sources [5], post-combustion capture using porous adsorbents is preferred because of its low energy consumption, low adsorbent material costs, cost-effective production design and high capacity to absorb CO_2. Gas-solid adsorption is one of the most promising strategies for both post-combustion and pre-combustion capture applications. Unlike liquid sorbents, solid sorbents can be used over a wide temperature range. An ideal CO_2 adsorbent must have high selectivity and adsorption capacity for CO_2, fast adsorption-desorption kinetics, adequate multicycle stability and good performance in the presence of competing species, such as water.

In response to these demanding requirements, a range of potential CO_2 adsorbents have previously been proposed. Various porous solids have been widely studied among which porous carbons are particularly best suited for use in post-combustion CO_2 capture systems, owning to their abundant porosity and feasibly in term of preparation adsorbent [6]. Graphene is an amazing 2D-carbon substance, a single-atom thick layer of a hexagonal structure, sp^2-bonded carbon atoms and until now, many have attempted to synthesize completely two-dimensional (2D) atomic crystal using an appropriate technique [7]. Due to its special and superior properties (mechanical, electrical, thermal, optical), graphene has become the main attraction among scientists for several years. Graphene is the thinnest, lightest and hardest substance (between 100-300 times stronger than steel) as well as the best heat and electrical conductors with a thermal conductivity of 5 $kW.m^{-1}.K^{-1}$ and an electron mobility of 15,000 $cm^2.V^{-1}.s^{-1}$, respectively [8][9]. As part from exploiting the properties of 2D graphene nanosheets at the nanometre scale especially in electronics, their high specific surface (2630 m^2/g), more than twice that of activated carbons makes graphene an ideal nanomaterial for environmental applications and especially CO_2 capture. Their assembly in hierarchized macroscopic structures or graphene based macroscopic materials GBMs has grown of interest among the scholars in recent years [10-13]. Figure 1 illustrates an idea how the self-assembly process been performed. Since the sp^2 carbon network can be functionalized in many ways, in terms of chemical affinity versatility of these GBMs is a remarkable tool for controlling interface interactions. For all these reasons, such substrates with beneficial surfaces are the focus of numerous studies in the scientific community. Various methodologies have been employed to construct graphene-based 3D nanostructures called here GBMs and in fact graphene alone can be viewed as a bridge between the nanoscale and the bulk material.

In many applications, hierarchically organized materials such as hydrogels, aerogels, foams, or sponges were a major concern compared to a finely divided graphene nanosheet powder.

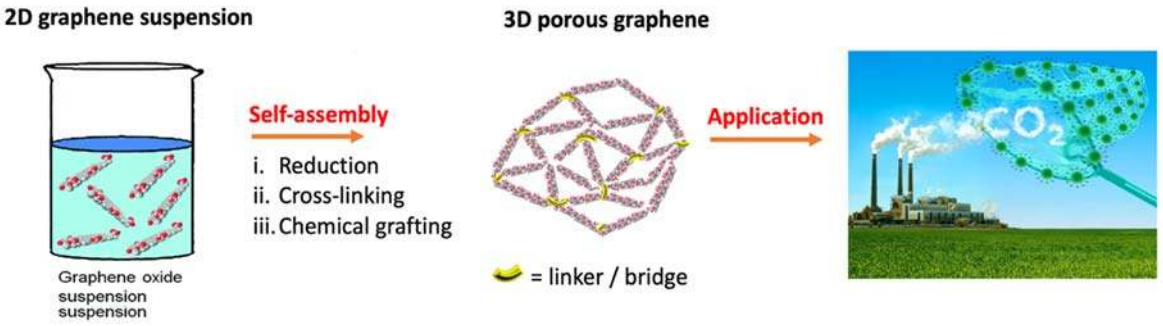

Figure 1. Self-assembly of individual graphene nanosheets to form 3D GBMs for CO_2 capture.

The already published works show GBMs exhibit large accessible surface area, high volume of pores, excellent stability, good flexibility, and sufficient mechanical strength due to the excellent properties of graphene. These materials can also work as effective adsorbents for capturing CO_2 originating from fossil fuel combustion. However, due to lack of control of the self-assembling mechanism, these graphene materials often suffer of restacking which significantly lessen the accessible surface and porosity they can offer [14].

RESEARCH CHALLENGES

Among all the graphene forms and types, graphene oxide (GO) is the mostly used starting materials in GBM domain [15-17]. In order to design 3D GBMs, chemical modifications particularly reduction provokes a decreasing in repulsive forces between the graphene nanosheets inducing their self-assembly in a controlled manner. GO is an interesting starting graphene to prepare GBMs since it can be easily synthesized in large quantities (several grams) in the laboratories and they easily disperse in water. However, GO bears a lot of surface functional groups which number cannot be really controlled. This leads to a lack of control of the GO self-assembling process and discrepancies between the published works. One of the key objectives of this domain study is to monitor the graphene intersheet interactions that are the driving force for the self-assembly process and possibly prevent or restrict the 2D graphene restacking to maximize the porosity of the prepared 3D GBMs. Besides, the self-assembly technique is sensitive to the experimental conditions used (concentration of graphene, temperature, drying phase) and to the graphene characteristics (size and shape, thickness, surface chemistry) which both have a major impact on the resulting properties of 3D GBMs. At the current stage of 3D GBM development, it is not clear which approach strategies leads to the best material in term of surface and physical properties. The chemistry and interaction forces involved in the process of self-assembly are far from being fully understood. The chemical procedures successfully applied to other carbon family, such as fullerenes and CNTs could be a comprehensive reference to further emerging the graphene functionalization concepts to develop 3D GBMs. Unfortunately, they cannot be directly transferred to graphene because chemical reactivity of graphene is different to that of fullerenes and carbon nanotubes (CNTs) which have both a curved sp^2 network. At last, the theoretical/calculation tools are rarely used to study GBMs and the mechanisms involved in their preparation. Further experimental investigations are needed in order to control the self-assembling mechanisms which play the major role on the structural properties of these 3D GBMs.

RESEARCH STRATEGY

GO is an interesting nanomaterial since it is a kind of reference in literature and its assembly into GBMs is efficient, but its high degree of functionalization hinders a deep understanding of the graphene nanosheet self-assembly phenomenon. Thus, for research strategy, two different graphene family of high-quality graphenes were proposed: low-layer graphene (FLG) and industrial graphene nanoplatelets (GNPs). Unlike GO, FLG and GNP, which have few defects, are not dispersible in water. The nature of functional groups with appropriate approach methods is crucial in order to both induce their dispersion and to assemble them to form GBM. Since FLG has never been used for the preparation of GBM, and its chemical reactivity is not yet well known, the preparation of these functionalized FLGs is one of the key challenges. The aim of the research study is to create stronger links to improve the handling of FLG / GNP-based GBMs compared to GO-based GBMs by using a chemically bound amide coupling approach [18-20]. The chemical reaction suggested below (Figure 2) shows how this strategy will work.

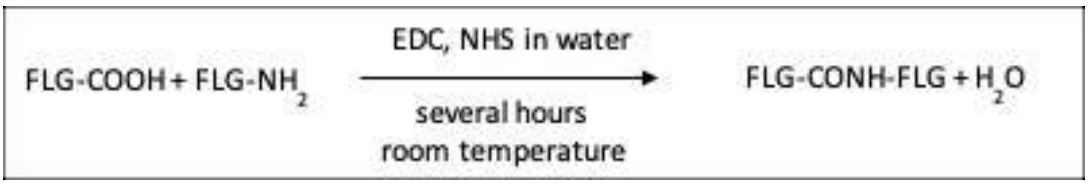

Figure 2. Amide coupling between functionalized FLGs to form GBMs.

CONCLUSION

The 3D GBMs exhibit interesting properties and are particularly highly promising materials for applications where surface exchanges play the major role. The areas of focus for these advanced nanostructured materials include energy technology (conversion and storage), environmental technology (CO_2 capture and water treatment), and catalysis. However, at this point it is not clear which approach leads to the best material in terms of surface and physical properties. Further fundamental investigations are needed in order to control and enhance both the preparation methods and the performance of these 3D GBMs.

ACKNOWLEDGEMENT

We acknowledge the financial support given by the Ministry of Education Malaysia through Universiti Sains Malaysia Fellowship, Hubert Curien Partnership France-Malaysia Hibiscus (PHC Hibiscus) Grant, and Institute of Postgraduate Studies Universiti Sains Malaysia.

REFERENCES

[1] A. Kaithwas, M. Prasad, A. Kulshreshtha & S.Verma, Chem Eng Res Des. 90(10), 1632-1641 (2012).
[2] D.P. Shepardson, D.Niyogi, S. Choi, U. Charusombat, Environ Educ Res. 18(4), 581-581 (2011).
[3] A. Al-Mamoori, A. Krishnamurthy, A.A Rownaghi & F. Rezaei, Energy Technol. 5(6), 834-849 (2017).
[4] J. Wang, L. Huang, R. Yang, Z. Zhang, J. Wu, Y. Gao & Z. Zhong, Energy Environ. Sci. 7(11), 3478-3518 (2014).
[5] R. Balasubramanian & S. Chowdhury, J. Mater. Chem. A. 3(44), 21968-21989 (2015).
[6] Y. Jin, S.C Hawkins, C.P Huynh & S. Su, Energy Environ. Sci. 6, 2591–2596 (2013).
[7] A.K. Geim & K.S Novoselov, J Nanosci Nanotechno. (11-19) (2010).
[8] A.A. Balandin, S. Ghosh, W. Bao, I. Calizo, D. Teweldebrhan, F. Miao & C.N Lau, Nano Lett. 8(3), 902-907 (2008).
[9] K.S Novoselov, A.K Geim, S.V Morozov, D. Jiang, Y. Zhang, S.V Dubonos & A.A Firsov, sci. 306(5696), 666-669 (2004).
[10] A.I. Pruna, A.C Cárcel, A. Benedito & E.Giménez, J. Nanomater. 9(3), 350 (2019).
[11] K. Xia, X. Tian, S. Fei & K. You, Int J Hydrogen Energ, 39(21), 11047-11054 (2014).
[12] A. Pruna, A.C Cárcel, A. Barjola, A. Benedito & E. Giménez, J. Nanomater. 9(8), 1077 (2019).
[13] Y. Zhang, Q. Wan & N. Yang, Small, 15(48), 1903780 (2019).
[14] R.M. Firdaus, N. Berrada, A. Desforges, A.R Mohamed, B Vigolo, Chem. Asian J. (2020).
[15] S. Chowdhury & R. Balasubramanian, Sci. Rep. 6, 21537 (2016)
[16] T. Khandaker, M.S Hossain, P.K Dhar, M. Rahman, M.A Hossain & M.B Ahmed, Processes, 8(6), 654, 2020.
[17] V. Rodríguez-Mata, J.M González-Domínguez, A.M Benito, W.K Maser & E. García-Bordejé, ACS Appl. Nano Mater. 2(3), 1210-1222 (2019).
[18] M.C. Bourkaib, Y. Guiavarc'h, I. Chevalot, S. Delaunay, J. Gleize, J. Ghanbaja & B. Vigolo, Catal. Today, 348, 26-36 (2020).
[19] M.H. Jazayeri, H. Amani, A.A Pourfatollah, H. Pazoki-Toroudi & B. Sedighimoghaddam, Sens Biosensing Res, 9, 17-22. (2016).
[20] K. Nam, T. Kimura & A. Kishida, Macromol. Biosci. 8(1), 32-37 (2008).

PGC_SCHE USM_2020_27

Plantwide Control of Biodiesel Production from Waste Cooking Oil

Rasheed Olakunle Kelani[1,a], Zainal bin Ahmad[1,b,*], Dipesh Patle[2,c]
[1]School of Chemical Engineering, Engineering Campus, Universiti Sains Malaysia, 14300 Nibong Tebal Penang, Malaysia
[2]Chemical Engineering Department, MNNIT Allahabad, UP, India, 211004
*E-mail:¨*chzahmad@usm.my*

Abstract. Biodiesel is one of the renewable energy sources alternative to hydrocarbon-based diesel fuel that is considered inimical to the environment. However, its high economic outlay limits its manufacture and utilization. In order to reduce its high cost of production, one attractive option is to use waste cooking oil (WCO) as the feedstock. The objective of the study is to develop a plantwide control (PWC) system for the enhancement of the process economics (i.e. profitability and yield) of a biodiesel plant. To this end, waste cooking palm oil containing 6% free fatty acids (FFA) was used as feedstock initiating a biodiesel production process involving acid esterification and alkali transesterification which was simulated rigorously in Aspen Plus simulator. For an effective use of rigorous process simulator and heuristics, the design of the PWC was based on the method of the integrated framework of simulation and heuristics (IFSH). Using performance indexes of settling time, deviation from the production target (DPT), and overall total variation (TV) in the manipulated variable, results of the dynamic simulation shows that the PWC system is stable and robust to disturbances.
Keywords: *Plantwide control; Biodiesel; Simulation and heuristics.*

INTRODUCTION

In the 21st century, bioprocess industry has become an essential integral part of the global economy for several reasons. Some of these reasons are related to the environmental problems caused by the use of fossil fuel as a primary source of energy to drive industrial processes and to power both commercial and private mode of transportation. Because of the negative impact of fossil fuel on the environment [1], and its gradual depletion [2], there has been a surge in biodiesel production in the last decade as it is seen as an attractive alternative to hydrocarbon-based fuel. Biodiesel is environmentally friendly and a renewable energy. To sustain biodiesel comparative environmental advantage over fossil fuel and improve its process economics (i.e., profitability and yield), waste cooking oil (WCO) is used as a feedstock for biodiesel production. Compared to other feedstocks for biodiesel production, it is cheaper to procure, and its use prevent the need for remediation process after disposal. However, the transesterification of WCO in the absence of esterification process leads to saponification and reduction in the yield of biodiesel because of the high contents of free fatty acids (FFA) in WCO.

To prevent this, [3] proposed two-step biodiesel production process, an acid-catalysed esterification process and alkali-catalysed transesterification process. In their two-part series papers, [4] investigated four approaches for biodiesel production: an alkali-catalysed process using pure oil, an alkali-catalysed process using WCO, an acid-catalysed process using WCO, and an acid-catalysed process using hexane extraction. They concluded that the acid-catalysed process using WCO required the least outlay cost [5]. Besides, there are studies that are focused on the optimal design of the whole biodiesel plant to reduce energy demand [6] [7]. In the area of process control, there have been studies based on the modelling and control of biodiesel reactors only [8], [9], [10] neglecting the effects of other unit operations on the biodiesel production process. However, plantwide control approach has been applied by few works to address improvement in the process economics of biodiesel production [11], [12]. [11] had designed a control system for a biodiesel plant within plantwide control framework using integrated framework of simulation and heuristics (IFSH). A proportionate-integral-derivative (PID) controller was used in their work to achieve the target setpoint. However, a PID controller is not as suitable as a model predictive controller for handling multivariable constrained nonlinear processes. Therefore, the performance of the PWC of the biodiesel process could be improved by using model predictive controller (MPC) which has not been fully adopted and utilised in the biodiesel plant [8] (Brásio et al., 2016). MPC is more suitable to controlling biodiesel production process because it can handle the nonlinearity and constraints present in the dynamics of the biodiesel process. This is a two-part series study. The present study replicates [11] and the second series in our future work will utilise MPC to realise an economic objective within plantwide control framework using IFSH method.

MATERIALS AND METHODS

Biodiesel Process Design

The study adapted the optimised process flowsheet of [11] with some modifications. The steady-state and dynamic simulation models of the biodiesel process were developed using Aspen Plus and Aspen Plus Dynamics

(APD) V11.0, respectively. Dortmund-modified UNIFAC was used to predict the physical properties of the considered components. The physical properties of the vapor phase were determined by the Soave−Redlich−Kwong equation of state (SRK EOS). Model parameters for thermophysical properties such as heat capacity, liquid molar volume, vapor pressure, heat of formation, heat of vaporization, and liquid viscosity for tri-, di-, and monoglycerides (TGs, DGs, and MGs, respectively) were taken from the biodiesel databank of Aspen Plus. The required critical pressure (Pc), critical temperature (Tc), and acentric factor (ω) for the SRK EOS were estimated by the Gani group contribution method [13]. Details of the constituents of the oil were taken from the Aspen Plus Biodiesel Model [13]. The composition of oil given in this model was adjusted to include 6% FFAs.

Plantwide Control Design

The IFSH methodology proposed by [14] was used to design the plantwide control for the biodiesel process. This systematic and hierarchical methodology has eight levels, where in addition to heuristics, both steady-state and dynamic process models are effectively utilized in decision making during the design of a control system; heuristics decisions are complemented with dynamic simulations. The main advantage of the IFSH methodology is that it overcomes an over-reliance on heuristics to design a decentralized regulatory control system. Each level of IFSH and its application to the biodiesel process are highlighted below. Details are available in [14].

Level 1.1. Define the PWC objectives
Level 1.2. Determine the number of control degrees of freedom (CDOF)
Level 2.1. Identify and analyse plantwide disturbances
Level 2.2. Set performance and tuning criteria
Level 3.1. Production rate manipulator selection
Level 3.2. Product quality manipulator selection
Level 4.1. Selection of manipulators for more severe controlled variables
Level 4.2. Selection of manipulators for less severe controlled variables
Level 5. Control of unit operation
Level 6. Check material components balance
Level 7. Effects of integration
Level 8. Enhance control system performance with remaining CDOF

RESULTS AND DISCUSSION

Figure 1. depicts the transient profile of biodiesel production rate for the disturbances D1, D2, D6 and D7. The plant settles down smoothly to a new throughput after some time. By and large, the change in WCO produces a proportionate change in the biodiesel production rate. Initially, the plant is run for 5 h, after which the disturbances are introduced, one at a time. It is clear from the figure that the developed PWC system can control the process for reasonably large disturbances i.e. +20% and -30% change in WCO. Transient responses are smooth and stable. Expectedly, D7 requires more settling time as compared to other disturbances as a result of larger throughput change, whereas D1 and D2 require relatively less settling time.

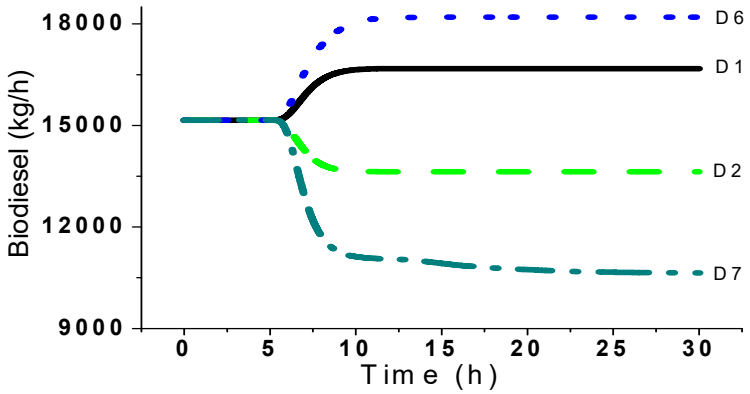

Figure 1. Transient profile of biodiesel production rate in the presence of selected disturbances.

Table 1. presents the performance of the control system for the disturbances D1 to D7. For the complete biodiesel plant, having a capacity of 120 kt/annum, the observed settling time of the biodiesel production rate in the presence of disturbances D1 to D6 is reasonable compared to the settling time of less than 10 h for a biodiesel plant processing 10 kmol/h of oil (i.e. nearly 71 kt/annum). Larger settling time of about 14.2 h is observed for the relatively

large disturbance D7 (-30% in the WCO). This settling time is required for the PWC system due to the more time required in phase separators and the larger holdup in reactors. DPT is the smallest for disturbance D3, wherein -10% change is introduced in the pre-exponential factor of reactions converting WCO to biodiesel. DPT for the disturbances D1 to D5 is comparable (Table 1.). As expected, DPT is the largest for D7, followed by D6 due to the magnitude of change in WCO. In general, increase in the magnitude of change in throughput leads to the increase in DPT. Note that smaller DPT is desired, which denotes that the PWC system is efficient in achieving the new production rate target, and so the economic loss is smaller.

Table 1. Performance of the PWC system designed for the complete biodiesel process

No.	Performance Criterion		
	Settling time (h)	**DPT (kg)**	**Overall TV**
D1	6.4	2123	445
D2	6.3	2042	429
D3	2.2	318	63
D4	7.4	2223	426
D5	7.2	2133	429
D6	8.7	4073	649
D7	13.2	7556	1104

CONCLUSION

A suitable PWC system is developed and evaluated for the complex multiunit biodiesel process using WCO as the feedstock. The IFSH methodology is used to design a PWC system for the biodiesel process where control loops are decided based on heuristics, simulations and ERGA analysis as this is a critical factor in the successful implementation of PWC. The main merits of IFSH methodology are effective use of rigorous process simulators and heuristics in developing a PWC system, and simplicity of application. The performance of the designed control system is investigated in terms of settling time of biodiesel production rate, deviation from the production target (that affects economics) and total variation in manipulated variables (that depicts the control effort needed to stabilize the process), for a number of disturbances. For these disturbances, the PWC system can maintain biodiesel purity under control as per EN standards, and is found to provide smooth, stable, and robust control.

ACKNOWLEDGEMENT

This research is not funded under any grant, but gratitude goes to the school of Chemical Engineering Universiti Sains Malaysia for the opportunity afforded in the colloquium.

REFERENCES

[1] A. N. Phan and T. M. Phan, Fuel. **87** 3490-3496 (2008).
[2] I. Fahmi and S. Cremaschi, Comput & Chem. Engineering. **46** 105-123 (2012).
[3] M. Canakci and J. Van Gerpen, Trans. ASAE. **44** 1429-1436 (2001).
[4] Y. Zhang, M. A. Dube, D. D. Mclean, M. Kates, Bioresour Technol. **89** 16 (2003a).
[5] Y. Zhang, M. A. Dube, D. D. Mclean, M. Kates, Bioresour Technol. **90** 229-240 (2003b).
[6] J. F. Granjo, B. P. M. Duarte, N. M. C. Oliveira, Energy. **129** 273-291 (2017).
[7] L. Simasatitkul, R. Gani, A. Arpornwichanop, Procedia Engineering. **42** 1292-1301 (2012).
[8] A. A. R. Brasio, A. Romanenko, N. C. P. Fernandes, L. O. Santos, Jour. of Process Control. **47** 11-21 (2016).
[9] R. Kern and Y. Shastri, Jour. of Process Control. **33** 127-139 (2015).
[10] A. A. R. Brasio, A. Romanenko, N. C. P. Fernandes, L. O. Santos, Jour. of Process Control. **23** 1471-1479 (2013).
[11] D. S. Patle, Z. Ahmad, G.P. Rangaiah, Industrial & Engineering Chemistry Research. **53** 14408-14418 (2014)
[12] C. Zhang, G. P. Rangaiah, V. Kariwala, Wiley Published Book (2012).
[13] Aspen Plus: Aspen Plus Biodiesel Model (Examples); Aspen Technology: Cambridge, MA, (2012).
[14] N. V. S. N. Murthy Konda, G. P. Rangaiah, P. R. Krishnaswamy, Ind. Eng. Chem. Res. **44** 8300−8313 (2005).

PGC_SCHE USM_2020_28

Sonophotocatalytic degradation of tetracycline antibiotic using ZnO quantum dots/CuO nanosheets composites; A novel hybrid system

Mohamed Hussein Abdurahman, Ahmad Zuhairi Abdullah*
School of Chemical Engineering, Universiti Sains Malaysia, Engineering Campus,
14300 Nibong Tebal, Penang, Malaysia
*Email :*chzuhairi@usm.my*

Abstract In this paper, in-situ fabrication of ZnO quantum dots/CuO nanosheets was performed via hydrothermal method to prepare ZnO/CuO nanocomposites and then coupled with visible light and ultrasound (US) irradiations for sonophotocatalytic removal of tetracycline (TC). The investigation of experimental parameters verified that 20 mg/L TC could be perfectly degraded at the optimum operational parameters (ZnO/CuO: 0.125 g/L, pH: 9.0, US power: 250 W/m^2, and light intensity: 120 W/m^2 over 60 min treatment.)
Keywords: *ZnO QDs/CuO NSs nanocomposite; Sonophotocatalytic, Tetracycline; Aquaculture wastewater*

INTRODUCTION

The inefficiency and long reaction time of traditional methods have motivated the application of alternative techniques, such as advanced oxidation process (AOP). AOPs are underline by the mechanism that are grounded in the production of non-selective reactive radicals, which mineralize organic matters into simple and oxidized components. Among the available AOPs, heterogenous photocatalysis has gained significant attention in recent decades, because its potential to produce numerous active radicals, excellent reusability, and minimal sludge production as well as lack of production of secondary pollutants [1]. Previous studies investigated the degradation of TC via photocatalysis process. Wu et al., for instance, degraded tetracycline antibiotic using TiO_2 under visible light and found that photocatalytic is more efficient than photolysis [2]. Huang et al. reported 87% removal of the tetracycline using $AgBr/Bi_2WO_6$ under visible light illumination [3].

Despite the progress made in identification of the effective degradation methods and materials, however, conventional photocatalysis has been comforted by certain limitations, such as required long reaction times for degradation, high catalyst consumption, low mass transfer, low light penetration, and undesirable aggregation of particles during catalytic processes [4]. These shortcomings prompted via the integration of photocatalytic and ultrasonic US irradiation, which is called sonophotocatalysis, that can improve degradation efficiency through synergistic effects [5]. In this study we used one of the most applied sort of surface modification (addition of ZnO QDs) to enhance the catalytic activity of CuO and utilize the synthesized nanocomposite for detoxification of TC under visible light and ultrasound irradiation.

MATERIALS AND METHODS

CuO nanosheets synthesis

In a typical synthesis process, 0.1 M aqueous solution (80 mL) of copper nitrate was mixed with 0.1 M aqueous solution of hexamethylenetetramine (80 mL) under vigorous stirring. In order to maintain a pH 12 of the solution, KOH was added drop by drop with continuous stirring. After stirring, the suspension was transferred to Teflon-lines stainless steel autoclave and heated to 180 °C for 8 h. The product formed was filtered, washed with ethanol–water mixture solution and finally dried at 70 C for 4 h in oven.

Synthesis of ZnO quantum dots

In a typical synthesis, 0.1 M zinc acetate solution by dissolving 0.55 g of zinc acetate in 25 ml of methanol and 1 M KOH solution by dissolving 2.8 g of KOH in 50 ml methanol were prepared separately. The reaction was carried out at room temperature by dropwise addition of KOH solution to zinc acetate solution with constant stirring. The final pH of the solution was maintained at 10. The resulting solution was homogenized by stirring continuously for 1 h with a magnetic stirrer. The solution thus obtained was found to show bright bluish-green luminescence under UV excitation, thereby indicating formation of ZnO particles. At this stage, 0.25 ml of tetraethylorthosillicate (TEOS) solution (98%, ACROS, USA) was added into the ZnO solution to control particle growth. Immediately after this, 0.5 ml of distilled water was injected to the colloidal solution for mild sol–gel reaction of silica on particle surfaces. The as-prepared colloid was separated by centrifuging and washed several times by methanol followed by distilled water to remove unreacted molecules.

ZnO quantum dots/CuO nanosheets synthesis

The composites were prepared by using hydrothermal synthesis method. In this method, the as prepared CuO nanosheet was added to the ZnO QD solution in water, with constant stirring for 2 h at room temperature to obtain a homogeneous suspension. After stirring, the suspension was transferred into a Teflon-lined stainless-steel autoclave, sealed tightly and maintained at 150 C for 6 h. After that we collected the white precipitate by centrifugation and dried in a vacuum oven at 80 C overnight. By varying the amount of ZnO QD as 1wt% (0.002 g), 2wt% (0.004 g) and 3wt% (0.006 g) in 0.198 g,0.196 g and 0.194 g of CuO NS, three heterojunctions were prepared and labelled as ZGQD1, ZGQD2, and ZGQD3, respectively.

RESULTS

Effect of ZnO QDs/CuO NSs

To investigate the effect of catalyst dosage on the degradation of TC over sonophotocatalysis process, the amount of sample varied from 0.05 to 0.15 g/L. The degradation rate of TC at different amounts of ZnO/CuO, at the selected operational conditions (pH of 9, TC initial concentration of 20 mg/L). With increasing the ZnO/CuO load from 0.05 to 0.125 g/L, the degradation rate elevated from 38.7 to 82%, which was followed by a slight reduction. This may be due to the fact that, enhancing the amount of catalyst leads to increasing surface area, the formation of more active sites (i.e., CuO), and the effective adsorption of light by the photocatalysts.

CONCLUSION

ZnO QDs/CuO NSs were synthesized as heterogeneous sonophotocatalysts through the sol-gel/hydrothermal method. A significant synergistic effect was observed for TC degradation when ZnO QDs/CuO NSs coupled with visible light and US waves. As reflected in the sonophotocatalytic degradation tests, TC was totally removed within 80 min at a ZnO QDs content of 3 wt.%, an initial pH value of 9, a catalyst loading of 0.125 g/L, an initial TC concentration of 20 mg/L.

ACKNOWLEDGEMENT

The Long-term Research Grant Scheme (67215001) from the Ministry of Higher Education of Malaysia is gratefully acknowledged.

REFERENCES

[1] A. Mirzaei, L. Yerushalmi, Z. Chen, F. Haghighat, Photocatalytic degradation of sulfamethoxazole by hierarchical magnetic ZnO@g-C_3N_4: RSM optimization, kinetic study, reaction pathway and toxicity evaluation, J. Hazard. Mater. 359 (2018) 516–526.

[2] A. Mirzaei, Z. Chen, F. Haghighat, L. Yerushalmi, Hierarchical magnetic petal- like Fe_3O_4-ZnO@g-C_3N_4 for removal of sulfamethoxazole, suppression of photocorrosion, by-products identification and toxicity assessment, Chemosphere 205 (2018) 463–474.

[3] A. Mirzaei, L. Yerushalmi, Z. Chen, F. Haghighat, J. Guo, Enhanced photocatalytic degradation of sulfamethoxazole by zinc oxide photocatalyst in the presence of fluoride ions: optimization of parameters and toxicological evaluation, Water Res. 132 (2018) 241–251.

[4] A. Mirzaei, Z. Chen, F. Haghighat, L. Yerushalmi, Magnetic fluorinated mesoporous g-C_3N_4 for photocatalytic degradation of amoxicillin: transformation mechanism and toxicity assessment, Appl. Catal. B 242 (2019) 337–348,

[5] S. Naraginti, Y. Li, G. L. Puma, Photocatalytic mineralization and degradation kinetics of sulphamethoxazole and reactive red 194 over silver-zirconium co-doped titanium dioxide: reaction mechanisms and phytotoxicity assessment, Ecotoxicol. Environ. Saf. 159 (2018) 301–309.

PGC_SCHE USM_2020_29

Comparative study of carbon nanotube dispersion using binary mixed polymers

J.G. Robinson[1,2], A.H. Kamaruddin[1,*], F.N. Gonawan[1]
[1]School of Chemical Engineering, Engineering Campus, Universiti Sains Malaysia, 14300 Nibong Tebal, Pulau Pinang, Malaysia
[2]Chemistry Department, School of Sciences, Adamawa State College of Education Hong, PM B 223, Yola, Adamawa State, Nigeria.
E-mail: *chazlina@usm.my*

Abstract. The recent research examined multiwalled carbon nanotube dispersion trait in aqueous suspensions subjected to sonication with the aid of mixed binary polymer solution of six types of dispersive agents, chitosan-glycerol, chitosan-glutaraldehyde, chitosan- polyethyleneimine, chitosan-gum Arabic, chitosan-triton x-100 and chitosan-polyvinyl alcohol. Among the six binary polymers chitosan-polyethyleneimine and chitosan- glutaraldehyde and chitosan-glycerol present maximum and minimum dispersion capacity respectively. The dispersion quality of multiwalled carbon nanotube has been analysed using uv-vis spectroscopy. The experimental results are in accordance with the chemical structure.
Keywords: *Multi-walled carbon nanotube; Polymer; Surfactant; Dispersion.*

INTRODUCTION

Carbon nanotubes have excellent properties such as optical, mechanical, electrical and thermal stability which made it one of the significant nanomaterials with promising broader applications in fields emission displays, high-strength and conductive composites [1] sensors [2], catalysis supports [1], biosensors [4], probe tips [5] and electronic components [6], photovoltaic devices, aircraft structures [7], water treatment [8] and the treatment of cancer [9]. The phenomenon of delocalization of the π-electrons is responsible for its conductivity and it also eases carbon nanotube adsorption of different chemicals moieties through π- π assembling [10]. However, several drawbacks pertaining to debundling and dispersion of carbon nanotubes is due to their high surface area with strong vander waals interaction energy of ca. 500 ev / μm of tube contact that results in low dispersion in common solvents and the formation of bundles and aggregates [11].

Presently, two methods are broadly utilized in nanotube dispersion which include mechanical method and chemical method. The mechanical method employs ultrasonication, calendaring process, ball milling or combined technique. Ultrasonication method is an efficient technique for dispersing carbon nanotubes in low-viscosity liquids which includes water, acetone, and ethanol. The generation of cavitation bubbles by implosion which releases enormous amount of energy in the form of shear forces and micro-shock waves and thereby assisting in splitting the carbon nanotubes agglomerates by dispersing the particles in aqueous solution. The resultant stability of the suspension is poor and the prolonged dispersion by applying ultrasonication techniques produces fragmentation of the nanotubes [12].

Currently, chemical dispersion involves covalent and non-covalent methods. This covalent technique employs the generation of flaws sites on carbon nanotubes. These flaws situated on the sidewalls as well as at the unclosed ends of the carbon nanotubes introduced by oxidative process induced by either strong acids such as nitric acid (HNO_3) or sulphuric acid or mixture of them. Consequently, these introduced numerous functional groups such as carboxylic (-COOH) and / or hydroxylic groups (-OH) integrated into the carbon nanotube structure [12,13 and 14]. After modifying the structure of carbon nanotube, its nature changes from hydrophobic to hydrophilic which enhances strong interfacial bonds with may polymers.

Also, the oxidative treatment helps to eliminate amorphous carbon and metallic oxide impurities produced during the synthesis process of the carbon nanotubes.

However, the main drawback to the covalent method as a result of chemical reaction comprises of formation of defects on carbon nanotubes structure. Furthermore, the over-sonication of carbon nanotubes results in its damage easily and sometimes the carbon nanotubes is broken into smaller pieces. These interrupt the π electrons mechanism in carbon nanotubes which have negative impact on the transport properties of the carbon nanotubes because the production of deformities can disperse electrons and phonons that are liable for the electrical and thermal behaviours respectively [12, 13 and 15]

The non-covalent method is especially significant, as it does not alter the carbon nanotubes physical properties but increases the carbon nanotube dispersion and processability. Polymers solution can be utilized to disperse the carbon nanotubes effectively with the help of a sonicator.

MATERIALS AND METHODS

The multi-walled carbon nanotube (MWCNTs) was purchased from commercial unit of Universiti Sains Malaysia with purity of 95 %. Various polymers such as chitosan, glycerol, polyethyleneimine, gum Arabic, polyvinyl alcohol was used as received. Surfactant Triton x-100 was also utilized as received. The deionized water 18 MΩ cm was used for the preparing of all solution. The chitosan solution was prepared by dissolving 1 % w/v of chitosan in 540 ml aqueous solution containing 1 % v/v acetic acid. The solution was heated for 3 h at temperature of 80 °C and accompany with stirring for 24 h to ensure that the chitosan completely dissolved. After the chitosan solution has been cooled overnight to temperature of 21°C, the resulting homogenous solution were filtered through a whatmann filter to get rid of any undissolved chitosan particles. The homogenous filtrate solution was divided into six portions. Each of the six-portion of chitosan solution was mixed with different polymers solution as follows: chitosan-glycerol, chitosan-glutaraldehyde, chitosan-polyethyleneimine, chitosan-gum Arabic, chitosan-Triton x-100 and chitosan-polyvinyl alcohol. Then the 50 mg multi-walled carbon nanotube were dispersed in the various binary mixtures of 20 ml each and sonicated for 3h. Before the quality of the dispersion of aqueous suspension was determined using UV-Visible spectroscopy from wavelength between 300-1100 nm with each baseline corrections.

RESULTS AND DISCUSSION

Since it is only individual carbon nanotubes that are active in the UV- Visible region, the dispersion of multi-walled carbon nanotubes was characterized using UV-visible absorbance spectroscopy. The UV-visible absorbance spectra as a function of wavelength for the dispersion of multi-walled carbon nanotubes in various 1 % w/v each of binary mixture of polymers and 1 % w/v binary mixture of polymer and surfactant are plotted in Figure 1. Most of the absorbance plots are similar with gradual increase in carbon nanotube peaks in the absorbance spectra which indicates the amount and quality of the dispersion attains by various binary mixture vary markedly. The maximum UV-Visible absorbance of MWNTs in suspension appears at 300 nm in this work.

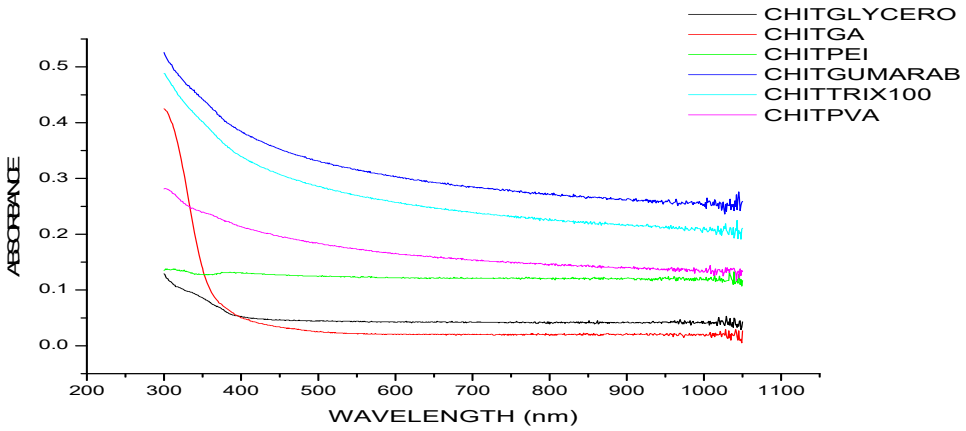

Figure 1. Six types of diluted polymers added to dilute chitosan

For chitosan-glycerol, the presence of more available -OH groups lead to generation of more hydrogen bonding interaction between chitosan and glycerol. These hydrogen bonding interaction in chitosan-glycerol bonded weakly to carbon nanotube due the presence of carboxyl and hydroxyl groups on its surface thereby reducing dispersive ability [16].

The free pendant amine groups of chitosan polymer interact with the aldehydic group of glutaraldehyde to form imine bonds, due to the resonance established with adjacent double ethylenic bonds [17]. This chitosan-glutaraldehyde interaction between carbon nanotube is the weakest that is why the absorbance spectra is the least.

The presence of OH, CH, and print of carbohydrates groups in chitosan-gum Arabic results in better dispersion of carbon nanotubes than chitosan-glycerol, which has been noted previously, though the difference is significant in these results. This hydroxyl and carboxyl groups are likely to cause hinderance in bonding chitosan-glycerol molecules to carbon nanotubes [18]. Therefore, the interaction between chitosan-gum Arabic and carbon nanotube is the greatest as a result of the strong interactive force acting. Consequently, the dispersing power of the six binary mixed polymers based on experimental results follows this trend:

chitosan-glutaraldehyde < chitosan-glycerol < chitosan-polyethyleneimine < chitosan-polyvinyl alcohol < chitosan-Triton x-100 < chitosan-gum Arabic

Dispersing power

CONCLUSION

The present investigation focused on the comparative evaluation of six binary mixture of polymers such as chitosan-glycerol, chitosan- glutaraldehyde, chitosan-polyethyleneimine, chitosan-gum Arabic, chitosan-Triton x-100 and chitosan-polyvinyl alcohol for the dispersion of multi-walled carbon nanotubes. The study examined the parameters influencing the degree of dispersion of the binary mixture polymers. UV-visible spectrophotometer was used to analyse the dispersion of MWNTs in the above binary polymer mixture. The chemical structure agreed with the experimental results of the binary polymer mixture.

REFERENCES

[1] P. Calvert, *Nature*, ***399*****(6733)** 210-211 1999.
[2] J. Kong, N.R. Franklin, C. Zhou, M.G. Chapline, S. Peng, K. Cho, and H. Dai, *science*, *287*(5453) 622-625 2000.
[3] P.G. Collins, K. Bradley, M. Ishigami, and D.A. Zettl, *science*, ***287*****(5459)**1801-1804 2000.
[4] X.Tang, S. Bansaruntip, N. Nakayama, E. Yenilmez, Y.L. Chang, and Q. Wang, *Nano letters*, ***6*****(8)**1632-1636 2006.
[5] H. Dai, J.H. Hafner, A.G. Rinzler, D.T. Colbert, and R.E. Smalley, *Nature*, ***384*****(6605)**147-150 1996.
[6] E. Frackowiak, and F. Beguin, *Carbon*, ***40*****(10)** 1775-1787 2002.
[7] O. Gohardani, M.C. Elola, and C. Elizetxea, *Progress in Aerospace Sciences*, ***70*** 42-68. 2014.
[8] D.K. Yadav, and S. Srivastava, *Materials Today: Proceedings*, ***4*****(2)** 4089-4094 2017.
[9] M. Sheikhpour, A. Golbabaie, and A. Kasaeian. *Materials Science and Engineering:* ***C 76*** 1289-1304 2017
[10] S. Liang, A.V. Subrahmanyam, M. Khadem, Y. Zhao, and A. Adronov, *RSC advances*, ***6*****(31)** 25733-25740 2016.
[11] P.C. Ma, N.A. Siddiqui, G. Marom, and J.K. Kim, a review. *Composites Part A: Applied Science and Manufacturing* 41**(10)** 1345-1367 2010
[12] J.A. Rojas, L.A. Ardila-Rodríguez, M.F. Diniz, M., Gonçalves, B. Ribeiro, and M.C. Rezende. *Materials & Design*, ***166*** 107612 2019.
[13] P. Alafogianni, K. Dassios, S. Farmaki, S.K. Antiohos, T.E. Matikas, and N.M. Barkoula, *Colloids and Surfaces A: Physicochemical and Engineering Aspects*, *495*,118-124. 2016.
[14] L.Y. Jun, N.M. Mubarak, L.S. Yon, C.H. Bing, M. Khalid, and E.C. Abdullah, Comparative study of acid functionalization of carbon nanotube via ultrasonic and reflux mechanism. *Journal of environmental chemical engineering*, ***6*****(5)** 5889-5896 2018.
[15] B. Sohrabi, N. Poorgholami-Bejarpasi, and N. Nayeri, *The Journal of Physical Chemistry B* ***118*****(11)** 3094-3103 2014.
[16] M.V. Debandi, C. Bernal, and N.J. Francois, *J. Tissue Sci. Eng* ***3*****(4172)** 2157-7552 2016.
[17] O.A. Monteiro Jr, and C. Airoldi, *International Journal of Biological Macromolecules* ***26*****(2-3)**119-128 1999
[18] C.A. Ibekwe, G.M., Oyatogun, T.A. Esan, and K.M. Oluwasegun, *American Journal of Materials Science and Engineering* ***5*****(1)** 28-36 2017

PGC_SCHE USM_2020_30

Surface modification of PTFE membrane for direct contact membrane distillation (DCMD) application

Mohamad Razif Mohd Ramli, Abdul Latif Ahmad*
School of Chemical Engineering, Engineering Campus, Universiti Sains Malaysia,
14300 Nibong Tebal, Pulau Pinang, Malaysia
E-mail:**chlatif@usm.my*

Abstract. This research aimed to improve surface hydrophobicity of polytetrafluoroethylene (PTFE) hollow fiber membrane by coating with low density polyethylene (LDPE) for direct contact membrane distillation (DCMD) application. The effect of coating solution was investigated. The coated membrane exhibited high water contact angle of 135.4 ° and permeation flux at 4.206 L m^{-2} h^{-1}.
Keywords: *Polytetrafluoroethylene (PTFE) and direct contact membrane distillation (DCMD).*

INTRODUCTION

Membrane distillation (MD) is a thermal driven separation process associated with membrane process. MD is an alternative to conventional distillation and RO separation where it is still in the phase of development, testing stages and not fully applied in industry [1]. The membrane is the key of the MD for practical application that could exhibited long term acceptable permeation flux and salt rejection. To achieve efficient operation of the MD process requires membrane which is superhydrophobic to prevent pore wetting phenomenon and penetration by liquid water [2][3]. Almost all the industrially used polymeric materials are hydrophobic which include polyethylene (PE), polypropylene (PP), polyvinylidene fluoride (PVDF) and polytetrafluorethylene (PTFE) [4]. Hydrophobic polymeric membrane made from PTFE and PVDF were commonly applied in MD [5]. Membrane with such high surface energy is subjected to pore wettability which reduces the membrane flux and rejection [6]. PTFE has lower surface energy compared to PVDF thus probably has high wetting resistance. In addition, commercial PTFE membrane with smaller pore size is resistant to irreversible fouling compared to PVDF with large pore size which could reduce the permeate flux and impact the output of direct contact membrane distillation (DCMD). In view of this, membrane was subjected to various modifications to acquire surface with low surface energy. In addition, the hydrophobicity of membrane could be altered by changing the morphology of the surface by creating hierarchical surface roughness. Thus, an attempt was made in this study on modification of PTFE surface via coating solution for desalination.

MATERIAL AND METHODS

Materials

The polytetrafluoroethylene (PTFE) hollow fiber membrane with size 0.8 mm OD/ 0.5 mm ID and 0.2-micron pore size was purchased from PLC Solution (Malaysia). The commercial- grade low density polyethylene (LDPE) pellets produced by Petlin Sdn. Bhd. (Malaysia) were used in this work. The polymer solvent adopted was xylene (> 98.5 % mixture isomers+ ethyl benzene basis, France) which was supplied by Sigma Aldrich Sdn. Bhd. Ethanol (> 99.9%, Germany) as non-solvent for indirect coating were purchased from Merck Sdn. Bhd. Sodium Chloride (NACl) was bought from Sigma-Aldrich (St. Louis., MO, United Stated) as feed solution.

Preparation of the LDPE coating solution

The LDPE coating solution was prepared according to literature with some modifications [7]. LDPE pellet was dried in an oven for 60 ºC for 24 h then were dissolved slowly in xylene without any further treatment at 85 ºC. The pellets and solvent were put in double jacket heating tank under continuous stirring at 300 rpm until the polymer dissolved completely for 2 h. PTFE hollow fiber membranes of 3 cm length were washed by distilled water followed by rinsing with ethanol to remove the contaminations from their surface. The fiber was dried in oven at 70 ºC for 24 h while at one end, the fibers were sealed with epoxy (Araldite, Hustsman Advance Materials, Belgium) to prevent the coating solution to flow inside the fiber lumen.

Characterization of LDPE coating layer and direct contact membrane distillation (DCMD) experiments

The obtained LDPE on membrane surfaces were characterized based on surface morphology and wettability. DCMD experiments were carried out to evaluate the separation performance of pristine and LDPE coated surface of hollow fiber membrane.

RESULT AND DISCUSSION

Characterizations

As shown in **Fig. 1** the membrane surface has a uniform topography and pore distribution for pristine (a) and significant change in coated PTFE membrane (b) with water contact angle 103.4º and 135.4° respectively. The indirect coating created a rough LDPE layer could promote to the interfacial interaction between the solvent and non-solvent on the surface of membrane. During the LDPE coating, phase inversion between solvent and non-solvent will cause tensions to shrink. As result, the smooth interface of the coating layer was partitioned into numerous curved surfaces. 5 leading to the precipitation of LDPE and micro-phase separation took place on the membrane surface [8]. In addition, fine nanostructure on the membrane surface was formed that created hydrophobic layer and high roughness of membrane and build up uniform LDPE network. Surface roughness and non-wettability of membrane material itself are general two major factors affecting WCA value of membrane surface hydrophobicity [9]. According to figure below, the shape of the water droplets on membrane is different from pristine PTFE hollow fiber membrane compared to PTFE coated layer due to rough hydrophobic surface. These results suggest that the coating of PTFE layer and the incorporation of LDPE in coating layer can effectively improve the surface hydrophobicity of PTFE hollow fiber membranes.

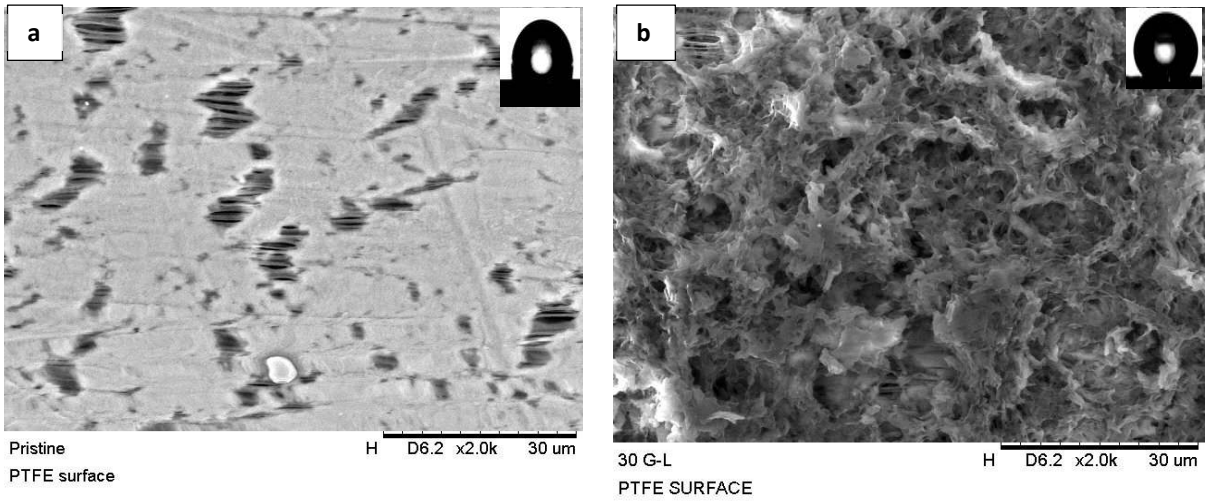

Figure 1. Pristine (a) and (b) LDPE coated on PTFE hollow fiber membranes

DCMD Performances

In the MD performance, the membrane structure play an important role in MD process. **Fig. 2** show the DCMD desalination performance of pristine and LDPE coated PTFE hollow fiber membrane. It can be seen the coated LDPE layer on membrane obviously improved the permeation flux of pristine membrane from 0.702 to 4.206 L m^{-2} h^{-1}. The rejection of NACl of both membranes remained at a high level in range of 99.12 to 99.98%. These results confirmed the LDPE coating on surface of PTFE hollow fiber membrane improved the membrane permeation water flux with great rejection of salt and can be applied for desalination performance test.

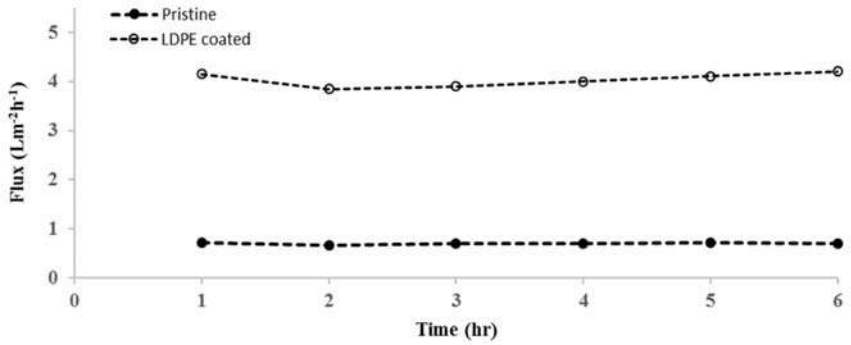

Figure 2. DCMD performance of Pristine (a) and (b) LDPE coated on PTFE hollow fiber membranes

CONCLUSION

LDPE coated on PTFE hollow fiber membrane was successfully prepared to enhanced membrane wettability and desalination performance in DCMD process. The water flux on membrane achieved 4.206 L m^{-2} h^{-1} at 70 ºC.

ACKNOWLEDGMENT

The authors would like to acknowledge the Ministry of Education Malaysia for the Trans-disciplinary Research Grant Scheme (TRGS) grant (203.PJKIMIA.67612001).

REFERENCES

[1] E. Shaulsky, V. Karanikola, A. P. Straub, A. Deshmukh, I. Zucker, and M. Elimelech, "Asymmetric membranes for membrane distillation and thermo-osmotic energy conversion," *Desalination*, vol. 452, no. November 2018, pp. 141–148, 2019.

[2] G. H. Teoh, J. Y. Chin, B. S. Ooi, Z. A. Jawad, H. T. L. Leow, and S. C. Low, "Superhydrophobic membrane with hierarchically 3D-microtexture to treat saline water by deploying membrane distillation," *J. Water Process Eng.*, vol. 37, p. 101528, 2020.

[3] E. Guillen-Burrieza, A. Servi, B. S. Lalia, and H. A. Arafat, "Membrane structure and surface morphology impact on the wetting of MD membranes," *J. Memb. Sci.*, vol. 483, pp. 94–103, 2015.

[4] F. Tibi, A. Charfi, J. Cho, and J. Kim, "Fabrication of polymeric membranes for membrane distillation process and application for wastewater treatment: Critical review," *Process Saf. Environ. Prot.*, vol. 141, pp. 190–201, 2020.

[5] M. Teoh and T.-S. Chung, "Membrane distillation with hydrophobic macrovoid-free PVDF–PTFE hollow fiber membranes," *Sep. Purif. Technol. - SEP PURIF TECHNOL*, vol. 66, pp. 229–236, Apr. 2009.

[6] A. Figoli *et al.*, "Innovative hydrophobic coating of perfluoropolyether (PFPE) on commercial hydrophilic membranes for DCMD application," *J. Memb. Sci.*, vol. 522, pp. 192–201, 2017.

[7] A. Rosli, A. L. Ahmad, and S. C. Low, "Anti-wetting polyvinylidene fluoride membrane incorporated with hydrophobic polyethylene-functionalized-silica to improve CO2 removal in membrane gas absorption," *Sep. Purif. Technol.*, vol. 221, no. March, pp. 275–285, 2019.

[8] X. Li *et al.*, "Preparation of a super-hydrophobic poly(vinyl chloride) surface via solvent–nonsolvent coating," *Polymer (Guildf).*, vol. 47, no. 2, pp. 506–509, 2006.

[9] Y. Liao, R. Wang, and A. G. Fane, "Engineering superhydrophobic surface on poly(vinylidene fluoride) nanofiber membranes for direct contact membrane distillation," *J. Memb. Sci.*, vol. 440, pp. 77–87, 2013.

PGC_SCHE USM_2020_31

Development of Food Waste-Derived Biochar for CO_2 Capture at Ambient Condition

Amirul Hazwan Nor Azazi, Abdul Rahman Mohamed*
School of Chemical Engineering, Engineering Campus, Universiti Sains Malaysia,
14300 Nibong Tebal, Pulau Pinang, Malaysia
*E-mail:*chrahman@usm.my*

Abstract. Carbon dioxide (CO_2) happened to be a major problem to the global warming crisis, and lots of attention had been garnered to find a solution to end this catastrophe. In this study, biochar derived from key-lime peel and was produced to test its capability on combating this problem. To enhance the performance of CO_2, a modification with different metal oxyhydroxide was performed. However, it was later found that the overall performance starts to deteriorate over time. Thus, a new modification method is in need to stabilise the biochar produced. The highest adsorption was recorded for the pristine biochar pyrolysed at 700°C at a rate of 30°C/min for 1 hour with 52.84 mg/g of CO_2.
***Keywords**: Biochar; Lime Peel; Metal oxyhydroxide; CO_2 capture.*

INTRODUCTION

Currently, global warming caused by the emission of greenhouse gases, mainly carbon dioxide (CO_2), into the atmosphere, is the top spoken environmental issue that needs an immediate solution. One of the key technologies to alleviate the challenge of climate change is Carbon Capture and Utilisation (CCU). In this regard, adsorption-based separation techniques using solid sorbents have attracted considerable attention. The development of solid sorbents from low-cost precursors can help to the commercialisation of the process. Globally, food waste accounts for the largest contributor to solid waste [1]. The high moisture content of food waste causes some difficulties for waste management. Disposal of the waste by incineration releases a significant amount of greenhouse gases, mainly CO_2, into the atmosphere. Apart of consuming much of land space [2], disposing of the food waste in the landfill without any treatment would also give bad odours to the nearby environment and attracts pests which would make the place unhygienic. Moreover, the development of gaseous by-products such as methane (CH_4) and carbon dioxide, CO_2 would give a much dire consequence to the environment [3]. In recent years, many thorough investigations have shown that food waste has a high potential to be converted into biochar. Reports show that biochar coming from food waste is rich in nutrients that would help to remediate the soil condition [4]. Besides, the produced biochar from food waste can be used for CO_2 capture. There are few well-known methods currently being practised [5] for producing biochar, namely pyrolysis, which can be divided into slow and fast pyrolysis, and hydrothermal carbonisation and microwave-assisted carbonisation. In this research, slow pyrolysis at different heating rates will be used to produce biochar from key-lime peel, a widely used ingredient in local cooking. The developed biochar will be characterised and used for CO_2 capture studies.

MATERIALS AND METHODS

In a typical synthesis [4], the lime peel was firstly dried at 105°C to remove moisture. The dried peel was then pyrolysed in a tubular furnace under N_2 flow at a different heating rate of 5, 10, 20, 30 and 50° C/min to the desired carbonisation temperature (700°C) and specific duration (60 min). Then, the biochar was let to cold down under N_2 to room temperature. The modification was done using one-step pyrolysis [6]. An amount of magnesium nitrate hexahydrate, $Mg(NO_3)_2.6H_2O$ was dissolved in 60 mL of deionised (DI) water. 5g of dried lime peel was added, and the solution was stirred until saturated. The mixture was dried completely at 60°C and pyrolysed at 700°C for 1 hour under N_2 flow. The samples were then dried and stored in a closed container. The same modification step was done using aluminium nitrate nonahydrate, $Al(NO_3)_3.9H_2O$. The CO_2 adsorption capacity of the biochar further tested using a Thermogravimetric Analyzer (TGA) at different adsorption temperatures.

RESULTS AND DISCUSSION

The adsorption capacity of the pristine biochar is presented in Fig 1. In general, rate 30 showed the best performance compared to others with the capture of 52.84 mg/g of CO_2. The trend of all rates showed that 90 minutes of adsorption time is sufficient to reach the maximum CO_2 capture. The trend is also almost linear as the maximum capacity increase linearly from rate 5 to rate 30. However, preparing the biochar at rate 50 lowers the capacity by a considerable amount as compared to rate 30. This may occur due to the rapid pore development, which causes bigger

pore size to form. It is known from previous studies that the optimum pore size is between 7-9 Å [7]. Therefore, some characterisation such as BET surface area and SEM is critical to investigate this.

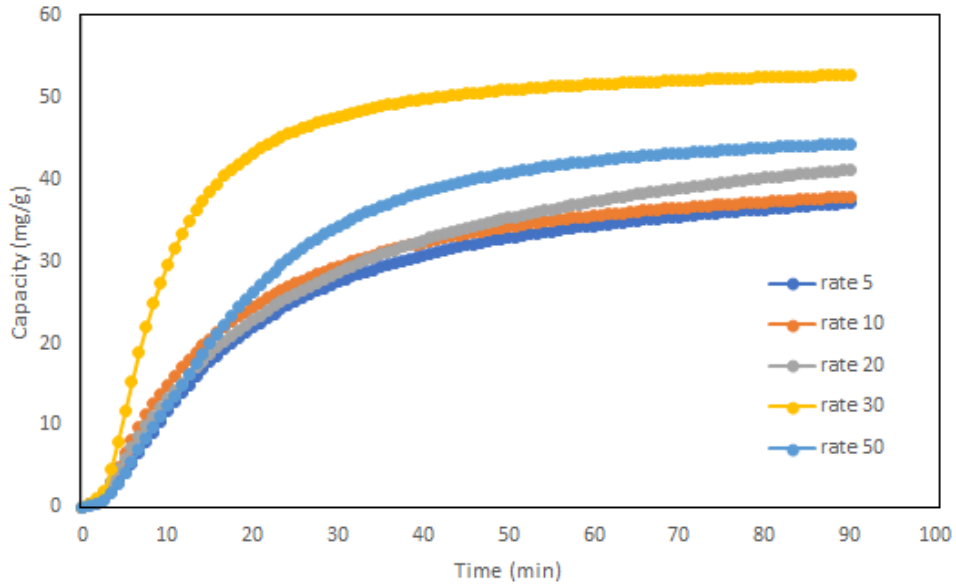

Figure 1: Adsorption capacity (mg/g) of lime peel biochar at different heating rates (°C/min)

Some modification was done to the pristine char with the desire to further increase its performance. Based on Fig 2, the modified char does not perform as well as the pristine char. Initial guess would be the pore developed had been clogged with the metal precursor, thus decreasing the active site for the adsorption process to take place. Therefore, new methods of modification need to experiment to sustain as well as improving the current performance. The pristine biochar prepared were tested again to see its performance. After several weeks of preparation, the performance of the same char started to deteriorate, as shown in Fig 3. Thus, raising the question of whether the biochar prepared from the lime peel is not suitable for the current application. Since CO_2 capture relies heavily on the pore size, it might have been that the pore developed does not sustain after some time. Nevertheless, more characterisation is needed to explain this phenomenon further.

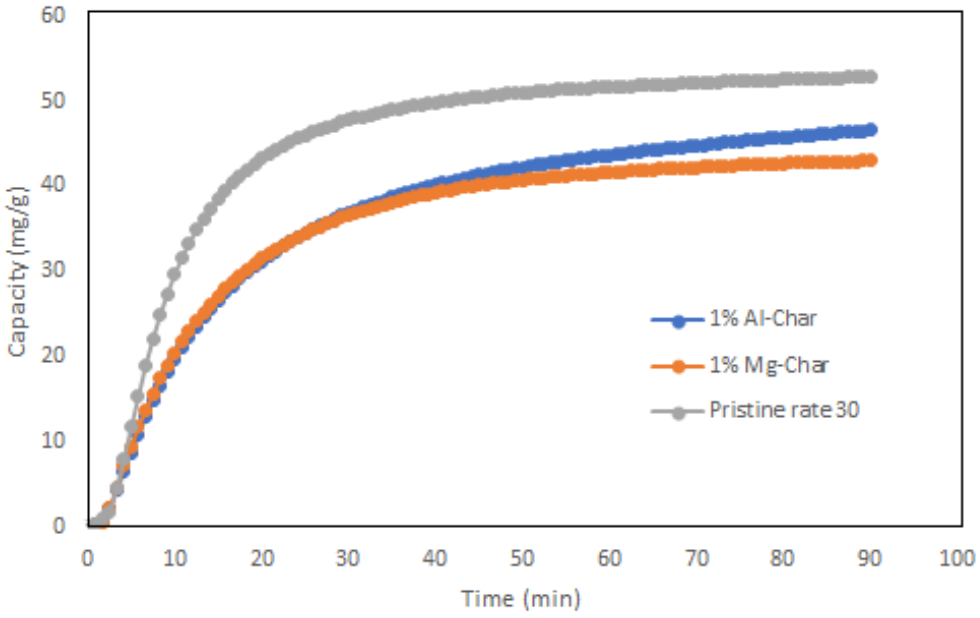

Figure 2: Adsorption capacity (mg/g) of modified char

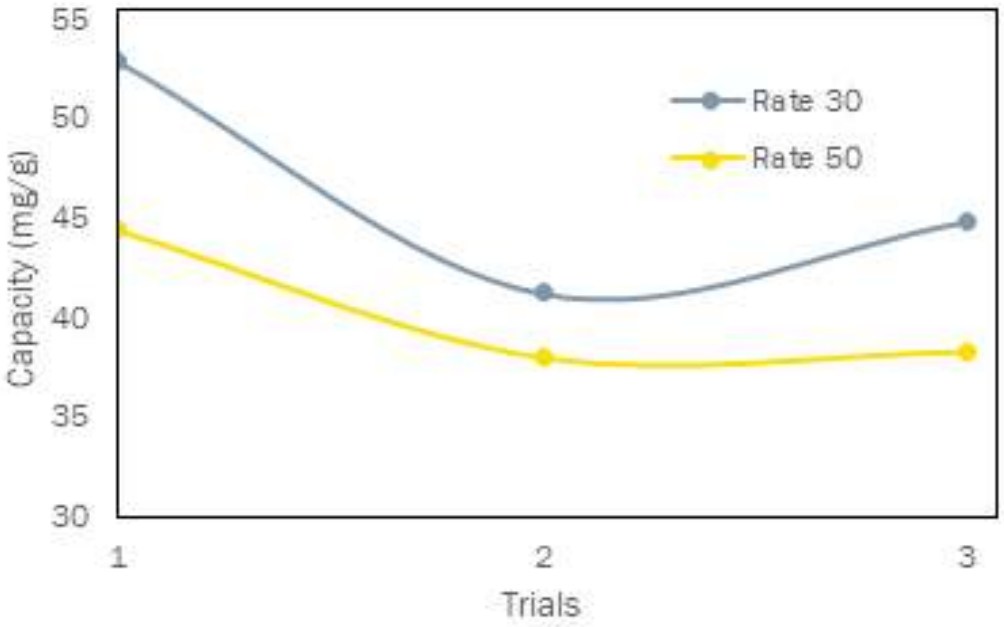

Figure 3: Adsorption capacity at different trials

CONCLUSION

Various biochar developed from key lime peel was done. The highest adsorption capacity obtained was at a heating rate of 30°C/min with a CO_2 capture of 52.84 mg/g.

ACKNOWLEDGEMENT

This research is funded under the Fundamental Research Grant Scheme (FRGS) (6071448) sponsored by the Ministry of Higher Education of Malaysia (MOHE).

REFERENCES

[1] M. Bagherzadeh, M. Inamura, and H. Jeong, "Food waste along the food chain," no. 71, 2014.
[2] D. Zhou, R. Wei, H. Long, J. Li, L. Qi, and C. Charles, "Combustion characteristics and kinetics of different food solid wastes treatment by blast furnace," *Renew. Energy*, vol. 145, pp. 530–541, 2020, doi: 10.1016/j.renene.2019.06.046.
[3] H. M. Kadlimatti, B. R. Mohan, and M. B. Saidutta, "Microwave-assisted pyrolysis of food waste : optimisation of fixed carbon content using response surface methodology," *Biofuels*, vol. 0, no. 0, pp. 1–8, 2019, doi: 10.1080/17597269.2019.1573609.
[4] M. Fu, C. Mo, H. Li, Y. Zhang, and W. Huang, "Comparison of physicochemical properties of biochars and hydrochars produced from food wastes," *J. Clean. Prod.*, vol. 236, p. 117637, 2019, doi: 10.1016/j.jclepro.2019.117637.
[5] S. Elkhalifa, T. Al-ansari, H. R. Mackey, and G. Mckay, "Food waste to biochars through pyrolysis : A review," *Resour. Conserv. Recycl.*, vol. 144, no. September 2018, pp. 310–320, 2019, doi: 10.1016/j.resconrec.2019.01.024.
[6] A. E. Creamer, B. Gao, and S. Wang, "Carbon dioxide capture using various metal oxyhydroxide – biochar composites," *Chem. Eng. J.*, vol. 283, pp. 826–832, 2016, doi: 10.1016/j.cej.2015.08.037.
[7] H. M. Coromina, D. A. Walsh, and R. Mokaya, "Biomass-derived activated carbon with simultaneously enhanced CO2 uptake for both pre and post combustion capture applications," *J. Mater. Chem. A*, vol. 4, no. 1, pp. 280–289, 2015, doi: 10.1039/c5ta09202g.

PGC_SCHE USM_2020_34

Environmental Evaluation of Bioplastic Extraction Methods from Bacteria Treating Palm Oil Mill Effluent

Rong-Er Lim, Vel Murugan Vadivelu*
School of Chemical Engineering, Engineering Campus, Universiti Sains Malaysia,
14300 Nibong Tebal, Pulau Pinang, Malaysia.
*E-mail: *chvel@usm.my*

Abstract. Polyhydroxyalkanoate (PHA) is a bioplastic naturally produced by bacteria but it is expansive due to the limited production. This study is to identify the most environment-friendly PHA extraction method among 5 extraction methods from bacteria treating Palm Oil Mill Effluent (POME) and identify the most contributing factor within the methods. The extraction methods were adopted from previous studies. 3 impact categories – climate changes, ozone depletion, and freshwater eutrophication were studied. Among the 3 selected impact categories, method 1 has the lowest impact for climate change and ozone depletion, while method 2 has the lowest impact for freshwater eutrophication. In conclusion, method 1 and 2 do not differ much but are outstanding compared to other methods. Method 4 and 5 have high impact in all impact categories because it does not undergo lyophilization process. In order to minimize the impact, the energy used for bacteria cultivation and PHA extraction need to be reduced. Further, the use of trichloromethane in extraction processes also need to be replaced or minimized.
Keywords: *Polyhydroxyalkanoate; environmental impact categories; bacteria; palm oil mill effluent*

INTRODUCTION

Plastic pollution has become an epidemic and is the great environmental challenge of our time. When plastic used ends up in the environment, it threatens nature. Finally, it can turn into micro-plastic fiber and enter our food chain. Besides recycling the plastic, the use of biodegradable plastic is another way to reduce plastic pollution. Among the various types of bioplastic, some can be composted in natural condition, but some only can be degraded in specific condition like in the facility. PHA is an outstanding natural degradable bioplastic. Besides, PHA is produced naturally by bacteria so it does not oppose the food scarcity issue. However, PHAs are expansive to make as only limited quantities can be produced from bacteria. To make PHA based plastic more practical, the production process should be improved or advanced. Most of the existing studies are focusing on life cycle assessment (LCA) of PHA production from different sources and waste. There is a lack of studies that is investigate the alternative ways to produce PHA from a single source. This study focuses on investigating the environmental impacts of different PHA extraction methods that are available. The study aims to identify and rank the environmental impacts of PHA extraction methods from the bacteria (aerobic granules) that are cultivated from POME treatment process. This study also identifies the most contributing process for each of the method and suggests mitigation steps to reduce the environmental impacts.

MATERIALS AND METHODS

The goal of this study is to evaluate the environmental impact of the methods to extract PHA from POME treating aerobic granules and thus identify the main process which caused the most impact on the life cycle impact assessment (LCIA). This work will identify the most optimum method for PHA extraction among the five methods. The system boundary of the study has shown as Figure 1. The function unit of the process is to produce lab scaled 1kg of dried PHA. SimaPro software version 8.5, developed by PRé Sustainability available in Malaysian Palm Oil Board (MPOB), was used. The ISO 14040:2006 and ISO 14044:2006 standards were followed in the study. The method used in this study is the ReCiPe Midpoint (E) V1.13 / World Recipe E. Top 3 impact categories have been selected using the normalization element available in the software. The 3 impact categories are climate change, ozone depletion and freshwater eutrophication. The evaluated 5 PHA extraction method was shown in Figure 2 and 3. The life cycle inventory (LCI) data collection is referred to previously published researches [1-6].

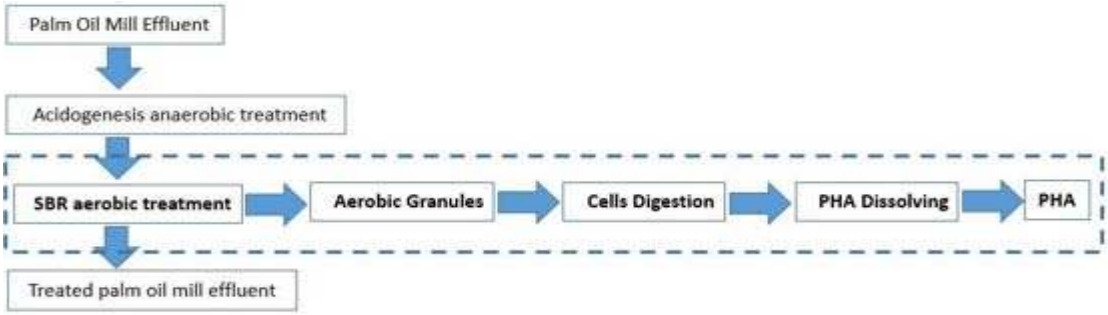

Figure 1: System Boundary

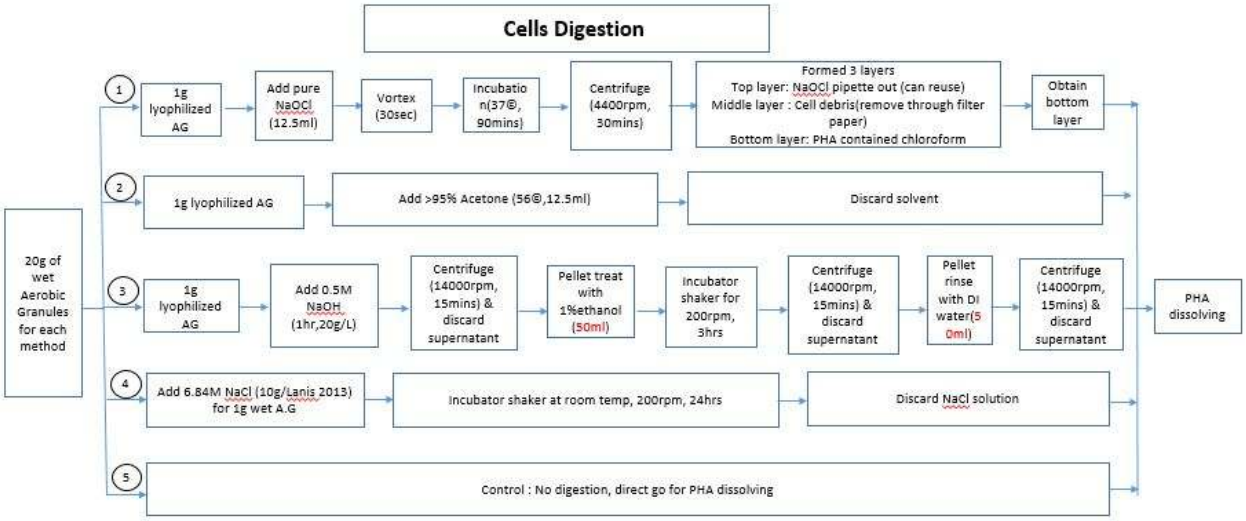

Figure 2: Cell Digestion methods

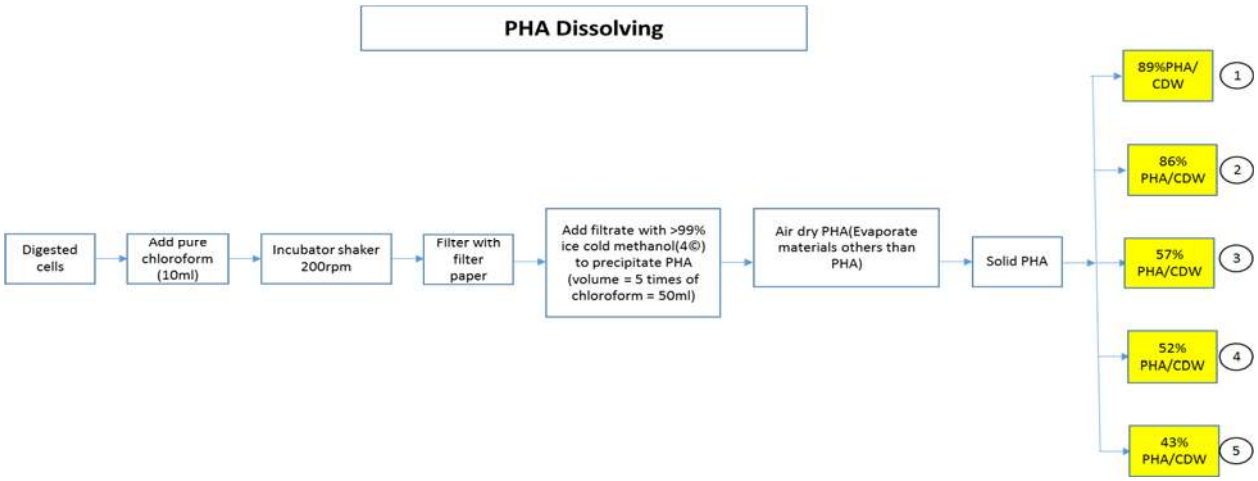

Figure 3: PHA dissolving and PHA yield

RESULTS AND DISCUSSION

In general, the PHA extraction methods can be categories into 3 main groups based on the impact categories. The first group consist of method 1 and 2 brings lowest impact among the 5 methods. The second group consist of method 3 bring medium impact, and the third group consist of method 4 and 5 bring highest impact to the impact categories. Method 1 and 2 gave lower impact and the impact categories brought by both methods were close to each other. In order to obtain 1kg of dried PHA, methods 1, 2, and 3 has lower impact because the aerobic granules

underwent lyophilization process. Lyophilization process is a process of drying in which water is sublimated from the aerobic granules after it is frozen [7]. In this study, lyophilization was applied to completely remove water content from the aerobic granules and it was able to reduce 90% to 95% of the aerobic granules weight. The amount of chemical used in the PHA extraction process is mainly weight per volume (w/v) basis. Therefore, the reduction in the weight of aerobic granules will reduce the amount of chemicals used in the extraction process. Consequently, when the amount of chemicals is reduced, the energy consumption for PHA extraction also reduce. The energy input is based on the power used by each piece of equipment such as vortex, incubator, centrifuge, evaporator, and freeze dryer. The calculation of energy use is based on equation stated below:

Energy consumption = Power Equipment × time × Capacity ratio of the samples occupying the equipment

Apart from that, methods 1 and 2 has the lowest impact because the extraction methods able to extract more PHA yield compare with Method 3, 4, and 5.

Table 1 shows the contribution of different PHA extraction methods to climate change in term of kg CO_2 equivalent. The result shows for climate change impact category, aerobic granules, electricity, and trichloromethane, are the top contributor for extraction methods of 1, 2, and 3. For the cultivation of aerobic granules, it required high input of aeration. The impact brought by aerobic granules is fully relying on the electricity use by the compressor. Electricity data used is based on Malaysia electricity generation data that is generated by the combustion of fossil fuel. Besides, trichloromethane contributed to climate change because the two common methods for commercial chloroform production are chlorination of methane and the chlorination of methyl chloride produced by the reaction of methanol and hydrogen chloride [8,9]. Chlorination of methane is a free radical substitution reaction. In this reaction, the use of methane caused the climate change impact since the global warming potential of methane is 21 CO_2 equivalent.

Table 1. Different PHA extraction methods contribute to climate change in term of kg CO_2 equivalent

Method	EPS digestion chemical	Trichlorom ethane	Methanol	Water	Wet Aerobic Granules	Electricity	Ethanol
1	30.84	37.73	17.40	0.01	468.04	171.71	-
2	22.94	39.05	18.00	0.01	484.37	180.12	-
3	4.45	58.92	27.16	0.17	730.80	486.78	0.78
4	436.30	1291.69	595.52	2.64	801.07	38.54	-
5	-	1562.03	720.17	0.42	968.70	0.17	-

Table 2 shows the contribution of the extraction methods to ozone depletion in term of kg CFC-11 equivalent. As shown in Table 2, for all 5 methods, the main contributor to ozone-depletion impact category is the use of trichloromethane. Trichloromethane is able to deplete the ozone layer due to the chlorine atom which has high potential to be chlorine radical. Chlorine radical has a high tendency to breaks bonds in ozone molecule. Although trichloromethane is not covered in Montreal protocol as long-lived ozone depleting substances, but according to [10], the rose of trichloromethane emission have pose a growing threat for ozone-layer recovery. Therefore, if ozone depletion impact needs to be lower down, substitution or replacement for trichloromethane is a must.

Table 2. Different PHA extraction methods contribute to ozone depletion in term of kg CFC-11 equivalent

Method	EPS digestion chemical	Trichlorom ethane	Methanol	Water	Wet Aerobic Granules	Electricity	Ethanol
1	1.7E-05	1.2E-02	6.2E-06	8.7E-09	1.7E-05	6.2E-06	-
2	3.8E-07	1.3E-02	6.4E-06	7.0E-09	1.8E-05	6.5E-06	-
3	2.6E-06	1.9E-02	9.6E-06	1.2E-07	2.7E-05	1.7E-05	2.5E-08
4	3.7E-05	4.2E-01	2.1E-04	1.8E-06	3.0E-05	1.4E-06	-
5	-	5.1E-01	2.5E-04	2.8E-07	3.6E-05	6.1E-09	-

Table 3 represents the impact of PHA extraction methods towards freshwater eutrophication in term of kg P equivalent. For freshwater eutrophication impact, method 2 is the lowest among the 5 methods followed by method 1, 3, 5 and the method 4. Aerobic granules and electricity consumption are the major two contributors for method 1,

2, and 3. According to the statistic from Malaysia Energy Information Hub (MEIH), by year 2018, 41%, 26%, and 22% of total energy supply was from the combustion of natural gas, crude oil, and coal coke respectively. Combusted fossil fuels release nitrogen oxides (NOx) into the environment and caused the deposition in freshwater and coastal ecosystem[11].Therefore, to lower down eutrophication impact for method 1, 2, and 3, the electricity consumption need to be reduced.

Table 3. Different PHA extraction methods contribute to freshwater eutrophication in term of kg P equivalent

Method	EPS digestion chemical	Trichlorom ethane	Methanol	Water	Wet Aerobic Granules	Electricity	Ethanol
1	0.01798	0.01550	0.00386	0.00001	0.18861	0.06910	-
2	0.00324	0.01604	0.00399	0.00001	0.19518	0.07248	-
3	0.00257	0.02421	0.00602	0.00012	0.29449	0.19589	0.00037
4	0.30546	0.53069	0.13208	0.00188	0.32281	0.01551	-
5	-	0.64176	0.15972	0.00030	0.39036	0.00007	-

CONCLUSION

As a conclusion, method 1 and 2 are better among the 5 methods studied. Methods 1 and 2 have close value for all impacts. Almost all impact categories were mainly contributed by aerobic granules, followed by electricity and thirdly is the use of trichloromethane. Ozone depletion impact categories was dominated using trichloromethane. In order to make method 4 and 5 to be more environmentally friendly, lyophilization process is suggested to take place for the wet aerobic granules. In order to minimize the impact, the energy used by aerobic granules cultivation and electricity needs to be reduced. The use of trichloromethane need to be replaced or minimized.

ACKNOWLEDGEMENT

This research is funded under the Research University Grant (RUI) 8014066, Universiti Sains Malaysia.

REFERENCES

[1] Mohammadi, M., Hassan, M.A., Shirai, Y., Man, H.C., Ariffin, H., Yee, L.N., Mumtaz, T., Chong, M.L. and Phang, L.Y. ***47*(3)** 534-541 (2012).
[2] Hahn, S.K., Chang, Y.K., Kim, B.S. and Chang, H.N. **44(2)** 256-261. (1994).
[3] Gamal, R.F., Abdelhady, H.M., Khodair, T.A., El-Tayeb, T.S., Hassan, E.A. and Aboutaleb, K.A., **44(2)** 539-549 (2013).
[4] Anis, S.N.S., Iqbal, N.M., Kumar, S. and Amirul, A.A. **102** 111-117 (2013).
[5] Duque, A.F., Oliveira, C.S., Carmo, I.T., Gouveia, A.R., Pardelha, F., Ramos, A.M. and Reis, M.A. **31(4)** 276-288 (2014).
[6] Gobi, K. and Vadivelu, V.M. **189** 169-176 (2015).
[7] Nireesha, G.R., Divya, L., Sowmya, C., Venkateshan, N.N.B.M. and Lavakumar, V. **3(4)** 87–98 (2013).
[8] Deshon, H., *m.* Kirk-Othmer **5** 693-703. (1979).
[9] Ahlstrom, R. and J. Steele **5** 677-685. (1979).
[10] King, A. *Chemistry World*. (2019).
[11] Selman, M. and Greenhalgh, S. **26(4)** 19–26 (2010).

PGC_SCHE USM_2020_37

Screening of Natural Coagulant from Fruit Peels for Turbidity Removal

Khadijah Md Noh, Suzylawati Ismail*
School of Chemical Engineering, Engineering Campus, Universiti Sains Malaysia,
14300 Nibong Tebal, Pulau Pinang, Malaysia.
*E-mail: *chsuzy@usm.my*

Abstract. Alum and ferric chloride are well known as an effective coagulant. However, there are many disadvantages associated, such as high operating costs, harmful effects on human health, production of large volumes of sludge and the fact that the pH of treated water is significantly affected. Therefore, it is beneficial to substitute these synthetic chemical coagulants with natural coagulants originated from fruit peels to counter the mentioned drawbacks. Therefore, the purpose of this study is to investigate the effectiveness of fruit peels as natural coagulants for turbidity removal in water treatment. The fruit peels screened in this study were the peel of orange, mango, papaya, pumpkin, rambutan, cucumber, lime, kaffir lime, pineapples and banana. These peels were prepared by washing, drying, grinding and finally sieving, and extracting using distilled water, thus the final product of natural coagulants was ready to be used. A series of jar test were then performed to determine the effect of individual natural coagulants on the efficiency of turbidity removal. Among the studied fruit peels' coagulants, banana peels coagulant gave the highest turbidity removal (57.2 %) followed by mango peels coagulant (53.1 % removal). Coagulant concentration of mango at 60 mg/L and banana peels at 80 mg/L were the minimum concentration obtained in order to get the highest turbidity removal for each material.
Keywords: *natural coagulant; fruit peels; turbidity removal.*

INTRODUCTION

Lots of impurities in water and wastewater are present as colloidal solids, which do not readily settle. The ordinary sedimentation not adequately remove fine dispersed suspended and colloidal particles which produce turbidity. Colloidal particles generally carry a negative electrical charge. Thus, these particles are surrounded by an electric double layer (diffuse layer and stern layer) which prevents contact between them [1]. Using a coagulant (usually positively charged) and adding water induces a double layer compression and hence neutralization of the electrostatic surface potential of the particles. The resulting destabilized particles stick together upon contact forming solids known as 'flocs'. Coagulation is an essential stage in conventional water and wastewater treatment process. Coagulation is a process that combines small particles into larger aggregates (flocs) and simultaneously adsorbing dissolved organic matter on to particulate aggregates so that these impurities can be removed in subsequent solid/liquid separation processes. Alum (aluminium sulphate), ferric chloride and cationic polymers are the common synthetic chemical coagulant that been used in the treatment process. [2], [3] However, there are also risks associated with the use of such coagulants, such as high maintenance costs, adverse effects on human health and a significant impact on the pH of treated water. Besides, the use of these synthetic chemical coagulants also tends to create end sludge product and usually, the sludge is toxic and hazardous. Due to such matter, proper treatment of the sludge before disposal is important. This sludge will normally be disposed to secured landfill, which then require a greater cost.

The alternative of synthetic chemical coagulant, natural coagulant; has been used in many countries as an option. These coagulants were produced from various plant materials such as plant seeds, leaves and roots [4]. Among the known natural coagulants are *Moringa oleifera, Jatropha curcas, Strychnos potatorum, Hibiscus sabdariffa* and many more [5]. These natural coagulants are sustainable because there are no health hazards and the cost of producing these natural coagulants was less expensive than the synthetic chemical coagulants since it is locally available. The natural coagulants can treat water of high turbidity and having remarkable removal efficiency [6]. It is beneficial to substitute these coagulants with more natural coagulants, such as fruit peels, which can overcome the above disadvantages. Therefore, this study aims to investigate the efficiency of fruits peels as natural coagulants in treating wastewater.

MATERIALS AND METHODS

Materials

Ten different fruit wastes namely orange peels, mango peels, papaya peels, pumpkin peels, rambutan peel, cucumber peels, lime peels, kaffir lime peels, pineapples peels, and banana peels were screened for the potential to be utilized as natural coagulant.

Preparation of Coagulant

The preparation of coagulant was conducted based on the methods described by Zurina and co-workers [7] with slight modifications. The samples were washed with distilled water several times to remove dirt and contaminants, followed by drying in a hot air oven at 80 °C for at least 24 hours. The dried samples were then ground or crushed using a blender, sieved well in a fraction of 150 µm. The powdered sample then was stored in an airtight container prior to coagulant extraction processes. In the preparation of coagulant, dried raw materials were soaked in distilled water at room temperature and stirred for 1 hour. The suspension was filtered through filter paper and the filtered extract was then used in the experiments.

Preparation of Synthetic Turbid Water

Stock kaolin suspension was prepared by dissolving kaolin in distilled water at room temperature. The suspension was then stirred under moderate speed for 30 minutes in a jar test apparatus to obtain a uniform dispersion of kaolin particles. The initial turbidity of synthetic turbid water before coagulation process was maintained between 250 - 280 NTU.

Coagulation Experiment

The coagulation testing was performed using a Jar Test unit. The study involved stages of rapid mixing, slow mixing and sedimentation in a batch process. For rapid mixing, the agitator was turned on at the speed of 80 rpm for 1 minutes once the coagulant from all fruit wastes was added into beakers containing 500 ml of synthetic turbid water each. Then, slow mixing was conducted at 30 rpm for approximately 30 minutes before the samples were left to sediment for 30 minutes. After sedimentation, a small volume of sample was collected without agitating the sediments at the bottom to measure the turbidity using a turbidity meter. The coagulation properties were evaluated by measuring the turbidity of the treated water. The percentage of turbidity removal was determined by using Equation (1):

$$\text{Turbidity removal percentage} = \frac{final\ turbidity - initial\ turbidity}{initial\ turbidity}\ x\ 100 \quad (1)$$

RESULTS AND DISCUSSION

In this study, ten fruit peels were selected, and crude extracts were prepared for coagulation activity analysis. Initially, all crude extracts were prepared with water solution to screen the coagulation activity from different materials. The fruit peels coagulant that showed coagulation activity is shown in Figure 1. Among the ten samples, there were only mango and banana peel extracts showed the turbidity removal more than 50 % and only orange-peel coagulant showed less than 40% turbidity removal.

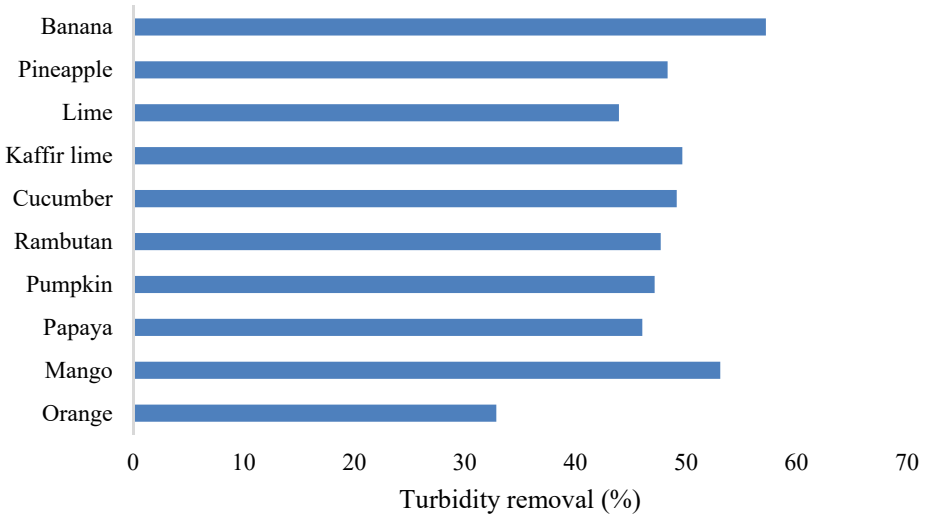

Figure 1: Percentage of turbidity removal using different fruit peels (coagulant concentration = 60 mg/L, rapid mixing = 80 rpm, slow mixing = 30 rpm, sedimentation time = 30 minutes)

Effect of Concentration on the Efficiency of Natural Coagulant

Two fruit peel extracts coagulants, banana and mango gave the highest turbidity removal (> 50%) were selected to study the effect coagulation concentration towards the turbidity removal from the synthetic turbid water. It is best to obtain optimum coagulant dosage that is sufficiently able to treat the water and at the same time does not give any adverse effect to the quality of the water. In this study, the coagulant concentration was varied at 0 mg/L, 20

mg/L, 40 mg/L, 60 mg/L, 80 mg/L, and 100 mg/L. These variations were conducted without any pH adjustment. Figure 2 showed the turbidity removal using banana and mango peel extracts, respectively, under various dosages.

Based on the result shown in Figure 2, both natural coagulants showed fluctuation in removing the turbidity. Based on the figure, coagulant dosage of 60 mg/L contributed to the highest turbidity removal for mango peels while banana peels at coagulant concentration of 80 mg/L. This dosage is taken as the best coagulant dosage to be used in later work. At 80 mg/L, banana peels indicated highest turbidity removal of 56.5%%, while at 60 mg/L, mango peels coagulant removed 52.3% turbidity from the synthetic turbid water. After 60 mg/L for mango and 80 mg/l for banana peel extracts, the turbidity removal showed decreases trend. This phenomenon might be due to all attractive charges of the particles have been fully attracted to each other before settling. If high dosage is used, the excess coagulants will simply get added thus, cause turbidity in water. The next stage of this research work is to improve the turbidity removal by modifying the banana and mango peel extracts.

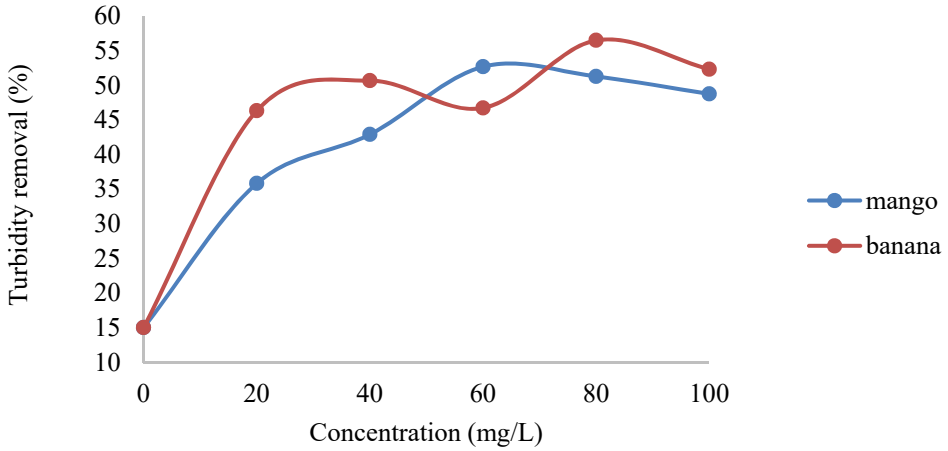

Figure 2: Percentage of turbidity removal using banana and mango peels at different coagulant concentration (rapid mixing = 80 rpm, slow mixing = 30 rpm, sedimentation time = 30 minutes)

CONCLUSION

In this study, ten fruit peel extracts were screened for turbidity removal from synthetic wastewater. Among the ten samples, banana and mango extracts show the highest turbidity removal. Highest turbidity removal was achieved at coagulant concentration of 80 mg/L for banana and 80 mg/L for mango.

ACKNOWLEDGEMENT

The authors would like to acknowledge the Long-Term Research Grant Scheme 1/2018, LRGS (203/PJKIMIA/6770005), under Ministry of Higher Education Malaysia for funding this research project.

REFERENCES

[1] B. Bolto and J. Gregory, "Organic polyelectrolytes in water treatment," *Water Research*. (2007).

[2] A. Sowmya and S. Meenakshi, "Zr(IV) loaded cross-linked chitosan beads with enhanced surface area for the removal of nitrate and phosphate," *Int. J. Biol. Macromol.*, vol. 69, pp. 336–343, Aug. (2014).

[3] F. P. Camacho, V. S. Sousa, R. Bergamasco, and M. Ribau Teixeira, "The use of Moringa oleifera as a natural coagulant in surface water treatment," *Chem. Eng. J.*, vol. 313, pp. 226–237, Apr. (2017).

[4] S. Y. Choy, K. M. N. Prasad, T. Y. Wu, M. E. Raghunandan, and R. N. Ramanan, "Utilization of plant-based natural coagulants as future alternatives towards sustainable water clarification," *J. Environ. Sci.*, vol. 26, no. 11, pp. 2178–2189, Nov. (2014).

[5] M. Pritchard, T. Mkandawire, A. Edmondson, J. G. O'neill, and G. Kululanga, "Potential of using plant extracts for purification of shallow well water in Malawi," *Phys. Chem. Earth, Parts A/B/C*, vol. 34, no. 13–16, pp. 799–805, (2009).

[6] H. Bhuptawat, G. K. Folkard, and S. Chaudhari, "Innovative physico-chemical treatment of wastewater incorporating Moringa oleifera seed coagulant," *J. Hazard. Mater.*, (2007).

[7] Z. A. Zurina, M. Mohd Fadzli, and L. A. Abdul Ghani, "Preliminary study of rambutan (Nephelium lappaceum) seed as potential biocoagulant for turbidity removal," in *Advanced Materials Research*, (2014).

PGC_SCHE USM_2020_38

Catalytic Co-pyrolysis of Plastic Waste and Biomass for the Production of Fuel Oil: Positive Synergistic Effect of Feedstock on Fuel Oil Yield and Quality –A Short Review

A.W., Gin, M.A., Ahmad, A.T., Mohd Din*
School of Chemical Engineering, Engineering Campus, Universiti Sains Malaysia,
14300 Nibong Tebal, Pulau Pinang, Malaysia.
*E-mail: *chazam@usm.my*

Abstract: Much interest has been shown recently in the co-pyrolysis of plastics and biomass for the production of fuel oil. Although considerable headway has been made in the investigation of the impact of experimental conditions on the yield of the fuel oil produced, studies on synergistic effect of the co-pyrolysis of plastic and biomass has not been considered much. Latest studies on the synergistic effect of co-pyrolysis of biomass with plastics are discussed in terms of liquid yield and quality.
Keywords: *Copyrolysis, fuel oil, plastic, biomass, synergistic effect*

INTRODUCTION

The growing demand for energy combined with the dwindling fossil fuel reserves, energy insecurity, and environmental challenges created by global warming and exacerbating air pollution necessitates a shift away from non-renewable fuels. Moreover, many countries are now facing the challenge of managing the increasing mass of plastic waste being accumulated in the environment due to the increasing population and changing lifestyle over the years. Thus, converting these plastic wastes to liquid fuels can be an attractive option to address these environment challenges while providing energy security. Pyrolysis of plastics with biomass wastes together to produce liquid fuels using a process called co-pyrolysis can be a promising option to reduce these wastes and the negative impact in the environment. Some set of investigations have been carried out by different researchers on synergistic effect of different biomass with plastic feedstock to verify or improve the yield and quality of the fuel oil produced during co-pyrolysis process [1].

The term of 'synergistic effect' has been commonly used to describe how thermal co-pyrolysis improves the yield of bio-oil, not the yield of non-polar fraction of bio-oil. A recent review carried out by Ryu *et al* [2] noted that the synergistic effect gives two benefits during co-pyrolysis of biomass . Firstly, co-pyrolysis of equal-mass feeds compared that obtained from pyrolysis of biomass alone leads to an improvement in the quantity of the liquid yield obtained, and the secondly, there is an improvement in the heating value of the co- pyrolytic oil compared to that obtained from pyrolysis of biomass alone. Thermal co-pyrolysis of biomass and plastics can lead to higher fuel-oil yield attributable to the free radical interaction of both feed charges

In most studies on co-pyrolysis of plastic waste and biomass, a substantial part of these studies has investigated the positive synergistic effect of the feedstock with the aim of improving the productivity and efficiency of the co-pyrolysis process. However most reviews [3], [4], have provided very limited discussion on this interesting aspect of co-pyrolysis studies. This review concisely discusses the positive synergistic effect of co-pyrolysis and catalytic co-pyrolysis of plastic and biomass using oil yield and quality as parameters.

SYNERGISTIC EFFECT OF CO-PYROLYSIS OF PLASTIC AND BIOMASS

Some researchers have observed positive synergetic effect during co-pyrolysis of biomass and plastics using increased production of bio-oil; reducing oxygenated compounds and alcohol content as parameters. Specific findings in these studies are summarized in Table 1. Generally, there exists a best mixing ratio of plastic and biomass to maximize the liquid production during co-pyrolysis.

SYNERGISTIC EFFECT OF CATALTIC CO-PYROLYSIS OF PLASTIC AND BIOMASS

Few researchers have investigated the effect of metals and catalyst on synergy between plastic and biomass during co-pyrolysis.[14]–[16] studied the co-pyrolysis of cellulose/ HDPE using TGA and Py-GC/MS. It was discovered that addition of potassium inhibited the synergy between cellulose and HDPE increasing the yields of furans and ketones. A contrary outcome was found in the co-pyrolysis of sugarcane bagasse and polystyrene in the presence of HZSM-5 and MgO/CaO catalysts. These catalyst promoted aromatic hydrocarbons formation and suppressed poly-aromatic hydrocarbon (PAH) and oxygenates in liquid yield [17]. Table 2 presents a summary of studies regarding synergistic effect of catalytic co-pyrolysis.

Table 1: Some findings regarding positive synergetic effects of co-pyrolysis of plastic and biomass

Biomass	Plastic	Pyrolysis environment and experimental conditions	Remarks	Ref
Corn cobs	PP	A stirred tank reactor was developed and used to carry out co-pyrolysis of feedstock containing 0%, 50%, and 100%PP	• Maximum synergistic effect was obtained in feed containing 50% PP	[5]
Frying oil	Plastic waste (PW)	Microwave (800 W) cooker was customised to carry out co-pyrolysis in continuous stirred batch pyrolysis reactor at ratios of 1:2, 1:1.5, 1:1, 1.5:1, and 2:1	• Co-pyrolysis reactions had engendered a high yield of liquid fuel (81 wt.%) and smaller amounts of pyrolysis gases (18 wt.% at 1:1	[6]
Micro Algae	PVC	Pyrolysis system with microwave assistance was used and microwave power adjusted from 800 W to 1000 W, heating rate 257 °C/min to 402 °C/min),	• Co-pyrolysis reaction caused high bio-oil yield when biomass-plastic ratios were 5:5 and 3:7 at 800 W and 5:5 at 1000 W, respectively.	[7]
Lignin	PP	Microwave cooker (CEM Corporation) model was adopted as reactor and used to carry out pyrolysis at different lignin/PP mass ratios of 1:0, 1:1, 1:2, 2:1, and 0:1	• Interaction between reactants appreciably enhanced as lignin/PP ratio varied from 2:1 to 1:2.	[8]
Grape seeds	PS	Fixed-bed apparatus, was used to conduct experiment at varied biomass-plastic ratio of 95/5; 90/10; 80/20; 60/40	• Noteworthy synergistic effects were found with the addition of 5–40 wt% polystyrene • Co-pyrolysis achieved over 80 wt% of organic phase yield, which is markedly higher than those obtained biomass pyrolysis (61 wt%).	[9]

Researchers have asserted that positive synergy exist during pyrolysis of biomass and plastics when the empirical value is higher than the computed values[10]–[13].

Table 2: Some findings regarding positive synergetic effects of catalytic co-pyrolysis of plastic and biomass

Biomass	Plastic	Catalyst	Pyrolysis environment and experimental conditions	Remarks	Ref
Lignin	PP	ZSM-5	A microwave reactor was developed and used to carry out co-pyrolysis of feedstock-catalyst ratio of 1:0, 1:1, 2:1, and 4:1	◗ Lignin-PP ratio of 4:1 gave the maximum bio-oil yield ◗ Increasing ZSM-5 -feedstock ratio lowered the bio-oil yield and proportion of cycloalkanes while increasing the proportion of aromatics	[8]
Pine sawdust	HDPE	HZSM-5	A fixed-bed reactor was developed and used to carry out co-pyrolysis of feedstock-catalyst ratio of 2.5– 10: 50	◗ HZSM-5-feed stock ratio of 0.2 gave maximum yield alkanes and aromatic hydrocarbon (benzene, toluene, xylene (BTX): (51.6–70.6 %)) ◗ Plastic to biomass ratio of 0.6 gave hydrocarbons yield of 18.3 % and the highest aromatic selectivity of 67.8 % at 400 °C, 1.5 MPa for 1 h ◗ Oxygenates were almost absent in bio-oil.	[18]

There is also a dire need to develop zeolites catalyst with functionalized groups which guarantees a high sensitivity as well as selectivity for desired quality components of pyrolytic oil produced from catalytic co-pyrolysis of plastic and biomass for use as liquid fuel. Currently, the functionalization of zeolite catalyst is the frontier of materials sciences. Such research will promote the development of innovative, low cost and highly capable zeolite catalyst. It must be pointed out that one notable attribute of functionalized zeolites may be their enhanced recyclability, which makes it possible for reutilization after many cycles. While some works aver that functionalization of zeolite could be achieved by introducing metallic oxides into the zeolite surface through chemical routes, others reports state that this can be also be realized through impregnation of zeolite with transition metals (Ni, Co, Fe or Mn). Besides modifying the zeolites with either metal or metallic oxides, the change of its physical structure through dealumination techniques (heat, chemical agents etc.) can improve the conversion for co-pyrolysis of plastic and biomass to produce high-grade fuel. Future research should carefully choose the functionalization route according to the properties of plastic-biomass feedstock and developed zeolite, as well as the operating conditions of the catalytic co-pyrolysis process. Although most plastic decomposes in a higher temperature range than biomass does, their melting temperature is below 300 °C, which overlaps with the decomposition temperature range of biomass. It is probable the biomass particles either stick to or is enclosed by melting plastic, which suppresses the transport of pyrolysis vapors out of reaction zone. This limited mass transfer increases the possibility of secondary reaction including dehydration, decarboxylation, decarbonylation and repolymerization, resulting in the production of solid and light gas at the expense of liquid products. Thus, increasing the mass transfer and product transport during co-pyrolysis of biomass and plastic could potentially minimize the negative synergistic effects

CONCLUSION

Findings on the synergistic effect of co-pyrolysis and catalytic co-pyrolysis of plastic and biomass have been presented and discussed. Future work should focus on developing zeolites catalyst with functionalized groups which guarantees a high sensitivity as well as selectivity for desired quality components of pyrolytic oil produced from catalytic co-pyrolysis of plastic and biomass for use as liquid fuel.

ACKNOWLEGMENT

The author gratefully acknowledges the support provided by Lotte Chemical Titan, Berhad, in symbiotic research collaboration with University Sains Malaysia (304/PJKIMIA/6050422/L128)

REFERENCES

[1] Y. Tang, Q. Huang, K. Sun, Y. Chi, and J. Yan, “Bioresource Technology Co-pyrolysis characteristics and kinetic analysis of organic food waste and plastic,” *Bioresour. Technol.*, vol. 249, no. September 2017, pp. 16–23, 2018, doi: 10.1016/j.biortech.2017.09.210.

[2] H. W. Ryu, D. H. Kim, J. Jae, S. S. Lam, E. D. Park, and Y. K. Park, “Recent advances in catalytic co-pyrolysis of biomass and plastic waste for the production of petroleum-like hydrocarbons,” *Bioresour. Technol.*, vol. 310, no. May, p. 123473, 2020, doi: 10.1016/j.biortech.2020.123473.

[3] B. B. Uzoejinwa, X. He, S. Wang, A. El-Fatah Abomohra, Y. Hu, and Q. Wang, “Co-pyrolysis of biomass and waste plastics as a thermochemical conversion technology for high-grade biofuel production: Recent progress and future directions elsewhere worldwide,” *Energy Conversion and Management*, vol. 163. pp. 468–492, 2018, doi: 10.1016/j.enconman.2018.02.004.

[4] M. H. M. Ahmed, N. Batalha, H. M. D. Mahmudul, G. Perkins, and M. Konarova, “A review on advanced catalytic co-pyrolysis of biomass and hydrogen-rich feedstock: Insights into synergistic effect, catalyst development and reaction mechanism,” *Bioresour. Technol.*, vol. 310, no. March, p. 123457, 2020, doi: 10.1016/j.biortech.2020.123457.

[5] D. Supramono, A. F. Sitorus, and M. Nasikin, “Synergistic effect on the non-oxygenated fraction of bio-oil in thermal co-pyrolysis of biomass and polypropylene at low heating rate,” *Processes*, vol. 8, no. 1, 2020, doi: 10.3390/pr8010057.

[6] W. Adibah *et al.*, “Production of value-added liquid fuel via microwave co-pyrolysis of used frying oil and plastic waste,” *Energy*, vol. 162, pp. 309–317, 2018, doi: 10.1016/j.energy.2018.08.002.

[7] M. Dai *et al.*, “Microwave-assisted fast co-pyrolysis behaviors and products between microalgae and polyvinyl chloride,” *Appl. Therm. Eng.*, vol. 136, no. February, pp. 9–15, 2018, doi: 10.1016/j.applthermaleng.2018.02.102.

[8] D. Duan *et al.*, “Bioresource Technology Ex-situ catalytic co-pyrolysis of lignin and polypropylene to upgrade bio-oil quality by microwave heating,” *Bioresour. Technol.*, vol. 241, pp. 207–213, 2017, doi: 10.1016/j.biortech.2017.04.104.

[9] A. Veses, M. V Navarro, J. M. López, R. Murillo, M. S. Callén, and T. García, “Drop-in biofuels from the co-

pyrolysis of grape seeds and polystyrene," *Chem. Eng. J.*, vol. 377, no. October 2018, p. 120246, 2019, doi: 10.1016/j.cej.2018.10.183.

[10] W. Chen, S. Shi, M. Chen, and X. Zhou, "Fast co-pyrolysis of waste newspaper with high-density polyethylene for high yields of alcohols and hydrocarbons," *Waste Manag.*, vol. 67, pp. 155–162, 2017, doi: 10.1016/j.wasman.2017.05.032.

[11] W. Chen, S. Shi, J. Zhang, M. Chen, and X. Zhou, "Co-pyrolysis of waste newspaper with high-density polyethylene: Synergistic effect and oil characterization," *Energy Convers. Manag.*, vol. 112, pp. 41–48, Mar. 2016, doi: 10.1016/j.enconman.2016.01.005.

[12] H. Hassan, B. H. Hameed, and J. K. Lim, "Co-pyrolysis of sugarcane bagasse and waste high-density polyethylene: Synergistic effect and product distributions," *Energy*, vol. 191, Jan. 2020, doi: 10.1016/j.energy.2019.116545.

[13] H. Yuan, H. Fan, R. Shan, M. He, J. Gu, and Y. Chen, "Study of synergistic effects during co-pyrolysis of cellulose and high-density polyethylene at various ratios," *Energy Convers. Manag.*, vol. 157, no. December 2017, pp. 517–526, 2018, doi: 10.1016/j.enconman.2017.12.038.

[14] X. Lin, L. Kong, H. Cai, Q. Zhang, D. Bi, and W. Yi, "Effects of alkali and alkaline earth metals on the co-pyrolysis of cellulose and high density polyethylene using TGA and Py-GC/MS," *Fuel Process. Technol.*, vol. 191, no. December 2018, pp. 71–78, 2019, doi: 10.1016/j.fuproc.2019.03.015.

[15] Y. Park *et al.*, "Catalytic co-pyrolysis of yellow poplar wood and polyethylene terephthalate over two stage calcium oxide-ZSM-5," *Appl. Energy*, vol. 250, no. April, pp. 1706–1718, 2019, doi: 10.1016/j.apenergy.2019.05.088.

[16] S. Xu *et al.*, "Synergistic effects of catalytic co-pyrolysis of macroalgae with waste plastics," *Process Saf. Environ. Prot.*, vol. 137, pp. 34–48, 2020, doi: 10.1016/j.psep.2020.02.001.

[17] H. Iftikhar, M. Zeeshan, S. Iqbal, B. Muneer, and M. Razzaq, "Co-pyrolysis of sugarcane bagasse and polystyrene with ex-situ catalytic bed of metal oxides/HZSM-5 with focus on liquid yield," *Bioresour. Technol.*, vol. 289, Oct. 2019, doi: 10.1016/j.biortech.2019.121647.

[18] W. Chen *et al.*, "Aromatic hydrocarbons production and synergistic effect of plastics and biomass via one-pot catalytic co-hydropyrolysis on HZSM-5," *J. Anal. Appl. Pyrolysis*, no. January, p. 104800, 2020, doi: 10.1016/j.jaap.2020.104800.

PGC_SCHE USM_2020_40

Quantifying Relationship between Chain Transfer Agent and Melt Flow Index for Low Density Polyethylene Tubular Reactor Production

Dinie Muhammad, Zainal Ahmad, Norashid Aziz*
School of Chemical Engineering, Engineering Campus, Universiti Sains Malaysia,
14300 Nibong Tebal, Penang, Malaysia
Email: * chnaziz@usm.my

Abstract. This paper presents the notion of relating reactor operating parameter, namely Chain transfer agent (CTA), with a Low Density Polyethylene (LDPE) commercial property, which is Melt flow index (MFI). In practice, MFI represents the polymer grade, and CTA flow rate is typically regulated to obtain the desired grade. However, the specific relationship between those two properties was not fully established. Thus, this study explores the basic theory of both parameters and establish a link to connect them. A mathematical model of the relationship using Matlab polynomial model is also proposed. The polynomial model has produced excellent results of R-Squared 0.9993 when compared with the simulated relationship data.
Keywords: *Low Density Polyethylene (LDPE); Melt Flow Index (MFI); Tubular reactor.*

INTRODUCTION

Low Density Polyethylene (LDPE) is a common commodity polymer with many applications in our daily life, such as packaging, adhesives, coatings, and films. One of the critical industrial end-use properties for LDPE is Melt Flow Index (MFI). MFI is defined as the weight of the polymer (g) extruded in 10 min through a capillary of specific diameter and length by pressure applied through dead weight under prescribed temperature conditions. MFI can also be regarded as a measure of the average polymer chain length and an inverse measurement of the viscosity. Polymer with different MFI values will have different mechanical properties and different processability in the customers' machines. Thus, MFI is mostly used as an indicator for LDPE production grade. Generally, in order to produce the polymer with desired MFI value, the regulation of Chain Transfer Agent (CTA) feed flow rate is performed. By adding CTA to the polymer mixture, the production of prohibitively large polymer molecules which could increase mixture viscosity, interfering with heat transfer, and thermal control of the reactor can be avoided [1].

However, MFI is a very complicated property and is influenced by many parameters, such as reactor pressure, reactor temperature, monomer concentration, CTA feed, and co-monomer feeds [2]. In practice, MFI is measured using an online rheometer, which can take up to 10 minutes (including measurement delay) or using standard lab testing, which takes 2 to 4 hours to complete [3]. Thus, faster and practical determination of MFI is needed. Based on the study by [4], weight average molecular weight (MWW) is found to be closely related to MFI with the addition of branching factor parameter. Previously, the branching factor can only be determined from experimental analysis using Gel Permeate Chromatography (GPC) [5]. At present, the branching factor can also be estimated using comprehensive deterministic model [6] and stochastic model [7]. Moreover, MWW also is a molecular property of LDPE, which can only be determined using experimental analysis or simulation model using method such as population balance, method of moments, and Monte Carlo. Thus, a mathematical model that can relate CTA amount (which relates to MWW) towards the desired MFI is significant for LDPE grade production monitoring and control.

In this work, MFI is predicted by using the equation from [8] which related it with MWW and branching factor. The MWW properties was obtained from LDPE tubular reactor state simulation model using Aspen Plus V10. As for branching factor, it was obtained from [6] study. Moreover, the relationship between MFI amount and MWW is attained from Aspen model sensitivity analysis

METHODOLOGY

Tubular reactor model

The reactor considered in this work was adapted from [1] work, which resembles a conventional industrial reactor with a length to diameter ratio of over 20000. The reactor operates at a high temperature around 300°C, pressure around 2200 bar, and axial velocity around 11 m/s. These severe conditions are needed for the free radical polymerization to take place inside the reactor. The feed to the reactor contains ethylene gas (monomer), oxygen, traces of hydrocarbon, and chain transfer agent (CTA). The addition of CTA will control the excessive production of large polymer molecules, which can escalate the polymer mixture viscosity. Thus, CTA is typically used to control the final grade of the polymer, which relates to the Melt Flow Index (MFI). The reactor is divided into five zones. The first two zones are used for preheating the reactor mixture to the optimal temperature for the first initiator injection.

An initiator is used to initiate the polymerization process by releasing free radicals into the process mixture. In the third zone, an initiator is injected to generate free radicals that will react with ethylene monomer to produce long growing chains of ethylene molecules (or polyethylene). At the same time, oxygen also decomposes to produce free radicals. The polymerization reaction will be stopped after the initiator is depleted. The fourth zone is regarded as a cooling zone. Since ethylene polymerization is an exothermic process, the excess heat needs to be removed to match the second initiator activation temperature. In the fifth and final zone, the second initiator is introduced, and the polymerization reaction resumed.

Aspen Plus model development

The modeling process began with the selection of feed components using Aspen Properties. Here, propane is used as CTA, *n*-butane as inerts, *tert*-butyl peroxy pivalate (TBPPI) as initiator 1 and *tert*-butyl 3,5,5 trimethyl-peroxy hexaonate (TBPIN) as initiator 2 [9, 10]. Property method selection in Aspen Plus was used to represent the thermodynamic and phase property of the process. Perturbed-chain statistical fluid theory (PC-SAFT) was chosen as it is known as one of the best equation of state (EOS) to represent the polymerization process [11]. The heat of polymerization of the process is calculated by adjusting the heat of formation (DHFVK) of the ethylene segment so that the calculated heat of polymerization matches the literature data in [1] work. The DHFVK value used in this study is -2.669 x 10^7 J/kmol. The process continued by building the process flowsheet. The tubular reactor design features and steady state operating condition can refer to [1] work. The pressure drop of the whole reactor was estimated to be around 10% from reactor inlet pressure as commonly observed in industrial tubular reactor operation [11]. Then, the reaction type and kinetic parameter of the process were defined in the simulation. The free radical polymerization kinetic mechanisms and parameters used in this study are presented in [12], which was based on [9, 10] study. In order to meet the validation data, some tunings are made to the kinetic parameters using optimization technique in Aspen Plus, which was explained in [12]. Finally, the model was ready to be simulated and validated.

MFI equation model

In order to predict the MFI, [8] has proposed the parameter, g, which is the branching factor with weight average molecular weight (MWW). The branching factor is defined as the ratio of root mean square radii of branched and linear polymers with the same molecular weight. The final equation is presented below as reported by [4]. In Eq. 1, two equations are provided which are for tubular and autoclave reactor application. The main characteristic that differentiates LDPE with High density polyethylene (HDPE) and even Linear LDPE (LLDPE) is its branching morphology. Thus, the application of the branching factor is considered necessary in predicting the accurate MFI value for LDPE.

$$MFI_{tubular} = 1.06\ x\ 10^{28}(g.MWW)^{-6.00}$$
$$MFI_{auto} = 3.15\ x\ 10^{25}(g.MWW)^{-5.41} \quad (1)$$

In this work, the branching factor was acquired from [6] work, and the MWW value was obtained from Aspen model simulation. In order to generate a mathematical equation to predict MFI based on MWW, curve fitting tool apps in Matlab 2015b was used.

RESULTS AND DISCUSSION

Model Validation

The final flowsheet for Aspen Plus steady state model and reactor temperature profile was presented in [12]. Here the validation for LDPE conversion and properties was displayed in Table 1. Based on the table, the current model fit within the range of the other researchers that are using a similar case study but with different modeling technique. The MWN and MWW properties are important for the LDPE molecular weight distribution (MWD) validation, and FSCB and FLCB are for molecular structure comparison.

Table 1: Validation for LDPE model conversion and properties

	Data [6]	Current model	Data [1]	Data [9]
Conversion (%)	25	28.9	30	29.7
MWN	23300	23290	21900	21901
MWW	172000	171978	n/a	n/a
FSCB	22.34	24.05	n/a	30.13
FLCB	2.40	1.38	n/a	n/a

*MWN = Number average molecular weight (kg/kmol), MWW = Weight average molecular weight (kg/kmol), FSCB = Short Chain Branch per 1000 carbon atoms, FLCB = Long Chain Branch per 1000 carbon atoms.

CTA and MFI Relationship

The relationship between Melt flow index (MFI) and Weight average molecular weight (MWW) is presented in Figure 1. Based on the figure, MWW has an inverse proportional correlation towards MFI. Based on Aspen model sensitivity analysis, the increasing of CTA flow rate has produced LDPE polymer with lower MWW. Thus, CTA can be assumed to be directly correlated with MFI [4, 13]. Similar behavior trend is also observed from MFI relation with polymer viscosity, which correlated with polymer density. Here, polymer density is a function of branching degree, particularly, the degree of short chain branching (which is generated by intramolecular chain transfer such as back-biting). If the short chain branching increase, the degree of crystallinity of the polymer decrease (less dense packing of a polymer chain), which resulted in decreasing of polymer density. Moreover, the relationship of MWW with polymer viscosity has already been established (Figure 2) [13].

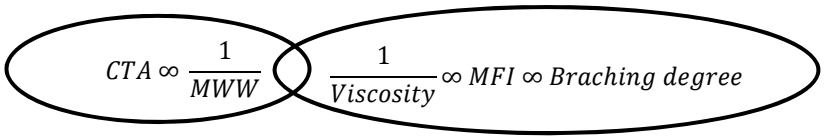

Figure 1: Combination of two theory to obtain relationship of CTA and MFI

Based on Matlab fitting analysis, the result was a 5th degree polynomial model as presented below where x is normalized by mean = 1.539 x 10^5 and Standard deviation = 3.797 x 10^4 with 95% confidence bounds:

$$f(x) = p(1) * x^5 + p(2) * x^4 + p(3) * x^3 + p(4) * x^2 + p(5) * x + p(6) \quad (2)$$

where: $p(1)$ = -4.911 (-5.481, -4.342); $p(2)$ = -7.986 (-9.577, -6.395); $p(3)$ = 1.788 (0.8902, 2.685); $p(4)$ = 9.514 (8.156, 10.87); $p(5)$ = -8.226 (-8.96, -7.493); $p(6)$ = 9.067 (8.774, 9.359). The polynomial model results have presented an excellent association with the simulated data with R-squared = 0.9993.

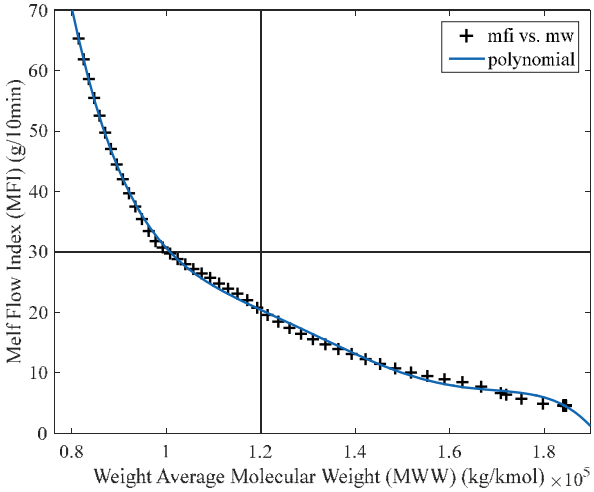

Figure 2: Melt flow index (MFI) vs Weight average molecular weight (MWW) from Aspen simulation. The polynomial model result is presented as a line.

CONCLUSION

This study has confirmed the established relationship of MFI with MWW. The relationship is further extended to CTA flow rate for practical usage of the correlation by developing a mathematical model using Matlab fitting functions. The polynomial model has produced R-squared of 0.9993 when compared with the simulated data. This new correlation is significant for online LDPE grade monitoring and transition control

ACKNOWLEDGEMENT

This work is supported by Ministry of Higher Education (MOHE) Malaysia through Fundamental Research Grant Scheme (Grant No: 203.PJKIMIA.6071368) and Universiti Teknologi Mara (UiTM) under Tenaga Pengajar Muda (TPM) scheme for the first author.

REFERENCES

[1] M. Asteasuain, S. M. Tonelli, A. Brandolin, and J. A. Bandoni, Comput Chem Eng. **25**, 509-515 (2001)
[2] S. Skålén, F. Josefsson, and J. Ihrström, IFAC-PapersOnLine. **49**, 562-567 (2016)
[3] R. Rallo, J. Ferre-Gine, A. Arenas, and F. Giralt, Comput Chem Eng. **26**, 1735-1754 (2002)
[4] A. V. Shenoy and D. R. Saini, Adv Polym Tech. **6**, 1-58 (1986)
[5] M. Teresa Rodríguez-Hernández, J. L. Angulo-Sánchez, and A. Pérez-Chantaco, J Appl Polym Sci. **104**, 1572-1578 (2007)
[6] M. L. Dietrich, C. Sarmoria, A. Brandolin, and M. Asteasuain, Ind Eng Chem Res. **58**, 4412-4424 (2019)
[7] D. Meimaroglou and C. Kiparissides, Macromolecules. **43**, 5820-5832 (2010)
[8] M. Rokudai and T. Okada, Nihon Reoroji Gakkaishi(Journal of the Society of Rheology, Japan). **8**, 154-160 (1980)
[9] N. Agrawal, G. P. Rangaiah, A. K. Ray, and S. K. Gupta, Ind Eng Chem Res. **45**, 3182-3199 (2006)
[10] A. Brandolin, M. H. Lacunza, P. E. Ugrin, and N. J. Capiati, Polym React Eng. **4**, 193-241 (1996)
[11] C. P. Bokis, S. Ramanathan, J. Franjione, A. Buchelli, M. L. Call, and A. L. Brown, Ind Eng Chem Res. **41**, 1017-1030 (2002)
[12] D. Muhammad, Z. Ahmad, and N. Aziz, Mater Today: Proceedings. **5**, 21612-21619 (2018)
[13] M. Teresa Rodríguez-Hernández, J. L. Angulo-Sánchez, and A. Pérez-Chantaco, J Appl Polym Sci. **104**, 1572-1578 (2007)

PGC_SCHE USM_2020_41

Morphology Studies of Kaolin Hollow Fiber Membrane: Effect of Different Bore Fluid Rates

M.I.M. Esham, A.L. Ahmad*
School of Chemical Engineering, Engineering Campus, Universiti Sains Malaysia,
14300 Nibong Tebal, Pulau Pinang, Malaysia
*Email: *chlatif usm.my*

Abstract: Recently, ceramic hollow fiber membrane (CHFM) has been paid so much attention to the treatment of oily wastewater because of its advantage to produce high quality filtered water. In this part of research, the aim is to study the effect of bore fluid rates on the morphology of the fabricated kaolin hollow fiber membrane (KHFM) before the sintering process. Kaolin was used as the starting material for the membrane fabrication. The membranes were prepared by the blending of the fine kaolin powder and polyethersulfone (PESf) via the combination of phase inversion technique and sintering process. During the phase inversion technique, the KHFM were spun with different bore fluid rates (5, 10 and 15 mL min^{-1}) at the fixed air-gap of 5 cm and solid loading of 53 wt%. The KHFM fabricated with bore fluid rate from 5 to 10 mL min^{-1} showed a deformation of inner layer, while a fully circular inner layer of KHFM was observed at the bore fluid rate of 15 mL min^{-1}.
***Keywords**: Ceramic hollow fiber membrane, Kaolin, Oily wastewater treatment*

INTRODUCTION

Ceramic hollow fiber membrane (CHFM) have been widely used in the application of separation and purification such as water desalination [1], wastewater treatment [2], purification of drinking water [3], removal of bacteria [4] and gas separation [5]. CHFM have the advantages of resisting harsh physical and chemical environment, high pressure and temperature also have the ability to resist membrane fouling [6]. Recently, pure alumina has become one of the most used starting material for CHFM. However, the refractory nature of the pure alumina showed that alumina needs a high sintering temperature which is usually greater than 1500 ºC to achieve the desired characteristic of CHFM. Also, the fabrication cost of pure alumina CHFM is relatively expensive [7]. Many researchers have changed their focus onto finding raw starting material which can reduce some issues related to the fabrication of CHFM. Some of the successful CHFM fabricated have been reported using raw minerals such as ball clay [8], bauxite [6], and kaolin[9-11]. So far as is known, kaolin has been widely used as the starting material to replace pure alumina since kaolin is cheaper than pure alumina in term of its fabrication cost. Kaolin hollow fiber membrane (KHFM) also have good hydrophilic characteristic for oily wastewater application [9]. Therefore, in this part of research, the aim of the study is to investigate the effect of bore fluid rate in the preparation of KHFM. In order to evaluate the optimum KHFM, three bore fluid rates (5, 10 and 15 mL min^{-1}) were applied. The morphology of the prepared KHFM were observed by scanning electron microscopy (SEM) (S-4800, Hitachi Ltd., Japan).

MATERIALS AND METHODS

Kaolin powder (1μm) purchased from Modern Lab Chemicals Sdn. Bhd. were used to prepare the KHFM. Kaolin powder and PESf (Polyethersulfone, Radel A300, Ameco Performance, USA) were dried for 24 hours to remove the moisture trapped in the powder. The preparation of dope suspension was based on the ratio of ceramic material and polymer binder which is fised to 8:1 [6]. The dope composition is shown in Table 1.

Table 1: Spinning suspension composition

Composition (wt.%)	Kaolin (g)	PESf (g)	Arlacel P135 (g)	NMP (g)
53	53.000	6.625	1.000	39.375

.

The KHFM were prepared via the combination of phase inversion extrusion and sintering technique. Firstly, the Arlacel P135 (Polyethyleneglycol 30-dipolyhydroxystearate, Uniqema) was added into the NMP (N-methyl-2-pyrrolidone, HPLC grade, Rathbone) under vigorous stirring. Kaolin powder was slowly added into the solution. Then, the solution was mechanically stirred at 300 rpm for 24 hours [10]. After that, dried PESf was added into the solution, then the mixing process was continued for another 48 hours to obtain the homogeneous suspension. After that, the suspension was loaded into the stainless-steel gas-tight reservoir and was degassed for 1 hour at room temperature. The suspension was forced with nitrogen pressure (1 bar) and spun through a single orifice spinneret based on the selected parameter and condition. The parameter and condition of the spinning process is shown in Table 2 and the

experimental setup of the spinning process is shown in Figure 1. The kaolin precursor was then left immersed in the water for 24 hours to complete the phase inversion process. After that, the kaolin precursor was cut into short fiber with length of 150 mm, straightened and dried at room temperature. The morphologies of the kaolin precursors were observed by scanning electron microscopy (SEM, TM3000, Hitachi Ltd, Japan).

Table 2: Spinning parameter and condition

Parameters	Case 1	Case 2	Case 3
Bore fluid rate (mL min^{-1})	5	10	15
Air gap (mm)	50	50	50
Spinneret orifice, OD/ID (mm)	3.0/2.8	3.0/2.8	3.0/2.8
Internal coagulant	Deionized water	Deionized water	Deionized water
External coagulant	Tap water	Tap water	Tap water
Temperature (ºC)	25	25	25

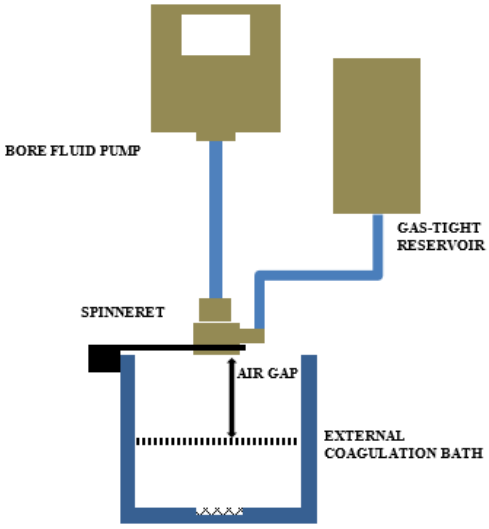

Figure 1: An illustration of spinning based phase inversion technique

RESULT AND DISCUSSION

Figure 2 showed the SEM images of the kaolin precursor with bore fluid rates (5, 10 and 15 mL min^{-1}) with a fixed solid loading of 53 wt.% and air gap distance of 5 cm. Based on the results, normal circular outer layer for all cases was obtained due to the function of surface tension [12]. All of the cases seem to possess the finger-like inner layer and thin sponge-like outer layer.

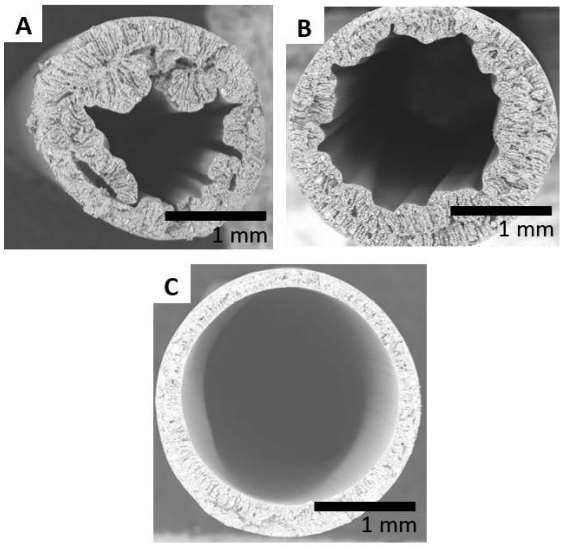

Figure 2: SEM images of the kaolin precursor with different bore fluid rates: (A) 5 mL min^{-1}, (B) 10 mL min^{-1} and (C) 15 mL min^{-1}, at a fixed solid loading of 53 wt.% and air gap distance of 5 cm.

However, the difference can be observed by formation of the inner layer of the precursor. At a bore fluid rates of 5 and 10 mL min^{-1}, the deformation of the inner layer of both precursors were observed, while the precursor spun at bore fluid 15 mL min^{-1} obtained the fully circular inner layer. This phenomenon can be explained by the shrinkage happened during the spinning process. Based on the previous paper, the diffusion rate of NMP from suspension usually quicker than the diffusion of water into the suspension [13]. Then, since of the bore fluid rates (5 and 10 mL min^{-1}) which is low, the diffusion of water become much slower than the diffusion of NMP which it could not generate the hydrodynamic force against the suspension while spinning, which then shrinkage happen and deformed of the inner layer of the kaolin precursor.

CONCLUSION

A kaolin precursor has been successfully spun via phase inversion technique. The morphology of the precursor was studied by adjusting the bore fluid rates during the spinning process. Based on the results, low bore fluid which are 5 and 10 mL min^{-1} showed a deformed inner layer even though both membrane have good thin sponge-like and thick finger-like layer structure, while a fully circular inner layer of KHFM was observed at the bore fluid rate of 15 mL min^{-1}.

REFERENCES

[1] Zhang, H., et al., Construction of MoS_2 composite membranes on ceramic hollow fibers for efficient water desalination. Journal of Membrane Science, 2019. **592**: p. 117369.
[2] Hubadillah, S.K., et al., Novel hydroxyapatite-based bio-ceramic hollow fiber membrane derived from waste cow bone for textile wastewater treatment. Chemical Engineering Journal, 2019: p. 122396.
[3] Wang, S., et al., Development of CuO coated ceramic hollow fiber membrane for peroxymonosulfate activation: a highly efficient singlet oxygen-dominated oxidation process for bisphenol a degradation. Applied Catalysis B: Environmental, 2019. **256**: p. 117783.
[4] Goswami, K.P. and G. Pugazhenthi, Credibility of polymeric and ceramic membrane filtration in the removal of bacteria and virus from water: A review. Journal of Environmental Management, 2020. **268**: p. 110583.
[5] Lee, H.J., et al., Study on CO2 absorption performance of lab-scale ceramic hollow fiber membrane contactor by gas/liquid flow direction and module design. Separation and Purification Technology, 2019. **220**: p. 189-196.
[6] Esham, M.I.M., et al., Effect of sintering temperature of bauxite hollow fiber membrane on flexural strength and water permeability. Malaysian Journal of Fundamental and Applied Sciences, 2019. **15**(2): p. 190-193.
[7] Abdullah, N., et al., Preparation and characterization of self-cleaning alumina hollow fiber membrane using the phase inversion and sintering technique. Ceramics International, 2016. **42**(10): p. 12312-12322.
[8] Abd Aziz, M.H., et al., Fabrication and characterization of mullite ceramic hollow fiber membrane from natural occurring ball clay. Applied Clay Science, 2019. **177**: p. 51-62.
[9] Hubadillah, S.K., et al., Fabrications and applications of low cost ceramic membrane from kaolin: A comprehensive review. Ceramics International, 2018. **44**(5): p. 4538-4560.
[10] Mohtor, N.H., et al., Synthesis of nanostructured titanium dioxide layer onto kaolin hollow fibre membrane via hydrothermal method for decolourisation of reactive black 5. Chemosphere, 2018. **208**: p. 595-605.
[11] Hubadillah, S.K., et al., A low cost hydrophobic kaolin hollow fiber membrane (h-KHFM) for arsenic removal from aqueous solution via direct contact membrane distillation. Separation and Purification Technology, 2019. **214**: p. 31-39.
[12] Wang, Z. and J. Ma, The role of nonsolvent in-diffusion velocity in determining polymeric membrane morphology. Desalination, 2012. **286**: p. 69-79.
[13] Li, L., et al., A low-cost alumina-mullite composite hollow fiber ceramic membrane fabricated via phase-inversion and sintering method. Journal of the European Ceramic Society, 2016. **36**(8): p. 2057-2066.

PGC_SCHE USM_2020_42

Modelling Performance of *Spirodela polyrhiza*, *Salvinia molesta,* and *Lemna minor* under Increasing Salinity

Daniel Nesan, Derek Chan Juinn Chieh*
School of Chemical Engineering, Engineering Campus, Universiti Sains Malaysia,
14300 Nibong Tebal, Pulau Pinang, Malaysia.
*E-mail: *chderekchan@usm.my*

Abstract. Phytoremediation is an effective and easily implemented technology that uses plants to remove pollutants from contaminated soils and wastewaters. However, one of the challenges in designing a phytoremediation system is the variation in uptake rates as a result of changes in the concentration of nutrients, plant growth and other environmental factors. In this paper, nutrient decay models are applied to the nutrient use data collected from three species of macrophytes under varying salinity stress. The median uptake rate (MUR) was determined then used to evaluate and compare the performance of each species of macrophyte under varying degrees of salinity stress.
Keywords: *phytoremediation, nutrient contamination, decay modelling*

INTRODUCTION

Nutrient pollution refers to a process where excess amounts of nutrients - primarily phosphorus and nitrogen are added to bodies of water [1]. Nutrients naturally enter waterways from the weathering of rocks and soils and the upwelling of nutrients by ocean currents [2]. However, an increase in human activity and urban development around coastal and riverine environments has led to a multifold increase in the quantity of nutrients that are drained into surrounding waters. A 2015 analysis on Malaysian water resources determined that 41% of rivers monitored were found to be affected by some degree of pollution with ammoniacal nitrogen and suspended solids [3]. Huang *et al*. further determined that 71.6 % of coastal monitoring stations reported moderate nutrient contamination and 5.8% of marine water stations were reported at poor water quality. An effective and sustainable approach to the management of these nutrient wastes is the application of phytoremediation; using the growth and natural nutrient uptake of living plants to recover and assimilate nitrogen and phosphorus species. Phytoremediation provides a low-impact, cost-effective, environmentally sound and easy to implement waste management technique for the treatment of nutrient pollution. [4] However, as a process that utilizes the metabolic functions of biological organisms, the exact rates of nutrient uptake by a phytoremediation system can be difficult to determine and are dependent on numerous biotic and environmental factors such as salinity concentration [5], [6]. To provide a clearer approximation of the effects of salinity stress on the uptake capacity of a phytoremediation system, this study uses a decay curve equation [7] to model the relationship between nutrient uptake, plant growth and time to evaluate uptake ability and compare performance between species.

MATERIALS AND METHODS

The macrophyte samples of *Spirodella polyrhiza*, *Salvinia molesta* and *Lemna minor.* used in this study were originally collected from the local waterways of the Kerian district in Perak, Malaysia as described by Ng & Chan (2018). Following initial sterilisation of the wild samples, these plantlets have continuously been subcultured into 250 ml glass jar filled with Hoagland no. 2 nutrient medium [9] and added sucrose (30g/L). Subculture of plantlets were performed approximately every 2 weeks.

Following the analysis of the farm effluent, we studied the effects of salinity on phytoremediation efficiency. To measure these exact effects, samples of *S. molesta*, *L. minor* and *S. polyrhiza* plantlets will be grown in synthetic culture media of known salinity. The conditions of the culture media will be based on the salinity results from measurements made on the collected aquaculture effluent. The starting concentrations of measured nutrients in the media were 100mg NO_3, 20 mg PO_4 and 20 mg NH_3. The salinity of the culture media will be increased through the addition of sodium chloride. 6 different salinities will be used; 2, 6, 10, 14, 16 and 18 g/L. For each salinity, approximately 2g of plantlets were placed in each glass jar (30 treatments) with 80 ml of medium. The medium was autoclaved at 121°C for 15 minutes prior to subculture with the plantlets to maintain aseptic conditions. The addition of plants was performed in a laminar flow cabinet to prevent contamination by algae, bacteria or fungi. The jars were kept in a controlled culture room maintained at 25°C. The plants spend 16 hours a day in 1500 lux lighting and 8 hours in the dark. 3 jars are harvested on day 0, 1, 2, 3, 4, 6, 8, 10, 12 and 14. The medium of each jar were assessed using nutrient uptake analysis. Throughout the same two-week growing period in saline medium the nutrient levels of the solution were analyzed to determine the relationship of uptake level with increasing salinity. Before removing the plantlets for measurement of mass, the medium in each jar was gently stirred and removed using a micropipette for

nutrient testing. The nutrient concentrations were measured using the following methods: Ammonia - Salicylate Method (Lovibond 66), Nitrate - Cadmium Reduction Method (HACH 8039) and Phosphate - Ascorbic Acid Method (HACH 8048). From this data we will be able to determine the consequences of increasing salinity on the uptake of ammonia, nitrate, and phosphate. To model the nutrient uptake under increasing salinity inhibition, an exponential decay curve was used [10]. This gives equation 1 in the form:

$$Y = (Y_0 - P)e^{-kt} + P \quad (1)$$

with the coefficients:

Y = Nutrient concentration per gram of dry plant biomass (mg/g)
Y_0 = Initial nutrient concentration per gram of dry plant biomass (mg/g)
P = Plateau, lowest estimated nutrient concentration achievable by plant uptake (mg/g)
k = Decay rate constant ($days^{-1}$)
t = Time (days)

The half-life of the equation, λ can also be determined at the point where the nutrient concentration decreases to half the initial value. As shown in equation 2 :

$$\lambda = t, when\ Y = \frac{1}{2} Y_0 \quad (2)$$

The exponential decay model was selected to represent the relationship because it has previously been shown that nutrients present as free compounds in the environment are measured to decrease in the form of exponential decay [7]. Furthermore, as this study uses the measures of concentration of nutrient in the medium surrounding the plantlets and not the nutrient content in the plant tissues, an exponential decay model would be a more accurate representation of the decline in nutrient concentrations over time. Additionally, by considering the relationship of the following coefficients from the exponential decay model in the form give in equation 3:

$$Median\ Uptake\ Rate\ (MUR) = \frac{Y_0 - P}{\lambda} \quad (3)$$

It is possible to determine the median nutrient uptake rate per gram of biomass per day (MUR), allowing for the comparative analysis of the time dependent nutrient removal profiles for each macrophyte species at different levels of salinity. The units of MUR are given as milligrams of nutrient uptake per gram of dry plant weight per time in days, mg/g/day. All curve fitting and statistical analysis was performed using RStudio [11] and graphs were made in Prism by GraphPad Software.

RESULTS AND DISCUSSION

Ammonia

Ammonia is the preferred nitrogenous source of aquatic plants [12] and is readily taken up by the macrophytes. From Fig 1 we can see that increasing salinity generally decreases the maximum uptake performance of all three macrophyte species. This relationship was to be expected as the negative effects of high salinity on plant nutrient uptake [13] and nutrient retention [14] have been previously established for photosynthetic macrophytes. The overall profiles also indicate that the maximum uptake rates of *S. molesta* even at the minimum salinity level of 2 g/L are lower compared to *S. polyrhiza* and *L. minor*. This suggests that the median nutrient uptake of *S. molesta* is lower per gram of mass when compared to the other two species. At the beginning of the experiment, *S. polyrhiza* has the largest median ammonia uptake rate at 63.07± 2.30 mg/g/day, but as salinity was increased this rate decreased to 10.96 ±5.29 mg/g/day at 18 g/L salinity, a performance reduction of 82.6%. The first significant decline in performance was observed at 14 g/L salinity, with a 72.7% reduction in ammonia uptake performance. This implies that optimum nutrient remediation with *S. polyrhiza* is best performed below 14 g/L salinity. In contrast, *L. minor* has a lower initial ammonia uptake rate of 29.21±2.88 mg/g/day. However, this rate does not decrease as significantly with increasing salinity compared to the two other plantlets until salinity reached 18g/L. By 16 g/L salinity, *L. minor* has the highest ammonia uptake rate of the three species, indicating the species' suitability for ammonia removal at high saline conditions.

The MUR of ammonia for *S. molesta* was noted to be lowest among the three species even at the control salinity of 2g/L. As salinity was increased, there was a statistically significant reduction in performance observed at 16g/L salinity with a 71.3% decline in ammonia MUR and this decline was also observed at 18g/L with a 79.3% reduction. One possibility for this observed difference in response to salinity is the variation in species sizes and surface area per unit of mass. One of the mechanisms by which salinity affects plants is by altering the water potential difference between plant cells and the external medium [6]. As *S. molesta* is the largest and most broad leaved of the three species; 20 - 40 mm in length, 10 – 60 mm wide [15], it is the most affected by increases in salinity, while *L.*

minor is the smallest species at 2 - 5 mm in length and 1.5 - 3.5 mm wide [16] and thus shows the least amount of change because of lower exposed surface area to a high saline environment and *S. polyrhiza* is between these other two species; round discs of 5 – 10 mm in diameter [17].

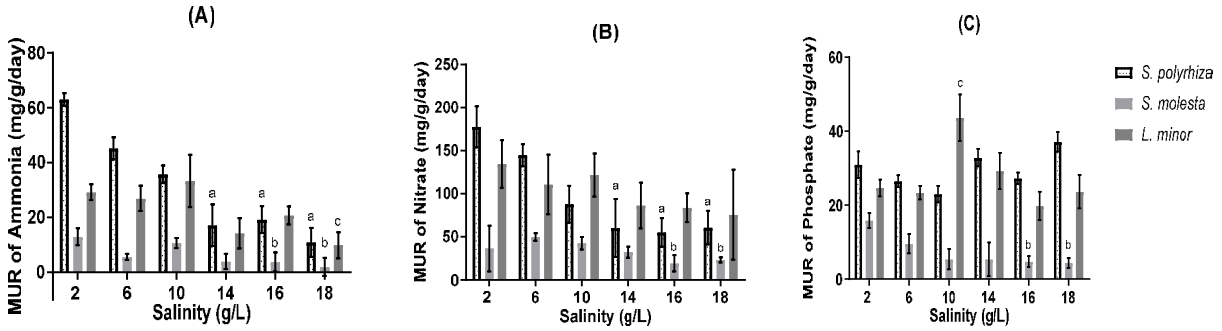

Figure 1: Median uptake rate (MUR) of ammonia (A), nitrate (B) and phosphate (C) in *S. polyrhiza* , *S. molesta* and *L. minor* . a, b and c symbols indicate results that deviate significantly from the control ($p < 0.05$) for each species respectively. Error bars indicate standard error.

Nitrate

As the initial concentration of nitrate was approximately 4.6 times greater than the concentration of ammonia in the medium; 101±0.5 mg/L compared to 22±0.1 mg/L, there was observable nitrate uptake by the plantlets from day 1 of the experiment. Fig. 1 (B) also shows the general trend that increasing salinity has a negative impact on the uptake of nitrate by all three macrophyte species, though all species show significantly higher uptake rates for nitrate compared to ammonia. This is likely a result of higher nitrate content in the experimental medium used or might indicate a higher physiological uptake capacity for nitrate over ammonia. The MUR of nitrate uptake of *S. polyrhiza,* as in the case of ammonia showed a significant decline in uptake performance at salinities greater than 14 g/L. With a reduction of 66.1% from 177.76±23.85 (at 2 g/L salinity) to 60.24±19.48 mg/g/day (at 14 g/L salinity), further suggesting that between 10 and 14 g/L salinity is the upper tolerance limit for *S. polyrhiza*. *S. molesta* also had lower median uptake rates compared to the other two species, however increasing salinity did not cause as great a decline to its nitrate uptake ability, with a decline of 36.2% by between the control and 18g/L. Nonetheless, *S. molesta* had the lowest nitrate uptake rates at all salinities when compared to the other two species. This was an unusual results as *S. molesta* has be regarded as one of the most noxious invasive aquatic species in the world [18], characterized by its rapid rates of growth and proliferation [19]. Nevertheless, it is shown that *S. molesta* had a lower nitrogen uptake capacity and probably nitrogen requirement than *L. minor* and *S. polyrhiza.* In the case of *L. minor*, maximum uptake was less affected by increases in salinity than *S. polyrhiza*. The total decline in performance between the control and 18 g/L was 43.7%. While its ammonia uptake performance is not as high as *S. polyrhiza* under normal conditions, *L. minor* is a superior choice for remediation in salinities above 14 g/L.

Phosphate

From the data presented in Figure 1 (C) there is no clear correlation between the increase in salinity and changes to the MUR of phosphate for *S. polyrhiza* or *L. minor*. Despite this apparently large degree of variation in uptake the only statistically significant results for these two species were obtained unusually for *L. minor*. at 10 g/L, with MUR increasing by 77.0% from 24.65±2.7 to 43.63±6.3 mg/g/day. In the case of *S. molesta*, a significant reduction in phosphate uptake was observed at salinities greater than 16 g/L, with MUR values decreasing from 15.9±2.02mg/g/day to 4.77±1.43mg/g/day; 70.0% reduction. In a previous study by Liu et al. (2017) on *L. minor*, the authors demonstrated that an increase in medium salinity above 100mM (5.8 g/L) results in an increase of total phosphate concentration by 200% after a 24 hr period as the plantlets begin to die and release phosphate into the medium. A study by Wendeou et al. (2013) on *S, polyrhiza* also shows a decrease in total phosphate removal by 62% when salinity is increased from the control to 30 mS/cm conductivity (~18.6 g/L). These results, however, were not reflected in the MUR data gathered here. This is likely because salinity causes a reduction in phosphate uptake indirectly by affecting the rate of duckweed growth instead of directly inhibiting the phosphate uptake process. As a result, the average per gram uptake rate as expressed by MUR remains generally unchanged despite the increasing concentrations of salinity. Alternatively, there was some degree of phosphate disassociation into forms that were not detectable by the phosphate test method used, [22].

CONCLUSION

For each of the three macrophytes species, median uptake rate of ammonia and nitrate were shown to be decreasing with increasing salinity. Additionally, salinity begins to significantly affects the ammonia, nitrate and phosphate

uptake of *S. polyrhiza* and *Lemna sp.* at concentrations of 14 g/L and above, while *S. molesta* was adversely affected from 6 g/L. It was also shown than while *S. polyrhiza* had the highest initial uptake rate of ammonia and nitrate, *Lemna sp.* begins to overtake this performance when salinity concentrations were increased to 16 g/L and 10 g/L salinity respectively. By modelling the nutrient uptake data using the methods outlined in this study it is possible to directly determine the time and mass dependent uptake rate for each macrophyte species and allows for the comparison of performance across varying concentrations of salinity.

ACKNOWLEDGEMENTS

The authors express their gratitude for the financial support provided to this research project from Long Term Research Grant, LRGS (203/PJKIMIA/6720015) and (Grant No. 4411/S01) from the Ministry of Education, Malaysia.

REFERENCES

[1] NOAA, "Nutrient Pollution - an overview," 2019.
[2] A. Huyer, "Coastal upwelling in the California current system," *Progress in Oceanography*, vol. 12, no. 3. pp. 259–284, 1983.
[3] Y. F. Huang, S. Y. Ang, K. M. Lee, and T. S. Lee, "Quality of Water Resources in Malaysia," in *Research and Practices in Water Quality*, InTech, 2015.
[4] R. Cropanzano and J. H. Stein, "Organizational Justice and Behavioral Ethics: Promises and Prospects," *Bus. Ethics Q.*, vol. 19, no. 02, pp. 193–233, Mar. 2009.
[5] M. Tkalec, J. Mlinarec, Z. Vidaković-Cifrek, B. Jelen, and I. Regula, "The effect of salinity and osmotic stress on duckweed Lemna minor L.," *Acta Bot. Croat.*, vol. 60, no. 2, pp. 237–244, 2001.
[6] R. Munns, "Comparative physiology of salt and water stress.," *Plant. Cell Environ.*, vol. 25, no. 2, pp. 239–250, 2002.
[7] J. Yuan, L. Hou, X. Wei, Z. Shang, F. Cheng, and S. Zhang, "Decay and nutrient dynamics of coarse woody debris in the Qinling Mountains, China," *PLoS One*, vol. 12, no. 4, pp. 1–24, 2017.
[8] Y. S. Ng and D. J. C. Chan, "Phytoremediation capabilities of Spirodela polyrhiza, Salvinia molesta and Lemna sp. in synthetic wastewater: A comparative study," *Int. J. Phytoremediation*, vol. 20, no. 12, pp. 1179–1186, Oct. 2018.
[9] D. R. Hoagland and D. I. Arnon, *The Water-Culture Method for Growing Plants without Soils*, vol. 347. 1950.
[10] G. F. Davies and G. F. Davies, "Exponential growth and decay," *Mantle Convect. Geol.*, pp. 208–210, 2011.
[11] RStudio Team, "RStudio: Integrated Development for R." RStudio, Inc., Boston, MA, 2015.
[12] D. L. Walstad, *Ecology of the planted aquarium : a practical manual and scientific treatise for the home aquarist*. Echinodorus, 2013.
[13] M. A. da C. Gomes, M. S. Suzuki, M. da Cunha, and C. F. Tullii, "Effect of salt stress on nutrient concentration, photosynthetic pigments, proline and foliar morphology of Salvinia auriculata Aubl.," *Acta Limnol. Bras.*, vol. 23, no. 2, pp. 164–176, 2011.
[14] M. Alldred, A. Liberti, and S. B. Baines, "Impact of salinity and nutrients on salt marsh stability," *Ecosphere*, vol. 8, no. 11, p. e02010, Nov. 2017.
[15] D. S. Mitchell and N. M. Tur, "The Rate of Growth of Salvinia molesta (S. Auriculata Auct.) in Laboratory and Natural Conditions," *J. Appl. Ecol.*, vol. 12, no. 1, p. 213, Apr. 1975.
[16] R. A. Leng, J. H. Stambolie, and R. Bell, "Duckweed - a potential high-protein feed resource for domestic animals and fish," *Livest. Res. Rural Dev.*, vol. 7, no. 1, 1995.
[17] USDA, "Plants Profile for Spirodela polyrrhiza (common duckmeat) - Natural Resources Conservation Service PLANTS Database.," 2015.
[18] S. Li *et al.*, "Endocide-Induced Abnormal Growth Forms of Invasive Giant Salvinia (Salvinia molesta)," *Sci. Rep.*, vol. 8, no. 1, pp. 1–15, Dec. 2018.
[19] J. D. Oliver, "A review of the biology of giant salvinia (Salvinia molesta Mitchell)," *J. Aquat. Plant Manag.*, vol. 31, pp. 227–231, 1993.
[20] C. Liu, Z. Dai, and H. Sun, "Potential of duckweed (Lemna minor) for removal of nitrogen and phosphorus from water under salt stress," *J. Environ. Manage.*, vol. 187, pp. 497–503, 2017.
[21] S. P. H. Wendeou, M. P. Aina, M. Crapper, E. Adjovi, and D. Mama, "Influence of Salinity on Duckweed Growth and Duckweed Based Wastewater Treatment System," *J. Water Resour. Prot.*, vol. 05, no. 10, pp. 993–999, 2013.
[22] HACH Co., "Differences between reactive , acid hydrolyzable, and total phosphorus.," 2018.

PGC_SCHE USM_2020_43

Effect of Particle Size on Bio-oil Production in Pyrolysis Process of Palm Wastes

M.A. Al-Maari[1,2], M.A. Ahmad[1,*], A.M. Alsobaai[2], H. Hassan[3], A.T.M. Din[1,a]
[1]School of Chemical Engineering, Engineering Campus, Universiti Sains Malaysia, 14300 Nibong Tebal, Pulau Pinang, Malaysia
[2]Chemical Engineering Department, Faculty of Engineering and Petroleum, Hadhramout University, Mukalla, Yemen.
[3]Faculty of Chemical Engineering, Universiti Teknologi MARA, Cawangan Pulau Pinang, 13500 Permatang Pauh, Pulau Pinang, Malaysia.
Email: chazmier@usm.my*

Abstract. This work investigates the effect of particle size of palm wastes on the yields of product in the pyrolysis process. Two types of palm waste namely, oil palm empty fruit bunches (EFB) and oil palm fronds (PF) were utilized. The experiments were conducted in a fixed-bed tubular reactor under various particle sizes in the ranges of 250-500, 500-1000 and 1000-2000 μm at a constant reaction temperature of 500 °C and holding time of 45 min. It was observed that with increase in particle size, the yields of bio-oil slightly increase and the gases decrease while char yield was not significantly affected by the particle size of both feedstocks. Only about 5% difference found for bio-oil yield between smaller and larger size particles.

Keywords: *Pyrolysis, Palm Wastes, Particle Size*.

INTRODUCTION

With the increasing of fossil fuel consumption, greenhouse gas emissions and air pollution, worldwide interest has been focused in the field of renewable alternative energy sources [1,2,3]. Biomass is considered to be one of the most favorable green alternative energy source [4, 5]. Biomass wastes, as a source of energy, has gained great interest as a potential renewable resource for green energy, because it is available worldwide, carbon–neutral and, meanwhile, increased biomass wastes cause many environmental issues due to the inadequate waste management systems [6]. Oil palm waste is one of the promising biomass source which is abundant in tropical countries [7]. Being a lignocellulosic biomass, palm wastes have a great potential to be converted into highly valuable [8]. These wastes can be obtained from oil milling activities such as palm kernel shell (PKS), empty fruit bunches (EFB), and mesocarp fibre (MF) and from harvesting activities in plantation sites such as oil palm frond (PF), oil palm trunk (OPT) [9]. With a tropical climate, Malaysia and Indonesia are the biggest palm oil producers in the world which both produce approximately 85 % of the worldwide production [10]. In Malaysia, the palm oil production has been increased through the past 10 years whereby the biomass waste could reach more than 100 million tons per year [11]. Therefore, Malaysian government stated many policies and plans to encourage biomass utilization to produce high valuable products [12].

Thermal conversion processes such as pyrolysis, liquefaction, gasification and combustion are the most promising technologies in the industrial utilization of biomass [13]. Pyrolysis can be considered as a promising process for utilization of biomass under slow and fast heating to produce useful products such as bio-oil and charcoal [14]. In pyrolysis process, the yield of the bio-oil, solid char, and gas is affected by many parameters such as temperature, biomass particle size, and residence time [15]. Many researchers studied the effect of operating conditions of the products yield they found that increasing the temperature of pyrolysis promotes biomass thermal degradation and accelerates the production of volatiles which subjected to a sequence of secondary reactions to generate pyrolytic gas [14, 16, 17, 18, 19]. Furthermore, Akhtar et al. [13] reported that pyrolysis of biomass at intermediate temperatures (500–550 ^{o}C) promote the production of liquid oil while low and very higher temperatures favours the production of char and gas, respectively [13]. Azduwin et al. [20] evaluated the effect of temperature on the pyrolysis of EFB in a vertical fixed bed reactor and reported that the maximum yield of bio-oil was produced at 500 ^{o}C. Dhanavath et al. [21] investigated the slow pyrolysis of Mahua press seed cake in a fixed bed batch reactor and found the optimum residence time is 45 min that produced maximum oil yield. Particle size is one the key parameters that affect the kinetics and mass transfer through the pyrolysis process [15]. Chandrasekaran et al. [22] investigated the effect of particle size on pyrolysis of prosopis juliflora fuelwood and explained that the smaller biomass particle offers a wide surface area for heat transfer, leading to faster heating rate which produces more light gases. The objective of this work was to investigate the effect of particle size on the bio-oil yield in the pyrolysis process of palm wastes. Empty fruit bunches (EFB) and oil palm frond (PF) were selected as representative of milling and plantation palm wastes, respectively. The experiments were carried out under various particle sizes in a fixed bed reactor.

MATERIALS AND METHODS

Materials

In this study, empty fruit bunches (EFB) and oil palm frond (PF) were selected as representative of milling and plantation palm wastes, respectively. The empty fruit bunch (EFB) and palm fond (PF) wastes were obtained from United Oil Palm Mill, Nibong Tebal, Penang, Malaysia. Initially, biomass was pre-treated by cleaning to remove visible impurities, washing and drying in the sun. The dried samples were grounded and screened to achieve particle sizes at various ranges (250-500, 500-1000 and 1000-2000 microns). Before use, the samples were again dried in the oven at 100 °C for 24 hours in order to remove the moisture. Nitrogen (N_2) gas (99.99%) supplied by Araztech Engineering, Penang, Malaysia was used as a carrier gas for volatile matter.

Experiment Setup

Pyrolysis of the samples were conducted in a vertical stainless steel fixed-bed reactor. The reactor has an internal diameter of 25 mm and height of 700 mm. It is suitable for maximum pressures of 2 bar, a maximum temperature of 850 °C and a flow rate of 300 ml / min of nitrogen gas. Nitrogen was used as gas carrier for purging the reactor from vapours. In each test, a layer of quartz wool was placed over the mesh in the middle of the reactor, after that 6.0 g of raw material was placed over the quartz layer in order to hold the raw material from the fall to the bottom of the reactor, then the reactor was closed tightly with connecting the nitrogen delivery tube and the output tubes related to liquid and gaseous products collection bottles. Before each run, nitrogen was purged by the reactor for 10 minutes to ensure the inert atmosphere. The reactor was heated externally by an electric furnace and the temperature was measured by a K-type thermocouple. At the end of experimental test, the electric furnace switch off and opened to cool the reactor but the carrier gas was still purging until the reactor cooled down to 40 °C. Volatile vapors inside the reactor were carried via the nitrogen stream and passed through the condenser to collect the liquid products. There is also a trap temperature of 170 °C to collect the wax under the reactor. The solid charcoal was collected when the reactor was cooled to room temperature. While the non-condensed gases were collected by bags.

Thermal pyrolysis

The experiments were conducted to study the effect of particle size on the products yield by varying the particle size at ranges of 250-500, 500-1000 and 1000-2000 microns at constant temperature of 500 °C and reaction time of 45 min. In each experimental test, about 0.1 g of quartz wool was placed over the mesh in the middle of the reactor in order to keep the raw materials from falling. The mass of the biomass in each batch was set at 6 g. The sample was putted inside the reactor over the quartz. The reactor was then closed tightly with other parts; thermocouple, inert gas tube, wax trap and condenser and it was installed in its place inside the electric furnace. The nitrogen gas (99.99% pure) was entered into the reactor at 250 mL/min for 10 min to ensure inert environment. Furthermore, N_2 was also applied to push the vapor products toward the condenser. The liquid products from the condenser and wax trap were collected and weighted. The gases were collected by gas bags through the vent valve after the condenser. When the reactor was cooled to room temperature the solid char recovered and weighted. The yield of the liquid and solid char products were calculated using the Equation (1) [23]:

$$Y_P = \frac{X_P}{X} X100 \quad (1)$$

where Y_P is the product yield, X_P is the mass of the product (bio-oil or bio-char), and X is the initial mass of the raw material. The gas yield was determined by difference: gas yield = 100 – (bio-oil yield + bio-char yield).

RESULTS AND DISCUSSION

Figure 1 showed the effect of the particle size of each biomass (EFB and PF) on the yields of the product. The particle size was varied in the range of 250-500, 500-1000 and 1000-2000 μm at a constant reaction temperature of 500 °C and holding time of 45 min. Empty fruit bunche (EFB) of particle size at range of 250-500, 500-1000 and 1000-2000 μm respectively produced a yield of 39 wt%, 40 wt% and 44% of bio-oil. Oil palm frond (PF) of particle size at ranges of 250-500, 500-1000 and1000-2000 μm produced a yield of 36 wt%, 39 wt% and 40% of bio-oil respectively. The effect of the particle size was consistent but small, where oil yields were on average 5% higher for the large particle than for the small. The both samples behave in the same manner, the yields of oil slightly increased with the increase of particle size while the gas yield decreased and the results show that the particle size parameter didn't exerted any influence on solid char under the conditions studied [17]. The effect of particle size on gas production can be explained by the fact that the smaller biomass particle offers a wide surface area for heat transfer resulting in a faster heating rate which leads to speed up secondary reactions such as decarbonization and cracking to form bio-gas [19].

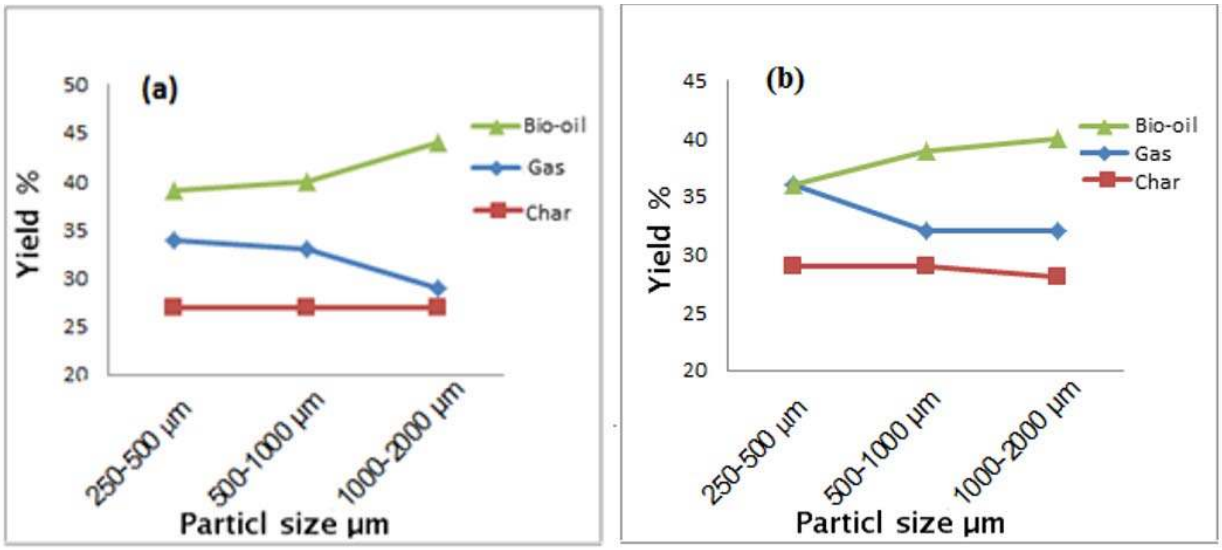

Figure 1: Effect of particle size on the product yields obtained from pyrolysis of (a) EFB and (b) PF at temperature of 500 ºC and reaction time of 45 min.

CONCLUSION

In this study, pyrolysis experiments of oil palm frond and oil palm empty fruit bunches were individually performed in a vertical fixed- bed reactor. The results were showed that the effects of the particle size were consistent but not significant. Both biomasses behave in the same manner where the yields of oil were slightly increased by increasing particle size.

ACKNOWLEDGEMENT

The authors thankfully acknowledge the support obtained from the Lotte Chemical Titan (M) Berhad and Universiti Sains Malaysia (Grant Number: 304/PJKIMIA/6050422/L128) in the form of research grant and facilities.

REFERENCES

[1] V. Dhyani and T. Bhaskar, "A comprehensive review on the pyrolysis of lignocellulosic biomass," *Renew. Energy*, vol. 129, pp. 695–716, 2018, doi: 10.1016/j.renene.2017.04.035.

[2] H. C. Ong, W. H. Chen, Y. Singh, Y. Y. Gan, C. Y. Chen, and P. L. Show, "A state-of-the-art review on thermochemical conversion of biomass for biofuel production: A TG-FTIR approach," *Energy Convers. Manag.*, vol. 209, no. March, p. 112634, 2020, doi: 10.1016/j.enconman.2020.112634.

[3] C. Gokcol, B. Dursun, B. Alboyaci, and E. Sunan, "Importance of biomass energy as alternative to other sources in Turkey," *Energy Policy*, vol. 37, no. 2, pp. 424–431, 2009, doi: 10.1016/j.enpol.2008.09.057.

[4] R. E. Guedes, A. S. Luna, and A. R. Torres, "Operating parameters for bio-oil production in biomass pyrolysis: A review," *J. Anal. Appl. Pyrolysis*, vol. 129, no. July 2017, pp. 134–149, 2018, doi: 10.1016/j.jaap.2017.11.019.

[5] P. McKendry, "Energy production from biomass (part 1): Overview of biomass," *Bioresour. Technol.*, vol. 83, no. 1, pp. 37–46, 2002, doi: 10.1016/S0960-8524(01)00118-3.

[6] C. N. Arenas, M. V. Navarro, and J. D. Martínez, "Pyrolysis kinetics of biomass wastes using isoconversional methods and the distributed activation energy model," *Bioresour. Technol.*, vol. 288, no. March, p. 121485, 2019, doi: 10.1016/j.biortech.2019.121485.

[7] S. P. Simanungkalit, D. Mansur, and M. A. Fitriady, "Effect of plastic blends on slow pyrolysis of oil palm empty fruit bunch," *AIP Conf. Proc.*, vol. 2024, 2018, doi: 10.1063/1.5064289.

[8] F. B. Ahmad, Z. Zhang, W. O. S. Doherty, and I. M. O'Hara, "The outlook of the production of advanced fuels and chemicals from integrated oil palm biomass biorefinery," *Renew. Sustain. Energy Rev.*, vol. 109, no. April, pp. 386–411, 2019, doi: 10.1016/j.rser.2019.04.009.

[9] M. A. Sukiran, F. Abnisa, W. M. A. Wan Daud, N. Abu Bakar, and S. K. Loh, "A review of torrefaction of oil palm solid wastes for biofuel production," *Energy Convers. Manag.*, vol. 149, pp. 101–120, 2017, doi: 10.1016/j.enconman.2017.07.011.

[10] M. J. Iskandar, A. Baharum, F. H. Anuar, and R. Othaman, "Palm oil industry in South East Asia and the

effluent treatment technology-A review," *Environ. Technol. Innov.*, vol. 9, pp. 169–185, 2018, doi: 10.1016/j.eti.2017.11.003.

[11] Y. H. Chan *et al.*, "An overview of biomass thermochemical conversion technologies in Malaysia," *Sci. Total Environ.*, vol. 680, pp. 105–123, 2019, doi: 10.1016/j.scitotenv.2019.04.211.

[12] A. A. Salema, R. M. W. Ting, and Y. K. Shang, "Pyrolysis of blend (oil palm biomass and sawdust) biomass using TG-MS," *Bioresour. Technol.*, vol. 274, no. October 2018, pp. 439–446, 2019, doi: 10.1016/j.biortech.2018.12.014.

[13] J. Akhtar and N. Saidina Amin, "A review on operating parameters for optimum liquid oil yield in biomass pyrolysis," *Renew. Sustain. Energy Rev.*, vol. 16, no. 7, pp. 5101–5109, 2012, doi: 10.1016/j.rser.2012.05.033.

[14] G. Kabir, A. T. Mohd Din, and B. H. Hameed, "Pyrolysis of oil palm mesocarp fiber and palm frond in a slow-heating fixed-bed reactor: A comparative study," *Bioresour. Technol.*, vol. 241, pp. 563–572, 2017, doi: 10.1016/j.biortech.2017.05.180.

[15] D. V. Suriapparao and R. Vinu, "Effects of Biomass Particle Size on Slow Pyrolysis Kinetics and Fast Pyrolysis Product Distribution," *Waste and Biomass Valorization*, vol. 9, no. 3, pp. 465–477, 2018, doi: 10.1007/s12649-016-9815-7.

[16] O. Onay, "Influence of pyrolysis temperature and heating rate on the production of bio-oil and char from safflower seed by pyrolysis, using a well-swept fixed-bed reactor," *Fuel Process. Technol.*, vol. 88, no. 5, pp. 523–531, 2007, doi: 10.1016/j.fuproc.2007.01.001.

[17] M. A. Sukiran, N. K. A. Bakar, and C. M. Chin, "Optimization of pyrolysis of oil palm empty fruit bunches," *J. Oil Palm Res.*, vol. 21, no. DECEMBER, pp. 653–658, 2009.

[18] M. Auta, L. M. Ern, and B. H. Hameed, "Fixed-bed catalytic and non-catalytic empty fruit bunch biomass pyrolysis," *J. Anal. Appl. Pyrolysis*, vol. 107, pp. 67–72, 2014, doi: 10.1016/j.jaap.2014.02.004.

[19] X. Hu and M. Gholizadeh, "Biomass pyrolysis: A review of the process development and challenges from initial researches up to the commercialisation stage," *J. Energy Chem.*, vol. 39, no. x, pp. 109–143, 2019, doi: 10.1016/j.jechem.2019.01.024.

[20] K. Azduwin, M. J. M. Ridzuan, A. R. Mohamed, and S. M. Hafis, "Pyrolysis of Empty Fruit Bunch (EFB) in a Vertical Fixed Bed Reactor," *Appl. Mech. Mater.*, vol. 695, pp. 228–231, 2014, doi: 10.4028/www.scientific.net/amm.695.228.

[21] K. N. Dhanavath, K. Shah, S. Bankupalli, S. K. Bhargava, and R. Parthasarathy, "Derivation of optimum operating conditions for the slow pyrolysis of Mahua press seed cake in a fixed bed batch reactor for bio-oil production," *J. Environ. Chem. Eng.*, vol. 5, no. 4, pp. 4051–4063, 2017, doi: 10.1016/j.jece.2017.07.034.

[22] A. Chandrasekaran, S. Ramachandran, and S. Subbiah, "Modeling, experimental validation and optimization of Prosopis juliflora fuelwood pyrolysis in fixed-bed tubular reactor," *Bioresour. Technol.*, vol. 264, no. May 2018, pp. 66–77, 2018, doi: 10.1016/j.biortech.2018.05.013.

[23] F. Abnisa and W. M. A. Wan Daud, "Optimization of fuel recovery through the stepwise co-pyrolysis of palm shell and scrap tire," *Energy Convers. Manag.*, vol. 99, pp. 334–345, 2015, doi: 10.1016/j.enconman.2015.04.030.

PGC_SCHE USM_2020_44

Biochar produce via liquid hot water (LHW) pretreatment and pyrolysis for CO_2 adsorption at low temperature

Nurul Azrin Zubbri, Abdul Rahman Mohamed*
School of Chemical Engineering, Engineering Campus, Universiti Sains Malaysia,
14300 Nibong Tebal, Pulau Pinang, Malaysia.
*E-mail: *chrahman@usm.my*

Abstract. The objective of this work is to convert rambutan (*Naphelium lappaceum*) peel waste into char via slow pyrolysis process. The biomass was initially pretreated with liquid hot water (LHW) treatment via hydrothermal carbonization (HTC) process in an autoclave reactor at elevated temperature and autogenous pressure. The HTC process was followed by pyrolysis at 450 °C for 60 min. Effect of HTC temperature was investigated to see the physicochemical influence on char structure. The experiments resulted with the highest CO_2 adsorption capacity of 94.03 mg g^{-1} by HTP200 (T_{HTC} = 200 °C) adsorbent while HTP150 (T_{HTC} = 150 °C) showed the lowest adsorption capacity of 63.39 mg g^{-1}. Raman spectra revealed that the I_D/I_G ratio increased as the HTC temperature increased, indicating that the adsorbent was transformed to amorphous material as exposed at higher temperature.
***Keywords**: CO_2 capture, Hydrothermal, Pyrolysis, Biochar, Liquid hot water*

INTRODUCTION

Due to huge consumption of fossil fuels such as coal, oil and natural gas, large emission of CO_2 that promoted the global warming effects to our atmosphere was critically focused [1]. Therefore, an efficient and economical technology is very important to be developed in capturing CO_2 from the governing emission sources. Among various technologies, chemical absorption using amine solutions was found to be the most appropriate technology [2]. However, this technology was experienced some drawbacks that could reduce the process efficiency such as corrosion effect on the equipment, large energy consumption for solution regeneration and ecotoxicological effect on the environment due to hazardous waste [3].

In recent years, solid adsorption process was found to be a potential technology for CO_2 capture thus was extensively studied as an alternative to the existing amine solution absorbent. Carbon porous material from natural biomass is among the solid adsorbent that becoming the focal interest in this recent year due to its environment-friendly properties and very abundant which make it as a low-cost adsorbent. Lignocellulosic materials are one of remarkable abundant renewable bioresource that available on our Earth.

In this research, rambutan peel waste was utilized as raw feedstock to produce biochar. Rambutan is one of tropical fruit that usually can be easily found in South East of Asia. Crop statistic has been conducted by Department of Agriculture of Malaysia in 2017 which revealed that around 37,215 MT of rambutan fruit was produced in that particular year [4]. Due to its large production, the peel waste was simply discarded once the flesh has been consumed. To reduce the effect of solid waste on the environment and cost of waste management, the rambutan peel was utilized to produce a beneficial product such as biochar.

Three primary components of lignocellulosic biomass were known as cellulose (30-60% dry matter), hemicellulose (14- 40% dry matter) and lignin 7-25 % dry matter) [5]. Due to its complex structure, biomass pretreatment is found to be very essential procedure at the beginning of any char production. There are several routes of biomass pretreatment such as comminution, biological pretreatment, chemical pretreatment and physicochemical pretreatment [6]. The most well-known pretreatment method is physicochemical pretreatment of biomass with hot water, known as liquid hot water (LHW) [6]. Usually, this kind of technique was carried out as hydrothermal carbonization (HTC) and the process was simply named as autohydrolysis. This kind of pretreatment is free from chemical reagent employment and economically efficient due to sole water consumption. During the pretreatment step, several processes tend to occur such as extraction of valuable product from biomass, transformation of the biomass structure which led to the improvement of the exposure area between biomass and chemicals or gases besides reducing the degree of crystallization [7]. LHW was conducted in an elevated temperature under autogenous pressure condition. This pretreatment usually carried out in a hydrothermal reactor at temperature of 150 – 250 °C for duration of more than one hour [8], [9].

In this work, an effort has been made to develop biochar from RP biomass. LHW pretreatment via hydrothermal carbonization (HTC) was carried out on the biomass prior facile slow pyrolysis process. The intention of HTC pretreatment in this study was to partially destruct the structure of biomass lignocellulosic which would help to improve the physicochemical properties of the char product. Effect of HTC temperature and time followed by pyrolysis temperature and time were studied in study.

MATERIALS AND METHODS

A. Biochar precursor

Rambutan (*Naphelium lappacium*) peel (RP) waste was used to produce biochar adsorbent. RP was initially washed with tap water and oven-dried at 110 °C for 24 hours to remove the moisture from the biomass. Proximate analysis was conducted on the raw RP using thermogravimetric analyzer (SDTQ-600) in order to measure the fraction of moisture, fixed carbon, volatile content and ash. Results of proximate analysis was shown in Table 1.

Table 1: Proximate Analysis of Raw RP

Parameter	Percentage (%)
Moisture	5.46
Fixed Carbon	27.00
Volatile matter	61.70
Ash	5.84

B. Methodology

Liquid hot water pretreatment was carried out at the first place via hydrothermal carbonization process. An amount of dried RP and 30 ml of water was place in an autoclave reactor (Figure 1) for the hydrothermal carbonization to begin at several temperature and time. The produced char (named as hydrochar) from LHW pretreatment was washed and kept in the oven overnight. Pyrolysis process was then carried out in a vertical reactor which was heated in a furnace under N_2 flow to pyrolysis temperature of 450 C and isothermally maintained at the same temperature for 60 min.

Figure 1: Autoclave reactor for hydrothermal carbonization (HTC)

C. CO_2 Capture

CO_2 adsorption study was conducted in a thermal gravimetric analyser (Perkin Elmer, SDTQ-600). An amount of sample was placed in the sample pan prior heated to 110 °C under N_2 flow (75 ml min^{-1}) purposely to purge any moisture and impurities from the biochar. The purging temperature was kept constant for 15 minutes. The CO_2 adsorption was then started when the temperature is fully equilibrated at 30 °C. The CO_2 adsorption process was kept at isothermal condition for 60 min to let the adsorption occurred until it was saturated.

D. Characterizations

The proximate analysis of RP biomass was conducted using thermal gravimetric analyzer SDTQ-600. The inherent carbon structure of hydrochar produce via LHW pretreatment was analysed by Renishaw inVia Raman Spectrometer.

RESULTS AND DISCUSSION

A. Effect of HTC pretreatment temperature

HTC pretreatment was conducted at several temperature (150 °C, 170 °C and 200 °C) for 120 min and coded as HTP150-120, HTP170-120 and HTP200-120, respectively. Effect of HTC pretreatment temperature towards CO_2 adsorption of biochar was shown in Figure 2. Overall, all three adsorbents possessed similar increasing

adsorption trend. The highest adsorption capacity was revealed by HTP200 with adsorption capacity of 86.73 mg g^{-1}, followed by HTP170 (86.44 mg g^{-1}) and HTP150-120 (63.39 mg g^{-1}). The adsorption was improved as the HTC temperature rise from 150 °C to 170 °C. Further increase the HTC temperature to 200 °C did not show any significant effect on the adsorption performance. It was also observed that high adsorption rate was happened to occur during the first 20 minutes of adsorption, followed by slow adsorption until adsorption time of 40 min. The adsorption curve was finally found to be plateaued after 40 min due to saturation of the adsorbent.

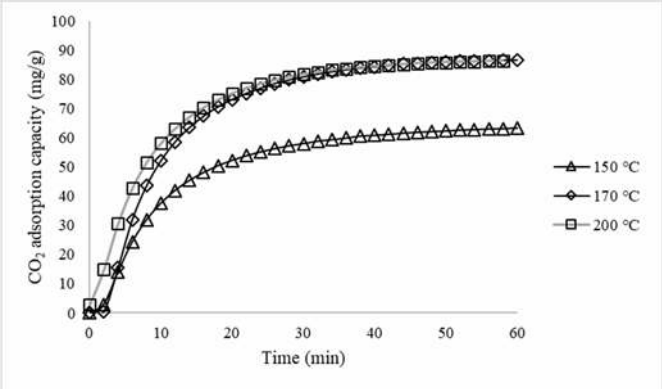

Figure 2: CO_2 adsorption capacity at different HTC temperature

During HTC process, the autoclave reactor was heated up until certain temperature (150 °C, 170 °C and 200 °C) and maintained for 120 min. During the hydrothermal process, autohydrolysis was the main governing phenomena occurred where organic acid was released from the hydrolysis of the hemicellulose. Auto-catalytic process tend to happen once these acidic compounds and the biomass extractives react with hydrolytic properties of water to initiate the hydrolysis reaction [11], [12]. Further increase the temperature to 170 °C and above will improve the adsorption performance of the adsorbent. It was suggested to be due to complete removal of hemicellulose from the biomass structure and defect of the crystalline of the graphitic structure.

In order to investigate the effect of HTC temperature to the structure of char, Raman spectroscopy analysis was carried out on the three samples. Figure 3 showed Raman spectra of biomass pretreated via HTC at different temperature of 150 °C, 170 °C and 200 °C. The peaks were analysed using Fityk software and the information was presented in Table 2. Overall, two major peaks were observed at around 1353 cm-1 and 1584 cm-1, which referred to D-band and G-band, respectively. The presence of these two peaks indicates that the adsorbents exhibit the non-graphitic carbon materials. D-band was attributed to the vibration of disordered graphitic lattice while G-band referred to the ideal graphitic lattice [13].

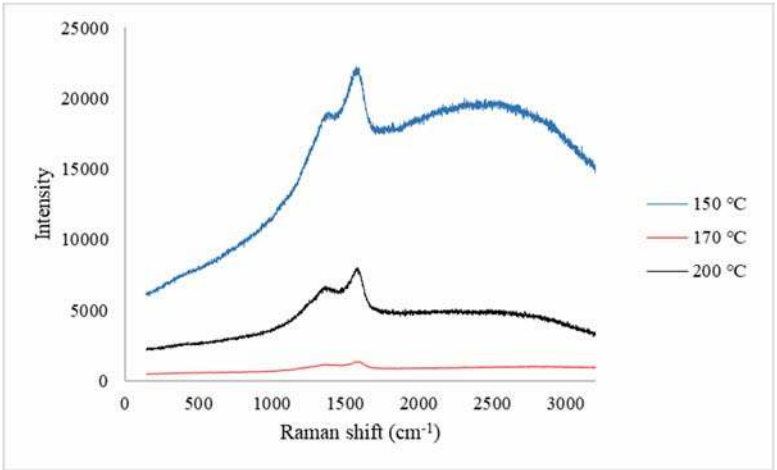

Figure 3: Raman spectra of char treated at HTC temperature of 150 °C, 170 °C and 200 °C

Table 2: Raman Spectra Information

Sample	D-band (cm^{-1})	G-band (cm^{-1})	ID	IG	ID/IG
HTP150	1361.64	1589.08	81.4	382.29	**0.21**
HTP170	1362.38	1590.58	88.63	372.67	**0.24**
HTP200	**1380.19**	**1578.34**	**130.02**	**215.914**	**0.60**

As the HTC temperature increased, the intensity of G-band was decreased with the growing of I_D. Obviously, the I_D/I_G ratio was increased from 0.21 to 0.60 as the HTC temperature increased. More carbon defect was suggested to present in adsorbent pretreated at higher temperature due to the breakdown of symmetric carbon atoms. Thus, it was expected that pretreatment of biomass at higher temperature in HTC could provide more surface exposure for the following pyrolysis process due to the extraction of lignocellulosic structure during HTC reaction. Even though HTP170 and HTP200 did not show significant different of CO_2 adsorption capacity, however the I_D/I_G ratio of HTP200 was 28% higher than HTP170. Therefore, HTC temperature of 200 °C was suggested to be the best condition due to the increment in D-band intensity from 1362.38 to 1380.19. Higher I_D indicate that the adsorbent structure was transitioning into amorphous phase.

B. Effect of HTC pretreatment retention time

Effect of HTC time was also observed in this research. Figure 4 show the CO_2 adsorption curves of biochar produced at different HTC time (30 min, 90 min, 150 min). The adsorbents were coded as HTP-200-30, HTP-200-60 and HTP-200-150, respectively. The results revealed that CO_2 adsorption was improved when HTC time increased from 30 min to 90 min with 72.12 mg g^{-1} to 90.35 mg g^{-1}, respectively. Further increase the duration of HTC reaction to 150 min will reduce the performance of CO_2 capture to 76.11 mg g^{-1}.

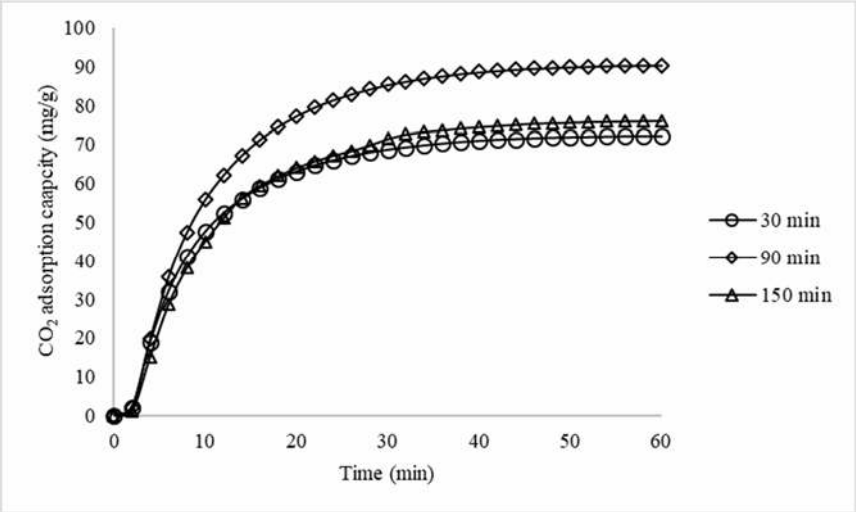

Figure 4:. CO_2 adsorption capacity at different HTC time

It was suggested that at the optimum HTC time (90 min), more than 90% of hemicellulose was extricated from the lignocellulosic polymer up to this reaction time, providing the extra surface contact for further carbonization to take place [14]. Further prolong the HTC time to 150 min was believed to decrease the yield of char which then reduce the CO_2 adsorption capacity.

CONCLUSION

Rambutan peel was processed to produce char via pretreatment of HTC and pyrolysis. HTC conditions were optimized at 200 °C for 90 minutes. As the HTC temperature increased, the I_D/I_G ratio was also improved, indicating that the structure of the adsorbent was transforming into amorphous materials. Therefore, LHW pretreatment via hydrothermal carbonization was a promising process in upgrading the physicochemical properties of biochar as CO_2 adsorbent.

ACKNOWLEDGEMENT

This research was supported by Ministry of Education of Malaysia and Universiti Sains Malaysia through LRGS Grant 203/PJKIMIA/672009.

REFERENCES

[1] G. Singh, I. Y. Kim, K. S. Lakhi, P. Srivastava, R. Naidu, and A. Vinu, "Single step synthesis of activated bio-carbons with a high surface area and their excellent CO_2 adsorption capacity," *Carbon*, vol. 116, pp. 448–455, 2017.

[2] G. T. Rochelle, "Amine Scrubbing for CO2 Capture," *Science*, vol. 325, no. 5948, pp. 1652–1654, 2009.

[3] A. E. Creamer, B. Gao, and M. Zhang, "Carbon dioxide capture using biochar produced from sugarcane bagasse and hickory wood," *Chemical Engineering Journal*, vol. 249, pp. 174–179, Aug. 2014.

[4] Department of Agriculture, "Statistik tanaman buah-buahan," *Crop Statistic*, 2017.

[5] Y. Sun and J. Cheng, "Hydrolysis of lignocellulosic materials for.pdf," vol. 83, pp. 1–11, 2002.

[6] W. Pruksakit and S. Patumsawad, "Hydrothermal Carbonization (HTC) of Sugarcane Stranded: Effect of Operation Condition to Hydrochar Production," *Energy Procedia*, vol. 100, pp. 223–226, 2016.

[7] M. Cozier, "Enzymatic conversion of lignocellulosic into fermentable sugars: challenges and opportunities," *Biofuels, Bioproducts and Biorefining*, vol. 8, no. 6, p. 743, 2014.
Y. Yu and H. Wu, "Understanding the primary liquid products of cellulose hydrolysis in hot-compressed water at various reaction temperatures," *Energy and Fuels*, vol. 24, no. 3, pp. 1963–1971, 2010.

[8] H. M. Coromina, D. A. Walsh, and R. Mokaya, "Biomass-derived activated carbon with simultaneously enhanced CO2uptake for both pre and post combustion capture applications," *Journal of Materials Chemistry A*, vol. 4, no. 1, pp. 280–289, 2015.

[9] P. Lahijani, M. Mohammadi, and A. R. Mohamed, "Catalytic CO 2 gasification of rubber seed shell-derived hydrochar : reactivity and kinetic studies," 2019.

[10] Y. Pu, T. Treasure, R. Gonzalez, R. Venditti, and H. Jameel, "Autohydrolysis pretreatment of mixed hardwoods to extract value prior to combustion," *BioResources*, vol. 6, no. 4, pp. 4856–4870, 2011.

[11] T. Ingram, T. Rogalinski, V. Bockemühl, G. Antranikian, and G. Brunner, "Semi-continuous liquid hot water pretreatment of rye straw," *Journal of Supercritical Fluids*, vol. 48, no. 3, pp. 238–246, 2009.

[12] A. B. Fuertes *et al.*, "Chemical and structural properties of carbonaceous products obtained by pyrolysis and hydrothermal carbonisation of corn stover," *Australian Journal of Soil Research*, vol. 48, no. 6–7, pp. 618–626, 2010.

[13] H. E. Putra, E. Damanhuri, K. Dewi, and A. D. Pasek, "Hydrothermal carbonization of biomass waste under low temperature condition," *MATEC Web of Conferences*, vol. 154, p. 01025, 2018.

PGC_SCHE USM_2020_45

Electrospun PET for Effective Air Filtration Media

Wei Lin Ng, Soon Huat Tan*
School of Chemical Engineering, Engineering Campus, Universiti Sains Malaysia,
14300 Nibong Tebal, Penang, Malaysia
*E-mail: *chshtan@usm.my*

Abstract. Electrospinning process is a proven technology to produce air filtration media with embedded nanofibers. The set-up of electrospinning process consists of three major components, which are high voltage power supply, a syringe containing polymer solution connected to a spinneret and a metallic collector. The electrospinning process parameter such as solution and processing parameters as well as ambient conditions could affect the resultant electrospun air filtration media. In this study, polyethylene terephthalate (PET) was used as the polymer. Two different types of PET polymers, which are the purchased PET granules containing 30% glass particles as reinforcer and recycle PET from water bottles were used to prepare the PET solutions. A pre-weighed amount of PET was dissolved in hexafluoro-2-propanol and stirred at room temperature with a stirring speed of 500 rpm for 24 hours. Different concentrations of PET polymer solutions were electrospinning on an aluminium foil placed on the collector. Other parameters such as electric field strength, distance between the spinneret and collector, syringe pump feed rate and ambient condition were fixed. The effects of PET polymer solutions on the electrospun nanofibers were observed through scanning electron microscope. The preliminary results showed that the resultant nanofibers prepared from 15 wt% PET granules and 10 wt% recycled PET were smooth and bead-free. Subsequently, the bead-free nanofibers will be electrospinning on the commercial PET support for further investigation of the air filter performances.
***Keywords**: Electrospining; Air filtration media; PET polymer*

INTRODUCTION

Electrospinning process is a relatively new technique to produce air filter with nanofibers to capture fine particles, volatile organic compounds and bacteria. The set-up of electrospinning process consists of three major components, which are high voltage power supply, a syringe containing polymer solution connected to a spinneret and a metallic collector. The polymer solution in electrospinning process will be electrically charged. The increase of electrical field intensity would cause the solutions to have stronger stretching. Then, a Taylor cone is formed on the tip of the syringe. A jet of solution is ejected from the syringe when the electric force overcome the surface tension of the solution. This charged jet is collected by oppositely charged metal collector that placed at certain distance from the tips of syringe. Then, the solvent evaporates eventually form solid fiber [1]. The electrospinning process parameters such as solution and processing parameters as well as ambient conditions could affect the resultant electrospun air filtration media [2].

Manipulate the polymer solution parameters such as the concentration, viscosity, molecular weight, solvent volatility, electrical conductivity and surface tension, would affect the formation of different nanofiber structure. Polymer concentration and viscosity will affect the surface tension of the solution. Low concentration tends to form beads on fiber during electrospinning. At very low concentration, no fiber is formed because of low viscosity. High concentration favors the increase in average fiber diameter and smooth fiber surfaces [1]. However, increasing the concentration beyond the concentration at which beadless electrospun nanofibers are formed will blocks the flow of solutions and make it dries at the tip of syringe [3]. Low molecular weight generates bead on the fibers. High conductivity brings to straighten the fiber and decrease its diameter. Conductivity can be increased by adding salts such as sodium chloride. In addition, low or high viscosity of the polymer solution will lead to the formation of beaded fibers [4]. High surface tension of polymer solution will result in instability of syringe flow; however, low surface tension might not always have fine fibers because the solvent evaporation rate influences the fiber diameter. Surface tension of polymer is mainly determined by solvent and also additional surfactants [1]. Solvents used for the polymer for electrospinning process should be able to completely dissolve the polymer, with moderate boiling point and conductivity. Boiling point gives an idea of the volatility of a solvent. Volatile solvent is preferred as they can easy travel from the tip of syringe to the metal collector. However, highly volatile (low boiling point) solvent should be avoided as it will be easily evaporated and block the tip of syringe. Less volatile (high boiling point) solvent will cause the deposition of solvent-containing nanofibers on the collector and formed the beaded nanofibers. Combination of solvents which have different evaporation rates leads to phase separation and favour for the fabrication of highly porous electrospun nanofibers [3].

Processing parameter such as electric field strength, flow rate and the distance between tip of the syringe and metal collector also affect the formation of nanofibers. Strong electric field strength is preferable for decrease in fiber diameter because polymer solution is stretched in correlation with the charge repulsion within the syringe [3]. High

applied voltage will cause the formation of beaded nanofibers because high voltage will decrease the size of Taylor cone and increase in the velocity for the same flow rate [3]. Polymer feed rate will affect the fiber diameter. Fast feed rate will increase fiber diameter and pore size, it also generates bead on the nanofiber because the flow cannot be fully stretched in the electrostatic field [2]. Besides that, increase in flow rate simultaneously increased the electric current and decreased the surface charge density. This will allow the merging of nanofibers during travelling toward the collector and forms garland like structure of nanofibers[5]. The distance between the collector and the tip could also affect the diameter and bead generation on the nanofibers. Shorter distance forms thicker or beaded fibers because the fibers yet to dry when reaching the collector, whereas longer distance might cause discontinuous fibers. Diameter and shape of the syringe changes the fibers diameter and fiber morphology, respectively. Increase in syringe gauge size effects the fibers of micro scale diameter meanwhile change in the shape of gauge will affect the fibers morphology [4]. Types of collector will affect the alignment or orientation of the fibers [4]. Pin, plate, cross bar, rotating rods or wheels, drum, liquid bath and disk are the options of the collectors.

Ambient parameter like humidity and temperature could affect the number of pores and fiber diameter [2]. Humidity effect the changes of nanofibers diameter by controlling the solidification process of the charged syringe, but it is depending on the chemical nature of the polymer. Normally, the increase in humidity will reduce the nanofiber diameter [3]. High humidity will also cause the formation of porous fiber [1]. The temperature cause two opposing effects where decrease the viscosity of the solution would increase the rate of evaporation, eventually decrease the fiber diameter [3]. Increase in temperature will also increase the fiber production rate [6].

Additives with the aim of boosting or enhancing gaseous pollutants-capturing could impregnate into the electrospinning polymer solution to produce functionalized nanofibers. Antibacterial nanofiber media is produced through the electrospinning process with additives derive either from inorganic or organic material from the natural plant extracts. In addition, the nanofiber mechanical strength also can be improved by adding additives [7].

Polyethylene terephthalate (PET) is well- known to be used as air filtration media. It is cheap but it has disadvantage in low filtration efficiency. Currently, PET filtration media can be produced in melt-blown process, spunbonded process, wet laid process, dry laid process, needle-punch process and spun laced process. Electrospinning technique is relatively a new technique to produce air filter with nanofiber to capture fine particles, volatile organic compounds and bacteria. Therefore, in this study, electrospinning is selected to produce PET nanofibers which with the aims that it can enhance the resultant filtration media efficiency.

MATERIAL AND METHODS

PET granules containing 30% glass particles as reinforcer was purchased from Sigma-Aldrich and the recycle PET was obtained from the “Spritzer” water bottles. Hexafluoro-2-propanol the solvent for the PET was purchased from the Haihang Industry Co. Ltd. A pre-weighed amount of PET was dissolved in hexafluoro-2-propanol and stirred at room temperature with a stirring speed of 500 rpm for 24 hours. Different PET polymer solutions were prepared namely10 wt% and 15 wt% PET granules and 10 wt% recycle PET. The resultant PET polymer solutions were electrospinning on an aluminium foil placed on the collector. The syringe pump (Cole Palmer Instrument Company) was adjusted to constant feed rate of 0.6mL/hours. The high voltage supply (ES30P-20W, Gamma High Voltage Research, Inc) was fixed at 20kV and 15kV. The distance between the tip of syringe to the aluminium foil collector was 19cm. The morphology of the electrospun nanofibers were observed through scanning electron microscope (SEM Hitachi TM3000 Tabletop).

RESULTS AND DISCUSSION

Two types of PET polymer solutions were obtained. A cloudy and opaque solution was found in the PET solution prepared from the purchased PET granules contains 30% glass particles as reinforcer. While the PET solution prepared from recycled PET showed a clear and transparent solution. This means that the PET solution prepared from PET granules might not be totally dissolved due to the glass particles in the PET granules. Different PET nanofibers were observed through the SEM. With a parameter was adjusted and other parameters were remained, the effects of parameter were observed. Figure 1 shows the SEM images of PET nanofibers prepared from the purchased and recycled PET polymers. Both PET polymer solutions were fixed at 10 wt% while the other parameters such as voltage supply, feed rate and distance between the tip of syringe and collector were remained constant. As shown in Figure 1, there were some beads formation observed in the fibers produced from the purchased PET, while the fibers produced from recycled PET were bead-less. The concentration of purchased PET shall be further increased to have bead-less nanofiber.

The nanofiber of 15 wt% purchased PET was prepared. The morphology of the nanofiber was observed under SEM as shown in Figure 2. It was proven that at higher polymer concentration will produce bead-less nanofiber. The nanofiber of 15 wt% PET polymer showed long and smooth fibers. The nanofiber of 15 wt% purchased PET has bigger diameter compare to 10 wt% purchased PET. Besides that, as compared to 10 wt% recycled PET, the diameter of the fiber in 15 wt% purchased PET was smaller. Even though high polymer concentration tends to increase the

fiber diameter [1], but the above observation might be due to the conductivity of 15 wt% purchased PET is better than 10 wt% recycled PET.

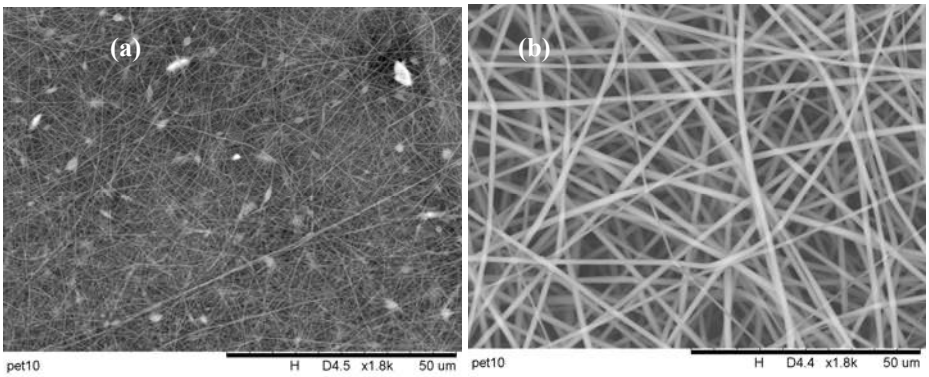

Figure 1: SEM images of nanofibers with different types of PET polymers under 10 wt% PET, feed rate 0.6mL/ h, applied voltage 20kV and distance between the tip of syringe and collector is 19cm: (a) Purchased PET, (b) Recycled PET.

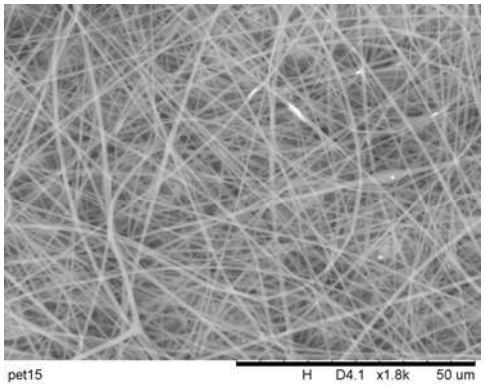

Figure 2: SEM images of nanofibers with 15 wt% of purchased PET polymers under 20kV applied voltage, feed rate 0.6mL/ hr and distance between the tip of syringe and collector is 19cm.

Another observation was done to compare the effect of applied voltage. The nanofiber of 10 wt% recycled PET was produced under 15kV and 20kV voltage as shown in Figure 3. Other processing parameters were remained. It was observed that the resultant fibers produced at 20kV voltage were denser than that produced at 15kV voltage. The electrospinning duration was fixed at 1.5 hours in both samples. This means that at higher applied voltage, the polymer solution easily to be stretched and produced larger quantity of fiber. Besides that, it can be observed that under these two applied voltages, the nanofibers produced was bead-less which means that the applied voltage of 15kV and 20kV were sufficient to decrease the size of Taylor cone on the tip of the syringe and increase the injected polymer speed under the same flow rate.

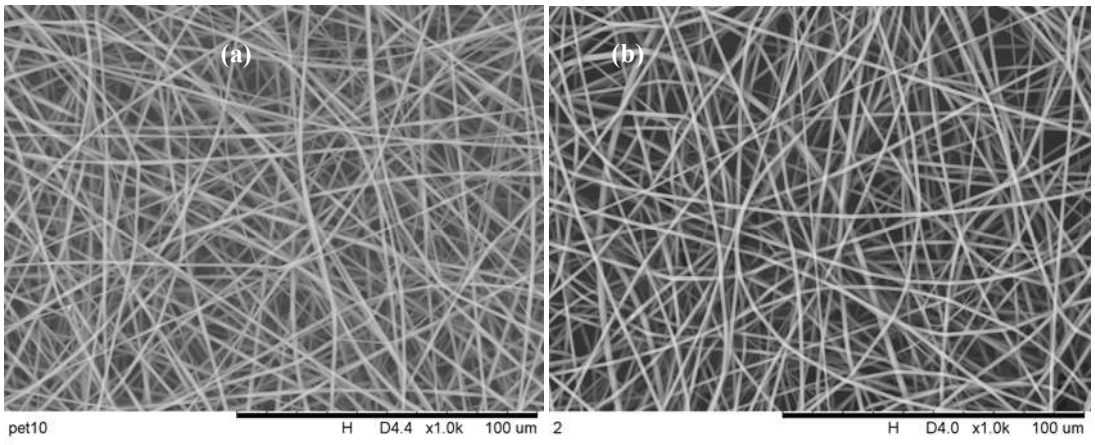

Figure 3: SEM images of nanofibers with different applied voltage on 10 wt% recycle PET polymers under feed rate 0.6mL/h and distance between the tip of syringe and collector is 19cm: (a) 20kV, (b) 15kV.

CONCLUSION

Both purchased and recycled PET can produce nanofibers via electrospinning process. The preliminary results showed that the resultant nanofibers prepared from 15wt% PET granules and 10wt% recycled PET were smooth and bead-free. Subsequently, the bead-free nanofibers will be electrospinning on the commercial PET support for further investigation of the air filter performances.

ACKNOWLEDGMENT

This research is funded under the Fundamental Research Grant Scheme (FRGS) (6071441) sponsored by the Ministry of Higher Education of Malaysia (MOHE).

REFERENCES

[1] E. Zdraveva, J. Fang, B. Mijovic, and T. Lin, *Electrospun nanofibers*. 2016.
[2] M. Zhu *et al.*, "Electrospun Nanofibers Membranes for Effective Air Filtration," *Macromol. Mater. Eng.*, vol. 302, no. 1, pp. 1–27, 2017.
[3] A. Haider, S. Haider, and I. K. Kang, "A comprehensive review summarizing the effect of electrospinning parameters and potential applications of nanofibers in biomedical and biotechnology," *Arab. J. Chem.*, vol. 11, no. 8, pp. 1165–1188, 2018.
[4] S. Thenmozhi, N. Dharmaraj, K. Kadirvelu, and H. Y. Kim, "Electrospun nanofibers: New generation materials for advanced applications," *Mater. Sci. Eng. B Solid-State Mater. Adv. Technol.*, vol. 217, pp. 36–48, 2017.
[5] S. A. Theron, E. Zussman, and A. L. Yarin, "Experimental investigation of the governing parameters in the electrospinning of polymer solutions," *Polymer (Guildf).*, vol. 45, no. 6, pp. 2017–2030, 2004.
[6] Chidchanok Mit-uppatham; Manit Nithitanakul; Pitt Supaphol, "Ultrafine Electrospun Polyamide-6 Fibers Effect of Solution Conditions on Morphology andAverage Fiber Diameter.pdf." pp. 2327–2338, 2004.
[7] V. V. Kadam, L. Wang, and R. Padhye, "Electrospun nanofibre materials to filter air pollutants – A review," *J. Ind. Text.*, vol. 47, no. 8, pp. 2253–2280, 2018.

PGC_SCHE USM_2020_46

Elucidation of Kinetics and Mechanism of Uncatalyzed Esterification of Acetic Anhydride with Isoamyl Alcohol in a Microreactor System

Cheong Sheng Lee, Syamsul Rizal Abd Shukor*
School of Chemical Engineering, Engineering Campus, Universiti Sains Malaysia,
14300 Nibong Tebal, Pulau Pinang, Malaysia.
E-mail: chsyamrizal@usm.my*

Abstract. Uncatalyzed esterification of acetic anhydride and isoamyl alcohol has been carried out in a miniaturized intensified reactor (MIR) to develop a kinetic equation using ideal homogenous model. The reaction was study towards the effect of temperature and reaction time. Based on the result, isoamyl acetate production increased with increase of reaction time and reaction temperature. High conversion of acetic anhydride was obtained in the absence of catalyst in a microreactor system in a short reaction time of 90 minutes compare to days in a traditional batch reactor. This show the advantages of microreactor with high surface to volume ratio which promotes perfect mixing and excellent proximate contact between the reactant which allow high heat and mass transfer. Three different kinetic model were proposed in which reversible reaction model were chosen as proper kinetic model to represent the esterification reaction. Hydrolysis toward acetic anhydride may be neglect for model simplification due to significant low rate constant upon simulation. The present of initial water in the reactant show effect toward the equilibrium and the yield of isoamyl acetate and it should be determined prior reaction and include in the simulation to improve the fitting of kinetic model.
Keywords: *Kinetic Modelling, Esterification, Solvent free, Non-enzymatic, Microreactor*

INTRODUCTION

Esters are compounds of the chemical structure R-COOR' whereby R and R' are either alkyl or aryl groups. It is one of the most natural occurring organic compound that can be found in essential oils of plant and animal fats as well as many biologically important molecules [1]. Isoamyl acetate is one of a naturally occurring short chain ester, which has drawn early interest of researchers and industry for its characteristic banana and peer like aroma. Industrially synthesized isoamyl acetate is commonly used in food, cosmetics and perfume industry. Due to consistently high demand and rising consumer expectations, the production process is under permanent pressure to improve [2]. Past research has focused on extraction from plants, Fischer esterification or synthesis in organic solvent. The former suffers from high production and handling cost [3] while the latter may lead to severe environmental issues and human health concerns if not handled properly. The current area of interest comprises solvent-free systems, enzymatic synthesis routes, ion exchange resin and process intensification by miniaturization. Solvent-free systems and the use of enzymes erase the toxicity concerns of previous methods, whereas the miniaturization is expected to improve process characteristics such as mixing and heat transfer. Nevertheless, enzymatic synthesis is restricted in temperature, as at higher temperatures enzyme denaturation leads to loss of catalytic function and isoamyl acetate yield declines. In line with this, latest research has shown that non-enzymatic continuous isoamyl acetate synthesis in a solvent-free microreactor system leads to lower yields in the temperature range of enzyme activity, but at higher temperatures, surpasses the highest achievable yield reached in the same synthesis process with immobilized Candida Antarctica lipase B [4]. Quitain et al. also showed that esterification between oleic acid and methanol can be proceed without any catalyst in less than 1 minutes by improve the mixing or molecular interaction of the reactant using supercritical carbon dioxide as a solvent and microfluidic device [5]. Narayan and Madras claim that catalysts are not absolutely necessary for esterification to occur [6]. These outcomes with the absence of expensive enzymes and toxic solvent or catalysts making such production method to be highly attractive for future application in industry.

Several papers have reported some kinetic data on the synthesis of isoamyl acetate by esterification in the presence of acid catalyst such as ion exchanges resin [7], enzyme [8] and ionic liquid [9] in which focus on reaction between acetic acid and isoamyl alcohol. However, to our knowledge, only a handful of studies were conducted towards kinetic model on uncatalyzed esterification of isoamyl acetate. In this study, elucidation on reaction kinetics modelling of non-enzymatic continuous isoamyl acetate synthesis in a microreactor system was established. For this purpose, isoamyl acetate had to be experimentally synthesized in a microreactor system. The effect of volumetric flow rate and temperature on the homogenous esterification reaction between acetic anhydride and isoamyl alcohol was also investigated. The obtained experimental results were verified using the developed kinetic equation based on ideal homogenous model for model validation.

MATERIALS AND METHODS

Isoamyl acetate synthesis was conducted under solvent-free condition and without the use of enzyme or acid catalyst in the microreactor system setup as shown in Figure 1. The red programmable syringe pump (VIT-FIT, LAMBDA, Czech Republic) and yellow programmable syringe pump (NE 1000, New Era, USA) pumped isoamyl alcohol and acetic anhydride respectively in a molar ratio of 2:1 at a continuous volumetric flow rate into the microreactor. The microreactor setup (as shown in Figure 1a) was placed in the blue thermal insulated water bath. Hot water was supplied by 4.5L water tank (CC-K6, Huber, Germany) and circulated in the water bath. The inlet temperature to the microreactor was measured by the thermocouple sensor and observed over a thermometer's display (DM6801A+, Vici, China). All the reactants and product compositions were analyzed by gas chromatography (7820A GC, Agilent Technologies, US). The retention peaks were as follows: isoamyl acetate, 3.519 minutes; isoamyl alcohol, 3.712 minutes; acetic anhydride, 4.007 minutes and acetic acid, 4.840 minutes. In evaluating the results, the arithmetic means of the results based on calibration curve of respective component were taken.

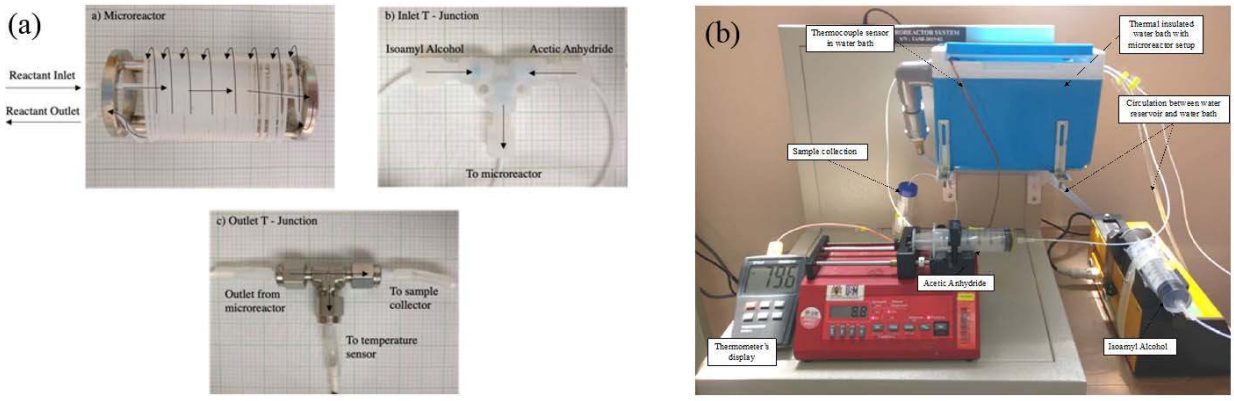

Figure 1: (a) Microreactor, T-junctions at the inlet and outlet from the microreactor, (b) Experiment setup of the Isoamyl Acetate synthesis

RESULTS AND DISCUSSION

Effect of reaction time and reaction temperature were shown in Figure 2(a) and 2(b) respectively. From Figure 2(a), it can be noticed that the concentration of isoamyl acetate increase from 0.8 mol/L to 2.64 mol/L (3.3 fold) when the reaction time increase from 7.9 minutes to 180 minutes at 80℃. At 90 minutes onwards, it is observed that the concentration of acetic anhydride nearly reaches zero which indicate almost 99% of acetic anhydride conversion has been achieved which far rapid compared to traditional batch reactor. Short diffusion path within the fluid stream in small volume microreactor channel led to very efficient mass transfer in mixing and much less energy input required to achieve mass transfer of reactant and product compared to the vigorously shaken batch reactor [10,11]. Increase of reaction time provide a greater contact time and allows effective diffusion of the reactants to take place, thus improve the conversion of acetic anhydride. This result is in agreement with the ones obtained by Mohammed Gumel and Annuar [12]. Increase in reaction temperature, increase the frequency of effective collision between the reactant hence enhance acetic anhydride conversion which shown in Figure 2(b). According to Arrhenius equation, it is understood that intrinsic rate constant is a strong function of temperature.

Three different kinetic model were proposed as stated in Table 1 to fit the experimental data. MATLAB's ode45s solver was implemented to solve the kinetic model of ordinary differential equation and algorithm of '*fmincon*' were applied to predict the rate constant, k in each kinetic model by minimizing the sum square error (SSE) with experimental concentration. The result was show in Table 2 in which second order model result in the lowest SSE. However, it is notice from experimental data in Figure 2(a), concentration of acetic acid was always higher compare to isoamyl acetate. Therefore, it is reasonable to suspect the hydrolysis of isoamyl acetate happened during esterification between acetic anhydride and isoamyl alcohol. Among three model, only reversible model contained term of water in the rate expression. Apparent value of k_3 and k_4 also represent there are hydrolysis reaction on isoamyl acetate and acetic anhydride respectively. Therefore, reversible model was used for further study and stimulate with different initial water concentration.

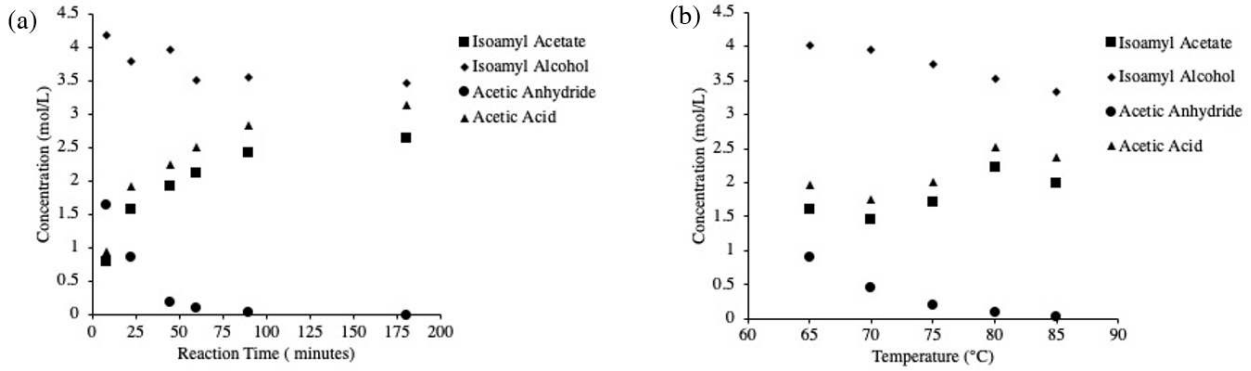

Figure 2: (a) Effect of reaction time at molar ratio of 2:1 (isoamyl alcohol : acetic anhydride), (b) Effect of reaction temperature at molar ratio of 2:1 (isoamyl alcohol : acetic anhydride) and 60 minutes reaction time.

Table 1: Reaction pathway and reaction rate expression for respective model

	Second Order Model	**Autocatalytic Model**	**Reversible Model**
Reaction Path way	$A + B \rightarrow C + D$	$A + B \rightarrow C + D$ $A + B + C \rightarrow 2C + D$	$A + B \rightarrow C + D$ $C + B \leftrightarrow D + H_2O$ $A + H_2O \rightarrow 2C$
Reaction Rate Expression	$r_s = k_1[A][B]$	$r_{A1} = k_1[A][B]$ $r_{A2} = k_2[A][B][C]$	$r_{r1} = k_1[A][B]$ $r_{r2} = k_2[B][C] - k_3[D][H_2O]$ $r_{r3} = k_4[A][H_2O]$

***A:** Acetic Anhydride; **B:** Isoamyl Alcohol; **C:** Acetic Acid; **D:** Isoamyl Acetate; **H_2O:** Water

Table 2: Rate constant and sum square error for respective model

Model	k_1	k_2	k_3	k_4	**SSE**
Second Order	0.0081615	-	-	-	4.8112
Autocatalytic	0.0081829	1.9506×10^{-9}	-	-	4.9012
Reversible	0.0081781	2.7882×10^{-5}	0.65011	0.11154	4.9038

Initial water concentration of 0.1, 0.2, 0.3, 0.4, 0.5 and 1.0 were stimulated with reversible model in MATLAB and the result was showed in Table 3. The initial concentration affects the rate constant of reversible reaction k_2 and k_3, whereas k_4 remain significantly lower which could be neglected for model simplification. All SSE value obtained were lower compare to result obtained with zero initial water concentration (show in Table 2) in which confirm the present of initial water concentration. Lowest SSE value of 4.3052 was observed with initial concentration of 0.4 mol/L. Figure 3a and 3b show the stimulated concentration curve against reaction time with 0 mol/L and 0.4 mol/L of initial water concentration respectively. It can be observed that Figure 3b more well fitted with experimental data and more reliable to represent the esterification of acetic anhydride and isoamyl alcohol. The deviation might due to non-ideal interaction behaviours between the reactant and product.

Table 3: Effect of initial water concentration toward rate constant and sum square error for reversible model

Initial Water concentration	k_1	k_2	k_3	k_4	**SSE**
0.1	0.0083068	6.7421×10^{-10}	0.013906	1.254×10^{-7}	4.5764
0.2	0.0083774	8.2647×10^{-10}	0.0085298	3.983×10^{-8}	4.4068
0.3	0.0083041	0.018439	0.33442	4.0174×10^{-7}	4.5548
0.4	0.008408	1.4363×10^{-8}	0.0037028	7.3674×10^{-8}	4.3052
0.5	0.0083201	0.064268	0.6362	7.2007×10^{-8}	4.4511
1.0	0.0083463	0.1252	0.57746	1.4822×10^{-5}	4.3129

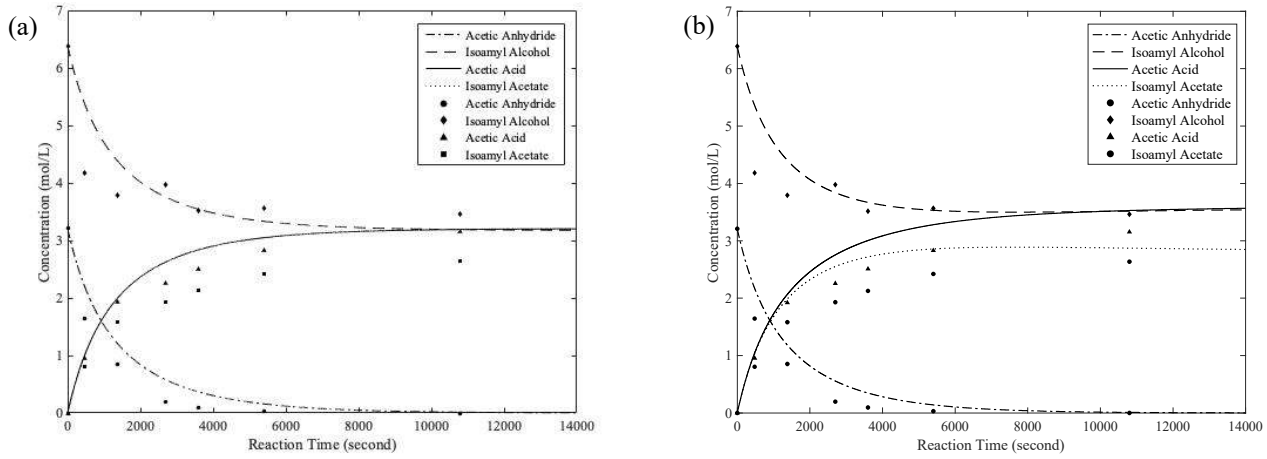

Figure 3: (a) Reversible model validation with 0 initial water concentration, (b) Reversible model validation with 0.4 mol/L initial water concentration.

CONCLUSION

The kinetic of uncatalyzed esterification between acetic anhydride and isoamyl alcohol at different temperature and reaction time at a molar ratio of 2:1 (isoamyl alcohol: acetic anhydride) was investigated experimentally in MIR. Three different kinetic model was proposed in developing the kinetic equation and compare with experimental data obtained for model validation. Result show that reversible model was the most suitable to represent the esterification between acetic anhydride and isoamyl alcohol in which having lowest sum square error of 4.3052 with stimulated 0.4 mol/L of initial water concentration. The hydrolysis of isoamyl acetate show more favorable compare to hydrolysis of acetic anhydride in which significant lower value of k_4 could be neglected for model simplification. Further improvement can be achieved in future studies by considering the initial water concentration analysis and online measurement which is suggested to provide a more reliable kinetic model of esterification.

ACKNOWLEDGEMENT

The authors would like to acknowledge Ministry of Education Malaysia for providing financial support via FRGS Grant (203. PJKIMIA 6071387) and MyBrain15 to sponsor scholarship for PhD study. The authors would also like to thank Universiti Sains Malaysia for the equipment and USM Post-Doctorate Research Fellow Scheme 2020-2021.

REFERENCES

[1] Y. A. Nurhazwani, M. D. Mashitah, and R. A. S. Syamsul, *J. Eng. Sci. Technol.*, vol. 10, no. Spec.issue8, pp. 78–87, (2015).
[2] M. J. Eisenmenger and J. I. Reyes-De-Corcuera, *Biotechnol. Lett.*, vol. 32, no. 9, pp. 1287–1291, (2010).
[3] H. Ghamgui, M. Karra-Chaâbouni, S. Bezzine, N. Miled, and Y. Gargouri, *Enzyme Microb. Technol.*, vol. 38, no. 6, pp. 788–794, (2006).
[4] N. Yusoff Azudin, S. Sangaran, and S. R. Abd Shukor, *J. Environ. Chem. Eng.*, p. 103186, (2019).
[5] A. T. Quitain, E. G. Mission, Y. Sumigawa, and M. Sasaki, *Chem. Eng. Process. - Process Intensif.*, vol. 123, pp. 168–173, (2018).
[6] R. C. Narayan and G. Madras, *React. Chem. Eng.*, vol. 2, no. 1, pp. 27–35, (2017).
[7] H. T. R. Teo and B. Saha, *J. Catal.*, vol. 228, no. 1, pp. 174–182, (2004).
[8] A. Güvenç, N. Kapucu, E. Bayraktar, and Ü. Mehmetoğlu, *Chem. Eng. Commun.*, (2003).
[9] X. Shao, Y. Zhang, J. Wang, Y. Liu, and W. Chen, vol. 44, pp. 1480–1485, Dec. (2015).
[10] M. Cvjetko, J. Vorkapić-Furač, and P. Žnidaršič-Plazl, *Process Biochem.*, vol. 47, no. 9, pp. 1344–1350, (2012).
[11] S. Watanabe *et al.*, *Adv. Powder Technol.*, vol. 28, no. 11, pp. 3104–3110, (2017).
[12] A. Mohammed Gumel and M. S. Annuar, *3 Biotech*, vol. 6, Dec. (2016).

PGC_SCHE USM_2020_47

Weight Impact of Integration of Sweetening Technologies onto FLNG

Li Chin Law[1,2], Masad Mezher Hasan[1,3], Irfan Ali Qazi[1], Mohd Roslee Othman[1,*]
[1]School of Chemical Engineering, Engineering Campus, Universiti Sains Malaysia 14300 Nibong Tebal, Pulau Pinang, Malaysia.
[2]Sembcorp Marine Ltd, 80 Tuas South Boulevard, Singapore 637051
[3]Department of fuel and energy, Basra Engineering Technical College, Southern Technical University.
E-mail: [*]chroslee@usm.my

Abstract. Global market trend is moving towards offshore exploration and production driven by the depletion of onshore oil and gas reservoirs. In recent years, natural gas has attracted more attention than the other fossil fuel resources. Oil and gas companies are shifting focus from developing landed natural gas plant to offshore floating liquefied natural gas platform or FLNG as a new technology for monetizing the offshore natural gas resources. Due to the stringent process requirement of LNG processing, installation of sweetening unit is considered a crucial strategy. The biggest challenge of integration of sweetening unit to FLNG is space and weight limitation on vessel and also the fact that the CO_2 content in the feed gas varies with times and location, and hence the sweetening unit needs to be designed with the ability to handle the variation in CO_2 content. In this paper, 3 different CO_2 removal technologies which are amine absorption, membrane and cryogenic units are compared in term of weight impact when the CO_2 content is changed. Considering the same natural gas feed condition (T = 25 °C, P = 30 bar) from the wellhead, and the variation of CO_2 content in the feed gas range from 5% to 50 %, the FLNG processes are simulated for the case where different sweetening units are used. For all simulations, the natural gas product's composition is fixed at a 97% of Methane product. Interesting finding based on the study is the membrane and cryogenic unit is very much lighter than amine absorption when the CO_2 content in the feed is high. The weight of membrane is the lowest among all the other technologies, and remain low even with CO2 increment, whereas the weight of the amine absorber unit has increased exponentially with CO_2 percentage in the feed gas. In the overall view of the technologies as part of a FLNG platform, the total weight of membrane and cryogenic is almost the same, with the latter being slightly heavier, thus membrane is found to be the most favourable as the sweetening unit for FLNG platform.
Keywords: *FLNG, CO_2 removal; energy; cost; natural gas; carbon capture; acid gas capture unit; Aspen Hysys.*

INTRODUCTION

FLNG has emerged as an attractive solution [1] to extract the natural gas resources at the deeper sea due to its floating feature which has helped to meet the global demand of cleaner energy [3]. Importantly, FLNG can be shifted from one field to another, so it could possibly serve different natural gas fields [2]. However, there are many challenges in the offshore exploration as compared to onshore LNG operation, and hence extra considerations are required in the design stage. One of the considerations is the weight control of the vessel. Weight has a direct impact on the construction cost and the vessel's structural design. A reduced weight and good weight distribution of vessel are important in assuring the stability of the ship in deep water which is exposed to the harsh sea movement is maintained at all time. Hence, this study has been carried out to compare the weight of the sweetening unit from 3 different technologies and the weight of the FLNG when these sweetening technologies are being integrated as part of the FLNG operation. The weight impact due to variation of CO2 content in the natural gas feed needs to be addressed to ensure that the vessel weight is accurately estimated in the design phase.

METHODS & MODEL DEVELOPMENT

Process design. In this study, three different sweetening units which are amine absorption, membrane and cryogenic units are compared in term of weight when the CO2 is varied from 5% to 50%. At the same time, the natural gas product's purity is being controlled and fixed at 97%. Increase of the CO2 percentage in the natural gas increases the workload of the CO2 sweetening unit and hence the design factors of the sweetening units need to be manipulated so that the sweet natural gas product obtained from the simulation can meet the methane product specification. The manipulated variables for amine absorption, membrane and cryogenic units are amine flow rate, membrane area, and reflux ratio of cryogenic tower respectively. Indirectly, the size and weight of the unit operations are affected. This change of weight is quantified and analysed in this study.

Simulation basis. The full simulation model is developed using Aspen Hysys. The model is divided into 3 main parts. The first part is the pre-treatment of natural gas feed, this part of simulation is to prepare the feed at the optimal condition for different CO_2 removal process, and part two of the simulation is the CO_2 removal which is the main

focus of this study. Part 3 of the simulation has included the natural gas processing until the end product methane is produced and then processed to reach the stable condition for storage in the cryogenic storage tanks. The natural gas is stored in liquid form at atmospheric pressure and an extremely low temperature of -162 °C [2]. For this study, the analysis is divided into 2 sections. First is the analysis on the weight of individual sweetening unit in general. Secondly, the full simulation of the FLNG is analysed to determine which CO_2 removal technologies that gives the lightest FLNG weight.

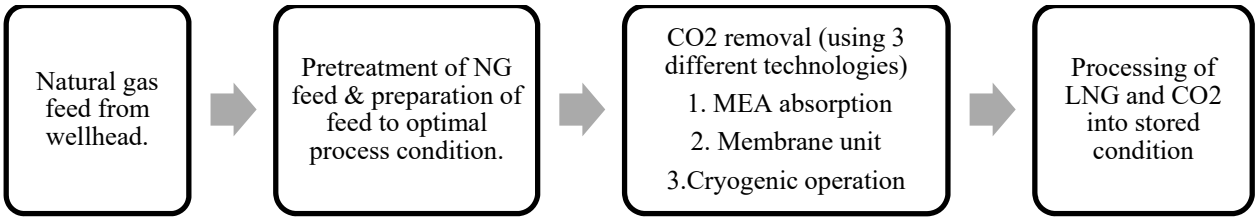

Figure 1: Illustration of simulation workflow for CO_2 removal from natural gas

The feed gas of the simulation is assumed to be gases directly extracted from the wellhead, with water content fixed at 10 volume % and other impurities are assumed to be negligible to simplify the computation. Table 1 shows the detail information of the natural gas feed from the wellhead. Full simulation workflow combining the pre-treatment, CO_2 removal and liquefied natural gas processing has been modelled in Aspen Hysys for three different CO_2 removal technologies. For different CO_2 removal unit, six scenarios with varied CO2% in the feed have been simulated as listed in Table 2.

Table 1. Natural gas feed from wellhead

Parameters	Values
Feed flow, m^3 (STP)/h	4213
Feed gas composition, vol %	Table 2
Feed temperature, °C	25
Feed pressure, bar	30

Table 2. List of different simulation scenarios

Scenarios	Feed Gas Composition, vol% *	
	CO_2	Methane
Case 1	5	85
Case 2	10	80
Case 3	20	70
Case 4	30	60
Case 5	40	50
Case 6	50	40

*10% H_2O for all cases

RESULTS AND DISCUSSION

Figure 2 shows the total weight of all the unit operations involved in the complete simulation including pre-treatment of feed gas, sweetening unit and LNG processing units. The total weight is also divided into three individual segments. The weight of the CO_2 removal unit is indicated by the second segments of the candlestick. As we can see, when the CO_2 % is at 10% or lower, the weight of membrane unit is the lowest, followed by amine absorption unit and lastly cryogenic technology. However, the weight of amine absorber unit increases exponentially with CO_2 %, making it heavier than the cryogenic technology when the CO_2 content in the feed is raised up to 20% and higher. This is due to the fact that amine unit involves usage of amine solvent, and the flow rate of amine increases with increasing amount of CO_2 in the feed. This results in larger size of amine absorber and regenerator units which incurs more weight. This has made amine technology less suitable for CO_2 content that is higher than 10%, partly because of the over-weighted towers, and also because of the taller towers generally results in ineffective solvent distribution thus, reduces the CO_2 removal efficiency.

Comparing between membranes and cryogenic tower, cryogenic technology is 30 to 50 times heavier than membrane unit due to the large cryogenic structure. However, the total weight of the whole process of these two technologies differs slightly. For the case with 50% of CO_2, the total weight of FLNG using cryogenic tower is just 12% heavier than membrane. This is due to the operating condition of membrane at a higher temperature that requires

additional cooler for the LNG processing, resulting in heavier LNG processing part. Considering the order of suitability of the sweetening unit in term of weight, membrane turns out to be the most suitable sweetening unit, followed by cryogenic tower and then amine absorber unit. In addition, when the percentage of CO_2 in the feed gas is increased from 5% to 50%, the weight for membrane has increased by 1%, weight for cryogenic tower increased by 58% and weight of amine absorber units has increased by 300%.

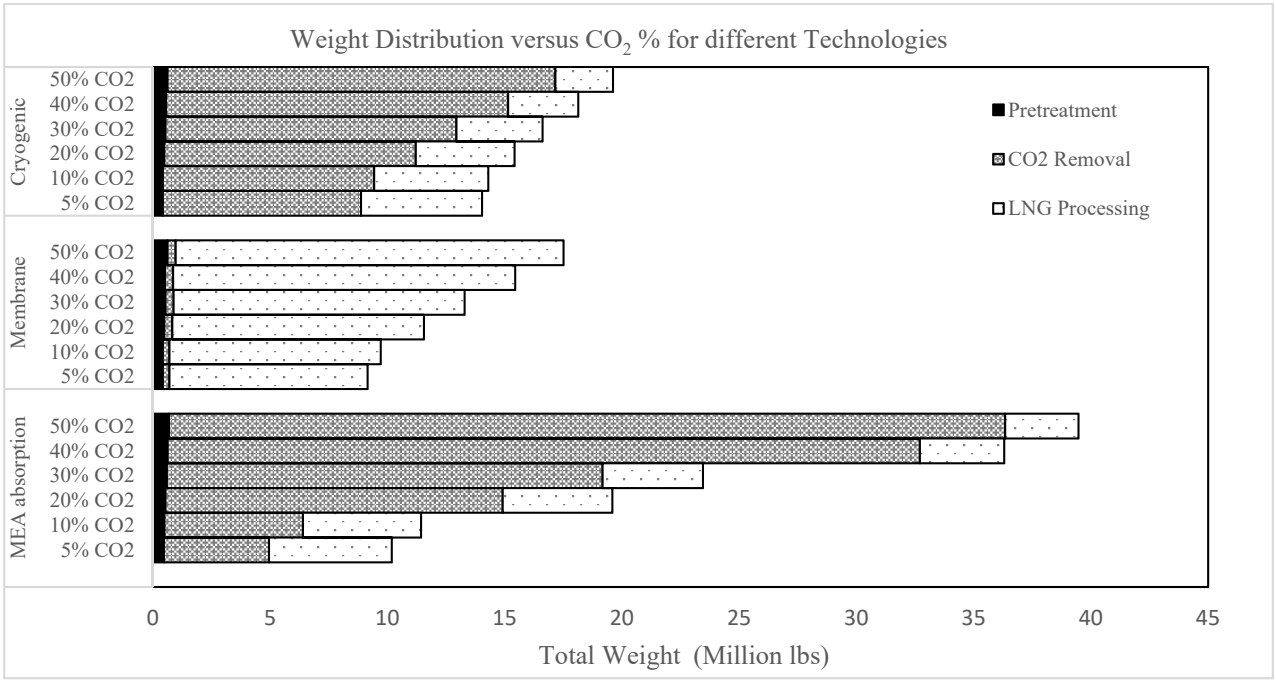

Figure 2: Weight distribution chart for three type of sweetening technologies at 6 different scenarios

CONCLUSION

This paper has compared the feasibility of integrating the amine absorption, membrane and cryogenic units in the FLNG for CO_2 removal. The CO_2 concentration in the feed is varied and the impact on the weight is analysed. Based on the analysis, membrane is the most suitable sweetening unit with its lowest total weight, followed by cryogenic tower and then the amine absorber unit. Amine absorber is not recommended for FLNG due to its exponential increase in weight which will adversely impact the weight distribution of the vessel and compromise the vessel's safety. Further study should be done on the other design factors such as the economic and energy penalty of the sweetening process, size of the equipment and the flexibility of the process under constant sea movement before recommending the most favourable sweetening technology for FLNG offshore operation.

REFERENCES

[1] Garside, M. Global natural gas consumption 1998-2019. Retrieved from Statista: https://www.statista.com/statistics/282717/global-natural-gas-consumption/). (2020, July 24).
[2] Khakzad, N., & Reniers, G. Floating Liquefied Natural Gas. ScienceDirect. (2018).
[3] Tham, S. xEngineringpro. Exploring the growth of the FPSO industry. (2019, Feb 20).

PGC_SCHE USM_2020_48

Comparing Different Data Reduction Techniques in the Development of Water Quality Index (WQI) Prediction Model

Danny Hartanto Djarum[1], Zainal Ahmad[1, *], Jie Zhang[2]
[1]School of Chemical Engineering, Engineering Campus, Universiti Sains Malaysia, 14300 Nibong Tebal, Penang, Malaysia
[2]School of Engineering, Merz Court, Newcastle University, Newcastle upon Tyne NE1 7RU, United Kingdom.
E-mail: [*]chzahmad@usm.my

Abstract. Many studies have shown that dataset with high dimensionality could give negative influenced to the performance and efficiency of most machine learning models. Thus, in this paper, seven different type of data reduction techniques were analysed and compared in order to optimize the water quality index (WQI) prediction model developed based on Perak and Penang river data. These include principle component analysis (PCA), kernel principle component analysis (kPCA), sparse principle component analysis (sPCA), linear discriminant analysis (LDA), singular value decomposition (SVD), independent component analysis (ICA), and factor analysis (FA). The analysis was carried out in four stages, in which the machine learning models were trained with a reduced input data of 12, 9, 6 and 3 dimensions respectively. The performance of the prediction model was compared based on their R^2 values, root mean squared error (RMSE) values, and the cumulative variance after the data reduction techniques were performed. **Major Findings**. The result from the data reduction analysis shows that LDA techniques yielded the best performance for the prediction models. This could be observed as even by utilizing the lowest input data shape (3 dimensions), extra tree regression (ETR) model still able to score an R^2 values of 0.85. This is due to the fact that even with the lowest dimensions the reduced data could still represent 95% of cumulative variance found in the original dataset. sPCA on the other hand is the worst performing data reduction technique of all, with the best performing model could only score an R^2 values of 0.67. Factor analysis (FA) interestingly displayed no clear relationship between the number of input data shape and the performance of the prediction models, as model trained with 6 dimensions performed better than model trained with 9 dimensions. This could be because FA searches for hidden variables that can explain the original features instead of transforming the whole dataset. The rest of the data reduction techniques (PCA, kPCA, SVD, and ICA) seemed to yield very similar results with performance of the prediction models not far from each other.

Keywords: *Water quality index, data reduction techniques, linear discriminant analysis, sparse principle component analysis, factor analysis.*

INTRODUCTION

Water quality plays an important role in human's wellfare, especially river water that has a direct relationship with health risk. Daily activites such as drinking, food production, domestic consumption, or any other activities that utilizes water is highly dependent on its quality. Unfortunately, rapid urbanization and climate change has led to changing waste and storm water flow patterns and associated pollutant loadings which in turn has caused significant degradation in water quality [1]. Poor water quality can give rise to disease outbreak which can cause instability in the ecosystem that not only affects human but also wildlife and plants [2]. Thus, it is very important to conitnuously assess and monitor the quality of water in the river. However, water quality measurement requires various biological, physical and chemical parameters, whereby some of the parameters are difficult and time consuming to measure. This has led to numerous studies being carried out to develop water quality prediction models based on various machine learning techniques. The size of the dataset fed into the machine learning model are often so large that it can cause enormous strain in the prediction model. High dimensional data could negatively impact the efficiency of the machine learning model, as the computational time increases exponentially with the dimensionality [4]. Therefore, perfoming dimensionality reduction (DR) on the water quality dataset is extremely crucial in order to generate a representation of the original data with a much smaller input dimensions. DR can be performed through two main techniques, *feature projection* which convert the high dimensional data into a lower dimensions by performing combination of linear transformation in the original dataset, *feature selection* on the other hand filters the input parameters based on their correlation strength to the output feature. Jun et al. [3] proposed a decision tree based model to predict water quality index (WQI) in Klang river, Malaysia, utilizing different set of input parameters. Their studies concluded that NH_3-N, pH, and suspended solid (SS) are insignificant in the WQI prediction, since the model could still score an R^2 values above 0.75 when these paramerets are ommited from the input dataset. Mangai et al. [5] developed a biological oxygen demand (BOD) prediction model coupled with principle component analysis (PCA) and correlation-features selection (CFS). Their work shows the two dimensionality reduction techniques PCA and CFS did not compromised the

performance of the BOD prediction models. In this study, seven different type of projection based DR techniques were analyzed and compared in order to optimize the WQI prediction model, namely principle component analysis (PCA), kernel principle component analysis (kPCA), sparse principle component analysis (sPCA), linear discriminant analysis (LDA), singular value decomposition (SVD), independent component analysis (ICA), and factor analysis (FA).

MATERIAL AND METHODS

Data collection. The dataset utilized for this study were obtained from Malaysia's department of environment (DOE) for Penang and Perak states from 2014 to 2018. The initial unprocessed dataset has 21 different parameters with 2843 data points for each parameters. Since the location attributes is a non-numerical attribute, this may cause some difficulty when developing the prediction model as most machine learning algorithms prefer to work with numerical values. In order to resolve this issue, the location attribute is converted into numerical binary attribute per category (one-hot encoding) [6]. BOD and chemical oxygen demand (COD) are also dropped from the input parameters, since they are difficult and time consuming to measure. The dataset was then randomly distributed into 80% training set and 20% test set. **Handling missing values**. The degree of missing values in the WQI data is quite insignificant with 1.2% being the highest recorded. Nevertheless, median value substitution was still performed, in which the missing values are imputed by the median value of said parameter. **Feature scaling**. The WQI dataset consist of parameters with highly varying magnitudes, units, and scales. This could unfortunately lead to bias and inaccuracy in the prediction model, as most machine learning models tend to favour parameters with larger scales by giving them more training weight. Power transformer was selected to scale the WQI dataset since our previous work shows that it led to a better prediction performance compared to other scaling techniques. **Dimensionality reduction**. After the preliminary data cleaning and preprocessing, the WQI dataset still has a considerably large dimensions at 16 X 2843 which translates to 45,488 individual data points. This include the following parameters: dissolved oxygen, 2 location attributes, 3-time attributes, suspended solids, E-coli, turbidity, conductivity, NH_3-NL, Zn, Cl, Cr, pH, and Cd. Thus, seven different DR techniques were compared and analyse (PCA, kPCA, sPCA, LDA, SVD, ICA, and FA). The analysis was carried out in four stages, in which the machine learning models were trained with a reduced input dimensions of 12, 9, 6 and 3 for the first, second, third, and fourth stages respectively. The objective here is to maintain the prediction performance while utilizing significantly smaller input shape. **Prediction model**. Four different regression-based machine learning models were assessed here: Multiple linear regression (MLR), random forest regression (FR), extra-tree regression (ETR), and decision tree regression with AdaBoost (BTR) model. The performance of each of these models were assessed by using the R^2 values and root mean square error (RMSE) metrics.

RESULTS AND DISCUSSION

Initially, the WQI prediction were carried out without performing any dimensionality reduction techniques, thus utilizing the full original dataset. The performance of the four regression models were assessed by comparing the R^2 and RMSE values. Table 1 shows the scores of the prediction models, we could immediately observe that in general all four prediction models performed reasonably good, with R^2 values consistently above 0.80. The best model accuracy could be observed from both ETR and BTR models with an R^2 values 0.89, both of these models are ensemble variation of decision tree regression model. ETR utilizes bagging technique in which vast number of decision trees were generated and the final prediction is computed from the average prediction of all the trees. Although, very similar to random forest regression model, ETR utilizes random splitting point instead of searching for optimal splitting point each time, this made ETR a more efficient algorithms [7]. BTR on the other hand consecutively build series of regressors based on the weight of sample that was adjusted according to the past prediction errors. This simply means that sample with higher degree of errors will receive larger training weight in the next iterations and vice versa. This process is then repeated until the overall prediction errors has been significantly reduced [8], which explained the better performance shown in Table 1.

Table 1. Prediction performance for different regression models without DR techniques

WQI prediction models	R^2	RMSE
MLR	0.84	5.576
FR	0.87	5.053
ETR	0.89	4.632
BTR	0.89	4.688

Dimensionality reduction techniques were then performed to reduce the input dataset to 12, 9, 6, and 3 dimensions which respectively is around 75%, 56%, 38%, and 19% of the original 16 X 2843 data size. The objective here is to maintain the prediction accuracy while utilizing a much smaller input dimension. The results of the WQI prediction after utilizing dimensionality reduction techniques are shown in Table 2 below. It is important to note that for some

of dimensionality reduction techniques, the variance of the reduced data cannot be retrieved since the cumulative variance attributes were not available within the scikit-learn dependency utilized for this study.

Table 2. Prediction performance for different regression models with DR techniques

Dimensions	Var	MLR		FR		ETR		BTR	
		R^2	RMSE	R^2	RMSE	R^2	RMSE	R^2	RMSE
PCA									
12	0.97	0.81	6.004	0.82	5.708	0.86	5.151	0.87	4.921
9	0.87	0.75	6.923	0.80	6.116	0.82	5.780	0.83	5.672
6	0.71	0.75	6.872	0.80	6.208	0.82	5.856	0.82	5.819
3	0.51	0.75	6.925	0.78	6.425	0.79	6.323	0.77	6.570
kPCA									
12	-	0.81	6.008	0.84	5.448	0.88	4.838	0.86	5.087
9	-	0.75	6.967	0.82	6.204	0.82	5.821	0.82	5.779
6	-	0.75	6.905	0.79	6.383	0.82	5.847	0.82	5.873
3	-	0.75	6.933	0.77	6.663	0.79	6.333	0.75	6.876
sPCA									
12	-	0.09	13.157	0.57	9.008	0.65	8.198	0.58	8.908
9	-	0.10	13.059	0.59	8.799	0.67	7.935	0.65	8.108
6	-	0.11	13.02	0.58	8.902	0.61	8.598	0.57	8.995
3	-	0.16	12.62	0.43	10.341	0.42	10.473	0.27	11.742
LDA									
12	0.99	0.84	5.584	0.86	5.142	0.88	4.860	0.88	4.811
9	0.98	0.83	5.590	0.86	5.236	0.87	4.918	0.87	4.887
6	0.97	0.83	5.595	0.85	5.287	0.86	5.147	0.87	4.929
3	0.95	0.83	5.596	0.85	5.344	0.85	5.339	0.85	5.396
SVD									
12	0.97	0.81	6.003	0.85	5.394	0.86	5.125	0.87	5.045
9	0.87	0.75	6.926	0.80	6.224	0.83	5.736	0.84	5.543
6	0.71	0.75	6.873	0.79	6.317	0.82	5.873	0.83	5.767
3	0.51	0.75	6.923	0.78	6.445	0.79	6.299	0.76	6.612
ICA									
12	-	0.81	6.003	0.81	5.955	0.86	5.206	0.84	5.516
9	-	0.75	6.927	0.79	6.294	0.82	5.837	0.82	5.926
6	-	0.75	6.872	0.79	6.316	0.83	5.805	0.82	5.901
3	-	0.74	6.925	0.78	6.447	0.79	6.374	0.77	6.566
FA									
12	0.59	0.82	5.797	0.84	5.523	0.87	4.940	0.87	5.065
9	0.59	0.77	6.499	0.81	6.076	0.84	5.577	0.83	5.747
6	0.57	0.79	6.262	0.85	5.421	0.86	5.161	0.86	5.213
3	0.41	0.74	7.108	0.76	6.759	0.78	6.545	0.74	7.028

Table 2 shows that the overall model performance for the reduced dataset appeared to perform reasonably well for most of the DR techniques (except for sPCA). Even at the lowest input data size of (3 dimensions), all four of the machine learning models could still score an R^2 values above 0.70. Considering that at 3 dimensions, the input data now only accounts for approximately 18.75% the size of the original dataset, the performance achieved by the prediction models is reasonably good. The best model performance could be observed when LDA technique was utilized with the highest achievable R^2 values of 0.88 for both ETR and BTR prediction models with 12 input dimensions. Surprisingly, when LDA were used to transform the dataset to only 3 dimensions, BTR, FR, and ETR could still achieve an R^2 values of 0.85, which is far better than any of the other DR techniques. This could be due to LDA ability in conserving majority of the discriminatory power from the original dataset when projecting the data into lower dimensional space, which allow LDA to maintain as much variance as possible. From Table 2, it could be observed that even at the lowest dimensional level, LDA could still explain 95% of the variance in the original dataset. sPCA on the other hand is the worst performing dimensionality reduction techniques, it causes significant performance decrease in all four prediction models. MLR seems to be the most affected of all the prediction model when sPCA is performed with an R^2 value as low as 0.09. In theory, sPCA does not search for the linear combination of all the input variables but instead it searches for the linear combination that contain just a few input variables by introducing sparsity structures to the input variables. Thus, it works best when the input dimension is extremely large (i.e. >1000),

which explained why the WQI prediction model suffered as sPCA seems to have neglected and removed important information from the input data set when performing the linear transformation. Interestingly, FA displayed no visible relationships between the number of dimensions in the input shape versus the performance of the WQI prediction model. This could be immediately seen from the model that has only 6 input dimensions appeared to perform better compared to models that has 9 input dimensions with the best achievable R2 values at 0.86 compared to 0.84. The results also show that the cumulative variance of the resulting dimensions does not affect the performance of the prediction model. Even though the resulting variance seems much lower compared to other DR techniques, the performance achieved are still reasonable. The reason could be due to the fact that FA does not perform linear transformation on the original data set but instead search for hidden variables that best represent the original dataset. As for the rest of the DR techniques namely PCA, kPCA, SVD, and ICA, a very similar prediction performance could be observed.

CONCLUSIONS

In the beginning, it is stated that the objective for the dimensionality reduction techniques here is to achieve the lowest possible dimensions of data shape while maintaining the prediction model performance. The results from this study shows that this is indeed possible, as most of the WQI prediction models could still score an R^2 value above 0.70 when only trained with 3 input dimensions instead of the original 16. LDA was concluded to be the best dimensionality reduction techniques as it could score an R^2 values of up to 0.85 even when only trained with 3 input dimensions. The worst performing dimensionality reduction technique is sPCA with an R^2 values as low as 0.09. FA on the other hand unable to depicts any clear relationships between the size of the input dimensions and the model performance, but still generate a reasonably good model performance with R^2 values up to 0.78 for 3 input dimensions. The rest of the data reduction techniques (PCA, kPCA, SVD, and ICA) seemed to yield very similar results with performance of the prediction models not far from each other.

ACKNOWLEDGMENT

This work was supported by Universiti Sains Malaysia (USM), special gratitude to Department of Environmental (DOE) Malaysia for providing the water quality data for this study and Kementerian Pendidikan Malaysia (KPM) through Fundamental Research Grant Scheme (FRGS) grant number PJKIMIA/6071414.

REFERENCES

[1]. M. Astaraie-Imani, Z. Kapelan, G. Fu, D. Butler. Journal of Environmental Management. **112**, 1–9 (2012).
[2]. I. B. Imneisi, M. Aydin. Lybian Journal of Ecological & Environemntal Sciences and Technology. **1(2)**, 22-30 (2019).
[3]. J. Y. Ho, H. A. Afan, Amr H. El-Shafie, S. B. Koting, N. S. Mohd, W. Z. Jaafar, H. L. Sai, M. A. Malek, A. N. Ahmed, W. H. M. W. Mohtar, A. Elshorbagy, A. El-Shafie. Journal of Hydrology. **575**, 148–165 (2019).
[4]. J. Fan and R. Li. Proceedings of the international Congress of Mathematicians. (2006).
[5]. J. A. Mangai and B. B. Gulyani. International conference on Modelling, Simulation and Intelligent Computing. 255-263 (2020)
[6]. Y. Qu, H. Cai, K. Ren, W. Zhang, Y. Wu, Y. Wen, J. Wang. IEEE 16th International Conference on Data Mining. 1149-1154 (2016)
[7]. P. Geurts, D. Ernst, L. Wehenkel. Machine Learning. **63(1)**, 3-42 (2006)
[8]. H. Drucker. Proceedings of the 14th International Conference on Machine Learning. (1997).

PGC_SCHE USM_2020_50

Exploring transition metals (Mn, Fe, Ni, and Cu) promoted Co/Al_2O_3 catalyst for dry reforming of methane

Yeejie Wong[a,b], N. Fazila Khairudin[a], Yoshitada Morikawa[b,c,d], Abdul Rahman Mohamed[a,*]
[a]Low Carbon Economy (LCE) Research Group, School of Chemical Engineering, Universiti Sains Malaysia, Engineering Campus, 14300 Nibong Tebal, Pulau Pinang, Malaysia
[b]Department of Precision Engineering, Graduate School of Engineering, Osaka University, 2-1 Yamadaoka, Suita, Osaka 565-0871, Japan.
[c]Elements Strategy Initiative for Catalysts and Batteries (ESICB), Kyoto University, Goryo-Ohara, Nishikyo-ku, Kyoto 615-8245, Japan.
[d]Research Center for Ultra-Precision Science and Technology, Graduate School of Engineering, Osaka University, 2-1 Yamadaoka, Suita, Osaka 565-0871, Japan.
*E-mail: *chrahman@usm.my*

Abstract: The promoting effect of transition metals in heterogeneous catalysis is an important yet challenging issue. In this work, Co/Al_2O_3 catalyst with different transition metal additives (Mn, Fe, Ni, and Cu) were studied for dry reforming of methane (DRM). XRD analysis revealed that the Co/Al_2O_3 was of Co metal supported on α-Al_2O_3. The promoters (additional transition metals) were able to incorporate into the lattice of Co, forming bi-metallic system. Catalytic study revealed that the addition of Ni slightly improved the CH_4 conversion, while, the addition of Mn slightly improved both the CH_4 and CO_2 conversion. Meanwhile, catalyst containing Fe reduces the CH_4 and CO_2 conversion. In addition, catalyst containing Cu was deactivated. However, it is worth noting that the Fe promotion reduces the carbon deposition and mitigate the formation of graphitic carbon.
Keywords: *Carbon dioxide, cobalt, dry reforming, promoters*

INTRODUCTION

Catalytic dry reforming of methane (DRM) is a good approach for converting carbon dioxide (CO_2) and methane (CH_4) into valuable syngas (H_2 and CO).[1] This reaction has the potential to mitigate environmental pollution associated with GHG emissions and has attracted tremendous attention along with the growing world biogas production, providing an inexpensive source of readily mixed CH_4 and CO_2. In addition, the syngas produced from DRM has a lower H_2/CO ratio than that from methane steam reforming (SRM) and is thus preferentially used in Fischer-Tropsch synthesis to produce long-chain hydrocarbons.

To date, active transition metals which are known to be capable of catalyzing DRM are mainly group VIII elements such as Ru, Rh, Ni, Co and Pt.[1] Precious metals such as Ru exhibit excellent performance but are scarce and expensive, shifting the research focus to alternative catalyst formulations based on earth-abundant 3d transition metals.[2] Among them, Ni was the most studied catalyst due to its low cost and availability.[3–5] Moreover, Co also shows a great potential as an alternative to Ni due to its great potential to suppress carbon deposition.[6] Nevertheless, issue of carbon deposition still persists, leading to catalytic deactivation and reactor plugging.

Recently, a popular approach to improve the performance and coke resistance of Co-based catalysts is by addition of other transition metals.[7,8] For instance, the bi-metallic CoNi system has been widely studied and the positive effects include reducing carbon deposition, increasing catalytic activity and stability.[9,10]

In our previous studies, Co/Al_2O_3 based catalysts were explored for DRM.[11,12] As inspired by the positive effect of promoters, the potential of transition metal close to the location of Co in the periodic table (Mn, Fe, Ni, and Cu) in promoting the catalytic performance of Co/Al_2O_3 was explored in this study. The structure characteristics and catalytic activity of transition element (Mn, Fe, Ni, and Cu) promoted Co/Al_2O_3 were established by a systematic comparison between the synthesized catalysts.

MATERIALS AND METHOD

Materials: $Co(NO_3)_2{\cdot}6H_2O$ (Merck, ≥99.0% purity), $Cu(NO_3)_2.3H_2O$ (Sigma-Aldrich, ≥99% purity), $Mn(NO_3)_2.4H_2O$ (Merck, ≥98.5% purity), $Fe(NO_3)_3.9H_2O$ (Merck, ≥99.0% purity), $Ni(NO_3)_2.6H_2O$ (Merck, ≥99.0% purity), citric acid (Merck, ≥99.5% purity). All chemicals were used as received without further purification.

Synthesis method: Co/Al_2O_3 catalyst was prepared using the above state metal precursors with the ratio of Co-to-Al (in mole) fixed at 3:97. The synthesized catalyst was denoted as Co3. In addition, a series of transition metal promoted Co/Al_2O_3 with fixed composition was synthesized. The metal contents in the catalysts were at the mole ratio of

3Co:1X:96Al, where X= Mn, Fe, Ni or Cu. The synthesized catalysts were denoted as Co3Mn1, Co3Fe1, Co3Ni1, and Co3Cu1.

All the catalysts were synthesized using sol-gel method. The molar ratio of total metal ions (Co, X, and Al ions) to citric acid was 1:2. Deionized water was added to the mixture and stirred continuously until all precursor compounds were dissolved. The solution was then aged for 1 h before heating at 90°C to form a xerogel. The obtained gel was then dried in the oven at 90°C for two days. The dried gel was then heated in the furnace at a heating rate of 10°Cmin^{-1} to 500°C and calcined at this temperature for 3 h before cooling to room temperature. Finally, the product was ground into powder form. The synthesized catalysts were treated at 1000°C under H2 gas flowing at 20 mLmin^{-1} for 3 h before being characterized and then used in DRM.

Catalyst characterization: X-ray diffraction (XRD) analysis was performed using a Bruker D8 ADVANCE X-ray diffractometer equipped with a Cu Kα radiation source operated at 40 kV and 40 mA. Samples were scanned over the diffraction range of $20° \leq 2\theta \leq 90°$ at a scanning rate of 0.015°s^{-1}. Carbon dioxide temperature-programmed desorption (CO_2-TPD) was conducted in a Micromeritic AutoChem II-2920. Firstly, 50 mg of catalyst was loaded in a U-shape quartz tube and reduced with pure H_2 at 300°C for 2 h. After cooling to 45°C, a pure CO_2 stream was introduced for adsorption for 1 h. After adsorption, the sample was flushed with He stream (10 mLmin^{-1}, 20 min) to remove weakly adsorbed CO_2. Finally, the sample was heated from room temperature to 900°C at a rate of 10 °Cmin^{-1}. The amount of CO_2 desorbed was recorded by a TCD. Thermogravimetric analysis (TGA) and differential thermal analysis were conducted on a TA Instrument SDT Q600. The furnace's temperature was increased at 10°Cmin^{-1} from room temperature to 900°C under purified air flowing at 100 cm^{3}min^{-1}.

Reactor setup: The experimental setup for DRM over transition metals doped Co/Al_2O_3 was discussed in our previous paper.[12] Experimental DRM was performed at 750°C, a pressure of 1 atm, a weight hour space velocity (WHSV) of 15 Lg^{-1}h^{-1}, a $CH_4/CO_2/N_2$ flow ratio of 2:2:1, and a time of 3 h using 100 mg of reduced catalysts. The performance of the catalysts was evaluated on the basis of CH_4 and CO_2 conversion.[12]

RESULTS AND DISCUSSION

The composition, structure, and crystallinity of catalysts after reduction treatment were analyzed using XRD and the diffraction patterns are shown in Figure 1. Sharp and distinct diffraction peaks of Co and α-Al_2O_3 were detectable in all the synthesized catalysts. The diffraction peaks of transition metal promoter (Mn, Ni, and Cu) were not distinguishable from the diffraction patterns, as they overlapped with Co (Figure 1 (b), (c), (e)).[13] Several literature studies reported that this synthesis method coupled with the XRD observations suggest the formation of bi-metallic (CoMn, CoNi, and CoCu) system.[14–16] The diffraction peak associated with Fe was detected for Co3Fe1 catalyst.[17] Meanwhile, the peaks position of Co of Co3Fe1 were shifted to lower diffraction angle, indicating the incorporation of Fe into Co lattice.

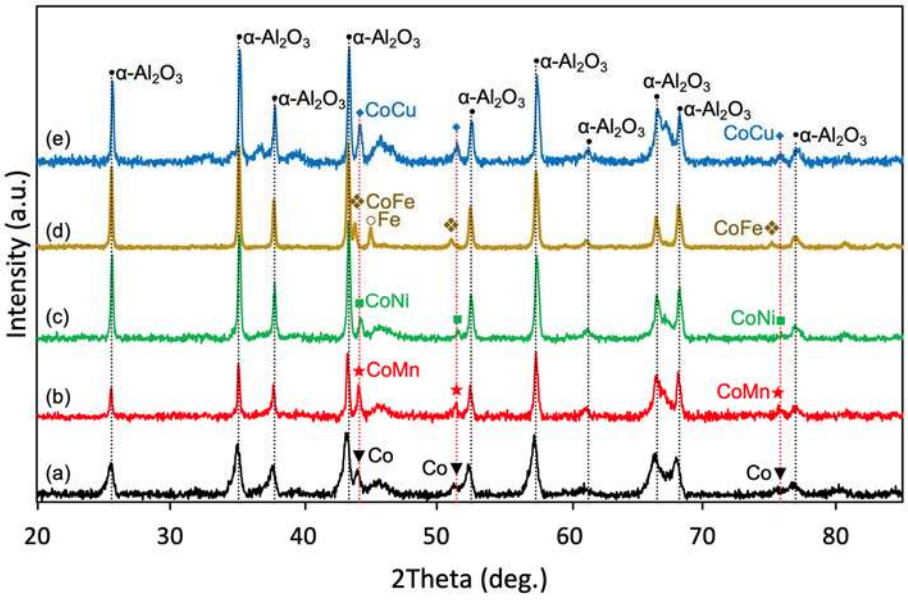

Figure 1: Powder XRD patterns of reduced (a) Co3 (b) Co3Mn1 (c) Co3Ni1 (d) Co3Fe1 (e) Co3Cu1

Figure 2 shows the CO_2 desorption profiles of all synthesized catalysts. Co3 showed a pronounced peak at 150°C, indicating the CO_2 desorption in the region of weak basicity and 3 peaks centered at around 250°C, 425°C, and 575°C, indicating the CO_2 desorption in the region of moderate-strong basicity.[18,19] The addition of transition metals (Mn, Fe, Ni, and Cu) does not significantly changes the overall basicity of Co3. However, as compared to Co3, the addition of Mn slightly increased the basicity as a broad peak started to emerge at the temperature region of >850°C. Meanwhile, the addition of Ni slightly decreased the basicity as the desorption peak which centered at 575°C for Co3 appeared at around 525°C for Co3Ni1. The addition of Fe also decreased the basicity as the height of the desorption peaks are reduced compared to that of Co3. The addition of Cu, on the other hand, reduced the height of desorption peak which centered at 575°C compared to that of Co3.

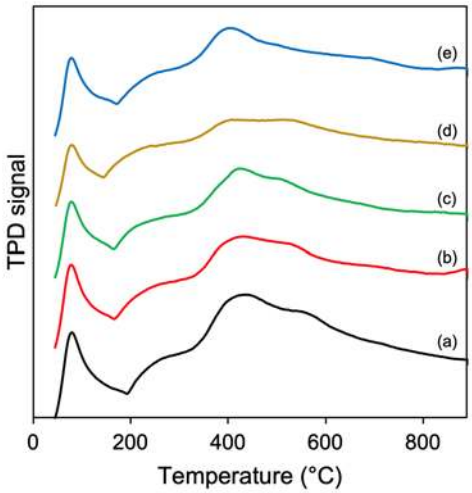

Figure 2: CO_2 TPD profile of reduced (a) Co3 (b) Co3Mn1 (c) Co3Ni1 (d) Co3Fe1 (e) Co3Cu1

Experimental reforming

The performance of Co/Al_2O_3 and the transition metal promoted catalysts for DRM was evaluated through CH_4 and CO_2 conversions and the results were summarized in Table 1. The average CH_4 and CO_2 conversion of Co3 was recorded at 83.87 and 86.32%, respectively. The addition of Mn and Ni promoters has a positive effect on the catalyst activity as compared to Co3. The addition of Mn slightly increased the CH_4 and CO_2 conversion to 85.23 and 88.14%, respectively. Meanwhile, the addition of Ni slightly increased to CH_4 conversion to 84.71%, however, changes in CO_2 conversion is negligible.

The addition of Fe, on the other hand, decreased the catalyst activity as compared to Co3. Co3Fe1 produced 55.66 and 67.53% of CH_4 and CO_2 conversion, respectively. The addition of Cu, however, greatly deactivated the catalyst where the CH_4 and CO_2 recorded were only 24.54 and 41.72%, respectively. In addition, catalyst with lower Fe addition, Co3Fe0.5 was tested and the CH_4 and CO_2 conversion recorded were 78.01 and 82.88%, respectively. Quantitatively, it is about 5.9 and 3.7% lower than the CH_4 and CO_2 conversion produced by Co3.

Table 1: Average CH_4 and CO_2 conversion of Co3, Co3Mn1, Co3Ni1, Co3Fe0.5, Co3Fe1, and Co3Cu1 in 3 h of reaction at 750°C, pressure of 1 atm, WHSV of 15 $Lg^{-1}h^{-1}$, and a $CH_4/CO_2/N_2$ flow ratio of 2:2:1.

Catalysts	CH_4 conv. (%)	CO_2 conv. (%)
Co3	83.87	86.32
Co3Mn1	85.23	88.14
Co3Ni1	84.71	86.23
Co3Fe0.5	78.01	82.88
Co3Fe1	55.66	67.53
Co3Cu1	24.54	41.72

TGA analysis was performed to determine the amount of carbon deposition on the spent catalysts and the results are shown in Figure 3. The carbon deposition for Co3Cu1 was not measured due to the inactivity of this catalyst in DRM. The weight loss below 400°C is attributed to the oxidation of amorphous carbon while the weight loss at around 500°C is attributed to the oxidation of graphitic carbon.[11] Meanwhile, the weight increment (Figure 3 (c), (d), and (e)) above 400°C is attributed to the oxidation of metals (Co and doped transition metals).

Analysis of Figure 3 revealed that the carbon deposited on Co3 was 0.85wt%. The addition of Mn increased the deposited carbon to 1.39wt%. The increase in carbon deposition by the addition of Mn is rationalized with the higher CH_4 and CO_2 conversion recorded by Co3Mn1 as compared to Co3. Meanwhile, the addition of Ni increased

the deposited carbon to a higher value of 1.56wt%, which can be rationalized with the higher CH_4 conversion but not CO_2 conversion recorded by Co3Ni1 as compared to Co3.

The addition of Fe, on the other hand, reduced the deposited carbon. The carbon deposited on Co3Fe1 was 0.39wt% while the carbon deposited on Co3Fe0.5 was 0.55wt%. The measured carbon deposition corresponds to their catalytic activity as recorded in Table 1, where the reduction in CH_4 and CO_2 conversion reduced the deposited carbon. In addition, it is worth noting that the TGA of Co3Fe1 and Co3Fe0.5 (Figure 3 (d) and (e)) showed no weight loss at around 500°C. This indicates that the carbon deposited on Fe promoted Co/Al_2O_3 was purely amorphous.

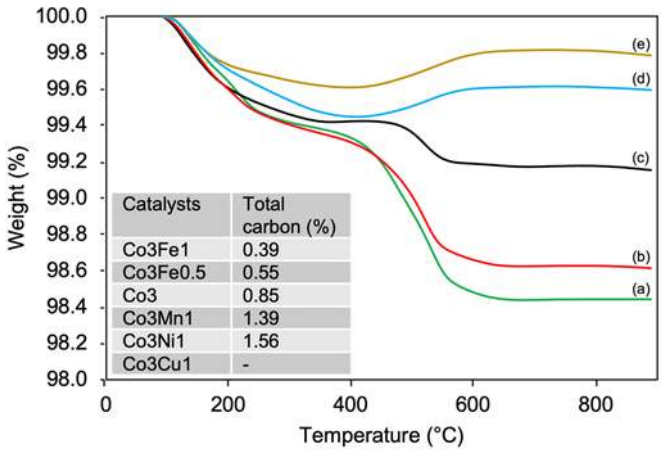

Figure 3: TGA of (a) Co3Ni1, (b) Co3Mn1, (c) Co3, (d) Co3Fe0.5, and (e) Co3Fe1 after 3 h of reaction at 750°C, pressure of 1 atm, WHSV of 15 $Lg^{-1}h^{-1}$, and a $CH_4/CO_2/N_2$ flow ratio of 2:2:1.

CONCLUSION

A series of transition metal (Mn, Fe, Ni, and Cu) promoted Co/Al_2O_3 (Co3) catalysts with fixed composition was synthesized and tested for dry reforming of methane. XRD analysis revealed that the Co3 was of Co metal supported on α-Al_2O_3. The promoters (additional transition metals) were able to incorporate into the lattice of Co, forming bi-metallic system. Meanwhile, CO_2-TPD analysis revealed that the basicity of Co3 were not significantly affected by promoters. As compared to the catalytic activity of pure Co3, the addition of Ni slightly improved the CH_4 conversion, while, the addition of Mn slightly improved both the CH_4 and CO_2 conversion. However, overall, the increment in activity was not significant. Moreover, the addition of Mn and Ni also increased the deposited carbon.

The addition of Fe, on the other hand, reduced the CH_4 and CO_2 conversion while the addition Cu deactivated the catalyst. Further study was conducted using catalyst with lower Fe content (Co3Fe0.5), where quantitatively, it produced 5.9 and 3.7% lower CH_4 and CO_2 conversion than that of Co3. However, it is worth noting that the Fe promotion reduces the carbon deposition and mitigate the formation of graphitic carbon. This present a possibility of preventing catalyst deactivation and reactor plugging caused by the formation of graphitic carbon during DRM.

ACKNOWLEDGEMENTS

The present study was supported by USM-NanoMITE under the Long-Term Research Grant Scheme (LRGS, 203/PJKIMIA/6720009) from the Ministry of Higher Education, Malaysia; Grants in Aid for Scientific Research on Innovative Areas "3D Active Site Science" (JP26105010) and a Grant-in-Aid for Scientific Research (B) (Grant No. 20H02569) from the Japan Society for the Promotion of Science (JSPS); the Elements Strategy Initiative for Catalysts and Batteries (ESICB) from the Ministry of Education, Culture, Sports, Science, and Technology, Japan (MEXT); and Osaka University's International Joint Promotion Program (Type B). We also gratefully acknowledge the financial support provided by USM fellowship and Marubun Research Promotion Foundation.

REFERENCES

(1) Pakhare, D.; Spivey, J. A Review of Dry (CO_2) Reforming of Methane over Noble Metal Catalysts. *Chem. Soc. Rev.* **2014**, *43*, 7813–7837.

(2) Jiang, C.; Akkullu, M. R.; Li, B.; Davila, J. C.; Janik, M. J.; Dooley, K. M. Rapid Screening of Ternary Rare-Earth – Transition Metal Catalysts for Dry Reforming of Methane and Characterization of Final Structures. *J. Catal.* **2019**, *377*, 332–342.

(3) Tang, Y.; Wei, Y.; Wang, Z.; Zhang, S.; Li, Y.; Nguyen, L.; Li, Y.; Zhou, Y.; Shen, W.; Tao, F. F.; et al. Synergy of Single-Atom Ni_1 and Ru_1 Sites on CeO_2 for Dry Reforming of CH_4. *J. Am. Chem. Soc.* **2019**, *141*,

7283–7293.

(4) Margossian, T.; Larmier, K.; Kim, S. M.; Krumeich, F.; Fedorov, A.; Chen, P.; Müller, C. R.; Copéret, C. Molecularly Tailored Nickel Precursor and Support Yield a Stable Methane Dry Reforming Catalyst with Superior Metal Utilization. *J. Am. Chem. Soc.* **2017**, *139*, 6919–6927.

(5) Kim, S. M.; Abdala, P. M.; Margossian, T.; Hosseini, D.; Foppa, L.; Armutlulu, A.; Van Beek, W.; Comas-Vives, A.; Copéret, C.; Müller, C. Cooperativity and Dynamics Increase the Performance of NiFe Dry Reforming Catalysts. *J. Am. Chem. Soc.* **2017**, *139*, 1937–1949.

(6) Li, D.; Lu, M.; Xu, S.; Chen, C.; Zhan, Y.; Jiang, L. Preparation of Supported Co Catalysts from Co–Mg–Al Layered Double Hydroxides for Carbon Dioxide Reforming of Methane. *Int. J. Hydrogen Energy* **2017**, *42*, 5063–5071.

(7) Park, J.-H.; Yeo, S.; HeO, I.; Chang, T.-S. Promotional Effect of Al Addition on the Co/ZrO_2 Catalyst for Dry Reforming of CH_4. *Appl. Catal. A Gen.* **2018**, *562*, 120–131.

(8) Park, J.-H.; Yeo, S.; Kang, T.-J.; Shin, H.-R.; Heo, I.; Chang, T.-S. Effect of Zn Promoter on Catalytic Activity and Stability of Co/ZrO_2 Catalyst for Dry Reforming of CH_4. *J. CO_2 Util.* **2018**, *23*, 10–19.

(9) Oliveira, A. C.; Viana, B. C.; Oliveira, A. C.; de Sousa, F. F.; Ayala, A. P.; Filho, J. M.; Junior, M. C. C.; de Sousa, H. S. A.; Barros, E. B. Nanostructured Ni-Containing Spinel Oxides for the Dry Reforming of Methane: Effect of the Presence of Cobalt and Nickel on the Deactivation Behaviour of Catalysts. *Int. J. Hydrogen Energy* **2011**, *37*, 3201–3212.

(10) Sengupta, S.; Deo, G. Modifying Alumina with CaO or MgO in Supported Ni and Ni–Co Catalysts and Its Effect on Dry Reforming of CH_4. *J. CO_2 Util.* **2015**, *10*, 67–77.

(11) Wong, Y. J.; Koh, M. K.; Khavarian, M.; Mohamed, A. R. Investigation on Cobalt Aluminate as an Oxygen Carrier Catalyst for Dry Reforming of Methane. *Int. J. Hydrogen Energy* **2017**, *42*, 28363–28376.

(12) Wong, Y. J.; Koh, M. K.; Khairudin, N. F.; Ichikawa, S.; Morikawa, Y.; Mohamed, A. R. Development of Co Supported on Co−Al Spinel Catalysts from Exsolution of Amorphous Co−Al Oxides for Carbon Dioxide Reforming of Methane. *ChemCatChem* **2019**, *11*, 5593–5605.

(13) Ishihara, A.; Andou, A.; Hashimoto, T.; Nasu, H. Steam Reforming of Ethanol Using Novel Carbon-Oxide Composite-Supported Ni, Co and Fe Catalysts. *Fuel Process. Technol.* **2020**, *197*, 106203.

(14) Claude, V.; Mahy, J. G.; Tilkin, R. G.; Lambert, S. D. Enhancement of the Catalytic Performances and Lifetime of $Ni/\gamma\text{-}Al_2O_3$ Catalysts for the Steam Toluene Reforming via the Combination of Dopants: Inspection of Cu, Co, Fe, Mn, and Mo Species Addition. *Mater. Today Chem.* **2020**, *15*, 100229.

(15) Chatla, A.; Ghouri, M. M.; El Hassan, O. W.; Mohamed, N.; Prakash, A. V.; Elbashir, N. O. An Experimental and First Principles DFT Investigation on the Effect of Cu Addition to Ni/Al_2O_3 Catalyst for the Dry Reforming of Methane. *Appl. Catal. A Gen.* **2020**, *602*, 117699.

(16) Zhao, L.; Han, T.; Wang, H.; Zhang, L.; Liu, Y. Ni-Co Alloy Catalyst from $LaNi_{1-x}Co_xO_3$ Perovskite Supported on Zirconia for Steam Reforming of Ethanol. *Appl. Catal. B Environ.* **2016**, *187*, 19–29.

(17) He, L.; Hu, S.; Yin, X.; Xu, J.; Han, H.; Li, H.; Ren, Q.; Su, S.; Wang, Y.; Xiang, J. Promoting Effects of Fe-Ni Alloy on Co-Production of H_2 and Carbon Nanotubes during Steam Reforming of Biomass Tar over $Ni\text{-}Fe/\alpha\text{-}Al_2O_3$. *Fuel* **2020**, *276*, 118116.

(18) Santos, R. C. R.; Braga, D. M. V.; Pinheiro, A. N.; Leite, E. R.; Freire, V. N.; Longhinotti, E.; Valentini, A. Role of Cu, Ni and Co Metals in the Acidic and Redox Properties of Mo Catalysts Supported on Al_2O_3 Spheres for Glycerol Conversion. *Catal. Sci. Technol.* **2016**, *6*, 4986–5002.

(19) Al-Fatesh, A. Suppression of Carbon Formation in CH_4 –CO_2 Reforming by Addition of Sr into Bimetallic $Ni–Co/\gamma\text{-}Al_2O_3$ Catalyst. *J. King Saud Univ. - Eng. Sci.* **2015**, *27*, 101–107.

PGC_SCHE USM_2020_51

Interface Interaction between g-C_3N_4 and Monolayer ZnO using First-Principles Calculations

Anis Natasha Shafawi,[1] Yoshitada Morikawa,[2] Abdul Rahman Mohamed[1,*]
[1]School of Chemical Engineering, Engineering Campus, Universiti Sains Malaysia, 14300 Nibong Tebal Penang, Malaysia
[2]Department of Precision Engineering, Graduate School of Engineering, Osaka University, 2-1 Yamadaoka, Suita, Osaka 565-0871, Japan
*E-mail: * chrahman@usm.my*

Abstract. g-C_3N_4 is known to be a good photocatalyst due to its moderate band gap energy (2.7 eV) with high thermal and chemical stability. To enhance the photocatalytic activity of pure g-C_3N_4, synthesis of a composite photocatalyst is a good approach to utilize higher portion of solar spectrum and improves separation of electron-hole pairs. Here, computational approach by using Density Functional Theory (DFT) may serve as the platform to understand the mechanism behind the improvement in the photocatalytic activity of the g-C_3N_4 upon coupling with another semiconductor. For the purpose of understanding the interfacial interaction between two semiconductors, composite made up of g-C_3N_4 and monolayer ZnO was constructed and compared with the previous studies. First-principles electronic structure calculations were performed by employing *STATE-Senri* code and the electronic properties of g-C_3N_4 and monolayer ZnO were compared before and after the construction of the composite. Hence, this computational study may provide insightful outlooks underlying the improved photocatalytic activity of g-C_3N_4 and other semiconductor materials upon the synthesis of a composite photocatalyst.
Keywords: *g-C_3N_4, monolayer ZnO, Density Functional Theory.*

INTRODUCTION

Due to the recalcitrance of organic pollutants against natural degradation in water, an effective wastewater treatment is required to break down the complex structure of organic pollutants, such as azo dyes. Compared to other conventional wastewater treatments, photocatalysis reaction is more favored as it may employs the use of renewable energy which is sunlight and is known for its ability to bring an almost total mineralization of organic pollutants in water. Recently, graphitic carbon nitride (g-C_3N_4) became an interest photocatalyst among other semiconductors due to its moderate band gap energy (2.7 eV) hence is able to absorb both UV and visible light portion, and has high reductive potential (~1.13 eV), hence is able to reduce oxygen into superoxide radical ($O_2^{\bullet-}$). Coupling of g-C_3N_4 with another semiconductor having suitable band edges position and moderate band gap energy would improve the performance of pure g-C_3N_4 as it may enlarge the absorption of light in the UV-vis light region and reduce the recombination of photo-generated charge carriers. Monolayer ZnO, one of the most established photocatalysts, is a suitable candidate to be coupled with g-C_3N_4 due to their matched band alignments [1]. For the purpose of understanding the interfacial interaction between two semiconductors, composite made up of g-C_3N_4 and monolayer ZnO was constructed and compared with the previous studies. The interface study between these two semiconductors were already studied extensively from experimental works, and it was proposed that the photo-generated charge carriers may follow either type-II or Z-scheme mechanism [2-5]. However, the mechanism of interfacial charge transfer upon coupling of two semiconductors are still unknown. Here, computational studies by using Density Functional Theory (DFT) may provide the fundamental understanding underlying the synergism effect of the interface between g-C_3N_4 and monolayer ZnO. The first-principles calculations were performed by using *STATE-Senri* code and the electronic properties of both g-C_3N_4 and monolayer ZnO were compared to propose the interfacial charge transfer upon coupling of these two materials. Hence, this computational study may provide insightful outlooks underlying the improved photocatalytic activity of g-C_3N_4 and other semiconductor materials upon the synthesis of a composite photocatalyst.

MATERIALS AND METHODS

The first-principles calculations were based on DFT implemented in the *STATE-Senri* code. The standard GGA Perdew-Burke-Ernzerhof (GGA-PBE) exchange correlation functional was used for the DFT calculations. Here, the energy cutoffs of the plane wave basis sets are 36 Ry and 400 Ry for the wave function and charge density, respectively. For the optimization, 6 × 6 × 6 K-point and 12 × 12 × 12 K-point were adopted for the primitive g-C_3N_4 and monolayer ZnO, respectively. Periodic boundary condition with large vacuum of 15 Å was introduced to minimize the interaction between neighboring slabs. In this study, vdW interactions proposed by Grimme (DFT-D2) was included to describe the weak

interaction between g-C_3N_4 and monolayer ZnO. For the interface study, 2 × 2-unit cell of triazine unit for g-C_3N_4 and 3 × 3 supercell of monolayer ZnO were constructed with small lattice mismatched of less than 4 % [1].

RESULTS AND DISCUSSION

The optimized lattice of triazine unit g-C_3N_4 and monolayer ZnO were calculated to be 4.784 Å and 3.285 Å, respectively, where these lattices are comparable with previous experimental and computational works with discrepancy of less than 1 % [1-3]. The optimized geometrical structures are shown in Figure 1a (primitive triazine unit of g-C_3N_4) and FIGURE 1b (repeated structure of 1x1 monolayer ZnO).

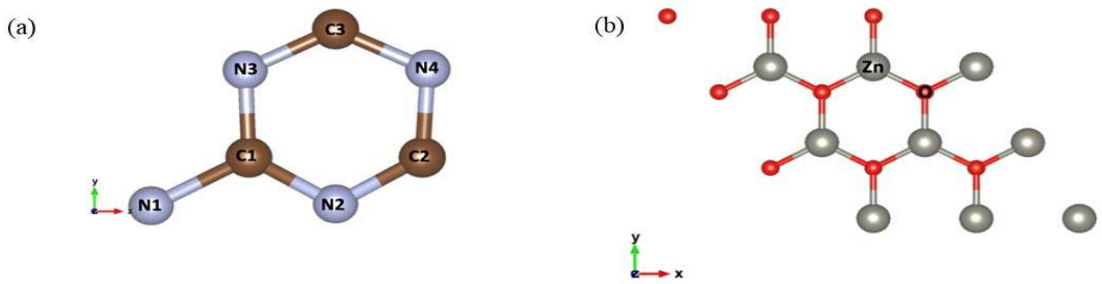

Figure 1. Optimized geometrical structures of **(**a) primitive triazine unit of g-C_3N_4 and **(**b) repeated structure of 1x1 monolayer ZnO.

The electronic properties based on the Partial Density of States (PDOS) are shown In Figure 2a (g-C_3N_4) and Figure 2b (monolayer ZnO). Here, the results are comparable with previous study where Conduction Band Minimum (CBM) of g-C_3N_4 are dominated by both C 2p and N 2p orbitals, while the Valence Band Maximum (VBM) of monolayer ZnO are contributed by O 2p and Zn 3d orbitals [1].

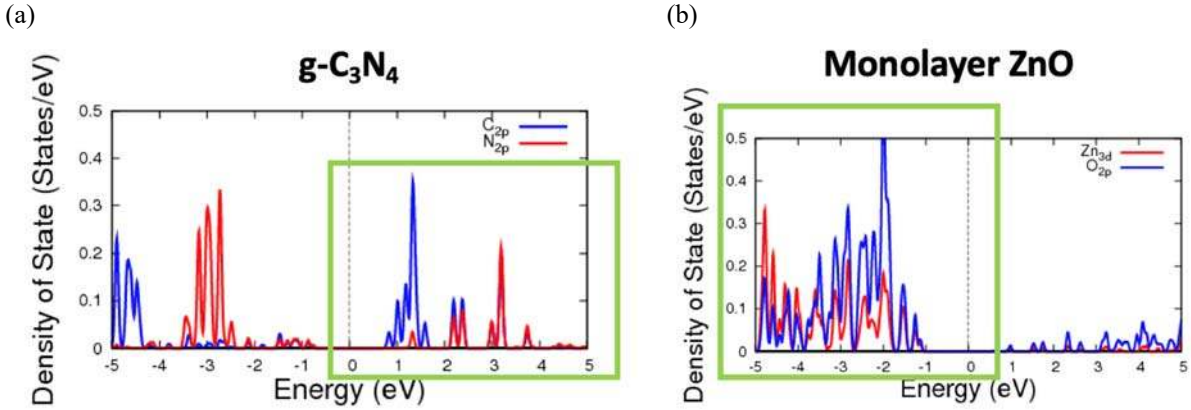

Figure 2. PDOS analysis of **(**a) g-C_3N_4 and **(**b) monolayer ZnO.

The band gap energies and work functions of both materials were also calculated to evaluate their electronic properties. In this calculation, the band gap of g-C_3N_4 and monolayer ZnO were calculated to be 1.60 eV and 1.73 eV, respectively. In comparison with previous theoretical studies, the calculated band gap energies of these materials are literally smaller because GGA-PBE functional are known for their underestimation in the band gap energy calculation for semiconductor materials [4-7]. Meanwhile, the work functions of g-C_3N_4 and monolayer ZnO were calculated to be 4.52 and 5.28 eV, which are almost similar with previous theoretical studies [4-7]. Generally, work function shows how much energy is required to remove an electron from the surface to infinity, hence showing that g-C_3N_4 needs smaller energy to remove an electron from its system. Thus, upon in contact, the electrons will be probably transferred from g-C_3N_4 to monolayer ZnO to make the fermi level becomes equilibrium. This hypothesis can be strengthened by plotting the charge density difference upon coupling of g-C_3N_4 and monolayer ZnO [1]. For the interfacial interaction between g-C_3N_4 to monolayer ZnO, the vertical separation was fixed to be 1.88 Å between g-C_3N_4 to monolayer ZnO. Two configurations were proposed, which is shown in Figure 3. Similar results with previous study was obtained, where configuration 1 achieved higher stability upon interface interaction due to smaller total energy [1]. Here, it is proposed that configuration 1 has higher stability as N atom is near to Zn atom, while C atom is near O atom, where they have opposite charge hence would have stronger interaction. Configuration 1 was then used for further calculation to get the binding energy.

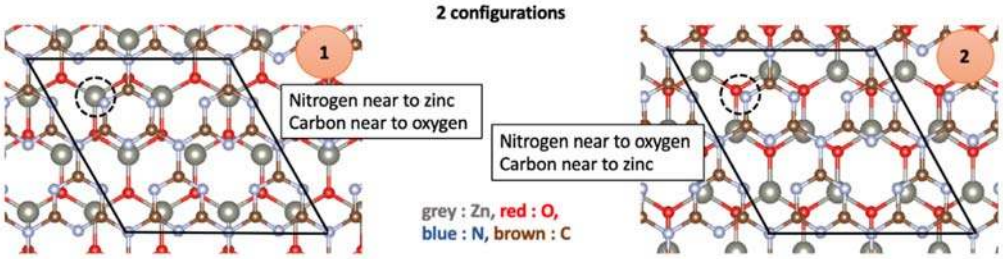

Figure 3. Two proposed configurations which are configuration 1 (left) and configuration 2 (right)

The binding energy of the optimized lattice upon coupling (9.50 Å) was calculated by using this equation:

$$\mathbf{E}_b = \mathbf{E}g\text{-}C_3N_4/g\text{-}ZnO - \mathbf{E}g\text{-}C_3N_4 - \mathbf{E}g\text{-}ZnO$$

where E_b is the binding energy, $\mathbf{E}g\text{-}C_3N_4/g\text{-}ZnO$ is the energy of the composite, and $\mathbf{E}g\text{-}C_3N_4$ and $\mathbf{E}g$-ZnO are the energies of the respective isolated materials. Here, the binding energy of the composite was calculated to be -28.24 meV/Å^2, which is considered as the typical vdW interaction between two materials [8-9]. However, compared to the previous study, the binding energy was calculated to be stronger with value -67 meV/Å^2 [1]. In their study, the authors concluded that they have stronger binding energy due to the formation of buckling between g-C_3N_4 and monolayer ZnO. Although buckle g-C_3N4 and monolayer ZnO were also produced upon coupling, the buckling distance (height) of isolated materials from previous study (reference) are larger than our optimized g-C_3N_4 and monolayer ZnO, which is shown in Figure 4. Hence, it is suggested to construct a corrugated (buckle) g-C_3N_4 by introducing molecular dynamic at high temperature which probably will increase the binding energy between g-C_3N_4 and monolayer ZnO.

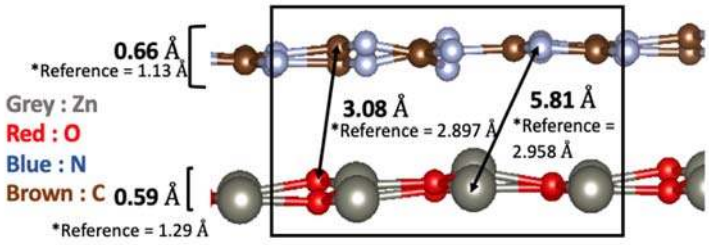

Figure 4. Interface interaction between g-C_3N_4 (top) and monolayer ZnO (bottom)

CONCLUSION

In conclusion, the geometrical structures and electronic properties were reproduced using *STATE-Senri* code. Additionally, it is expected that electrons from g-C_3N_4 will be transferred to monolayer ZnO upon in contact based on the work function calculations. Lastly, the binding energy predicted by this calculation shows that the interfacial interaction between g-C_3N_4 and monolayer ZnO possesses vdW interaction instead of chemical interaction.

ACKNOWLEDGEMENTS

Financial support provided by Japan Student Services Organization (JASSO) along Quantum Engineering Design Course (QEDC) attachment and USM-NanoMite under the Long-Term Research Grant Scheme (LRGS, 203/PJKIMIA/6720009) along master study are highly appreciated.

REFERENCES

[1] J. Cui, S. Liang, S. Sun, X. Zheng, J. Zhang, Journal of Physics: Condensed Matter. **30**, 175001 (2018).
[2] C. Tusche, H.L. Meyerheim, J. Kirschner, J., Physical review letters. **99**, 026102 (2007).
[3] D.M. Teter, & R.J. Hemley, Science. **271**, 53-55 (1996).
[4] J. Liu., B. Cheng, J. Yu, Physical Chemistry Chemical Physics**. 18**, 31175-31183 (2016).
[5] J. Liu, The Journal of Physical Chemistry C, **119**, 28417-28423 (2015).
[6] S.Y. Wakhare, M.D. Deshpande, Bulletin of Materials Science. **42**, 206 (2019).
[7] L. Chen, Y. Cui, Z. Xiong, M. Zhou, Y. Gao, RSC advances. **9**, 21831-21843 (2019).
[8] T. Bjorkman, A. Gulans, A.V. Krasheninnikov, R.M. Nieminen, Physical review letters. **108**, 235502 (2012).
[9] Y. Lin, H. Shi, Z. Jiang, G. Wang, X. Zhang, H. Zhu, R. Zhang, C. Zhu, International Journal of Hydrogen Energy. **42**, 9903-9913 (2017).

PGC_SCHE USM_2020_52

A Theoretical Study by Density Functional Theory (DFT) on Interface Structure of Graphene/ZnO (001) Surface

Rabiatul Aliah Mahmud,[1] Abdul Rahman Mohamed,[1,*] Yoshitada Morikawa[2]
[1]School of Chemical Engineering, Engineering Campus, Universiti Sains Malaysia, 14300 Nibong Tebal Penang, Malaysia
[2]Department of Precision Engineering, Graduate School of Engineering, Osaka University, 2-1 Yamadaoka, Suita, Osaka 565-0871, Japan.
*E-mail: * chrahman@usm.my*

Abstract. Wastewater crisis has been worsening and pollution abatement should be taken seriously to reduce the pollutant content in the water stream. Advanced oxidation processes (AOPs) is known to be an effective method to overcome this raised issue and photocatalysis is the best option among all. This is due to the utilization of renewable energy by using semiconductor and at the same time mineralized the harmful pollutant into non-toxic CO_2 and H_2O. The experimental finding has exhibited an outstanding photodegradation results using graphene-based with ZnO composite, however the band gap energy of graphene-based remained unclear hence showing the importance of computational studies. The limitation of experimental analysis is due to the physical properties of graphene (dark colour) allowing it to absorb all wavelength of light and the band gap energy cannot be determined. Hence, computational study using Density Functional Theory (DFT) is needed to confirm the mechanism in photodegradation to study the interaction between low density oxygen functional group of graphene and ZnO in the composites. Here, the band alignment of each materials and composites can be investigated and provides better understanding in charge transfer. As for now, simulations of graphene/ZnO (001) surface have been reproduced by using *STATE-Senri* code and compared with previous computational calculations. Therefore, the lattice parameters, work function, electronic properties of graphene and ZnO polar surface and binding energy of graphene/ZnO are in a good agreement with reported literatures.
Keywords: *DFT, ZnO, graphene, charge transfer, work function*

INTRODUCTION

ZnO semiconductor is widely used in light emitting diode and the study of its structure-dependent electronic properties through experimental work and computational study can be considered as an established one. In the case of photocatalyst, ZnO is a n-type semiconductor and with its well-known high band gap energy, 3.2 eV, whereby the band gap energy of a semiconductor is typically a crucial preliminary study [1,2]. To date, graphene has been proposed as one of the rising materials in photocatalytic activity, but graphene alone is a weak photocatalyst [2]. Based on the theoretical findings, it has been proven that graphene has metallic properties where its half-filled electron band touches the fermi level producing gapless energy [3,4]. Thus, heterojunction of graphene with other semiconductors does enhance the photocatalytic process. Graphene has a great property in the adsorption capability because of its high surface area and relatively gives a high impact in the photocatalysis [5]. The formation graphene/ZnO semiconductor is lacking in providing information on interfacial binding energy and its charge transfer, hence making computational studies in demand. Therefore, we have simulated graphene, ZnO polar surfaces and graphene/ZnO.

MATERIALS AND METHODS

The calculation of individual graphene, bulk ZnO, polar surfaces of ZnO and graphene/ZnO is carried out by using *STATE-Senri* package which is based on plane waves and pseudopotential. The well-known GGA Perdew-Burke-Ernzerhof (GGA-PBE) exchange-correlation functional is used for density functional theory calculations. Vanderbilt's ultrasoft pseudopotentials are used to describe the electron-ion interaction. The energy cutoffs of the plane wave basis sets are 36 Ry and 400 Ry for wave function density, respectively. The models of specific materials are 4 x 4 graphene and 3 x 3 of 3 bilayer ZnO of (001) surface with the lattice mismatch of only 0.7%. The lateral size of the interface models adopted the lattice of ZnO. The dangling bond at the bottom layer of polar ZnO surface are saturated with artificial hydrogen with charge of 0.5 for Zn-terminated, similar to previous studies. The vacuum layer of interface is set to be 50 Bohr. There are three different graphene/ZnO configurations that has been studied in this work where CH, CZ and CO. Besides that, DFT-D2 by Grimme was adopted to describe the long-range interaction (van der Waals).

RESULTS AND DISCUSSION

The results and discussion comprised of lattice constant, binding energy, density of states, and work function for graphene, ZnO and graphene/ZnO structure. The computed lattice constants for graphene and ZnO was compared with experimental values and tabulated in Table 1. Hence, it can describe the discrepancies between computational data and experimental values. Experimentally, lattice constant of graphene is 2.46 A, whereas the calculated lattice constant is 2.47 A with only 0.4% discrepancy. Similarly, wurtzite ZnO was reported with lattice constant of a = b = 3.25 A and c = 5.20 A, while computed lattice constant of ZnO is a = b = 3.27 A and c = 5.28 A with discrepancy 0.61% and 1.52% of lattice a and c, respectively. The calculated band gap energy from this work was obtained with value of 0.74 eV, which is likely to be similar to the previous computational study. However, the band gap energy for ZnO based on experimental work is larger with 3.2 eV [1,6,7]. This is due to the well-known GGA-PBE functional that underestimate the energy of Zn 3d orbital, hence giving out smaller gap energy of ZnO [6].

Table 1. Lattice constants of graphene and ZnO.

Lattice constant	Graphene		ZnO	
	This work	Experimental	This work	Experimental
a (A)	2.47	2.46	3.27	3.25
c (A)	-	-	5.28	5.20
Discrepancy a (%)	0.4	-	0.61	-
Discrepancy c (%)	-	-	1.52	-
Band gap (eV)	-	-	0.74	0.73

Three different configurations of graphene/Zn-terminated ZnO has been computed to determine the most stable configuration with the lowest total energy [6,7]. There are CH, CZ and CO that specifies 1 carbon atom on top of hollow ZnO ring, 1 carbon atom on top Zn atom and 1 carbon atom on top of oxygen atom, respectively (Figure 1).

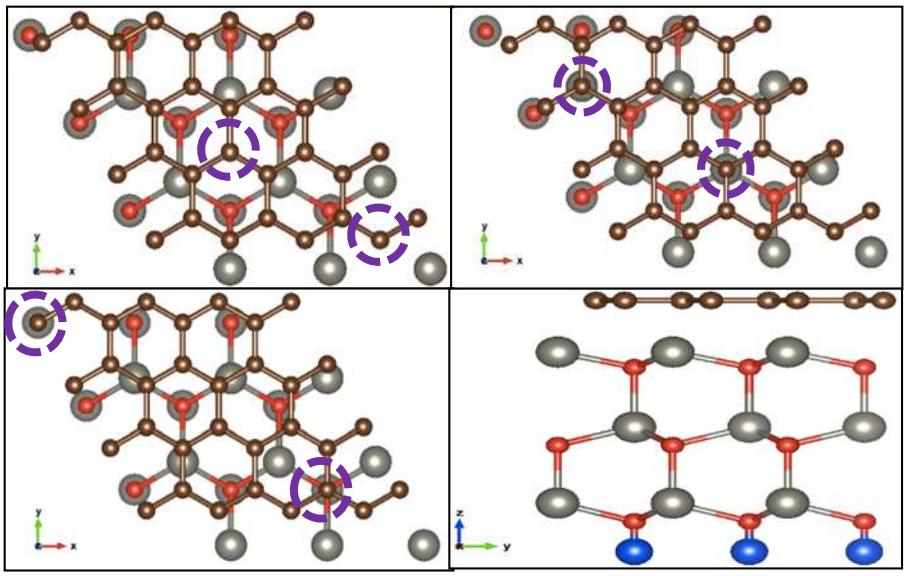

Figure 1. Three different configurations of graphene/ZnO: (a) CH (b) CZ, (c) CO and (d) front view all model.

The interfacial distance between graphene and ZnO was first computed by using CH model and obtained its equilibrium distance, which then were used for calculating other configurations (CZ and CO). Thus, the equilibrium distance obtained is 2.69A, that can be confirmed as the vdW interaction (Figure 2). It can be concluded that the total energy is likely to be similar even though by using different configurations of graphene/Zn-terminated ZnO interfacial study [6,7]. In addition, DOS was plotted to determine the electronic properties of each materials and illustrated in Figure 3. For materials consisting of graphene, ZnO and graphene/Zn-terminated ZnO are all showing metallic behavior with no band gap energy. Basically, graphene has no gap energy due to its massless Dirac point, while ZnO polar surface is known to exhibits metallic properties [6-8]. ZnO polar surface in real has high stability due to the surface reconstruction or introduction of defects [9]. However, the calculations that was conducted has ignored this parameter.

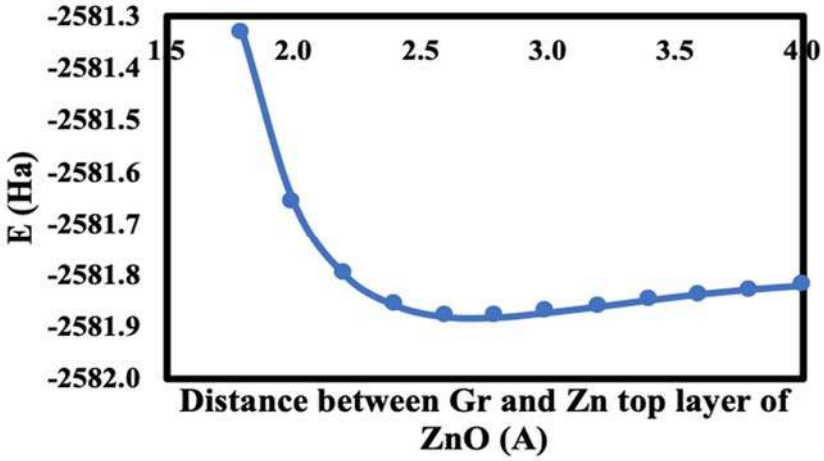

Figure 2. Interfacial distance of graphene and ZnO.

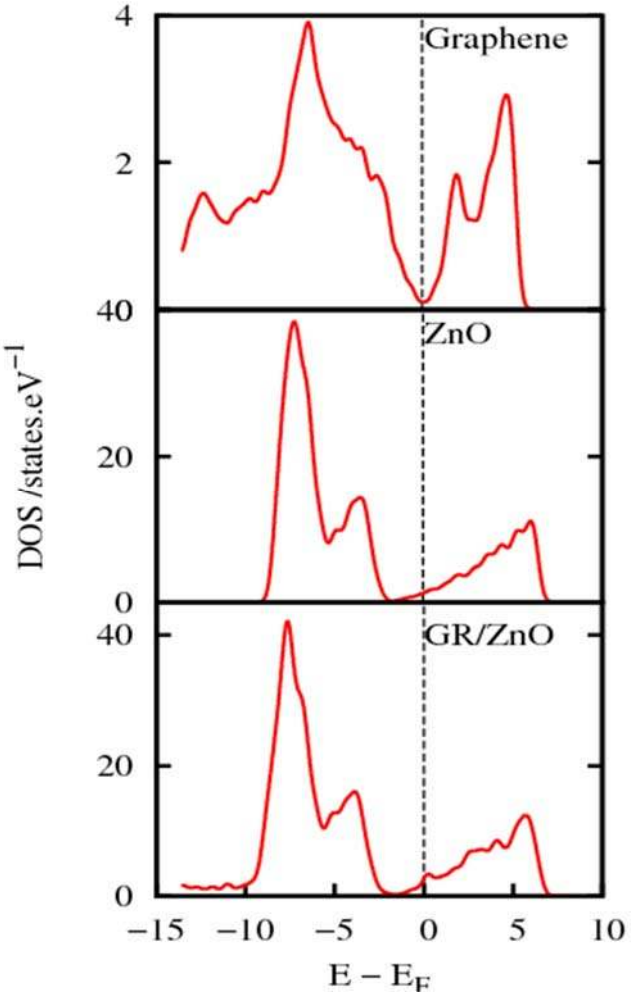

Figure 3. DOS profile of clean graphene, ZnO and graphene/ZnO.

Work function is the energy required for an electron to be extracted from the system. Therefore, it is important to investigate work function in order to enlighten on the charge transfer between graphene and ZnO. For the work function calculation of ZnO, the dipole correction (ESM) is included to eliminate the artificial electrostatic field between periodic supercells. The effect of bilayers number of ZnO on work function is calculated and the data has been summarized in Table 2. Here, the work function is reduced as the number of bilayers increases, similarly with the previous study [11]. On the other hand, work function of graphene was calculated with 4.26 eV, hence showing that the charge is transfer from ZnO to graphene.

Table 2. The calculated work function with different number of bilayers

Bilayer	Work function (eV)
3	3.412
4	3.371
5	3.323
6	3.316

CONCLUSION

Firstly, we have demonstrated an overview on the formation of graphene/ZnO interface, where the vdW forces between graphene and ZnO ensure a close but non-destructive contact. Secondly, the charge transfer was evaluated based on the work function which proven that the pathway of charge is from ZnO to graphene. Lastly, computational studies using *STATE-Senri* is in a good agreement with previous computational works.

ACKNOWLEDGEMENTS

Financial support provided by USM-NanoMite under the Long-Term Research Grant Scheme (LRGS, 203/PJKIMIA/6720009) and Japan Student Services Organization (JASSO) are really appreciated.

REFERENCES

[1] K. Dai, L. Lu, C. Liang, J. Dai, G. Zhu, Z. Liu, Q. Liu, Y. Zhang, Materials Chemistry and Physics, **143**, 1410-1416 (2014).
[2] T. Xu, L. Zhang, H. Cheng, Y. Zhu, Applied Catalysis B: Environmental, **101**, 382-387 (2011).
[3] C. A. Celaya, C. Delesma, P. J. V. Pelayo, O. A. J. Quintero, C. O. C. Araiza, L. Ramos, P. J. Sebastian, J. Muniz, Fuel, **271**, 117616 (2020).
[4] C. N. Peter, W. W. Anku, S. K. Shukla, P. P. Govander, Theoretical Chemistry Accounts, **137**, 75 (2018).
[5] S. Conejeros, N. L. Allan, F. Claeyssens, J. N. Hart, Nanoscale Advances, **1**, 1924-1935 (2019).
[6] P. Xu, Q. Tang, Z. Zhao, Nanotechnology, **24**, 305401 (2013).
[7] F. Nasehnia, S. M. Lima, M. Seifi, E. Mehran, Computational Materials Science, **114**, 112-120 (2016).
[8] W. Geng, X. Zhao, H. Liu, X. Yao, Journal of Physical Chemistry C, **117**, 10536-10544 (2013).
[9] J. M. Carlsson, Computational Material Science, **22**, 24 (2001).
[10] A. Ghosh, P. Guha, R. Thapa, S. Selvaraj, M. Kumar, B. Rakshit, T. Dash, R. Bar, S. K. Ray, P. V. Satyam, Nanotechnology, **27**, 125701 (2016).

PGC_SCHE USM_2020_53

Review of Feedwater Treatments for Steam Boilers at Palm Oil Factory in Perak

Muhammad Rufaizal Izham Rusdi, Zainal Ahmad*
School of Chemical Engineering, Engineering Campus, Universiti Sains Malaysia,
14300 Nibong Tebal, Pulau Pinang, Malaysia.
*E-mail: *chzainal@usm.my*

Abstract. Steam boilers commonly used in oil palm mills are intended to produce steam for process use in the factory. The steam was produced through the process of heat transfer from the combustion of fuel in the furnace that directly heating the water. Heating water in the boiler physically transforms the water into steam and at the same time will produce solid waste such as potassium, calcium, magnesium, silica and ions that remain in the boiler which consequently will coat the tubes and boilers. This solid coat increases the heating surface of the boiler and resulting in reducing the heat transfer efficiency. This condition will also increase fuel consumption which will cause overheating in the boiler that leads to tube failure. Despite having to incur high costs for tube repairs, this problem will lead to the losses of oil palm plantation due to having unscheduled plant shut down. To avoid this problem, water quality should always be maintained and monitored according to parameters.
Keywords: *Feedwater, steam boilers, palm oil*

INTRODUCTION

The history of early development of boilers, water treatment is not so much causing problems because the temperature and pressure are very low so that layers of scale and rust will not form so much if the boiler is cleaned and blow down is done through a blow down valve. Usually, the installation of zinc plates or the use of alkaline chemicals done to reduce corrosion in the boiler. Many tests have been performed to try to determine the cause and possibility of protection from corrosion in boilers using distilled water, various chemicals, and use of metals. One way is to add silver nitrate into feed water samples to detect contamination by seawater. The use of lime for alkalinity control was mentioned as early as 1900 and was used by French and British Navies until around 1935. In modern boilers, boiler feed water treatment is very critical because many problems can lead to the use of untreated water in extreme pressure and ambient temperature. This includes the lower efficiency in terms of heat transfer, overheating, damage, and highly cleaning cost. Water has a higher thermal capacity than most materials. This quality makes it a raw material ideal for boiler operation. Boilers are part of the system closed compared to open systems in gas turbines. Closed system used is the Rankine cycle. This means that the water is turned on throughout the system and never come into contact with the atmosphere. The water was reused, and it need to be treated to continue operated efficiently. Boiler water must be treated to be proficient in producing steam. Boiler water treated to prevent entrapment, corrosion, fertilization, and bleaching. Chemicals are introduced into the boiler water through a feed tank for store water in a chemical environment. These chemicals are mostly is an agent that removes oxygen and phosphate. Boiler operation as well including draining through a blow down valve to reduce total dissolved solids to increase boiler efficiency. The scale is a residue dissolved solid in the water formed and will stick to the shell and tubes that will reduce the heat transfer efficiency between water and heating surface. This condition increases the boiler temperature and the possibility of failure of tubes and boilers can occur. Erosion is caused by the oxygen content in the water. Oxygen causing the metal to oxidize which lowers the melting point of the metal. Thus, this present work was aimed to review to study parameters that need to be controlled such as pH follow by ASME Code for steam boilers at Palm Oil Factory in Perak.

PH RELATED METAL PROTECTIVE LAYER STABILITY

The stability of the passivating iron oxide layer is critically dependent on pH and temperature. Any contaminants in the system that cause the pH to decrease cause dissolution of the oxide layer and increased corrosion. Carbon dioxide (CO_2) is the primary cause of decreased condensate pH. Carbon dioxide enters the system with air leaking in condensate vacuum areas, in atmospheric condensate tanks or from decomposition of feedwater alkalinity. The latter should not be a problem in refinery and petrochemical industry using demineralized makeup water. Low pH causes a generalized loss of metal rather than the localized pitting caused by oxygen corrosion. Figure 1 shows a graph of pH boiler data in Palm Oil Factory at Perak. A total of 39 pH data boiler water of the oil palm factory has been taken since January 2017 until September 2019.

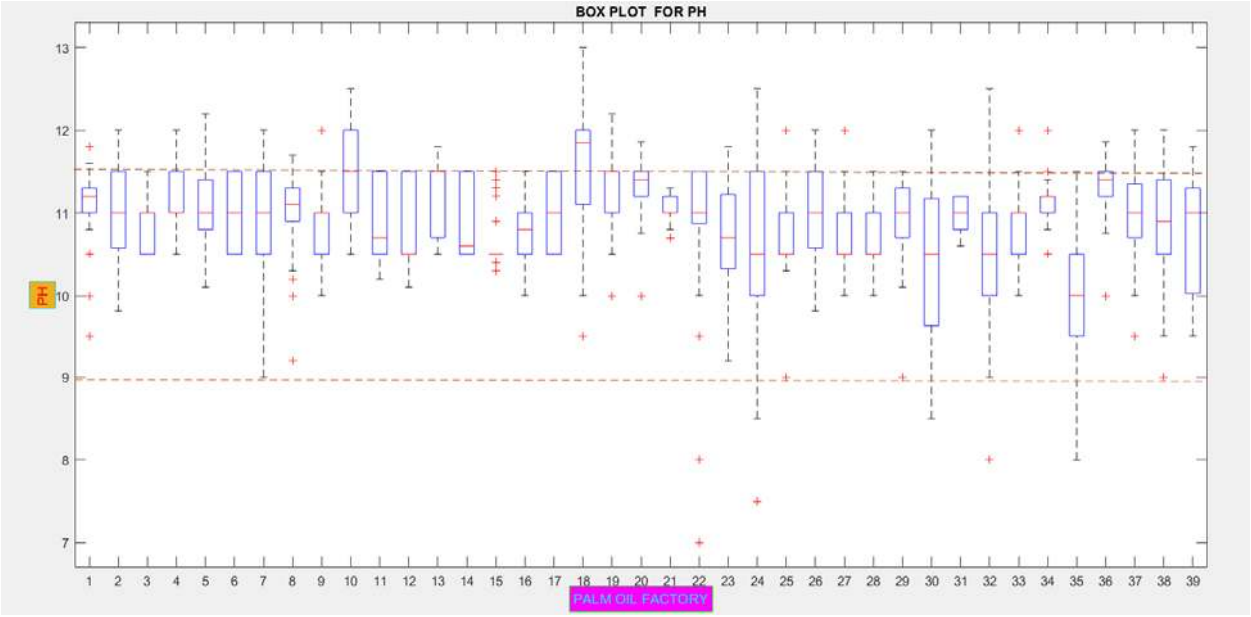

Figure 1. pH range for different Palm Oil Factory in Perak

From the graph shows the suggested parameter pH range is between 9 to 11.5 for water tube boiler based on ASME Guidelines. It is found that factories no. 10 and no. 18 exceed the set range of pH 12. Commonly, pH should not be less than 9 to avoid acidic conditions that can cause corrosion. At lower pH values hydrogen ions are discharged, whereas at values greater than 12 the magnetite layer thickens, peptizes to some extent, and is made porous by the diffusion of ions from the underlying metal. Above pH 14 the protective film is destroyed rapidly and may diffuse into the metal, blistering and weakening it severely.

CONCLUSION

The suggestions for feedwater pH are based on values that will protect the pre-boiler system from corrosion and consistent with the indicated pretreatment and internal boiler water treatment. Generally, pH for all boiler at Palm oil Factory in Perak are in range pH 9 -11.5.

REFERENCES

[1] ACT 139, Factory And Machinery Act 1967.
[2] Steam Boiler and Unfired Pressure Vessel Regulations of Factory And Machinery Act 1970
[3] Improvement of Steam Quality," A. L. Jacoby and W. H. Thompson, Seventh Annual Conference, Engineers' Society of Western Pennsylvania.
[4] Igberaharha, L.O., 1998. Zero Discharge Layout of Palm oil mill Effluent (POME). Research Project, Depart. Of Chemical Engineering University of Port Harcourt, pp: 1-5.
[5] Practical Boiler Water, Treatment Including Air Conditioning Systems Leo I. Pincus (McGraw-Hili Book Company)
[6] Journal Article Boiler Feed Water Purification Sheppard T. Powell and Harold Farmer Journal (American Water Works Association) Vol. 19, No. 1 (January, 1928), pp. 95-97
[7] The Chemical Treatment of Boiler Water, James W. McCoy. 12-66
[8] Consensus on Operating Practices for the Control of Feedwater and Boiler Water Chemistry in Modern Industrial Boiler

PGC_SCHE USM_2020_55

A Treatment of Hand-drawn Batik Effluent using Zwitterionic Adsorbent Coating: COD and Color (ADMI) Removal Approach

Syahida Farhan Azha, Suzylawati Ismail *
School of Chemical Engineering, Engineering Campus, Universiti Sains Malaysia,
14300 Nibong Tebal, Pulau Pinang, Malaysia.
*E-mail: *chsuzy@usm.my*

Abstract. A novel adsorbent-based coating with zwitterionic functionality (ZwitAd) was employed to study the removal performance of hand-drawn Batik effluent. The adsorbent was prepared as a coating and supported onto cotton cloth by application of a simple procedure which based on combined use of clay-based adsorbent, polymer-based binder and cationic polyelectrolyte. The Batik wastewater known to be high in COD and color intensity has undergone treatment processed using ZwitAd. Result shown a significant reduction of COD (147 mg/L), color (128 ADMI) and pH (7.34) based on Standard B of mixed effluent discharged limit. This has proved that ZwitAd is applicable to reduce the COD, colour intensity and stabilized the pH of water as well as low cost, simple treatment operation and lack of sludge generated.
Keywords: *Hand-drawn Batik Effluents, Zwitterionic Adsorbent Coating, Color Removal, COD, ADMI*

INTRODUCTION

Textiles industry in Malaysia featuring as a matured industry since country started an export-oriented industrial transformation since early of 1970s [1]. The textile industry has been a significant contributor to Malaysia's economy and was regarded as the backbone to be one of the active developing industry to the country. One of the best-known traditional textile industries in Malaysia including Southeast Asia region (Indonesia, Thailand) is the batik industry [2]–[4]. Batik production is expanding, been commercialized and it contributes positive economic growth to Malaysia [3]. Above 1000 batik factories are disseminated mainly throughout Kelantan and Terengganu on the East Coast of Malaysia, where it became a significant source of occupation and generated income for the local people.

Nevertheless, behind the positive, successful and growing progress of textile industries in Malaysia, it also acts as a double-edge sword. The ruinous is, development of the textile industries has left a large footprint to the environment. The sources of pollution significantly due to the discharged of large volume of water containing synthetic waste dyes, colour residues, catalytic chemicals (wax, sodium silicate as fixing agents), excess nutrients (nitrogen, phosphorus), organic matters (sodium, potassium, magnesium, calcium, copper, lead, nickel and zinc) [5], [6]. Throughout the production of batik, there are three major consecutive steps involved, ie., soaking, boiling and rinsing (Figure 1). Each of the step lead to their own contaminant and complexity of wastewater, resulting in higher pH, chemical oxygen demand (COD), biological oxygen demand (BOD), total dissolved solid (TDS) and suspended solid (TSS) [3], [4], [7]. The arising problem may threaten whole system include biota (flora and fauna), environment and the worst assuredly towards human health.

Therefore, this study was aimed to portray at different way of batik wastewater treatment using a novel approach of zwitterionic adsorbent coating or in short "ZwitAd". The ZwitAd is modifying the classical adsorption concept, which then transform in a form of coating layer with a simpler synthesis procedure and flexible working application. This new innovative solutions aimed at simultaneous increase of performances in terms of dyes removal and decrease of the energetic footprint by bringing to cost minimization in operation and secondary waste generated [8], [9].

MATERIALS AND METHODS

The wastewater samples were provided by a local batik manufacturer (Fauzi Batik, Ipoh, Malaysia). Sampling bottles were rinsed with samples before the collection was done. The samples were manually collected in a 30-L plastic container and preserved in the refrigerator at 4 °C in accordance with the standard method. The Batik effluent were collected from four main discharged points (as shown in Figure 1 at i, ii, iii, iv) in the batik process: soaking, boiling, and two rinsing steps. The physico-chemical characteristics of the wastewater were studied in terms of the pH value, COD and color (ADMI unit). The main characteristics of the wastewater are presented in Table 1. It exemplifies that the batik wastewater was a dark bluish-color wastewater with a high content of organic compounds.

The complete preparation method of ZwitAd can be referred in previous study [10], [11]. Briefly, ZwitAd is an adsorbent coating in a flat sheet layer which compounded with binder from acrylic polymer emulsion (APE) based, bentonite as additive and epichlorohydrin-dimethyl amine (EPIDMA) as surfactant. The mixture of these three components were then coated onto a (20 cm x 5 cm) cotton cloth which act as a support. The coated adsorbent was

then dried in oven at 80 °C and ready to undergo adsorption process to treat the Batik effluent (Figure 2). The physicochemical parameters such as COD, pH and color (ADMI) were analysed based on Standard Methods for the examination of wastewater before and after the treatment.

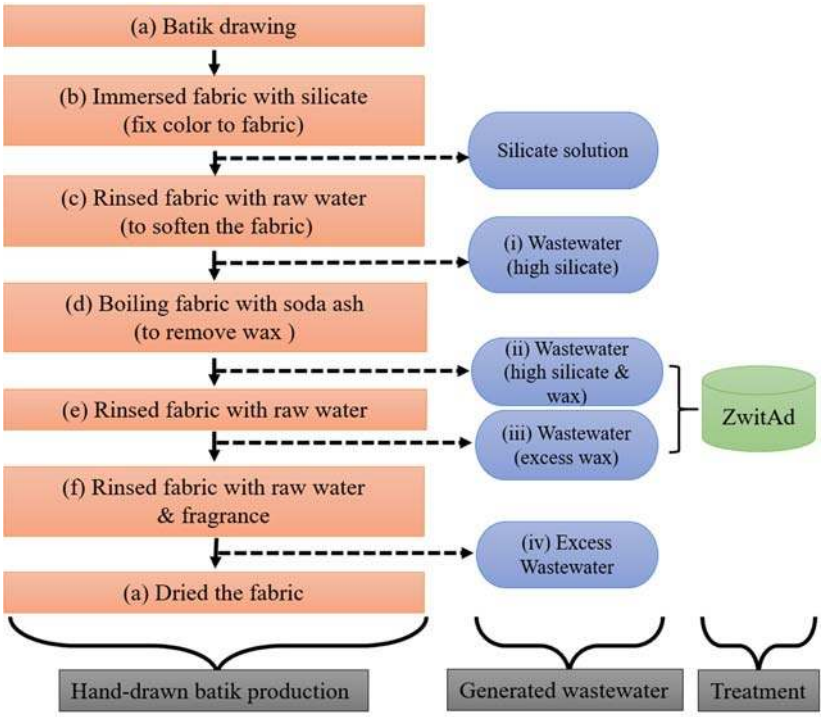

Figure 1 : Major consecutive steps involved in Batik production, the generated waste and suggested treatment using ZwitAd at two wastewater released points.

RESULTS AND DISCUSSION

Based on the schematic diagram shown in Figure 1, the focused treatment involved in this study were collected at point (ii) and (iii). At point (ii), wastewater is coming from a boiling pan where the fabric being boiled with a soda ash. This is one of the procedures to remove the wax that being painted on a fabric during the painting at a beginning of the process. The effluent contained high concentration of silicate and waxes. Besides, at point (ii), the wastewater was collected after the rinsing process of the fabric with the raw water. In this study, the wastewater at point (ii) and (iii) were mixed at 1:9 ratio before undergone adsorption using ZwitAd strip. The uv-Vis absorption spectra of mixed Batik wastewater showed absorption peak at 437 nm as in Figure 2. The pick appeared in visible region (437 nm) indicated the existence of chromophore that is responsible to impart colour to the batik effluent [12]. The value of COD concentration, pH and ADMI for each of the collected samples were shown in Table 1. The effluents of each step have different contents of COD, color and pH values. Each sample were compared with the acceptable conditions of mixed industrial effluent discharge according to Standard B. After the 1st treatment using one strip of ZwitAd, the value of COD reduced about 67.9 % and passed the allowable discharged limit. However, at first stage of adsorption process, the colour was not effectively removed (remaining color was found to be > 250 ADMI). Second stage of adsorption was carried out in order to obtain a value under allowable discharged limit especially for colour reduction. In second treatment, the value of COD, ADMI and pH has passed the standard limit by having 147 mg/L, 128 ADMI and pH 7.34, respectively.

The photographic image of ZwitAd strips were taken before and after the adsorption treatment. The original ZwitAd strips is characterized by white color, while ZwitAd strips appeared greenish after the Batik effluent has been adsorbed onto the strips (Figure 3 (a)). The colour pigment from Batik wastewater was equally distributed onto the ZwitAd surface and imparted the greenish colour. The complete decolorization of Batik Effluent can be analysed using Uv-Vis spectrum. The reduction in adsorption peak (λmax) at 437 nm of Batik effluent was shown in Figure 3 (b). The SEM-EDX test were performed to investigate the surface morphology of ZwitAd with low and high magnification, 100x and 2500x. The dried adsorbent coated onto a weaving linkage pattern with loosely spiral cellulose fiber of cotton cloth can be observed clearly from the images. At 2500x magnification, the single thread can be seen visibly and the coated adsorbent was covering well onto the cotton cloth. Looked into the SEM image after the adsorption process, the morphology of ZwitAd shown not much changes than before the treatment (Figure 4).

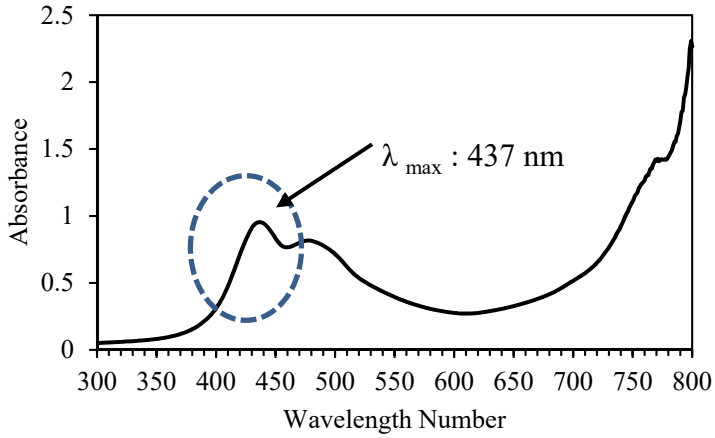

Figure 2: Uv-Vis absorption spectra of mixed Batik wastewater (absorption peak at 437 nm)

Table 1: Properties of Batik wastewater at point (i), (ii), and mix points, the Standard B discharge limit and result after treatments

Parameters	Point (i)	Point (ii)	Mixed point (i) & (ii) before treatment	Standard B discharged limit	Mixed point (i) & (ii) after 1st treatment	Mixed point (i) & (ii) after 2nd treatment
COD	2180	412	496	200	159	147
Color (ADMI)	16900	500	9800	200	258	128
pH	11.5	9.8	10.9	5.5-9.0	8.75	7.34

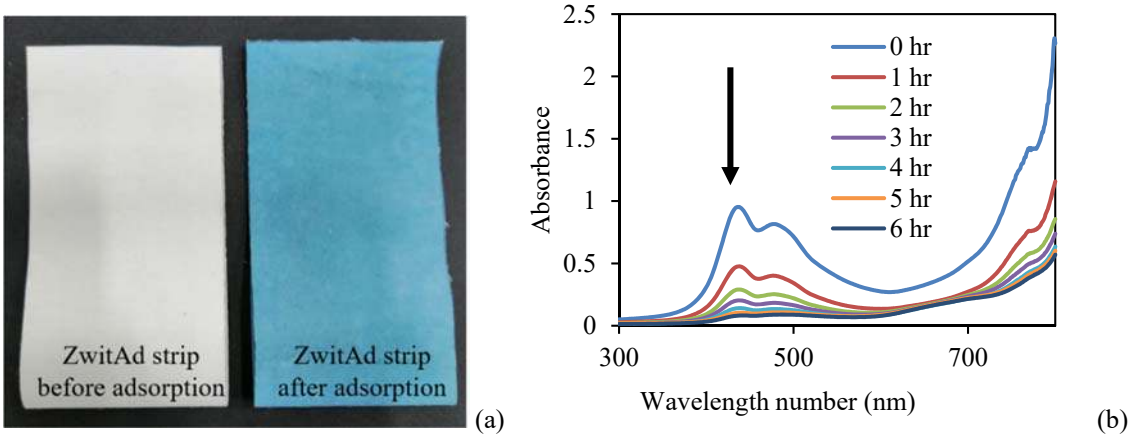

Figure 3: Images of ZwitAd strip before adsorption and ZwitAd strip after adsorption (a), Uv-vis spectrum analysis of Batik effluent

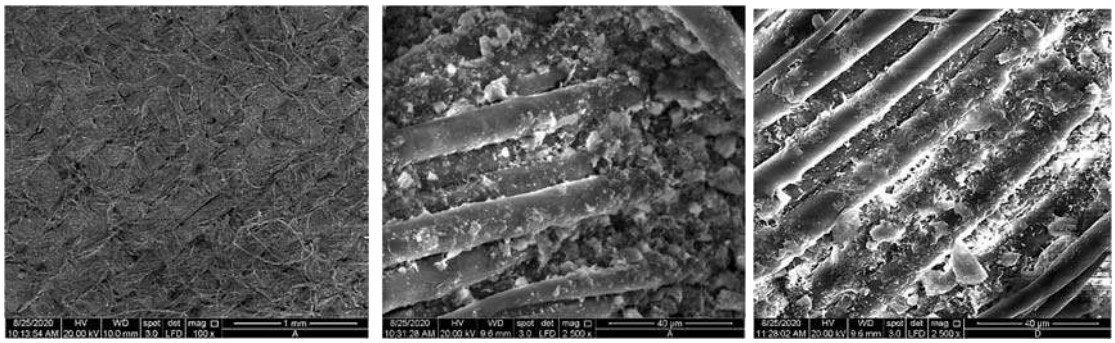

Figure 4: SEM images of ZwidAd before adsorption at 100x (left side) and 2500x magnifications (middle side), and ZwitAd after Batik treatment (right side).

CONCLUSION

The physical treatment using zwitterionic adsorbent coating was successfully applied for the decolorization of Batik wastewater. The result indicated that the removal of colour and COD for the mixture of wastes from boiling and rinsing discharged points achieved the acceptable limit by Standard B. The implementation of ZwitAd shown a as a promising and applicable treatment for the Batik wastewater. Less of generated sludge, efficient and lower treatment cost will be a good strategy for the industrial player to execute the ZwitAd as one of the alternatives in wastewater treatment procedure.

ACKNOWLEDGEMENT

The authors acknowledge the Prototype Research Grant Scheme (PRGS) (203/PJKIMIA/6740049) provided by the Ministry of Higher Education, Malaysia.

REFERENCES

[1] MIDA, "Malaysian Investment Development Authority (MIDA) 2018," 2018. [Online]. Available: http://www.mida.gov.my/home/textiles-and-textile-products/posts/?lg=EN. [Accessed: 06-Dec-2018].

[2] N. Sridewi, L. Tan, and K. Sudesh, "Solar Photocatalytic Decolorization and Detoxification of Industrial Batik Dye Wastewater Using P (3HB) -TiO 2 Nanocomposite Films," *Clean-Soil, Air, Water*, vol. 39, no. 3, pp. 265–273, (2011).

[3] A. Buthiyappan, A. Aziz, A. Raman, W. Mohd, and A. Wan, "Development of an advanced chemical oxidation wastewater treatment system for the batik industry," *RSC Adv.*, vol. 6, pp. 25222–25241, (2016).

[4] W. F. Khalik, L. Ho, S. Ong, C. Voon, Y. Wong, and S. Y. Yusuf, "Enhancement of simultaneous batik wastewater treatment and electricity generation in photocatalytic fuel cell," *Environ. Sci. Pollut. Res.*, vol. 25, pp. 35164–35175, (2018).

[5] Y. L. Pang and A. Z. Abdullah, "Current status of textile industry wastewater management and research progress in malaysia: A review," *Clean - Soil, Air, Water*, vol. 41, no. 8, pp. 751–764, (2013).

[6] K. Siddique, M. Rizwan, M. J. Shahid, S. Ali, R. Ahmad, and Hina Rizvi, "Textile Wastewater Treatment Options: A Critical Review," *Enhancing Cleanup Environ. Pollut.*, pp. 183–207, (2017).

[7] P. Moradi *et al.*, "An efficient and economical treatment for batik textile wastewater containing high levels of silicate and organic pollutants using a sequential process of acidi fi cation , magnesium oxide , and palm shell- based activated carbon application," *J. Environ. Manage.*, vol. 184, pp. 229–239, (2016).

[8] L. Junyi *et al.*, "Immobilization of dye pollutants on iron hydroxide coated substrates: kinetics, efficiency and the adsorption mechanism," *J. Mater. Chem. A*, vol. 4, no. 34, pp. 13280–13288, (2016).

[9] A. H. Jawad, M. Azharul Islam, and B. H. Hameed, "Cross-linked chitosan thin film coated onto glass plate as an effective adsorbent for adsorption of reactive orange 16," *Int. J. Biol. Macromol.*, vol. 95, pp. 743–749, (2017).

[10] S. F. Azha *et al.*, "Synthesis and characterization of a novel amphoteric adsorbent coating for anionic and cationic dyes adsorption : Experimental investigation and statistical physics modelling," *Chem. Eng. J.*, vol. 351, no. June, pp. 221–229, (2018).

[11] S. F. Azha, M. S. Shamsudin, M. Shahadat, and S. Ismail, "Low cost zwitterionic adsorbent coating for treatment of anionic and cationic dyes," *J. Ind. Eng. Chem.*, vol. 67, pp. 187–198, (2018).

[12] W. Fadhilah, W. Mohd, L. Ho, and Y. S. Wong, "Decolorization and Mineralization of Batik Wastewater through Solar Photocatalytic Process Decolorization and Mineralization of Batik Wastewater through Solar Photocatalytic Process," *Sains Malaysiana*, no. April, (2015).

PGC_SCHE.USM_2020_56

Preliminary studies on material selection for developing new polymeric water shut off agent emphasized on Malaysian average wellbore condition

Siti Nuraffini Kamarulizam, Suzylawati Ismail*
School of Chemical Engineering, Engineering Campus, Universiti Sains Malaysia,
14300 Nibong Tebal, Pulau Pinang, Malaysia
*E-mail: *chsuzy@usm.my*

Abstract. The preliminary selection of material was studied in term of apparent structure of synthesized polymer. The synthesized polymers were undergoing in situ polymerization reaction at 60°C to determine solid form polymer indicate the feasible material to be developed as water shut off agent. The best backbone polymer were Guar Gum (GG), the polymer strengthener were Acrylic Acid (AA) and the time delayer were Chitosan (CHI) were selected as these materials showed the most cooperative synergism to work with the present of Acrylonitrile (AN) and Cerium Ammonium Nitrate (CAN) in a given concentration range.
Keywords: *Water Shut Off Agent, Oil Recovery, Guar Gum*

INTRODUCTION

The production of excess water during the process of oil extraction has emerged as a problem that has been identified in the oil wells across the world and with the passage of them, there have evolved a number of efficient ways to control or reduce the same so as the improve the profile of oil, assist in better oil recovery and enhance economical oil extraction from the wells (Karimi et al., 2014). Salimi et al., (2014) had stated particularly with the use of low concentration high molecular weight polymers, cross-linked with organic crosslinker as the remediating factor to address the problems associated with excess production of water. However, owing to the problems associated with the high temperature reservoir and compatibility problems with adducts paved the way of developing new formulation. The implementation into the process served to be a cost effective and highly efficient means to address the problems and also, the crosslinkers in the gel recipe can reduced the synergistic issues could also be resolved (Sengupta et al., 2012). In this current research, materials suggestion for new environmental friendly hydrogel for meeting water shut off requirement were studied.

MATERIALS AND METHOD

For this preliminary selection, polymer was categorized into four apparent observation upon reacted polymer structure. The polymer was blended together in the test tubes, shake well, and place into oven for 60°C for 24 hours. This was to meet the first characteristic of water shut off polymer which able to become polymer that fit onto enclosed channel, which in this experiment were the bottles' wall. The four categories were fluid physical forms that were free flow liquid, slurry, solid and syneresis as shown in Figure 1, the appearance of polymer after 24 hours reaction time at 60°C condition. The aim was the polymer appeared in solid form which indicate the feasible of materials to be developed as WSO agent.

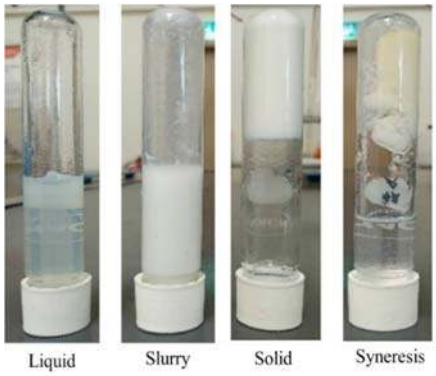

Figure 1: Synthesized polymer appearance after 24 hours at 60°C

For functioning monomer, Acrylonitrile, AN, was selected base on the acknowledgement of AN as hydrophobic nature to add into hydrophilic backbone polymer. The selection of this polymerization was based on

literature (Thimma et al., 2003), and the presence of a little amount of vinyl group is necessary for synthesizing hydrogel (Ismail et al., 2013). This functioning monomer, AN, was selected based on potential of becoming one of polymeric WSO (Lymar et al., 2011). The vinyl monomer, AN were grafted into backbone to become macromolecules with help of CAN.

RESULT AND DISCUSSION

Selection of backbone polymer was important to set initial viscosity of polymer. Backbone polymer was needed to be similar to water viscosity or near to water viscosity in order to get good injectable polymer. The effect of using different backbone polymer (GG, XG, and LBG) at 1000ppm with AN concentration ranging from 1v%, 4v%, 7v% and 10v% and a constant of 0.5v% CAN concentration. Figure 2 shows the polymer appearance of different backbone polymer. GG shows a change in its physical formation with the increase in AN concentration. This was illustrated at 4v% AN concentration, it was solidified after 24 hours and change to syneresis once AN concentration increased at 10v%. GG showed the most cooperative polymer to function under the given condition with present of AN and CAN. GG was reported to be high molecular weight polysaccharide, thus efficient in producing highly viscous polymer at very low GG concentrations.

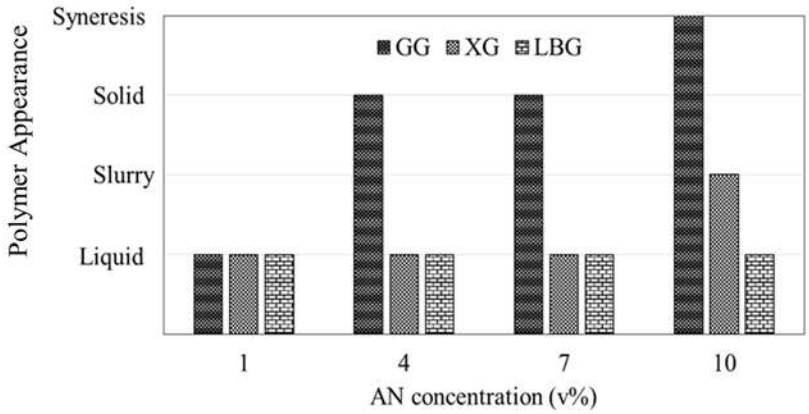

Figure 2: Different type of natural polymer at different concentration of functioning monomer, AN.

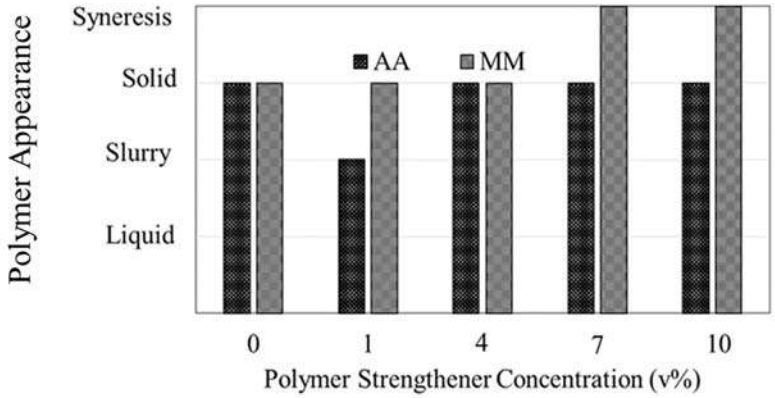

Figure 3: Polymer appearance using different type of polymer strengthener at different concentration.

The hydrophobicity had modified by polymerization of GG-AN, the polymer strength does not meet the expectation as polymeric WSO. The monomer selected were acrylic acid (AA) and methyl methacrylate (MM) selection had been studies to understand morphology and polymer strength enhancement and meet water shut off requirement. Figure 3, both polymer strengthener give good conversion into solid state gel by addition of same concentration of secondary monomer. Even though both polymers were well cooperated with initial composition, the visualization analysis was done to study the justification for selecting AA. Figure 4 shows the morphology of AA and MM addition into initial polymer composition. The addition of AA turned the polymer to elastic 3D structure (white rubber texture). Meanwhile, by the addition of MM, it improved the polymer strength to unbreakable stiff structure (strong hard plastic). The structure was inflexible. According to Nietzsche et al., (1973), hard or soft polymer is depending on polymer chain mobility. Adding AA, polymer chains can jiggle, thus soften the polymer. While adding

MM, methyl group spikes in polymer chains thus restrict the chain mobility. Furthermore, because of AA addition allowed polymer chain to slither around, it able to hold more to its current weight. Due to these justifications, the addition of AA was selected since synthesized polymer are needed to be flexible and able to preserve water as much as it could.

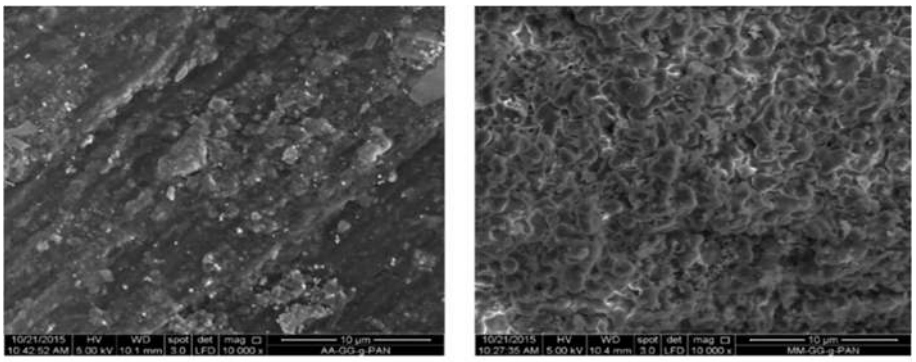

Figure 4: Morphology of AA addition and MM addition into 1000ppm GG, 0.5v% CAN and 4v% AN using SEM.

Inhibitor/ retarder was added to ensure gelation happen on targeted time. The range for this research was between 120 minutes to 180 minutes before gelation start. In order to achieve this target, small amount of inhibitor or retarder was added to obstruct polymerization process of GG-AN. However, this inhibitor was function as time disturbance and do not significantly change the characteristic of present polymer. Figure 5 showed, addition of CHI and LCT turn into solid state and do not give any polymerization effect on present polymer. It was determined that time hindrance was resolute by addition of secondary long chain polymer. These were welcomed since the effect into current polymer was not disturbed. However, by the addition of BRX and APS, the polymerization of current polymer was disturbed due to unwanted reaction kinetic, hence, cause polymer to be slurry rather than solid. Therefore, only CHI and LCT were selected for further study. Figure 6 presents the preliminary test result of gelation time for CHI and LCT at 60ºC. It is known that CHI work in required time frame and can be adjusted according to required time frame selection. Comparing to the use of LCT, the polymerization was delayed so long before it started to solidify, and this can jeopardize the function of initiator which can partially oxidized before polymerization started. Developing steric hindrance on pre-set polymer can elongate relaxation time before polymerization start. This was due to expression of intermolecular activities between added polymers that cause CHI suppression over current polymer before its combine and synthesized to become one good functioning polymer.

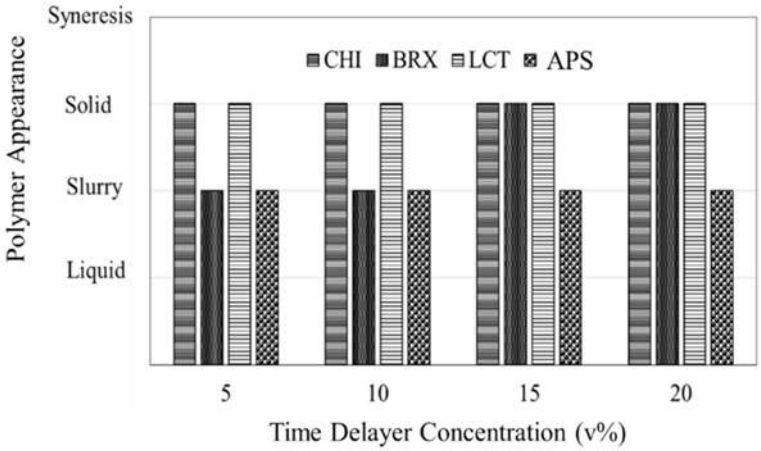

Figure 5: Polymer Appearance using different type of time delayer at 1000ppm

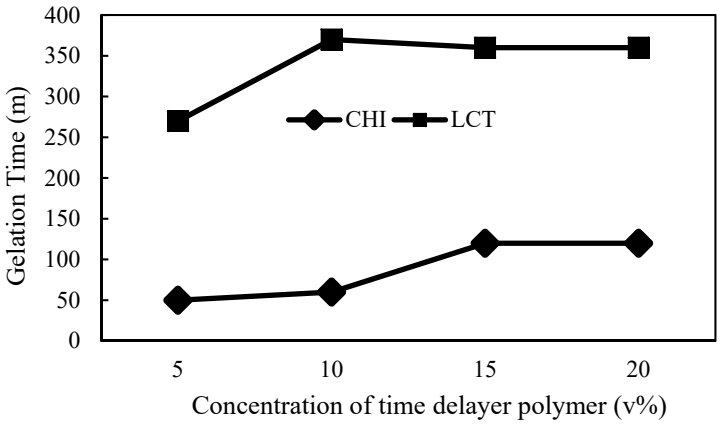

Figure 6: Gelation time for different CHI and LCT concentration at 60°C

CONCLUSION

The preliminary studied showed that GG were the best selection to become polymer backbone, AA as polymer strengthener and CHI as time delayer to synthesize a new hydrogel to be functioned as a water shut off agent.

ACKNOWLEDGEMENT

The authors acknowledge the Prototype Research Grant Scheme (PRGS) (203/PJKIMIA/6071413) provided by the Ministry of Higher Education, Malaysia.

REFERENCES

[1] Karimi, S., Esmaeilzadeh, F., & Mowla, D. J. Nat. Gas. Sci. & Eng., 21, 940–950(2014).
[2] Sengupta, B., Sharma, V. P., & Udayabhanu, G., J. Pet. Sci. & Eng., 81, 145–150 (2012).
[3] Ismail, H., Irani, M., & Ahmad, Z. Int. J. Pol. Mat. & Biomat., 62(7), 411–420 (2013).
[4] Thimma, R. T., Reddy, N. S., & Tammishetti, S. Pol. Adv. Tech., 14(10), 663–668 (2003)
[5] Lymar, I., UDC 622.276 (476) Lymar I.V. (Vol. 276, pp. 133–142) (2011).
[6] Arici M , Gumus T, Sukrus A, Mirik M, , Aysan Y., Food Sci. Biotech.; 19: 201-206 (2010).
[7] Zhang, X., Wang, X., Li, L., Zhang, S., & Wu, R., Rea & Func. Pol., 87, 15–21 (2015).
[8] Shah, S. B., Patel, C. P., & Trivedi, H. C., Carb. Pol., 26(1), 61–67 (1995).
[9] Akhtar, M. F., Hanif, M., & Ranjha, N. M., Saudi Phar. J., 24(5), 554–559(2016).
[10] Guo, S., Jia, H., & Chen, H., Fuel, 210(August), 207–216 (2017).

PGC_SCHE USM_2020_57

Co-Pyrolysis Process of Palm Kernel Shell and Polypropylene for Bio-Oil Production: Effect of Blending Ratio

Aizatul Hikmah Zulkafli[1], Hamizura Hassan[1], Mohd Azmier Ahmad[2,*], Azam Taufik Mohd Din[2]
[1]Faculty of Chemical Engineering, Universiti Teknologi MARA,
Cawangan Pulau Pinang, 13500, Permatang Pauh, Pulau Pinang, Malaysia
[2]School of Chemical Engineering, Engineering Campus, Universiti Sains Malaysia,
14300 Nibong Tebal, Pulau Pinang, Malaysia.
*E-mail: *chazmier@usm.my*

Abstract. This research examines the co-pyrolysis of palm kernel shell (PKS) and polypropylene (PP) in a fixed-bed reactor. The effect of PKS-to-PP ratio on the bio-oil yield was discussed. The highest bio-oil of 62.7 wt% was achieved at blending ratio of PKS-to-PP ratio of 25:75, temperature of 500℃ within 45 minutes. The proximate analysis shows the volatile matter of PKS with PP and without PP are 75.3 wt% and 61.7 wt%, respectively, indicating the PKS and PP could be potential sources of energy. The co-pyrolysis of PKS and PP produced higher yield of bio-oil compared to pyrolysis of PKS alone.
Keywords: *Co-pyrolysis; bio-oil; palm kernel shell; polypropylene.*

INTRODUCTION

Pyrolysis oil or called bio-oil has been receiving significant attention of researchers due to its potential application as fuel. Bio-oil can be useful chemicals, such as resins and flavourings [1]. Palm kernel shell (PKS) has a high potential to use as a biomass resources for bio-oil generation as it is abundant, inexpensive, high in lignin (50.7%) and low in moisture content (12 %) compared to another biomass [2]. PKS is a fraction of the shell remaining after the kernel has been extracted from the palm oil factory [1]. However, the pyrolysis of biomass produced bio-oil with undesirable properties such as low calorific value, corrosive, and instable [3]. Co-feeding of biomass with polymer might significantly enhanced the yield and quality of bio-oil in order to circumvent the problem of low quality of bio-oil. [4]. Previous studies show that biomass and polymer could increase the bio-oil yield and quality. In addition, the hydrocarbon produced was within the diesel fraction range. Chi et al. [5] investigated co-pyrolysis of cellulose and propylene and found that the addition of polypropylene lowered the oxygenated compound in bio-oil and increased yield of olefins and aromatics. Therefore, the objective of this study is to examine the co-pyrolysis of PKS and PP to produce greater yield of bio-oil. The effect of blending ratio on the product fractional yield was evaluated.

MATERIALS AND METHODS

Palm kernel shell (PKS) was obtained from United Oil Palm mill in Nibong Tebal, Penang, Malaysia and the polypropylene (PP) was obtained from Lotte Chemical Titan. The particle diameter size of feedstock was fixed from 1 mm to 250 μm. The pyrolysis experiments were performed using a stainless steel fixed-bed type reactor with a slow heating rate at atmospheric pressure. The reactor was heated by electric furnace. The K-type thermocouple was used inside the reactor to measure the temperature. Some amount of glass wool was placed inside the reactor and PKS/PP mixture was loaded. The total mass mixture PKS/PP was fixed at 6 g. High purity of nitrogen gas (99.99%) was flowed inside the reactor, to build an inert atmosphere. The ratio of PKS to PP in the feedstock were varied at 100:0, 75:25, 50:50, 25:75 and 0:100 at a constant reaction temperatures and times. Wax trap was the first collector and constant at 170℃. The pyrolysis vapour was collected and deposited in a condenser in an ice bath. The heater has been switched off, then quickly cooled to 24℃, while flowrate of the nitrogen gas was managed to circumvent the oxidation of the char after the experiment completed.

RESULTS AND DISCUSSION

Generally, proximate analysis of biomass is classified in of moisture content, volatile matter, fixed carbon and ash content and the result is shown in Table 1. In pyrolysis, volatile matter is factor that influence the production of liquid yield which converted biomass to bio-oil after condensation [6]. The volatile matter of PKS is 61.7 wt% suggesting that PKS could be potential sources of energy. The higher the volatile matter, the higher yield of pyrolysis oil produced due to its high volatility and reactivity. The ash content of PKS and PP are 9.3 wt% and 0.363, respectively, which is less than 10 wt%. High ash content favoured the production of char. The lower the fixed carbon content in the samples, the lower the bio-char generated. High fixed carbon content contributes to the production of

bio-char in the pyrolysis process and decrease the bio-oil yield [7]. On the other hand, the high moisture content could reduce the production of pyrolysis oil. Bridgwater [8] reported that the total moisture content of the dry feedstock should be less than 10%, since this parameter effect the yield and quality of the pyrolysis oil produced.

Table 1: Proximate analysis of biomass

Biomass/Plastic	**Proximate Analysis (wt%)**			
	Moisture content	Fixed carbon	Volatile matter	Ash
PP	41.07	-	-	0.36
PKS	4.8	24.3	61.7	9.3

Blending ratio of biomass-to-plastic play a crucial role in bio-oil production. The experiments were performed at fixed temperature and reaction time of 500℃ and 45 minutes, respectively. The results on the effects of blending ratio of PKS and PP is shown in Table 2. As the PP ratio increased from 25% to 75%, the liquid yield increased steadily from 32.4 wt% to 62.7 wt%. On the other hand, the pyrolysis oil produced from pyrolysis of PKS alone is only 32.1 wt% which is lower than co-pyrolysis of PKS with PP. The higher the loading of PP in co-pyrolysis of PKS, the higher the yield of bio-oil produced since high plastic could donate more hydrogen to PKS and enhanced the production of bio-oil [9].

Table 2: Effect on blending ratio of palm kernel shell and polypropylene

Palm Kernel Shell : Polypropylene	**Yield (wt%)**
100:0	32.1
75:25	32.4
50:50	53.3
25:75	62.7
0:100	69.7

CONCLUSION

In conclusion, an addition of plastic such as polypropylene gives high yield of bio-oil in co-pyrolysis process. The higher bio-oil yield of 62.7 wt% was achieved at PKS-to-PP ratio of 25:75, reaction temperature of 500℃ within 45-minute reaction time. High volatile matter of PKS signify that these feedstocks could be potential sources of energy.

ACKNOWLEDGEMENT

The authors thankfully acknowledge the support obtained from the Lotte Chemical Titan (M) Berhad and Universiti Sains Malaysia (Grant number: 304/PJKIMIA/6050422/L128) in the form of research grant and facilities.

REFERENCES

[1] S. Zafar, Consult. (2020). https://www.bioenergyconsult.com/palm-kernel-shells.
[2] N. Hamzah, K. Tokimatsu, K. Yoshikawa, Sustain, (2019) 1–23.
[3] G. Ozsin, Clean. Product., **205** (2018) 1127–1138.
[4] M.H.M. Ahmed, N. Batalha, H.M.D. Mahmudul, G. Perkins, M. Konarova, Bioresour. Technol. **310** (2020) 123457.
[5] Y. Chi, J. Xue, J. Zhuo, D. Zhang, M. Liu, et al., Sci. Total Environ. **633** (2018) 1105–1113.
[6] F. Abnisa, W.M.A. Wan Daud, Energy Convers. Manag. **87** (2014) 71–85.
[7] M. Mierzwa, H. Krzysztof, G. Marcin, J. Krzysztof, J. Mater. Cycles Waste Manag. **21** (2019) 786–800.
[8] A. V Bridgwater, Biomass and Bioenergy. **38** (2011) 68–94.
[9] A. Dewangan, D. Pradhan, R.K. Singh, Fuel. **185** (2016) 508–516.

PGC_SCHE USM_2020_58

Investigation on Activated Carbon Pre-treatment in Catalytic Cracking of Waste Cooking Oil

Tavayogeshwary Thangadurai, Ching Thian Tye*
School of Chemical Engineering, Engineering Campus, Universiti Sains Malaysia,
14300 Nibong Tebal, Pulau Pinang, Malaysia.
*E-mail: *chcttye@usm.my**

Abstract. Activated carbon is the waste-derived material serves as economical catalyst in various applications. Its catalytic performance varies with the source and surface modification via chemical pretreatment. Acid and alkali treatment are the commonly adapted method which were noticed to influence its catalytic activity. Hence, commercially available wood-based and coconut shell-based activated carbon were pre-treated with nitric acid (HNO_3) and sodium hydroxide (NaOH) to study its effect in catalytic cracking of waste cooking oil.
Keywords: *Activated carbon; source; chemical treatment; catalytic cracking.*

INTRODUCTION

The demand for energy has been rapidly escalating but the fuel resource is seemingly depleting. This has led to development of alternative renewable biofuel which is environmental friendly and economical [1]. However, fatty acid methyl ester (FAME) and bio-oil generated via transeterification and pyrolysis, respectively, exhibited higher oxygen content and acidic value. Hydroprocessing and catalytic cracking produce green fuel that has properties close to petroleum-based fuel and hence ideal for conventional engines.

Catalytic cracking requires no hydrogen supply which is more economical in terms of operation than hydroprocessing reaction. Catalyst plays an important role in improving conversion and selectivity for better product quality. Activated carbon has attracted attention of recent researches for its significant catalytic performance in plant oil cracking activity [2]. Its catalytic activity can be manipulated via chemical treatment which changes its physicochemical properties such as surface area, porous structure and surface functional group [3]. Acid (HNO_3, H_2SO_4 and H_3PO_4) and alkali (KOH and NaOH) are the widely known reagents for chemical treatment of activated carbon. Therefore, the effect of activated carbon source and its chemical treatment were investigated in this study. Nitric acid (HNO_3) and sodium hydroxide (NaOH) were used in pretreatment of activated carbon which were sourced from wood and coconut shell.

MATERIALS AND METHODS

Materials

Waste cooking oil was collected from the cafeteria in Universiti Sains Malaysia and activated carbon (wood and coconut shell) was obtained from KI Carbon Solutions, Kapar. The waste cooking oil was filtered and heated overnight at 105°C to eliminate impurities and moisture. Nitric acid (HNO_3) of 69% purity was purchased from QReC whereas sodium hydroxide (NaOH) was acquired from Friendemann Schmidt Chemicals.

Chemical treatment of activated carbon

The nitric acid and sodium hydroxide were diluted with distilled water to 250 ml of 6 M solution. Wood-based (w-AC) and coconut shell-based (c-AC) activated carbon powder were stirred overnight with the solution at 80°C in a reflux system. The activated carbon was washed with distilled water until the pH is 7 and then dried overnight in an oven at 105°C.

Catalyst activity test

Carburization of activated carbon was carried out prior to the reaction where 1 g of activated carbon was loaded into a tubular reactor placed in a tube furnace. A mass flow controller was used to pass nitrogen gas (99.9995%) through the reactor. Reactor temperature was raised gradually to 550° at a heating rate of 10°C/minute. The temperature was maintained for 5 hours and then allowed to drop to reaction temperature of 450°C. Waste cooking oil was fed into the reactor for 60 minutes and the liquid product formed at the outlet was weighed.

Liquid product analysis

Liquid product collected in the reaction was diluted with hexane and was analyzed in a gas chromatography equipped with flame ionization detector (GC-FID) that operated at 300°C with a HP-5 column (30 m x 0.25 mm x 0.25 μm). Helium (99.999%) was used as the carrier gas and the injection temperature was set at 250°C. The oven

temperature was retained at 40°C for 6 minutes and then ramped to 270°C at a rate of 7°C/minute, followed by holding for 5 minutes [4]. The liquid yield and C5 – C20 hydrocarbon yield were calculated using the following equations:

$$Liquid\ yield\ (wt.\%) = \frac{Weight\ of\ liquid\ product\ (g)}{Weight\ of\ oil\ feed\ (g)} \times 100\ \% \quad (1)$$

$$Hydrocarbon\ yield\ (\%) = \frac{Area\ of\ C_5{-}C_{20}\ hydrocarbons}{Total\ area{-}Area\ of\ hexane} \times 100\% \quad (2)$$

RESULTS AND DISCUSSION

Table 1 shows the liquid yields for the thermal and catalytic cracking of waste cooking oil using activated carbon.

Table 4. Thermal cracking and catalytic cracking of waste cooking oil using activated carbon at 450°C; WHSV 9 hour^{-1} and 60 minutes.

Reaction	Liquid yield (wt. %)
Thermal	45.09
Wood-AC (HNO_3)	44.48
Coconut-AC (HNO_3)	45.63
Wood-AC (NaOH)	40.88
Coconut-AC (NaOH)	43.81

The highest liquid yield was obtained by coconut shell-based activated carbon treated with nitric acid. More liquid product was obtained in reaction by acid-treated activated carbon than that of the alkali-treated AC. Coconut shell-based activated carbon exhibited better catalytic performance than that of the wood-based AC as well. Although thermal reaction had higher liquid yield, its hydrocarbon yield was very much lower than that obtained in catalytic cracking using activated carbons.

Figure 1 shows the C_5 – C_{20} hydrocarbons yield in the liquid product detected via GC-FID obtained in reaction with different material as the catalyst. The hydrocarbon yield of coconut shell-based activated carbon was slightly higher (~1%) for alkali treatment than that of acid treatment. But, wood-based activated carbon gave lower C_5 – C_{20} hydrocarbons yield with NaOH treatment than did HNO_3. The hydrocarbon yield was also higher for coconut shell-based activated carbon than that of wood-based activated carbon. This could be due to the variation in their surface area and porous structure which holds the active sites for the reaction [5].

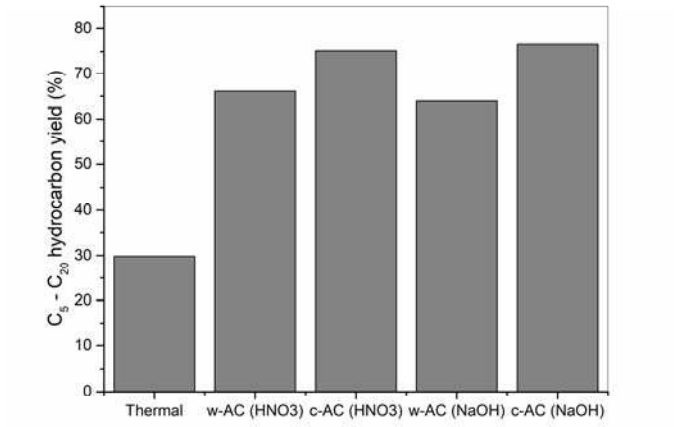

Figure 1: C_5 - C_{20} hydrocarbon yield of liquid product in catalytic cracking of waste cooking oil at 450°C; WHSV 9 hour^{-1} and 60 minutes.

CONCLUSION

The source and chemical treatment indeed affected the catalytic performance of activated carbon. It was noted that nitric acid as the chemical reagent for activated carbon treatment gave better catalytic activity than the sodium hydroxide. Coconut shell-based activated carbon also gave more liquid product with higher C_5 – C_{20} hydrocarbon yield than the wood-based activated carbon.

ACKNOWLEDGEMENT

This study was supported by Ministry of Education Malaysia under FRGS grant (A/C: 203.PJKIMIA.6071445).

REFERENCES

[1] M. F. Othman, A. Adam, G. Najafi, and R. Mamat, "Green fuel as alternative fuel for diesel engine: A review," *Renew. Sustain. Energy Rev.*, **80**, June, pp. 694–709, 2017.

[2] G. Abdulkareem-Alsultan, N. Asikin-Mijan, H. V. Lee, U. Rashid, A. Islam, and Y. H. Taufiq-Yap, "Review on thermal conversion of plant oil (Edible and inedible) into green fuel using carbon-based nanocatalyst," *Catalysts*, **9** (4), MDPI AG, 01-Apr-2019.

[3] W. Dilokekunakul, P. Teerachawanwong, N. Klomkliang, S. Supasitmongkol, and S. Chaemchuen, "Effects of nitrogen and oxygen functional groups and pore width of activated carbon on carbon dioxide capture: Temperature dependence," *Chem. Eng. J.*, **389**, February, p. 124413, 2020.

[4] G. Abdulkareem-Alsultan, N. Asikin-Mijan, G. Mustafa-Alsultan, H. V. Lee, K. Wilson, and Y. H. Taufiq-Yap, " Efficient deoxygenation of waste cooking oil over Co 3 O 4 –La 2 O 3 -doped activated carbon for the production of diesel-like fuel ," *RSC Adv.*, **10**, pp. 4996–5009, 2020.

[5] Z. M. Yunus, Y. G, A. Al-Gheethi, N. Othman, R. Hamdan, and N. N. Ruslan, "Advanced methods for activated carbon from agriculture wastes; a comprehensive review," *Int. J. Environ. Anal. Chem.*, 00, pp. 1–25, 2020.

APPENDIX

FINAL YEAR PROJECT 2020 ABSTRACT

ID: FYP2020/1

RECYCLE POLYETHYLENE TEREPHTHALATE REINFORCED ACTIVATED CARBON ADSORBENTS FOR METHYLENE BLUE DYE REMOVAL

ALSHIDDIQ ALLAZMI & TAN SOON HUAT
School of Chemical Engineering, Engineering Campus, Universiti Sains Malaysia,
14300 Nibong Tebal, Pulau Pinang, Malaysia

ABSTRACT

Water pollution is one of the most undesirable environmental problems in the world and it requires solutions. Textile industries produce a lot of wastewater, which contains a number of contaminants, including acidic or caustic dissolved solids, toxic compounds, and dyes such as methylene blue (MB). The aim of this project is to study the adsorption of MB dyes on recycle polyethylene terephatalate (rPET) and recycle polyethylene terephthalate reinforced activated carbon (rPET/AC) composite ring adsorbents. Various parameters such as initial concentration, contact time and adsorbent dosage were investigated in a batch adsorption technique. rPET and rPET/AC composite ring adsorbents were prepared by the dropping method. The resultant composite rings were employed as adsorbents for MB removal from aqueous solution. The removal efficiency for rPET/AC was found to be higher at 65% compared to rPET rings which is only 26% at the initial MB concentration of 10 mg/L. The equilibrium data were evaluated using Langmuir, and Freundlich isotherms. The Langmuir model best described the uptake of MB dye, which implies that the adsorption of MB dyes in this study onto composite ring adsorbents is a single layer adsorption. The single layer maximum adsorption capacity of MB onto rPET/AC was 0.35 mg/g while for rPET only 0.16 mg/g.

ID: FYP2020/2

EFFECTS OF DIP COATING PARAMETERS OF POLYDIMETHYLSILOXANE (PDMS) DENSE LAYER ON POROUS POLYETHERSULFONE (PES) HOLLOW FIBER MEMBRANE FOR CO_2/N_2 SEPARATION

AMIR IKMAL HASSAN & ABDUL LATIF AHMAD
School of Chemical Engineering, Engineering Campus, Universiti Sains Malaysia,
14300 Nibong Tebal, Pulau Pinang, Malaysia

ABSTRACT

Polydimethylsiloxane (PDMS) has been commonly used as separating layer in gas separation membrane, hydrocarbon separation process, pervaporation and recently as a viable gutter layer in composite membrane fabrication. As PDMS is rubbery, a porous substrate is needed to mechanically support the polymer, especially when fabricated in hollow fiber form. Therefore, in this study, the combination of polydimethylsiloxane (PDMS) dense layer on porous polyethersulfone (PES) hollow fiber membrane as a support was chosen to be analyzed with varying dip coating parameters. Coating parameters which includes speed of coating (5 – 15 mm/s) and holding time (10 – 900 s) of PES membrane in PDMS coating solution were varied by using automated dip coating machine. The performance of coated and uncoated membranes was tested in the separation of carbon dioxide (CO_2) and nitrogen (N_2) gases. Effect of the parameters on permeation and selectivity were measured under transmembrane pressure of 1 to 3 bars for both gases. Scanning Electron Microscopy (SEM) characterization was also conducted for the investigation of membrane morphology and confirmed the presence of coating after coating procedure was applied. For gas permeation, both gases resulted in flux decrement reaching to 13434.3 GPU from initial 23149 GPU as coating speed increased. Starting from 5 mm/s speed, initial selectivity of the gases was at 0.842 and then gradually increased by 10% at 10 mm/s. As speed increased above 10 mm/s, the selectivity slightly dropped to 0.876. This suggested that single coating at this range speed was not able to fully coat the porous PES fibers. Despite that, the decrease of gas permeance with coating speed confirms the increased amount of coated PDMS on the substrate. On the other hand, holding time in coating solution also showed significant effects on the membrane performance. Coated membrane showed good balance of permeation and selectivity at 200 s ranging from 25000 GPU and 0.911 respectively at fixed coating speed. However, membrane exhibits drop in permeance at high holding time, suggesting a more complete covering of the support with PDMS layer. This is suggested to be caused by increased in viscosity during the PDMS crosslinking reaction as time passed, allowing more PDMS solution to be retained on the PES fiber's surface.

ID: FYP2020/3

SIMULATION OF CARBON BLACK PRODUCTION VIA THERMAL DECOMPOSITION OF METHANE IN A PLUG FLOW REACTOR

CARANI NARAYANASAMY & NORASHID AZIZ
School of Chemical Engineering, Engineering Campus, Universiti Sains Malaysia,
14300 Nibong Tebal, Pulau Pinang, Malaysia

ABSTRACT

Production of carbon black via thermal decomposition of methane is becoming the center of attraction among the researchers, thus this process needs to be studied in detail so that the yield of carbon black will be promising to be implemented in the industrial scale. In this study with the aid of simulating software such as Aspen Plus version 10, thermal decomposition of methane was simulated and the reactor length was optimized. Aspen Plus was used to simulate the reaction where methane is thermally cracked and converted into desirable product which is carbon black and a by-product namely hydrogen gas. The simulation was acceptable as the error percentage was less than 10% obtained when a comparison was made between the simulated and literature results. Next, sensitivity analysis that was carried out on the RPLUG model showed that methane feed flow rate and reactor temperature had a notable effect on the conversion of methane and carbon black yield. It was found that the carbon black yield increases when the reactor temperature increases up to 1840 K and methane feed flow rate decreases to 3.67 l/min. Finally, reactor length optimization study showed that the maximum carbon black yield which was 33.33% can be achieved when the reactor length was 0.52 m instead of 0.6 m at optimum variables of 1840 K and 3.67 l/min.

ID: FYP2020/4

METHYLENE BLUE DYE REMOVAL USING PARKIA SPECIOSA POD BASED ACTIVATED CARBON

CHANG CHEE HOE & MOHD AZMIER AHMAD
School of Chemical Engineering, Engineering Campus, Universiti Sains Malaysia,
14300 Nibong Tebal, Pulau Pinang, Malaysia

ABSTRACT

Textile industry comprises one of the key supporters to the growth of Malaysia's economy. However, crucial environment issues arise related to water pollution due to textile effluent discharged consisting dyes. Effective methods such as adsorption is applied in treating textile wastewater while activated carbon (AC) is commonly used. In this study, low-cost AC was developed from Parkia speciosa pods (PSP) using microwave-assisted activation technique for the methylene blue (MB) dye adsorption. Optimization on activating conditions in terms of MB removal and AC yield was performed using response surface methodology (RSM). Optimized results found that microwave irradiation power (MIP) has significance effect on MB removal while MIP has more prominent effect followed by activation time on AC yield. The optimized conditions obtained were 416.50 W and 2 minutes. Characterization results depicted that PSPAC possesses intermediate surface area and total pore volume (51.3 m^2/g and 0.0681 cm^3/g). Surface morphology analysis showed that PSPAC was mesoporous and consists highly porous structure with great number of pores, indicating characteristics of good AC. Batch adsorption studies with various initial concentrations (50 mg/L to 300 mg/L) and contact time (0 to 24 hours) discovered that MB adsorption increased with increasing initial concentrations and contact time. Isotherm studies discovered that the experimental data was in close fit using Langmuir isotherm. Kinetics studies provided MB adsorption onto PSPAC followed pseudo-first-order kinetic models. Intraparticle diffusion analysis depicted that MB dye adsorption process was governed by simultaneous surface adsorption and intraparticle diffusion. The results of studies proved that PSPAC is a potential adsorbent for dye-contaminated wastewater.

ID: FYP2020/5

CRITICAL REVIEW ON KINETICS OF SOLID-LIQUID EXTRACTION PROCESS OF TOTAL POLYPHENOL, ANTIOXIDANTS AND EXTRACTION YIELD FROM PLANT

CHIN YOONG WEI & KHAIRIAH ABD. KARIM
School of Chemical Engineering, Engineering Campus, Universiti Sains Malaysia,
14300 Nibong Tebal, Pulau Pinang, Malaysia

ABSTRACT

Antioxidants and polyphenol compounds are useful resources to human in many aspects. The acquisition of these compounds is challenging because of the nature of extraction process efficiency that is affected by multiple variables. The use of these compounds could be beneficial to the medical and the science research field if the sources of antioxidants are more commonly available and efficient. Natural plants, especially those with medicinal effect has a potential to be a good source of antioxidant and phenolic compounds. Despite Malaysia being a tropical country with rich and unique biodiversity, there are relatively little research done on solid-liquid extraction of antioxidants from local traditional medicinal plants and their kinetic modelling. In this critical review, the steps to carry out the study of solid-liquid extraction of antioxidant in plants and its kinetic modelling are discussed. Detailed steps of the experiment are included such as preliminary testing, analysis of antioxidants and total phenolic compounds, available potential kinetic model for trial, and the factors affecting the extraction process. The common practice and aspects of carrying out the experiment of plant solid-liquid extraction and their kinetic modelling are being identified and reviewed.

ID: FYP2020/6

SEDIMENTATION KINETIC OF ELECTROSTERICALLY STABILIZED MAGNETIC NANOPARTICLE: INFLUENCES OF DEPLETION FORCES

CHONG CI EN & LIM JIT KANG
School of Chemical Engineering, Engineering Campus, Universiti Sains Malaysia,
14300 Nibong Tebal, Pulau Pinang, Malaysia

ABSTRACT

Nanotechnology is recently implemented in the wastewater treatment to improve the quality of water for daily human needs. The mixed valence iron magnetite, Fe_3O_4 research is aimed to determine the influence of the aggregation and sedimentation kinetic of the MIOPs exposed to the freely suspended polyelectrolyte. The study of sedimentation of the magnetic nanoparticles was done in anionic condition. The measurement was done using UV vis as the absorbance of the FMIOPs suspension undergoes aggregation and sedimentation in without influence by magnetic field. The mathematical analysis was also conducted to determine whether the settling of the cluster was affected by not only depletion force, but also the molecular weight and the viscosity of the medium. For the FMIOPs cluster, the sedimentation phase was divided into 2 phases when the concentration of the MIOPS is high. This might be due to the hydrodynamic size of the nanosphere cluster. The Mathematical analysis was conducted revealing the relationship between the settling velocity of the FMIONP clusters and the depletion force. In the condition of high concentration of the FMIOPs, two distinctive sedimentation stage was obtained. This might be due to the packing density of the FMIOPs cluster. In PSS1000k, the system showed more stable as the aggregation time taken was longer and the sedimentation rate was lower than PSS70k as well as DI.

ID: FYP2020/7

STUDY ON THE GREEN COAGULANT FOR DYES REMOVAL IN TEXTILE INDUSTRY

CHONG SOON XIN & SUZYLAWATI ISMAIL
School of Chemical Engineering, Engineering Campus, Universiti Sains Malaysia,
14300 Nibong Tebal, Pulau Pinang, Malaysia

ABSTRACT

This research investigated and evaluated mung bean and pigeon pea as natural coagulants to eliminate cationic dye (methylene blue) and anionic dye (direct yellow) for textile industry wastewater treatment. Plant seeds were chosen due to low-cost and high accessibility. Pre-treatment of the plant seeds using ethanol was performed to avoid the cloudiness in the coagulation activity. Response surface methodology (RSM) built with four-variables, central composite design (CCD) was utilised to analyse and optimise the treatment activity. The effect and interaction among the process parameters towards the removal of dyes namely pH, initial dye concentration, coagulant dosage and mixing time in an orbital shaker were analysed. Three reduced quadratic model equations were built independently for three distinct conditions. The results obtained employing the developed model suggested that the optimum conditions for removing methylene blue using mung bean were pH at 11, initial dye's concentration 50 mg/L, 3 g of dosage and 135 minutes mixing time. The optimised conditions for removing methylene blue using pigeon peas were similar to using mung bean except for the pH at 9.792. The removal efficiency was predicted by the RSM model as high as 98.491% and 96.974% for mung bean and pigeon pea. Results indicating pH contributes to the dramatic effect in the removal efficiency while natural coagulant tend to regulate to the initial pH dye solution during the treatment process. In short, mung bean and pigeon pea are more suitable for removing cationic dye (methylene blue) compared to anionic dye (direct yellow) in which mung bean depicts a slightly better performance in methylene blue dye removal efficiency.

ID: FYP2020/8

MODELLING OF GAS DIFFUSION IN MESOPOROUS BASED GAS SENSOR

ERFAN HAKIM AZMAL ZAID & MOHAMAD ZAILANI ABU BAKAR
School of Chemical Engineering, Engineering Campus, Universiti Sains Malaysia,
14300 Nibong Tebal, Pulau Pinang, Malaysia

ABSTRACT

Influences of gas diffusion phenomena have been theoretically studied on the sensitivity of a mesoporous thick film tin dioxide gas sensor. Diffusion equation was formulated as a function of Knudsen diffusion constant (D), film thickness (L) and gas concentration (C_{A_S}) under steady-state first-order kinetic reaction. Further, assuming that the temperature dependence of Arrhenius rate constant (k) and sensitivity coefficient (a) was derived from a general expression of sensitivity (S) involving temperature and gas concentration. Previous research shows that sensitivity versus sensor operating temperature resulted in a bell-shaped graph variability with optimum temperature, whereas increasing gas concentration resulted in increased sensitivity before saturation was reached. Based on the simulation result, the sensitivity analysis is increase with the concentration of target gas increase. The modification of the model was done by introducing Thiele Modulus. By comparing the previous result and simulation by MATLAB, it is noticed that the sensitivity will increase with the increasing of temperature and this is not following the trend. This can be said the model is not suited for the stimulated various operating temperature. Sensitivity analysis was performed base on film thickness, L and pore radius, r. Based on the simulation, the sensitivity increasing with the increase with the thickness of film decrease due to stronger contact between target gas and the surface of the sensor. for the simulation of pore radius in model, the sensitivity increases with the pore radius increase at the fixed temperature and can be explained by Knudsen equation, D_k.

ID: FYP2020/9

ROLE OF NUTRIENTS IN INCREASING MICROALGAE SETTLEABILITY

FARAH YASMIN MOHD NAWAWI & VEL MURUGAN VADIVELU
School of Chemical Engineering, Engineering Campus, Universiti Sains Malaysia,
14300 Nibong Tebal, Pulau Pinang, Malaysia

ABSTRACT

The usage of microalgae in industrial application not only shows prominent features of microalgae, but also increasing the demand of its cultivation. However, the current microalgae technologies faced with some issue including harvesting of microalgae biomass to separates microalgae from the culture medium. Settleability of microalgae are among the features that can cause the difficulty in separation step. Properties and configuration of various species microalgae have been analysed and explored by the researchers in effort to increase the efficiency of microalgae settleability. This work study the effects of nutrients on microalgae growth and settling efficiency

by provided different amount of nutrients for each different biomass concentration. During the continuous feed study, the results show that microalgae experience a lag growth during the beginning of experiment due to the prolong adaptation phase. The settleability still increase for all three reactors since the nutrients were provided daily and this could enhance the microalgae flocculation. In the starvation study, the nutrients were consumed completely in the first three days. Hence, the growth shows increment until reached saturation. The settleability in starvation study also show increment for all reactors due to growth increment. Excessive feeding study shows unstable trend for both growth curve and settling efficiency.

ID: FYP2020/10

EFFECT OF MEMBRANE POST-TREATMENT TOWARDS PORE COLLAPSE PHENOMENA DURING DRYING PROCESS OF FLAT SHEET ASYMMETRIC POLYETHERSULFONE (PES) MEMBRANE

HO HAI PING & ABDUL LATIF AHMAD
R3School of Chemical Engineering, Engineering Campus, Universiti Sains Malaysia,
14300 Nibong Tebal, Pulau Pinang, Malaysia

ABSTRACT

Recently, membrane-based processes have become one of the most dominant technology and advances at a remarkable speed in industrial separation applications. Compared to conventional technology, membrane-based processes offer better performance in terms of treatment efficiency and product quality which makes it more preferable. Polyethersulfone (PES) has emerged as one of the most important commercial polymeric materials that is widely used as a promising material for membrane fabrication in gas separation field due to its excellent mechanical strength, wide temperature limits as well as great chemical and thermal stability. One of the phenomena that has high impact on performance of PES membranes is pore collapse. For flat sheet PES membrane to be implemented in gas separation application, the membrane needs to undergo drying process. However, PES membrane usually subjected to pore collapse due to loss of pore filling fluid with high surface tension (usually water) during membrane drying process, which eventually leads to irreversible loss of flux and decrease in membrane permeability. In order to solve this issue, it is crucial for flat sheet PES membrane to undergo post-treatments via solvent exchange method to retain its porous structure and permeability flux to optimize membrane performance in industrial gas separation applications. The objective of this study is to study the effects of membrane post-treatment on pore collapse of polyethersulfone (PES) flat sheet membrane. In this current study, prior to membrane drying process, flat sheet PES membrane samples were allowed to carry out post-treatments via solvent exchange method, where the water inside membrane pores was replaced with fluids of lower surface tension. The post-treatments of membrane were carried out by immersing PES membrane samples in ethanol, hexane and glycerol prior to drying. Fabricated membrane samples were characterized by SEM, FTIR-ATR, contact angle and porosity measurement along with gas permeation test for performance evaluation. The results were then compared with air-dried PES membrane samples without post-treatments. From the results of gas permeation test, it is shown that PES membrane samples that undergone post-treatments had improved nitrogen permeance ranges from 346.36% to 1980.56% as compared to air-dried PES membrane. Among the post-treatment solvent, hexane-treated membrane had the highest nitrogen permeance with permeance improvement of more than 1000%, which is supported by its highest surface porosity and surface pore size, along with highest bulk porosity as mentioned in characterization results. This proves that hexane-treated membrane was the least collapsing membrane with lowest degree of pore collapse. On the other hand, due to high viscosity, glycerol did not evaporate during membrane drying, which results in membrane pore blockage, thus causes unavailability of data in nitrogen permeate flux.

ID: FYP2020/11

METHANE AND CARBON DIOXIDE ENRICHMENT FROM STRANDED NATURAL GAS BY MEMBRANE GAS SEPARATION: EFFECTS OF SELECTIVITY ON PURITY AND RECOVERY OF THE GASES

JANICE NG JIA YEE & MOHD ROSLEE OTHMAN

School of Chemical Engineering, Engineering Campus, Universiti Sains Malaysia,
14300 Nibong Tebal, Pulau Pinang, Malaysia

ABSTRACT

Simulated methane and carbon dioxide enrichment from stranded natural gas by gas separation membrane has been presented in this thesis. The simulation was carried out to study the effect of carbon dioxide composition in feed gas, stage cut and pressure ratio on purity and recovery of CH_4/CO_2 and effect of separation factor (selectivity) on purity and recovery of CH_4/CO_2 of stranded natural gas. Complete mixing model was used to simulate the results by using Mathcad and optimization of performance was conducted by using Response Surface Methodology in Design Expert. The optimized CH_4 purity and recovery at retentate were 71.02% and 75.77% whereas for CO_2 in permeate were 56.13% and 89.71% respectively at 0.284 CO_2 feed composition in mol fraction, 0.45 of stage cut and pressure ratio of 10. As for stranded natural gas with CO_2:CH4 ratio constant at 7:3, CH_4 purity of 82.50% and 100% of recovery were obtainable at separation factor α_{CH_4/CO_2} of 849.5, stage cut of 0.39 and pressure ratio of 36.7. At this condition, the optimized CO_2 purity was obtainable at 76.15% and recovery at 95.26%. This study showed that the membrane with superior methane permeability than carbon dioxide permeability is needed in order to surpass the performance of PSA in methane enrichment process.

ID: FYP2020/12

STUDY ON THE ADSORPTION OF THIN COATED ADSORBENT FORMULATION ON SULFAMETHOXAZOLE

JEREMY MUSA & SUZYLAWATI ISMAIL
School of Chemical Engineering, Engineering Campus, Universiti Sains Malaysia,
14300 Nibong Tebal, Pulau Pinang, Malaysia

ABSTRACT

The influence of three different physical factors on the adsorption of sulfamethoxazole (SMX) on a zwitterionic adsorbent composite coating (ZACC) has been studied, namely; pH, initial concentration and temperature. Adsorption is a method proposed to remove SMX from pharmaceutical effluents which has multiple pros over other removal methods. The ZACC studied is low in cost and simple to fabricate. This gives it an edge a cost-effective treatment method for SMX. In this study, SMX removal percentage and adsorption capacity of ZACC is evaluated. The results show that the highest removal percentage was achieved by initial concentration of 10 ppm while the lowest is percentage removal is seen for initial concentration of 50 ppm which are 58.8 % and 50.11 % respectively. For the study of varied pH values, the best SMX removal percentage was achieved at pH 7 (58.48 %). Increasing and reducing pH values both affected the removal percentage of SMX negatively. Among all the temperatures at which the experiments were conducted, the highest temperature of 75 ^{0}C achieved the best removal of SMX.

ID: FYP2020/13

ULTRASOUND ASSISTED EXTRACTION OF ANTHOCYANINS FROM *CLITORIA TERNATEA* USING GREEN SOLVENTS: OPTIMIZATION AND STORAGE STABILITY STUDY

KANAGESVARI A/P K. ANNAMALAI & MASRINA MOHD NADZIR
School of Chemical Engineering, Engineering Campus, Universiti Sains Malaysia,
14300 Nibong Tebal, Pulau Pinang, Malaysia

ABSTRACT

A step-by-step optimization of the ultrasound assisted extraction (UAE) process was carried out to establish an eco-friendly and sustainable methodology for anthocyanin recovery from *Clitoria ternatea* (*C. ternatea*) flowers that is commonly used as natural coloring in food and cosmetic industries. The solvent screening for UAE was performed using water, 60% (w/v) glycerol and 90% (w/v) glycerol. The results revealed that 60% (w/v) glycerol extracted the highest amount of anthocyanins of 104.90 ± 3.73 mg/L. In this research, further optimization of anthocyanin extraction using 60% (w/v) glycerol was designed using Taguchi method by applying a L27 orthogonal array and signal to noise ratio to investigate the performance of parameters, which are the extraction time (30-50 mins), temperature (40-60^{o}C) and solvent to solid ratio (10:1-30:1) and find the most

influencing parameters in the extraction. The optimal combination of these factors on the ultrasound assisted extraction is an extraction time of 30 min, a temperature of 50°C and a solvent to solid ratio equal to 10:1. The anthocyanin yield obtained from the optimal combination is 115.22 ± 4.20 mg/L. Changes in color and storage stability of the *C. ternatea* extract affected by light, temperature and pH were further evaluated. Results indicated that *C. ternatea* anthocyanins had good color stability with lower percentage degradation of anthocyanins when stored in the dark (11.43%), temperature of 4°C (10.57%) and pH 1.0 (11.29%) to pH 4.5 (20.89%) during the 7 days of storage. The color of *C. ternatea* anthocyanin extract varied according to the changes in pH. The anthocyanin in *C.ternatea* gave intense red, purplish blue, deep blue and bluish green at pH 1.0-9.0.

ID: FYP2020/14

DYNAMIC ADSORPTION OF PHENOL USING MICROWAVE INDUCED COCONUT SHELL ACTIVATED CARBONS

KARTIKAH A/P SELLAPPAN & AZAM TAUFIK MOHD DIN
School of Chemical Engineering, Engineering Campus, Universiti Sains Malaysia,
14300 Nibong Tebal, Pulau Pinang, Malaysia

ABSTRACT

Phenolic compounds are organic pollutants that pose a serious threat due to its high toxicity and carcinogenicity even at low concentrations. Several methods were introduced for the separation process of phenol, however, adsorption is preferred for its low cost and high quality treated wastewater especially for well-designed sorption processes. In this study, the adsorption of phenol in aqueous solution using coconut shell activated carbons (CSACs) was investigated. Characterization of CSACs before and after adsorption was done by using Fourier Transform Infrared (FTIR) and Scanning Electron Microscopy-Energy Dispersive X-Ray Spectroscopy (SEM-EDX). The results of FTIR and SEM-EDX have confirmed the presence of phenol molecules on the surface of CSACs after adsorption. Column adsorption studies were performed to evaluate the effects of some parameters such as initial concentration of phenol (10, 20, 30, 40 and 50 ppm), flow rate of phenol solution (5, 6, 7, 8 and 10 mL/min) and column's bed height (3, 4 and 5 cm). It was found that the breakthrough time, t_b and adsorption capacity, $q_{e(exp)}$, decreased with increasing initial concentration and flow rate and increased with increasing height of column bed. Besides, three dynamic models namely, Adams-Bohart, Thomas and Yoon-Nelson models were used to predict the breakthrough characterisitics and the result was compared with experimental data. The data of continuous adsorption of phenolic compounds on CSACs agreed well with Yoon-Nelson model with highest r^2 of 0.9877 and lowest SSE of 0.002. Finally, scale up adsorption column study was conducted to predict the mass-transfer zone and concentration profiles in the bed. It was evident that unused bed height, H_{UNB} increased as the initial phenol concentration and flow rate increase but decreased as the bed height of the column increase.

ID: FYP2020/15

NANOSTRUCTURED LIPID CARRIER: RECENT REVIEW ON TOPICAL DRUG DELIVERY APPLICATION

KAWIN PATTARANUKUL & NUR AYSHAH ROSLI
School of Chemical Engineering, Engineering Campus, Universiti Sains Malaysia,
14300 Nibong Tebal, Pulau Pinang, Malaysia

ABSTRACT

The development of lipid nanocarriers is an alternative to polymeric nanoparticles, emulsions and liposomes. Further, solid lipid nanoparticles (SLN) was introduced as the first generation of lipid nanoparticles, while nanostructured lipid carriers (NLC) is the second generation which was developed from SLN. NLCs were developed to overcome problems associated with SLN and are utilized in various therapeutic applications. Characterization of NLCs is a major challenge due to the small particle size that results in system complexity. It is an essential requirement for product quality control and necessary to consider the parameters that directly affect the stability and release kinetics of NLCs such as particle size, zeta potential and polydispersity index. There are currently various techniques for the preparation of NLC using in industries such as high-pressure homogenization technique, phase inversion techniqu, microemulsion technique and ultrasonication technique. There are many products using NLC incorporation which has been launched into the market such as NanoRepair Q 10 Cream and

Serum and NanoVital. This article describes the NLC in terms of structures, preparation methods, characterisation, stability and its advantages over lipid nanoparticles of first generation. The article also provides an overview of relevant application studies, such as the cosmetic benefits of lipid nanoparticles, food applications of NLC which can enhance the chemical and physical properties of products. Review focuses primarily on the different therapeutic applications of NLCs and their sensitivity to various physiological proximities.

ID: FYP2020/16

PHYSICOCHEMICAL PROPERTIES OF CHOLINE CHLORIDE BASED NATURAL DEEP EUTECTIC SOLVENTS

KHO LI JIA & FADZIL NOOR GONAWAN
School of Chemical Engineering, Engineering Campus, Universiti Sains Malaysia,
14300 Nibong Tebal, Pulau Pinang, Malaysia

ABSTRACT

Deep eutectic solvent (DES) is the mixture of two components that can associate with each other through hydrogen bonding and form homogeneous liquid at room temperature. Nowadays, DESs have emerged as an alternative solvent to replace conventional solvent in extraction process. However, DES with high viscosity has affected the efficiency of the extraction process. In order to solve this problem, water as co-solvent is added to enhance the viscosity of deep eutectic solvents but adding water will also affect others physicochemical properties of solvent. Therefore, physicochemical properties of pure DES and DES with water have to be studied. Choline chloride was used as hydrogen bond acceptor to mix with different hydrogen bond donors such as urea, glucose and citric acid to form choline chloride based deep eutectic solvent by using heating method. Eutectic composition of these DESs will be determined by using trial and error method. Physicochemical properties of DESs at different water content and temperature are being studied by using appropriate equipment such as rheometer and conductivity meter. Choline chloride-based DES with citric acid is having highest viscosity (11200cP) and density (1.4741g/mL) as well as lowest conductivity (228.4μS/cm) due to strong hydrogen bonding network between choline chloride and citric acid that restrict the movement of molecules. Effect of temperature on these three DESs can be well described by using Andrade's equation. Increase in water content will cause the density to decrease and the conductivity to increase. In a nutshell, suitable solvents for extraction process could be produced by altering the factors such as temperature, water content and nature of HBDs.

ID: FYP2020/17

STUDY OF EQUILIBRIUM AND NON-EQUILIBRIUM MODEL OF REACTIVE DISTILLATION COLUMN FOR THE PRODUCTION OF METHYL TERTIARY BUTYL ETHER (MTBE)

KHOO CHING YI & MUHAMAD NAZRI MURAT
School of Chemical Engineering, Engineering Campus, Universiti Sains Malaysia,
14300 Nibong Tebal, Pulau Pinang, Malaysia

ABSTRACT

Methyl Tertiary Butyl Ether (MTBE) is a valuable gasoline's octane number booster. Reactive distillation column is usually used to produce MTBE as high yield of MTBE can be obtained. However, due to the high cost of practical experiment on reactive distillation column, the development of MTBE reactive distillation model is an essential tool to study the process as well as to investigate the optimum production of MTBE. This report was carried out to develop a MTBE distillation column model using Aspen Plus and study the equilibrium model as well as the non-equilibrium model of reactive distillation column. A simulation of reactive distillation column has been developed and validated by comparing the simulation results obtained with the data collected from the literature. The validated model is then further used to study the effect of Methanol feed flow rate, mixed Butene feed flow rate and reflux ratio on the MTBE purity and Isobutene conversion. Then, optimization was carried out to determine the optimum operating parameter of the reactive distillation column. 209.3 mol/s of Methanol feed flow rate, 583.2 mol/s of mixed Butene feed flow rate and reflux ratio of 7 able to achieve 99.99% MTBE purity and 96.92% of Isobutene conversion. Lastly, a non-equilibrium model has been developed. Simulation results obtained from equilibrium model and non-equilibrium model were compared with industrial MTBE plant data and it is found that non-equilibrium model is more accurate to the real system.

ID: FYP2020/18

REMOVAL OF PHOSPHORUS USING *POLYMESODA EXPANSA* AND *POMACEA CANALICULATA* SHELLS

KISHENTAR A/L RAJA KUMAR & MASRINA MOHD NADZIR
School of Chemical Engineering, Engineering Campus, Universiti Sains Malaysia,
14300 Nibong Tebal, Pulau Pinang, Malaysia

ABSTRACT

Approximately 70 million tons of organic waste are estimated to be produced annually and such waste is either incinerated or dumped to landfill, all of which have significant environmental impacts. In this present work, the kinetic of phosphorus removal by *P.caniculata* and *P.expansa* shell were investigated and their characteristics as an adsorbent were also evaluated. *Pomacea Canicualta (P.canalicualata)* and *Polymesoda expansa(P.expansa)* prepared at 250ºC,500°C and 750ºC temperatures through pyrolysis was characterized for physicochemical properties and potential for removal of phosphorus. Elemental study shows that *P.expansa* in addition to silicon (Si) as a component, Polymesoda expansa is composed primarily of carbon (C), oxygen (O), and calcium (Ca). The *P.canalicuta* shell which undergo pyrolysis at 750°C removed almost 56% of phosphate in KH_2PO_4 solution. The *P.expansa* which undergo pyrolysis at 750°C removed almost 70% in KH_2PO_4 solution. The phosphate removal was rapid for all concentration (25–100 mg/L) tested at the beginning of the studies until the first 20 min and gradually reached equilibrium within the first 120 min of the sorption phase. Values ranging from 64% to 72% phosphate removal were obtained in the initial concentration ranging from 25 to 100 mg/L of phosphate at the first 30 minutes of the sorption cycle, while only 10 to 25% of the additional removal occurred within 120 minutes of the contact period before the equilibrium state. The linearity of the reversible kinetic first order model was poor where the R^2 range (0.3763–0.4289). The overall reaction rate, K,(min^{-1}) decreased from 0.475 min^{-1} to 0.257 min^{-1} with an improvement in the initial phosphate concentration from 25 mg/L to 100 mg/L while the forward reaction rate, k_1, was slower than the backward reaction rate, k_2 (min^{-1}) at all the concentrations tested. When the initial concentration of phosphate increased from 25 to 100 mg/L, it was found that I_{resp} increase from 39.17 to75.77 min. It can be concluded that the adsorbents from *P.expansa* shell which undergo pyrolysis at 750°C shows a good potential to be used for removal of phosphorus

ID: FYP2020/19

PRODUCTION OF ETHYL ACETATE BY ESTERIFICATION BETWEEN ETHYL ALCOHOL AND ACETIC ANHYDRIDE IN A SOLVENT FREE SYSTEM USING MINIATURISED INTENSIFIED REACTOR

KOKILAN A/L BALAN & SYAMSUL RIZAL ABD SHUKOR
School of Chemical Engineering, Engineering Campus, Universiti Sains Malaysia,
14300 Nibong Tebal, Pulau Pinang, Malaysia

ABSTRACT

Ethyl acetate is an important commodity feedstock for a variety of industrial products, and it is also used as an industrial solvent in the manufacture of various chemicals. Ethyl acetate is used primarily as a solvent and diluent, being favoured because of its low cost, low toxicity, and agreeable odour. Ethyl acetate is the most common ester in wine, being the product of the most common volatile acetic acid and the ethyl alcohol generated during the fermentation. Over the time, the esterification process is conducted using enzyme because consumers highly prefer naturally synthesized ester compared to chemically synthesized ester. On the other hand, lately process intensification is gaining momentum among the researchers. This is because the maximum conversion and yield can be achieved in shorter time in miniaturised intensified reactors compared to the large conventional reactors. Thus, this study is conducted to investigate the effect of process parameters in the synthesis of ethyl acetate in a solvent-free system. Acetic anhydride is reacted with ethyl alcohol in miniaturised intensified reactor of internal diameter 2mm to produce ethyl acetate. The effect of operating parameters such as reaction temperature, reaction time and alcohol-acid ratio were studied using One-Factor-At-A-Time (OFAT) method. Moreover, optimization process for operating parameters also done using statistical tool was also investigated using Response Surface Methodology (RSM) method. The trend of the final concentration of isoamyl acetate is

also related to the by-product of this reaction which is the acetic acid. The optimum operating conditions for high yield of ethyl acetate based on OFAT analysis were reaction time of 120 minutes, reaction temperature of 65°C and alcohol-acid ratio of 1:1; meanwhile reaction time of 93.27 minutes, reaction temperature of 64.15°C and alcohol-acid ratio of 1.4881:1 based of RSM analysis.

ID: FYP2020/20

A COMBINATION OF CANONICAL CORRELATION ANALYSIS (CCA) – CONVOLUTIONAL NEURAL NETWORK (CNN) BASED FAULT DETECTION SYSTEM FOR TENNESSEE EASTMAN PROCESS

LEE JIA YING & NORAZWAN MD NOR
School of Chemical Engineering, Engineering Campus, Universiti Sains Malaysia,
14300 Nibong Tebal, Pulau Pinang, Malaysia

ABSTRACT

Fault detection and diagnosis (FDD) is one of the significant elements in the process monitoring system, especially in the chemical process that involved such complex processes and hazardous chemicals. This system secures the safety of the plant by early detection of faults and the advanced management of faults which reduce the possibility of severe accidents. This project focuses on the development and application of CCA-CNN based FDD system in detecting and diagnosis various faults in the Tennessee Eastman Process (TEP). TEP is a commonly used case study that simulated an actual chemical process with multivariate system. Meanwhile, the multilayer of Convolutional Neural Network (CNN) is employed as the neural classifier and Canonical Correlation Analysis (CCA) is applied as the feature extraction mechanism. Hence, the performance of CCA-CNN model for detection and diagnosis of faults on TEP was investigated in the present study to ensure its applicability to correctly classify the faults with a relatively huge volume of input variables. The detection was based on the fault-free and faulty conditions that available in the database while the classification through the model will be trained, validated, and tested using the neural net pattern recognition tool in MATLAB. An optimum CCA-CNN configuration was acquired by using the proposed approach in this report with the highest accuracy of 95.8 % and minimal error rate at 4.2 %.

ID: FYP2020/21

SYNTHESIS OF POLYETHYLENE TEREPHTHALATE/MULTIWALLED CARBON NANOTUBES ADSORBENT FOR METHYLENE BLUE ADSORPTION

LEE SIEW MUN & TAN SOON HUAT
School of Chemical Engineering, Engineering Campus, Universiti Sains Malaysia,
14300 Nibong Tebal, Pulau Pinang, Malaysia

ABSTRACT

Dyes produced by textile and chemical industries have brought along with it many detrimental effects to our ecosystem. Water pollution is one of the typical undesirable environmental problems and it requires effective solutions. The aims of this study were to synthesis polyethylene terephthalate/multiwalled carbon nanotubes (PET/MWCNTs) adsorbent and to examine its performance in comparison with PET adsorbent which was without any functionalization on the adsorption of methylene blue (MB). Both adsorbents were synthesised via phase inversion. Several variables on the adsorption of MB such as contact time, amount of adsorbent and initial dye concentration was studied in a batch adsorption method. It was found out that 2880 minutes was the optimized contact time for the adsorption. PET/MWCNTs with removal efficiency of 51.53% and adsorption capacity of 0.3162 mg/g was found to be higher than PET which was only 23.05% and 0.1421 mg/g respectively at initial MB concentration of 6 mg/L, showing that PET/MWCNTs was a better adsorbent than PET. The adsorption capacity for both adsorbents decreased while the MB dye removal percentage increased with increasing adsorbent dosage. When the initial concentration rose from 2 mg/L to 10 mg/L, the adsorption capacity increased but the removal percentage decreased for both adsorbents. The data obtained were well fitted with Langmuir (Type II) adsorption isotherm model and the R_L values were in the range of 0 to 1. Kinetic studies of adsorption by using both adsorbents were better described by pseudo-second-order model. Overall, the results of this study showed

that PET/MWCNTs can be a potential adsorbent to remove dyes from wastewater. The outcome of this research project has triggered a potential to recycle waste PET bottles to produce adsorbents for dye removal.

ID: FYP2020/22

EFFECT OF REACTOR CONFIGURATION ON MICROALGAE SETTLEABILITY

LIM KEE SHIAN & VEL MURUGAN VADIVELU
School of Chemical Engineering, Engineering Campus, Universiti Sains Malaysia,
14300 Nibong Tebal, Pulau Pinang, Malaysia

ABSTRACT

Over the past decades, microalgae have been identified as a potential alternative resource for biofuel production. The increasing demand for microalgae accelerates the scientific research related to microalgae production. Microalgae are generally low density and small in particle size, these make the harvesting and separation processes of microalgae energy-intensive, thus reduces feasibility of scale-up. The primary purpose of this project is to study the effect of height to diameter (H/D) ratio of reactor on the cultivation of microalgae with improved settleability. In this study, the microalgae were cultivated in two 8L photobioreactors with different dimensions, namely H5 (H/D: 4.67) and H8 (H/D: 15). Different analyses such as sludge volume index (SVI), extra polymeric substances (EPS), particle size distribution and settling efficiency were used to study the interconnectivity between H/D ratio of reactors and settleability of microalgae. In addition, nutrient consumption and growth phase of the microalgae were also investigated in this research. The results showed that the lowest SVI (12.73 mL/g) and highest settling efficiency (95.02%) were obtained in reactor H8 which has a higher H/D ratio. The good flocculation performance of reactor H8 was caused by the high protein to polysaccharide (PN/PS) ratio in EPS. It was also shown that the microalgae in reactor H8 were larger in particle size (percentile d(0.9)= 266.54μm) compared to reactor H5 (percentile d(0.9)= 121.86μm) on Day 70. These proved that H/D ratio of the reactors have notable impact of microalgae settleability.

ID: FYP2020/23

OZONATION OF METHYLENE BLUE AND RHODAMINE B: PARAMETERS STUDY AND MODELLING THE REACTION KINETIC

LIM RUEI JIA & AHMAD ZUHAIRI ABDULLAH
School of Chemical Engineering, Engineering Campus, Universiti Sains Malaysia,
14300 Nibong Tebal, Pulau Pinang, Malaysia

ABSTRACT

Ozone application has been emerged to be a reliable approach on dye removal due to its extraordinary high oxidation potential. However, the performance of ozone process is much affected by operational parameters. In this study, the factors affecting the colour removal rate of two basic dyes, methylene blue (MB) and rhodamine B (RB) were investigated. From the result, the ozone successfully removes up to 95% of colour within reaction time of 30 minutes and applied ozone dosage at 500cm3/min for both dyes with initial dye concentration ranging from 5mg/L to 15mg/L. However, MB required longer time to decolourised in all sets of experiment. This showed that thiazine structure (MB) is less susceptible to electrophilic attack than xanthene (RB). Both initial dye concentration and applied ozone dosage has significant effect on dye removal, with similar trend for both dye. The colour removal efficiency increases with increasing ozone dosage and decreasing initial dye concentration. Meanwhile, the decolourization of MB and RB was favourable at pH of 11 and 3 respectively. This is due to different oxidizing species where molecular ozone is predominant under acidic condition whilst reactive hydroxyl is more pronounce at alkali condition. Molecular ozone was found to be more selective towards certain dye structure during ozonation process, as in this case, RB. Kinetic study verified that ozonation of both MB and RB was in accordance to pseudo-first-order reaction with an average $R2$ of 0.986. This study may provide insights on enhancement of ozone performance via identification of preferable operating condition, mechanism and characteristic of dye. The outcomes may help in designing a practical system in real scenario.

ID: FYP2020/24

DESIGN OF A MECHANICALLY DRIVEN MAGNETIC STEERING SYSTEM FOR RAPID MAGNETOPHORESIS CONTROL AND SWITCHING

LIM XIU XIAN & LIM JIT KANG
School of Chemical Engineering, Engineering Campus, Universiti Sains Malaysia,
14300 Nibong Tebal, Pulau Pinang, Malaysia

ABSTRACT

This study discussed about the design and the implementation of the permanent magnetic steering system comprising of four neodymium-boron-ferrite magnets in quadrupole arrangement, and four Arduino servo motors to magnetically guiding a 1mm stainless steel s304 bead onto the targeted pathway in a 1.2cm × 1.2cm dimension workspace. In recent advancements, electromagnetic steering system has frequently been used as the tools for the cell manipulation. However, the significant weaknesses of the electromagnetic steering system are high energy consumption, high installation cost and operation cost and the high chances for the cells subjected to the joule heating and thus, permanent magnetic steering system has been proposed as a solution for the issues caused by the electromagnetic steering system. In this study, the main concerns are to develop a fully automated permanent magnetic steering system which shows the capability of guiding the stainless-steel bead and to analyse the impacts of the magnetic actuations towards the magnetophoretic control pathways of the bead. The strategies used in this study are first constructing the permanent magnetic steering system to implement mechanical actuation on the magnets via the servo motors, followed by the recording the trajectories of the bead in the workspace via 60fps camera to generate the time lapsed images of the bead under magnetophoretic control. The information on the position of the bead via the images enable the instantaneous velocity, the magnetophoretic force onto the bead and the magnetic flux density generated via the magnetic steering system being recovered. Furthermore, the magnetic flux density generated is then predicted via the numerical analytical solutions and being compared with the experimental results. The study's results depict the successful control over the bead towards the desired path within the working space through both cases i.e. the actuation of single magnet and the actuation of pair magnets. However, it is observed that due to the synchronous errors between servo motors in which the maximum time delay at 0.067s, the position of the bead deviates from the references path as obtained from ideal cases. The permanent magnetic steering system proposed can generate the magnetic flux density of 0.0015T for actuation of single magnet and 0.003T for actuation of pair magnets at the centre of the workspace of the bead. Based on the experimental results, it can be deduced the permanent magnetic steering system proposed is able to guide the bead towards the desired paths which are horizontal, vertical and diagonal path, but further improvements are needed to resolve the synchronous errors from the motors issue.

ID: FYP2020/25

PREPARATION OF OIL PALM FROND BASED ACTVATED CARBON VIA MICROWAVE IRRIADATION FOR METHYLENE BLUE AND REMAZOL BRILLIANT VIOLET 5R REMOVAL

LOH CHIAN YONG & MOHD AZMIER AHMAD
School of Chemical Engineering, Engineering Campus, Universiti Sains Malaysia,
14300 Nibong Tebal, Pulau Pinang, Malaysia

ABSTRACT

The production of activated carbon (AC) made from renewable and cheap agricultural waste had been studied as an alternative to existing commercial AC. In this study, oil palm fronds (OPF) had been chosen as precursor because of its high carbon content and readily available in Malaysia. Oil palm fronds based activated carbon (OPFAC) was prepared through a physical activation process involving microwave irradiation and carbon dioxide gasification. Efficiency of the OPFAC was determined by batch adsorption study of methylene blue (MB) and Remazol Brilliant Violet 5R (RBV) groups. The optimum preparation conditions obtained from Response Surface Methodology (RSM) were obtained at 264 W irradiation power and 4 minutes of activation time resulting in 98.36% MB and 31.72% RBV removal. The optimized OPFAC was characterized through Brunauer-Emmett-Teller (BET) surface area, proximate and elemental analysis, Scanning Electron Microscopy (SEM) and Fourier transform infrared spectroscopy (FTIR). High BET surface area, total pore volume and fixed carbon content for OPFAC were found at 425.40 m^2/g, 0.3252 cm^3/g and 75.20 %, respectively. The OPFAC had heterogenous pore

size in mesoporous region with average pore diameter of 2.86 nm. For batch adsorption study, the effect of initial dye concentration (50 – 300 mg/L) and contact time (0 – 24 hours) were evaluated. The MB and RBV adsorption uptake by optimized OPFAC were increased as the initial dye concentration and contact time increased. OPFAC was found to have better performance in removing MB compared to RBV dye due to presence of azo bond in chemical structure of RBV which was stronger and more resistant than any physio-chemical bonds existing in MB. The obtained equilibrium data for MB dye was best fitted by Langmuir model while Temkin and Freundlich model exhibited better fit for RBV adsorption equilibrium. Meanwhile, the kinetic data of both adsorbent-adsorbate systems were best represented by pseudo first order model. All the adsorption processes were controlled by film diffusion mechanism.

ID: FYP2020/26

IMMOBILIZED LIPASE-CATALYZED ESTERIFICATION OF FORMIC ACID AND ETHANOL FOR SYNTHESIS OF ETHYL FORMATE: PROCESS OPTIMIZATION

LOW TING PENG & AZLINA HARUN @ KAMARUDDIN
School of Chemical Engineering, Engineering Campus, Universiti Sains Malaysia,
14300 Nibong Tebal, Pulau Pinang, Malaysia

ABSTRACT

The common method for esterification synthesis, either by chemical synthesis or natural sources extraction often involved several drawbacks such as massive spent acids, poor yields and environmental issues. Hence, lipases which has proven to have tremendous potential as biocatalyst in the production of ester through enzymatic esterification is the main alternative. In this study, ethyl formate, a commercially valuable formate ester, was synthesis by direct esterification reaction catalysed by immobilised lipase from Candida *rugosa* in batch system using *n*-hexane as organic solvent. The free Candida *rugosa* lipase was successfully immobilised on Amberlite MB-1 support with catalytic activity of 582.3 U/g. The influence of optimizing parameters including reaction time, enzyme loading, temperature, agitation speed and formic acid:ethanol molar ratio were studied using one-at-a-time (OFAT) method. Optimal conversion yield for ethyl formate of 91.2 % ± 0.59% was obtained at 1.5 hours incubation time with 20 U/ml of enzyme loading at 40 ℃ and 150 rpm with a substrate molar ratio of 1:3 (formic acid to ethanol). Response surface methodology (RSM) based on five-level-four-factor central composite rotatable design (CCRD) was further used to study the interactive effects of synthesis, of enzyme loading (10-40 U/ml), temperature (30-50 ℃), agitation speed (100-200 rpm) and substrate molar ratio (1:1-1:5, formic acid:ethanol). The study reveals that substrate molar ratio was the most effective parameter for ethyl formate synthesis followed by enzyme loading. The optimum conditions derived from RSM were of temperature 40 ℃, enzyme loading of 35 U/ml, agitation speed of 150 rpm and substrate molar ratio of 1:2.75 with an experimental yield of 92.7 % under optimum condition, which compared well to the maximum predicted value of 93.87 %. The comparison between bisubstrate kinetic models of enzyme catalyzed esterification by correlating experimental findings from reported research study was also investigated using non-linear regression analysis. A model of Ping Pong Bi Bi with inhibition by both substrate was found to exhibit the best fit with the experimental data with R^2 value of 0.9993 where the model parameters were obtained as V_{max} = 53.27 mmol g^{-1} h^{-1}, $K_{m,A}$ = 55.2 mmol L^{-1}, $K_{m,B}$ = 14.19 mmol L^{-1}, K_{iA} = 14.77 mmol L^{-1}, and K_{iB} = 224.17 mmol L^{-1} which shows good agreement to the reported findings.

ID: FYP2020/27

GROWING *SCHIZOPHYLLUM COMMUNE* THROUGH SOLID-STATE FERMENTATION, SSF AND TOWARDS CELLULASE ENZYME PRODUCTION

MASLIANA MOHAMED SABIB & MOHAMAD HEKARL UZIR
School of Chemical Engineering, Engineering Campus, Universiti Sains Malaysia,
14300 Nibong Tebal, Pulau Pinang, Malaysia

ABSTRACT

Schizophyllum Commune, split-gilled mushroom is an edible mushroom grown on woody plants. This study was carried out to investigate the cultivation of *Schizophyllum Commune* on different wood substrates and to identify the cellulase enzyme production. Dried banana leaves, which alternative substrate was compared with

sawdust which is the commonly used substrate for commercial production of *Schizophyllum Commune*. A pure culture of *Schizophyllum Commune* used to be got by the way of developing a tissue of the mushroom on Potato Dextrose Agar (PDA) medium. *Schizophyllum Commune* was cultivated on sawdust of rubber and sawdust of oil palm with 5g, 10g, and 15g of dried banana leaves. The suitable incubating temperature for *Schizophyllum Commune* growth on the substrate was obtained at 30℃. Among all cultivation of *Schizophyllum Commune*, the highest rate for *Schizophyllum Commune* growth and cellulase enzyme production was observed in mixtures containing 15g of dried banana leaves on sawdust of rubber. It was 2.1174g of *Schizophyllum Commune* in 20 days and 1.4 mg/ml.

ID: FYP2020/28

SIMULATION ON COVID-19

MOHAMAD ZUL AQIMAN SHUKERI & SUHAIRI ABDUL SATA
School of Chemical Engineering, Engineering Campus, Universiti Sains Malaysia,
14300 Nibong Tebal, Pulau Pinang, Malaysia

ABSTRACT

Coronavirus is virus from wild animals such as snake or bat that been transmitted to human, This Covid-19 virus can spread using surface and air. Health Organisation (WHO), announced outbreak in Wuhan, the province of Hubei, People's Republic of China (PRC), that globally become pandemic to overall world. This aim of work to study of collected total case detected in 4 four country. The research will evaluate daily case, total recovered and total death. Situation, geological or another parameter that main key for spreading Covid-19 inside Country. Malaysia that have high total recovery rate and lowest death rate which is 97.3% and 1.4 % respectively. This efficiency of lockdown or Perintah Kawalan Pergerakan (PKP) show successful to handle of Covid-19 situation. In modern world, country that have high technology as United states of America that cannot handle of Covid-19 situation which as 46.7 % recovered rate. As death rate, Indonesia show highest death rate which is 4.8 %, factor that may be affected of lack of equipment and geological or high-density population affected to handle Covid-19.

ID: FYP2020/29

CORROSION INHIBITION PERFORMANCE OF *Dillenia sp.* LEAVES EXTRACT ON ALUMINIUM IN 1.0 M HYDROCHLORIC ACID SOLUTION

MOHD SYAHMI AZMIN AZMAN & KHAIRIAH ABD. KARIM
School of Chemical Engineering, Engineering Campus, Universiti Sains Malaysia,
14300 Nibong Tebal, Pulau Pinang, Malaysia

ABSTRACT

Aluminium is currently widely used in both industrial and domestic applications due to its light weight, strength, durability and formability. Aluminium is especially suitable in many applications due to the presence of oxide layer and is chemically relatively inert. The excellent resistance to corrosion of aluminium is based on the ground film's inactivity. Corrosion is a natural phenomenon in which metals and alloys are exposed to the surrounding environment. Corrosion is costly due to loss of characteristics of goods, which leads to maintenance loss of resources, device downtime and severe failure of some characteristics, which in some instances can be dangerous to harm. There are many methods and research have been discovered in order to inhibit corrosion of aluminium from occur. One of them that is suitable and environmentally sustainable is by using green corrosion inhibitor. Therefore, in this research study, *Dillenia sp.* leaves extract has been used to discover inhibitive action on aluminium surface in 1.0 M hydrochloric acid using weight loss method by varying the concentration of inhibitor (1.0 – 2.0 g/L) and temperature of solution (30°C - 70°C). Fourier Transform Infrared Spectroscopy (FTIR) analysis was carried out to determine the functional groups of *Dillenia sp.* leaves extract in corrosion inhibition. It can be concluded that the inhibition ability of *Dillenia sp.* leaves extract was influenced by compound with alkene, azide and carboxylic acid functional groups. From the experiment, it was found that the percentage of inhibition efficiency increased as the concentration of inhibitor increased. Meanwhile, the inhibition efficiency decreased when the temperature of the solution was increased. The optimum concentration of this study was obtained at 1.2 g/L of *Dillenia sp.* leaves extract where 99.48% of inhibition efficiency at 30°C was achieved.

Then, adsorption isotherm study has been carried out using Langmuir, Temkin and Freundlich isotherms. Langmuir adsorption isotherm was determined to be the best fit line among other adsorption isotherm where the value of correlation coefficient (R^2) obtained is 0.9994. However, the values of correlation coefficient for Temkin and Freundlich isotherm obtained were lower than Langmuir which are 0.7987 and 0.7985, respectively. Thermodynamic parameters such as activation energy E_a, enthalpy $\Delta H°$ and entropy $\Delta S°$ were calculated and analyzed based on the data obtained from the varying of temperature in corrosion inhibition studies. Activation energy (*Ea*) obtained in the presence of *Dillenia sp.* leaves extract was 62.00 kJ/mol which was higher than the uninhibited corrosion system 51.41 kJ/mol. The increase in metal dissolution activation energy was due to an increase in inhibitor concentration and adsorption. Enthalpy $\Delta H°$ calculated for inhibited and uninhibited corrosion system were 59.37 kJ/mol and 6.52 kJ/mol, respectively. The positive values of ΔH show an endothermic aspect of the process of dissolution that is related to the rise in metal corrosion levels at high temperatures. Entropy $\Delta S°$ also has been calculated for inhibited and uninhibited corrosion systems where the values were -489.26 kJ/mol and -288.61 kJ/mol, respectively.

ID: FYP2020/30

SOLVENT-FREE AND NON-ENZYMATIC ISOAMYL ACETATE SYNTHESIS VIA MINIATURIZED INTENSIFIED REACTOR

MUGELEN RANGASAMY & SYAMSUL RIZAL ABD SHUKOR
School of Chemical Engineering, Engineering Campus, Universiti Sains Malaysia,
14300 Nibong Tebal, Pulau Pinang, Malaysia

ABSTRACT

Isoamyl acetate is a type of ester that has similar flavour to banana which is widely used as banana flavouring in food industries. At first, isoamyl acetate was extracted using tradition method through plants and fruits. Then, production of isoamyl acetate through chemical synthesis has been introduced. However, consumers highly prefer naturally synthesized ester compared to chemically synthesized ester. Lately, researchers giving attention to process intensification due to its numerous advantages in the production of isoamyl acetate. This is because, it is known that maximum conversion and yield can be achieved in miniaturized intensified reactor in short period of time compared to the conventional reactors. Therefore, this study is conducted to investigate the performance of isoamyl acetate production in a miniaturized intensified reactor. The effect of operating parameters such as alcohol to acid ratio, retention time and operating temperatures were studied using One-Factor-at-A-Time (OFAT) method. In addition, optimization process for operating parameters also done using statistical tool which is Response surface Methodology (RSM) method. Then, the results of OFAT and RSM were compared. The results of both OFAT and RSM were reliable because the regression coefficient of both methods is very close to unity.

ID: FYP2020/31

THE SYNTHESIS OF MANGROVE BASED ACTIVATED CARBON AND ITS APPLICATION TO ADSORB ZINC ON THE WASTEWATER INDUSTRY

MUHAMAD AISAR NAFIZ ASWAN & RIDZUAN ZAKARIA
School of Chemical Engineering, Engineering Campus, Universiti Sains Malaysia,
14300 Nibong Tebal, Pulau Pinang, Malaysia

ABSTRACT

Most of the waste from the wastewater industry contains hazardous heavy metals that need to be treated properly. In the developing county, heavy metal contamination is a major concern as most of the industrial activities led to the increase of the heavy metal contamination into lakes, rivers and other water sources. Due to that concern, a significant amount of research has been conducted on the low-cost adsorbent to evaluate their capability in the heavy metal removal. Thus, in this critical review report, summary and evaluation on the mangrove as the low-cost adsorbent has been done. This review evaluates the potential of the mangrove based activated carbon on the specific heavy metal removal which is zinc. Other than that, the evaluation on the major

factor that affects the heavy metal removal is also being discussed which the effect of pH, temperature, initial concentration and contact time on the removal of heavy metal. Optimum pH for the removal of zinc is between 5-7, the optimum temperature is 60ºC, while for the initial concentration, the higher the initial concentration decreasing the zinc adsorption. Lastly, optimum contact time is at 30 minutes to give the highest percentage or zinc removal.

ID: FYP2020/32

MULTIWALLED CARBON NANOTUBES/POLYETHYLENE TEREPHTHALATE (MWCNTs/PET) ADSORBENTS SYNTHESIS FROM WASTE BOTTLES FOR METHYLENE BLUE DYE REMOVAL

MUHAMAD AMMAR SYAHMI MOHD ALI SHAHBANA & TAN SOON HUAT
School of Chemical Engineering, Engineering Campus, Universiti Sains Malaysia,
14300 Nibong Tebal, Pulau Pinang, Malaysia

ABSTRACT

Large proportion of colouring emission into waterway can affect the aquatic life. This main objective of this research project is to evaluate the performance of recycle of polyethylene terephthalate (PET) mineral bottle incorporated with multiwalled carbon nanotube (MWCNTs) to form the PET/MWCNTs adsorbents for methylene blue (MB) dye removal. The scopes of the study included the evaluation of the adsorption performance of MB dyes molecule on PET and PET/MWCNTs adsorbents in a batch process. This project was conducted with the effect of various parameters such as initial concentration, contact time and adsorbent dosage on the adsorption process. The percentage of MB removal was found to be higher at 10mg/L of initial concentration which is 74.1% for PET/MWCNTs and 29.42% for PET adsorbents, respectively. The equilibrium data were evaluated by using Langmuir and Freundlich isotherm model to determine the adsorption behaviour. Freundlich model was found to be the best to describe the uptake of MB dyes. The maximum adsorption capacities by the multi-layer adsorption were 0.67mg/g and 0.84 mg/g onto PET and PET/MWCNTs adsorbents, respectively.

ID: FYP2020/33

CARBON-BASED CONDUCTIVE INK ON ELECTRONIC TEXTILES: RECENT VIEWS ON MATERIALS, METHODS AND APPLICATIONS

MUHAMAD ZULHELMI MOHAMAD SOBRI & LEO CHOE PENG
School of Chemical Engineering, Engineering Campus, Universiti Sains Malaysia,
14300 Nibong Tebal, Pulau Pinang, Malaysia

ABSTRACT

Without changing the natural properties of textile, the electronic textile (E-textile) give the conductive performance to textile. The development of usable chemicals and innovative of their methods of production making the growth of E-textile is demand. It is crucial to develop the innovative methods efficiently by applying these useful chemicals to textiles that can relay additional capability to the textile since textile is a three-dimensional material, porous and anisotropic. Useful carbon-based materials are widely used for comparative low-cost production processes and for the value of their raw materials. Plus, a review of the various carbon-based would be very important to understand and compare their conductive chemicals and their methods of application on textiles for the effective use of those materials in various E-textile applications. This thesis evaluates the common manufacture procedures electronic carbon-based materials, ink formulation methods for producing conductive inks and methods for applying inks on textile substrates. A critical analysis was discussed for comparison and collection of specific carbon-based materials and their textile application methods which is dip coating, screen printing and inkjet printing for the scalable manufacturing process and the electrical properties desired. A critical analysis was discussed for comparison and collection of specific carbon-based chemicals.

ID: FYP2020/34

ADSORPTION OF METHYLENE BLUE DYE AND CHLORAMPHENICOL BY OF ACTIVATED CARBON PREPARED FROM PAPER MILLS SEWAGE SLUDGE

MUHAMMAD AFIQ AHMAD ISMAIL & MOHD AZMIER AHMAD
School of Chemical Engineering, Engineering Campus, Universiti Sains Malaysia,
14300 Nibong Tebal, Pulau Pinang, Malaysia

ABSTRACT

In this research, the paper mills sewage sludge (PMSS) as a precursor for activated carbon (AC) for methylene blue (MB) dye and chloramphenicol (CPA) adsorption has been investigated. The paper mills sewage sludge based activated carbon (PMSSAC) has been prepared using the physical activation and microwave irradiation and the optimization of operating condition which are radiation temperature (W) and activation time (min) has been investigated using response surface methodology (RSM). The result obtained for optimum parameters are 440W and 3 minutes for radiation temperature and activation temperature. The effect of the initial concentration for MB and CPA adsorption has been investigated at from 50 mg/L to 300 mg/L and 24 hours for contact times. The PMSS and optimized PMSSAC has been further studied about the characterization of the samples by using Scanning Electron Microscope (SEM), Simultaneous Thermal Analyzer (STA) and Elemental Analyzer. The SEM image showed that the rough and cratered surface for the PMSS, after activation process, the surface was changed to the formation of the numerous numbers of pores. For proximate analysis, it showed that the result of BET surface area, mesopores surface area, total pore volume and fixed carbon content for PMSSAC were 411.9 m^2/g, 235.0 m^2/g, 0.241 cm^3/g and 72.6 %, respectively. Equilibrium and kinetic adsorption studies for optimized PMSSAC were followed the Freundlich isotherm and pseudo-second order model due to the best fit that found from the calculated graph. In conclusion, the PMSS portrays good potential to be as AC's precursor for dye and drug removal from aqueous solution.

ID: FYP2020/35

BIOSORPTION OF CADMIUM (II) IONS FROM AQUEOUS SOLUTION UTILIZING MODIFIED TAMARIND FRUIT SHELL AS BIOSORBENT

MUHAMMAD AKMAL MOHAMED ARIFFIN & KHAIRIAH ABD. KARIM
School of Chemical Engineering, Engineering Campus, Universiti Sains Malaysia,
14300 Nibong Tebal, Pulau Pinang, Malaysia

ABSTRACT

Biosorption is an effective method for the removal of heavy metals from wastewaters by using agriculture wastes. In this study, tamarind fruit shell (TFS) was chosen as the biosorbent for cadmium (II) ions removal from aqueous solution since they are abundant and can be obtained at almost no cost. Batch experiments were conducted to determine the effects of pre-treatment TFS (acid and alkali), varying value of pH (5-10), dosage of biosorbent (0.2-1.0 g), initial metal concentration (50-300 ppm) and contact time of biosorption (15-240 minutes). The FTIR result shows that the functional group of hydroxyl, alkane, amine and fluro compound. The results proved that the suitable conditions for high biosorption capacity, i.e. 97.6% removal using alkali pre-treated TFS was achieved at pH 8, biosorbent dosage of 0.4 g and initial metal concentration of 100 ppm in 60 minutes contact time. The adsorption isotherm studies were done by using Langmuir, Freundlich and Temkin models and kinetics reaction was studied by pseudo-first order and pseudo-second order kinetic reaction. The biosorption process fitted well with the Langmuir isotherm model (R^2=0.9925) than the other isotherm models. Meanwhile, the second order reaction kinetics fitted well the biosorption process showing that the R^2=0.9992. In conclusion, TFS has the potential to be developed as a low-cost biosorbent to remove cadmium (II) ions from industrial wastewater.

ID: FYP2020/36

DYNAMIC ADSORPTION OF METHYLENE BLUE USING MICROWAVE INDUCE COCONUT SHELL ACTIVATED CARBON

MUHAMMAD FARIS AFIQ ZAINAL AZMAN & AZAM TAUFIK MOHD DIN
School of Chemical Engineering, Engineering Campus, Universiti Sains Malaysia,
14300 Nibong Tebal, Pulau Pinang, Malaysia

ABSTRACT

Most of industries nowadays release waste to the environment and lead to water contamination. Consuming fresh water daily is important as it is a natural source of survival for human health and to run daily activities. Hence, a research study has been carried out study the adsorption of methylene blue dyes as adsorbate onto coconut shell activated carbon (CSAC) as adsorbent. This research will first be highlighting the fixed bed adsorption study to compute the optimum conditions to be used for different parameters such as the initial concentration of methylene blue dyes that is range from 10,20,30,40 and 50 ppm, the inlet flow rate range from 3,4,5,6 and7 ml/min and bed height of adsorbent range from 3,4 and 5 cm. The research studies show that faster breakthrough time will occur if the initial concentration is higher, bed height is lower and inlet flow rate is higher. The research studies continuous will column dynamic analysis using 3 different type of dynamic models which are Adam-Bohart model, Thomas model and Yoon and Nelson model. The analysis shows that Yoon and Nelson showing the most significant model to be used as it fitted well with the presented experimental data compared to Adam-Bohart and Thomas model. Finally, the analysis continues with scale up study of adsorption column in order to find the mass transfer zone and concentration profile in bed. The research studies show that increasing initial concentration and inlet flow rate will decrease the used-up bed height (H_B), while increasing bed height of adsorbent will increase the used-up bed height (H_B).

ID: FYP2020/37

SIMULATION AND OPTIMIZATION OF SINGLE-STEP PROPYLENE OXIDATION FOR ACRYLIC ACID PRODUCTION

MUHAMMAD IMRAN SAZALI & NORASHID AZIZ
School of Chemical Engineering, Engineering Campus, Universiti Sains Malaysia,
14300 Nibong Tebal, Pulau Pinang, Malaysia

ABSTRACT

The production of acrylic acid using the single-step oxidation of propylene is becoming more prominent as the industry grows hence the process should be thoroughly studied and optimized to insure both the production yield and acrylic acid quality are assured prior to its implementation in the industry. Through the use of Aspen Plus V10 simulation software, it is now possible to simulate and optimize the process with the desired end products to maximize the production of acrylic acid. In this study, Aspen Plus V10 is used to simulate and optimize the fluidized bed oxidation reactor (FBR), where the feed propylene undergoes a single-step oxidation to convert into acrylic acid with side products of acetic acid, carbon dioxide and water. The simulation was conducted using parameter obtained from literature to simulate the process using RPLUG reactor model. The simulation results achieved were first compared to that from literature, which showed acceptable errors results of less than 3% for the final composition of the product stream. A sensitivity analysis conducted on the same process model showed that the reactor temperature, reactor pressure, and mole flow of oxygen in the feed has significant effect on the production yield of acrylic acid. From the analysis the highest achieved yield for the three variables were at 240°C, 10 bar, 450 kmol/hr for each case respectively. Lastly, optimization of the reactor model was conducted which yielded a maximum yield of acrylic acid production at 93.397% which was achieved at the optimized operating variables at 210°C reactor temperature, 10 bar reactor pressure, and 450 kmol/hr oxygen mole flow in feed.

ID: FYP2020/38

UTILIZATION OF HYDROTHERMAL CARBONIZATION TO CONVERT COCONUT RESIDUE INTO HYDROCHAR

MYRA SHAHIRA LAU MUHAMMAD ASRAF & NOORASHRINA A HAMID
School of Chemical Engineering, Engineering Campus, Universiti Sains Malaysia,
14300 Nibong Tebal, Pulau Pinang, Malaysia

ABSTRACT

Coconut residue was used in producing hydrochar via hydrothermal carbonization (HTC). The hydrochar was experimentally conducted in the range of 6 h to 48 h at 200°C. The chemical and structural properties of hydrochar products were investigated. Oxygen to Carbon ratio (O/C), and Hydrogen to Carbon ratio (H/C) in all hydrochars product were 0.36-0.16 and 1.78-1.17, respectively. Higher heating value (HHV) of hydrochar product were in range of 28.79 MJ/kg to 28.73 MJ/kg. The highest rate of removal of methylene blue was approximately 70-80% for all concentrations. The predicted functional group that presence in hydrochars were hydroxyl and carbonyl group with increasing aromatic structure with longer residence time. The diameter of microspheres of hydrochars increased with residence time. Overall, residence time exhibited small effect on the chemical properties of hydrochars. However, the hydrochar products developed better characteristics as the time increase.

ID: FYP2020/39

SYNTHESIS AND PHYSICOCHEMICAL CHARACTERIZATION OF NIOSOMES AS NANOPARTICLULAR DRUG CARRIERS FOR QUERCETIN

MYTHILI LIM A/P TAMIL CHELVAN & NUR AYSHAH ROSLI
School of Chemical Engineering, Engineering Campus, Universiti Sains Malaysia,
14300 Nibong Tebal, Pulau Pinang, Malaysia

ABSTRACT

This study aimed to formulate stable niosomes loaded with quercetin by using different types of surfactant and surfactant ratio in terms of average particle size and high encapsulation efficiency by using thin layer hydration method. Quercetin was dissolved in chloroform, followed by the preparation of niosomes with the mole ratio of mixture of surfactant to cholesterol of 1:1. Span 20, Span 60 and Span 80 were used with Hydrophilic-Lipophilic Balance (HLB) values of 8.6, 4.7, and 4.3 respectively. The combination of Span 80 and Tween 80 was incorporated with the ratio of 4:6, 3:7, 2:8, 1:9 and 0:10 with Hydrophilic-Lipophilic Balance (HLB) values of 10.7, 11.8, 12.8, 13.9 and 15.0 respectively. Dynamic light scattering was performed on the synthesized niosomal formulations to investigate the physical characteristics of quercetin-loaded niosomes in terms of surface characteristics. Quercetin-loaded niosomes were characterized for size, zeta potential, encapsulation efficiency and storage stability. It was showed that formulation with Span 60, and the formulation with Span 80 to Tween 80 ratio of 3:7 has superior quercetin entrapment efficiency with small particle size, high zeta potential and best stability during storage under different temperature conditions. The results demonstrated that appropriate selection of non-ionic surfactant types and ratio of Span 80 to Tween 80 was necessary for the formation of small and stable quercetin-niosomes.

ID: FYP2020/40

SIMULATION OF FERMENTATION OF GLUCOSE TO PRODUCE BIOETHANOL USING BATCH FERMENTER BY ASPEN PLUS V10 SIMULATOR

NAJIHAH ROSLAN & NORASHID AZIZ
School of Chemical Engineering, Engineering Campus, Universiti Sains Malaysia,
14300 Nibong Tebal, Pulau Pinang, Malaysia

ABSTRACT

A fermentation of glucose is a promising process to convert glucose into bioethanol. However, it suffers from the relatively low selectivity of bioethanol at high glucose conversion. In this study, simulation software, Aspen Plus is applied to simulate the reaction, study the effect of operating conditions on the performance of the fermentation of glucose reactor and optimization of the reaction. The simulation results obtained are acceptable since the error calculated for the product is less than 1%. Sensitivity analysis conducted shows that the conversion of glucose and selectivity of bioethanol was maximum at reactor temperature, pressure and glucose flow rate at 215 °C, 1 atm and 300.3972818 kg/sec respectively. The influences of key operating parameters such as temperature, pressure, and glucose flow rate on the fermentation of glucose reactor performance are further analyzed. From the optimization, it shows that the maximum glucose conversion and bioethanol selectivity are 99% and 28% respectively. The reactions have been optimized at 222°C, 1 atm, and 480.3972818 kg/sec glucose feed flow rate.

ID: FYP2020/41

STEADY STATE SIMULATION OF REACTIVE DISTILLATION COLUMN FOR THE PRODUCTION OF METHYL ACETATE - STUDY OF KINETIC PARAMETERS AND OPTIMIZATION OF SELECTED OPERATING CONDITIONS

NEERUHSHA A/P MUNIANDY & MUHAMAD NAZRI MURAT
School of Chemical Engineering, Engineering Campus, Universiti Sains Malaysia,
14300 Nibong Tebal, Pulau Pinang, Malaysia

ABSTRACT

The usage of reactive distillation column has gained increased attention because of its high potential for process intensification and therefore this process needs to be studied and optimized fully so that the reaction conversion and purity of the product are assured before its implementation in industrial scale. In this work, Aspen Plus was used to simulate and optimize a reactive distillation column where methanol and acetic acid undergo esterification reaction to produce methyl acetate and water and undergo continuous separation process. Firstly, the obtained simulation results were compared with that from literature. The simulated results obtained by Aspen Plus showed that it is acceptable since the simulation values obeyed that of the literature with an average conversion and purity errors of 0.77% and 0.19% respectively. Sensitivity analysis on the same RadFrac model showed that reflux ratio, number of rectifying stages, number of reactive stages, number of stripping stages and reboiler have significant effects on methanol conversion and methyl acetate purity. Lastly, optimization study on the reactive distillation model resulted in maximum methyl acetate purity of 96.5% which was achieved at reflux ratio of 8.5, reboiler duty of 0.28 kW and total 10 stages.

ID: FYP2020/42

PHOTOCATALYTIC CARBON DOT DOPED TiO_2 NANOPARTICELS FOR DYED WATER TREATMENT

NG WENG YEE & LEO CHOE PENG
School of Chemical Engineering, Engineering Campus, Universiti Sains Malaysia,
14300 Nibong Tebal, Pulau Pinang, Malaysia

ABTRACT

Dyed wastewater is one main issue contributing to water pollution, causing increase of chemical oxygen demand (COD) and toxicity to water. Therefore, developing an effective, sustainable and economic way to remove dye is important to sustainability of environment. Photodegradation by TiO_2 is one of the effective ways in removing dye from wastewater. This photocatalyst could be improved through doping with multiple materials to improve its performance in removal of dye from wastewater. In this study, carbon dot (CD) was successfully prepared from citric acid via microwave assisted method and doped to TiO_2 nanoparticles through conventional and microwave assisted hydrothermal process at 120 °C and 200°C respectively. The photocatalytic activity of carbon dot doped TiO_2 were measured by the degradation rate of methylene blue (MB) under UV light irradiation at λ=365 nm. The results show that carbon dot doped TiO_2 (C/TiO2) has improved adsorption capacity due to presence of oxidized functional group on carbon dot surface doped to TiO_2. The degradation rate of MB by C/TiO_2

can reach up to 96.3 %. It is also determined that doping condition of C/TiO_2 such as concentration of carbon dot solution and heating time has significant effect on the photocatalytic performance of C/TiO_2 as excessive doping of carbon on TiO_2 can reduce the exposure of light to active site and inhibit migration of substances.

ID: FYP2020/43

EFFECTS OF ENHANCED MIXING TOWARDS THE PRODUCTION OF FATTY ACID METHYL ESTERS BY IN-SITU TRANSESTERIFICATION OF *EUCHEUMA COTTONII*

NISHA A/P NAVAINTHRAN & ZAINAL AHMAD
School of Chemical Engineering, Engineering Campus, Universiti Sains Malaysia,
14300 Nibong Tebal, Pulau Pinang, Malaysia

ABSTRACT

Biodiesel is proposed to replace the conventional fossil fuel-based diesel as the demand for energy is increasing with the increasing world population. The production of fatty acid methyl esters (FAME) from macroalgae (*Eucheuma cottonii*) is focused in this study. Conventionally, production of FAME will be carried out through the two-step transesterification process, which consists of extraction of lipid and subsequent acid or base-catalysed transesterification. However, the two-step transesterification method is a time and energy consuming process. With the advancement in technology, a more economical approach for the biodiesel production has been investigated, which is the in-situ transesterification reaction. Several studies have suggested that enhanced mixing can improve the yield of biodiesel produced through ISTE. In this study, the effects of reaction time and mixing intensity on the ISTE of FAME production in being investigated. The ISTE reaction was carried out at the ratio of biomass:MeOH:HCl (w/v/v) of 1:20:5 and a reaction temperature of 60°C. The total reaction time for the reaction was 90 minutes, where samples were collected at 30minutes interval. Two types of FAME were identified from the ISTE of *E. cottonii*, which are Methyl Palmitate and Methyl Stearate. The increase in reaction time and mixing intensity gave a significant positive impact on the production of FAME. At 90 minutes of reaction time and impeller rotational speed of 900rpm, the maximum amount of methyl palmitate and methyl stearate produced were 0.5729 wt% and 0.0559 wt% respectively. The results of contour of volume fraction of palmitic acid obtained from CFD analysis from the Aspen Fluent Software have a good agreement to the experimental results of the research.

ID: FYP2020/44

EFFECT OF POLYVINYLPYRROLIDONE (PVP) CONCENTRATION ON THE MORPHOLOGY AND COMPACTION STRENGTH OF POLYETHERSULFONE (PES) BASED MEMBRANE

NOR RABIATUL HUSNA AZMI & ABDUL LATIF AHMAD
School of Chemical Engineering, Engineering Campus, Universiti Sains Malaysia,
14300 Nibong Tebal, Pulau Pinang, Malaysia

ABSTRACT

Formation of composite membranes consist of a porous substrate as the back support of a denser selective layer. Polyvinylpyrrolidone (PVP) modified polyethersulfone (PES) asymmetric porous membranes which are normally used in ultrafiltration process would be suitable for this purpose. Introduction of PVP has been noted to enhance the porosity which would limit the flow resistance contribution of the substrate and increase its hydrophilicity which would improve coating interaction during composite formation. In addition, the use of PVP could also induce macropore formation which may limit the compaction strength of the PES membrane. In this work, the influence of feed pressure on the morphology and water flux across PVP modified PES flat sheet membranes were studied. Distilled water was pressurized at 2, 4, 6, and 8 bars using nitrogen gas at the feed to induce compaction for PES membranes modified with PVP concentration ranging from 0 to 4 wt%. The fabricated membranes were then characterized by SEM and FTIR while its contact angle and porosity were measured. The results suggested that the introduction of 4wt% PVP reduced the water flux by 96.07% from 187.05 to 7.34 $kg/m^3.h$ for 8 bar due to the formation of denser surface as measured through SEM and analysed with ImageJ software. This in turn would increase the membrane flow resistance which would contribute to the reduction in flux when used as a substrate for composite structure (Wu et al., 2018). On the other hand, while no samples were burst during the period of testing, compaction under the maximum 8 bar pressure suggested significant decrease in thickness with reduction of 32.03% from 191.74 to 130.33 um thickness at 8 bar for PES/PVP membrane. The

introduction of PVP decreases the solvent-nonsolvent exchange during phase inversion process, which minimize the formation of weak macropores that could weaken the membranes.

ID: FYP2020/45

PAPAYA PEELS AS SOURCE OF HYDROCHAR VIA HYDROTHERMAL CARBONIZATION

NOR ZAFIRAH ZULKIFLI & NOORASHRINA A HAMID
School of Chemical Engineering, Engineering Campus, Universiti Sains Malaysia,
14300 Nibong Tebal, Pulau Pinang, Malaysia

ABSTRACT

Papaya peels was used in this report because it can be renewable, easily collected and quite abundant as well as freely obtainable. It has been observed that papaya was produced broadly in Malaysia and consumed the fruits. Thermochemical conversion is one of technology used to form a carbonaceous end solid product. A higher carbon content in the product produced can be observed. In general, the hydrothermal carbonization (HTC) process will be emphasized in this paper and the product was called as hydro char. Basically, it was chosen due to its low energy consumption and ability to increase the carbon content in the feedstock. The carbonization of the papaya peels was executed at six different temperatures, 150, 160, 170, 180, 190 and 200°C and the reaction time of 120 minutes mainly to study the effect of the carbonization temperature on the hydro char formed via HTC. The end product was soaked in deionized water to reduce the amount of chlorophyll contained in the waste. The hydro char was assessed its properties into several analysis, mass yield, elemental composition and higher heating value (HHV). Apart from the characterization of the hydro char, the adsorption ability of the hydro char using methylene blue solution also included in this research. For all experiments, the mass yield of the hydro char reduced as the reaction temperature increase and the carbon contents showed an opposite trend where it increases as the HTC temperature increase. The HHV in general also increases as the carbonization temperature rise, but it was observed a slight decline of the HHV for hydro char formed at 170°C, 15.26 MJ Kg^{-1} from 15.65 MJ Kg^{-1} which as a consequence of the carbon content in the hydro char. When the initial MB concentration was 200 mg L^{-1}, the removal percentage increase along with the carbonization temperature.

ID: FYP2020/46

IMPROVED KERNEL PRINCIPAL COMPONENT ANALYSIS (KPCA) - SUPPORT VECTOR MACHINE (SVM) FAULT CLASSIFICATION MODEL FOR BATCH PENICILLIN FERMENTATION PROCESS

NORLIANA YENNIWAL & NORAZWAN MD NOR
School of Chemical Engineering, Engineering Campus, Universiti Sains Malaysia,
14300 Nibong Tebal, Pulau Pinang, Malaysia

ABSTRACT

Batch penicillin fermentation process is one of the bioprocesses in industry. In the biotechnology industry, the optimization and operation of fermentation processes play a key role due to heavy competition among the companies. Besides, fault detection and classification in the industrial of batch penicillin fermentation are important due to high demand for improved the product quality and economic operation of the penicillin fermentation process. Hence, the fault should to be noticed early to reduce the impact to the penicillin fermentation process. In this study, the machine learning method, support vector machine (SVM) and feature extraction method, kernel principal component analysis (KPCA) are developed and combined as a fault classification model for penicillin fermentation process. The batch penicillin fermentation process was simulated in the MATLAB software, where 10 batches of process faults with 35 variables from the penicillin fermentation database are used in the KPCA-SVM model development. The results of the models are analyzed by comparing the confusion matrix of both KPCA-SVM and SVM models. Based on the results, SVM model gained 56.042% for correct classification, while 43.958% for incorrect classification. After the KPCA is developed and introduced to SVM model, the percentage of correct and incorrect classification become 80.972% and 19.028% respectively. Therefore, KPCA-SVM model has higher percentage of correct classification compared to the SVM model.

ID: FYP2020/47

BATCH ADSORPTION OF METHYLENE BLUE DYE BY CARBONIZED CHILLI STALK ADSORBENT

NUR ADIRA AMIRNA MUHAMAD AMERR ABD RAHMAN & MOHD AZMIER AHMAD
School of Chemical Engineering, Engineering Campus, Universiti Sains Malaysia,
14300 Nibong Tebal, Pulau Pinang, Malaysia

ABSTRACT

The wide and fast growth of the textile industry has become one of the benefactors to the polluted environment, especially in water pollution. The emission of dyes into the environment poses health threats to the ecosystem and human, due to the characteristics of being carcinogenic and mutagenic. Adsorption process is the most utilized approach in treating textile wastewater, which also has become the aim of this study. Carbonized chilli stalk adsorbent (CCSA) is produced by the carbonization process of chilli stalk at various temperatures (350 °C, 370 °C and 400 °C) for the adsorption of methylene blue (MB). Dye batch adsorption studies were conducted to evaluate the effects of initial dye concentration (25 – 300 mg/L), contact time (0 – 24 hours) and carbonization temperature (350 °C, 370 °C and 400 °C). The surface area and pore characteristics, proximate and elemental analysis, surface morphology and surface chemistry were studied on both chilli stalk and carbonized chilli stalk adsorbent (CCSA). The maximum dye removal was 97.04% at 400 °C of carbonization. The data resulted from the experiment were analysed by three isotherm model equations: Langmuir, Freundlich and Temkin. The Freundlich isotherm model fitted the best to the adsorption data at all carbonization temperature range studied. Adsorption kinetic studies were resolved using pseudo-first-order, pseudo-second-order and intra-particle diffusion models. The results showed that the adsorption process of MB dye onto CCSA followed pseudo-second-order kinetic model, with film diffusion mechanism involved.

ID: FYP2020/48

ANALYSIS OF SINGLE-USED BIOMASS-RESIDUE-BASED FOR THE COGENERATION POWER PLANT IN PALM OIL MILL VIA ASPEN PLUS

NUR AFINI RAMZI & SYAMSUL RIZAL ABD SHUKOR
School of Chemical Engineering, Engineering Campus, Universiti Sains Malaysia,
14300 Nibong Tebal, Pulau Pinang, Malaysia

ABSTRACT

Nowadays, the biomass residue is way preferable than the fossil fuels as the fossil fuels can contribute to global warming and climate change. The usage of biomass residue as fuel for the boiler at palm oil mill is getting popular day by day since it gives a lot of benefits such as reducing the palm oil wastes, reducing global warming and save cost. In this study, it will be focus on the newly built boiler at my internship company which need to increase the amount biomass to generate saturated steam according to the new demands. The boiler at the company was upgraded from 15 ton/hr to 50 ton/hr to accommodate the process capacity of the mill at 30 ton/hr. The objective of this study was to model, validate and optimize the boiler in Aspen Plus software. Besides, the other objective is to find the most suitable biomass to be used as fuel sources for the boiler at the palm oil mill. The research starts by referring the published article to obtain the input operating conditions and the ultimate analysis of the biomass for the combustion process. Then, the whole process flow of the boiler was simulated, validated and optimized by using Aspen Plus software. From the simulation results, the power generated from each of the biomass such as fiber, shell and dry empty fruit bunch were 5117.57 kW, 5123.43 kW and 5019.01 kW respectively. The power generated for those biomasses exceed the power generated at the palm oil mill of the internship company which is only 570 kW. At the end of the study, fiber was chosen as the most suitable fuel sources to generate saturated steam at the palm oil mill.

ID: FYP2020/49

SUPERHYDROPHOBIC POLYURETHANE COATING INCORPORATED WITH SILICA NANOPARTICLE FOR WATER PROOFING

NUR AIN BINTI ZAKARIA & LEO CHOE PENG
School of Chemical Engineering, Engineering Campus, Universiti Sains Malaysia,
14300 Nibong Tebal, Pulau Pinang, Malaysia

ABSTRACT

Superhydrophobic surface has various applications such as waterproofing, self-cleaning and anti-corrosion. Thus, superhydrophobic surfaces were developed from silica nanoparticle and polyurethane paint in this study. The effects of silica content and silane post-treatment in blending spray coating as well as the effects of solvent type and nanoparticle size in dual-layer spray coating were studied. The highest water contact angle (WCA) of 155.60 ± 1.75 º was obtained using dual-layer spray coating method with the silica nanoparticle content of 2 wt%, paint thinner as the solvent and the particle size of 20-30 nm. The superhydrophobic surface minimized the water contact due to the air captivation on top of rough surface generated by the nanoparticles.

ID: FYP2020/50

LIPID ACCUMULATION IN *Lemna minor*

NUR ELLIANA MAZALAM & DEREK CHAN JUINN CHIEH
School of Chemical Engineering, Engineering Campus, Universiti Sains Malaysia,
14300 Nibong Tebal, Pulau Pinang, Malaysia

ABSTRACT

Nowadays, development of biofuels and biochemical resources of high commercial value from duckweed can replace petroleum as the main component source. Another importance of *Lemna minor* is in food source of animals also humans, which the lipids play important role for health of organisms. Hence, lipid content based on the growth of the *L. minor* has been studied from the others literature to study on how to produce large yield of lipid for the next generation. Large yield of lipids is obtained by changing the effect of the solvent system, long the period of extraction time, cultured in high nutrient water and the concentration of the solvent should be considered both polar and non-polar. Thus, *L. minor* would be one of useful duckweed in various applications due to high lipid content produced.

ID: FYP2020/51

RECOVERY OF BRACKISH WATER VIA VACUUM MEMBRANE DISTILLATION AND ITS FOULING STUDY

NUR RAFIQAH MOHAMAD TARJI & OOI BOON SENG
School of Chemical Engineering, Engineering Campus, Universiti Sains Malaysia,
14300 Nibong Tebal, Pulau Pinang, Malaysia

ABSTRACT

As water scarcity has increasingly become a serious global problem, desalination process via membrane distillation (MD) is considered as a non-energy intensive process that used to produce clean water as it can be operated efficiently at lower temperature. However, membrane fouling and scaling are major obstacles to its long-term stability and it subsequently affect the efficiency and performance of vacuum membrane distillation (VMD). In this study, effect of feed temperature and concentration on permeation flux were analysed by employing propylene (PP) hollow fiber membrane in VMD at constant pressure for 40 hours. Permeation flux is increasing as the temperature is raised from 55 to 65°C due to an increase in driving force of permeation which influenced by the saturated water vapor pressure. In addition, reduction of flux was substantially observed over the time caused by polarization and membrane fouling. Fouling rate was higher at 65°C as crystals of NaCl salt and Mg scalant are deposited on the membrane surface from the SEM coupled with EDS analysis. Meanwhile, a decrease in permeation flux was observed in a 2 wt% of NaCl with a large amount of $MgCl_2$ as a feed solution which is

likely due to reduced vapor pressure and membrane fouling. No membrane wetting was observed as permeate conductivity is constant at lower value and no foulants detected in the cross section of the membrane.

ID: FYP2020/52

CONCENTRATING FISH FARM EFFLUENT FOR ITS NUTRIENT RECOVERY VIA NANOFILTRATION AND ITS POTENTIAL AS LIQUID FERTILIZER

NUR ZAHIDAH ZAHID & OOI BOON SENG
School of Chemical Engineering, Engineering Campus, Universiti Sains Malaysia,
14300 Nibong Tebal, Pulau Pinang, Malaysia

ABSTRACT

The aquaculture industry in Malaysia is expanding rapidly and this leads to an increase on the threat that is possibly caused by this industry. Eutrophication and production of pond effluents are some of the threats from this industry. High amount of nitrogen and phosphorus in the effluents cause negative impact to the water body if there are not treated properly. In this study, a nanofiltration membrane will be used to test on the ability of the membrane to separate and concentrate the nutrients in the effluents. Two types of effluent will be used which are synthetic effluent and real fish farm effluent collected from Sungai Udang, Nibong Tebal. The synthetic effluent (ammonium, phosphate and nitrate) was used to study the effect of concentration, pressure and type of membrane on the separation efficiency and concentrating capabilities. The increase in concentration from 10 mg/L to 25 mg/L gave a strong influence on the permeate flux and concentrating percentage of the nutrients. For ammonium and phosphate, increase in concentration cause the permeate flux to increase. Meanwhile, for nitrate, the increase in concentration will make the permeate flux to decrease due to the high repulsion forces between the membrane surface and the anion. Same pattern happened on the effect of pressure where the permeate flux will increase when the pressure increase. In this study, it was observed that NF270 gives a higher permeate flux because of the characteristic of the membrane where it has a more open polymeric structure. The real fish farm effluent was used to study the concentrating capabilities of nutrients using the nanofiltration membrane. It is found that the membrane was able to concentrate the nutrient with a concentrating factor up to 90.53% for phosphate and 41.46% for ammonium. Then, the retentate will be used as liquid fertilizer on a plant and the effectiveness will be observed. The growth of the plants was being observed for 25 days and it shows that the retentate from a raw fish farm effluent gives the highest growth rate where it is up to 65.71%. This indicate that the nanofiltration membrane is able to concentrate the nutrients and can be used as a liquid fertilizer effectively.

ID: FYP2020/53

OPTIMIZATION STUDY ON THE PARAMETERS IN KINETIC MODEL OF REACTIVE DISTILLATION COLUMN FOR METHYL ACETATE SYNTHESIS

NUR ZAIDATUL AKMA ZULPAIDI & MUHAMAD NAZRI MURAT
School of Chemical Engineering, Engineering Campus, Universiti Sains Malaysia,
14300 Nibong Tebal, Pulau Pinang, Malaysia

ABSTRACT

Reactive distillation (RD) had attracted many attentions due to its high potential for process intensification. Apart from that, RD has many potential benefits which make people more interested in it. Due to that, the study of methyl acetate synthesis in reactive distillation column (RDC) was studied and a model was proposed by using the Aspen Plus V10. Before the simulation was started, the analysis of kinetic model parameters was conducted in order to find the actual data of kinetic model which in continuous process. The kinetic model parameters involved in this analysis are activation energy and reaction constant rate. After analysis, the activation energy and reaction rate constant were obtained at 8650 cal/mol and 2.15 accordingly. Later, the model was verified by comparing the simulation results with the literature used as reference. The proposed model was accepted when the simulation results almost similar with the literature. Then, the simulation was proceeded further by performing the optimization analysis on the proposed model in order to find the operating condition which gave significant changes on the conversion of methanol and purity of methyl acetate. The operating conditions

that were manipulated in the reactive distillation column such as reflux ratio, feed flowrates and number of stages. Based on the analysis results, the reflux ratio and feed flowrates were chosen as the most significant operating conditions which were affecting the methanol conversion and purity of the product.

ID: FYP2020/54

SUSPENDED SOLID REMOVAL DURING PHYTOREMEDIATION OF FISH FARM WASTEWATER

NURSYAZANA OMAR & DEREK CHAN JUINN CHIEH
School of Chemical Engineering, Engineering Campus, Universiti Sains Malaysia,
14300 Nibong Tebal, Pulau Pinang, Malaysia

ABSTRACT

Phytoremediation uses plants to remove contaminants in wastewater. The effluents from aquaculture especially in fish farm water contains large amount of suspended solids and has high concentration of nitrogen and potassium. The conventional wastewater treatment, which is recirculating aquaculture system is expensive to run and high cost in maintenance. Phytoremediation can be another alternative in wastewater treatment process but there might be limitation for this process to achieve the desired quality of fish farm water. Thus, the effect of suspended solid removal during phytoremediation was analysed to determine which combination technology could achieve a better outcome. A part form that, the performance of phytoremediation was also studied. Different types of suspended solid removal in aquaculture have been analysed such as sedimentation, filtration and coagulation. Each type has their own pros and cons in wastewater treatment. Thus, based on the advantages and disadvantages of the suspended solids removal technology, the horizontal flow sedimentation tank with adding natural coagulants is chosen to be combine with phytoremediation that will be able to treat the fish farm effluent.

ID: FYP2020/55

PHYSICOCHEMICAL PROPERTIES OF USED VEGETABLE COOKING OIL

NURUL AIN KHAIRUNNISA AZHARI & TYE CHING THIAN
School of Chemical Engineering, Engineering Campus, Universiti Sains Malaysia,
14300 Nibong Tebal, Pulau Pinang, Malaysia

ABSTRACT

The vegetable palm cooking oil is generally used in any household or industry. It is due to the vegetable palm cooking oil is relatively low cost compared to other sources. However, there are limitation in the usage of vegetable cooking oil as it may not good to human consumption when it starts to degrade. More likely, the waste vegetable cooking oil will be discarded in which may cause some environmental issues. To enhance the usage of the waste vegetable cooking oil, it can be a substitute as feedstock in biodiesel production. In order to get a good quality of waste vegetable cooking oil, this study explores the effect of types of foods and heating methods towards the physicochemical properties of vegetable cooking oil during frying process. Density, Kinematic Viscosity, Acid Value, Free Fatty Acid and Saponification Value are the physicochemical properties tested on used vegetable cooking oil in the present study. Potato cubes and Fish crackers were two types of food used in the study. At the same time, two types of oil heating method to be studied are collective heating and continuous heating. The collective heating refers to frying the foods for 30 minutes each day for four consecutive days while continuous heating refers to frying the foods for 2 hours straight. Cooking oils which underwent different condition such as frying time and types of food had a significantly different of physicochemical properties. The analysis results showed the density of waste vegetable cooking oil for both foods are 1.3 g/ml due to small amount of food use. Kinematic viscosity much higher compared to standard value in previous study, since Potato is one of deep-fat fried food. The Acid value and free fatty acid value for Fish crackers is significant due to the ratio of weight of food to the oil. The Saponification value deviates from previous study. It can be concluded that, collective heating has a significant change towards the acid value, free fatty acid, kinematic viscosity, saponification value and density of cooking oil and the used vegetable cooking oil is suitable for alternative in biodiesel production.

ID: FYP2020/56

A STUDY ON THE REMOVAL OF METHYLENE BLUE AND METANIL YELLOW DYE USING AN OZONE BASED OXIDATION PROCESS

NURUL IZZATI ZAIDAE & AHMAD ZUHAIRI ABDULLAH
School of Chemical Engineering, Engineering Campus, Universiti Sains Malaysia,
14300 Nibong Tebal, Pulau Pinang, Malaysia

ABSTRACT

Dyes are used in the various industries which acts as the colouring agents. The discharge of dyes especially synthetic dyes leads to the serious environmental problem and issue to public. In this study, there are several parameters that were investigated including initial concentration of dye, the solution pH and reaction of ozone with aids of a UV lamp (O_3/UV). There are two type of dyes investigated, the water-soluble basic dye, methylene blue (MB) and water-soluble azo acid dye, metanil yellow (MY) by supply the ozone using ozone generator. The ozone output supply in constant which is 500 mg/h. The decolourization of dye was achieved by using an advanced oxidation processes (AOPs), the single ozonation process and combination of ozone with UV light which promising an efficient removal and the friendly method that have been develop. For an initial concentration of dye, the results obtained shown that ozone can degrade dyes faster at a very low concentration where at 20 mg/L of MB and MY, the removal efficiency was 99.64% and 96.44% respectively for 30 minutes' reaction. The results shown that for higher concentration, the reaction time need to increase. At an initial pH of 11, the decolourization of dye showed higher percentage of removal efficiency. More than 99% of colour was removed after 30 minutes of the reaction. Kinetic analysis showed that the ozonation of the both water soluble dyes represented the first order reaction. There result reaction of O_3/UV was more effective compared to ozone alone. The removal efficiency of methylene blue at low concentration at 5 minutes of reaction was 80% with UV and 75% for ozone alone. For higher concentration show the same trend as it gives 56% removal for O_3/UV process and 36% for ozone alone. This concluded that ozone-based oxidation reaction could serve as an effective method to reduce the colour intensity from the polluted water.

ID: FYP2020/57

BINARY ADSORPTION OF TEXTILE DYES ONTO ZWITTERIONIC ADSORBENT COATING

NURUL NADIRAH BINTI MUHAMAD NASIR & SUZYLAWATI ISMAIL
School of Chemical Engineering, Engineering Campus, Universiti Sains Malaysia,
14300 Nibong Tebal, Pulau Pinang, Malaysia

ABSTRACT

It is about 800,000 tons of synthetic coloring are manufactured annually and about half of this comes from azo coloring. Azo dyes providing a wide variety of industrial uses, including clothing, medicinal, and cosmetics. Triarylmethane dyes form one of the oldest synthetic color groups. They are brilliant in color, have a high tincture strength, are relatively cheap, and can be applied to a wide variety of substrates. They are seriously deficient in the properties of pace, particularly light and washing fastness. Textile wastewater is considered the most polluting of all industrial sectors, both the amount produced and the effluent composition. Most of the previous researches only concentrates on extracting dyes from water in a single solution. In real applications, the colored effluents contain more than one removable component. In this study, the adsorption of two textile dyes (Acid Red 1 and Brilliant Green) was investigated in a binary mixture. The derivative spectrophotometry for each dye was used to determine the precise wavelength. Consideration was given to the effect of pH, contact time, initial dye concentrations, and temperature. The findings show that the zwitterionic adsorbent coating has a strong potential to simultaneously remove both dyes. Equilibrium was achieved within 300min and to obtain a higher percentage removal of Acid Red Brilliant Green, ARBG, the optimal condition has been achieved. The higher percentage of removal for AR1 and BG was reported at 92.14% and 90.18% respectively at 10BG-40AR (ppm) initial concentration. While, the optimum elimination is at pH 11 and 30°C, since both AR1 and BG were at 100% of removal.

ID: FYP2020/58

REAL-TIME DYNAMIC SIMULATION OF HEAT EXCHANGER NETWORK (HEN) USING PYTHON

ONG XHIN CI & SUHAIRI ABDUL SATA
School of Chemical Engineering, Engineering Campus, Universiti Sains Malaysia,
14300 Nibong Tebal, Pulau Pinang, Malaysia

ABSTRACT

Heat exchanger network, HEN has been extensively being studied in chemical engineering owing to the main driving aim for improving energy recovery and lowering the consumption of hot and cold utilities by means of process streams energetic integration. HEN modelling and simulation was treated as the domain of interest of study because it provides the automatic analysis of output variables and trends when the operating conditions change as a function of time. HEN simulation was conducted and explored through Python acting as an alternative as it is a liberal open source license. Several required extension libraries were imported into Python to give their specialized functions. The mathematical model implemented for describing the variation of process stream temperature passing through heat exchangers was validated with small error percentage reported compared to theoretical values extracted from literature. The HEN simulator was successfully being developed via Python software and proven its functionality through conducting simulation study on steady state, dynamic and introduced input variable step change condition to obtain the real-time results. The effects caused by the manipulation of operating variables towards outlet port temperature were studied and interpreted to obtain the interaction between heat exchangers.

ID: FYP2020/59

CRACKING OF USED COOKING OIL TO BIOFUEL IN THE PRESENCE OF ZEOLITE-BASED CATALYST

PAVITHRAN RAVINDRAN & TYE CHING THIAN
School of Chemical Engineering, Engineering Campus, Universiti Sains Malaysia,
14300 Nibong Tebal, Pulau Pinang, Malaysia

ABSTRACT

The insecure supply of fossil fuel coerces the scientific society to keep a vision to boost investments in the renewable energy sector. Among the many renewable fuels currently available around the world, biofuel offers an immediate impact in our energy. In fact, a huge interest in related research indicates a promising future for the biofuel technology. This paper reports studies on ultrasound-assisted catalytic cracking of biofuel from used palm oil in the presence of H-ZSM zeolite catalyst. A statistical experimental design has been used to optimize the process conditions for the study. Three different variables including catalyst loading (1.0-5.0 wt.%), ultrasonic amplitudes (20,40,6,75&90%) and pulse of ultrasonic irradiation (1:1s,2:1s&9:3s) were investigated. The study shows that the ultrasonic significantly improves the catalytic cracking process. The product gas yield (wt%) and liquid yield (wt%) was measured and calculated to determine the optimal conditions of biofuel production. The highest gas yield (wt%) were obtained with catalyst loading of 5 wt% with 2.00 wt%, amplitude of 90% with 1.12 wt% and the ultrasonic pulse of 9:3 s with 1.08 wt%. Further study was done to learn the effect of ultrasonic irradiation on the viscosity of product yields. As a conclusion, ultrasonic energy irradiation lowered the viscosity, and ultrasonic energy irradiation has an enormous effect on production of biofuel.

ID: FYP2020/60

PROPERTIES OF DEEP EUTECTIC SOLVENT (DES)

SAKTHINATHAN A/L BALAKRISHNAN & FADZIL NOOR GONAWAN
School of Chemical Engineering, Engineering Campus, Universiti Sains Malaysia,
14300 Nibong Tebal, Pulau Pinang, Malaysia

ABSTRACT

Deep eutectic solvents (DES) are organic solvents which can be formed by mixing two solid hydrogen bond donor and hydrogen bond acceptor at the right ratio. When a clear liquid forms, it is an identification of a deep eutectic solvent. DES components like decanoic acid, thymol and betaine are reviewed for the preparation of DES. Several report evidences are collected here to support the validity of these compounds as the component of DES. The properties of the DESs like the viscosity, density, melting point and the conductivity is then studied. The data taken from the experiment shows the relationship of viscosity with water content (0%, 5% and 10%) in the betaine-based DES. The density of the menthol: thymol DES is also reviewed with the change in temperature from 298.15 K to 353.15 K. Other reports that were reviewed in this study also showed the trend of conductivity with the increase in temperature (295 K to 330 K). The application of DES is also reviewed in metal-catalyzed reaction, electrochemistry, biodiesel synthesis and sample preparation via liquid-liquid extraction.

ID: FYP2020/61

MANIPULATING MEMBRANE HYDROPHOBICITY AND SWELLING TENDENCY BY INTEGRATING FUNCTIONALIZED FUMED SILICA NANOPARTICLES

SAMUEL ANAND STEPHEN PAUL & LOW SIEW CHUN
School of Chemical Engineering, Engineering Campus, Universiti Sains Malaysia,
14300 Nibong Tebal, Pulau Pinang, Malaysia

ABSTRACT

Membrane gas absorption (MGA) as an emerging technology exhibits superior advantages in comparison to conventional carbon dioxide (CO_2) absorption processes. However, the decrease in membrane flux, induced by membrane wetting is a significant issue to be pondered upon. Thus, in this work, silica nanoparticles were first functionalized with hydrophobic low-density polyethylene (LDPE). Integrating LDPE functionalized fillers into polyvinylidene fluoride (PVDF) membrane matrix increases membrane hydrophobicity and to prevent severe alterations in membrane morphology upon membrane swelling. In this study, to better understand the wetting mechanism of a nanocomposite PVDF membranes towards amines, a 20-day swelling analysis was done, in which, 1M monoethanolamine (MEA), diethanolamine (DEA) and amino methyl propanol (AMP) solutions were used as amine absorbents. The incorporation of LDPE-functionalized silica into PVDF polymer enhanced the contact angle values from 90.6° to 103.1°. These increments indicate an improvement in hydrophobicity for the LDPE-silica/PVDF composite membrane, thus, enhancing membrane anti-wetting ability. Nevertheless, the characterization results revealed that all three amine absorbents diffused into the membranes during the membrane swelling test, resulting in membrane swelling. The reduction of contact angle for all four membranes stipulated that membrane surface hydrophobicity depreciated during 20-day immersion in amine. Membrane surface morphologies were also observed to suffer from noticeable and complicated changes after immersion in absorbents. Among the amine absorbents, DEA with the highest surface tension had demonstrated the lowest swelling percentages with minimal changes in membrane surface morphology. From the experimental results, the choice of using DEA amine as an absorbent is proved to affect the least upon the membrane properties and morphology. Indeed, the increased surface hydrophobicity of TS-610 nanocomposite membranes ultimately plays a pivotal role in overcoming membrane wetting drawbacks when in contact with the liquid absorbents. The enhanced hydrophobic property of membrane is a highly regarded property especially during the application of membrane gas absorption as the sustainability of the membrane (excellent hydrophobic property) would affect the overall performance of MGA throughout a sustained period.

ID: FYP2020/62

SYNTHESIS AND CHARACTERISATION OF WASTE DERIVED SILICEOUS MAGNETIC METAL ORGANIC FRAMEWORK-5

SARAVANAKUMARA A/L M. MARAPPAN & IRVAN DAHLAN
School of Chemical Engineering, Engineering Campus, Universiti Sains Malaysia,
14300 Nibong Tebal, Pulau Pinang, Malaysia

ABSTRACT

MOF-5 is an important metal organic framework that is widely being studied in the field of absorption and separation. The aim of this research is to study the surface properties of MOF-5 and the effect of silica and magnetic properties to the structure of metal organic framework. In this study we synthesised the MOF-5 using $\boldsymbol{Zn(NO_3)_2 \cdot 6H_2O}$ N, N-dimethylformamide (DMF) as solvent and 1, 4-benzenedicarboxylic acid (1, 4-BDC). The Langmuir surface area and BET surface area were obtained via nitrogen adsorption and desorption. Scanning electron microscopy (SEM) were carried out on MOF-5 using Zeiss Supra 35VP to study the surface morphology and to verify the presence of porosity on the surface of the MOF-5. SEM images show thin loose microplates of MOF-5 collected after two hour of reaction. After 16h reaction the particles were cube in shape. Thus, increased time of reaction lead to increase in crystallinity of the cubic crystals. When a comparison is made between the SEM image of MOF-5 and the magnetic MOF-5 it can be said that Fe_3O_4 nanoparticles are successfully coated on the surface of metal organic framework. The image also indicates the presence of large number of nanoparticles on the surface of the metal organic framework. XRD pattern shows that the area under the peaks are wider which indicates that the MOF crystals formed under surface of coal fly ash crystals are relatively smaller in size compared to the pure phase. SEM image of MOF-5 with rice husk ash (RHA) also showed that the silica nanoparticles begin to stick and fuse together to form porous structure. It was also noticed that the silica nanoparticles begin to stick on the surface forming thicker walls of MOF-5.

ID: FYP2020/63

CARBON DIOXIDE ABSORPTION VIA MEMBRANE GAS ABSORPTION AS A FUNCTION OF SILICA LOADING IN COMPOSITE MEMBRANE

SARVVESWARAN PARANTHAMAN & LOW SIEW CHUN
School of Chemical Engineering, Engineering Campus, Universiti Sains Malaysia,
14300 Nibong Tebal, Pulau Pinang, Malaysia

ABSTRACT

The aim of this research is to study carbon dioxide absorption via membrane gas absorption as a function of silica loading in composite membrane. One pristine polyvinylidene fluoride (PVDF) membrane and three silica/PVDF composite membrane with different silica loading (1wt%, 3wt% and 5wt%) is synthesized to evaluate carbon dioxide absorption via membrane gas absorption process. The membranes were characterized using a scanning electron microscopy (SEM), thermogravimetric analysis (TGA), porometer and energy dispersive X-ray spectroscopy (EDX) to determine the morphology, thermal stability, liquid entry pressure (LEP_W), silica nanoparticles dispersion and concentration. SEM result shows that the membranes have thicker sponge-like layer than finger-like layer with rough surface. TGA results indicate that the membranes experience a significant change in weight percentage between temperatures of 460° C to 490° C. The EDX results showed that the silica nanoparticles are well dispersed throughout the membrane with relatively equal concentration in both sponge-like layer and finger-like layer. The liquid entry pressure (LEP_W) of the membranes increases as the silica loading in the composite membrane increases. The surface contact angle of the membranes was also analysed, with the contact angle of the membrane increases as the percentage of silica loading increases in the composite membrane. The membranes were also subjected to porosity analysis, where the analysis show that the silica/PVDF composite membrane with silica loading of 1% have the highest porosity compared to other membranes. Finally, the membrane gas absorption results show that the silica/PVDF membrane with 3% and 5% silica loading having better carbon dioxide permeability and better carbon dioxide selectivity compared to other membranes.

ID: FYP2020/64

REMOVAL OF PHOSPHOROUS BY USING CALCIUM RICH BIOCHAR PREPARED FROM *ANADARA GRANOSA* SHELL

SEE KHAI TENG & MASRINA MOHD NADZIR
School of Chemical Engineering, Engineering Campus, Universiti Sains Malaysia,
14300 Nibong Tebal, Pulau Pinang, Malaysia

ABSTRACT

Cockle shell or *Anadara granosa* is a natural source of calcium carbonate other than limestone. This study explored the potential application of biochar derived from cockle shells to adsorb phosphate from aqueous solution. The calcium rich biochar (CRB) prepared at various temperature by pyrolysis of cockle shells were characterized to study its physiochemical properties. EDX analysis showed that raw cockle shell as well as its CRB was rich in calcium (28.4 – 40.4 %) while FTIR results showed that CRB prepared at temperature > 700 ℃ could be classified as lime-based CRB. The phosphate removal experiment results revealed that CRB prepared at 700 ℃ manage to achieve phosphate removal up to 93% in 80 mg/L phosphate solution. Adsorption kinetics study was conducted, and the results indicated that pseudo second order model best describe the phosphate adsorption onto CRB700 (R^2 = 0.9960) and time to reach equilibrium was around 2 hours. This implied that the adsorption of phosphate onto CRB700 particle was caused by chemical actions. On the other hand, adsorption isotherm study disclosed that phosphate adsorption onto CRB700 fitted both Langmuir and Freundlich isotherm fairly well, however, Freundlich model fitted better with higher correlation coefficient (R^2 = 0.9995). Thus, this result indicated that adsorption of phosphate onto CRB700 particles was dominated by multilayer adsorption. In brief, these results proposed that cockle shell biochar could be applied for wastewater treatment to remove phosphate from aqueous solution due to its cost-effectiveness and simplicity.

ID: FYP2020/65

UNDERWATER SUPER OLEOPHOBIC LIGNIN MODIFIED PVDF MEMBRANE FOR OIL/WATER SEPARATION

SITI NURZALIKHA AHMAD ZAINI & LEO CHOE PENG
School of Chemical Engineering, Engineering Campus, Universiti Sains Malaysia,
14300 Nibong Tebal, Pulau Pinang, Malaysia

ABSTRACT

Lignin is phenolic polymer with abundant of hydrophilic groups which are widely available for different uses. Lignin is helpful to improve the hydrophilicity and antifouling properties of the PVDF membrane. In this work, lignin was coated on the commercial and fabricated polyvinylidene fluoride (PVDF) membranes for filtration of oily water. Sodium hydroxide, NaOH solution is been used as solving agent in lignin modification. PVDF membranes were immersed in the lignin solution containing varied NaOH content (0.25-1.0 wt%) overnight. The PVDF and lignin modified PVDF membranes were characterized with Fourier-transform infrared (FTIR), spectroscopy and scanning electron microscope (SEM) for comparison. The water permeability of lignin modified PVDF membrane (506.23 $L.m^{-2}.h^{-1}.bar^{-1}$) was improved compared to the neat PVDF membrane. The PVDF/lignin membrane exhibit antifouling properties with oil rejection up to 99.88% and permeate flux 361.00 $L.m^{-2}.h^{-1}.bar^{-1}$ at 1 bar in the filtration of oily water. The presence of lignin as hydrophilicity agent has a huge impact to the performance of the PVDF membrane and one of the suitable materials used for oil/water separation.

ID: FYP2020/66

KERNEL INDEPENDENT COMPONENT ANALYSIS (KICA) -ARTIFICIAL NEURAL NETWORK (ANN)-BASED FAULT DETECTION OF METHYL METHACRYLATE POLYMERIZATION PROCESS

SITI ZULAIKHA AZMI & NORAZWAN MD NOR
School of Chemical Engineering, Engineering Campus, Universiti Sains Malaysia,
14300 Nibong Tebal, Pulau Pinang, Malaysia

ABSTRACT

Methyl methacrylate (MMA) is a significant monomer which is widely used for producing acrylic plastics (polymethyl methacrylate) or producing polymer dispersions for paints and coatings. The increasing demand has led to significant automation to provide the desired quality of MMA. Therefore, the process needs to be safeguarded against the faults. The objective of this work is to detect and identify any faults in the process as soon as possible so that the fault can be handled before any disastrous incident occurred. An approach using Kernel Independent Component Analysis (KICA) is one of the techniques that have been introduced to diagnose the fault in any of the processes. However, KICA is difficult to diagnose the fault in the nonlinear problem. This is due to the unknown mapping function from input space into feature space. Thus, to overcome this drawback, Artificial Neural Network (ANN) which is the learning strategy is proposed to diagnose the fault. The polymerization process of MMA was developed in the Matlab software. The normal and fault operation introduced to the system. Feedforward neural networks without feature extraction (ANN model) are implemented by using Matlab Neural Network Toolbox. Based on the ANN model developed, the KICA-ANN model is created. The percentage of correct classification is obtained from the confusion matrix. For the ANN model, the percentage of correct classification is 51%, 75%, and 89% with the number of one, two, and three hidden nodes employ on the neural network. For the KICA-ANN model, the percentage of correct classification is 94% with one hidden node employ to the neural network. Both ANN and KICA-ANN model was able to detect and isolate faults that have been considered in this work. However, with the KICA-ANN model, the higher percentage of correct classification can be obtained compared to the ANN model.

ID: FYP2020/67

OPTIMIZATION OF MICROWAVE-ASSISTED EXTRACTION (MAE) OF *MORINGA OLEIFERA* LEAVES USING RESPONSE SURFACE METHODOLOGY (RSM)

SRI WAHYUNI MOHAMMAD ZAIN & NUR AYSHAH ROSLI
School of Chemical Engineering, Engineering Campus, Universiti Sains Malaysia,
14300 Nibong Tebal, Pulau Pinang, Malaysia

ABSTRACT

Extraction is widely used in various industries such as food and pharmaceutical industries as they need to achieve certain level of nutrients in their products. Conventional extraction takes longer time and large amount of solvent to get similar yield compared to advanced extraction. Microwave assisted extraction is one of the advanced extraction methods which widely used in extracting bioactive compound from plants. In this study, the extraction of phenolics compound from *Moringa oleifera* leaves using microwave assisted extraction by using water as a solvent. In order to improve the extraction efficiency in term of extraction yield and phenolic content recovery, optimization using RSM were done. The optimisation was done to get optimum microwave power and extraction time with maximum responses. The chosen model for RSM was Central Composite designs (CCD) which was fairly fitted for both responses. The optimisation was done and the optimum extraction condition which at microwave power of 264 W and 2 minutes of extraction were obtained. The optimized processing parameters were then verified by comparing predicted responses and experimental responses. The experimental data obtained of the maximum yield of extract and TPC were at 53.67% and 118.1 µg/mL whereas the predicted responses were at 53.72% and 115.1 µg/mL, which had small deviation of 0.053% and 3.024 µg/mL, respectively. In other words, the percentage errors for both were obtained at 9.87% and 2.63% respectively.

ID: FYP2020/68

MANIPULATING GEOMETRICAL OF CARBON ELECTRODE THROUGH SCREEN PRINTING FOR ENHANCED ELECTROCHEMICAL SENSING DETECTION

TAN CI JUN & LOW SIEW CHUN
School of Chemical Engineering, Engineering Campus, Universiti Sains Malaysia,
14300 Nibong Tebal, Pulau Pinang, Malaysia

ABSTRACT

Screen-printed carbon electrodes (SPCEs) are widely used for electrochemical sensing of organic and inorganic compound to replace conventional carbon electrode. The production cost of SPCE is lower and able to analyse samples with a much smaller volume. However, the main challenges of SPCE is that its effectiveness is highly relied on the formulation of the printed ink that affect its conductivity and the printed morphology. In this work, the SPCEs is printed by using a water-based carbon ink with the top layer coated with viscous solvent-based carbon ink on a mesh template. Printing was carried out manually by using a squeegee on a flat surface. The aim of this work was to compare the electroactivity of both conventional carbon electrodes and SPCEs, in order to prove that SPCE can replace the conventional carbon electrode for amperometric sensor work. The changes in topology, surface chemistry and electrochemical behaviour of SPCE in detection of ascorbic acid (AA) were analysed by SEM, optical microscope and cyclic voltammetry. Moreover, different concentrations of AA (5 to 50 mM) were prepared to evaluate the effect of concentration against current for conventional carbon electrode. It was found that the SPCE has the same functionality as the conventional carbon electrodes, although SPCE exhibits lower current but it displayed a more significant oxidation peak. Optimization of SPCE is done by several factors such as active length (1 cm, 1.6 cm and 2 cm), width (1 mm, 2mm and 4 mm) and thickness (1, 3, 5 layers). The result obtained shows that when the active length, width and thickness increases, the electrochemical activity increases as well. Findings from this work may contribute to the development of SPCE, to replace the conventional carbon electrode, since both type of electrodes have shown similar electrochemical behaviour.

ID: FYP2020/69

ANTHOCYANIN PRODUCTION IN *Spirodela polyrhiza*

TAN HOOI YEI & DEREK CHAN JUINN CHIEH
School of Chemical Engineering, Engineering Campus, Universiti Sains Malaysia,
14300 Nibong Tebal, Pulau Pinang, Malaysia

ABSTRACT

Anthocyanins are pigments that can be found in flowers and the fruits of many plants. The nutraceutical properties of this pigment such as antioxidative activities and antiangiogenic effect enable the industrial application in food, pharmaceutical and cosmetics. In recent years, more and more attention has been paid to study the factors that affect anthocyanin production in many plant cell and tissue cultures but not much in *Spirodela polyrhiza.* In this paper, we focus to determine the conditions for the enhancement of anthocyanin accumulation in *S.polyrhiza.* We suggested that the anthocyanin accumulation is potentially enhanced when the conditions of medium culture is at around pH 6, lack of nitrogen and phosphorus, available of sucrose concentration in the range of 131 mM to 219 mM, expose to red light and cultivate at a temperature between 20^{o}C to 24^{o}C. However, the current study on the strategy to enhance the anthocyanin accumulation in *S.polyrhiza* is not feasible enough. Therefore, further studies and researches are required.

ID: FYP2020/70

BINARY ADSORPTION OF PHENOL AND METHYLENE BLUE USING MICROWAVE INDUCED COCONUT SHELL ACTIVATED CARBON

TAN YAT SING & AZAM TAUFIK MOHD DIN
School of Chemical Engineering, Engineering Campus, Universiti Sains Malaysia,
14300 Nibong Tebal, Pulau Pinang, Malaysia

ABSTRACT

Coconut shells are cheap and sustainable resources for making activated carbon for adsorption process. In this study, the adsorption performance of the microwave induced coconut shell activated carbon is tested on the continuous adsorption of phenol and methylene blue in aqueous solution. A series of characterization tests are carried out to gain a better understanding of the adsorption mechanism of the activated carbon such as SEM, EDX and FTIR. The effects of the pH, flow rate, bed height and initial concentration of phenol and methylene blue are investigated, and the results shown that the effects of all 4 parameters are significant. The breakthrough time and the breakthrough adsorption capacity are used to evaluate the adsorption performance of phenol and methylene blue. Higher amounts of adsorbates are adsorbed on the activated carbon when low flow rate is utilized. As the initial concentration of adsorbates and the bed height increased, the amounts of adsorbates adsorbed also increased. Three kinetic models, Adam-Bohart, Thomas as well as Yoon and Nelson are applied to predict the breakthrough behaviour for the adsorption of phenol and methylene blue. Both Thomas model and Yoon and Nelson model are capable of providing a good fit to the experimental data.

ID: FYP2020/71

TANG SZE KHAI & RIDZUAN ZAKARIA

School of Chemical Engineering, Engineering Campus, Universiti Sains Malaysia,
14300 Nibong Tebal, Pulau Pinang, Malaysia

REVIEW: REMOVAL OF IRON ION IN INDUSTRIAL WASTEWATER USING MANGROVE ACTIVATED CARBON

ABSTRACT

Activated carbon is a highly sustainable alternative for adsorption comparable to efficiency of membranes, in term of cost effective. Mangrove as a widely available carbon source in Malaysia are converted to activated carbon using physical or chemical activation. Few studies are picked with different activation properties. It is proved that suitable functional group must be added to surface of pore to allow adsorption of heavy metal ion. Though there is insufficient time to perform iron adsorption study, mangrove activated carbon shows good absorbent properties to other heavy metal ion such as nickel and copper. Destroying original mangrove ecosystem brings side effects to sea coastal area.

ID: FYP2020/72

ADSORPTION OF COPPER (II) IONS BY USING MANGROVE-BASED ADSORBENT: OPERATION FACTORS AND KINETIC STUDIES

TEO PUI KUAN & RIDZUAN ZAKARIA
School of Chemical Engineering, Engineering Campus, Universiti Sains Malaysia,
14300 Nibong Tebal, Pulau Pinang, Malaysia

ABSTRACT

With the embarkment on finding the most suitable materials for effective adsorption and massive adsorbents production, several options of wood-based agricultures were proposed as adsorbents' raw material and compared for its removal efficiency based on its adsorption capacity. In conjunction, modified mangrove bark, was added as subject of studies to explore its potential as adsorbent after intrigue value in its adsorption capacity (6.95 mg/g $_{adsorbent}$) being reviewed from the previous work. Therefore, the studies of Cu(II) adsorption using modified mangrove bark was extended by studying the mesh size suitable for adsorption at different initial ion concentration and the results obtained were compared together with FTIR and BET test done with the mangrove bark before and after modification done to justify the importance of modification step. In the process, the adsorption kinetic for all adsorbents were investigated in relation with the effect of change in initial concentration. In the studies, the effect of modification done on carbon with mesh size 355 μm mesh size is most significant as it shows good overall removal percentage in high and low concentration without having polar opposite effect on adsorption. Also, the adsorption kinetic shows promising result whereby equilibrium can be achieved in 1.5 hrs under 100 ppm. In the adsorption kinetic model analysis, adsorption kinetic behaves differently at different initial

concentration. In higher initial concentration, all adsorbent fits well in Pseudo Second-Order (PSO) model. On the other hand, when lower ion centration applied, unmodified 250 µm adsorbent favour more on Pseudo First-order (PFO) model while others fits better at PSO model.

ID: FYP2020/73

ON THE GROWTH PROFILE AND TANNASE PRODUCTION FROM *PENICILLIUM VARIABLE* USING DIFFERENT TANNIC ACID SOURCES

TING SING KIONG & MOHAMAD HEKARL UZIR
School of Chemical Engineering, Engineering Campus, Universiti Sains Malaysia,
14300 Nibong Tebal, Pulau Pinang, Malaysia

ABSTRACT

Penicillium variable is one of species that has potential to produce tannase enzyme. Tannase is an inducible enzyme and it only can be produced in the presence of tannic acid. The purpose of this experiment was to study the growth of *Penicillium variable* under different tannic acid sources and determine the tannase production amount of *Penicillium variable* under different tannic acid source. In this experiment, tea leaves and mango leaves were used as the sources of tannic acid. *Penicillium variable* was grown in a modified Czapek's Dox medium and incubated at 30 ±1 °C in a shaker at 150 rpm. Under this condition, *Penicillium variable* experienced lag phase from day 0 to day 2 when grew in medium using mango leaves as a tannic acid source. The exponential phase occurred after day 2 and reached maximum cell concentration on day 4. On the other hand, *Penicillium variable* experienced lag phase from day 0 to day 1 when grew in medium using tea leaves as a tannic acid source. The exponential phase occurred after day 1 and reached maximum cell concentration on day 4. Then, *Penicillium variable* entered death phase after 4 day of incubation for both conditions. Through the growth profile, it is known that specific growth rate of *Penicillium variable* under mango leaves as a tannic acid source and *Penicillium variable* under tea leaves as a tannic acid source were 0.61 day^{-1} and 0.62 day^{-1} respectively. Tannase activity achieved 4.76 µmol/ml on the 3rd day of cultivation period when using mango leaves as a tannic acid source. As for tannase activity using tea leaves as a tannic acid source, it achieved 4.13 µmol/ml on the 3rd day of cultivation time. It proved that mango leaves and tea leaves are potential tannic acid source.

ID: FYP2020/74

CONCENTRATING NUTRIENTS FROM FISH FARM EFFLUENT VIA FORWARD OSMOSIS

VOO YEE XING & OOI BOON SENG
School of Chemical Engineering, Engineering Campus, Universiti Sains Malaysia,
14300 Nibong Tebal, Pulau Pinang, Malaysia

ABSTRACT

The fish farm effluent was studied its plausibility of using forward osmosis (FO) to treat the water discharge that was abundant with nutrients. Its lower pressure operation and less fouling tendency compared to conventional wastewater treatment could potentially help to concentrate the nutrients like ammonia, and phosphate. It would be testing with synthetic feed solution that contained the ammonia and phosphate with varying DS concentration for its concentration efficiency test prior to using real fish farm effluent. Meanwhile, observing the decline of flux to look for any fouling behaviors especially scaling the membrane surface in the form of struvite. This entire configuration would be conducted in cross-flow orientation and closed-loop, with the membrane active layer facing the feed side. It was found that the higher the DS concentration, the higher the concentration factor within 2 hours. At 2M of DS concentration, the concentration factors were 1.41 and 1.31 for ammonia and phosphate respectively, while using a real fish farm effluent had 1.24 and 1.72 for ammonia and phosphate respectively, which showed good retention for phosphate and vice-versa for ammonia. This could be CTA membrane was poor at retaining ammonia because the Xue, Yamamoto, and Tobino (2016) explained ammonia might undergo nitrification or oxidation by microbes in a long run, while Xue (2015) described another reason was ammonia was poorly retained in high pH. As for the fouling while using mixing nutrients and fish farm effluent had shown a decline in flux over the 6 hours operation.

ID: FYP2020/75

PROCESS CONTROLLABILITY OF AN INTENSIFIED SYSTEM

WONG YING SHIUAN & SYAMSUL RIZAL ABD SHUKOR
School of Chemical Engineering, Engineering Campus, Universiti Sains Malaysia,
14300 Nibong Tebal, Pulau Pinang, Malaysia

ABSTRACT

Intensified system has very fast responding time compare to conventional system and therefore each control element in control loop significantly affect its control performance. The controller was designed via IMC approach where it included all the dynamic of control elements in control loop. In intensified system, all the control elements are interacting with each other where variation of time constant of measurement, τ_m and time constant of actuator, τ_v were prove affecting the control performance. The best control performance was obtained with smallest value of τ_m and τ_v at 0.02s due to lowest percent of overshoot and smallest IAE value. Order of process is one of parameter influencing the control performance of intensified system in which process of first order without time delay showed the most satisfactory control performance. The compatibility of conventional sensor and actuator in intensified system were investigated. The results obtained signified that both conventional sensor and valve are not compatible with intensified system as they have poor control performance in term of percent of overshoot and IAE value. Improvement of intensified control system was made by changing the controller structure to PIDDD to PIDD and PID structure. It was concluded that changes in controller structure enhance the intensified system where the most satisfactory performance was shown by simplest controller structure (PID structure).

ID: FYP2020/76

ADSORPTION OF MALACHITE GREEN DYE IN AQUEOUS MEDIUM USING MAGNETIC MOF-5: EFFECT OF SILICA CONTENT AND MAGNETIC Fe_3O_4 MICROPARTICLES

YAZRI AZDI BIN RASDI & IRVAN DAHLAN
School of Chemical Engineering, Engineering Campus, Universiti Sains Malaysia,
14300 Nibong Tebal, Pulau Pinang, Malaysia

ABSTRACT

Nowadays, the amount of coloured wastewater released by many industries that are sent to the ecosystem were difficult to degrade. The research for effective and improved separation methods by using metal organic frameworks (MOFs) continues. In this study, the effects of the parameters carried out in liquid phase batch operations such as the adsorptions of malachite green dye by using different adsorbent, the silica content, magnetization, contact time and adsorbent dosage were used to investigate the efficiency of removal of the dye. Silica content was added to the unstable structure of MOF-5 and magnetic properties was added for better separation between the adsorbent and the dye solution. Data obtained from literature such as the characterization which include SEM and FTIR analysis were some of the techniques used on the MOF-5 to estimate the surface area and porosity etc. Based on the experimental result, non-magnetized MOF-5 with RHA burnt at 800°C have the lowest final concentration of dye solution as it had the highest reactivity due to its' amorphous phase with controlled burning and low amount of unburnt carbon in the ash. Non-magnetized samples have higher efficiency of dye removal compared to the magnetized samples.

ID: FYP2020/77

EFFECT OF DIFFERENT AERATION INTENSITY ON CULTURE SETTLEABILITY

YOKISENRAW A/L CHANDRARAO & VEL MURUGAN VADIVELU
School of Chemical Engineering, Engineering Campus, Universiti Sains Malaysia,
14300 Nibong Tebal, Pulau Pinang, Malaysia

ABSTRACT

Microalgae is a renewable resource which can cater to the demand of fuel and chemicals in this world. However, mass cultivation and harvesting of microalgae could be very challenging. In order to mass cultivate

microalgae, better microalgae biomass concentration and better settleability is needed. In this study, the effect of different aeration intensity on the settleability of the microalgae is studied using three photobioreactor. R1, R2 and R3 with 0.5 L/min, 2.0 L/min and 4 L/min aeration intensity respectively. The biomass growth, settleability (in terms of sludge volume index, SVI), extracellular polymeric substances (EPS) content were measure throughout the study. Reactors R2 and R3 showed better performance in terms of biomass growth and settleability. Reactor R2 has the highest biomass concentration and biomass recovery. Reactor R3 has the highest EPS content which positively influences the microalgae settleability. Nevertheless, the utilization of highest aeration intensity of 4 L/min (R3) in cultivating microalgae is not suitable as the high aeration intensity damages the cells and the higher dissolved oxygen concentration in the reactor inhibits photosynthesis process. Higher aeration intensity is also not sustainable as it relatively consumes higher energy and will not be economically feasible.

ID: FYP2020/78

MANGOSTEEN PEEL-DERIVED HYDROCHAR PREPARED VIA HYDROTHERMAL CARBONIZATION FOR METHYLENE BLUE REMOVAL

YOU JIN JIE & NOORASHRINA A HAMID
School of Chemical Engineering, Engineering Campus, Universiti Sains Malaysia,
14300 Nibong Tebal, Pulau Pinang, Malaysia

ABSTRACT

The interest of transforming mangosteen peel into useful adsorbent via conventional pyrolysis method has been established in the recent years. Hydrothermal carbonization (HTC) arises as an improved carbonization step developed to enhance the carbon porosity and reduce the production cost by thermally treating feedstock under milder operating conditions. Therefore, this research work aimed to generate hydrochar from mangosteen peel (MPHTC) via hydrothermal carbonization for the removal of methylene blue from aqueous solution. Also, it was targeted to perform kinetic and isotherm studies on the experimental result. In the study, hydrochar was synthesized at an optimized carbonization temperature (200 °C) with a production yield of 82.75% and a methylene blue removal of 75.93%. Batch adsorption of methylene blue has been conducted on resultant hydrochar at varied operating parameters such as initial dye concentration (50 mg/L to 250 mg/L) and solution pH (3 to 11). The adsorption capacity of adsorbent enhanced with the increasing initial dye concentration due to high driving force for efficient mass transfer. The hydrochar could attain its maximum adsorption capacity at 131.58 mg/g. The derived hydrochar performed a higher uptake of dye molecules under basic conditions rather than acidic conditions owing to the presence of OH group for the attachment of cationic dye. It was determined that Freundlich isotherm and pseudo second order kinetic models best fitted the experimental data. External film diffusion was found to be the rate-controlling step for the batch adsorption process. The results revealed that MPHTC is a promising adsorbent for treatment of cationic dye in effluent wastewater.

ID: FYP2020/79

BIOFUEL PRODUCTION FROM USED COOKING OIL VIA CATALYST CRACKING PROCESS WITH ALUMINA SUPPORTED METAL OXIDE CATALYSTS

YU JIA XIN & TYE CHING THIAN
School of Chemical Engineering, Engineering Campus, Universiti Sains Malaysia,
14300 Nibong Tebal, Pulau Pinang, Malaysia

ABSTRACT

Depletion of fossil fuels in the recent years has led to an urge to develop the potential renewable energy as the useful fossil fuel substitute. Moreover, the environmental issue that raised by the combustion process of fossil fuels becomes a major concern worldwide. Used cooking oil as the most economical candidate for biofuel production is believed to reduce dependency on fossil fuels as well as mitigate emission of greenhouse gases. In the present study, the performances of Fe_2O_3/Al_2O_3, MgO/Al_2O_3 and ZnO/Al_2O_3 catalysts were investigated to produce liquid biofuels via catalytic cracking of used cooking oil. The catalytic cracking reaction was carried out in a fixed bed reactor. Among the three catalysts, Fe_2O_3/Al_2O_3 gave the highest liquid product yield of 34.80%. On the other hand, the influence of variation of reaction temperature between 450°C and 550°C to the biofuel

production has been evaluated. The results revealed that Fe_2O_3/Al_2O_3 catalyst achieved highest liquid product yield at reaction temperature of 500°C. The composition of liquid product was analysed using a GC-FID and categorized into three groups, which were gasoline, kerosene and diesel fractions. The catalyst deactivation over with time also rendered a significant effect towards the catalytic activity whereby a high catalytic activity was at the beginning of cracking reaction, and gradually loss of catalytic activity over the time.

ID: FYP2020/80

GROWTH KINETIC OF PENICILLIUM GLABRUM DURING A SOLID-STATE FERMENTATION

MUHAMMAD AZRI BIN A. NORIZAN & MOHAMAD HEKARL UZIR
School of Chemical Engineering, Engineering Campus, Universiti Sains Malaysia,
14300 Nibong Tebal, Pulau Pinang, Malaysia

ABSTRACT

Penicillium glabrum also has been used widely as enzyme production in food and medical industry such as instant tea, acorn wine and drug trimethoprim in the gallic acid. Additionally, this fungus rate of kinetic growth depends on the environmental factors to keep survive and response to the stress exposed. Besides, sufficient back mixing, spore transfer is an essential for the sterile feed and inoculation to entering the reactor to prevent growth of the undesirable microorganisms. For a further study, linking of the fungal uptake, growth kinetics, inoculation mechanism behaviour and washout condition to achieve optimal condition should be considered and focus for future studies.

ID: FYP2020/81

PARAMETERS AFFECTING MICROALGAE GROWTH AND KINETIC MODELS OF MICROALGAE CULTIVATION FOR BIOFUEL PRODUCTION

SITI QARIYAH ISMAIL & VEL MURUGAN VADIVELU
School of Chemical Engineering, Engineering Campus, Universiti Sains Malaysia,
14300 Nibong Tebal, Pulau Pinang, Malaysia

ABSTRACT

Biofuel which derived from biomass has been recognized as one of alternative source to replace fossil fuel. Biomass comes from plant, algae material or animal waste. Microalgae appears to possess high potential in production of biofuel due to high value of lipid and biomass productivity compare to another feedstock. The important key in gaining high production of biofuel from microalgae include the identification of parameters that influence the microalgae cultivation, the cultivation system and kinetic models of microalgae growth. Parameters (light, temperature, pH, salinity, and nutrient) are the major factors that affecting the growth rate and photosynthesis activity of microalgae. The different type of microalgae cultivation system (phototrophic, heterotrophic, mixotrophic, and photoheterotrophic) and type of kinetic models for microalgae cultivation (Monod and Droop) are compared and critically discussed in this study.

ACKNOWLEDGEMENTS

SCIENCE & ENGINEERING RESEARCH CENTRE (SERC)

Universiti Sains Malaysia

Engineering Campus

14300, Nibong Tebal

Seberang Perai Selatan

Pulau Pinang

Malaysia

http://serc.eng.usm.my/index.php/ms/

Published by,

School of Chemical Engineering
Engineering Campus
Universiti Sains Malaysia
14300, Nibong Tebal
Penang, Malaysia

UNIVERSITI SAINS MALAYSIA

APEX™